Chemical composition of scheelite and its application as an indicator mineral

Thèse de doctorat

Ana Carolina Rodrigues Miranda

Sous la direction de:

Georges Beaudoin, directeur de recherche

Bertrand Rottier, codirecteur de recherche

Résumé

La scheelite est un minéral de tungstène ($CaWO_4$) qui est présent dans plusieurs gisements magmatiques-hydrothermaux et qui est associé temporellement et spatialement à l'or dans certains gisements d'or orogéniques dans le monde. Comme la scheelite est un minéral résistant et lourd, et qu'elle est facile à identifier en raison de sa propriété luminescente, sa présence dans les sédiments a été utilisée comme outil pour cibler les gisements de tungstène et, plus récemment, les gisements d'or orogéniques dans les régions où l'exposition du substratum rocheux est rare. La scheelite contient certains éléments traces clés (Sr, Mo, REE, Na, As) dont la distribution et la concentration sont contrôlées par le contexte géologique dans lequel la scheelite s'est formée. Par conséquent, comprendre les facteurs qui contrôlent la distribution des éléments traces dans la scheelite permet d'utiliser la composition de la scheelite pour cibler les gisements minéraux.

Cette thèse de doctorat étudie la composition en éléments traces de la scheelite associée aux principaux gisements magmatiques-hydrothermaux contenant de la scheelite, tels que les skarns oxydés et réduits, les veines de quartz/greisen à Sn-W, les porphyres à W-Mo et les systèmes aurifères liés à des intrusions réduites, afin d'identifier les principaux facteurs qui contrôlent la distribution des éléments mineurs et traces dans la scheelite. Ces nouvelles données sont combinées avec les données de la littérature sur les gisements d'or orogéniques contenant de la scheelite et étudiées à l'aide de l'analyse discriminante des moindres carrés partiels (PLS-DA) pour trouver les variables chimiques qui permettent de distinguer la scheelite des différents types de gisement et de les utiliser pour cibler les gisements de minerai d'or et de tungstène.

Les résultats montrent que la fugacité de l'oxygène, la composition des fluides et des intrusions, les minéraux co-précipités et la salinité des fluides sont les principaux paramètres qui contrôlent l'incorporation des éléments traces dans la scheelite provenant de gisements magmatiques-hydrothermaux. Les résultats de l'analyse PLS-DA montrent que les teneurs élevées en Mo, As et V dans la scheelite sont caractéristiques des dépôts magmatiques-hydrothermaux formés sous une fugacité élevée de l'oxygène, tels que les skarns oxydés, tandis que les teneurs élevées en Nb, Mn, Y et U sont caractéristiques de la scheelite formée dans des conditions réduites, qui sont généralement associées aux skarns réduits et aux veines de quartz/greisen à Sn-W. La scheelite provenant de gisements d'or orogéniques présente une anomalie positive prédominante en Eu, une teneur élevée en Sr, et de faibles

teneurs en Mo, Mn et Nb, ce qui la distingue de la scheelite liée aux gisements magmatiques-hydrothermaux. De telles différences permettent de discriminer la scheelite associée à l'or orogénique de celles des dépôts magmatiques-hydrothermaux.

En plus de l’analyse PLS-DA, deux modèles de Random Forest sont proposés pour évaluer la source de la scheelite et la fertilité en or des gisements d'or orogéniques contenant de la scheelite. La grande justesse obtenue par les deux modèles renforce l'utilisation des éléments traces dans la scheelite non seulement comme un outil robuste et efficace pour cibler les gisements contenant de la scheelite, mais aussi pour évaluer la fertilité des gisements d’or orogéniques contenant de la scheelite.

Abstract

Scheelite is a tungsten mineral ($CaWO_4$) that is present in several magmatic-hydrothermal deposits and occurs temporally and spatially associated with Au in some orogenic Au deposits worldwide. Because scheelite is a resistant, heavy mineral, and easy to identify due to luminescence propriety, its occurrence in unconsolidated sediments has been used as a tool for targeting tungsten and orogenic Au deposits in areas where the bedrock exposition is rare. Scheelite hosts some key trace elements (Sr, Mo, REE, Na, As) those distribution and concentration are controlled by the geological settings where scheelite formed. Therefore, understanding the factors that control the distribution of trace elements in scheelite provides insights for using scheelite composition to target mineral deposits.

This PhD thesis investigates the trace element composition of scheelite associated with the main scheelite-bearing magmatic-hydrothermal deposits such as oxidized and reduced skarns, quartz-vein/greisen Sn-W, porphyry W-Mo and reduced intrusion-related gold systems (RIRGS) to identify the principal factors that control the distribution of minor and trace elements in scheelite. This new data is combined with literature data of scheelite-bearing orogenic Au deposits and investigated using partial least square-discriminant analysis (PLS-DA) to find the chemical variables that allow for discriminating scheelite from different deposit types and use these to target for Au and W ore deposits.

The results show that oxygen fugacity, fluid and intrusion compositions, co-precipitated minerals and fluid salinity are the main parameters that control the incorporation of trace elements in scheelite from magmatic-hydrothermal deposits. The PLS-DA results show that high Mo, As and V contents in scheelite are characteristic of magmatic-hydrothermal deposits formed under high oxygen fugacity such as oxidized skarns, whereas high Nb, Mn, Y and U contents are features of scheelite formed under reduced conditions, which are commonly associated with reduced skarns and quartz-veins/greisen Sn-W deposits. Scheelite from orogenic Au deposits displays predominantly positive Eu anomaly, high Sr and low Mo, Mn and Nb contents which differ from scheelite related to magmatic-hydrothermal deposits. Such differences allow discriminate scheelite associated with orogenic gold from those of magmatic-hydrothermal deposits.

In addition to PLS-DA, two Random Forest models are proposed to assess the source of scheelite and the Au endowment of scheelite-bearing orogenic Au deposits. The high

accuracy obtained by the two models enhances the use of trace element in scheelite not only as a robust and efficient tool for targeting scheelite-bearing deposits, but also to assess the fertility of scheelite-bearing orogenic Au deposits.

Table of Contents

List of Figures

List of Tables

List of Appendices

List of Abbreviations

CL: Cathodoluminescence

EPMA: Electron Probe Microanalysis

LA-ICP-MS: Laser ablation-inductively coupled plasma-mass spectrometry

PLS-DA: Partial least squares-discriminant analysis

RF: Random Forest

RIRGS: Reduced Intrusion Related Gold Systems

Acknowledgments

First, my sincerely thank to my supervisor Prof. Georges Beaudoin for giving me the opportunity to pursue this PhD research, for his constant support and guidance. Also many thanks my co-supervisor Prof. Bertrand Rottier for sharing his enthusiasm and knowledge.

An enormous thanks to all collaborators who provided the samples to conduct this study. Many thanks to Émilie Bédard and Enzo Caraballo for their support with R and everything related to coding. Edmond Rousseau and Marc Choquette for the patient with my terrible French and the support with the samples and microprobe analysis. Audrey Lavoie and Dany Savard from UQAC for the LA-ICP-MS analysis. This project wouldn't have been possible without all of you.

I thank all colleagues in the chair and on the third floor of the Adrien Pouliot (Alex, Enzo, FX, Victor, Chao, Haiming, Jeremie, Samuel, Cecile, Flor, Julie, Isaac and Bruna) for providing enjoyable environment. Special thanks to Vinicius Boico, a wonderful Brazilian soul that I've met in the first day I arrived in Ulaval, for his friendship.

A huge thank to all friends that I've made in the 2059 in Chicoutimi (Doudou, Charley, Renato, Yan, Omi, Georgia, Ben, Vincent, Alizée, Pierre, Nancy). Thanks for sharing special, fun and friendly moments (soirées, barbecue, canoeing and snowshoeing) and good food. You have made my time in Canada even better. Special thanks to Doudou, especially during the COVID, who made this hard time lighter and less sad.

An enormous thank to my family for all support, even with the distance. Mom and Dad thanks for everything that you've done for us (Marco and I). I couldn't have gotten this far without you two. Marco, my annoying big brother, thank you for taking care of our parents (and Acerola) in the difficult times that I couldn't be there. I love you all.

Finally, a thousand thanks to the group, my dear partner Eduardo Mansur. Your endless love, support and patience over the last 10 years have helped me to be a better person every day. Thank you for believing in me (someone in the group must believe), for always being you (sincere, no matter what), for our daily philosophical and geological conversations, and for pushing me to get out of my comfort zone and to do my best, always. As the group knows *la vie est plus belle ensemble*. I love you.

Foreword

This thesis is an original work by the author Ana Carolina Rodrigues Miranda. It is composed of introductory section, three research articles and one study in progress organized in the form of chapters (chapters 1, 2, 3 and 4), a general discussion and conclusion. All tasks related to realization of this thesis, which include the collection and preparation of samples for thin sections, chemical analysis, compilation and interpretation of the data, and writing were conducted by the author and supervised by Dr. Georges Beaudoin and co-supervised by Dr. Bertrand Rottier, who co-authored the three articles.

This PhD project was funded by Natural Sciences and Engineering Research Council (NSERC) of Canada, Agnico Eagle Mines Ltd., and Ministère de l'Énergie et des Ressources Naturelles du Québec. It is part of the research projects of the NSERC-Agnico Eagle Industrial Research Chair in Mineral Exploration held by Prof. Georges Beaudoin, which objective is the development of robust and effective tools for the mineral exploration. Also, this project has been made possible due to samples provided by national and international geological surveys, mining companies and academic researchers.

Introduction is an original work by the author.

The **chapter 1,** entitled *Scheelite chemistry from skarn systems: implications for ore-forming processes and mineral exploration* by Miranda, A.C.R., Beaudoin, G. and Rottier, B., was published in the journal Mineralium Deposita on May 2022. This article highlights how scheelite composition varies in skarn-type deposits according to different conditions of formation, which lead to distinct mineral assemblage and metal content. All the co-authors collaborated with relevant discussions for the improvement of the manuscript.

The **chapter 2**, entitled *Trace element signatures in scheelite associated with various deposit types: a tool for mineral targeting* by Miranda, A.C.R., Beaudoin, G., Rottier, B., Pašava, J., Bohdálek, P., and Malec, J., will be submitted for publication in Journal of Geochemical Exploration. This chapter integrates new chemical composition data of scheelite in various magmatic-hydrothermal deposits and compiled literature data. The objective is to build a model based on scheelite composition to discriminate deposit types. This paper counted with the collaboration of Pašava, J., Bohdálek, P., and Malec J., Geological Survey of Czech Republic), who provided several samples and significant scientific approach for the realization of this study.

The **chapter 3,** entitled *Prediction of metal endowment in orogenic Au deposits based on scheelite trace element composition and Random Forest classifier* by Miranda, A.C.R., Beaudoin, G., and Rottier, B., will be submitted for publication in journal “Geology”. This study is a compilation of scheelite chemistry data from several orogenic Au deposits of different sizes aiming to use scheelite composition as an indicator of Au endowment of orogenic Au deposits. The data compilation and writing were done by the author, and the co-authors collaborated with insightful discussions.

The **chapter 4**, entitled *In situ Sm-Nd analysis in scheelite from magmatic-hydrothermal deposits,* is a work in progess that consists of preliminary results of in situ Sm-Nd analysis in scheelite from nine magmatic-hydrothermal deposits.The objective of this study is to investigate Nd isotopes in scheelite from magmatic-hydrothermal and orogenic Au deposits and determine the source of the metals (W and Au) in few W and Au provinces. However due to COVID-19 issues, only few data have been acquired until submission of this thesis.

Discussion is an original work by the author.

Conclusion is an original work by the author.

Introduction

Overview of scheelite occurrence and chemistry

Scheelite, a calcium tungstate mineral ($CaWO_4$), is a common mineral in skarn, quartz-vein/greisen Sn-W and porphyry Mo-W deposits, as well as an accessory mineral in reduced intrusion-related gold systems (RIRGS) and orogenic Au deposits (Brown and Nesbitt 1986; Groves et al. 1998; Brugger et al. 2000; Hart 2007; Song et al. 2014; Guo et al. 2016; Xu et al. 2019; Craw et al. 2015). Scheelite also occurs in metasediments as a product of breakdown of rutile during regional metamorphism (Cave et al. 2017; Palmer 2021). Additionally, because scheelite is a heavy mineral (specific gravity of 5.9-6.1), it can easily be concentrated in sediments thus forming placer type deposits (Willden and Hotz 1995).

Scheelite crystal structure accommodates key trace elements such as Mo, Nb, Sr, REE, for which abundance is controlled by physico-chemical parameters and composition of the fluids (Hsu and Galli 1973; Tyson et al. 1988; Raimbault et al. 1993; Brugger et al. 2008; Zhao et al. 2018; Poulin et al. 2018; Sciuba et al. 2020; Miranda et al. 2022). Consequently, scheelite composition has been widely used to constrain the path and source of fluids (Kent et al. 1995; Voicu et al. 2001; Scanlan et al. 2018; Elongo et al. 2022), age (Bell et al. 1989; Darbyshire et al. 1996; Wintzer et al. 2022) and as a proxy for physico-chemical conditions in several geological settings (Brugger et al. 2008; Song et al. 2014; Kozlik et al. 2016a; Zhao et al. 2018). Additionally, because of its occurrence in distinct geological settings, scheelite composition has been used to discriminate different types of deposits (Song et al. 2014; Poulin et al. 2018; Sciuba et al. 2020; Miranda et al. 2022).

Skarns are calc-silicate rocks which form in or at the contact with calcium-rich rocks, as a result of their interaction with magmatic-hydrothermal fluids (Einaudi et al. 1981). In skarn deposits, scheelite is commonly associated with garnet, clinopyroxene, wollastonite, amphibole, epidote and biotite, besides of sulfides and oxides (Newberry 1982). Two types of tungsten skarns, where scheelite is the main W mineral, have been recognized: reduced and oxidized skarns (Einaudi et al. 1981). Reduced skarns are closely associated with reduced intrusions and occur in pure carbonate rocks, whereas oxidized skarns show a strong association with relatively oxidized intrusions, and are generally hosted in Fe-rich carbonaceous sedimentary rocks (Newberry 1983; Newberry and Swanson 1986).

Quartz-vein/greisen Sn-W deposits consist of simple to complex fissure fillings or replacement quartz-veins that occur within or near granitic intrusions (Pirajno, 1992). Such fissures may occur accompanied by gresen alteration, which results in the alteration of feldspar to quartz-muscovite with disseminated Sn (cassiterite) and/or W (scheelite/wolframite) minerals (Taylor 1979; Reed 1986). In general, quartz-vein/greisen Sn-W deposits are associated with highly fractionated and silica-rich intrusions, which range from peraluminous to peralkaline compositions, and are enriched in lithophile (Rb, Li, Be, Sn, W, Mo, Ta, Nb, U, Th, and REEs) and volatile elements (B and F; Tischendorf 1977; Pollard et al. 1987).

Porphyry W-Mo deposits are typically medium to low grade deposits (0.1-0.4% WO_3) associated with late phase subvolcanic rhyolite porphyry or deeper monzogranite stocks (Noble et al. 1984; Sinclair et al. 1986). In porphyry W-Mo deposits, scheelite (and/or wolframite) and molybdenite occur commonly as disseminated grains, in veins and veinlets, and in breccia pipes in or above the granitic rocks.

As the name itself says, RIRGS are Au deposits related to granitic intrusions. They share many similarities in terms of fluid composition (low-salinity and CO_2-rich fluids), metal association and alteration with the genetically distinct orogenic Au deposits (Hart and Goldfarb 2005). Moreover, RIRGS differ from Au-Cu porphyry deposits mainly due to reduced character of the intrusions. In RIRGS, Au(±W) mineralization is commonly found in intrusion-hosted sheeted quartz veins or in the immediate wall rocks of intrusions, which comprise skarn-, replacement- and veinmineralization (Lang and Baker 2001; Hart and Goldfarb 2005; Goldfarb et al. 2005; Hart et al. 2007).

Orogenic Au deposits occur in metamorphic rocks (metasedimentary and/or metavolcanic rocks) of all ages, generally formed in the mid- to shallow crust (5-15 km), at temperatures of 200-650°C and pressures of <1-5 kbar during compressional to transpressional deformation processes linked to orogens (Groves et al. 1998; Goldfarb et al. 2005). The Au mineralization is structurally controlled and occurs mostly in quartz-carbonate veins and sulfides, with traces of albite, paragonite, white mica or fuchsite, chlorite, scheelite, and tourmaline (Groves et al. 1998).

Scheelite as an indicator mineral

Indicator minerals are mineral species whose presence in clastic sediments indicates the occurrence of a specific mineralization, hydrothermal alteration or lithology (McClenaghan 2005). Indicator mineral technique has been widely used in the initial stages of mineral exploration aiming to target new ore deposits. Among the requirements for an effective indicator mineral for mineral exploration are: (1) occurrence in rocks related to an ore deposit; (2) a sufficiently wide compositional range that allows accessing genetic information about the metallogenetic environment; (3) the ability to survive extensive surficial weathering and transport, and (4) being relatively easy to identify, separate and analyze (Averill 2001; McClenaghan 2005; McClenaghan & Kjarsgaard 2007). Among the well-known indicator minerals are: pyrope garnet, pyroxene, olivine, Cr-Mg chromite, spinel, Mg-ilmenite and diamond, for diamond targeting (Gurney 1984; McClenaghan & Kjarsgaard 2001); gold, pyrite, rutile, tourmaline and scheelite for Au deposits (McClenaghan and Cabri 2011); alunite, apatite, magnetite, barite and sulfides for porphyry Cu (Averill 2001); scheelite, wolframite and sulfides for intrusion-related W deposits (McClenaghan et al. 2017).

Because scheelite is a direct evidence of tungsten mineralization, it has been used as an indicator mineral for targeting primary tungsten-bearing deposits (Toverud 1984; Averill 2001). Around known tungsten deposit, studies have demonstrated the ability of scheelite to resist to long transport (approximately 10 km down ice of deposit), which enhances its use an efficient mineral for targeting primary tungsten-bearing deposits (McClenaghan et al. 2017). Studies have shown that scheelite can be effectively used to target orogenic Au (Maneglia et al. 2017; Grzela et al. 2019; Sciuba et al. 2020; de Bronac de Vazelhes 2019; Mendizabal 2022).

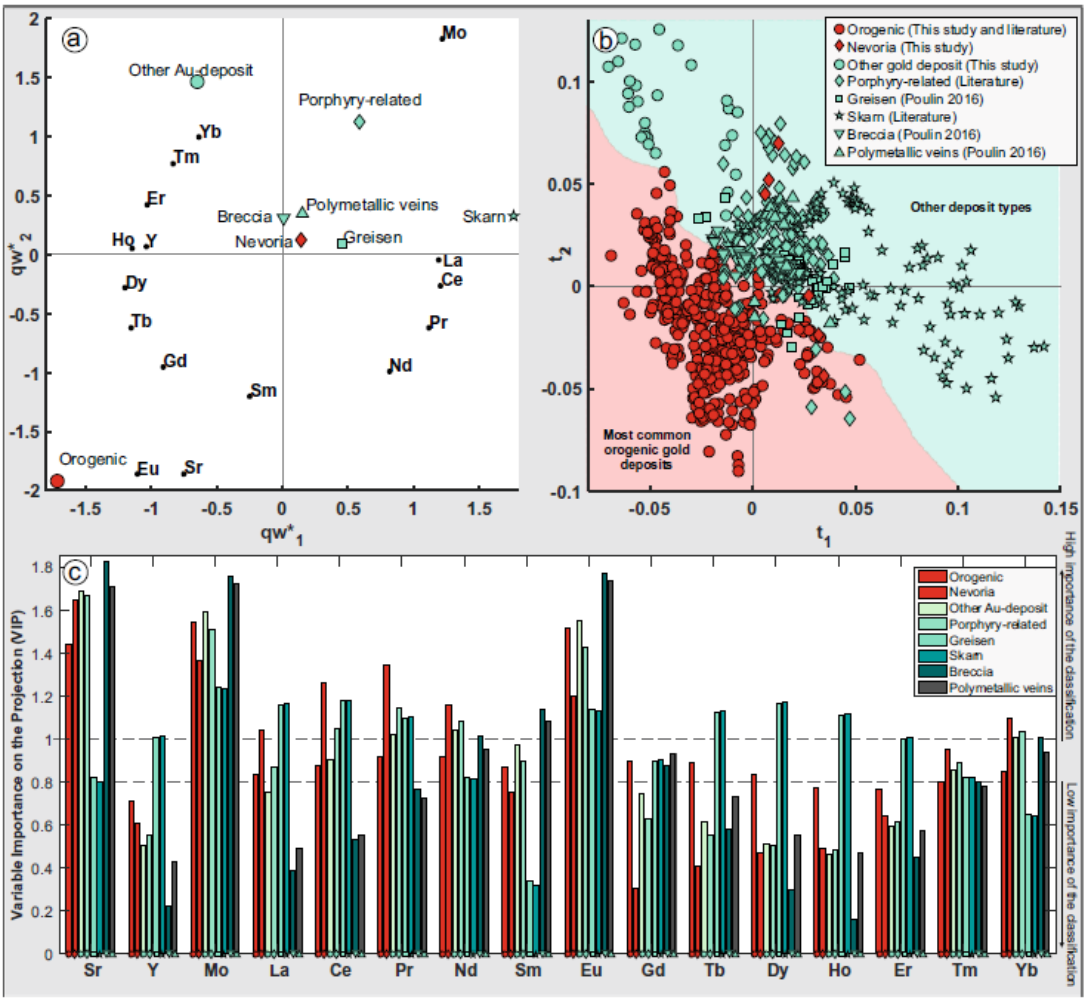

Figure 1. Partial least square-discriminant analysis of LA-ICP-MS data for scheelite from different deposit types. The PLS-DA was performed with limited set of analysed trace elements (Sr, Mo and REE). a The qw*1-qw*2 loadings plot shows correlations among elemental variables and deposit types. b The t1-t2 scores plot shows the distribution of scheelite samples in the qw*1- qw*2 space. c Variable importance of the projection (VIP) per deposit types shows the detailed element contribution per deposit. Diagram from Sciuba et al. (2020).

Problems and objectives

Few studies have shown the potential of scheelite trace element composition to discriminate distinct deposit types, even with a limited dataset (Song et al. 2014; Poulin et al. 2018; Sciuba et al. 2020; Fig. 1). However, most of these studies have concentrated on scheelite from skarn and orogenic gold deposits. The characterization of the chemical composition of scheelite in other deposit types such as porphyry W-Mo, quartz-veins/greisen Sn-W and RIRGS remains poor. The main focus of this PhD is to develop, based on scheelite chemistry, effective tools for mineral exploration to target W and Au deposits.

This thesis addresses two main questions: (1) can scheelite composition be effectively used to discriminate different deposit types?; and (2) whether scheelite trace element composition can be used to assess the metal endowment of mineral deposit. To answer these questions, two hypotheses are tested: (i) scheelite trace element composition varies following magmatic-hydrothermal deposits; and (ii) metal endowment is reflected in scheelite composition from orogenic Au deposits. To test the risen hypotheses, the steps below were followed:

- Investigation of mineral assemblage and textural relationships for scheelite-bearing samples from well-known magmatic-hydrothermal deposits;
- Analysis of the concentration and distribution of major, minor and trace elements in scheelite from these various ore deposits;
- Combination of the results with literature data to improve the application of scheelite as an indicator mineral;
- Use of multivariate statistical method such as PLS-DA to find discriminant variables that may help to fingerprint scheelite from each type of deposit;
- Use of machine learning approach such as Random Forest (RF) algorithm to classify scheelite-bearing deposits, and then predict the source of unkown scheelite recovered from sediments for mineral exploration of Au and W deposits in order to optimize the exploration strategies;
- Assess the chemical composition of scheelite as an indicator mineral of the Au endowment in orogenic Au deposits.

Methodology

This section provides a synthesis of the methods used to investigate the aforementioned hypotheses and thus attain the established objectives. More details on the analytical methods are provided in the individual chapters.

The prior characterization of the scheelite-bearing deposit is an essential information to guide us in the correct classification of each deposit type and assist in the interpretation of the trace element results. The sampling strategy was focused on selecting well-documented magmatic-hydrothermal scheelite-bearing deposits worldwide, where scheelite occurs both as major and accessory mineral, and that could cover different conditions of formation (i.e., different fO_2, and fluid salinity), host rock compositions, hydrothermal

alteration and mineral assemblage. The selected scheelite-bearing samples were obtained through the collaboration of academic and geological survey researchers, and geologists from mining companies worldwide.

Major and minor element composition of scheelite and silicates minerals (garnet and clinopyroxene), and cathodoluminescence (CL) images of scheelite were obtained by electron probe micro-analyser (EPMA) at Université Laval, using a CAMECA SX-100 instrument equipped with five wavelength-dispersive spectrometers (WDS). All analyses were performed using a 10-µm-diameter beam. Analytical conditions for major elements analyses were 20 nA for beam current and 15 kV for accelerating voltage, with a counting time of 20 s at the peak and 10 s at the background. For minor elements in scheelite (Na, Sr, Mo, Y and Fe), the analytical conditions were 100 nA beam current, 15 kV of accelerating voltage, and counting times of 120 s at the peak and 30 s at the background.

The concentration and distribution of the minor and trace elements in scheelite and silicate minerals (garnet and pyroxene) were determined by laser ablation-inductively coupled plasma mass spectrometry (LA-ICP-MS) at LabMaTer (UQAC), using an Excimer 193-nm RESOlution M-50 laser ablation system (Australian Scientific Instrument) equipped with a double volume cell S-155 (Laurin Technic) and coupled with an Agilent 7900 mass spectrometer. The LA-ICP-MS tuning parameters for each analytical section, isotopes measures, and the results for reference materials are reported in chapters 1 and 2. Data reduction was carried out using the Iolite package for Igor Pro software (Paton et al. 2011).

Scheelite compositional data were then investigated using basic and multivariate statistics using Rstudio v4.04 (R Core Team 2021). Elements with ≤ 40% below detection limit (bdl) or left-censored data were imputed using log-ratio Expectation-Maximisation (lrEM) algorithm from the R package zCompositions (Palarea-Albaladejo and Martín-Fernández 2015) before the statistical analysis. After imputation, the dataset was transformed using centred-log ratios (clr) to overcome the closure effect in compositional data (Aitchison, 1986).

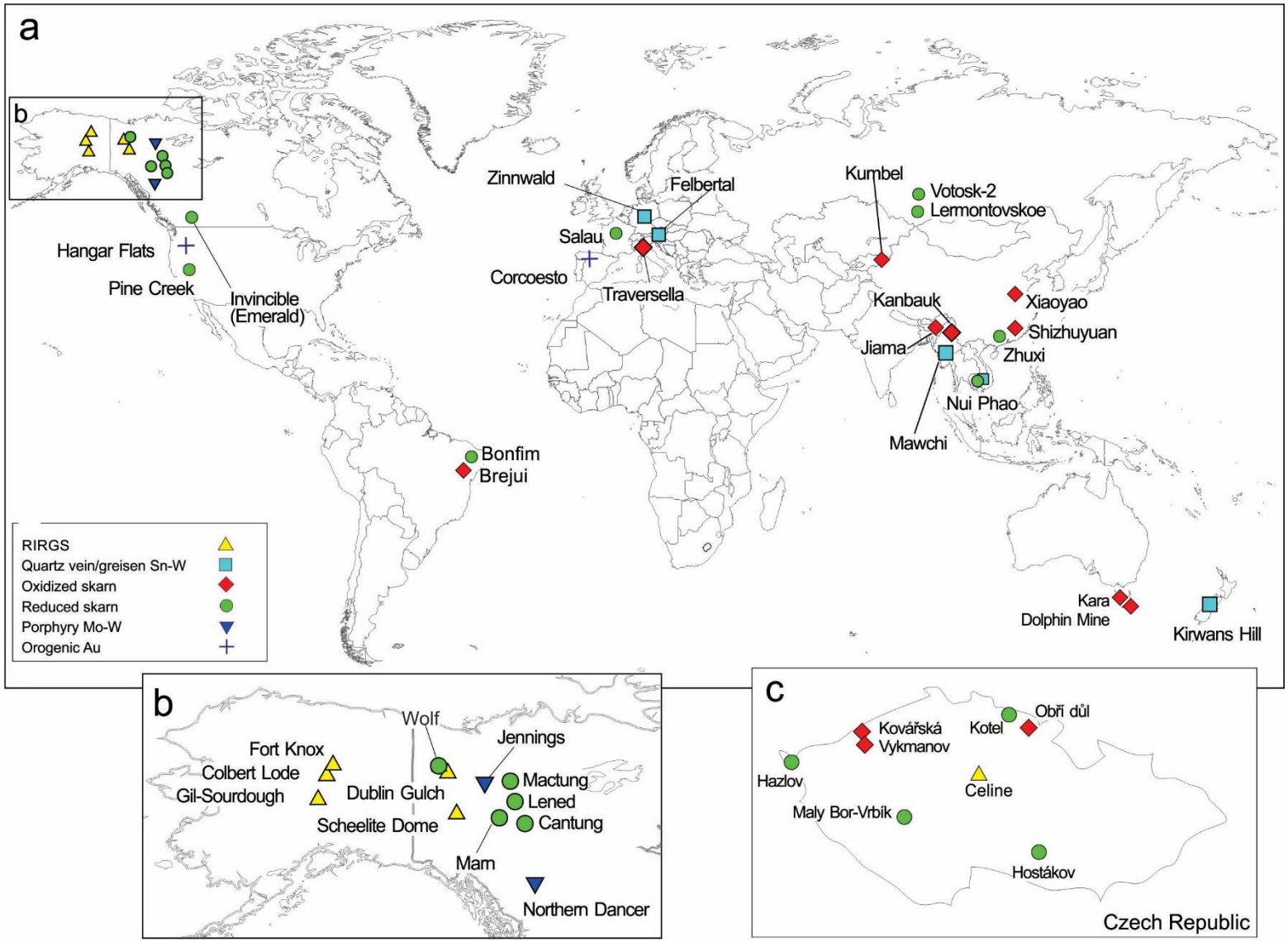

Figure 2. (a) World distribution of scheelite-bearing ore deposits samples considered in this study. In (b) samples location from Alaska-Yukon, and in (c) samples location in Czech Republic.

Table 1. List of the selected scheelite-bearing deposits for this study.

Deposit name	Country	Major metal	Reference
Quartz-vein/Greisen W-Sn			
Felbertal	Austria	W	Kozlik et al. (2016a,b)
Kirwans Hill	New Zealand	W	Pirajno and Bentley (1985)
Mawchi	Myanmar	Sn-W	Myint et al. (2018)
Nui Phao	Vietnam	W-Bi-Cu-F-(Au)	Nguyen et al. (2020)
Zinnwald	Germany	Sn-W-Li	Webster et al. (2004); Breiter et al. (2017)
Oxidized skarn			
Brejui	Brazil	W	Souza Neto et al. (2008)
Jiama	China	Cu-polymetallic	Zheng et al. (2016)
Kanbauk	Myanmar	Sn-W-F	Zhang et al. (2022)
Kara	Australia	Fe-W	Zaw and Sinogyi (2000); Sinogyi and Zaw (2001)
King Island	Australia	W	Kwak and Tan (1981)
Kovářská	Czech Republic	F-Ba-Fe-W	Štemprok and Mašková (1992)
Kumbel	Kyrgyzstan	W-Mo-Cu-Bi	Soloviev (2015)
Obří důl	Czech Republic	Fe-Cu-As-W	Veselovský et al. (2018)
Shizhuyuan	China	W-Mo-Sn-Bi-F	Lu et al. (2003)
Traversella	Italy	Cu-Fe-W	Dubru et al. (1988); Auwera and Andre (1991)
Vykmanov	Czech Republic	Zn-Pb-W	Štemprok and Mašková (1992)
Xiaoyao	China	W-Mo-Cu	Su et al. (2020)
Reduced skarn			
Bonfim	Brazil	W-Au	Souza Neto et al. (2008)
Cantung	Canada	W-Cu	Mathieson and Clark (1984)
Hazlov	Czech Republic	W	Štemprok and Mašková (1992)
Hostákov	Czech Republic	W	Štemprok and Mašková (1992)
Invincible Mine/Emerald	Canada	W-Mo(Au-Pb-Zn)	Ball (1954)
Kotel	Czech Republic	Cu-Fe-Zn	Žacek (2008)
Lened	Canada	W-Cu	Dick and Hodgson (1982)
Lermontovskoe	Russia	W-Cu(Au)	Soloviev et al. (2015)
Mactung	Canada	W-Cu	Dick and Hodgson (1982)
Marn	Canada	Au-Cu-W	Brown and Nesbitt (1986)
Pine Creek	USA	W	Newberry (1982); Porter (2013)
Ray Gulch or Mar	Canada	W	Brown et al. (2002)
Salau	France	W-Au	Poitrenaud et al. (2019)
Vostok-2	Russia	W-Cu(Au)	Soloviev et al. (2017)
Maly Bor-Vrbík	Czech Republic	W	J. Pasava pers. comm.
Zhuxi	China	W-Cu	Pan et al. (2020)
RIRGS			
Celine	Czech Republic	Au	Lang and Barker (2001)

Deposit name	Country	Major metal	Reference
RIRGS			
Dublin Gulch	Canada	Au-W	Maloof et al. (2001)
Fort Knox-Colbert Lode	USA	Au-W	Thompson et al. (1999)
Gil-Sourdough	USA	Au	Allegro (1987); Blum (1985)
Scheelite Dome	Canada	Au-W	Mair et al. (2006)
Porphyry W-Mo			
Jennings	Canada	W-Mo	Yukon Open File (2018)
Northern Dancer	Canada	W-Mo	Noble et al. (1984)
Orogenic Au			
Corcoesto	Spain	Au	Boiron et al. (2003); Cepedal et al. (2014)
Hangar Flats	USA	Au-Sb-W	Wintzer et al. (2022)

Two principal methods, Partial Least Squares-Discriminant Analysis (PLS-DA) and Random Forest (RF), commonly used for classification and prediction purpose were used in this study. PLS-DA is a multivariate dimensionally-reduction tool that was applied in scheelite chemistry data to reveal hidden correlations between the variables and the deposit types, and to identify potential elements useful to classify scheelite from different geological settings/sources. Random Forest was mostly used for classification and prediction purpose and to test whether scheelite trace element composition could be effectively used to predict different deposits types and metal endowment.

Structure of the thesis

This thesis consists of an introduction, three research articles organized in the form of chapters that have been or will be submitted, a general conclusion and appendices. The introduction provides a general view about indicator mineral, scheelite occurrence and chemistry in addition to its use as an indicator mineral, followed by a description of the research problems and objectives and the overall methodology.

Chapter 1 consists of a manuscript published in the journal “Mineralium Deposita” on May 2022 as: as: ‘Miranda, A.C.R., Beaudoin, G. and Rottier, B. *Scheelite chemistry from skarn systems: implications for ore-forming processes and mineral exploration’.* This article highlights how scheelite composition varies in skarn-type deposits according to different conditions of formation that lead to distinct mineral assemblage and metal content. This study also provides new insights for discrimination of deposit types based on scheelite composition which served as a support for the second article in this thesis.

Chapter 2 consists of a manuscript submitted for publication in *Journal of Geochemical Exploration* as: Miranda, A.C.R., Beaudoin, G., Rottier, B., Pašava, J., Bohdálek, P., and Malec, J., *Trace element signatures in scheelite associated with various deposit types: a tool for mineral targeting'*. This manuscript integrates new chemical composition data of scheelite in various magmatic-hydrothermal deposits and compiled literature data. The objective is to build a model based on scheelite composition and machine learning to discriminate different scheelite-bearing deposit types.

Chapter 3 consists of a manuscript that will be submitted to the journal "Geology" as: 'Miranda, A.C.R., Beaudoin, G., and Rottier, B. '*Prediction of metal endowment in orogenic Au deposits based on scheelite trace element composition and Random Forest classifier'*. This study brings a compilation of scheelite chemistry data from several orogenic Au deposits of different sizes aiming to use scheelite composition as an indicator of Au endowment of orogenic Au deposits, using a RF classifier algorithm.

Chapter 4 consists of preliminary results of in situ Sm-Nd analysis in scheelite from nine magmatic-hydrothermal deposits. The objective of this study is to investigate Nd isotopes in scheelite from magmatic-hydrothermal and orogenic Au deposits and determine the source of the metals (W and Au) in few W and Au provinces. However due to COVID-19 issues, only few data have been acquired until submission of this thesis.

The discussion consists of an interpretation, explanation and application of the results presented in this thesis.

The conclusion consists of a concise summary of the major findings presented in this thesis.

Detailed information regarding samples, and EPMA and LA-ICP-MS results are presented in Appendices.

References

Allegro, G.L., 1987. The Gilmore Dome tungsten mineralization, Fairbanks mining district, Alaska: University of Alaska Fairbanks, M.S. thesis, 150 p., illust. maps, 7 folded maps.

Auwera, J.V., and Andre, L., 1991. Trace elements (REE) and isotopes (O, C, Sr) to characterize the metasmatic fluids sources: evidence from the skarn deposit (Fe, W, Cu) of Traversella (Ivrea, Italy). Contrib Mineral Petrol, 106:325-339.

Averill, S. A., 2001. The application of heavy indicator mineralogy in mineral exploration with emphasis on base metal indicators in glaciated metamorphic and plutonic terrains. Geological Society, London, Special Publications, 185:69-81.

Ball, C.W., 1954. The Emerald, Feeney and Dodger tungsten ore-bodies, Salmo, British Columbia, Canada. Economic Geology, 49, 625–638.

Bell, K., Anglin, C.D., and Franklin, J.M., 1989. Sm-Nd and Rb-Sr isotope systematics of scheelites: Possible implications for the age and genesis of vein-hosted gold deposits. Geology, 17:500-509.

Boiron, M.C., Cathelineau, M., Banks, D.A., Fourcade, S., Vallance, J., 2003. Mixing of metamorphic and surficial fluids during the uplift of the Hercynian upper crust: consequences for gold deposition, Chemical Geology, Volume 194, Issues 1–3, Pages 119-141, https://doi.org/10.1016/S0009-2541(02)00274-7

Breiter, K, Korbelová, Z., Chládek, Š., Uher, P., Knesl, I., Rambousek, P., Honig, S., Šešulka, V., 2017. Diversity of Ti–Sn–W–Nb–Ta oxide minerals in the classic granite-related magmatic–hydrothermal Cínovec/Zinnwald Sn–W–Li deposit (Czech Republic). *European Journal of Mineralogy,* 29 (4): 727–738. doi: https://doi.org/10.1127/ejm/2017/0029-2650

Brown, I., and Nesbitt, B., 1987. Gold-copper-bismuth mineralization in hedenbergitic skarn, Tombstone Mountains, Yukon. Can J Earth Sci 24:2362-2372

Brown, V.S., Baker, T., Stephens, J.R., 2002. Ray Gulch tungsten skarn, Dublin Gulch, central Yukon: Gold-tungsten relationships in intrusion-related ore systems and implications for gold exploration. In: Yukon Exploration and Geology 2001, DS Emond, LH Weston and LL Lewis (eds), Exploration and Geological Services Division, Yukon Region, Indian and Northern Affairs Canada, p 259-268

Brugger , J., Lahaye, Y., Costa, S., Lambert, D., Bateman, R., 2000. Inhomogeneous distribution of REE in scheelite and dynamics of Archaean hydrothermal systems (Mt Charlotte and Drysdale gold deposits, Western Australia). Contrib Mineral Petrol 139:251–264.

Brugger, J., Etschmann, B., Pownceby, M., Liu, W., Grundler, P., Brewe, D., 2008. Oxidation state of europium in scheelite: tracking fluid–rock interaction in gold deposits. Chem Geol 257:26–33.

Bulm, J.D., 1985. A petrologic and Rb–Sr isotopic study of intrusive rocks near Fairbanks, Alaska. Canadian Journal of Earth Sciences, 22, 1314-1321.

Cave, B.J., Pitcairn, I.K., Craw, D., Large, R.R., Thompson, J.M., Johnson, S.C., 2017. A metamorphic mineral source for tungsten in the turbidite-hosted orogenic gold deposits of the Otago Schist, New Zealand. Miner Deposita 52, 515–537. https://doi.org/10.1007/s00126-016-0677-5

Cepedal, A., Fuertes-Fuente, M., Martin-Izard, A., Boixet, L., 2014. Tellurides, sulfides and sulfosalts in the mineral paragenesis of the Corcoesto orogenic gold deposit, NW Spain. Conference: IMA 2014 At: Sudafrica Volume: Abstract Volume ISBN: 978-0-620-60082-8, p 14.

Darbyshire, D.P.F., Pitfield, P.E.J., Campbell, S.D.G., 1996. Late Archean and Early Proterozoic gold-tungsten mineralization in the Zimbabwe Archean craton: Rb-Sr and Sm-Nd isotope constraints. *Geology*, 24 (1): 19–22. doi: https://doi.org/10.1130/0091-7613(1996)024<0019:LAAEPG>2.3.CO;2

Dave Craw, D., Mortensen, J., MacKenzie, D., Pitcairn, I., 2015 Contrasting geochemistry of orogenic gold deposits in Yukon, Canada and Otago, New Zealand. *Geochemistry: Exploration, Environment, Analysis* 15 (2-3): 150–166. doi: https://doi.org/10.1144/geochem2013-262

De Bronac de Vazelhes V., 2019. Étude de la dispersion d'un gisement d'or dans les sédiments glaciaires: Le cas d'Amaruq (Nunavut, Canada). M.Sc. thesis, Université Laval, 213p.

Dick, L., and Hodgson, C., 1982. The MacTung W-Cu(Zn) contact metasomatic and related deposits of the northeastern Canadian Cordillera. Econ Geol 77:845-867

Dubru, M., Vander Auwera, J., Van Marcke De Lummen, G., and Verkaeren, J., 1988. Distribution of scheelite in magnesian skarns at Traversella (Piemontese Alps, Italy) and Costabonne (Eastern Pyrenees, France): Nature of the associated magmatism and influence of fluid composition. In Mineral Deposits within the European Community (J. Boissonnas & P. Omenetto, eds.). Society for Geology Applied to Mineral Deposits, Special Publication 6, Springer-Verlag, Berlin, Germany (117–134).

Einaudi, M., Meinert, L., Newberry, R., 1981. Skarn deposits. Econ Geol 75:317-391

Elongo, V., Falck, H., Rasmussen, K.L., Robbins, L.J., Creaser, R.A., Luo, Y., Pearson, D.G., Sarkar, C., Adlakha, E., Palmer, M.C., Scott, J.M., Hickey, K., Konhauser, K., Lecumberri-Sanchez, P., 2022. Ancient roots of tungsten in western North America. *Geology*, 50 (7): 791–795. doi: https://doi.org/10.1130/G49801.1

Goldfarb, R.J., Bake, T., Dubé, B., Groves, D.I., Hart, C.J.R., and Gosselin, P., 2005. Distribution, character, and genesis of gold deposits in metamorphic terranes. Economic Geology, 100th Anniversary Volume, p. 407–450.

Groves, D.I., Goldfarb, R.J., Gebre-Mariam, M., Hagemann, S.G., Robert, F., 1998. Orogenic gold deposits: A proposed classification in the context of their crustal distribution and relationship to other gold deposit types. Ore Geol Rev 13, 7-27, doi: https://doi.org/10.1016/S0169-1368(97)00012-7.

Grzela, D., Beaudoin, G., Bedard, E., 2019. Tourmaline, scheelite, and magnetite compositions from orogenic gold deposits and glacial sediments of the Val-d'Or district (Quebec, Canada): implications to mineral exploration. J Geochem Explor 206:106355.

Guo, Z., Li, J., Xu, X., Song, Z., Dong, X., Tian, J., Yang, Y., She, H., Xiang, A., Kang, Y., 2016. Sm/Nd dating and REE composition of scheelite for the Honghuaerji scheelite deposit, Inner Mongolia, Northeast China. Lithos 261:307–321

Gurney, J.J., 1984. A correlation between garnets and diamonds in kimberlites. In: Kimberlite Occurrence and Origin: a Basis for Conceptual Models in Exploration. Publication, 8. Geology Department and University Extension, University of Western Australia, 143–166.

Hart, C., 2007. Reduced Intrusion-Related Gold Systems. In W D Goodfellow, Mineral Deposits of Canada: a synthesis of major deposittypes, district metallogeny, the evolution of geological provinces, and exploration methods (pp 95–112) Geological Association of Canada, Mineral Deposits Division.

Hart, C.J.R., and Goldfarb, R.J., 2005. Distinguishing intrusion-related from orogenic gold systems: Proceedings of the 2005 New Zealand Minerals Conference, Auckland, November 13–16, 125–133.

Hsu, L., 1977. Effects of oxygen and sulfur fugacities on the scheelite tungstenite and powellite-molybdenite stability relations. Econ Geol 72:664–670

Kent, A.J.R., Campbell, I.H., McCulloch, M.T., 1995. Sm-Nd systematics of hydrothermal scheelite from the Mount Charlotte Mine, Kalgoorlie, Western Australia; an isotopic link between gold mineralization and komatiites. *Economic Geology*; 90 (8): 2329–2335. doi: https://doi.org/10.2113/gsecongeo.90.8.2329

Kozlik, M., Gerdes, A., Raith, J.G., 2016a. Strontium isotope systematics of scheelite and apatite from the Felbertal tungsten deposit, Austria – results of in-situ LA-MC-ICP-MS analysis. Miner Petrol 110, 11–27. https://doi.org/10.1007/s00710-015-0416-0

Kozlik, M., Raith, J.G., Gerdes, A., 2016b. U–Pb, Lu–Hf and trace element characteristics of zircon from the Felbertal scheelite deposit (Austria): New constraints on timing and source of W mineralization. Chemical Geology, 421, 112-126, https://doi.org/10.1016/j.chemgeo.2015.11.018.

Kwak, T., and Tan T., 1981. The geochemistry of zoning in the skarn minerals at the King Island Dolphin mine. Econ Geol 76:468–497

Lang, J.R., and Baker, T., 2001. Intrusion-related gold systems: the present level of understanding. Min Dep 36, 477–489. https://doi.org/10.1007/s001260100184

Lu ,H-Z., Liu, Y., Wang, C., Xu, Y., Li, H., 2003. Mineralization and Fluid Inclusion Study of the Shizhuyuan W-Sn-Bi-Mo-F Skarn Deposit, Hunan Province, China. Econ Geol 98:955–974

Mair, J.L., Goldfarb, R.J., Johnson, C.A., Hart, C.J.R., Marsh, E.E., 2006. Geochemical constraints on the genesis of the Scheelite dome intrusion-related gold deposit, Tombstone gold belt, Yukon, Canada. Economic Geology, 101, 523-553.

Maloof, T.L., Baker, T. & Thompson, J.F., 2001. The Dublin Gulch intrusion-hosted gold deposit, Tombstone plutonic suite, Yukon Territory, Canada. Min Dep 36, 583–593. https://doi.org/10.1007/s001260100190

Mathieson, G., and Clark, A., 1984. The Cantung E Zone Scheelite Skarn Orebody, Tungsten Northwest Territories: A Revised Genetic Model. Econ Geol 79:883-901

McClenaghan, M. B., 2005. Indicator mineral methods in mineral exploration, geochemistry: Exploration, Environment, Analysis, 5(3):233-245.

McClenaghan, M. B., and Cabri, L. J., 2011. Review of gold and platinum group element (PGE) indicator minerals methods for surficial sediment sampling, Geochemistry: Exploration, Environment, Analysis, 11(4):251-263.

McClenaghan, M. B., and Kjarsgaard, B. A., 2007. Indicator mineral and surficial geochemical exploration methods for kimberlite in glaciated terrain; Examples from Canada, p. 983-1006, in Goodfellow, W. D., ed., Mineral Deposits of Canada: A Synthesis of Major Deposit-Types, District Metallogeny, the Evolution of Geological Provinces, and Exploration Methods, Vol. Special Publication No. 5, Geological Association of Canada, Mineral Deposits Division.

McClenaghan, M., Parkhill, M., Pronk, A., Seaman, A., McCurdy, M., Leybourne, M., 2017. Indicator mineral and geochemical signatures associated with the Sisson W-Mo deposit, New Brunswick,Canada. Geochem Explor Environ Anal 17:297–313

McClenaghan, M.B. and Kjarsgaard, B.A. 2001. Indicator mineral and geochemical methods for diamond exploration in glaciated terrain in Canada. In: MCCLENAGHAN, M.B., BOBROWSKY, P.T., Hall, G.E.M., and Cook, S.J. (eds) Drift Exploration in Glaciated Terrain. Special Publication, 185. Geological Society, London, 83–123.

Mendizabal, A., 2022. Étude de la composition des minéraux indicateurs et de la géochimie du till en aval d'un gisement d'or : Le cas d'Amaruq (Nunavut, Canada). M.Sc. thesis, Université Laval, 196p.

Miranda, A.C.R., Beaudoin, G., Rottier, B., 2022. Scheelite chemistry from skarn systems: implications for ore-forming processes and mineral exploration. Miner Deposita. https://doi.org/10.1007/s00126-022-01118-y

Myint, A.Z., Yonezu, K., Boyce, A.J., Selby, D., Scherstén, A., Tindell, T., Watanabe, K., Swe, Y.M., 2018. Stable isotope and geochronological study of the Mawchi Sn-W deposit, Myanmar: Implications for timing of mineralization and ore genesis. Ore Geology Reviews, 95, 663-679, https://doi.org/10.1016/j.oregeorev.2018.03.014

Newberry, R., 1982. Tungsten-bearing skarns of the Sierra Nevada I The Pine Creek Mine, California. Econ Geol 77:823-844

Newberry, R., and Swanson, S., 1986. Scheelite Skarn Granitoids: An evaluation of the roles of magmatic source and process. Ore Geol Rev 1:57-81

Nguyen, T.H., Nevolko, P.A., Pham, T.D., Svetlitskaya, T.V., Tran, T.H., Shelepaev, R.A., Fominykh, P.A., Pham, N.C., 2020. Age and genesis of the W-Bi-Cu-F (Au) Nui Phao deposit, Northeast Vietnam: Constrains from U-Pb and Ar-Ar geochronology, fluid inclusions study, S-O isotope systematic and scheelite geochemistry, Ore Geology Reviews, 123, 103578. https://doi.org/10.1016/j.oregeorev.2020.103578

Noble, S.R, Spooner, E.T.C., Harris, F.R., 1984. The Logtung large tonnage, low-grade W (scheelite)-Mo porphyry deposit, south-central Yukon Territory. *Economic Geology* 79(5):848–868. doi: https://doi.org/10.2113/gsecongeo.79.5.848

Palarea-Albaladejo, J., and Martín-Fernández, J., 2015. zCompositions — R package for multivariate imputation of left-censored data under a compositional approach. Chemometr Intell Lab Syst 143:85–96

Palmer, M.C., 2021. Geochemical characterisation of scheelite from New Zealand (Thesis, Doctor of Philosophy). University of Otago. Retrieved from http://hdl.handle.net/10523/12254

Pan, X., Hou, Z., Zhao, M., Li, Y., Ouyang, Y., Wei, J., Yang, Y., 2020. Fluid inclusion and stable isotope constraints on the genesis of the worldclass Zhuxi W(Cu) skarn deposit in South China. J Asian Earth Sci 190:104192

Paton, C., Hellstrom, J., Paul, B., Woodhead, J., and Hergt, J., 2011, Iolite: freeware for the visualization and processing of mass spectrometric data: Journal of Analytical Atomic Spectrometry, 26, p. 2508–2518. https:// doi. org/ 10. 1039/ c1ja1 0172b

Pirajno, F., 1992. Greisen systems, Hydrothermal Mineral Deposits. Springer, pp. 280-324.

Pirajno, F., and Bentley, P.N., 1985. Greisen-related scheelite, gold and sulphide mineralisation at Kirwans Hili and Bateman Creek, Reefton district, Westland, New Zealand. New Zealand Journal of Geology and Geophysics, 28, 97-109.

Poitrenaud, T., Poujoi, M., Augier, R., Marcoux, E., 2019. The polyphase evolution of a late Variscan W/Au deposit (Salau, French Pyrenees): insights from REE and U/Pb LA-ICP-MS analyses. Mineral Deposita 55:1127–1147

Pollard, P.J., Pichavant, M., and Charoy, B., 1987. Contrasting evolution of fluorine- and boron-rich tin systems. Mineralium Deposita 22:315-321.

Porter, J.P., 2013. Source, emplacement and evolution of the Morgan Creel Pluton, Sierra Nevada Batholith, California, USA PhD thesis, Salt Lake City, USA, The University of Utah, 201 p.

Poulin, R., Kontak, D., McDonald, A., McClenaghan, M. 2018. Assessing scheelite as an ore-deposit discriminator using its trace element and REE chemistry. Can Mineral 56:265–302

Raimbault, L., Baumer, A., Dubru, M., Benkerrou, C., Crose, V., & Zahm, A. 1993. REE fractionation between scheelite and apatite in hydrothermal conditions. American Mineralogist 78:1275–1285.

Reed, B.L. 1986. Descriptive model of Sn greisen deposits; & Mineral Deposit Models, (ed.) D.P. Cox and D.F. Singer; United States Geological Survey, Bulletin 1693, p. 70.

Scanlan, E.J., Scott, J.M., Wilson, V.J., Stirling, G.H., Reid, M.R., Le Roux, P.J., 2018. In Situ $^{87}Sr/^{86}Sr$ of Scheelite and Calcite Reveals Proximal and Distal Fluid-Rock Interaction During Orogenic W-Au Mineralization, Otago Schist, New Zealand. *Economic Geology*; 113 (7): 1571–1586. doi: https://doi.org/10.5382/econgeo.2018.4603

Sciuba, M., Beaudoin, G., Grzela, D., Makvandi, S., 2020. Trace element composition of scheelite in orogenic gold deposits. Miner Deposita 55:1149-1172

Sinclair, W.D., 1986. Molybdenum, tungsten and tin deposits and associated granitoid intrusions in the northern Canadian Cordillera and adjacent parts of Alaska; in Morin, J.A., Mineral Deposits of Northern Cordillera: The Canadian Institute of Mining and Metallurgy, Special Volume 37, p. 216-233

Singoyi, B., and Zaw, K., 2001. A petrological and fluid inclusion study of magnetite–scheelite skarn mineralization at Kara, Northwestern Tasmania: implications for ore genesis. Chem Geol 173:239–253

Soloviev, S., 2015. Geology, mineralization, and fluid inclusion characteristics of the Kumbel oxidized W-Cu-Mo skarn and Au-W stockwork deposit, Tien-Shan, Kyrgyzstan. Mineral Deposita 50:187–220

Soloviev, S., Kryazhev, S., Dvurechenskaya, S., 2017. Geology, mineralization, stable isotope, and fluid inclusion characteristics of the Vostok-2 reduced W-Cu skarn and Au-W-Bi-As stockwork deposit, Sikhote-Alin, Russia. Ore Geol Rev 86:338–365

Soloviev, S., Kryazhev, S.G., Dvurechenskaya, S.S., 2015. Geology, mineralization, and fluid inclusion characteristics of the Lermontovskoe reduced-type tungsten (±Cu, Au, Bi) skarn deposit, Sikhote-Alin, Russia. Ore Geol Rev 89:15-39

Song, G., Qin, K., Li, G., Evans, N., Chen, L., 2014. Scheelite elemental and isotopic signatures: Implications for the genesis of skarn-type W-Mo deposits in the Chizhou area, Anhui Province Eastern China. Am Mineral 99:303–317

Souza Neto, J.A., Legrand, J.M., Volfinger, M., Pascal, M-L., Sonnet, P., 2008. W–Au skarns in the Neo-Proterozoic Seridó Mobile Belt, Borborema Province in northeastern Brazil: an overview with emphasis on the Bonfim deposit. Miner Deposita 43:185-205

Štemprok, M., and Mašková, A., 1992. Scheelite mineral of the Bohemian Massif. Zbl. Geol. Palaont. Teil (1/2): 117-129.

Su, Q., Mao, J., Sun, J., Zhao, L., Xu, S., 2020. Geochemistry and Origin of Scheelites from the Xiaoyao Tungsten Skarn Deposit in the Jiangnan Tungsten Belt, SE China. Minerals 10:271

Taylor, R.G. 1979. Geology of Tin Deposits, Elsevier, Amsterdam, 544 p.

Thompson, J., Sillitoe, R., Baker, T., Lang, J.R., Mortensen, J.K., 1999. Intrusion-related gold deposits associated with tungsten-tin provinces. Mineral. Deposita 34, 323–334. https://doi.org/10.1007/s001260050207

Tischendorf, G., 1977. Geochemical and petrographic characteristics of silicic magmatic rocks associated with rare-element mineralisation. In M. Stemprok, L. Burnol and G. Tischendorf (eds.) Metallization associated with acid magmatism (Geo. Surv. Prague) 2:41-96.

Toverud, O., 1984. Dispersal of tungsten in glacial drift and humus in Bergslagen, southern central Sweden. Journal of Geochemical Exploration, 21:261–272.

Tyson, R.M., Hemphill, W.R., Theisen, A.R., 1988. Effect of the W:Mo ratio on the shift of excitation and emission spectra in the scheelite-powellite series. *American Mineralogist* 73 (9-10): 1145–1154.

Veselovský, F., Ackerman, L., Pašava, J., Žák, K., Haluzová, E., Creaser, R.A., Dobeš, P., Erban, V., Tasler, R., 2018. Multiphase formation of the Obří důl polymetallic skarn deposit, West Sudetes, Bohemian Massif: Geochemistry and Re–Os dating of sulfide mineralization. Miner Deposita 53, 665–682. https://doi.org/10.1007/s00126-017-0766-0

Voicu, G.M., Bardoux, M., Stevenson, R., Jebrak, M., 2001 Nd and Sr isotope study of hydrothermal scheelite and host rocks at Omai, Guiana Shield: implications for ore fluid source and flow path during the formation of orogenic gold deposits Mineralium Deposita 35: 302-314

Webster, J., Thomas, R., Förster, H.J., Seltmann, R., Tappen, C., 2004. Geochemical evolution of halogen-enriched granite magmas and mineralizing fluids of the Zinnwald tin-tungsten mining district, Erzgebirge, Germany. Miner Deposita 39, 452–472. https://doi.org/10.1007/s00126-004-0423-2

Willden, C.R., and Hotz, P.E., 1955. A gold-scheelite-cinnabar placer in Humboldt County, Nevada. *Economic Geology*; 50 (7): 661–668. doi: https://doi.org/10.2113/gsecongeo.50.7.661

Wintzer, N.E., Schmitz, M.D., Gillerman, V.S., Vervoort, J.D., 2022. U-Pb Scheelite Ages of Tungsten and Antimony Mineralization in the Stibnite-Yellow Pine District, Central Idaho. *Economic Geology*; doi: https://doi.org/10.5382/econgeo.4953

Xu, J., Ciobanu, C., Cook, N.C., Slattery, A., 2019. Crystals from the powellite-scheelite series at the nanoscale: a case study from the Zhibula Cu skarn, Gangdese Belt. Tibet Minerals 9:340

Žáček, V., 2008. Cu-skarn v Kotli v Krkonoších (Česká republika). - Bull. mineral.-petrolog. Odd. Nár. Muz. (Praha) 16/2, 230-237. ISSN: 1211-0329

Zaw, K., and Singoyi, B., 2000. Formation of Magnetite-Scheelite Skarn Mineralization at Kara, Northwestern Tasmania: Evidence from Mineral Chemistry and Stable Isotopes. Econ Geol 95:1215–1230

Zhang, Q., Zhao, K.D., Li, W-Q., Palmer, M.R., Jiang, S-Y., Jaing, H., Zhang, W., Zhang, D., Hussian, A., 2022. Timing and tectonic setting of tin mineralization in southern Myanmar: constraints from cassiterite and wolframite U–Pb ages. Miner Deposita 57, 977–999. https://doi.org/10.1007/s00126-021-01083-y

Zhao, W., Zhou, M-F., Williams-Jones, A., Zhao, Z., 2018. Constraints on the uptake of REE by scheelite in the Baoshan tungsten skarn deposit, South China. Chem Geol 477:123–136

Zheng, W., Tang, J., Zhong, K., Ying, L., Leng, Q., Ding, S., Lin, B., 2016. Geology of the Jiama porphyry copper–polymetallic system, Lhasa Region, China. Ore Geol Rev 74:151–169

Chapter 1 - Scheelite chemistry from skarn systems: Implications for ore-forming processes and mineral exploration

Ana Carolina R. Miranda[1,2], Georges Beaudoin[1,2] and Bertrand Rottier[1,2]

[1]Département de Géologie et Génie Géologique, Université Laval, Québec, Canada

[2]Centre de recherche sur la géologie et l'ingénierie de ressources minérales (E4m), Université Laval, Québec, Canada

(published in Mineralium Deposita v. 57: 1469-1497)

1.1 Résumé

La composition en éléments traces de la scheelite provenant de 19 systèmes de skarns réduits et oxydés bien documentés a été mesurée par ablation laser-spectrométrie de masse à plasma à couplage inductif (LA-ICP-MS) afin d'établir des critères chimiques pour l'application de la scheelite comme minéral indicateur efficace pour le ciblage de l'exploration minérale. Dans les systèmes de skarns réduits et oxydés, la scheelite se forme au cours de phases prograde et rétrograde. La scheelite prograde est zonée texturalement et chimiquement, tandis que la scheelite rétrograde est principalement homogène texturalement, mais peut présenter une zonation chimique. Cinq modèles d'ETR normalisés à la chondrite, présentant des anomalies positives et négatives en Eu, sont identifiés dans les données : (i) pentes négatives raides et (ii) peu profondes, (iii) formes concaves, (iv) plates à légèrement concaves et (v) convexes. Les différents modèles d'ETR sont liés à la salinité variable des fluides et à l'association avec du grenat ou du clinopyroxène co-précipité. Les résultats de l'analyse discriminante des moindres carrés partiels (PLS-DA) montrent que la composition de la scheelite varie en fonction du redox du skarn, de la composition de l'intrusion et de l'association des métaux. Ces résultats appuient le fait que la composition en éléments traces de la scheelite est en partie fonction de la composition de la roche ignée et de la fugacité de l'oxygène, en plus de la salinité, des minéraux co-génétiques et de la composition des fluides minéralisateurs. La scheelite provenant de skarns réduits et oxydés peut être distinguée de celles provenant de gisements d'or orogéniques et liés à des intrusions, en raison de leur concentration plus faible en Sr et plus élevée en Mo, Ta et Nb. La composition en éléments traces de la

scheelite étudiée par PLS-DA est efficace pour discriminer les différents types de gisements, soutenant l'utilisation de la scheelite comme minéral indicateur pour le ciblage de l'exploration.

Mots clés: scheelite, élément trace, systèmes de skarn, minéral indicateur, analyse discriminante partielle des moindres carrés.

1.2 Abstract

The trace element composition of scheelite from 19 well-documented reduced and oxidized skarn systems was measured by laser ablation-inductively coupled plasma-mass spectrometry (LA-ICP-MS) to establish chemical criteria for the application of scheelite as an efficient indicator mineral for mineral exploration targeting. In both reduced and oxidized skarns systems, scheelite forms during prograde and retrograde stages. Prograde scheelite is texturally and chemically zoned, whereas retrograde scheelite is predominantly texturally homogeneous, but may display chemical zonation. Five chondrite-normalized REE patterns, displaying both positive and negative Eu anomalies, are identified in the data: (i) steep and (ii) shallow negative slopes, (iii) concave, (iv) flat to slightly concave and (v) convex shapes. The different REE patterns are related to variable fluid salinity and association with co-precipitated garnet or clinopyroxene. Results of partial least square-discriminate analysis (PLS-DA) show that scheelite composition varies according to skarn redox, intrusion composition, and metal association. These results support the fact that the trace element composition of scheelite is in part a function of igneous rock composition and oxygen fugacity, in addition to salinity, co-genetic minerals and composition of the mineralizing fluids. Scheelite from reduced and oxidized skarns can be discriminated from those from orogenic and intrusion-related gold deposits due to their lower Sr and higher Mo, Ta, and Nb concentrations. Scheelite trace element composition investigated by PLS-DA is effective in discriminating different deposit types, supporting the use of scheelite as an indicator mineral for exploration targeting.

Keywords: scheelite, trace element, skarn systems, indicator mineral, partial least square-discriminant analysis

1.3 Introduction

Scheelite ($CaWO_4$) is a common tungsten ore mineral in skarn, greisen Sn, porphyry (Mo-W and Sn-W) and polymetallic deposits, as well as an accessory mineral in reduced intrusion-related gold systems (RIRGS), orogenic gold, Au skarns, and porphyry-skarn Cu deposits (Brown and Nesbitt 1986; Brugger et al. 1998,2000; Uspensky et al. 1998; Hart 2007; Song et al. 2014; Guo et al. 2016; Fu et al. 2017; Poulin et al. 2018; Wintzer 2019; Xu et al. 2019; Sciuba et al. 2020). Because scheelite is a resistant mineral and occurs in several geological settings, it has been used as an indicator mineral for targeting primary tungsten bearing deposits (Toverud 1984; Averill 2001; McClenaghan et al. 2017) in addition to orogenic gold deposits (Uspensky et al. 1998; Maneglia et al. 2017; Grzela et al. 2019; Sciuba et al. 2020; de Bronac de Vazelhes et al. 2021).

The advances of micro analytical techniques (LA-ICP-MS) allow a wide range of trace elements in various minerals to be measured (Cook et al. 2016; Sylvester and Jackson 2016). Studies on mineral chemistry are essential to understand ore-forming processes, since the mineral trace element composition varies as a function of the origin, composition, and physicochemical conditions of hydrothermal fluids or melts from which it precipitates (Gaspar et al. 2008; Dare et al. 2012; Andersson et al. 2019; Mansur et al. 2021). Since the composition and physicochemical conditions of hydrothermal fluids are determined by the geological settings, and the chemical composition of minerals reflects this environment, the compositional variation of minerals is used to discriminate among magmatic or hydrothermal environments (Duran et al. 2015; Huang et al. 2019), deposit types (Dupuis and Beaudoin 2011; Boutroy et al. 2014; Dare et al. 2014; George et al. 2015a,b; O'Brien et al. 2015; Duran et al. 2016; Makvandi et al. 2016a, 2020; Mao et al. 2016; Gregory et al. 2019; Porter et al. 2020; Liu and Beaudoin 2021), hydrothermal alteration (Wilkinson et al. 2015), and mineralized and barren rocks (Gregory et al. 2019; Shu et al. 2019). Trace element chemistry of indicator minerals is used to vector towards ore bodies (Barker et al. 2020; Cook et al. 2020; Wilkinson et al. 2020; Rottier and Casanova 2021) and for exploration for diamonds (Gurney and Zweistra 1995; Grütter et al. 2004) and concealed deposits (Eppinger et al. 2011; Kelley et al., 2011; Duran et al. 2019). Several contributions have shown the potential use of scheelite chemistry for indicating different deposit types and the source of hydrothermal fluids (Ghaderi et al. 1999; Song et al 2014; Poulin et al. 2018; Sciuba et al. 2020).

Skarn deposits, where garnet and clinopyroxene are common minerals, are the main worldwide source of tungsten, and scheelite is one of the most common W ore mineral in these systems (Einaudi et al. 1981). Based on garnet and clinopyroxene major element compositions, skarns are classified following different redox states, reduced and oxidized, which is a result of magma and host rock compositions and depth of formation (Einaudi and Burt 1982; Newberry and Swanson, 1986; Meinert 1997; Chang et al. 2019). For instance, hedenbergitic clinopyroxene and grossular-spessartite garnet commonly occur in reduced skarns, whereas andradite garnet and diopisidic clinopyroxene are typically found in oxidized skarns (Einaudi et al. 1981; Einaudi and Burt 1982). Scheelite occurs in both redox skarn types and can be temporally and spatially associated with several other metals such as Au, Cu, Mo, and Sn (Lu et al. 2003; Hart 2007; Song et al. 2014). Therefore, scheelite chemistry may be used to target not only tungsten as the primary commodity, but also other metals (Au, Cu, Mo, and Sn) found in association with tungsten. Although scheelite major element chemistry has been studied in some detail (Raimbault et al. 1993; Ghaderi et al. 1999; Robert et al. 2006; Dostal et al. 2009; Song et al. 2014; Poulin et al. 2018; Zhao et al. 2018; Sciuba et al. 2020), its trace element composition remains poorly documented in several settings, and our understanding of the controls of its chemical composition and the application for the exploration for skarn deposits remains limited.

In this contribution, we document the chemical signature of scheelite, garnet, and clinopyroxene from various skarn systems to develop compositional fingerprints that allow discrimination of scheelite from reduced and oxidized skarns, skarn deposits with different metal associations, and other scheelite-bearing deposit types. The results are explored using basic and multivariate statistical methods, which establish chemical criteria for the scheelite as an efficient indicator mineral for mineral targeting.

1.4 Selected tungsten skarns deposits

Scheelite crystals and co-genetic minerals (garnet and clinopyroxene) from exoskarn samples from thirteen W(±Au-Cu-Mo-Sn) skarn deposits were investigated (Fig. 1.1; Table 1.1). Typical examples of scheelite-bearing skarn samples related to RIRGS (Scheelite Dome, Ray Gulch, Lermontovskoe and Vostok-2), Au skarn (Marn), and Cu-polymetallic porphyry-skarn deposit (Jiama) were also included in our dataset (Table 1.1). In total, scheelite-bearing skarn samples from 19 localities formed in varied geological settings,

metal associations, from a range of deposit sizes, and mineralization ages ranging from Neoproterozoic to Miocene were selected (Table 1.1; Fig. 1.1).

According to Einaudi et al. (1981), scheelite skarns are classified in oxidized and reduced types, based on skarn mineralogy (Fe^{3+} versus Fe^{2+} bearing minerals, Fig. 1.2), which depends on the host rock composition, the redox state of the hydrothermal fluids, and on the depth skarn formation. In general, reduced skarns are hosted in pure limestone, and are associated with ilmenite-series intrusions (Ishihara 1977), emplaced at greater depth (> 2 kbar) relative to, for example, skarns associated with porphyry Cu systems (Newberry and Swanson 1986; Chang et al. 2019). In contrast, oxidized skarns are closely associated with magnetite-series intrusions emplaced at shallow crustal levels (<2 kbar; Newberry 1983; Newberry and Swanson 1986; Chang et al. 2019) and developed in impure carbonates and/or hematite-rich metasedimentary host rocks (Newberry 1983; Newberry and Swanson 1986).

Newberry (1983) and Zaw and Singoyi (2000) showed that scheelite skarns might also be classified as moderately reduced (e.g. Pine Creek, California) to moderately oxidized (e.g. King Island, Tasmania) because they show intermediate characteristics between end-member of oxidation state, host rock composition and depth of formation (Kwak and Tan 1981; Newberry 1983). For simplicity, in this study we grouped the moderately oxidized skarns with oxidized, and moderately reduced with reduced skarns, respectively (Table 1.1). Typical examples of reduced scheelite-bearing skarns include Sangdong (South Korea) and Cantung and Mactung (Canada), whereas Kara (Australia) and Costabonne (France) are examples of oxidized W skarns (Einaudi et al. 1981; Dick and Hodgson 1982; Zaw and Singoyi 2000; Table 1.1).

The reduced skarn prograde mineral assemblage is dominated by hedenbergitic (Fe^{2+}-rich) clinopyroxene over grossular-spessartite (Al-rich) garnet (Fig. 1.2). The retrograde assemblage comprises hornblende and/or biotite, and sulfides such as pyrrhotite, chalcopyrite, molybdenite, sphalerite and arsenopyrite (Dick and Hodgson 1982; Mathieson and Clark 1984). In oxidized skarns, andradite (Fe^{3+}-rich) garnet is more abundant than diopsidic clinopyroxene in the prograde stage (Fig. 1.2), whereas the retrograde assemblage consists mainly of epidote, hornblende, magnetite, and pyrite (Kwak and Tan 1981; Zaw and Singoyi 2000). In both redox type skarns, fine-grained, Mo-rich (> 1000 ppm) scheelite occurs in the prograde stage, whereas coarse-grained, Mo-poor (< 1000 ppm) scheelite

occurs commonly in the retrograde stage (Kwak and Tan 1981; Liu et al. 2020; Su et al. 2020).

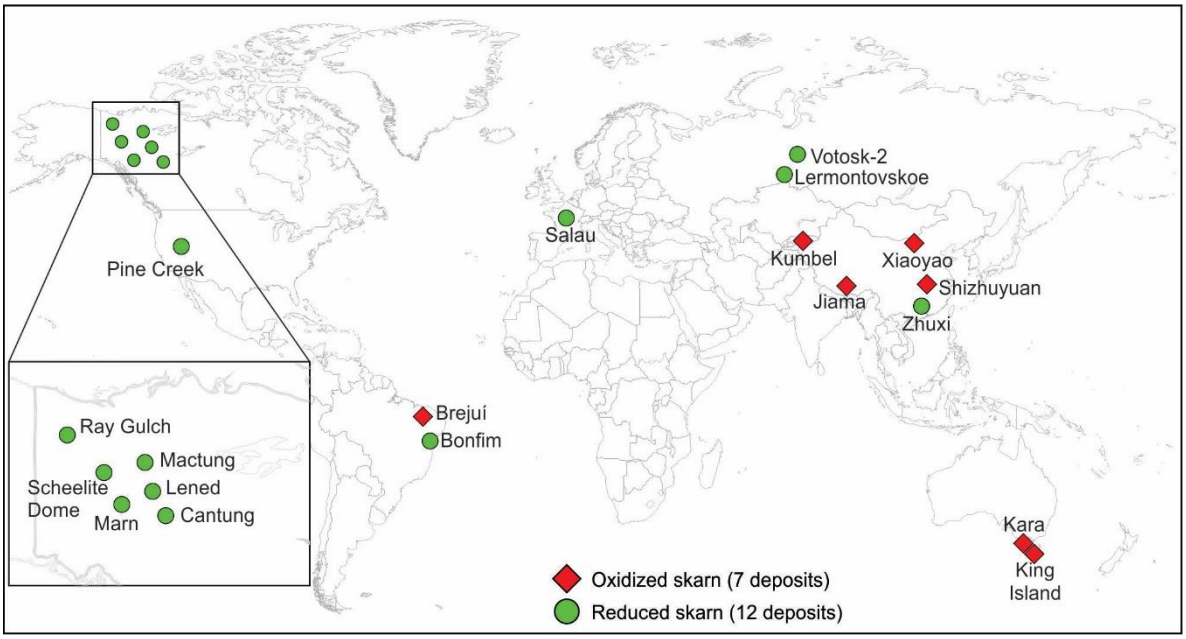

Figure 1.1. World distribution of sampled scheelite-bearing skarn deposits (references included in Table 1.1).

1.5 Methodology

1.5.1 Sample selection

Fifty-three scheelite-bearing skarn samples from 19 well-documented deposits distributed worldwide were investigated (Fig. 1.1 and Table 1.1). Garnet and clinopyroxene compositions from literature and this study were used as proxies for redox conditions (Appendix 1.1B; Fig. 1.2). Twelve are classified as reduced, and 7 as oxidized skarns (Table 1.1, Fig. 1.2). In total, 70 polished thin sections were studied to constrain mineralogy, morphology, texture, and chemical composition of scheelite and co-existing minerals in different skarn facies.

Table 1.1. Summary of the main geological characteristics of scheelite-bearing skarn samples.

Deposit/Country	Metal association	Host rocks	Intrusive rocks	Alumina Saturation Index (ASI) and redox state of intusive rocks	Skarn facies
Tungsten skarn deposits					
Shizhuyuan/China	W-Mo-Sn-Bi-F	Devonian limestone	Jurassic biotite K-feldspar granodiorite	peraluminous, magnetite-series	grt, amph
Kumbel/Kyrgyzstan	W-Mo-Cu-Bi	Devonian and Carboniferous sandy limestones and sandstones	Carboniferous monzogabbro–monzonite–granodiorite–granite pluton	magnetite-series	grt
Xiaoyao/China	W-Mo-Cu	Cambrian limestone	Jurassic granodiorite	metaluminous, magnetite-series	grt
Brejui/Brazil	W	Neoproterozoic marble and gneiss	Neoproterozoic biotite granite	-	grt, mag
Kara/Australia	Fe-W	Ordovician limestone	Denovian highly fractionated granite	peraluminous, magnetite-series	grt, mag
King Island/Australia	W	Cambrian dolomite	Devonian mozogranite to granodiorite	magnetite-series	grt-px
Pine Creek/USA	W	Cambrian carbonate-rich metasedimentary rocks	Cretaceous quartz monzonite	titanite-bearing granite	px-grt

Deposit/Country	Metal association	Host rocks	Intrusive rocks	Alumina Saturation Index (ASI) and redox state of intusive rocks	Skarn facies
Tungsten skarn deposits					
Zhuxi/China	W-Cu	Carboniferous carbonaceous shales and limestones	Mesozoic biotite granite	peraluminous, ilmenite-series	grt-wo, amph
Lened/Canada	W-Cu	Cambrian limestone	Cretaceous biotite quartz monzonite	peraluminous, ilmenite-series	grt, px, amph, po-bt
Cantung/Canada	W-Cu	Cambrian limestone	Cretaceous biotite granite and biotite-rich dikes	peraluminous, ilmenite-series	px-grt, amph, po
Mactung/Canada	W-Cu	Cambrian limestone	Cretaceous biotite granite	peraluminous, ilmenite-series	px, po
Salau/France	W-Au	Ordovician carbonate rocks	Variscan granodiorite	ilmenite-series	grt, po
Bonfim/Brazil	W-Au	Neoproterozoic marble and schist	Neoproterozoic biotite granite		px
Tungsten skarns associated with RIRGS					
Ray Gulch or Mar or Wolf/Canada	W	Proterozoic-Early Cambrian Quartz-biotite schist and carbonate	Cretaceous granodiorite	metaluminous, titanite-bearing granite	px
Vostok-2/Russia	W-Cu(Au)	Paleozoic limestone	Cretaceous granodiorite	peraluminous, ilmenite-series	po, bt

Deposit/Country	Metal association	Host rocks	Intrusive rocks	Alumina Saturation Index (ASI) and redox state of intusive rocks	Skarn facies
Tungsten skarns associated with RIRGS					
Lermontovskoe/Russia	W-Cu(Au)	Paleozoic limestone	Cretaceous granodiorite-granite	peraluminous, ilmenite-series	po, bt
Scheelite Dome/Canada	Au-W	Proterozoic-Cambrian marble	Cretaceous quartz monzonite to granodiorite	metaluminous, titanite-bearing granite	px-po
Gold skarn					
Marn/Canada	Au-Cu-W	Permin sedimentary and limestone	Cretaceous monzonite	metaluminous, magnetite-series	px-po
Cu porphyry-skarn system					
Jiama/China	Cu-polymetallic	Jurassic limestone	Miocene granite-granodiorite porphyries	metaluminous, magnetite-series	grt, qtz-cc

* Garnet and clinopyroxene EPMA analysis from this study and literature
** Temperature range of prograde and retrograde stages

Table 1.1 (continued)

Deposit/Country	Garnet component (mole %)*	Clinopyroxene component (mole %)*	Skarn type	Tonnage and grade	Temperature**	Salinity (wt.% NaCl)	Reference
Tungsten skarn deposits							
Shizhuyuan/China	Ad15-76	Hd10-47	Oxidized	0.8 Mt WO3, 0.3% W, 0.5 m.t. Sn (metal), 0.2 m.t. Bi (metal), 0.1 m.t. Mo (metal)	350 - 535°C	26 - 41	Mao et al. (1996); Lu et al. (2003)
Kumbel/Kyrgyzstan	Ad40-98	Hd0-22	Oxidized	10 Mt, 17 000 t of WO3, (0.4% WO3); 100000 t Cu (0.25% Cu); 2500 t Bi (0.02% Bi); 500 t Mo (0.05 % Mo)	120 - 600°C	18 - 60	Soloviev (2015)
Xiaoyao/China	Ad78-100	-	Oxidized	50000t of WO3, 0.2% WO3, 6700t Cu, 360t Mo	-	-	Su et al. (2020)
Brejui/Brazil	Ad19-49	Hd30-60	Oxidized	17 Mt, 0.5-1% WO3	200 - 550°C	<15	Souza Neto et al. (2008)
Kara/Australia	Ad70-100	Hd0-25	Oxidized	0.4 Mt, 0.75% WO3	240 - 600°C	2 - 45	Zaw and Sinogyi (2000); Sinogyi and Zaw (2001)
King Island/Australia	Ad43-98	Hd23-98	Oxidized	9.6 Mt, 0.9% WO3	180 - 800°C	3 - 65	Kwak and Tan (1981)

Deposit/Country	Garnet component (mole %)*	Clinopyroxene component (mole %)*	Skarn type	Tonnage and grade	Temperature**	Salinity (wt.% NaCl)	Reference
Tungsten skarn deposits							
Pine Creek/USA	Ad30-65	Hd47-80	Reduced	16 Mt, 0.5% WO3	350 - 550°C	-	Newberry (1982); Porter (2013)
Zhuxi/China	Ad7-15	-	Reduced	6.37 Mt, 0.54% WO3, 0.57% Cu	280 - 500 °C	1.6 - 6.0 (few with 60)	
Lened/Canada	Ad20-40	Hd55-98	Reduced	0.7 Mt, 1% WO3, 0.15% Cu	-	-	
Cantung/Canada	Ad30-49	Hd75-99	Reduced	E-zone: 0.77 Mt, 1.75% WO3; Open pit: 3.4 Mt, 0.55% WO3	270 - 520 °C	4 - 14	Dick and Hodgson (1982); Mathieson and Clark (1984)
Mactung/Canada	Ad15-20	Hd40-83	Reduced	33 Mt, 0.88% WO3	350 - 470 °C	<5	Dick and Hodgson (1982)
Salau/France	Ad7-14	Hd35-97	Reduced	0.01 Mt, 1.44% WO3, 2 g/t Au	-	-	Poitrenaud et al. (2019)
Bonfim/Brazil	-	Hd17-53	Reduced	>0.3 Mt, 4.8 % WO3, 0.5-1.5 t Au	400 - 580 °C	4.8	Souza Neto et al. (2008)
Tungsten skarns associated with RIRGS							
Ray Gulch or Mar or Wolf/Canada	-	Hd60-92	Reduced	12.6 Mt at 0.31 % WO3	-	-	Brown et al. (2002)

Deposit/Country	Garnet component (mole %)*	Clinopyroxene component (mole %)*	Skarn type	Tonnage and grade	Temperature**	Salinity (wt.% NaCl)	Reference
Tungsten skarns associated with RIRGS							
Vostok-2/Russia	Ad10-25	Hd25-80	Reduced	180 Kt WO3 and 10 -15 t Au, averaging 1.7% WO3, 0.64% Cu, and 1.9 g/t Au	420 - 460 °C	5.4 - 12	Soloviev et al. (2017)
Lermontovskoe/Russia	-	Hd70-90	Reduced	0.048 Mt, 2.6% WO3, 0.23 g/t Au	360 - 500 °C	low salinity	Soloviev et al. (2015)
Scheelite Dome/Canada	-	Hd80-90	Reduced	Drilling in 1979 intersected 1.5 m grading 0.35% WO3 and 1.2 g/t Au	300 - 500 °C	4	Meinert et al. (2005); Mair et al. (2006)
Gold skarn							
Marn/Canada	-	Hd80-100	Reduced	0.3 Mt, 8.6 g/t Au, 1% Cu, 0.1% WO3 and 17 g/t Ag	-	-	Brown and Nesbitt (1986)
Cu porphyry-skarn system							
Jiama/China	Ad60-100	Hd0-20	Oxidized	7.4 Mt Cu, 0.6 Mt Mo, 1.8 Mt Pb+Zn, 6.65 Moz Au, 350.32 Moz Ag	225 - 550 °C	<36.2	Zheng et al. (2016)

* Garnet and clinopyroxene EPMA analysis from this study and literature

** Temperature range of prograde and retrograde stages

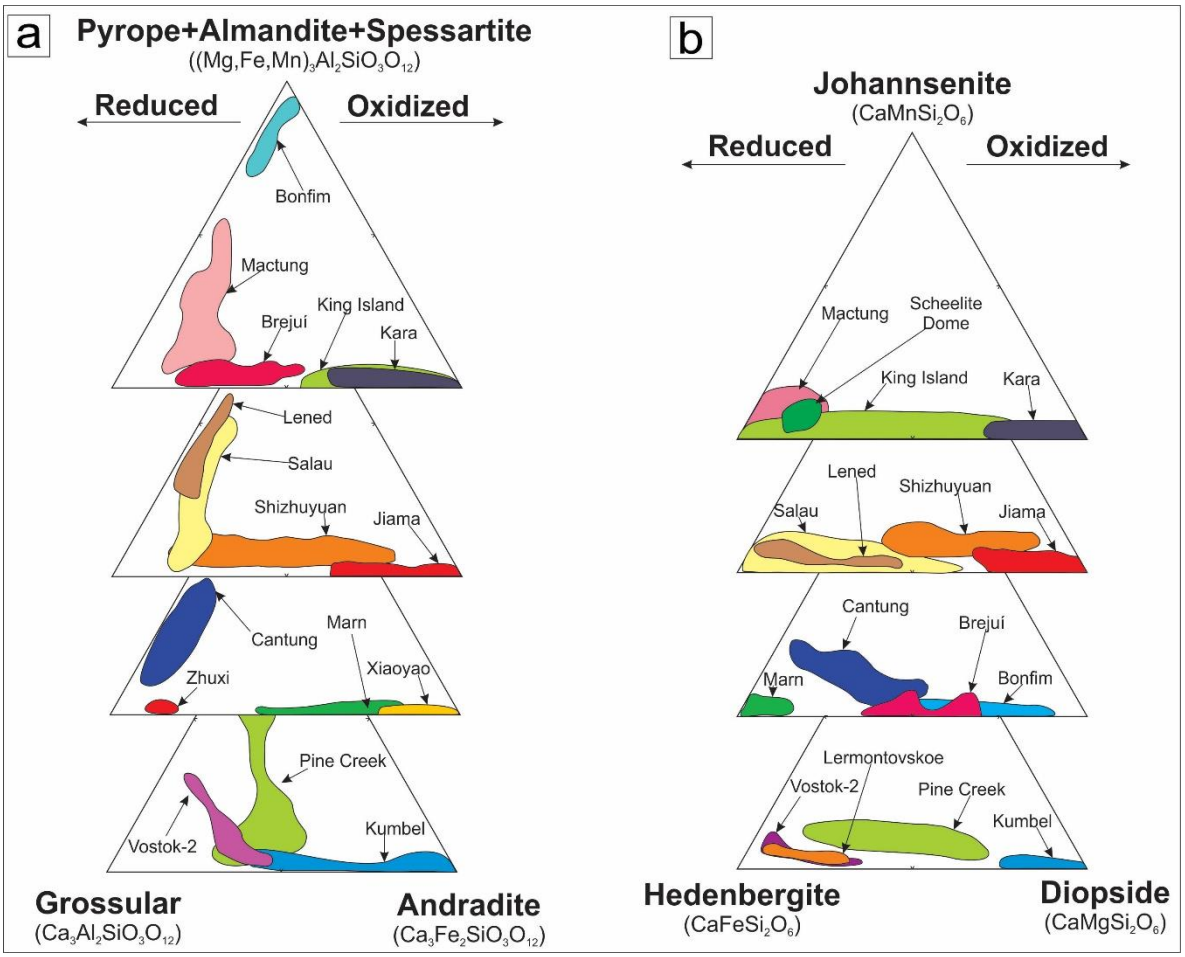

Figure 1.2 Ternary diagrams for garnet (a) and clinopyroxene (b) compositional variations from the studied scheelite-bearing skarn deposits. Data from literature (references included in Table 1) and this study (Appendix 1.1B).

1.5.2 Electron probe micro-analyses (EPMA) and cathodoluminescence images (CL)

Major and minor element composition of scheelite (n= 164 analysis), garnet (n= 84) and clinopyroxene (n= 32) (Appendix 1.1B), and cathodoluminescence (CL) images of scheelite were obtained by electron probe micro-analyser (EPMA) at Université Laval, using a CAMECA SX-100 instrument equipped with five wavelength-dispersive spectrometers (WDS) and a CL detector. The analyses were performed using a 10-µm-diameter beam. Analytical conditions for major elements analyses were 20 nA for beam current and 15 kV for accelerating voltage, with a counting time of 20 s at the peak and 10 s at the background. For minor elements in scheelite (Na, Sr, Mo, Y and Fe), the analytical conditions were 100

nA beam current, 15 kV of accelerating voltage, and counting times of 120 s at the peak and 30 s at the background. Metal tungsten (W), metal molybdenum (Mo), MgO (Mg), diopside (Ca), quartz (Si), celestite (Sr), YPO4 (Y), magnetite (Fe), albite (Na), plagioclase (Al), rutile (Ti), Cr (chromite), sphalerite (Zn), rhodochrosite (Mn), zircon (Zr), apatite (P) and orthoclase (K) were used as standards. For CL investigation, the accelerating voltage was set at 15 kV, the beam current at 20 nA, and work distance fixed at 2 mm. The dwell time of each pixel was 0.03 ms. The CL images were recorded in gray-scale in order to document texture and zonation patterns in scheelite prior to other micro-analyses.

1.5.3 Laser ablation-inductively coupled plasma-mass spectrometry (LA-ICP-MS)

The concentration and distribution of the minor and trace element in scheelite (n = 382), and in garnet (n= 32), and clinopyroxene (n= 31), were determined by LA-ICP-MS at the LabMaTer, Université du Québec à Chicoutimi (UQAC), using an Excimer 193 nm RESOlution M-50 laser ablation system (Australian Scientific Instrument) equipped with a double volume cell S-155 (Laurin Technic) and coupled with an Agilent 7900 mass spectrometer. The LA-ICP-MS tuning parameters were a laser frequency of 15 Hz, a fluence of 3 J/cm2, and rastering speed of 10µm/s for the line scans. Spots and line scans across the surface of scheelite grains were made with beam sizes of 33 and 55 µm, depending on grain size. Given the distinct textures in scheelite, the spots were performed in all distinct CL zones to obtain most variance as possible in scheelite composition. For garnet and clinopyroxene, spot analyses were made with beam size of 55 µm. Data reduction was carried out using the Iolite v3 running in Igor Pro 6.37 (Paton et al. 2011). The 44Ca was used for internal standardisation for scheelite and silicates, based on EPMA results (Appendix 1.1B). Synthetic glass reference material NIST-610 were used as external standard for all elements using preferred values from the GeoReM database (Jochum et al. 2005). In addition, GSE-1g, GSD-1g and Gprobe6-A, which are basalt glasses and NIST-612, which is a synthetic glass, were used as secondary reference materials for quality control. They were analyzed at the beginning, throughout and the end of each analytical session, to monitor a potential instrumental drift. The following isotopes were measured: 11B, 23Na, 24Mg, 39K, 44Ca, 49Ti, 51V, 55Mn, 57Fe, 59Co, 61Ni, 63Cu, 66Zn, 75As, 85Rb, 88Sr, 89Y, 93Nb, 95Mo, 137Ba, 139La, 140Ce, 141Pr, 146Nd, 147Sm, 153Eu, 157Gd, 159Tb, 163Dy, 165Ho, 166Er, 169Tm, 172Yb, 175Lu, 181Ta, 182W, 183W, 208Pb,

209Bi, 232Th and 238U. Silicon and S were also monitored to identify possible silicate and sulfide inclusions, respectively. Analyses affected by inclusions were discarded.

Maps of element distribution of individual scheelite grain used a laser frequency of 15 Hz and power of 3 mJ/pulse. Different beam size (19 and 25 μm) and stage movement speed (10 to 20 μm/s) were used to optimize spatial resolution according to grain size. The maps were generated using Iolite v3 based on the time-resolved composition of each element. The maps indicate the relative concentration of the elements and are semi-quantitative. Detailed information about laser setting and results for reference material are presented in Appendix 1.2B and 1.3B, respectively.

1.5.4 Statistical analysis

Scheelite compositional data were investigated using basic and multivariate statistics using Rstudio v4.04 (R Core Team 2021). Elements with ≤ 40% below detection limit (bdl) or left-censored data were imputed using log-ratio Expectation-Maximisation (lrEM) algorithm from the R package zCompositions (Palarea-Albaladejo and Martín-Fernández 2015). The lrEM algorithm replaces left-censored values by expected values conditional to the information provided by the compositional dataset (Palarea-Albaladejo and Martín-Fernández 2013,2015). Elements with over 40% left-censored data were excluded from further analysis. After imputation, the dataset was transformed using centred-log ratios (clr) to overcome the closure effect in compositional data (Aitchison, 1986). The clr-transformed values were investigated using partial least squares-discriminant analysis (PLS-DA, mixOmics package in R) to reveal hidden correlations among elements, and to identify potential elements useful to classify scheelite from different geological settings.

The PLS-DA is a supervised method that combines linear regression with classification technique. It consists of making a regression model from a predictive matrix X (variables/elements) to a response matrix Y (known groups/samples). To separate the known groups, the model finds the maximum covariance of uncorrelated linear transformations (latent components) of X and Y matrices, and the variables that best describe their differences. The results are visualized on scatter plots referred to as loading and scores plots (Makvandi et al. 2016b), and in bar plots referred to as scores contribution and as variable importance on projection (VIP) (Makvandi et al. 2016b). The loadings plot displays the correlations among the variables and illustrates the relationship between

variables and groups. Variables that plot in the same quadrant are positively correlated, whereas those plotting on opposite quadrants are negatively correlated. Additionally, the farther an element plots from the origin of the diagram, the greater its contribution to the model. The scores plot displays the distribution of the samples and the relationship among the groups, where samples with similar features are grouped together (Eriksson et al. 2001). The score contribution plot is used to highlight the differences between each group and the average of the entire dataset. In compositional data, the element contribution reflects its concentration. The VIP plot emphasizes the importance of each element for the model. Elements with VIP values ≥1 have major controls in the discriminant analysis, whereas those between 0.8 and 1, and <0.8 have intermediate and minor contributions to the model, respectively (Eriksson et al. 2001).

1.6 Results

1.6.1 Texture and scheelite composition

In oxidized and reduced skarns, scheelite associated with prograde assemblages is commonly fine grained (<1 mm), and varies from rounded to euhedral, occurring as inclusions within garnet, less commonly within clinopyroxene, and as disseminated crystals (Figs. 1.3a-c). Scheelite associated with retrograde stages varies from fine- to coarse-grained (from 1 to 5 mm), rounded to euhedral and is mostly disseminated (Figs. 1.3d-f). Mineral inclusions such as amphibole, biotite, pyrrhotite, apatite in reduced skarns, and magnetite in oxidized skarns, are commonly found in scheelite, especially in retrograde stages (Figs. 1.3e-f).

Cathodoluminescence (CL) and backscatter electron (BSE) photomicrographs reveal three different internal textures in scheelite: (i) homogeneous, (ii) zoning and (iii) dissolution fronts (Fig. 1.4). Homogenous scheelite is commonly associated with retrograde stages, and less often with prograde stages (Figs. 1.4a-b), whereas zoned scheelite commonly occurs in prograde stages (Figs. 1.4c-f). Two zoning patterns were identified: (i) oscillatory and (ii) patchy. Oscillatory zoning is the most common and is characterized by alternation of darker- and lighter-grey micrometric bands (Figs. 1.4c-d). Patchy zoning is less common and consists of irregular zones (Fig. 1.4e). Dissolution fronts are observed in zoned (Figs. 1.4e-f) and in homogenous crystals (Fig. 1.4b), and are characterized by resorption/dissolution of external parts of scheelite crystals, leading to variably rounded shapes with overgrown rims.

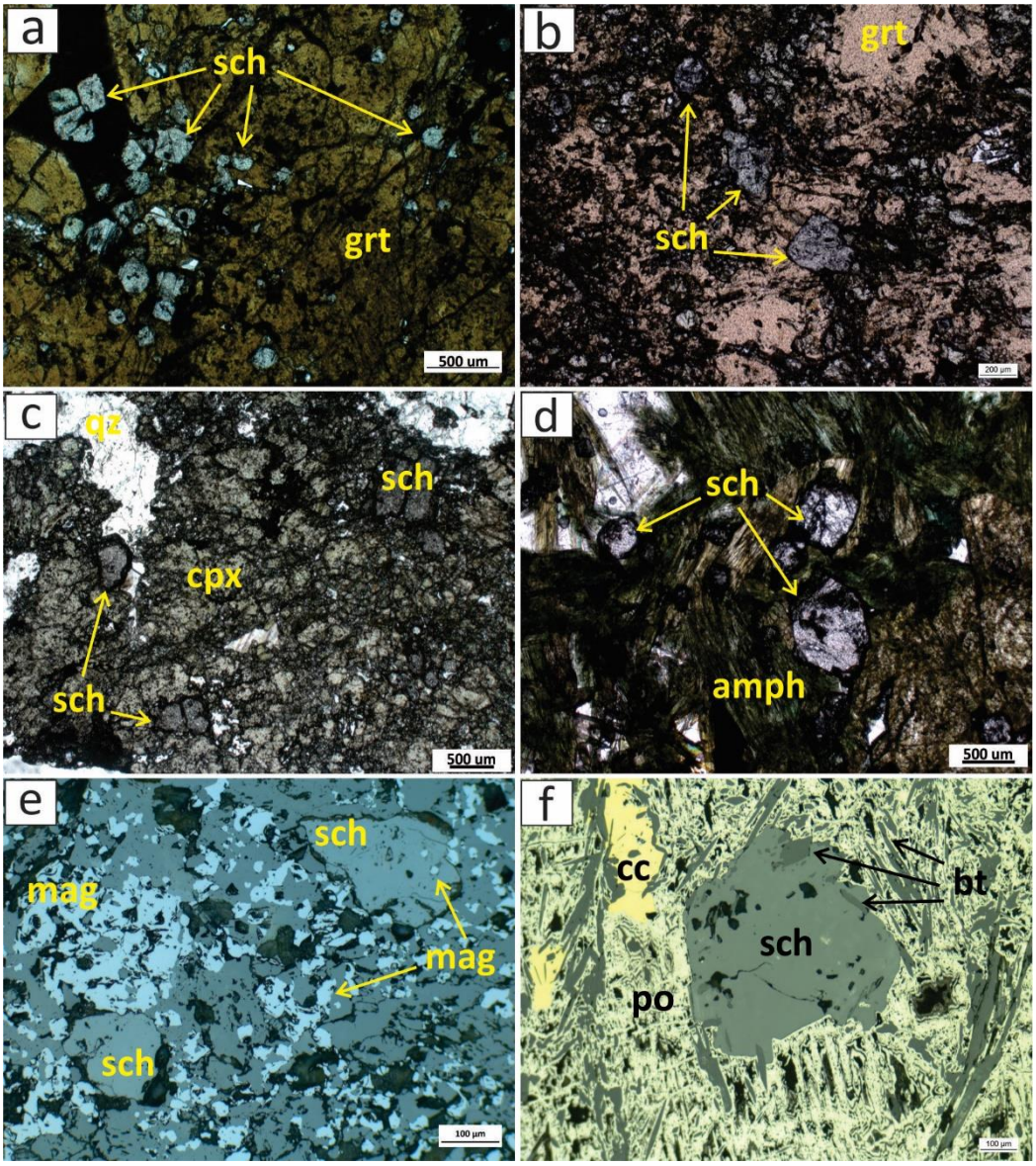

Figure 1.3 Photomicrographs under transmitted light **a-c** and reflected light **d-e** of scheelite-bearing skarn samples. **a.** Scheelite associated with garnet (King Island). Scheelite occurs as inclusions in andradite, and as disseminated grains in the matrix. **b.** Scheelite inclusions in garnet from garnet-clinopyroxene skarn facies (Lened). **c**. Scheelite associated with clinopyroxene (Mactung). **d**. Disseminated scheelite associated with amphibole (Cantung). **e**. Scheelite grains associated with magnetite and amphibole from magnetite skarn (Kara). **f**. Scheelite with pyrrhotite, biotite and chalcopyrite (Lened). Note biotite and pyrrhotite inclusions close to scheelite grain boundaries. sch: scheelite; grt: garnet; cpx; clinopyroxene; qz: quartz; mag: magnetite; amph: amphibole.

Compositional data for scheelite, and ΣREE for garnet and clinopyroxene are reported in supplementary data (Appendix 1.4B and 1.5B). In scheelite, Mo is the only trace

element with median concentration above 100 ppm. Cerium, Sr, Nd, Nb, La, Y, Mn and Na have median concentrations between 10 and 100 ppm, whereas B, Mg, K, As, Pr, Sm, Eu, Gd, Dy, Er, Yb and Pb have median contents between 1 and 10 ppm. Titanium, V, Co, Ni, Ba, Tb, Ho, Tm, Lu, Ta, Bi, Th and U have the lowest median concentrations, which are all below 1 ppm. The concentration ranges for each element are shown in box and whisker plot grouped according to skarn redox (Fig. 1.5).

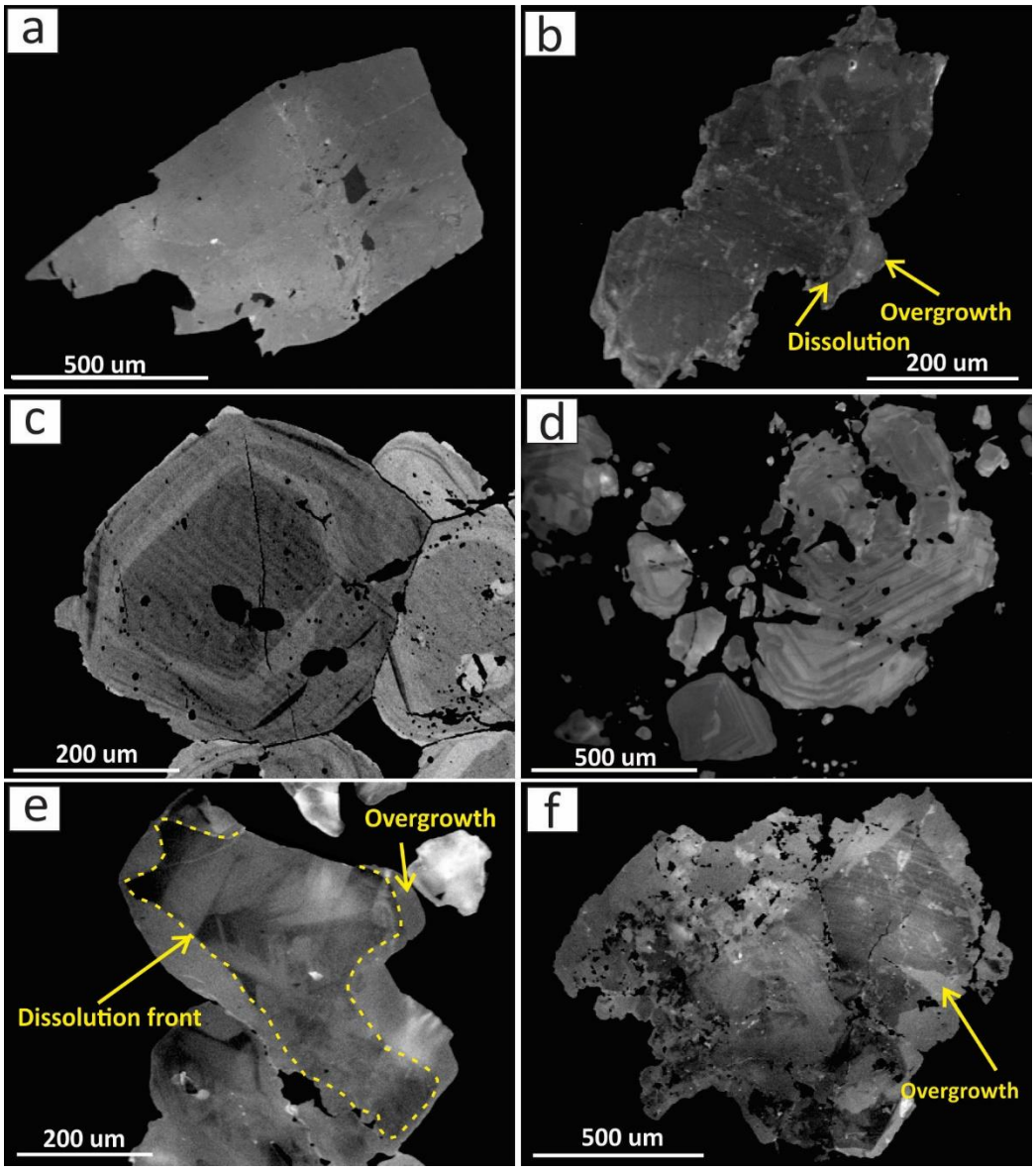

Figure 1.4 Cathodoluminescence (a-b, d-f) and backscattered electron (c) images of scheelite crystals. a. Homogeneous scheelite from Zhuxi. b. Homogeneous scheelite cut by late, brighter CL scheelite (Kara). c. and d. scheelite with oscillatory zoning from King Island and Jiama, respectively.

e. Scheelite with irregular zoning and with an overgrown of brighter CL scheelite (Mactung). f. Scheelite with narrow oscillatory zoning with an overgrown of brighter CL scheelite (Mactung).

Trace element concentrations of scheelite from oxidized and reduced skarns show significant differences (Fig. 1.5). Scheelite from oxidized skarns has higher concentrations of Mo (<18.1 wt.%), As (<103 ppm), Ti (<42 ppm), V (<16 ppm) and Pb (<52 ppm) compared to those from reduced skarns (Mo <7 wt.%, As <27 ppm, Ti <28 ppm, V <3 ppm and Pb <18 ppm; Fig. 1.5). Yttrium, Nb, Ta and HREE display higher contents in reduced skarn scheelite (Y <1980 ppm, Nb <970 ppm, Ta<11 and HREE <1450 ppm; Fig. 1.5), and lower concentrations in oxidized skarn scheelite (Y <197 ppm, Nb <77 ppm, Ta<2 and HREE <206 ppm; Fig. 1.5). Boron, K, Sr, Na, Mg, Co, Ni, Mn, Ba, LREE, Th and U have similar concentration ranges in scheelite from both skarn types (Fig. 1.5). Given these differences, scheelite from oxidized skarns has higher LREE/HREE (up to 510) and Mo/Nb (from 5 to 40,577) ratios relative to reduced skarn scheelite (LREE/HREE from 0.6 and 65, and Mo/Nb <324; Figs. 1.6a-b). Significant positive correlations exist between ΣREE-Eu+Y and Na, As+V and Nb+Ta (Figs. 1.6c-e) in both reduced and oxidized skarns scheelite. The MoO3 and WO3 contents are negatively correlated (Fig. 1.6f). Weak to no correlations are noticed between U and Mo (Fig. 1.6g), ΣREE-Eu+Y and K (Appendix 1.1A) in reduced and oxidized skarns. Europium anomaly and Mo display a weak negative correlation in reduced skarn scheelite, and no correlation in oxidized skarns (Fig. 1.6h). A positive correlation is observed between U and Th in scheelite from both reduced and oxidized skarns (Fig. 1.6i).

Appendix 1.2A and Fig. 1.7 show representative LA-ICP-MS multielement maps of scheelite grains found in (i) prograde stage oxidized tungsten skarn (King Island; Appendix 1.2A), and (ii) retrograde stage from reduced tungsten skarn (Cantung; Fig. 1.7). The maps revel that Mo is the main element mirroring the CL zoning in scheelite. The CL-darker domains coincide with Mo-rich bands, and the lighter domains represent Mo-poor sectors (Appendix 1.2A and Fig. 1.7). In contrast, more homogenous grains display flat Mo signal (Fig. 1.8). Some of the darkest CL zones coincide with high Nb, U, and Th concentrations (Appendix 1.2A and Fig. 1.7). Strontium, As, Y, and ΣREE distributions do not correlate with the internal textures revealed by CL imaging, even though these elements also show a heterogeneous distribution in the elemental maps. Strontium varies from zoned Appendix 1.2A and Fig. 1.7) to homogenous (Figs. 1.8c-d). Arsenic exhibits a zoned distribution in scheelite from oxidized skarn, which roughly matches the Mo zonation (Appendix 1.2A). However, it tends to be more homogenously distributed in scheelite from reduced skarns

(Figs. 1.7 and 1.8c), and in unzoned scheelite from oxidized retrograde skarns (Fig. 1.8d). Yttrium and Yb have a similar distribution and differ from that of Eu and La (Appendix 1.2A and Fig. 1.7). Cores of zoned crystals are depleted in Y and Yb relative to the younger rims. In contrast, La is higher in the core relative to the rims (Appendix 1.2A; Figs. 1.7 and 1.8c-d), whereas Eu displays variable distribution relative to La and Y.

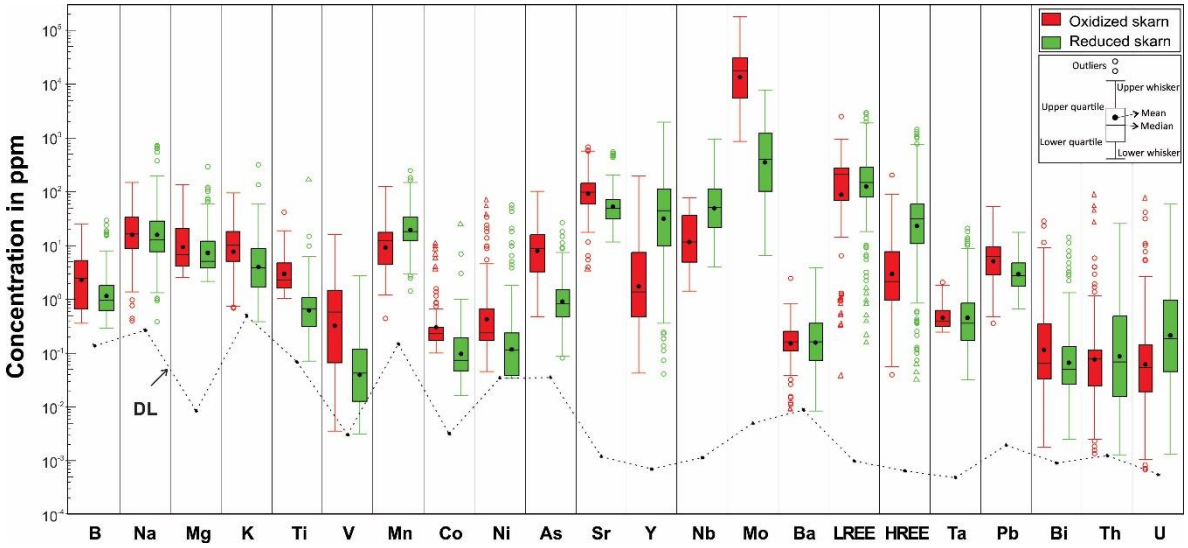

Figure 1.5 Box and whisker diagram of trace elements concentrations in scheelite from reduced and oxidized skarns. Dashed line represents the detection limit (DL). Note that scheelite from oxidized skarns contains higher concentrations of Ti, V, As and Mo, whereas scheelite from reduced skarns contains higher concentrations of Nb, Y and HREE.

1.6.2 Garnet and clinopyroxene composition

Figure 1.2 shows a compilation of major elements composition of garnet and pyroxene from this study and literature (Table 1.1 for references). These data show that garnet from reduced skarn varies in composition mostly from grossular to spessartite ($Gr_{88}Ad_{12}Sp_0$ - $Gr_{63}Ad_{10}Sp_{27}$), whereas in oxidized skarns garnet composition ranges from andradite to grossular ($Gr_0Ad_{100}Sp_0$ – $Gr_{20}Ad_{80}Sp_0$), but being predominantly andraditic in composition (>50% mol of andradite). Clinopyroxene was analyzed for major and trace elements only in reduced skarns, since it is rare in oxidized skarns. Clinopyroxene from reduced skarns varies in composition from diopside to dominantly hedenbergite (Fig. 1.2; $Di_{80}Hd_{18}Jo_2$ – $Di_8Hd_{88}Jo^4$).

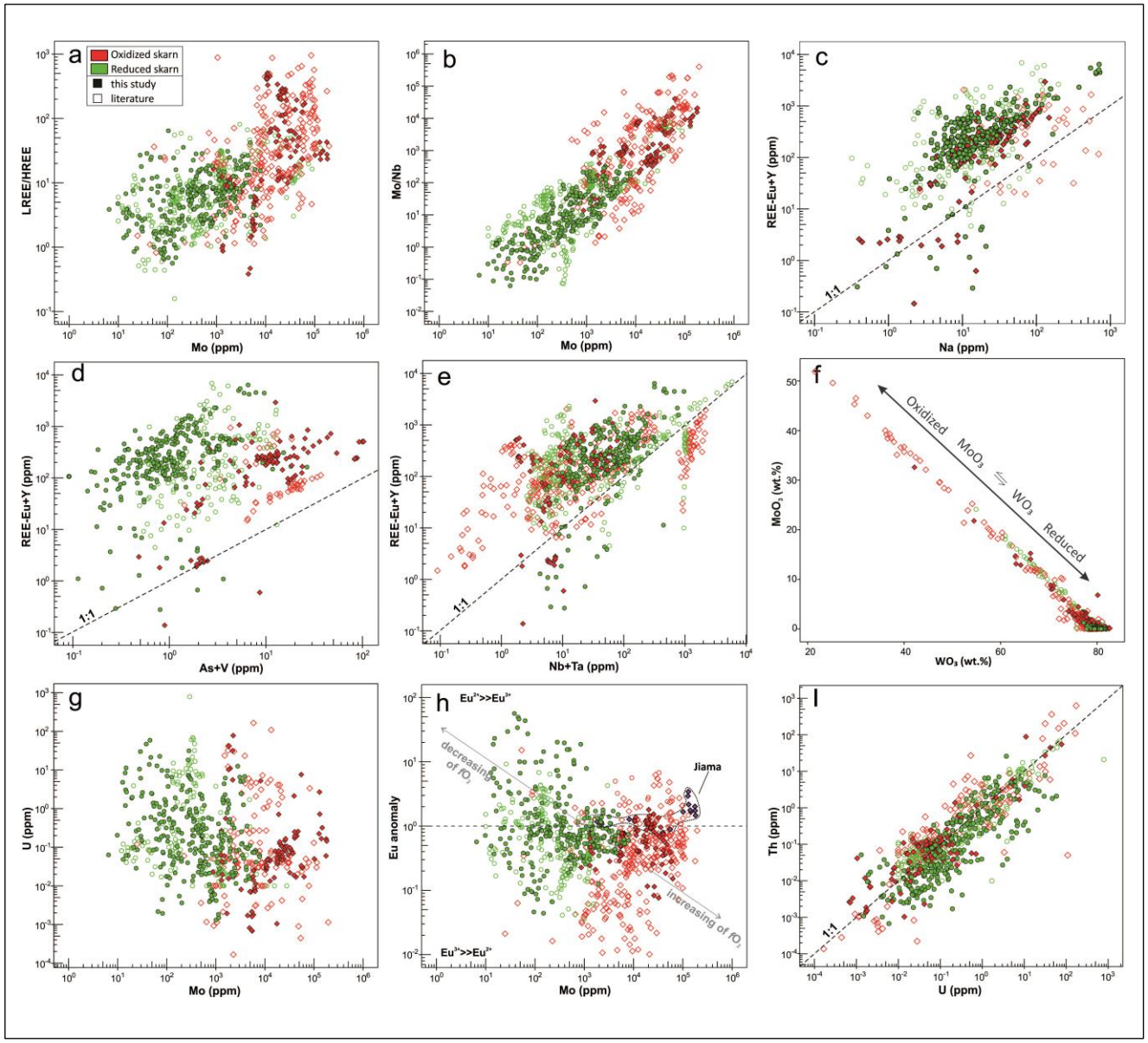

Figure 1.6 Binary plots of minor (f) and trace (a-e, g-i) elements composition scheelite. a. Mo versus LREE/HREE, b. Mo versus Mo/Nb, c. Na versus ΣREE-Eu+Y, d. V+As versus ΣREE-Eu+Y, e. Nb+Ta versus ΣREE-Eu+Y, f. WO_3 versus MoO_3, g. Mo versus U, h. Mo versus Eu anomaly, and i. U versus Th. Data from: Song et al. (2014), Fu et al. (2016), Guo et al. (2016), Ding et al. (2018), Zhao et al. (2018), Li et al. (2019), Wu et al. (2019), Yuan et al. (2019), Xu et al. (2019), Chen et al. (2020), Seo et al. (2020), Song et al. (2020) and Su et al. (2020).

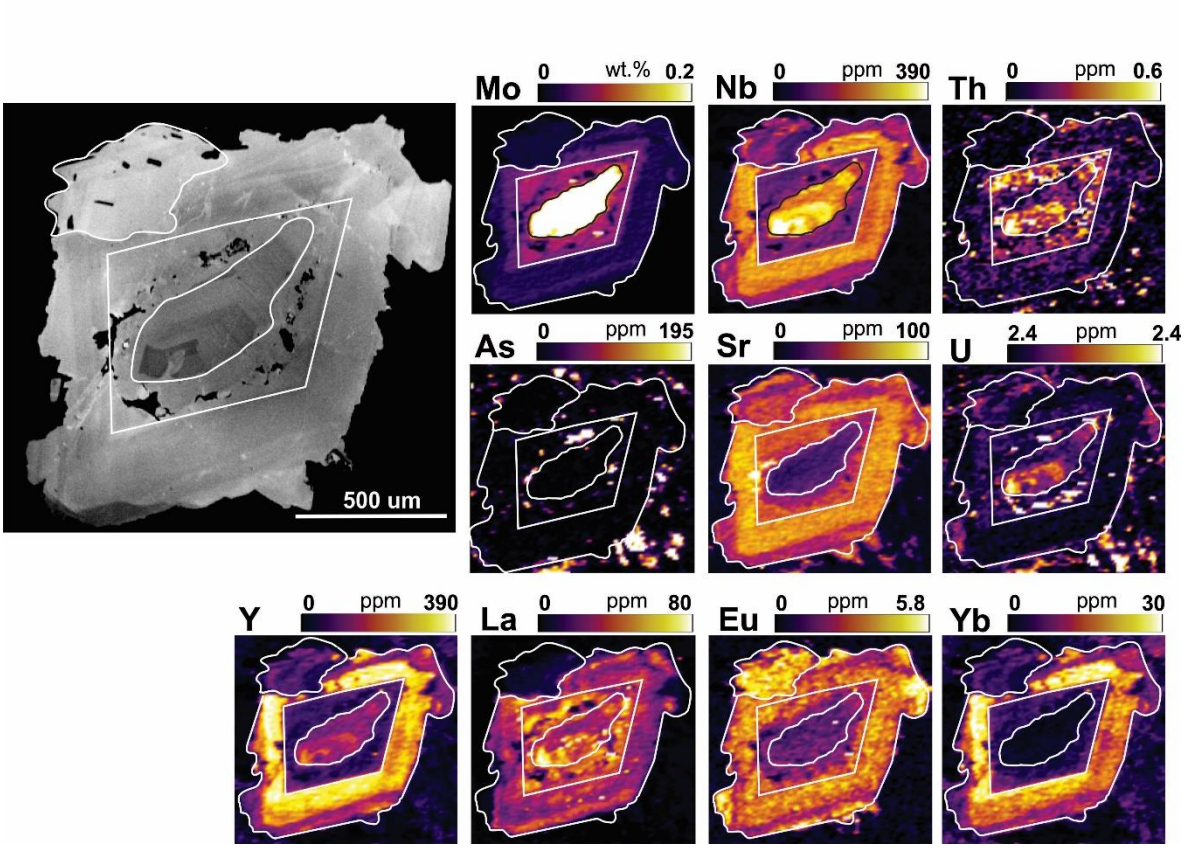

Figure 1.7 Cathodoluminescence image (grey scale) and LA-ICP-MS multi-element maps (white-violet scale) showing zoning, dissolution and overgrown textures in scheelite from amphibole facies, Cantung. Note the homogenous distribution of As. The concentrations of the elements in the LA-ICP-MS maps are semi-quantitative. The white lines show the grain outline.

Garnet and clinopyroxene have much lower ΣREE content compared to scheelite. In garnet, ΣREE contents vary from 0.01 to 134.5 ppm, whereas in clinopyroxene these vary from 0.2 to 8.8 ppm (Appendix 1.5B). Grossular-spessartite garnet from reduced skarns, contains lower LREE contents (<7 ppm) relative to HREE (<127 ppm; Appendix 1.3A). Andradite garnet from oxidized skarn has relatively higher LREE contents (12 to 29 ppm) compared to HREE (0.3 to 10.5 ppm). Light REE contents in clinopyroxene vary from 0.115 to 6.7 ppm and HREE vary from 0.06 to 2.6 ppm (Appendix 1.3A).

1.6.3 REE patterns

Scheelite displays five main REE patterns: (i) steep and (ii) shallow negative slope, (iii) concave, (iv) flat to slightly concave and (v) convex shape (Fig. 1.9). The steep negative slope pattern is characterized by high (La/Sm)CN and (Gd/Lu)CN ratios (i.e., >10; Fig. 1.10),

negative to slightly positive Eu anomalies, and is restricted to oxidized skarns scheelite (Fig. 1.9a). The shallow negative slope pattern has (La/Sm)CN and (Gd/Lu)CN ratios >1 (Fig. 1.10), negative and positive Eu anomalies, and occurs in scheelite from both oxidized and reduced skarns (Figs. 1.9b-c).

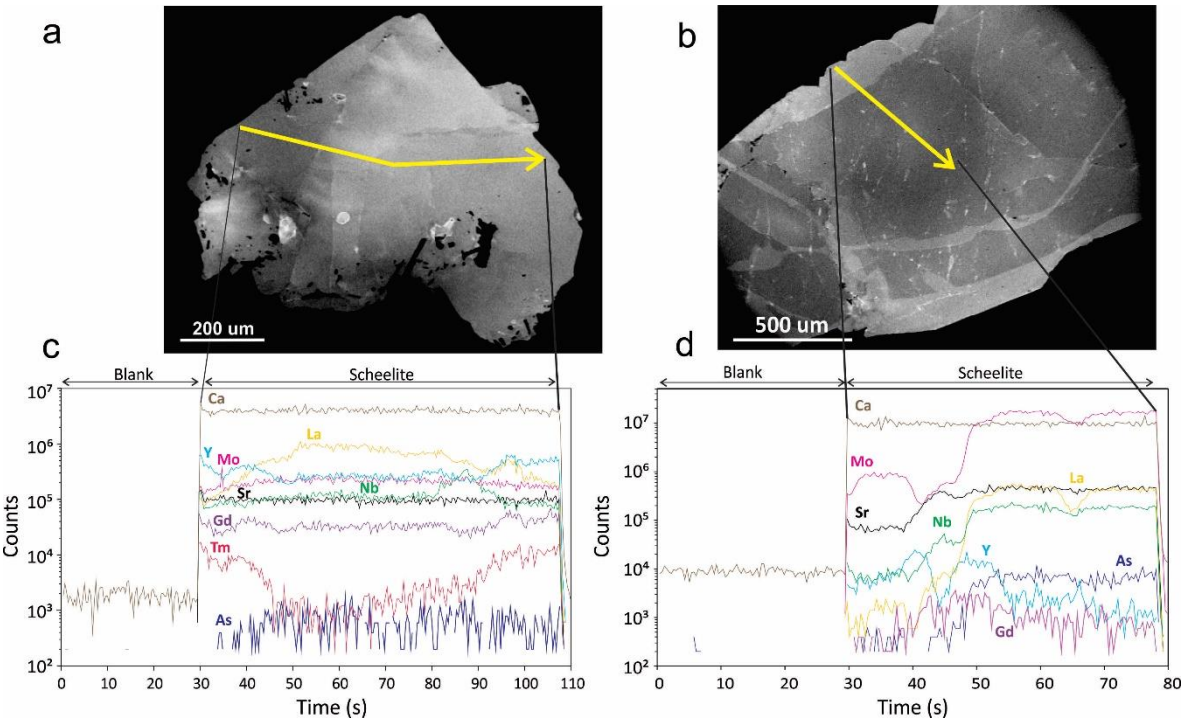

Figure 1.8. Cathodoluminescence image showing homogeneous scheelite from Lened in a, and homogenous grain overgrown and cut by brighter CL scheelite (Kara) in b. The yellow lines indicate the laser-ablation trenches. c-d. Time-signal diagram showing the trace element distribution in scheelite along the ablation trenches. Flat patterns indicate homogeneous trace element distribution, whereas irregular profiles indicate heterogeneous element distribution.

The concave pattern is characterized by an enrichment of Pr-Dy relative to La-Ce and Ho-Lu, with (La/Sm)CN <1 and (Gd/Lu)CN >10 ratios (Figs. 1.9d and 1.10). It occurs mostly in reduced skarn scheelite, with a few samples from oxidized skarns (i.e., Brejui and Shizhuyuan). The Eu anomaly is predominantly negative, with a few samples displaying positive Eu anomaly (Fig. 1.9d).

The flat to slightly concave pattern is characterized by (La/Sm)CN <1 and (Gd/Lu)CN between 1 and 10 (Figs. 1.9e and 1.10). It commonly has a negative Eu anomaly and occurs in both reduced and oxidized skarn scheelite, however, reduced skarns have REE

scheelite/chondrite ratio >1, whereas oxidized skarn scheelite has predominantly REE scheelite/chondrite ratio <1 (Fig. 1.9e).

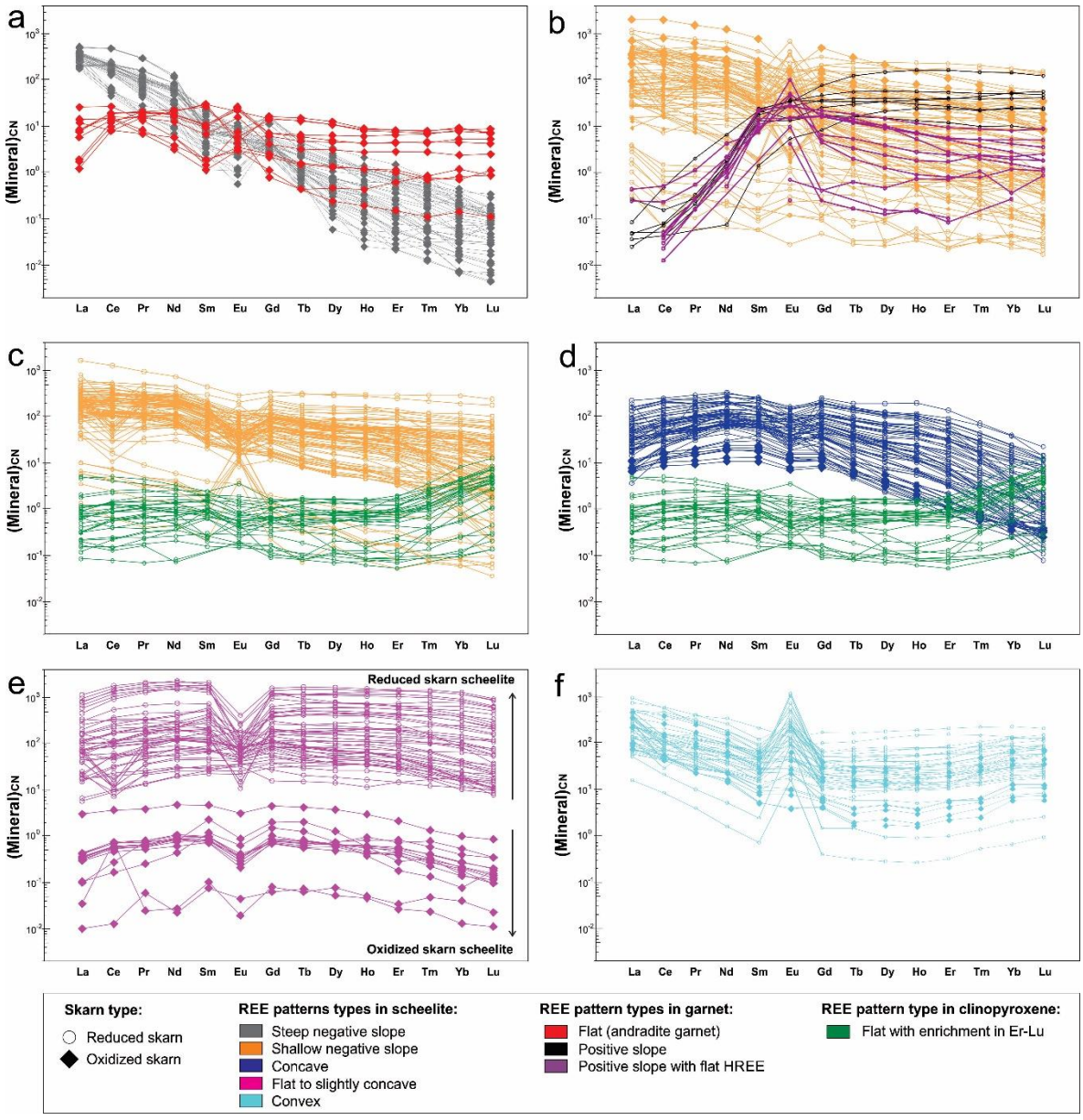

Figure 1.9 Chondrite-normalized REE patterns of scheelite, garnet and clinopyroxene. Chondrite normalized values from McDonough and Sun (1995). a. steep negative slope in scheelite coexisting with flat pattern in garnet. b. shallow negative slope in scheelite coexisting with positive slope pattern in garnet, c. shallow negative slope with a slight depletion between Er-Lu pattern in scheelite coexisting with flat pattern with a slight enrichment among Er-Lu in clinopyroxene. d. concave shape with a depletion among Er-Lu coexisting with flat pattern with a slight enrichment among Ho-Lu in

clinopyroxene. e. flat to slightly concave shapes with scheelite/chondrite ratio > 1 for reduced skarns and < 1 for oxidized skarns. f. convex shape.

The convex pattern, characterized by (La/Sm)CN >1 and (Gd/Lu)CN <1 and a positive to slightly negative Eu anomaly, is commonly associated with scheelite from retrograde stages in reduced skarns (Fig. 1.9d and Appendix 1.4Ai). One exception is the Jiama oxidized porphyry-skarn Cu deposit, where retrograde scheelite displays a convex pattern (Fig. 1.9f).

Garnet displays three different REE patterns according to its composition (Fig. 1.9 and S4). Andradite garnet displays a (i) flat to shallow negative slope pattern with (La/Sm)CN and (Gd/Lu)CN ratios >1 and positive and negative Eu anomalies (Fig. 1.9a). In contrast, grossular-spessartite garnet displays a (ii) positive slope with (La/Sm)CN <1 and (Gd/Lu)CN varying from 0.3 to 2, and (iii) positive slope with flat HREE, which is characterized by (La/Sm)CN <1 and (Gd/Lu)CN >2 (Fig. 1.9b). The Eu anomaly in grossular-spessartite garnet is predominantly positive with few slightly negative values. The Fe-rich clinopyroxene has a flat pattern between La and Ho and a small enrichment from Er to Lu. The Eu anomaly varies from positive to negative (Fig. 1.9c-d).

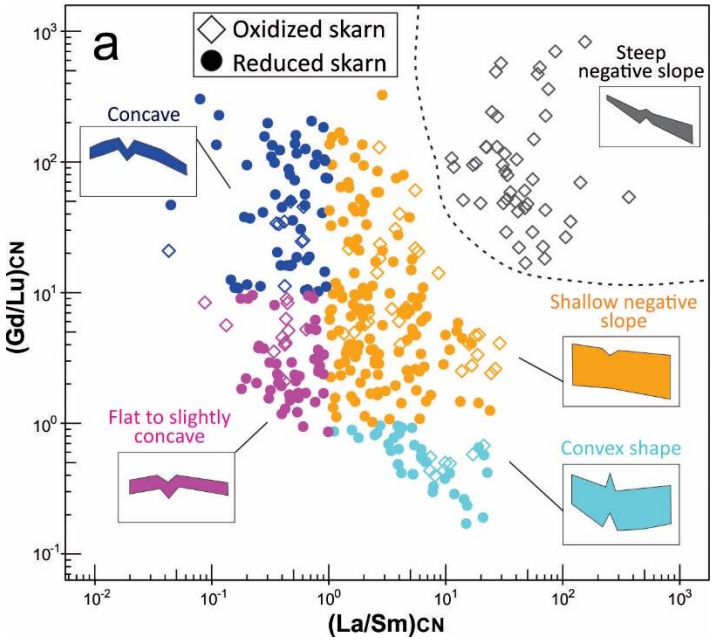

Figure 1.10 Binary plot $(Gd/Lu)_{CN}$ versus $(La/Sm)_{CN}$ showing the relation between these ratios and the REE patterns on scheelite.

Appendix 1.4A shows REE patterns of coexisting scheelite, garnet, and clinopyroxene. Scheelite associated with andradite garnet has steep negative slope, whereas garnet displays a flat REE pattern (Appendix 1.4A a-c). Positive slope REE pattern scheelite coexists with shallow negative slope pattern grossular-spessartite garnet (Appendix 1.4A d-f). Where scheelite and clinopyroxene coexist, scheelite displays both shallow negative slope and concave patterns with a depletion among Er-Lu, whereas pyroxene shows a flat pattern with an enrichment among Er-Lu (Appendix 1.4A g-i).

1.7 Multivariate Statistical Analysis of Scheelite Composition

1.7.1 Scheelite from oxidized and reduced skarns

Figure 1.11 shows PLS-DA results for LA-ICP-MS scheelite analyses classified according to skarn redox type. The loadings plot (Fig. 1.11a) of the first and second PLS-DA components (qw*1-qw*2) displays the relationship among variables and groups, whereas the scores plot (Fig. 1.11b) shows the distribution of the samples in t1-t2 space. In general, positive correlations exist among Mo, As and V in negative qw*1 and positive qw*2; Th, U, ΣREE, Ta and Na in positive qw*1 and qw*2; Nb, Mn and Y, and Ba and Eu anomaly in positive qw*1 and negative qw*2; B, Co, Ni, Ti and Sr in negative qw*1 and qw*2 (Fig. 1.11a).

Oxidized skarns plot in the negative qw*1 and positive qw*2, as a result of correlated Mo, As, V and Ti (Fig. 1.11a). In contrast, reduced skarns plot at positive qw*1 and negative qw*2 because of correlated Mn, Y and Nb (Fig. 1.11a). Therefore, oxidized and reduced skarn classes are mostly discriminated by qw*1 (Fig. 1.11a). Figure 1.11b shows that oxidized skarn scheelite plots at negative t1 and spreads in negative and positive t2 due to high Mo, As, V and Ti concentrations (Fig. 1.11c). Scheelite from reduced skarns plots mostly at positive t1, and negative and positive t2 because of high Mn, Y, Nb, U, and Eu anomaly contents (Fig. 1.11b,d). However, few scheelite analyses from reduced skarns plot in negative t1, which overlaps with few samples of oxidized skarn scheelite (Fig. 1.11b). The elements that best discriminate for redox state skarn classification are Ti, V, Mn, As, Y, Nb and Mo (VIP >1) followed by Co, Th, U and Eu anomaly (VIP between 0.8 and 1) (Fig. 1.11e).

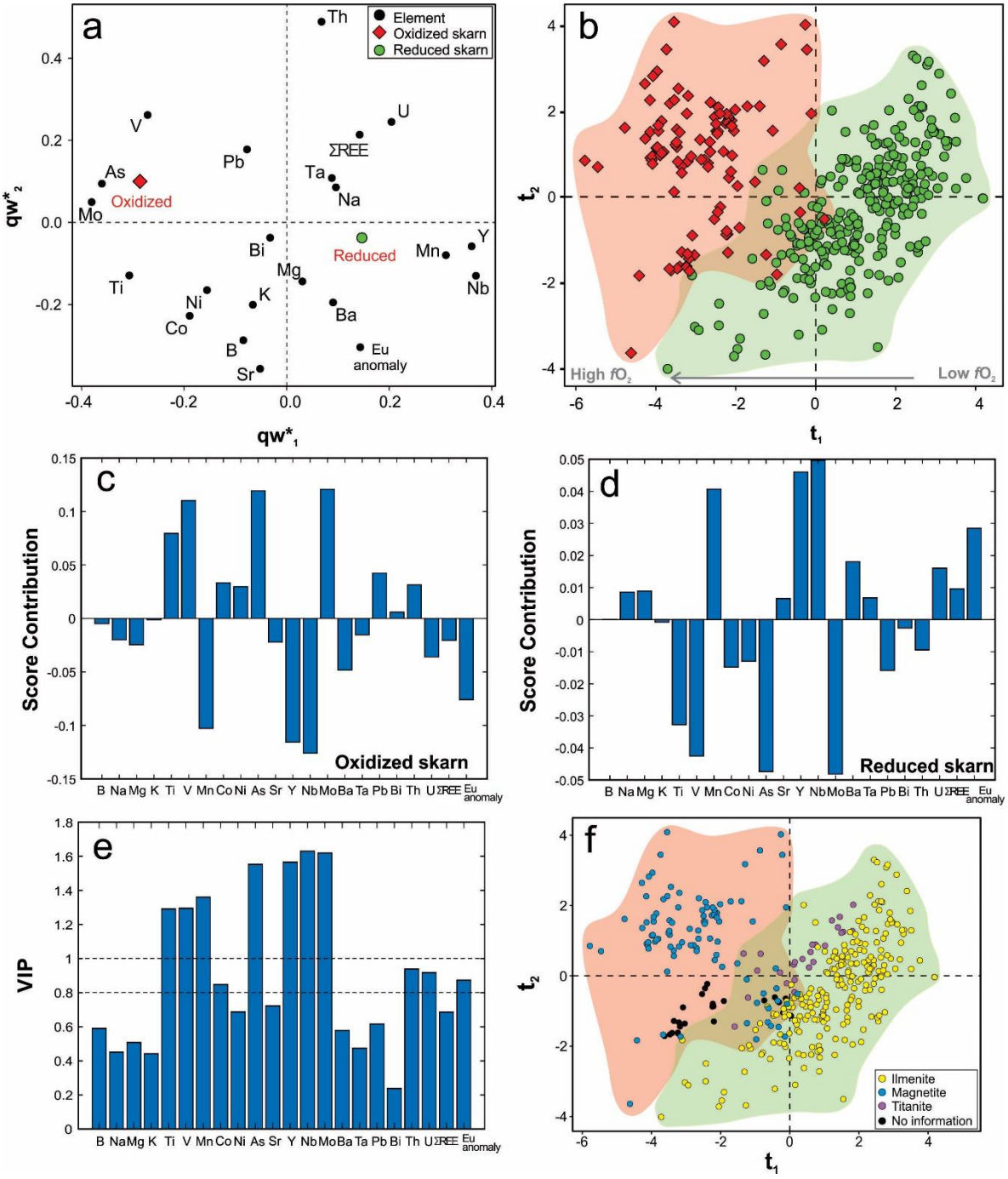

Figure 1.11 Partial least squares discriminant analysis (PLS-DA) of LA-ICP-MS data for scheelite from skarn systems. a. qw*1–qw*2 (first and second loadings) plot showing the correlations among elemental variables and skarn types (oxidized vs reduced). b. t1–t2 (first and second scores) plot showing the distribution of scheelite analyses in the latent variable space defined by qw*1–qw*2. c-d Score contributions of scheelite associated with oxidized (c) and reduced (d) skarns indicating the main elements that contribute to classification. e. Variable Importance on Projection (VIP) plot showing the importance of compositional variables in classification of the model in (b). f. Projection

of the compositional data of scheelite analyses labeled by the oxidation state of the intrusion related to skarn mineralization in the t1-t2 plot (b).

Figure 1.11f displays the same scheelite analyses plotted in the t1-t2 space (Fig. 1.11b), labeled according to redox state of the granitic intrusions that are associated with the formation of oxidized and reduced skarns. Figure 1.11f shows a direct relationship between the redox states of skarns and granites, where scheelite associated with magnetite-series granite plots in the oxidized skarn field and scheelite associated with ilmenite(titanite)-series granite plots in the reduced skarn field.

1.7.2 Intrusion composition

Figure 1.12 displays PLS-DA results of LA-ICP-MS data for scheelite related to the aluminum saturation index of their source felsic intrusions. Figure 1.12a highlights that peralunimous granites plot at negative qw*1 due to correlated Mn, Mg and Nb, and at negative qw*2 very close to the qw*2 axis. In contrast, metaluminous granites plot at positive qw*1 because of correlated As and V, and at positive qw*2 because of correlated U, Th, Y and Pb, and Sr and ΣREE. Therefore, peraluminous and metaluminous granites are mainly discriminated by qw*1 (Fig. 1.12a).

In the t1-t2 scores plot (Fig. 1.12b), scheelite related to peraluminous granitic intrusions plots mostly at negative t1 because of high Mn, Sn and Nb contents and scattered through negative and positive t2. Few analyses plot at negative t1, likely due to higher V and As concentrations relative to the others elements of the peraluminous intrusions (Figs. 1.12b-c). In contrast, scheelite related to metaluminous granitic intrusions plots mostly at positive t1 and t2, due to high V and As, and U and Th concentrations, respectively (Figs. 1.12b-d). A few analyses scatter at negative t2, which causes an overlap with analyses of scheelite related to peraluminous granitic intrusions. Figure 1.12e shows that the most important elements for classification are Mg, V, Mn, As, Nb, Mo and Ta for VIP >1, and Ti, Pb, B and U with VIP between 0.8 and 1.

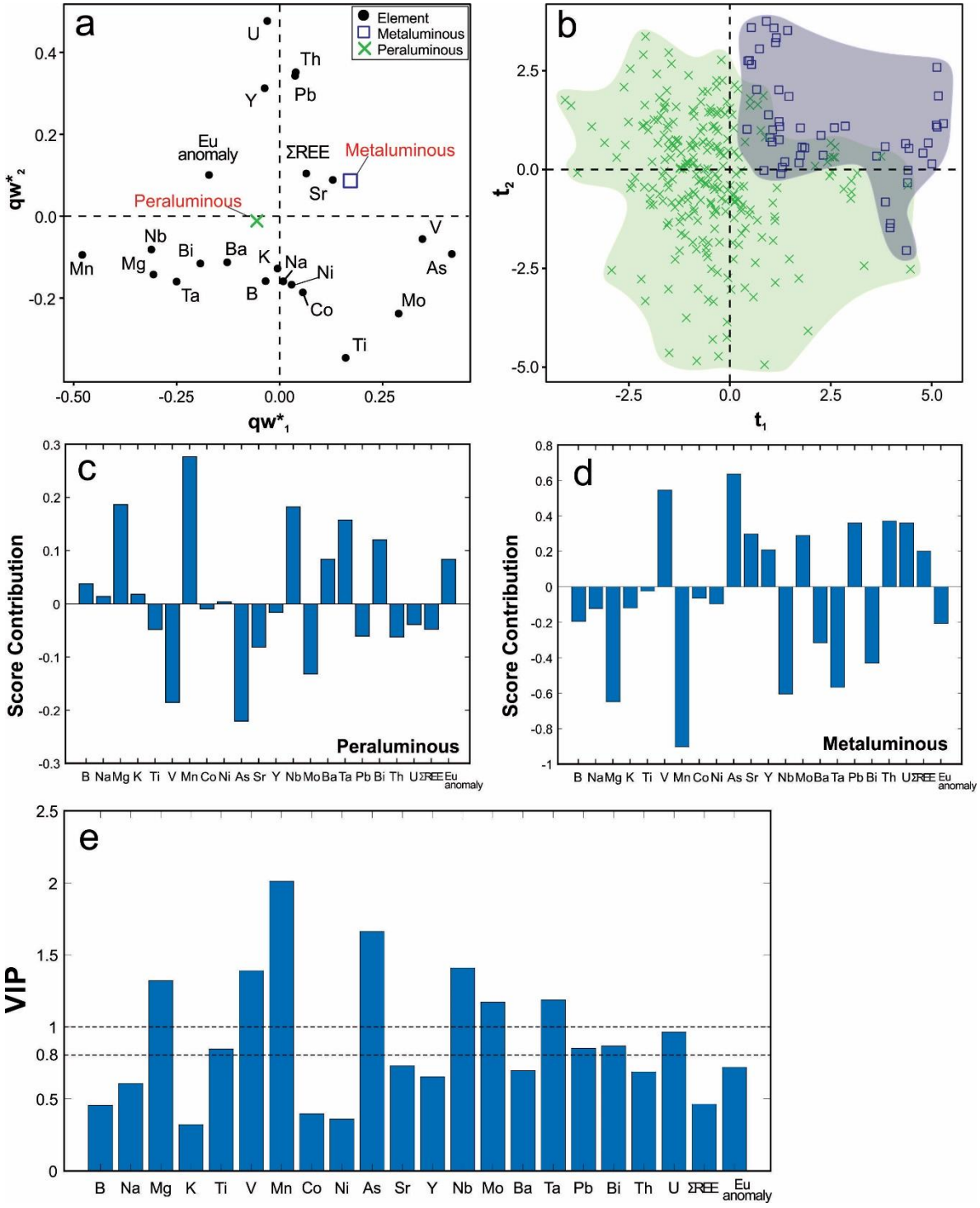

Figure 1.12 Partial least squares discriminant analysis (PLS-DA) of LA-ICP-MS data for scheelite from skarn systems. a. qw*1–qw*2 (first and second loadings) plot showing the correlations among elemental variables and intrusion composition (peraluminous and metaluminous). b. t1–t2 (first and second scores) plot showing the distribution of scheelite analyses in the latent variable space defined by qw*1–qw*2. c-d. Score contributions of scheelite associated with peraluminous (c) and

metaluminous (d) intrusions indicating that each group is discriminated by distinct mean composition, and the main elements that contribute for each group. f. VIP plot showing the importance of compositional variables in classification of the model in b.

1.7.3 Metal association

Figure 1.13 displays PLS-DA results of LA-ICP-MS data for scheelite classified in 5 deposit types according to the metal association (Cu-polymetallic, W, W-Au, W-Cu, W-Mo(Sn); Table 1.1). Figure 1.13a shows that W-Mo(Sn) and Cu-polymetallic deposits plot at negative qw*1 and positive qw*2 as they correlate with As and Ti, and Co and Ni. The W deposits plot at negative qw*1 and qw*2 because of correlated Mo and V. The W-Au and W-Cu deposits plot at positive qw*1 because of correlated Nb and Mn. The W-Au deposits plot at positive qw*2 due to Na, Th, U and, Y ΣREE correlation and W-Cu deposits plot at negative qw*2 owning to correlated Eu anomaly, Mg and Ba. Overall, qw*1 discriminates W-Mo(Sn), Cu-polymetallic and W deposits from W-Cu and W-Au deposits and qw*2 discriminates Mo(Sn), Cu-polymetallic and W-Au from W and W-Cu deposits.

Figure 1.13b shows that scheelite associated with W-Mo(Sn) and Cu-polymetallic deposits overlap in negative t1 and positive t2. Scheelite from W-Mo(Sn) and Cu-polymetallic deposits has in common higher contents of Co, Ni, As and Ti relative to the other deposits. Scheelite from W-Au deposits plots mostly at positive t1 and t2 because of high Y and ΣREE, and low Pb and Sr contents, with few samples plotting at negative t1 and t2, close to the origin. Scheelite from W-Cu deposits shows a wide spread, where most analyses plot at positive t1 and negative t2 due to higher Nb and Mn concentrations, and with few scheelite analyses with positive t1 and t2. Few scheelite analyses from W-Cu deposits plot at negative t1 and t2 overlapping with scheelite from W deposits (Figs. 1.13a-b). Scheelite from W deposits plots mostly at negative t1 and t2, because of higher Mo and Pb concentrations relative to the origin. A small group of few scheelite analyses plot at negative t1 and positive t2 due to their higher Co and Y concentrations relative to the others scheelite from W deposits.

Figure 1.13c displays the first and third components (qw*1-qw*3), where W-Mo(Sn) deposits are better discriminated from Cu-polymetallic deposits relative to qw*1-qw*2 plot (Fig. 1.13a). Scheelite from Cu-polymetallic and W deposits plot at negative qw*1 and qw*3 as they correlated to V and Mo. The W-Mo-(Sn) deposits plot at negative qw*1 because of Ti, As, and Mo correlation, but qw*3 is not discriminant. Tungsten-Au and W-Cu deposits

plot close to each other at positive qw*1 and qw*3 owing to correlated Ta, Eu anomaly, ΣREE, Mg and Na.

Figure 1.13d shows significant overlaps between: (i) scheelite from W-Cu and W-Au deposits that spread from positive t1 and negative t3 toward negative t1 and positive t3, and have in common high Nb, Mn and Y concentrations and; (ii) scheelite from W-Mo(Sn) and W deposits that plot at negative side of t1, but through positive and negative t3. Scheelite Cu-polymetallic deposits plots separately from the others scheelite at negative t1 and t3, due to high V and Mo concentration (Fig. 1.13d).

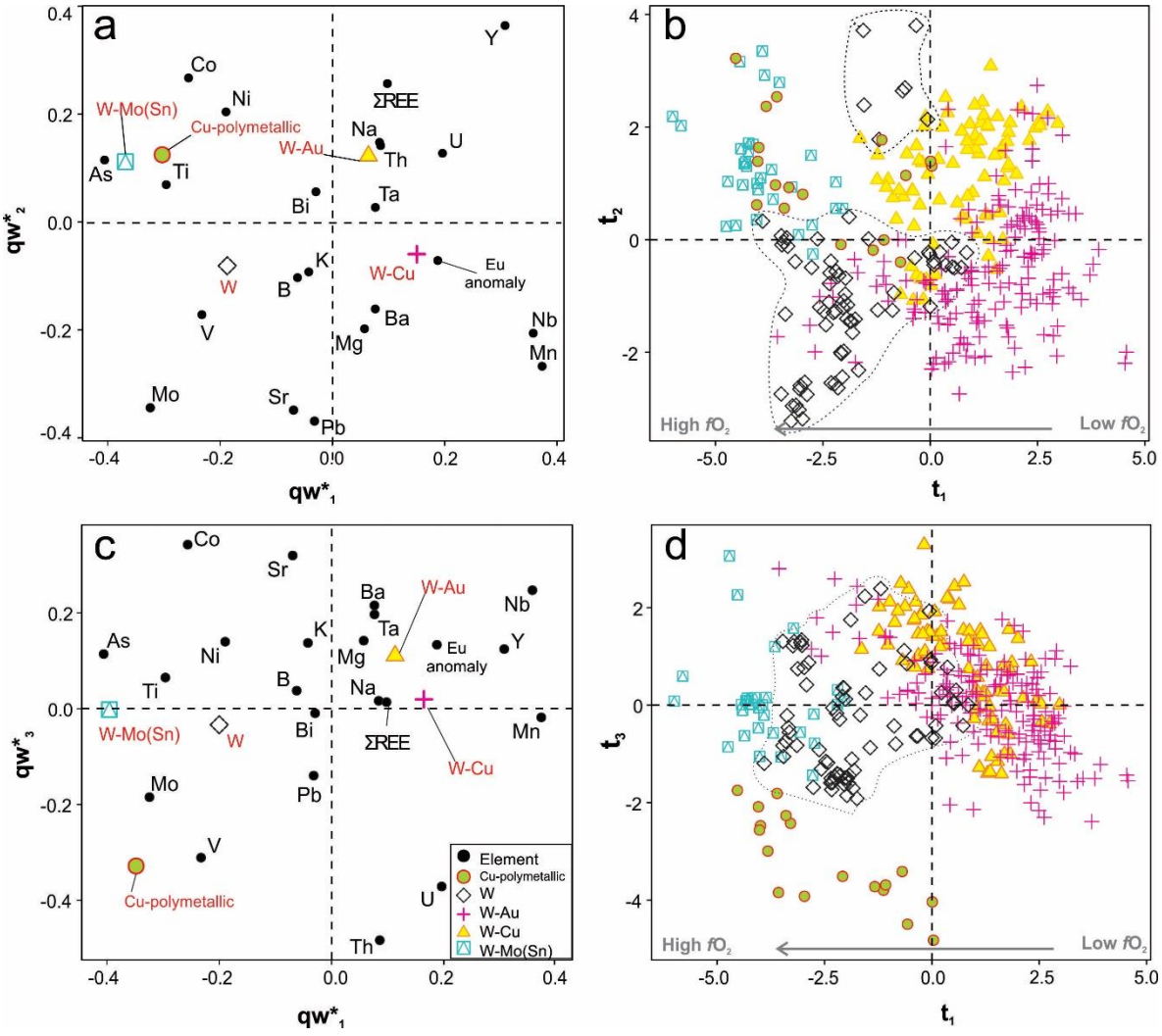

Figure 1.13 Partial least squares discriminant analysis (PLS-DA) of LA-ICP-MS data for scheelite from skarn systems. a. qw*1–qw*2 (first and second loadings) plot showing correlations among elemental variables and metal associations. b. t1–t2 (first and second scores) plot showing the distribution of scheelite analyses in the latent variable space defined by qw*1–qw*2. c. qw*1–qw*3

(first and third loadings) plot showing the correlations among elemental variables and metal association. d. t1–t3 (first and third scores) plot showing the distribution of scheelite analyses in the latent variable space defined by qw*1–qw*3.

1.8 Discussion

1.8.1 Scheelite trace element substitution

Scheelite has a tetragonal structure with two cation sites: a dodecahedral coordination occupied by $[CaO_8]^{14-}$ groups, and a tetrahedral coordination occupied by $[WO_4]^{2-}$ groups. Elements with similar electron configuration and ionic radii to Ca (i.e., Sr, Pb, Mn, ΣREE) and W (i.e., Y, Mo, V, As, Nb, Ta) commonly substitute into the scheelite lattice (Ghaderi et al. 1999; Poulin et al. 2018; Sciuba et al. 2020).

The ΣREE^{3+} and Y^{3+} are incorporated as follow (Nassau 1963; Burt 1989; Ghaderi et al. 1999):

(i) $2Ca^{2+} = (REE,Y)^{3+} + (Na)^{+}$;

(ii) $Ca^{2+} + W^{6+} = (REE,Y)^{3+} + (V,As,Nb,Ta)^{5+}$

(iii) $3Ca^{2+} = 2(REE,Y)^{3+} + Ca_{vac}$, where $Ca_{va}c$ is a vacancy site.

For substitution (i) the sum of monovalent cations must be equal to all trivalent REE and Y, since 1+ cations provide the charge balance in scheelite structure. The MREE (Sm-Dy) are preferentially incorporated in the dodecahedral site relative to LREE (La-Nd) and HREE (Ho-Lu), which characterizes the bell-shaped/MREE-enriched pattern as exemplified by Ghaderi et al. (1999) in scheelite from Archaean gold deposits in Western Australia. For equation (ii) the sum of Nb, Ta, As and V also needs to be similar to that of REE and Y (Dostal et al. 2009).

Among the monovalent cations hosted in scheelite (K and Na), only Na is positively correlated with trivalent REE and Y (Fig. 1.6c and Appendix 1.1A a). Niobium, Ta, As and V also display a positive correlation with REE and Y (Figs. 1.6d-e), suggesting that REE and Y are, at least in part, incorporated through mechanism (ii). However, the sum of Na, Nb, Ta, As and V is lower than the sum of REE and Y (Appendix 1.1A b), which suggests that part of the REE and Y are incorporated by substitution (iii). In this case, as substitution (iii)

does not depend on a coupled substitution to maintain crystal neutrality, the scheelite REE signature is directly controlled by that of the fluid (Ghaderi et al. 1999; Song et al. 2014).

Strontium^{2+} and Pb^{2+} are readily incorporated into Ca^{2+} site as they have similar ionic radii and valence state (Dostal et al. 2009; Sciuba et al. 2020). The Mn^{2+} and Mg^{2+} incorporation is limited because they have smaller cations relative to Ca^{2+} ($^{[VIII]}Mn^{2+}$: 0.96; $^{[VIII]}Mg^{2+}$: 1.03; $^{[VIII]}Ca^{2+}$: 1.12) and prefer monoclinic structure (Ghaderi et al. 1999; Dostal et al. 2009). This may explain their lower contents in scheelite (Fig. 1.5). Although Mn occurs in low content, it is an important element (VIP> 1) for discrimination of reduced and oxidized skarn scheelite (Fig. 1.11). Manganese is widely accepted to be transported as $MnCl_2$ or $MnCl^-$ complexes in crustal fluids (Tian et al 2014; Brugger et al. 2016). Stokes et al. (2019) and Bromiley et al. (2021) showed that the magma fO_2 does not affect the concentration of Mn in magmatic apatite, which is commonly found as Mn^{2+} form. Given that Mn occurs as MnCl2 or MnCl- complexes in crustal fluids (Tian et al. 2014; Brugger et al. 2016) and assuming that magma fO_2 does not affect the Mn redox state, a possible explanation for the higher Mn concentration in reduced skarns relative to oxidized skarn could be magma composition because the majority of reduced skarns are related to peraluminous felsic intrusions that have high Mn concentration (Table 1.1; Fig. 1.12).

Scheelite forms a solid solution with powellite ($CaMoO_4$) through the simple substitution of W^{6+} for Mo^{6+} (Fig. 1.6f). This substitution is strongly favored by high fO_2 in the hydrothermal system, where Mo migrates as Mo^{6+} and thus substitutes for W^{6+} in scheelite (Hsu 1977). Scheelite associated with high fO_2 systems has higher Mo content than that associated with low fO_2 systems (Figs. 1.5, 1.6f and 1.11) as confirmed by our dataset and Xu et al. (2020).

Molybdenum is the main element that causes different textural zonings in scheelite revealed by CL imaging (Figs. 1.4, 1.7-1.8; Appendix 1.2A), and Nb, Th and U are often concentrated in few zones through the scheelite crystal (Fig. 1.7; Appendix 1.2A). Oscillatory zoned scheelite grains commonly occurs during the prograde stage, and less commonly during the retrograde stage (Fig. 1.4). As Mo incorporation in scheelite is mainly controlled by the fO_2 of hydrothermal fluids (Hsu 1977), the oscillatory zoning (Appendix 1.2A; Fig. 1.7) is likely due to fluctuations of the redox conditions. Scheelite crystallized from retrograde fluids is predominantly homogeneous, which suggest more constant hydrothermal fluid fO_2. Retrograde stage scheelite has relatively lower Mo content relative to prograde stage (Figs.

1.7-1.8) due to Mo depletion as a result of earlier deposition of scheelite (Einaudi et al. 1981; Choi et al. 2020; Su et al. 2020).

Arsenic, V, Nb and Ta are incorporated in the scheelite lattice according to (ii) substitution mechanism (Nassau 1963; Burt 1989; Brugger et al. 1998; Ghaderi et al. 1999), as shown by their broad correlation with ΣREE (Fig. 1.6d-e). Similar to Mo, As and V incorporation in scheelite is dominantly controlled by the redox conditions. At high fO_2, As^{5+} and V^{5+} form $H_3AsO_{4(aq)}$ and $H_3VO_{4(aq)}$ complexes (Testemale et al. 2004; James-Smith et al. 2010; Brugger et al. 2016) which have similar ionic radii to W ($^{[IV]}W^{6+}$: 0.42 Å; $^{[IV]}As^{5+}$: 0.335 Å; $^{[IV]}V^{5+}$: 0.355 Å; Shannon 1976). At lower fO_2 As and V (less soluble) are transported in more reduced forms $^{[VI]}As^{3+}$ (0.58 Å) and V ($^{[VI]}V^{4+}$: 0.58 Å; $^{[VI]}V^{3+}$: 0.64 Å; Shannon 1976) as $As(OH)_{3(aq)}$ and VO2+/VOH2+ complexes (Testemale et al. 2004; James-Smith et al. 2010; Brugger et al. 2016), which are less compatible to enter scheelite structure. This may explain their lower concentration in scheelite from reduced skarns (Figs. 1.5 and 1.11).

Unlike As and V, the Nb concentrations are higher in scheelite from reduced relative to oxidized skarns (Figs. 1.5 and 1.11). Higher Nb contents coincide with lower Mo concentrations (Appendix 1.2A; Fig. 1.7). According to Zhao et al. (2018), the presence of Mo in hydrothermal fluid has a negative effect on Nb incorporation into the scheelite structure as $^{[IV]}Nb^{5+}$ (0.48 Å) and $^{[IV]}Mo^{6+}$ (0.41 Å) occupy the same $^{[IV]}W^{6+}$ (0.42 Å; Shannon 1976) site and scheelite-powellite solid solution results from the preferential incorporation of Mo6+ into scheelite at high fO_2. At moderate to low fO_2 conditions, Mo is dissolved in the hydrothermal fluid as both $^{[IV]}Mo^{5+}$ (0.46 Å) and $^{[VI]}Mo^{4+}$ (0.65 Å) states (Hsu 1977; Zhao et al. 2018), which form the coupled substitution:

(iv) $Ca^{2+} + Mo^{6+} = \Sigma REE^{3+} + (1 - x)\, Mo^{5+} + xNb^{5+}$ $(0 \leq x \leq 1)$ (Zhao et al. 2018).

High $Mo^{6+}/(Mo^{5+} + Mo^{4+})$ ratios in hydrothermal fluids inhibit Nb incorporation into scheelite whereas lower $Mo^{6+}/(Mo^{5+} + Mo^{4+})$ ratios favor it. Such correlation is supported by low Mo/Nb ratios in scheelite from reduced skarns (0.06 to 324) relative to higher Mo/Nb ratios in oxidized skarns (from 5 to 40,577; Fig. 1.6b).

Higher U and Th concentrations coincide with darker zones in CL images in both skarn types (Appendix 1.2A; Fig. 1.7). Su et al. (2019) showed similar features with CL images of scheelite from the Dabaoshan porphyry Mo-W deposit, suggesting that U replaces W in scheelite, since U6+ has similar ionic configurations to W^{6+}, and displays a negative

correlation with Mo. Thorium is incorporated into the Ca site because Th has a similar ionic radii ($^{[VIII]}Th^{4+}$: 1.05 Å and $^{[VIII]}Ca^{2+}$: 1.12 Å; Shannon 1976; Sun et al. 2019). Uranium and Mo show weak negative correlations in reduced skarns, and display no correlation in oxidized skarn scheelite (Fig. 1.6h). Such weak correlations suggest that U may not necessarily substitute for W but instead for Ca. Given that U also exist as U^{4+} ($^{[VIII]}U^{4+}$: 1 Å) and is positively correlated to Th (Fig. 1.6i), we suggest that both U and Th may be incorporated together as follows:

(v) $2Ca^{2+} = (U,Th)^{4+} + Ca_{vac}$, where Ca_{vac} is a vacancy site.

This substitution may explain the low concentration of both U and Th in skarn scheelite (Fig. 1.5), given the valence state differences between $(U,Th)^{+4}$ and Ca^{2+}. However, more work is required to better understand U and Th incorporation in scheelite.

Titanium concentration is higher in oxidized relative to reduced skarn scheelite (Fig. 1.5), yet its distribution is not affected by fO_2. In hydrothermal fluids Ti is commonly transported as Ti^{4+} and its solubility increases with increasing fluid salinity, temperature, and pressure (Ayers and Watson 1993; Purtov & KoteVnikova 1993; Ryzhenko et al. 2006). Given that oxidized skarns are formed from higher salinity fluids relative to reduced skarns (Table 1.1), and Ti^{4+} can be incorporated into either W or Ca sites ($^{[IV]}Ti^{4+}$: 0.42 Å versus $^{[IV]}W^{+6}$: 0.42 Å, and $^{[VIII]}Ti^{4+}$: 0.74 Å versus $^{[VIII]}Ca^{2+}$: 1.12 Å; Shannon 1976), the salinity is likely a contributing factor for the higher Ti concentrations in oxidized skarn scheelite (Figs. 1.5 and 1.11).

1.8.2 REE patterns

Negative slope REE patterns are the most common in scheelite from skarn systems (Song et al. 2014; Guo et al. 2016). Li et al. (2019) observed that less fractionated REE patterns (slightly concave to flat) are commonly associated with retrograde stage scheelite. This study confirms these findings, but also shows that the negative slope REE pattern can be divided in two types, steep and shallow negative slope REE patterns, with distinct (La/Sm)CN and (Gd/Lu)CN ratios (Fig. 1.10), with the steep negative slope REE pattern being restricted to oxidized skarn scheelite (Figs. 1.9a and 1.10).

Song et al. (2014) suggested that the steep negative slope REE pattern in scheelite from oxidized skarns at Chizhou (China) is caused by co-precipitation of andradite garnet.

In this case, garnet incorporates preferentially HREE over LREE causing HREE depletion in hydrothermal fluids (Song et al. 2014). Our results show that Fe-rich garnet, associated with steep negative slope REE pattern, has a flat REE pattern with no enrichment in HREE relative to LREE (Fig. 1.9a), which is a typical REE pattern for andradite garnet (Gaspar et al. 2008; Ismail et al. 2014; Xu et al. 2020). For this sample suite, garnet crystallisation cannot explain the REE fractionation in scheelite.

Factors such as fluid composition, redox, and salinity can lead to the fractionation of REE during transport (Haas et al. 1995; Migdisov et al. 2016). In high salinity fluids, LREE are more stable as chloride complexes relative to HREE (Migdisov et al. 2016). Given that prograde oxidized skarn scheelite formed from fluids with higher salinities than those of reduced skarns (up to 60 wt.% NaCl equiv. versus up to 14 wt.% NaCl equiv. for reduced skarns; Table 1.1), such differences of salinity would explain the stronger REE fractionation in oxidized skarn prograde scheelite.

In reduced skarns, the typical grossular-spessartite garnet displays a strong HREE enrichment relative to LREE (Fig. 1.9b) and clinopyroxene has a flat REE pattern from La to Dy, with a slight enrichment from Ho to Lu (Figs. 1.9c-d). In cases where scheelite co-crystallized with garnet (Fig. 1.9b; Appendix 1.4A d-f) scheelite displays a shallow negative slope REE pattern and in cases where it co-crystallizes with clinopyroxene (Figs. 1.9c-d; Appendix 1.4A d-f), the scheelite REE pattern is depleted in Er to Lu. Unlike in oxidized skarn, we suggest that the co-crystallization of grossular-spessartite garnet and clinopyroxene in reduced skarns fractionate HREE in the fluids, yielding scheelite REE patterns slightly depleted from Ho-Lu relative to La-Dy (Figs. 1.9b-d; Appendix 1.4A d-i).

Brugger et al. (2000) showed that scheelite from Mt. Charlotte orogenic gold deposit (Australia) has concave and convex REE patterns, where the convex REE pattern is the result of fractional crystallization of scheelite in a closed system. Because the partition coefficients for MREE (Sm-Dy) between scheelite and the fluid are relatively higher than for LREE and HREE (Brugger et al. 2000), the early scheelite to crystallize has a concave REE pattern, causing depletion of MREE in the fluid resulting in the latest scheelite with a convex REE pattern. Zhang et al. (2018) reported similar findings for scheelite from the vein and disseminated Shimensi W deposit in South China. Given that the convex REE pattern is restricted to scheelite crystallized during the late stages of skarn systems, this pattern probably results from MREE incorporation in early scheelite (Appendix 1.4A and 1.5A).

1.8.3 Eu anomaly

The Eu anomaly is commonly used as a qualitative indicator to track the redox conditions of fluids or melts (Sverjensky 1984; Zhang et al. 1990). A positive Eu anomaly indicates an abundance of Eu^{2+} relative to Eu^{3+} in the fluids, suggesting more reduced conditions, and a negative Eu anomaly indicates abundance of Eu^{3+}, and more oxidized conditions. In the case of scheelite caution is in order in interpreting redox conditions as Eu is incorporated into the Ca site of scheelite, regardless of its oxidation state, Eu^{2+} is more readily incorporated over Eu^{3+} because of its valence and ionic radii similarity to Ca^{2+} (Ghaderi et al. 1999; Brugger et al. 2000, 2008).

Scheelite from reduced and oxidized skarns system displays both positive and negative Eu anomalies (Fig. 1.6h). Strong negative Eu anomalies are limited to oxidized skarn scheelite and strong positive Eu anomalies are limited to reduced skarns, which matches with the redox state of each system (Fig. 1.6h). A broad negative correlation between the Eu anomaly and Mo content suggests that the Eu^{2+}/Eu^{3+} ratio of scheelite increases with decreasing fO_2 (Fig. 1.6h), given that low Mo content is an indicative of low fO_2 (Hsu 1977). The Eu anomaly in scheelite does not seem to be totally controlled by the fO_2, given that negative Eu anomalies are also observed in reduced skarn scheelite. A plausible explanation could be that the Eu anomaly is inherited from the mineralizing fluid extracted from the residual melt of felsic intrusions, which commonly have a negative Eu anomaly due to crystallization of feldspar (Drake and Weill 1975; Baker et al. 2004).

In oxidized skarn scheelite, positive Eu anomalies (from 2 to 3.4) are associated with the highest Mo concentrations (Jiama porphyry-skarn Cu deposit, 12 to 17 wt.% of Mo; Fig. 1.6h). The felsic intrusion related to mineralization at Jiama displays weak negative Eu anomalies (Zheng et al. 2016), so the positive Eu anomalies in Jiama scheelite cannot be explained by high Eu content of mineralizing fluid sourced from this intrusion. Salinity and the nature of the REE ligands can cause changes in the Eu anomaly (Migdisov et al. 2016), since the Eu^{2+} cation is more stable in Cl-rich fluids whereas Eu^{3+} is more easily mobilized by OH^- complexes (Sverjensky 1984; Bau 1991; Haas et al. 1995). The Jiama porphyry-skarn Cu deposit is dominated by Cl-rich saline fluids (<36 wt.% NaCl eq.; Zheng et al. 2016), so Eu^{2+} would be preferentially transported as chloride complexes relative to Eu^{3+}, yielding positive Eu anomalies in scheelite. The positive Eu anomalies can also be related

to local variation of the pH of mineralizing fluids due to fluid-rock interaction (Brugger et al. 2008).

1.9 Use of scheelite chemistry as discriminant of skarn type, source of mineralizing fluids and deposit types

1.9.1 Skarn type and source of the mineralizing fluid

The PLS-DA results show that scheelite composition varies following skarn redox state, intrusion composition and metal association (Figs. 1.11-1.13). Scheelite from oxidized skarns, metaluminous felsic intrusions, and from Cu-polymetallic, W-Mo(Sn), and W deposits have in common high concentrations of Mo, As, and V. Scheelite from reduced skarns, peralunimous felsic intrusions, and W-Au and W-Cu deposits have in common low Mo, As and V, and high Mn, Nb and Ta concentrations (Fig. 1.13). These results suggest that scheelite chemistry is strongly dependent on composition of mineralizing fluids, which are partially controlled by the chemical composition of the felsic intrusion, consequently the chemical variations of scheelite can be used to discriminate skarn redox state, fluids source, and deposit types.

The redox state of skarns depends either on the redox potential of the host rocks or the fO_2 of the source magma (Einaudi et al. 1981; Newberry and Swanson 1986; Chang et al. 2019). The redox potential of the different rocks hosting the investigated scheelite skarn deposits is difficult to estimate. The majority are hosted in limestone and/or carbonaceous-rich (reduced) rocks having a relatively similar redox potential. The fO_2 of magmas controls skarn redox state as reduced skarns are dominantly associated with ilmenite- and titanite-bearing intrusions, and oxidized skarn with magnetite-bearing intrusions (Table 1.1). The control of magmas fO_2 on scheelite composition is supported by the concentration of elements sensitive to the oxidation state of the fluid (e.g., Mo, As, V) that correlates with the oxidation state of magma (Fig. 1.11f).

The metal association is largely controlled by the redox state and fractionation degree of the magma in magmatic-hydrothermal systems (Chang et al. 2019). Intrusion-related Cu-Mo deposits are commonly associated with more oxidized magmas and Sn and some Au deposits are commonly related to more reduced magmas (Ishihara 1977; Belvin and Chappell 1992; Thompson et al. 1999). Tungsten deposits can be related to both redox type magmas. Because scheelite records both fO_2 and the chemical affinity of granitic

magma (Figs. 1.11a-b and 1.12a-b), our results show that scheelite can be used to discriminate different metal association in intrusion-related deposits (Figs. 1.13a-d).

1.9.2 Scheelite from different deposit types

Several discrimination diagrams based on Mo, Sr, and REE concentrations in scheelite have been proposed (Song et al. 2014; Poulin et al. 2018; Sciuba et al. 2020). Song et al. (2014) suggested that the differences in LREE (La-Nd), MREE (Sm-Dy) and HREE (Ho-Lu) concentrations in scheelite may be used to separate skarn-porphyry and Au-W quartz vein deposits. Poulin et al. (2018) and Sciuba et al. (2020) showed that the Sr/Mo ratio versus Eu anomaly discriminate scheelite from metamorphic environments from those from magmatic-hydrothermal settings, although there is a considerable overlap. Sciuba et al. (2020) showed that multivariate statistical methods (PLS-DA) allow better discrimination of scheelite from magmatic-hydrothermal systems from those from orogenic gold deposits.

A PLS-DA of LA-ICP-MS scheelite composition from this study and literature (n = 711 in total) using 18 elements, ΣREE and Eu anomaly, is applied to compare scheelite composition from intrusion related gold, orogenic gold, reduced skarn and oxidized skarn deposits (Fig. 1.14). Other deposit types in our sample suite had insufficient data to be included in this PLS-DA. Figure 1.14a shows that orogenic gold deposits plot at negative qw*1 and qw*2, as result of the Sr, Pb, Na, Ba and Eu anomaly correlation. An intrusion-related gold deposit (Crusader deposit) plots at negative qw*1 and positive qw*2 due to correlated As and V, and oxidized skarn deposits plot at positive qw*1 and qw*2, as it correlates with Ti and Mo (Fig. 1.14a). Reduced skarns deposits plot at positive qw*1 and negative qw*2 due to correlation of Nb and Mn. Overall, orogenic gold deposits are mainly discriminated from intrusion-related gold, oxidized and reduced skarns deposits by qw*1.

Figure 1.14b shows that scheelite from orogenic gold deposits forms a cluster at negative t1 due to high Sr and Pb concentrations, but also scatters from negative and positive t2 because of high Y and As concentrations, respectively (Figs. 1.14a-b). Scheelite from oxidized skarns plots mostly at positive t1 and t2 due to high Mo content, but few analyses have negative t2. Reduced skarn scheelite plots at positive t1 and negative t2 due to high contents or Nb and Mn. Some of the analyses of reduced skarn scheelite plot at positive t1 and overlap with scheelite from oxidized skarns. Scheelite from intrusion-related

gold deposit forms a cluster in negative t1 and positive t2 due to high As and V concentrations.

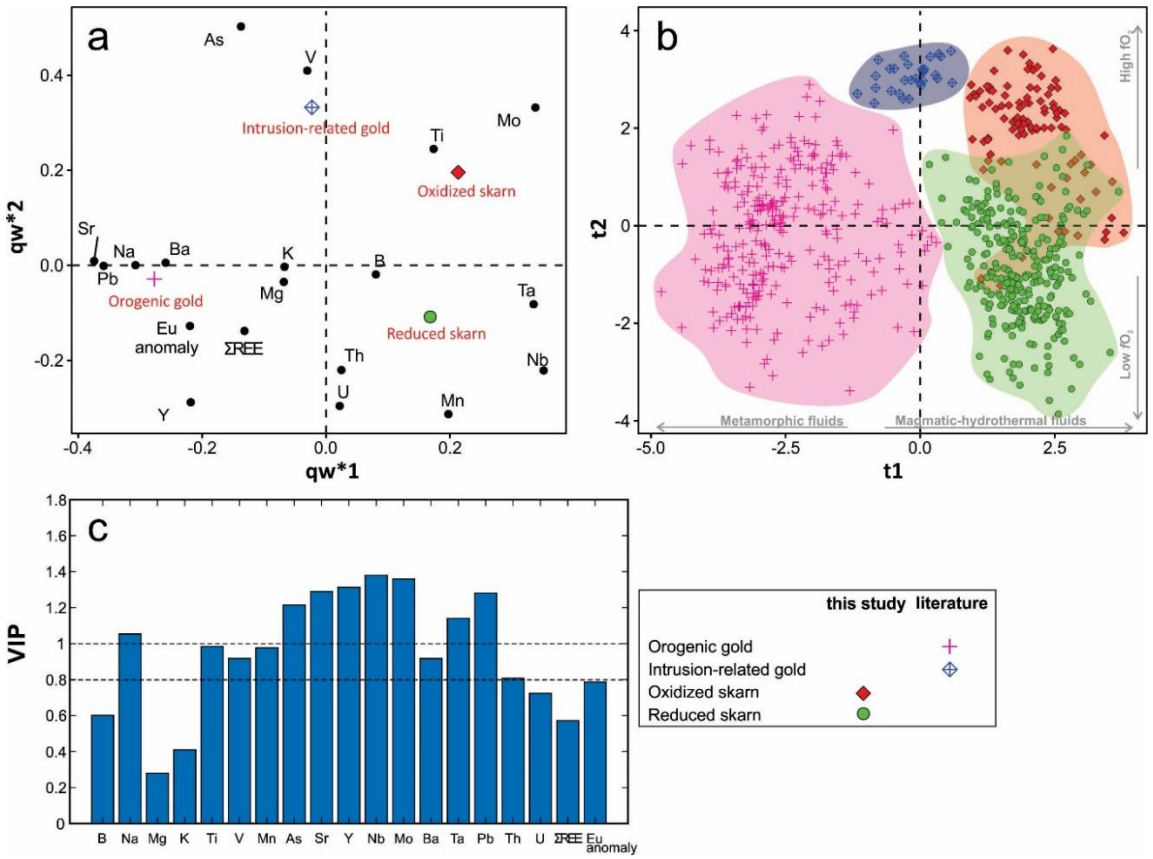

Figure 1.14 Partial least squares discriminant analysis (PLS-DA) of LA-ICP-MS data for scheelite from orogenic gold and intrusion-intrusion related gold deposits (from Sciuba et al. 2020 and De Bronac de Vazelhes et al. 2021; Appendix 1.6B) and skarn systems (this study). a. qw*1–qw*2 (first and second loadings) plot showing the correlations among elemental variables and different deposit types. b. t1–t2 (first and second scores) plot showing the distribution of scheelite analyses in the latent variable space defined by qw*1–qw*2. Note that qw*1 separates fluid origin whereas qw*2 separates oxygen fugacity. c. The Variable Importance on Projection (VIP) plot shows the importance of compositional variables in classification of the model.

The high Sr concentration in scheelite from orogenic gold deposit is likely because of higher content of Sr in hydrothermal fluids derived from dehydration of metasediments and/or mafic-ultramafic volcanic rocks associated with orogenic gold deposits (Kempe et al. 2006; Poulin et al. 2018; Sciuba et al. 2020). Given that Sr is compatible during fractional crystallization, scheelite crystallized from fluids exsolved from felsic magmas has low Sr concentration (<<1000 ppm, Poulin et al. 2018). High Nb, Ta, and Mo contents characterize

scheelite formed from fluids exsolved from felsic magmas (Figs. 1.14a-b) due to the incompatibly of these elements during fractional crystallization and to higher fO_2 of magmatic-hydrothermal, relative to metamorphic fluids. Given that Sr and Pb are negatively correlated with Mo, Nb and Ta, qw*1 allows discrimination of scheelite formed from distinct hydrothermal fluid sources, i.e., metamorphic vs magmatic. High As and V concentrations characterize the intrusion-related deposit (Crusader gold deposit; Sciuba et al. 2020) and oxidized skarns (this study), and Mn characterizes scheelite from more reduced environments. The negative correlation between As-V and Mn in qw*2 discriminates scheelite crystallized from contrasting fO_2 (Figs. 1.14a-b).

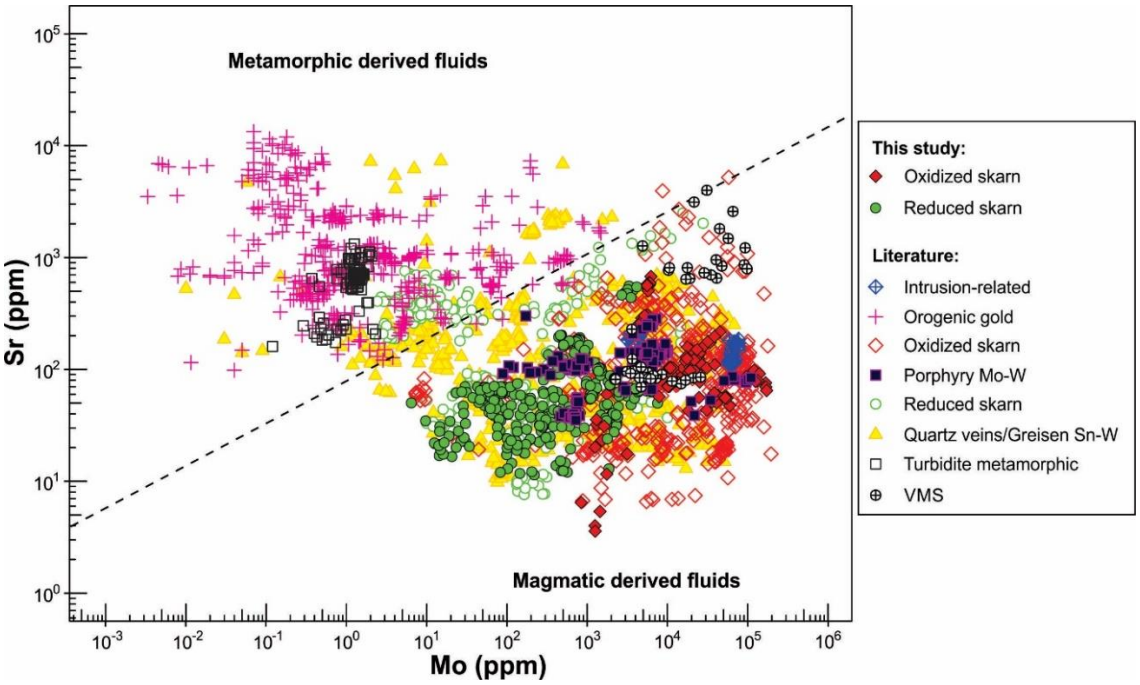

Figure 1.15 Binary plot of Mo versus Sr showing that scheelite formed from metamorphic fluids can be discriminated from that of magmatic derived fluids due to lower Mo and higher Sr concentrations. Data from: Song et al. (2014), Fu et al. (2016), Guo et al. (2016), Poulin (2016), Sun and Chen (2017), Cave et al. (2017), Plotinskaya et al. (2017), Li et al. (2018,2019), Ding et al. (2018), Song et al. (2019), Zang and Gao (2018), Zhao et al. (2018), Liu et al. (2019), Wu et al. (2019), Xu et al. (2019), Yuan et al (2019), Chen et al. (2020), Sciuba et al. (2020), Seo et al. (2020), Su et al. (2020) and de Bronac de Vazelles et al. (2021).

Given that Mo and Sr are the main elements used for discriminating the source of hydrothermal fluids (Fig. 1.14a) and because Mo and Sr are commonly analyzed, we propose that, although there are some overlaps, the relation between these elements can

be used to discriminate scheelite derived from metamorphic and magmatic fluids (Fig. 1.15). Scheelite from magmatic-hydrothermal settings such as intrusion-related gold, oxidized and reduced skarns, Sn-W quartz-veins/greisen, and Mo-W porphyry deposits have high Mo, and low to intermediate Sr concentrations (Fig. 1.15), as does scheelite associated with VMS hydrothermal deposits. Similar to scheelite associated with orogenic gold deposits, metamorphic scheelite from W occurrence in metasediments has low Mo and intermediate to high Sr contents. The Mo and Sr correlation does not discriminate scheelite from different magmatic-hydrothermal deposits, however, reinforcing the advantage of PLS-DA.

1.10 Conclusions

This work shows the efficiency of scheelite chemical composition as a tool for mineral exploration targeting. Texturally, scheelite may display complex zoning patterns and dissolution front textures, which indicate changes in physicochemical conditions of hydrothermal fluids during scheelite crystallisation. Skarn prograde scheelite is zoned, whereas retrograde scheelite is commonly homogeneous in CL and BSE images. The trace element composition of scheelite reflects compositional features inherited from the magmatic-derived fluids and the nature of co-precipitated minerals. Scheelite displays five main REE patterns with positive and negative Eu anomalies: steep and shallow negative slopes, concave, flat to concave and convex shapes. These different REE patterns reflect differences in salinity of hydrothermal fluids, type of co-precipitating minerals, and amount of early scheelite precipitation. Niobium, Ta, Mn, Mo, V and As are the best elements to discriminate scheelite according to redox skarn types, felsic intrusion composition, and metal association. High Mo, As and V contents characterize scheelite from oxidized skarns, metaluminous felsic intrusions, Cu-polymetallic, W-Mo(Sn), and W deposits. High Mn, Nb, and Ta concentrations are typically of scheelite from reduced skarns, peraluminous felsic intrusions, W-Au, and W-Cu deposits. The PLS-DA results show that scheelite from magmatic-hydrothermal settings can be discriminated from those from orogenic gold deposits due to higher Mo, Nb and, Ta and lower Sr abundances. Overall, our results support the use of scheelite as an indicator mineral for exploration targeting.

1.11 Acknowledgments

This research was supported by the Natural Sciences and Engineering Research Council (NSERC) of Canada, Agnico Eagle Mines Ltd., and Ministère de l'Énergie et des

Ressources Naturelles du Québec. We would like to thank Hendrik Falck (Northwest Territories Geological Survey), Nilson Botelho (University of Brasília), Khin Zaw (University of Tasmania), Sergey Soloviev (Int'l GeoSol Consulting Inc.), Lara Lewis (Yukon Geological Survey) and Sun Jia (Chinese Academy of Geological Sciences) for providing some of the samples, and Marc Choquette (Université Laval), Dany Savard and Audrey Lavoie (Université du Quebec à Chicoutimi) for their assistance with EPMA and LA-ICP-MS analyses.

1.12 References

Aitchison J (1986) The Statistical Analysis of Compositional Data. (C a Hall, Ed) London.

Andersson S, Wagner T, Jonsson E, Fusswinkel T, Whitehouse M (2019) Apatite as a tracer of the source, chemistry and evolution of ore-forming fluids: The case of the Olserum-Djupedal REE-phosphate mineralisation, SE Sweden. Geochim Cosmochim Acta 255:163–187

Averill S (2001) The application of heavy indicator mineralogy in mineral exploration with emphasis on base metal indicators in glaciated metamorphic and plutonic terrains. Geological Society, London, Special Publications, 185:69-81

Ayers JC, Watson EB (1993) Rutile Solubility and Mobility in Supercritical Fluids. Contrib Mineral Petrol 114:321–330

Baker T, Achterberg EV, Ryan CG, Lang JR (2004) Composition and evolution of ore fluids in a magmatic-hydrothermal skarn deposit. Geology 32(2):117–120

Baker JM, Wilkinson JJ, Wilkinson CC, Cooke DR, Ireland T (2020) Epidote Trace Element Chemistry as an Exploration Tool in the Collahuasi District, Northern Chile. Econ Geol 115(4): 749–770

Bau M, (1991) Rare earth element mobility during hydrothermal and metamorphic fluid-rock interaction and the significance of the oxidation state of europium. Chem Geol 93:219–230

Boutroy E, Dare S, Beaudoin G, Barnes S-J, Lightfoot P (2014) Magnetite composition in Ni-Cu-PGE deposits worldwide and its application to mineral exploration. J Geochem Explor 145:64-81

Bromiley GD (2021) Do concentrations of Mn, Eu and Ce in apatite reliably record oxygen fugacity in magmas? Lithos 384-385:105900

Brown I, Nesbitt B (1987) Gold-copper-bismuth mineralization in hedenbergitic skarn, Tombstone Mountains, Yukon. Can J Earth Sci 24:2362-2372

Brown VS, Baker T, Stephens JR (2002) Ray Gulch tungsten skarn, Dublin Gulch, central Yukon: Gold-tungsten relationships in intrusion-related ore systems and implications for gold exploration. In: Yukon Exploration and Geology 2001, DS Emond, LH Weston and LL Lewis (eds), Exploration and Geological Services Division, Yukon Region, Indian and Northern Affairs Canada, p 259-268

Brugger J, Giere R, Grobety B, Uspensky E (1998) Scheelite-powellite and paraniite-(Y) from the Fe-Mn deposit at Fianel, Eastern Swiss Alps. Am Mineral 83:1100–1110

Brugger J, Lahaye Y, Costa S, Lambert D, Bateman R (2000) Inhomogeneous distribution of REE in scheelite and dynamics of Archaean hydrothermal systems (Mt Charlotte and Drysdale gold deposits, Western Australia). Contrib Mineral Petrol 139:251–264

Brugger J, Etschmann B, Pownceby M, Liu W, Grundler P, Brewe D (2008) Oxidation state of europium in scheelite: Tracking fluid–rock interaction in gold deposits. Chem Geol 257:26-33

Brugger J, Liu W, Etschmann B, Mei Y, Sherman DM, Testemal D (2016) A review of the coordination chemistry of hydrothermal systems, or do coordination changes make ore deposits? Chem Geol 447:219-253

Burt D (1989) Compositional and phase relations among rare earth elements. Rev Mineral 21:259–307

Chang Z, Shu Q, Meinert L, (2019) Skarn deposits of China. In: Chang, Zhaoshan, and Goldfard, Richard J (ed) Mineral Deposits of China. Special Publications of the Society of Economic Geologists, 22 Society of Economic Geologists, Littleton, CO, USA, pp 189-234

Choi W, Park C, Song, Y (2020) Multistage W-mineralization and magmatic-hydrothermal fluid evolution: Microtextural and geochemical footprints in scheelite from the Weondong W-skarn deposit, South Korea. Ore Geol Rev 116:103219

Cooke DR, Wilkinson JJ, Baker M, Agnew P, Phillips J, Chang Z, Chen H, Wilkinson CC, Inglis S, Hollings P, Zhang L, Gemmell B, White NC, Danyushevsky L, Martin H (2020) Using mineral chemistry to aid exploration: A case study from the Resolution porphyry Cu-Mo deposit, Arizona. Eco Geol 115(4):813-840

Cook N, Ciobanu CL, George L, Zhu Z-Y, Wade B, Ehrig K (2016) Trace Element Analysis of Minerals in Magmatic-Hydrothermal Ores by Laser Ablation Inductively-Coupled Plasma Mass Spectrometry: Approaches and Opportunities. Minerals 6(4):111

Dare SAS, Barnes SJ, Beaudoin G, Méric J, Boutroy E, Potvin-Doucet C (2014) Trace elements in magnetite as petrogenetic indicators. Mineral Deposita 49:785–796

Dare SAS, Barnes SJ, Beaudoin G, (2012) Variation in trace element content of magnetite crystallized from a fractionating sulfide liquid, Sudbury, Canada: Implications for provenance discrimination. Geochim Cosmochim Acta 88:27-50

de Bronac de Vazelhes V, Beaudoin G, McMartin I, Côté-Mantha O, Boulianne-Verschelden N (2021) Assessment of the Amaruq gold deposit signature in glacial sediments using multivariate geochemical data analysis and indicator minerals. J Geochem Explor 228:106800

Dick L, Hodgson C (1982) The MacTung W-Cu(Zn) contact metasomatic and related deposits of the northeastern Canadian Cordillera. Econ Geol 77:845-867

Dostal J, Kontak D, Chatterjee A (2009) Trace element geochemistry of scheelite and rutile from metaturbidite-hosted quartz vein gold deposits, Meguma Terrane, Nova Scotia, Canada: genetic implications. Mineral Petrol 97:95–109

Drake MJ, Weill DF (1975) Partition of Sr, Ba, Ca, Y, Eu2+, Eu3+, and other REE between plagioclase feldspar and magmatic liquid: an experimental study. Geochim Cosmochim Acta 39:689-712

Dupuis C, Beaudoin G (2011) Discriminant diagrams for iron-oxide trace element fingerprinting of mineral deposit types Mineral Deposita 46: 319-335

Duran C, Barnes S-J, Corkerybc J (2016) Trace element distribution in primary sulfides and Fe–Ti oxides from the sulfide-rich pods of the Lac des Iles Pd deposits, Western Ontario, Canada: Constraints on processes controlling the composition of the ore and the use of pentlandite compositions. J Geochem Explor 166:45-63

Duran C, Dubé-Loubert H, Page P, Barnes S-J, Roy M, Savard D, Cave BJ, Arguin J-P, Mansur E (2019) Applications of trace element chemistry of pyrite and chalcopyrite in glacial sediments to mineral exploration targeting: Example from the Churchill Province, northern Quebec, Canada. J Geochem Explor 196:105-130

Einaudi M, Burt D (1982) Introduction, terminology, classification, and composition of skarn deposits. Econ Geol, 77(4):745-754

Einaudi M, Meinert L, Newberry R (1981) Skarn deposits. Econ Geol 75:317-391

Eppinger, R.G., et al., 2011 Exploration case study using indicator minerals in till at the giant Pebble porphyry Cu-Au-Mo deposit, southwest Alaska, USA, in Indicator mineral methods in mineral exploration: Workshop in the 25th International Applied Geochemistry Symposium 2011, 22-26 August 2011 Rovaniemi, Finland p 41-48 https://pubs.er.usgs.gov/publication/70156777

Eriksson L, Johansson E, Kettaneh-Wold N, Wold S (2001) Multi- and megavariate data analysis, principles and applications. UMETRICS, Umea, 425 p

Fu Y, Sun X, Zhou H, Lin H, Jiang L, Yang T (2017) In-situ LA-ICP-MS trace elements analysis of scheelites from the giant Beiya gold-polymetallic deposit in Yunnan Province, Southwest China and its metallogenic implications. Ore Geol Rev 80:828–837

Gaspar M, Knaack C, Meinert L, Moretti, R (2008) REE in skarn systems: A LA-ICP-MS study of garnets. Geochim Cosmochim Acta 72:185–205

George L, Cook N, Ciobanu C, Wade B (2015) Trace and minor elements in galena: A reconnaissance LA-ICP-MS study. Am Mineral 100: 548–569

George L, Cook N, Crowe B, Ciobanu C (2018) Trace elements in hydrothermal chalcopyrite. Mineral Mag 82(1):59–88

Ghaderi M, Palin J, Campbell I, Sylvester P (1999) Rare earth element systematics in scheelite from hydrothermal gold deposits in the Kalgoorlie-Norseman region, Western Australia. Econ Geol 94:423–437

Gregory DD, Cracknell MJ, Large RR, McGoldrick P, Kuhn S, Maslennikov VV, Baker MJ, Fox N, Belousov I, Figueroa MC, Steadman JA, Fabris AJ, Lyons TW (2019) Distinguishing Ore Deposit Type and Barren Sedimentary Pyrite Using Laser Ablation-Inductively Coupled Plasma-Mass Spectrometry Trace Element Data and Statistical Analysis of Large Data Sets. Econ Geol 114 (4): 771–786

Grütter HS, Gurney JJ, Menzies AH, Winter F (2004) An updated classification scheme for mantle-derived garnet, for use by diamond explorers. Lithos 77:841-857 doi: 101016/jlithos200404012

Grzela D, Beaudoin G, Bédard É (2019) Tourmaline, scheelite, and magnetite compositions from orogenic gold deposits and glacial sediments of the Val-d'Or district (Québec, Canada): Applications to mineral exploration. J Geochem Explor 206:106355

Guo Z, Li J, Xu X, Song Z, Dong X, Tian J, Yang Y, She H, Xiang A, Kang Y (2016) Sm/Nd dating and REE composition of scheelite for the Honghuaerji scheelite deposit, Inner Mongolia, Northeast China. Lithos 261:307–321

Gurney JJ, Zweistra P (1995) The interpretation of the major element compositions of mantle minerals in diamond exploration. J Geochem Explor 53:293-309

Haas J, Shock EL, Sassani D (1995) Rare earth elements in hydrothermal systems: estimates of standard partial molal thermodynamic properties of aqueous complexes of the rare earth elements at high. Geochim Cosmochim Acta 59:4329–4350

Han J, Chen H, Hing C, Hollings P, Chu G, Zang L, Sun S (2020) Texture and geochemistry of multi-stage hydrothermal scheelite in the Tongshankou porphyry-skarn Cu-Mo(-W) deposit, eastern China: Implications for ore-forming process and fluid metasomatism. Am Mineral 105:945–954

Hart C (2007) Reduced Intrusion-Related Gold Systems. In W D Goodfellow, Mineral Deposits of Canada: a synthesis of major deposit-types, district metallogeny, the evolution of geological provinces, and exploration methods (pp 95-112) Geological Association of Canada, Mineral Deposits Division

Hsu L (1977) Effects of oxygen and sulfur fugacities on the scheelite-tungstenite and powellite-molybdenite stability relations. Econ Geol 72:664–670

Huang X-W, Boutroy E, Makvandi S, Beaudoin G, Corriveau L, De Toni A (2019) Trace element composition of iron oxides from IOCG and IOA deposits: Relationship to hydrothermal alteration and deposit subtypes. Mineral Deposita 54:525-552

Ishihara S (1981) The magnetite-series and ilmenite-series granitic rocks. Min Geol 27:293-305

Ismail R, Ciobanu CL, Cook NJ, Teale GS, Giles D, Mumm AS, Wade B (2014) Rare earths and other trace elements in minerals from skarn assemblages, Hillside iron oxide–copper–gold deposit, Yorke Peninsula, South Australia. Lithos 184:456-477

James-Smith J, Cauzid J, Testemale D, Liu W, Hazemann J, Proux O, Etschmann B, Philippot P, Banks D, Williams P, Brugger J, (2010) Arsenic speciation in fluid inclusions using micro-beam X-ray absorption spectroscopy. Am Mineral 95(7):921–932

Jochum KP, Nohl U, Herwig K, Lammel E, Stoll B Hofmann AW (2005) GeoReM: a new geochemical database for reference materials and isotopic standards. Geostand Geoanal Res 29:333-338

Kelley,K.D. et al. 2011 Porphyry Cu indicator minerals in till as an exploration tool: example from the giant Pebble porphyry Cu-Au-Mo deposit, Alaska, USA, Geochemistry: Exploration, Environment, Analysis, 11(4):321 http://dx.doi.org/10.1144/1467-7873/10-IM-041

Kempe U, Belyatsky B, Krymsky R, Kremenetsky A, PA I (2001) Sm-Nd and Sr isotope systematics of scheelite from the giant Au(-W) deposit Muruntau (Uzbekistan): implications for the age and sources of Au mineralization. Mineral Deposita 36:379–392

Kwak T, Tan T (1981) The geochemistry of zoning in the skarn minerals at the King Island Dolphin mine. Econ Geol 76:468–497

Li J, Li X, Xiao R (2019) Multiple-stage tungsten mineralization in the Silurian Jiepai W skarn deposit, South China: Insights from cathodoluminescence images, trace elements, and fluid inclusions of scheelite. J Asian Earth Sci 181:103898

Liu H, Beaudoin G (2021) Geochemical signatures in native gold derived from Au-bearing ore deposits. Ore Geol Rev 132:104066

Liu J, Li W, Zhu X, Li C, Zhou Q, Yang F (2020) Origin and evolution of ore-forming fluids of the Larong W-(Mo) deposit, eastern Tibet: Constraints from fluid inclusions, H-O isotopes, and scheelite geochemistry. Ore Geol Rev 124:103620

Lu H-Z, Liu Y, Wang C, Xu Y, Li H (2003) Mineralization and Fluid Inclusion Study of the Shizhuyuan W-Sn-Bi-Mo-F Skarn Deposit, Hunan Province, China. Econ Geol 98:955–974

Mair J, Goldfarb R, Johnson C, Hart C, Marsh E (2006) Geochemical constraints on the genesis of the Scheelite Dome intrusion-related gold deposit, Tombstone gold belt, Yukon, Canada. Econ Geol 101:523−553

Makvandi S, Ghasemzadeh-Barvarz M, Beaudion G, Grunsky E, McClenaghan M, Duchesne C (2016a) Principal Component Analysis of magnetite composition from volcanogenic massive sulfide deposits: Case studies from the Izok Lake (Nunavut, Canada) and Halfmile Lake (New Brunswick, Canada) deposits. Ore Geol Rev 72:60-85

Makvandi S, Ghasemzadeh-Barvarz M, Beaudion G, Grunsky EC, McClenaghan MB, Duchesne C (2016b) Partial Least Squares Discriminant Analysis of trace element compositions of magnetite from various VMS deposit subtypes: Application to mineral exploration. Ore Geol Rev 78:388-408

Makvandi S, Huang X, Beaudoin G, Quirt D, Ledru P, Fayek M (2020) Trace element signatures in hematite and goethite associated with the Kiggavik-Andrew Lake structural trend U deposits (Nuvanut, Canada). Mineral Deposita 56:509-535

Manéglia N, Beaudoin G, Simard M (2017) Indicator minerals of the Meliadine orogenic gold deposits, Nunavut (Canada), and application to till surveys. Geochem Explor Environ Anal 18:241-251

Mansur ET, Barnes S-J, Duran C (2021) An overview of chalcophile element contents of pyrrhotite, pentlandite, chalcopyrite, and pyrite from magmatic Ni-Cu-PGE sulfide deposits. Mineral Deposita 56:179-204

Mao M, Rukhlov A, Rowins S, Spence J, Coogan L (2016) Apatite Trace Element Compositions: A Robust New Tool for Mineral Exploration. Econ Geol 111:1187-1222

Mathieson G, Clark A (1984) The Cantung E Zone Scheelite Skarn Orebody, Tungsten Northwest Territories: A Revised Genetic Model. Econ Geol 79:883-901

McClenaghan M (2005) Indicator mineral methods in mineral exploration. Geochem Explor Environ Anal 5(3):233-245

McClenaghan M, Parkhill M, Pronk A, Seaman A, McCurdy M, Leybourne M (2017) Indicator mineral and geochemical signatures associated with the Sisson W-Mo deposit, New Brunswick, Canada. Geochem Explor Environ Anal 17:297–313

Meinert L (1997) Application of Skarn Deposit Zonation Models to Mineral Exploration. Explor Mining Geol 6(2):185-208

Meinert L, Dipple G, Nicolescu S (2005) World skarn deposits. In J Hedenquist, J Thompson, R Goldfarb, and J Richards. Econ Geol 100th Anniversary Volume, pp 299–336, Littleton, CO: Society of Economic Geologists

Migdisov A, Williams-Jones AE, Brugger J, Caporuscio F (2016) Hydrothermal transport, deposition, and fractionation of REE: experimental data and thermodynamic calculations. Chem Geol 439, 13–42

McDonough WF, Sun SS (1995) The composition of the earth. Chem Geol 120:223–253

Nassau K (1963) Calcium tungstate--IV: The theory of coupled substitution. J of Physics and Chemistry of Solids, 24:1511-151

Newberry R, (1982) Tungsten-bearing skarns of the Sierra Nevada I The Pine Creek Mine, California. Econ Geol 77:823-844

Newberry R (1983) The formation of subcalcic garnet in scheelite-bearing skarns. Can Mineral 21:529-544

Newberry R, Swanson S (1986) Scheelite Skarn Granitoids: An evaluation of the roles of magmatic source and process. Ore Geol Rev 1:57-81

O'Brien J, Spry P, Teale G, Jackson S, Koenig A (2015) Gahnite composition as a means to fingerprint metamorphosed massive sulfide and non-sulfide zinc deposits. J Geochem Explor 159:48–61

Palarea-Albaladejo J, and Martín-Fernández J A (2013) Values below detection limit in compositional chemical data, Anal. Chim. Acta 764:32–43

Palarea-Albaladejo J, and Martín-Fernández J (2015) zCompositions — R package for multivariate imputation of left-censored data under a compositional approach. Chemometr Intell Lab Syst 143:85–96

Pan X, Hou Z, Zhao M, Li Y, Ouyang, Y, Wei J, Yang Y (2020) Fluid inclusion and stable isotope constraints on the genesis of the worldclass Zhuxi W(Cu) skarn deposit in South China. J Asian Earth Sci 190:104192

Paton, C, Hellstrom, J, Paul, B, Woodhead, J, and Hergt, J., 2011, Iolite: Freeware for the visualization and processing of mass spectrometric data: Journal of Analytical Atomic Spectrometry, v. 26, p. 2508-2518. doi:10.1039/c1ja10172b

Poitrenaud T, Poujoi M, Augier R, Marcoux E (2019) The polyphase evolution of a late Variscan W/Au deposit (Salau, French Pyrenees): insights from REE and U/Pb LA-ICP-MS analyses. Mineral Deposita 55:1127–1147

Plotinskayaa O, Baksheevb I, Minervina EA (2018) REE Distribution in Scheelite from the Yubileinoe Porphyry Gold Deposit, South Urals: Evidence from LA-ICP-MS Data. Geol Ore Depos 60(4):355–364

Porter JP (2013) Source, emplacement and evolution of the Morgan Creel Pluton, Sierra Nevada Batholith, California, USA PhD thesis, Salt Lake City, USA, The University of Utah, 201 p.

Porter J, McNaughtona, N, Evansa N, McDonald J (2020) Rutile as a pathfinder for metals exploration. Ore Geol Rev 120:03406

Poulin R, Kontak D, McDonald A, McClenaghan, M (2018) Assessing scheelite as an ore-deposit discriminator using its trace element and REE chemistry. Can Mineral 56:265–302

Purtov VK, KoteVnikova AL (1993) Solubility of Titanium In Chloride And Fluoride Hydrothermal Solutions. Intern Geol Rev 35:3279-287

R Core Team (2021). R: A language and environment for statistical computing. R Foundation for Statistical Computing, Vienna, Austria. URL https://www.R-project.org/.

Raimbault L, Baumer A, Dubru M, Benkerrou C, Croze V, Zahm A (1993) REE fractionation between scheelite and apatite in hydrothermal conditions. Am Mineral 78:1275–1285

Roberts S, Palmer M, Waller L (2006) Sm-Nd and REE characteristics of tourmaline and scheelite from the Bjorkdal gold deposit, northern Sweden: Evidence of an intrusion-related gold deposit? Econ Geol 101(7):1415-1425

Rottier B, Casanova V (2020) Trace element composition of quartz from porphyry systems: a tracer of the mineralizing fluid evolution. Miner Deposita 55:843-862

Sciuba M, Beaudoin G, Grzela D, Makvandi S (2020) Trace element composition of scheelite in orogenic gold deposits. Miner Deposita 55:1149-1172

Shannon RD (1976) Revised effective ionic radii and systematic studies of interatomic distances in halides and chalcogenides. Acta Cryst A 32:751–767

Seo J, Yoo B, Yang Y (2020) Scheelite geochemistry of the Sangdong W-Mo deposit and W prospects in the southern Taebaeksan metallogenic region. Korea Geosci J 24:701-721

Shu Q, Chang Z, Lai Y, Hu X, Wu H, Zhang Y, Wang P, Zhai D, Zhang C (2019) Zircon trace elements and magma fertility: insights from porphyry (-skarn) Mo deposits in NE China. Miner Deposita 54:645–656

Singoyi B, Zaw K (2001) A petrological and fluid inclusion study of magnetite–scheelite skarn mineralization at Kara, Northwestern Tasmania: implications for ore genesis. Chem Geol 173:239–253

Soloviev S (2015) Geology, mineralization, and fluid inclusion characteristics of the Kumbel oxidized W-Cu-Mo skarn and Au-W stockwork deposit, Tien-Shan, Kyrgyzstan. Mineral Deposita 50:187–220

Soloviev S, Kryazhev SG, Dvurechenskaya SS (2015) Geology, mineralization, and fluid inclusion characteristics of the Lermontovskoe reduced-type tungsten (±Cu, Au, Bi) skarn deposit, Sikhote-Alin, Russia. Ore Geol Rev 89:15-39

Soloviev S, Kryazhev S, Dvurechenskaya S (2017) Geology, mineralization, stable isotope, and fluid inclusion characteristics of the Vostok-2 reduced W-Cu skarn and Au-W-Bi-As stockwork deposit, Sikhote-Alin, Russia. Ore Geol Rev 86:338–365

Song G, Qin K, Li G, Evans N, Chen L (2014) Scheelite elemental and isotopic signatures: Implications for the genesis of skarn-type W-Mo deposits in the Chizhou area, Anhui Province Eastern China. Am Mineral 99:303-317

Song G, Cook NJ, Li G, Qin K, Ciobanu CL, Yang Y, Xu Y (2019) Scheelite geochemistry in porphyry-skarn W-Mo systems: A case study from the Gaojiabang Deposit, East China. Ore Geol Rev 113:103084

Souza Neto JA, Legrand JM, Volfinger M, Pascal M-L, Sonnet P (2008) W–Au skarns in the Neo-Proterozoic Seridó Mobile Belt, Borborema Province in northeastern Brazil: an overview with emphasis on the Bonfim deposit. Miner Deposita 43:185-205

Su Q, Mao J, Sun J, Zhao L, Xu S (2020) Geochemistry and Origin of Scheelites from the Xiaoyao Tungsten Skarn Deposit in the Jiangnan Tungsten Belt, SE China. Minerals 10:271

Su Q, Mao J, Wu S, Zhang Z, Xu S (2018) Geochronology and geochemistry of the granitoids and re-forming age in the Xiaoyao tungsten polymetallic skarn deposit in the Jiangnan Massif tungsten belt China: Implications for their petrogenesis, geodynamic setting, and mineralization. Lithos 29:365–381

Sun K, Chen B (2017) Trace elements and Sr-Nd isotopes of scheelite: Implications for the W-Cu-Mo polymetallic mineralization of the Shimensi Deposit, south China. Am Mineral 102:1114–1128

Sun K, Chen B, Deng J (2019) Ore genesis of the Zhuxi supergiant W-Cu skarn polymetallic deposit, South China: Evidence from scheelite geochemistry. Ore Geol Rev 107:14-29

Sverjensky D (1984) Europium redox equilibria in aqueous solution. Earth Planet Sci Lett 67:70–78

Sylvester PJ, Jackson SE (2016) A brief history of laser ablation inductively coupled plasma mass spectrometry (LA–ICP–MS). Elements 12(5):307-310

Testemale D, Hazemann JL, Pokrovski GS, Joly Y, Roux J, Argoud R, Geaymond O (2004) Structural and electronic evolution of the As(OH)3 molecule in high temperature aqueous solutions: an X-ray absorption investigation. J Chem Phys 121(18):8973–8982

Thompson J, Sillitoe R, Baker T, Lang J, Mortensen J (1999) Intrusion-related gold deposits associated with tungsten-tin provinces. Miner Deposita 34(4):323-334

Tian Y, Etschmann B, Mei Y, Grundler PV, Testemale D, Hazemann J-L, Elliott P, Ngothai Y, Brugger J (2014) Speciation and thermodynamic properties of manganese(II) chloride complexes in hydrothermal fluids: in situ XAS study. Geochim Cosmochim Acta 129:77–95

Toverud O (1984) Dispersal of tungsten in glacial drift and humus in Bergslagen, southern central Sweden. J Geochem Explor 21:261–272

Uspensky E, Brugger, J, Graeser, S (1998) REE geochemistry systematics of scheelite from the Alps using luminescence spectroscopy: from global regularities to facies control. Schweiz Mineral Petrogr Mitt 78:33–56

Wilkinson J, Chang Z, Cooke D, Baker M, Wilkinson C, Inglis S, Gemmell J (2015) The chlorite proximitor: A new tool for detecting porphyry ore deposits. J Geochem Explor 152:10–26

Wilkinson J, Baker M, Cooke D, Wilkinson C (2020) Exploration targeting in porphyry Cu systems using propylitic mineral chemistry. Econ Geol 115:771–791

Wintzer NE (2019) Geology, Geochronology, and Geochemistry of the Stibnite-Yellow Pine Gold-Antimony-Tungsten Mining Area, Idaho. PhD thesis, Pullman, USA Washington State University 297p

Wu S, Mao J, Ireland T, Zaho Z, Yao F, Yang Y, Sun W (2019) Comparative geochemical study of scheelite from the Shizhuyuan and Xianglushan tungsten skarn deposits, South China: Implications for scheelite mineralization. Ore Geol Rev 109:448–464

Xu J, Ciobanu C, Cook NC, Slattery A (2020) Crystals from the Powellite-Scheelite Series at the Nanoscale: A Case Study from the Zhibula Cu Skarn, Gangdese Belt, Tibet. Minerals 9:340

Yuan L, Chi G, Wang M, Li Z, Xu D, Deng T, Geng J, Hu M, Zhang, L (2019) Characteristics of REEs and trace elements in scheelite from the Zhuxi W deposit, South China: Implications for the ore-forming conditions and processes. Ore Geol Rev 109:585–597

Zang Z, Xie G, Mao J, Liu W, Olin P, Li, W (2019) Sm-Nd Dating and In-Situ LA-ICP-MS Trace Element Analyses of Scheelite from the Longshan Sb-Au Deposit, Xiangzhong Metallogenic Province, South China. Minerals 9:87

Zaw K, Singoyi B (2000) Formation of Magnetite-Scheelite Skarn Mineralization at Kara, Northwestern Tasmania: Evidence from Mineral Chemistry and Stable Isotopes. Econ Geol 95:1215–1230

Zhang Q, Zhang RQ, Gao JF, Lu JJ, Wu JW (2018) In-situ LA-ICP-MS trace element analyses of scheelite and wolframite: Constraints on the genesis of veinlet-disseminated and vein-type tungsten deposits, South China. Ore Geol Rev 99:166-179

Zhao W, Zhou M-F, Williams-Jones A, Zhao Z (2018) Constraints on the uptake of REE by scheelite in the Baoshan tungsten skarn deposit, South China. Chem Geol 477:123–136

Zheng W, Tang J, Zhong K, Ying L, Leng Q, Ding S, Lin B (2016) Geology of the Jiama porphyry copper–polymetallic system, Lhasa Region, China. Ore Geol Rev 74:151–16

Chapter 2 - Trace element signatures of scheelite associated with various deposit types: a tool for mineral targeting

Ana Carolina R. Miranda[1,2], Georges Beaudoin[1,2], Bertrand Rottier[1,2], Jan Pašava[3], Petr Bohdálek[3] and Jan Malec[3]

[1]Département de Géologie et Génie Géologique, Université Laval, Québec, Canada

[2]Centre de recherche sur la géologie et l'ingénierie de ressources minérales (E4m), Université Laval, Québec, Canada

[3]Czech Geological Survey, Geologická 6, CZ-15200 Praha 5, Czech Republic

(Submitted to the Journal of Geochemical and Exploration, Feb 2023)

2.1 Résumé

La scheelite est un minéral fréquent dans plusieurs contextes géologiques et sa composition en éléments traces fournit des informations précieuses sur la source et la composition des fluides hydrothermaux. La scheelite provenant de 22 gisements magmatiques-hydrothermaux et de 2 gisements orogéniques d'Au (Hangar Flats et Corcoesto) a été analysée par EPMA et LA-ICP-MS. La scheelite magmatique-hydrothermale, ainsi que les données de la littérature sont étudiées à l'aide de l'analyse discriminante des moindres carrés partiels (PLS-DA) et de la Random Forest (RF), afin d'évaluer l'utilisation de la scheelite comme minéral indicateur robuste pour le ciblage des gisements contenant du W. Les images de cathodoluminescence montrent que la scheelite est texturalement homogène dans les systèmes aurifères liés à des intrusions réduites (RIRGS) et varie d'homogène à hétérogène dans d'autres gisements magmatiques-hydrothermaux et d'or orogéniques. La scheelite présente six modèles normalisés par la chondrite pour les ETR, qui sont fonction de la source et de la composition (principalement la salinité) des fluides minéralisateurs et du partage avec les minéraux cogénétiques (p. ex., grenat, clinopyroxène). Le PLS-DA met en évidence que la composition en éléments traces de la scheelite provenant de gisements magmatiques-hydrothermaux varie selon les différents types de gisements (skarns oxydés et réduits, porphyre W-Mo, RIRGS, quartz-vein/greisen Sn-W), et que cette variation de composition reflète principalement la différence de fO_2 et de composition des fluides minéralisateurs exsolus des intrusions liées au minerai. De plus, la scheelite des gisements

magmatiques-hydrothermaux est chimiquement distincte de celle des milieux orogéniques, comme le montrent leurs teneurs plus élevées en Mo, Nb et Mn, et plus faibles en Sr, ainsi que leurs anomalies Eu négatives prédominantes. Dans les contextes orogéniques, la scheelite métamorphique peut être distinguée de celle des gisements orogéniques d'or par ses teneurs plus faibles en Pb, As et ETR et ses rapports LREE/HREE, qui sont liés à la composition de la roche hôte locale et au grade métamorphique. En utilisant les concentrations de Na, Mg, Mn, As, Sr, Y, Nb, Mo, Pb, ΣREE et l'anomalie Eu comme prédicteurs, le modèle RF donne une précision de prédiction globale de 97% pour les données de test en fonction des types de gisement (89,2% pour RIRGS, 100% pour le porphyre W-Mo, 97,8% pour le quartz-veine/greisen Sn-W, 96,9% pour le skarn oxydé, 98,1% pour le skarn réduit et 99,3% pour les gisements d'Au orogéniques). L'application du classificateur RF à la composition de la scheelite provenant de gisements orogéniques d'Au et de gisements de W de type skarn et greisen de la littérature donne une prédiction globale de ~79% (91% pour le skarn oxydé, 71,4% pour le quartz-veine/greisen Sn-W et 74,2% pour les gisements orogéniques d'Au) montrant que la scheelite est un minéral indicateur efficace pour le ciblage des gisements d'Au et de W. La scheelite métamorphique est prédite principalement comme la scheelite d'or orogénique (83%), reflétant la genèse des fluides métamorphiques et un cadre géologique similaire, suggérant que le classificateur RF peut également être utilisé pour prédire les sources de fluides.

Mots clés: scheelite, élément trace, minéral indicateur, PLS-DA, forêt aléatoire.

2.2 Abstract

Scheelite is a widespread mineral in several geological settings and its trace element composition provides valuable information about the source and composition of the hydrothermal fluids. In this study, scheelite from 22 magmatic-hydrothermal deposits and 2 orogenic Au deposits (Hangar Flats and Corcoesto) were analyzed by EPMA and LA-ICP-MS. Magmatic-hydrothermal scheelite, together with literature data are investigated using partial least square-discriminant analysis (PLS-DA) and Random Forest (RF) classifier, to evaluate the use of scheelite as a robust indicator mineral for W-bearing deposit targeting. Cathodoluminescence images show that scheelite is texturally homogeneous in reduced intrusion-related gold systems (RIRGS) and varies from homogeneous to heterogeneous in other magmatic-hydrothermal and orogenic Au deposits. Scheelite displays six REE chondrite-normalized patterns, which are a function of the source and composition (mainly

salinity) of the mineralizing fluids and partitioning with co-genetic minerals (e.g., garnet, clinopyroxene). The PLS-DA highlights that scheelite trace element composition from magmatic-hydrothermal deposits varies following different deposit types (e.g., oxidized and reduced skarns, porphyry W-Mo, RIRGS, quartz-vein/greisen Sn-W), and that such compositional variation reflects mainly the difference of fO_2 and composition of mineralizing fluids exsolved from the ore-related intrusions. Additionally, scheelite from magmatic-hydrothermal deposits are chemically distinct to those formed dominantly by metamorphic fluids in orogenic settings as shown by their higher Mo, Nb and Mn, and lower Sr contents and predominantly negative Eu anomalies. Metamorphic scheelite can be discriminated from that of orogenic Au deposits by their lower Pb, As and REE contents and LREE/HREE ratios, which are related to local host rock composition and metamorphic grade. Using Na, Mg, Mn, As, Sr, Y, Nb, Mo, Pb, ΣREE concentrations and Eu anomaly as predictors, the RF model yields an overall prediction accuracy of 97% for test data as function of deposit types (89.2% for RIRGS, 100% for porphyry W-Mo, 97.8% for quartz-vein/greisen Sn-W, 96.9% for oxidized skarn, 98.1% for reduced skarn and 99.3% for orogenic Au deposits). Application of RF classifier to scheelite composition from orogenic Au and skarn- and greisen-type W deposits from literature yields an overall prediction of ~79% (91% for oxidized skarn, 71.4% for quartz-vein/greisen Sn-W and 74.2% for orogenic Au deposits) showing that scheelite is an efficient indicator mineral for Au and W deposits targeting. Metamorphic scheelite is predicted mostly as orogenic Au scheelite (83%), reflecting the genesis of metamorphic fluids and similar geological setting, suggesting that RF classifier can be also used to predict the fluid sources.

Keywords: scheelite, trace element, indicator mineral, PLS-DA, random forest

2.3 Introduction

Advances in micro analytical techniques have allowed a better chemical characterization of minerals and consequently, a better understanding of ore-forming processes (Gaspar et al. 2008; Dare et al. 2012; Andersson et al. 2019; Mansur et al. 2021). Such approach has been applied in several fields of economic geology to assess the fertility of igneous rocks to form mineral deposits (e.g., zircon, Ballard et al. 2002 and Wade et al. 2022; epidote, Cooke et al. 2014), vector towards mineralized systems (Cooke et al. 2014; Wilkinson et al. 2015; Rottier and Casanova 2020), discriminate and indicate distinct types of mineral deposits (Belousova et al. 2002; Dupuis and Beaudoin 2011; Boutroy et al. 2014;

Dare et al. 2012, 2014; George et al., 2015, 2018; Pašava et al. 2016; Huang et al. 2019; Mansur et al. 2020; Barnes et al. 2022; Mansur et al. 2023) and to prospect/target mineral deposits in regional exploration surveys (Duran et al. 2019; de Bronac de Vazelhes et al. 2021). Others studies have shown that multivariate statistical and machine learning methods combined with mineral chemistry are successful not only in classification and prediction of deposit types (O'Brien et al. 2015; Mao et al. 2016; Gregory et al. 2019; Makavandi et al. 2019; Porter et al. 2020; Sciuba et al. 2020,2021; Liu et al. 2021; Zhao et al. 2021; Bédard et al. 2022; Caraballo et al. 2022; Ghosh and Upadhyay 2022; Miranda et al. 2022; Nathwani et al. 2022; Sun et al. 2022) but also to predict the fertility for ore deposits (O'Brien et al. 2015).

Scheelite is commonly found in skarn, quartz-vein/greisen Sn-W, porphyry W-Mo, reduced intrusion related gold systems (RIRGS) and orogenic Au deposits, and in metasedimentary rocks (Štemprok and Mašková 1992; Brugger et al. 2000; Uspensky et al. 1998; Hart 2007; Song et al. 2014; Guo et al. 2016; Cave et al. 2017; Poulin et al. 2018; Sciuba et al. 2020; Miranda et al. 2022; Wintzer et al. 2022). It hosts a wide range of minor and trace elements (Mo, Sr, As, Na, REE, HFSE), which abundances are controlled by host rock composition, fluid physico-chemical conditions (i.e., fO2, pH, P, T, salinity) and partitioning with co-genetic minerals (Hsu 1977; Gadheri et al. 1999; Song et al 2014; Cave et al. 2017; Zhao et al. 2018; Sciuba et al. 2020; Miranda et al. 2022). Because these factors are strongly dependent on the geological setting, scheelite trace element composition has been used to constrain the source of hydrothermal fluids and the genesis of diverse mineral deposits (Kent et al. 1995; Darbyshire et al. 1996; Voicu et al. 2000; Kempe et al. 2001; Song et al. 2014; Scanlan et al. 2018; Zhao et al. 2018; Palmer et al. 2022; Elongo et al. 2022; Wintzer et al. 2022). In addition, its physical properties (resistant mineral, high density and easily identified) are favorable to recover it from stream and glacial sediments, making it a powerful indicator mineral (McClenaghan et al. 2017; Maneglia et al. 2018; Grzela et al. 2019; Sciuba et al. 2020; de Bronac de Vazelhes et al. 2021).

The chemical composition of scheelite in orogenic Au and skarns deposits has been documented in detail by few studies (Gadheri et al. 1999; Song et al. 2014; Poulin et al. 2018; Xu et al. 2019; Sciuba et al. 2020; Miranda et al. 2022). These contributions have shown the potential of scheelite chemistry as a useful exploration tool to discriminate, for instance, orogenic Au and skarn-related deposits. However, the chemical characterization of scheelite in several other ore deposit types such as RIRGS, quartz-vein/greisen Sn-W

and porphyry W-Mo remains incomplete limiting its application as an efficient indicator mineral of the source of detrital scheelite.

This contribution aims to use the minor and trace elements composition of scheelite and assess its efficiency to predict deposit types using detrital scheelite in overburden sediments. Scheelite chemical composition from RIRGS, porphyry W-Mo, quartz-veins/greisen Sn-W and skarn-type deposits are combined with literature data to show that trace element in scheelite varies between different deposit types and settings. These data are investigated by partial least squares-discriminant analysis (PLS-DA) and random forest (RF) classifier to discriminate mineral deposit types and other geological settings. The PLS-DA and RF classifier models are tested with scheelite chemistry data from two orogenic Au deposits (Hangar Flats and Corcoesto) and other deposit data from literature to assess their effectiveness. The results show that compositional variations of scheelite chemistry can be used to discriminate different deposit types, enabling its application in mineral exploration.

2.4 Geological features of scheelite-bearing samples

Scheelite from polymetallic skarn, quartz-vein/greisen Sn-W, porphyry W-Mo, RIRGS, and orogenic Au deposits, which cover the main scheelite-bearing ore deposits, were analysed (Fig. 2.1 and Table 2.1). Scheelite skarn samples are classified as oxidized and reduced skarns based on mineral assemblage and scheelite composition following Miranda et al. (2022). Reduced skarns are characterized predominantly by clinopyroxene, amphibole (Fig. 2.2a-b) and sulfides with minor garnet, whereas oxidized skarns consist mainly of garnet, clinopyroxene, amphibole and oxides (Table 2.1). Reduced and oxidized skarn scheelite samples comprise mainly exoskarns surrounding intermediate to felsic intrusions (Table 2.1). Skarn host rocks vary from dolostone/limestone to metasedimentary rocks and gneiss (Table 2.1). Five of the localities contain major W, Fe and Cu skarns deposits (Obří důl, Traversella, Kanbauk, Invincible Mine and Nui Phao), whereas six other investigated localities represent small deposits/showings. Nui Phao is the only deposit where scheelite mineralization occurs in both skarn and quartz-veins/greisen (Nguyen et al. 2020).

Machwi, Kirwans Hill, Zinnwald and Nui Phao contain typical greisen-type Sn-W mineralization associated with highly evolved F- or B-rich intrusions (Table 2.1). Scheelite occurs disseminated and associated with micas, cassiterite, wolframite and fluorite in greisenized cupolas of felsic intrusions. At Felbertal, scheelite mineralization occurs mainly

in quartz-veins and disseminated throughout orthogneiss and amphibolite (Kozlik et al. 2016a, b), and was formed at 335 Ma from W-rich fluids derived from orthogneiss (Raith et al. 2011). Late metamorphic events at 330 Ma and 30 Ma are recorded in scheelite, which caused its partial recrystallization (Raith et al. 2011; Kozlik et al. 2016a,b). The analyzed Felbertal samples comprise primary scheelite and recrystallized crystals from the first metamorphic event (Fig. 2.2c).

The RIRGS samples are from the Tintina Gold belt, located between Yukon (Canada) and Alaska (USA), and the Čelina deposit (Czech Republic; Fig. 2.1). Reduced IRGS comprise a variety of deposit styles, which range from intrusion-hosted sheeted quartz veins and skarn to proximal thermal aureole-hosted replacement/disseminated, and distal Au-As-Sb veins (Thompson et al. 1999; Hart et al. 2000, 2002; Lang and Barker 2001). The scheelite-bearing samples cover the majority of these deposit styles with intrusion-hosted sheeted quartz-veins from Dublin Gulch and Fort Knox; scheelite-bearing clinopyroxene/amphibole skarn (Fig. 2.2d) and marble from Fort Knox, Scheelite Dome and Colbert Lode; and disseminated/quartz-veins from Čelina and Gil-Sourdough (Alaska; Table 2.1).

The two porphyry W-Mo examples investigated are Northern Dancer and Jennings, located in Yukon, Canada (Table 2.1). Both deposits are derived from the same suite of quartz monzonite to monzogranite rocks emplaced in sedimentary strata at 110 – 120 Ma (Noble et al. 1984; Mihalynuk and Heaman 2002). The tungsten mineralization occurs as a system of quartz-scheelite veins with variable amounts of plagioclase, pyrite and beryl, which is hosted in both intrusion and nearby hornfels (Noble et al. 1984; Minfile Yukon).

Table 2.1 Summary of the main geological characteristics of scheelite-bearing samples.

Deposit/Country	Major metal	Mineral association	Intrusion	Host rock	Age
Quartz-vein/Greisen W-Sn					
Mawchi (Myanmar)	Sn-W	wo+sch+moly+apy+py+fl+dn	Peraluminous biotite granite and tourmaline granite	Granite and metasedimentary rocks	42 Ma
Nui Phao (Vietnam)	W-Bi-Cu-F-(Au)	qz+sch+fl	Peraluminous granite	Shales, sandstones, siltstones, marbles, and siliceous rocks	85 Ma
Kirwans Hill (New Zealand)	W	qz+sch+ms+fl+tz+tm	Granite	Granite and metasediments	382-358 Ma
Felbertal (Austria)	W	qz+sch+fl	Orthogneisses	Orthogneisses and amphibolites	335 Ma
Zinnwald (Germany)	Sn-W-Li	sch+qz	Strongly fractionated and slightly peraluminous rare metal A-type granites	Cínovec-Zinnwald granite cupola and rhyolite	312 Ma
Oxidized skarn	-	-	-	-	-
Obří důl (Czech Republic)	Fe-Cu-As-W	grt+cpx+amph+sch	Krkonoše-Jizera granite	Dolomite	312 Ma
Traversella (Italy)	Cu-Fe-W	cpx+sch+mag	Diorite	dolomic marbles	30 Ma
Kanbauk (Myanmar)	Sn-W-F	grt+px+amph+fl+sch	Biotite granite	metasedimentary rocks	61 Ma
Kovářská (Czech Republic)	F-Ba-Fe-W	cpx+grt+fl+sch	Bohemian massif/ Saxothuringian unit	metamorphic crystaline basement (gneiss)	Variscan
Vykmanov (Czech Republic)	Zn-Pb-W	cpx+fl+sph+gl+sch+grt	Bohemian massif/Saxothuringian unit	metamorphic crystaline basement (gneiss)	Variscan

Deposit/Country	Major metal	Mineral association	Intrusion	Host rock	Age
Reduced Skarn					
Invincible Mine/Emerald (Canada)	W-Mo(Au-Pb-Zn)	grt+cpx+sch	Cretaceous granite	limestone	-
Nui Phao (Vietnam)	W-Bi-Cu-F-(Au)	amph+py+fl+sch	Peraluminous granite	shales, sandstones, siltstones, marbles, and siliceous rocks	85 Ma
Kotel (Czech Republic)	Cu-Fe-Zn	grt+cpx+sch	Krkonoše-Jizera granite	limestone	312 Ma
Hostákov (Czech Republic)	W	cpx+fl+grt+ph+sch	Třebíče massif, Ilmenite series	metamorphic crystaline basement (gneiss)	Variscan
Hazlov (Czech Republic)	W	ves+cpx+pl+wo+sch	Smrčiny granite massiv/Moldanubian unit	limestone	Variscan
Vrbík (Czech Republic)	W	sch+bt+amph+cc+po	Variscan Belt/Central Bohemian granite pluton/Moldanubian unit	metamorphic crystaline basement (gneiss)	Variscan
Reduced Intrusion Related Gold Systems (RIRGS)					
Dublin Gulch (Canada)	Au-W	qz+sch+tn	Monzonite	Monzonite and limestone	94 Ma
Scheelite Dome (Canada)	Au-W	cpx+sch	Monzonite	Limestone	94 Ma
Celine-Mokrsko (Czech Republic)	Au	qz+sch	Tonalite-granodiorite	Amphibolite	320 - 360 Ma
Fort Knox-Colbert Lode (USA)	Au-W	qz+sch±amph±cc	Granodiorite	Monzonite and limestone	92 Ma
Gil-Sourdough (USA)	Au	qz+ms+sch+py+apy	Granodiorite	Metasedimentary rocks	92 Ma
Porphyry					
Northern Dancer (Canada)	W-Mo	qz+py+sch+brl	Monzonite	Monzonite and limestone	110 Ma

Deposit/Country	Major metal	Mineral association	Intrusion	Host rock	Age
Porphyry					
Jennings (Canada)	W-Mo	qz+py+sch	Monzonite	Limestone	100 Ma
Orogenic gold					
Corcoesto (Spain)	Au	qz+sch+apy	-	Orthogeniss, biotitic gneiss and schists.	
Hangar Flats/Yellow Pine (USA)	Au-Sb-W	st+sch+pl	-	Brecciated granodiorite	56-45 Ma

Deposit/Country	Number of analysis	Deposit size	Temperature and salinity of the fluids	Reference
Quartz-vein/Greisen W-Sn				
Mawchi (Myanmar)	15	-	260-345 °C; 4.5-15.7 wt% NaCl eq.	Myint et al. (2018)
Nui Phao (Vietnam)	10	87.9 Mt at 0.19% WO_3, 7.95% CaF_2, 0.18% Cu, 0.19 g/t Au, and 0.09% Bi	275 - 337 °C; 4.7 - 11.7 wt% NaCl eq.	Nguyen et al. (2020)
Kirwans Hill (New Zealand)	12	-	-	Pirajno and Bentley (1985)
Felbertal (Austria)	62	6.1 Mt at 0.5% WO_3	-	Kozlik et al. (2016a,b)
Zinnwald (Germany)	12	-	370 - 410 °C; 0.4 - 5.6 wt.% NaCl eq.	Webster et al. (2004); Breiter et al. (2017)
Oxidized skarn				
Obří důl (Czech Republic)	79	0.1 Mt of ore with 0.43–0.47% W; 0.85 Mt of ore with 0.41-0.43% Cu and 0.19–0.49% Bi	-	Veselovský et al. (2018)
Traversella (Italy)	12		300 - 625 °C	Dubru et al. (1988); Auwera and Andre (1991)
Kanbauk (Myanmar)	11	122 Mt at 0.14% WO_3, 0.23% Sn, 11.57% CaF_2	-	Zhang et al. (2021); Technical report Savitar 2018
Kovářská (Czech Republic)	3	showing	-	Štemprok and Mašková (1992)
Vykmanov (Czech Republic)	7	showing	-	Štemprok and Mašková (1992)

Deposit/Country	Number of analysis	Deposit size	Temperature and salinity of the fluids	Reference
Reduced Skarn				
Invincible Mine/Emerald (Canada)	12	-	-	Ball (1954)
Nui Phao (Vietnam)	9	87.9 Mt at 0.19% WO_3, 7.95% CaF_2, 0.18% Cu, 0.19 g/t Au, and 0.09% Bi	275 - 337 °C; 4.7 - 11.7 wt.% NaCl eq.	Nguyen et al. (2020)
Kotel (Czech Republic)	12	showing	-	Žacek (2008)
Hostákov (Czech Republic)	12	showing	-	Štemprok and Mašková (1992)
Hazlov (Czech Republic)	11	showing	-	Štemprok and Mašková (1992)
Vrbík (Czech Republic)	12	showing	-	J. Pasava pers. comm.
Reduced Intrusion Related Gold Systems (RIRGS)				
Dublin Gulch (Canada)	8	50.3 Mt at 0.93 g/t Au	141 - 345 °C; <15 wt.% NaCl eq.	Maloof et al. (2001)
Scheelite Dome (Canada)	22	4.1 Moz Au	300 - 550 °C; <4 wt.% NaCl eq.	Mair et al. (2006)
Celine-Mokrsko (Czech Republic)	8	11t Au	-	Lang and Barker (2001)
Fort Knox-Colbert Lode (USA)	41	3.3 Moz Au	-	Thompson et al. (1999); NI-43-101 report (2018)
Gil-Sourdough (USA)	23	0.53 Moz Au (Mesured and Indicated, Resources)	-	Allegro (1987); Blum (1985); NI-43-101 report (2018)

Deposit/Country	Number of analysis	Deposit size	Temperature and salinity of the fluids	Reference
Porphyry				
Northern Dancer (Canada)	13	242 Mt at 0.10% WO_3 and 0.047% MoS_2	-	Noble et al. (1984); Mihalynuk and Heaman (2002)
Jennings (Canada)	7	drillhole intersected 234.0 m of 0.092%MoS_2 and 0.110% WO_3.	-	Yukon Open File (2018)
Orogenic gold				
Corcoesto (Spain)	9	4.2 Mt at 1.32 g/t, over 1Moz	170 - 390 °C; 0.5 - 2.2 wt.% NaCl eq.	Boiron et al. (2003); Cepedal et al. (2014)
Hangar Flats/Yellow Pine (USA)	17	1.6 Moz Au, 3.4 Moz Ag; 111.7 Mlb Sb; tungsten past production: 0.48 t W	-	Wintzer et al. (2022)

Corcoesto (NW Spain) is an orogenic Au deposits where Au mineralization is related to extensional zones, which represent second order dextral shear bands. Scheelite crystals (Fig. 2e) occur in quartz-arsenopyrite veins within leucocratic orthogneiss that pre-dates Au mineralization (Boiron et al. 1996,2003; Cepedal et al. 2014). Hangar Flats (Idaho, USA) is also an orogenic Au deposit (Wintzer et al. 2022) that hosts significant Sb, Ag and W resources (Table 2.1). The Au-Sb-W mineralization is controlled by faults and is hosted in brecciated granodiorite (Wintzer 2019). The W mineralization (57 Ma) post-date the Au mineralization (67-58 Ma), and both are crosscut by late W-Sb veins (45 Ma) (Gillerman et al. 2019; Wintzer et al. 2022), and are interpreted as distinct mineralizing event. The analysed scheelite-bearing samples are from the early W mineralization event. Stibnite occurs mostly in the matrix of brecciated scheelite of the first W mineralization (57 Ma), indicating that this stibinite was deposited after scheelite (Wintzer et al. 2022) (Fig. 2.2f). In the late W-Sb veins (45 Ma), scheelite is intergrown with stibnite in a single veins (Wintzer et al. 2022).

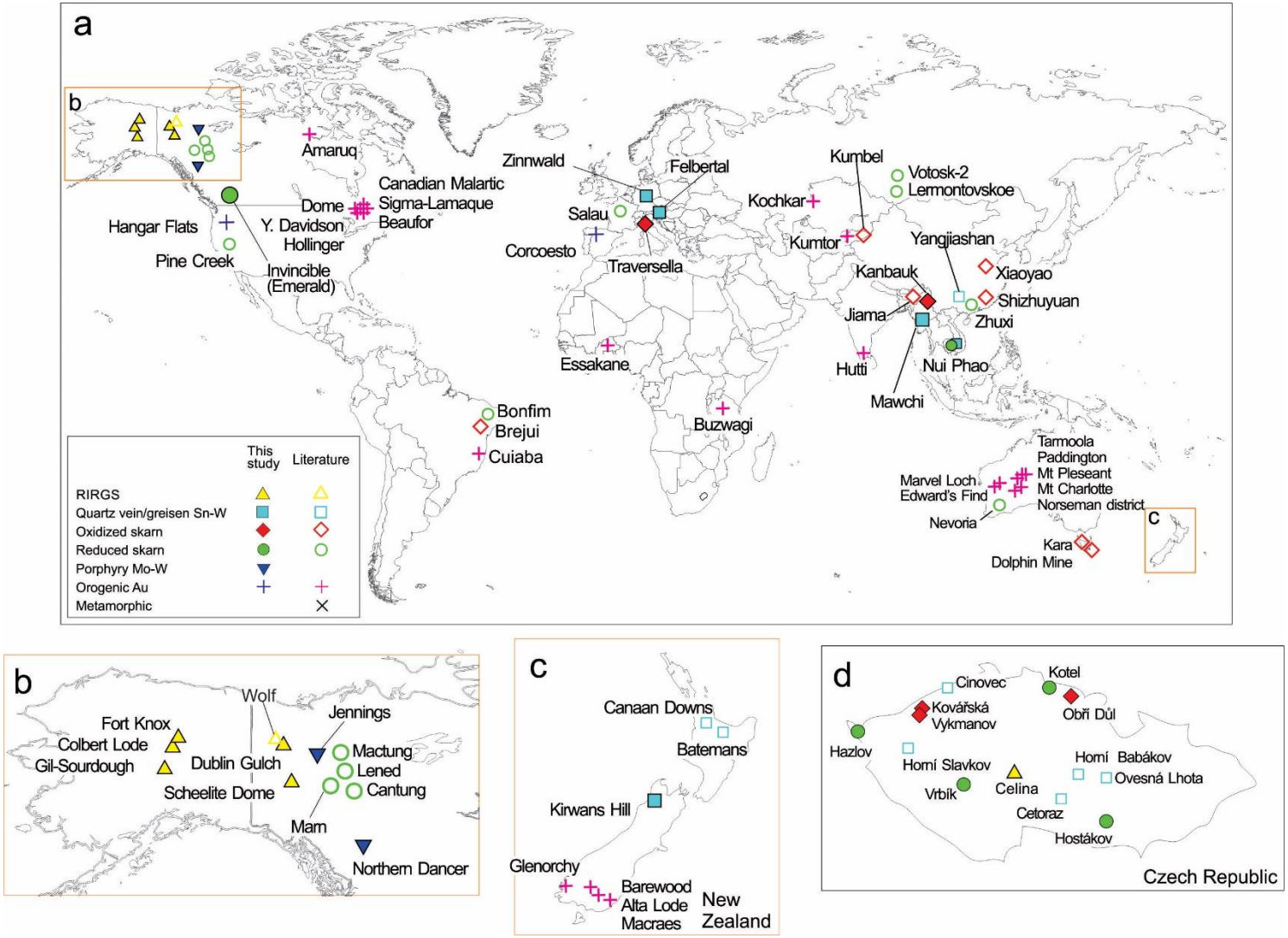

Figure 2.1. a. World distribution of scheelite-bearing ore deposits samples considered in this study. Filled symbols represent scheelite-bearing ore deposit analyzed in this study, whereas empty symbols refer to scheelite-bearing ore deposits compiled from literature. b-d. Samples location from Alaska-Yukon (b), New Zealand (c), and Czech Republic (d).

2.5 Methodology

2.5.1 Samples

Sixty scheelite-bearing samples from 16 well-documented mineral deposits and 6 showings distributed worldwide were investigated (Fig. 2.1). The selected samples cover distinct deposit types, which include eleven skarns, five quartz veins/greisen Sn-W, four RIRGS districts and two porphyry W-Mo (see Table 2.1). Moreover, we also analysed scheelite from two orogenic Au deposits: Corcoesto (2 samples) and Hangar Flats (2 samples; Fig. 2.1; Table 2.1).

2.5.2 Analytical Methods

Cathodoluminescence (CL) images and major (CaO and WO_3) and minor (Na, Sr, Mo and Fe) element composition (n= 140 analysis) of scheelite were determined using a CAMECA SX-100 electron probe micro-analyser (EPMA), equipped with five wavelength-dispersive spectrometers (WDS) and a CL detector, at Université Laval, Canada. The analytical conditions for CL images were using an accelerating voltage set at 15 kV and the beam current at 20 nA with a working distance of 2 mm. The major elements were determined using a 10-µm-diameter beam, 20 nA for beam current and 15 kV for accelerating voltage. The counting times were of 20 s at the peak and 10 s at the background. The analytical conditions for minor elements were using a 10-µm-diameter beam, 100 nA beam current, 15 kV of accelerating voltage, and counting times of 120 s at the peak and 30 s at the background. Metal tungsten (W), diopside (Ca), metal molybdenum (Mo), celestite (Sr), albite (Na) and magnetite (Fe) were employed as standards.

The minor and trace element concentrations in scheelite (n = 432 analyses) were determined by LA-ICP-MS using an Excimer 193 nm RESOlution M-50 laser ablation system equipped with a double volume cell S-155 and coupled with an Agilent 7900 mass spectrometer at the LabMaTer, Université du Québec à Chicoutimi (UQAC). The LA-ICP-MS tuning parameters were a laser frequency of 15 Hz, a fluence of 3 J/cm2, and scanning speed of 10µm/s for the line scans. Depending on scheelite grain size, spots and line scans were made with beam sizes of 33 and 55 µm. Given the heterogeneous textures in scheelite revealed by CL images, the spots were performed in all distinct CL zones to obtain most variance as possible in scheelite composition. Iolite v3 running in Igor Pro 6.37 was used for

data reduction (Paton et al. 2011). The following isotopes were measured: ^{11}B, ^{23}Na, ^{24}Mg, ^{39}K, ^{44}Ca, ^{49}Ti, ^{51}V, ^{55}Mn, ^{57}Fe, ^{59}Co, ^{61}Ni, ^{63}Cu, ^{66}Zn, ^{75}As, ^{85}Rb, ^{88}Sr, ^{89}Y, ^{93}Nb, ^{95}Mo, ^{137}Ba, ^{139}La, ^{140}Ce, ^{141}Pr, ^{146}Nd, ^{147}Sm, ^{153}Eu, ^{157}Gd, ^{159}Tb, ^{163}Dy, ^{165}Ho, ^{166}Er, ^{169}Tm, ^{172}Yb, ^{175}Lu, ^{181}Ta, ^{182}W, ^{183}W, ^{208}Pb, ^{209}Bi, ^{232}Th and ^{238}U. The ^{44}Ca was used for internal standardisation for scheelite based on EPMA results (Appendix 2.1B), whereas Si and S were monitored to identify possible silicate and sulfide inclusions, respectively. The NIST-610 synthetic glass reference material was employed as external standard for all elements using preferred values from the GeoReM database (Jochum et al. 2005). The basalt glasses GSE-1g, GSD-1g and Gprobe6-A and the NIST-612 (synthetic glass) were used as secondary reference materials for quality control. The reference materials were analyzed at the beginning, throughout and the end of each analytical session, to monitor a potential instrumental drift. The results obtained for the monitors were allowing for standard deviations on the working values. Detailed information about laser setting and reference material results for quality control are presented in ESM Tables 1.2B and 1.3B, respectively.

2.5.3 Statistical analysis

2.5.3.1 Data compilation and pre-processing

Laser ablation-ICP-MS scheelite trace element composition data from this study and from Scanlan (2018), Sciuba et al. (2020), Li et al. (2021), Palmer (2021), Miranda et al. (2022) and Pašava (unpublished data) were compiled and investigated with basic and multivariate statistics using Rstudio v4.04 (R Core Team 2021). The literature data comprise 1,620 trace element analyses of scheelite from eight quartz veins/greisen W-Sn, eighteen skarns, two RIRGS and twenty-eight orogenic Au deposits, and metamorphic scheelite (Fig. 2.1; Appendix 2.2B).

Log-ratio Expectation-Maximisation (lrEM) algorithm from R package zCompositions (Palarea-Albaladejo and Martín-Fernández 2013, 2015) was used to impute elements with less than 40% below detection limit (bdl) values. Elements with over 40% bdl values were excluded from further analysis. After imputation, the dataset was transformed using centred-log ratios (clr) to overcome the closure effect in compositional data (Aitchison 1986).

2.5.3.2 Partial Least-Squares Discriminant Analysis (PLS-DA)

The PLS-DA is a supervised multivariate dimensionality-reduction tool used for classification/clustering purpose. The method consists in finding the maximum variance of two matrices X (variables/elements) and Y (classes) that can be linked. Hence, the objective of PLS-DA method is to optimize the separation between the classes of samples and find the variables that best describe their differences. The results are visualized on scatter plots (loadings and scores plots) and bar plots (score contributions and variable importance on projection). The loadings plot illustrates the relationship between elements and groups, and the correlations among the elements. Hence, elements that plot in the same quadrant display a positive correlation, whereas those plotting on opposite quadrants display a negative correlation. The farther an element plots from the origin of the loading plot, the greater its contribution to the model, whereas the closer an element plot from the origin, the smaller its contribution for the classification. The scores plot displays the distribution of the samples in the space created by the variables and classes. Samples with similar features are grouped together (Eriksson et al. 2001). The score contribution plot highlights the differences between classes in relation to the average of the entire dataset. The Variable Importance on Projection (VIP) plot emphasizes the importance of each element for the model. Elements with VIP values ≥1 have major controls in separating the classes, whereas those between 0.8 and 1, and <0.8 have intermediate and minor contributions in the discriminant analysis, respectively (Eriksson et al. 2001). The PLS-DA was conducted using the mixOmics package in R (Rohart et al. 2017).

2.5.3.3 Random Forest

To test whether scheelite composition can be used for discrimination and prediction of deposit types, we employed a Random Forest (RF) classifier algorithm. Random Forest is a supervised machine learning algorithm that is commonly used for classification, regression and prediction (Breiman 2001). The algorithm consists of a large number of decision trees (forest) that operate as an ensemble. Each tree is individually built from a random sampling subset with replacement (bootstrapping) from the training dataset (i.e., analysis), and from randomly selected predictor variables (i.e., elements). The number (N) of predictor variables in each tree is set to be equal to the square root of the total variables of the training data (Breiman 2001). The predictor variables and their values define each split (nodes) of the tree. Each decision tree searches through all candidates the optimal split

that maximizes the purity of the resulting tree. Gini decrease is a measure that shows the contribution importance of each variable in the model. The higher the mean decrease Gini score, the higher importance of the variable in the model. The outcome of RF model is visualized through a confusion matrix. The confusion matrix is built with the testing data, which is used to express the predictions of the classifier. The rows represent the true classes, whereas the columns indicate predicted classes.

Random Forest was performed using untransformed data and the Caret package in R. To build the RF model 70% of the scheelite dataset was used as training data and 30% was used for testing. The best results for the RF model were acquired using 11 predictor variables (Na, Mg, Mn, As, Sr, Y, Nb, Mo, Pb, ΣREE and Eu anomaly) and 500 trees. In addition, scheelite from Corcoesto and Hagnar Flats (this study), orogenic Au (Cave 2016; Cave et al. 2017; Liu et al. 2021) and W greisen and oxidized skarn deposits (Huang et al. 2022), and metamorphic scheelite (Cave et al. 2017; Palmer 2021) (Appendix 2.3B) were used as blind data to assess the effectiveness of the model. This additional dataset had few missing elements that were imputed using missForest algorithm from missForest package in R (Stekhoven and Buehlmann 2012). Similar to Random Forest algorithm, the missForest algorithm consists of building a random forest for each variable based on the input dataset and uses it to predict the missing variables.

2.6 Results

2.6.1 Cathodoluminescence and texture

In general, scheelite varies from fine to coarse grains regardless the deposit type (Fig. 2.2). Cathodoluminescence (CL) reveal textures varying from homogeneous to oscillatory zoning with less common recrystallization textures (Fig. 2.3). In quartz-vein/greisen Sn-W deposits, scheelite crystals are homogeneous or zoned (Fig. 2.3a), whereas at Felbertal, scheelite shows recrystallizations textures characterized by sub grains at the border of scheelite crystals (Fig. 2.3b). Under ultra-violet (UV) light, quartz-vein/greisen Sn-W deposits scheelite grains commonly display bluish colors. Scheelite from oxidized and reduced skarns are characteristically zoned, with common dissolution textures under CL (Fig. 2.3c-d). Under UV light skarn scheelite shows a yellow-greenish to bluish luminescence for oxidized skarns, and mostly bluish for reduced skarns.

Scheelite from RIRGS is predominantly homogenous under CL (Fig. 2.3e) and commonly display bluish color under UV light. At the Northern Dancer and Jennings porphyry W-Mo deposits, scheelite crystals vary from homogenous to zoned under CL (Fig. 2.3f) and displays mostly bluish luminescence color under UV light. At the Corcoesto orogenic Au deposit, CL reveals that scheelite crystals are commonly homogeneous (Fig. 2.3g). At Hangar Flats, scheelite occurs as aggregates of microcrystals and as coarse grains (Fig. 2.2f), and commonly displays oscillatory zoning under CL (Fig. 2.3h).

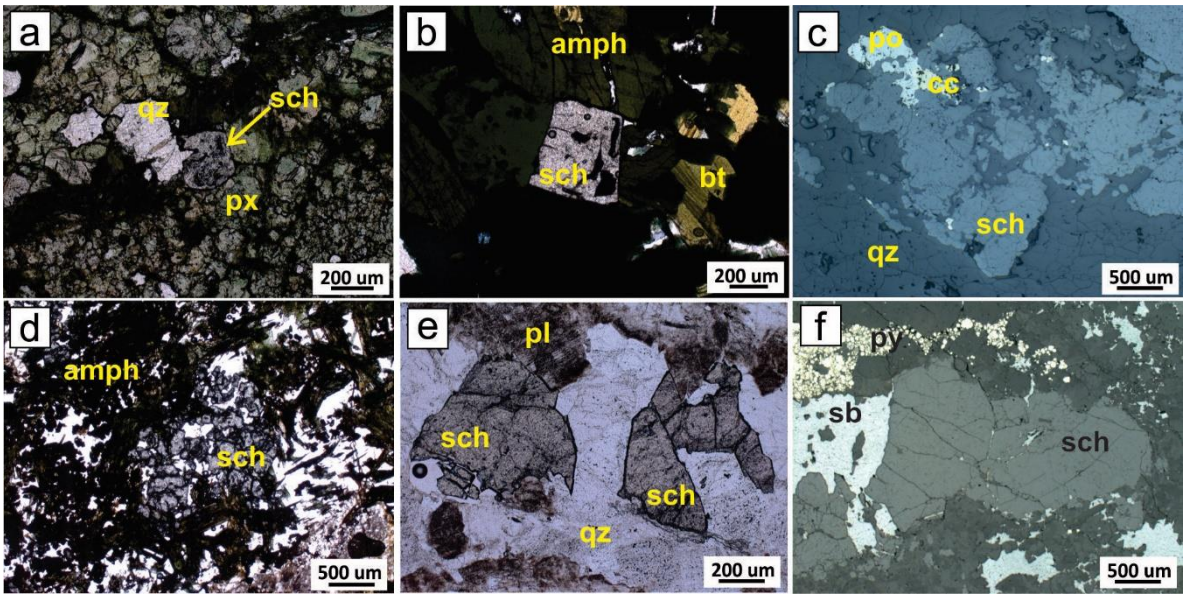

Figure 2.2 Photomicrographs under transmitted light (a-b, d-e) and reflected light (c and f) of scheelite-bearing samples. a. Scheelite associated with clinopyroxene and few biotite from pyroxene skarn facies at Kanbauk. b. Scheelite crystal associated with amphibole and biotite from Nui Phao skarn. c. Coarsed scheelite grains associated with chalcopyrite, pyrrhotite and quartz from Felbertal quartz-vein W deposit. d. Scheelite associated predominantly with amphibole at Fort Knox. e. Scheelite crystals in a quartz-vein hosted in a granodiorite (Corcoesto). f. Scheelite with pyrite, stibnite and plagioclase from Hangar Flats. Abreviations: sch: scheelite; grt: garnet; cpx: clinopyroxene; qz: quartz; mag: magnetite; amph: amphibole; po: pyrrhotite; cc: chalcopyrite; sb: stibnite; py: pyrite.

2.6.2 Composition variation in relation to deposit type

The full compositional data for scheelite is reported in Appendix 2.4B. The concentration ranges for each element grouped by deposit type are shown in box and whisker plots (Fig. 2.4) and Table 2.2. Also, the chemical variation of minor and trace elements of Hangar Flats and Corcoesto gold deposits are reported apart. In general, Mo is

the most abundant minor element in scheelite from magmatic-hydrothermal deposits with concentrations ranging from 0.07 ppm to 5.4 wt.%, followed by Nb (0.43 to 3211 ppm), Y (0.03 to 2182 ppm), Sr (10 to 1721 ppm), Th (0.002 to 625 ppm), As (0.054 to 363 ppm), Na (0.4 to 361 ppm), U (bdl to 263 ppm), Mg (0.02 to 259 ppm), Pb (0.03 to 236 ppm), Mn (0.25 to 225 ppm), Ta (0.03 to 86 ppm), K (0.28 to 83 ppm), Ti (0.14 to 60 ppm) and V (0.001 to 16 ppm).

The highest Mo content (from 21 ppm to 5.4 wt.%) is associated with scheelite from oxidized skarns. Quartz vein/greisen Sn-W scheelite displays the second highest Mo concentration which is up to 1.5 wt.%, followed by reduced skarns (<6300 ppm), RIRGS (<5015 ppm) and porphyry W-Mo (<1500 ppm). The highest Nb content is associated with scheelite from quartz vein/greisen Sn-W (<3211 ppm), followed by porphyry W-Mo (<1204 ppm), oxidized and reduced skarns (<1168 ppm and <602 ppm, respectively), and RIRGS (<212 ppm). Yttrium content is higher in quartz-vein/greisen Sn-W (74 to 2182 ppm) relative to oxidized skarn (0.03 to 1476 ppm), porphyry W-Mo (341 to 1223 ppm), and RIRGS (21 to 1120 ppm). Reduced skarn scheelite displays the lowest Y concentrations, ranging from 0.38 to 264 ppm.

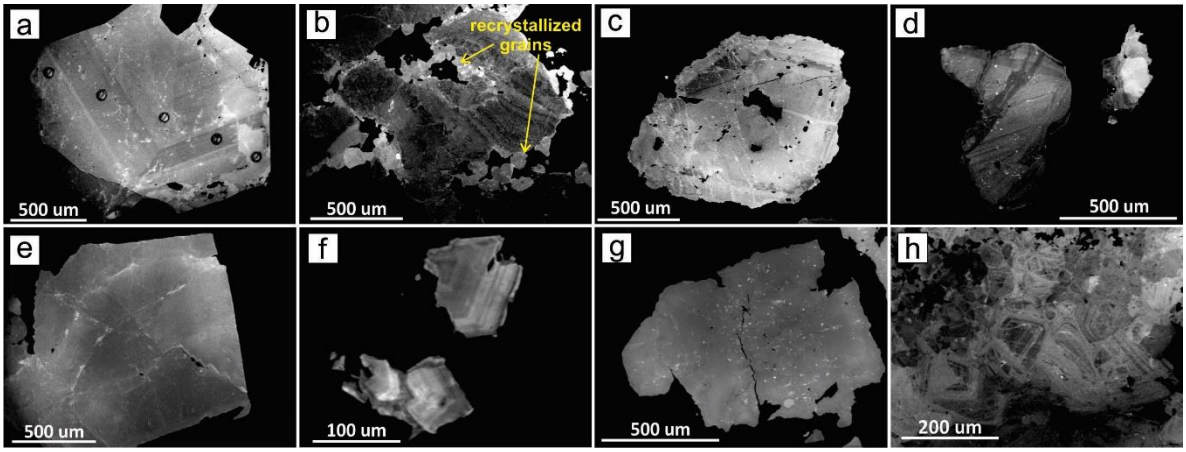

Figure 2.3 Cathodoluminescence images of scheelite crystals. a. Scheelite with oscillatory zoning from Mawchi quartz-vein/greisen Sn-W. Laser spots on the grain. b. Zoned scheelite grain from Felbertal. Note recrystallized grains on the border with a light grey CL color. c. and d. scheelite with oscillatory zoning from Obří důl and Kotel (Krkonoše), respectively. e. Homogeneous scheelite crystal from Dublin Gulch (RIRGS). f. Oscillatory zoning in scheelite from Northern Dancer (W-Mo porphyry). g. Homogeneous scheelite crystal from Corcoesto orogenic gold deposit. h. Aggregate of zoned scheelite grains from Hangar Flats.

Scheelite from reduced skarns and quartz vein/greisen Sn-W contain higher Sr content (1720 ppm and 1380 ppm, respectively) relative to scheelite from RIRGS (553 ppm), oxidized skarns (159 ppm) and porphyry (144 ppm). Thorium content varies from 0.1 to 625 ppm in porphyry W-Mo and from 0.003 to 151 ppm quartz-vein/greisen Sn-W scheelite. Scheelite from oxidized and reduced skarns and RIRGS display similar range of Th content, which varies between 0.002 and 11 ppm, with medians of 0.13 ppm, 0.05 ppm, and 0.04 ppm, respectively (Fig. 2.4). Arsenic concentration is higher in oxidized skarn (<362 ppm), quartz-vein/greisen Sn-W (<64.3 ppm) and porphyry W-Mo (<40.3 ppm) scheelite relative to RIRGS (<16 ppm) and reduced skarns (<8 ppm) scheelite, which display the lowest As contents.

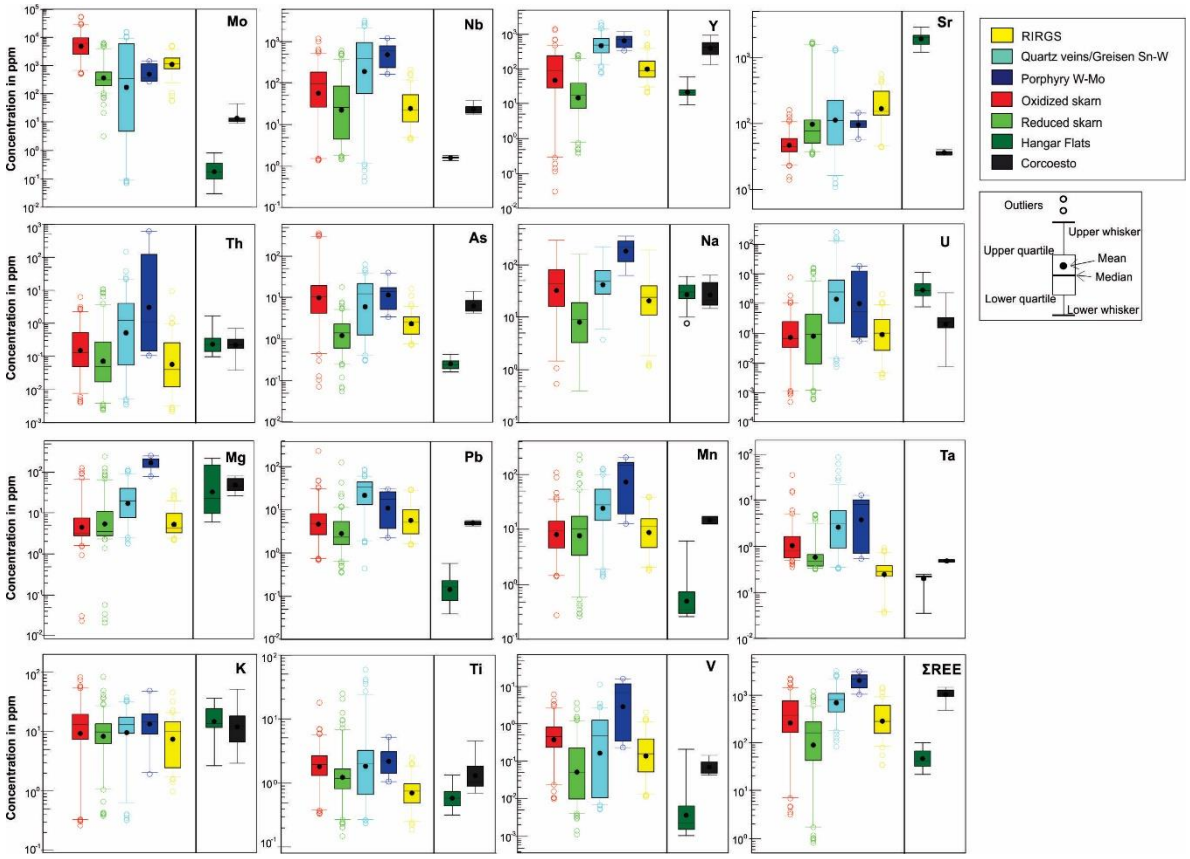

Figure 2.4 Box and whisker diagram of trace elements concentrations in scheelite from magmatic-hydrothermal deposits and from Hangar Flats and Corcoesto.

The highest Na contents occur in scheelite associated with porphyry W-Mo (<361 ppm), followed by oxidized skarns (<305 ppm) and quartz-vein/greisen Sn-W (<225 ppm). Reduced-IRGS and reduced skarns scheelite display the lowest Na concentration, <195

ppm and <85 ppm, respectively. The highest U content occur in quartz-vein/greisen Sn-W (<263 ppm). Porphyry W-Mo and reduced skarns scheelite contain <19 ppm and <16 ppm, respectively, and oxidized skarns and RIRGS scheelite display the lowest U concentration, <8 ppm and <2.15 ppm, respectively. The highest Mg concentration occurs in scheelite from porphyry W-Mo (<258 ppm), followed by reduced skarns (<244 ppm) and oxidized skarns (<130 ppm). Quartz-vein/greisen Sn-W and RIRGS scheelite have the lowest content, up to 117 ppm and 35 ppm of Mg, respectively.

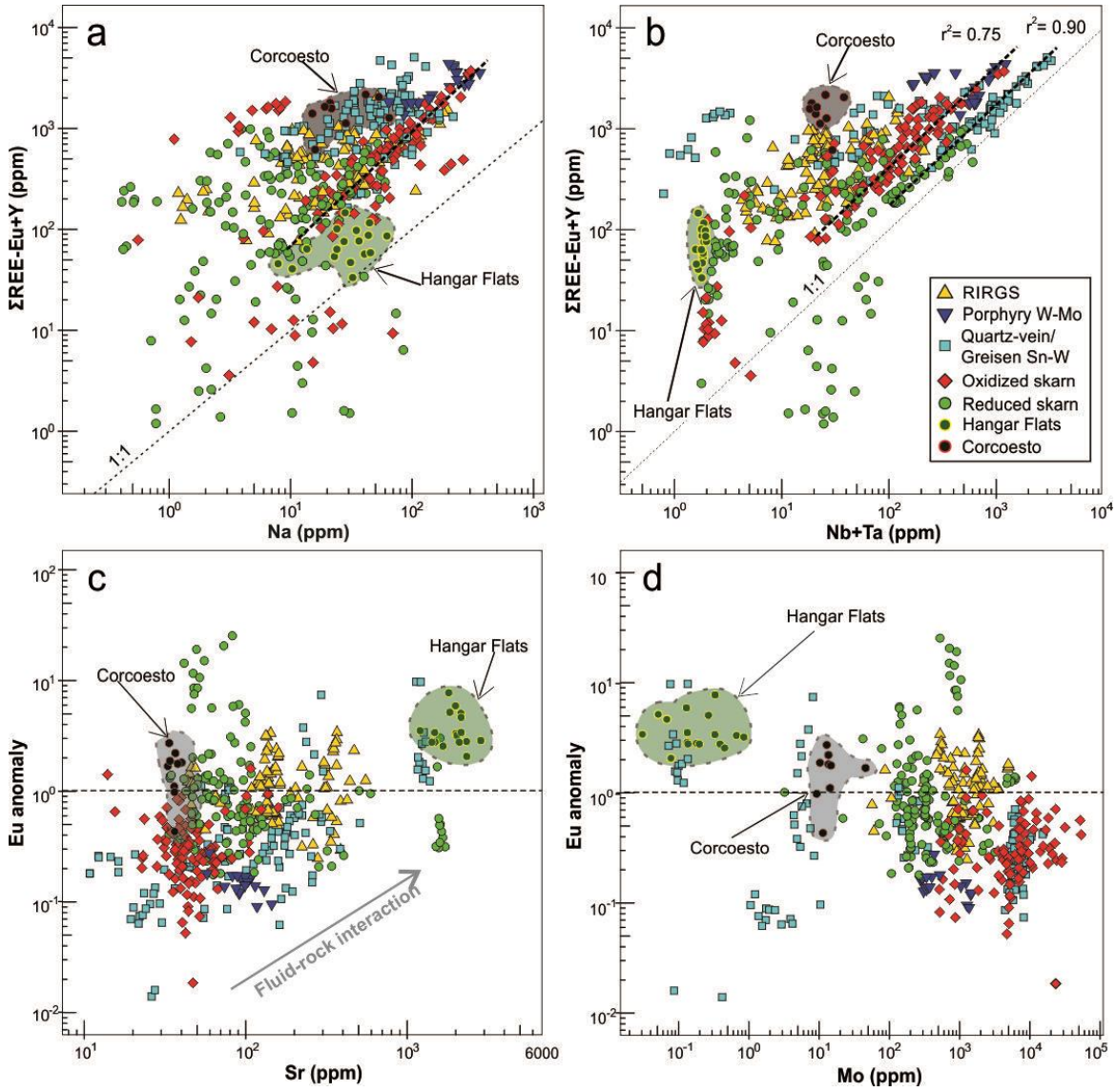

Figure 2.5 Binary plot showing the correlation between a. Na versus ΣREE-Eu+Y; b. Nb+Ta versus ΣREE-Eu+Y; c. Sr versus Eu anomaly and d. Mo versus Eu anomaly.

Table 2.2 Summary of LA-ICP-MS data of scheelite.

Deposit		Na (ppm)	Mg (ppm)	K (ppm)	Ti (ppm)	V (ppm)	Mn (ppm)	As (ppm)	Sr (ppm)	Y (ppm)
RIRGS	N	95	95	95	95	95	95	95	95	95
	Min	1.19	2.14	0.98	0.19	0.01	1.77	0.71	43.85	21.29
	Max	195.71	35.03	45.87	2.50	2.04	39.10	16.47	553.22	1120.34
	Median	24.74	4.34	10.01	0.75	0.16	11.19	2.63	151.51	92.16
Porphyry W-Mo	N	20	20	20	20	20	20	20	20	20
	Min	64.50	79.79	1.91	1.06	0.23	12.57	3.42	57.69	341.38
	Max	361.12	258.96	48.65	5.28	16.12	203.91	40.31	144.84	1223.2
	Median	224.49	205.93	14.39	2.25	6.83	146.58	14.07	97.65	722.8
Quartz vein/Greisen Sn-W	N	111	111	111	111	111	111	111	111	111
	Min	3.84	1.78	0.32	0.24	0.01	1.36	0.31	10.83	74.64
	Max	225.18	117.87	37.53	59.63	11.26	125.80	64.36	1380.27	2182.3
	Median	50.04	19.60	13.07	2.00	0.48	27.86	12.52	111.76	492.1
Oxidized skarn	N	112	112	112	112	112	112	112	112	112
	Min	0.55	0.02	0.26	0.33	0.01	0.27	0.07	13.96	0.03
	Max	305.80	129.27	83.40	18.07	6.12	224.90	362.79	159.16	1476
	Median	47.26	3.20	12.37	1.96	0.49	8.66	12.04	44.62	94.7
Reduced skarn	N	68	68	68	68	68	68	68	68	68
	Min	0.44	0.02	0.37	0.20	0.001	0.26	0.27	33.92	0.39
	Max	84.79	244.64	41.70	12.51	1.39	52.50	7.37	1720.82	264.7
	Median	9.40	3.54	9.80	1.20	0.05	10.19	1.44	77.01	17.94
Hangar Flats	N	17	17	17	17	17	17	17	17	17
	Min	7.88	6.03	2.66	0.32	0.001	0.26	0.16	1203.7	9.59
	Max	62.13	223.79	36.14	1.33	0.21	6.12	0.44	2855.1	61.16
	Median	31.14	22.94	13.76	0.58	0.00	0.35	0.24	2000	21.41
Corcoesto	N	9	9	9	9	9	9	9	9	9
	Min	15.10	26.69	2.92	0.70	0.04	12.52	4.23	32.93	134.55
	Max	64.91	80.76	51.43	4.59	0.14	17.39	14.18	40.18	950.76
	Median	21.70	45.15	12.23	1.04	0.06	14.91	5.53	36.28	430.21

Deposit		Nb (ppm)	Mo (ppm)	Ba (ppm)	Ta (ppm)	Pb (ppm)	Th (ppm)	U (ppm)	REE (ppm)
RIRGS	N	95	95	95	95	95	95	95	95
	Min	4.24	56.71	0.02	0.04	1.53	0.00	0.00	34.64
	Max	212.25	5015.12	2.50	0.93	29.47	9.59	2.15	1469.6
	Median	21.98	1182.89	0.17	0.29	5.13	0.04	0.10	283.8
Porphyry W-Mo	N	20	20	20	20	20	20	20	20
	Min	165.41	277.58	0.01	0.54	2.27	0.11	0.06	1034
	Max	1203.74	1473.40	6.89	12.95	30.57	625.50	18.90	3163
	Median	604.65	366.82	0.23	8.22	17.74	1.14	0.56	2200
Quartz vein/Greisen Sn-W	N	111	111	111	111	111	111	111	111
	Min	0.43	0.07	0.01	0.33	0.44	0.00	0.01	84.08
	Max	3210.90	15721	6.67	86.18	87.15	151.51	262.71	3234.79
	Median	387.81	351.67	0.21	3.14	34.37	1.28	2.57	805.64
Oxidized skarn	N	112	112	112	112	112	112	112	112
	Min	1.37	21.82	0.01	0.36	0.67	0.00	0.00	3.24
	Max	1167.60	53932	48.65	35.31	236.30	8.28	16.68	2231.94
	Median	97.86	5281	0.12	0.83	4.92	0.15	0.07	409.46
Reduced skarn	N	68	68	68	68	68	68	68	68
	Min	1.43	3.22	0.01	0.34	0.64	0.00	0.00	0.82
	Max	601.87	6296.7	3.61	4.96	127.88	11.13	15.82	965.80
	Median	25.82	325.82	0.18	0.48	2.36	0.05	0.09	163.84
Hangar Flats	N	17	17	17	17	17	17	17	17
	Min	1.36	0.03	0.33	0.04	0.04	0.10	0.80	22.30
	Max	1.77	0.85	1.97	0.25	0.57	1.71	11.76	100.57
	Median	1.61	0.18	0.64	0.22	0.17	0.23	2.77	42.69
Corcoesto	N	9	9	9	9	9	9	9	9
	Min	17.79	9.24	0.01	0.45	4.24	0.04	0.01	488.10
	Max	37.67	45.87	0.14	0.52	5.70	0.72	2.36	1483.21
	Median	22.42	13.59	0.02	0.48	5.05	0.23	0.25	1049.23

The highest Pb contents occur in scheelite from oxidized (<236 ppm) and reduced skarns (<128 ppm), followed by quartz-vein/greisen Sn-W (<87 ppm), porphyry W-Mo (<30.5 ppm), and RIRGS (<29.5 ppm). Manganese contents are higher in oxidized skarns (0.27 to 224 ppm), porphyry W-Mo (12 to 203 ppm), quartz-vein/greisen Sn-W (1.36 to 125 ppm) and reduced skarn scheelite (0.27 to 52.5 ppm) compared to scheelite from RIRGS (1.7 to 40 ppm). The Ta content is higher in quartz-vein/greisen Sn-W scheelite (<86 ppm for) relative to oxidized skarn (<35 ppm), porphyry W-Mo (<13 ppm), reduced skarn (<5 ppm) and RIRGS (<1 ppm) scheelite. The K contents are higher in oxidized skarn scheelite (<82 ppm), compared to porphyry W-Mo (<49 ppm), RIRGS (<46 ppm), reduced skarn (<42 ppm) and quartz-vein/greisen Sn-W (<38 ppm).

Titanium content varies from 0.23 to 60 ppm in quartz-vein/greisen Sn-W scheelite, from 0.33 to 18 ppm in oxidized skarn, and from 0.12 to 12.5 ppm in reduced skarn. The lowest Ti concentration occurs in scheelite from porphyry W-Mo (<5.3 ppm) and RIRGS (<2 ppm). Vanadium is less abundant element with concentrations not exceeding <16 ppm for porphyry W-Mo, <11.3 ppm for quartz-vein/greisen Sn-W, <6.1 ppm for oxidized and <2 ppm for both reduced skarns and RIRGS scheelite.

The ΣREE contents in scheelite are variable, ranging from 0.81 to 3235 ppm. The highest concentrations occur in scheelite from quartz-vein/greisen Sn-W (84 to 3234 ppm), followed by porphyry Mo-W (1033 to 3163 ppm), oxidized skarn (3 to 2231 ppm) and RIRGS (34 to 1470 ppm). The lowest ΣREE content occurs in reduced skarn scheelite, with concentrations ranging from 0.81 to 966 ppm (Fig. 2.4).

A significant positive correlation occurs between Na and ΣREE-Eu+Y in scheelite from most oxidized skarn deposits, and few scheelite from RIRGS (Fig. 2.5a). No correlations are observed for RIRGS and oxidized and reduced skarns scheelite with low ΣREE-Eu+Y and Na contents (<30 ppm for ΣREE-Eu+Y, and <10 ppm for Na). A positive correlation between Nb-Ta and ΣREE-Eu+Y is visible for most quartz-vein/greisen Sn-W, reduced and oxidized skarns and porphyry W-Mo scheelite (Fig. 2.5b).

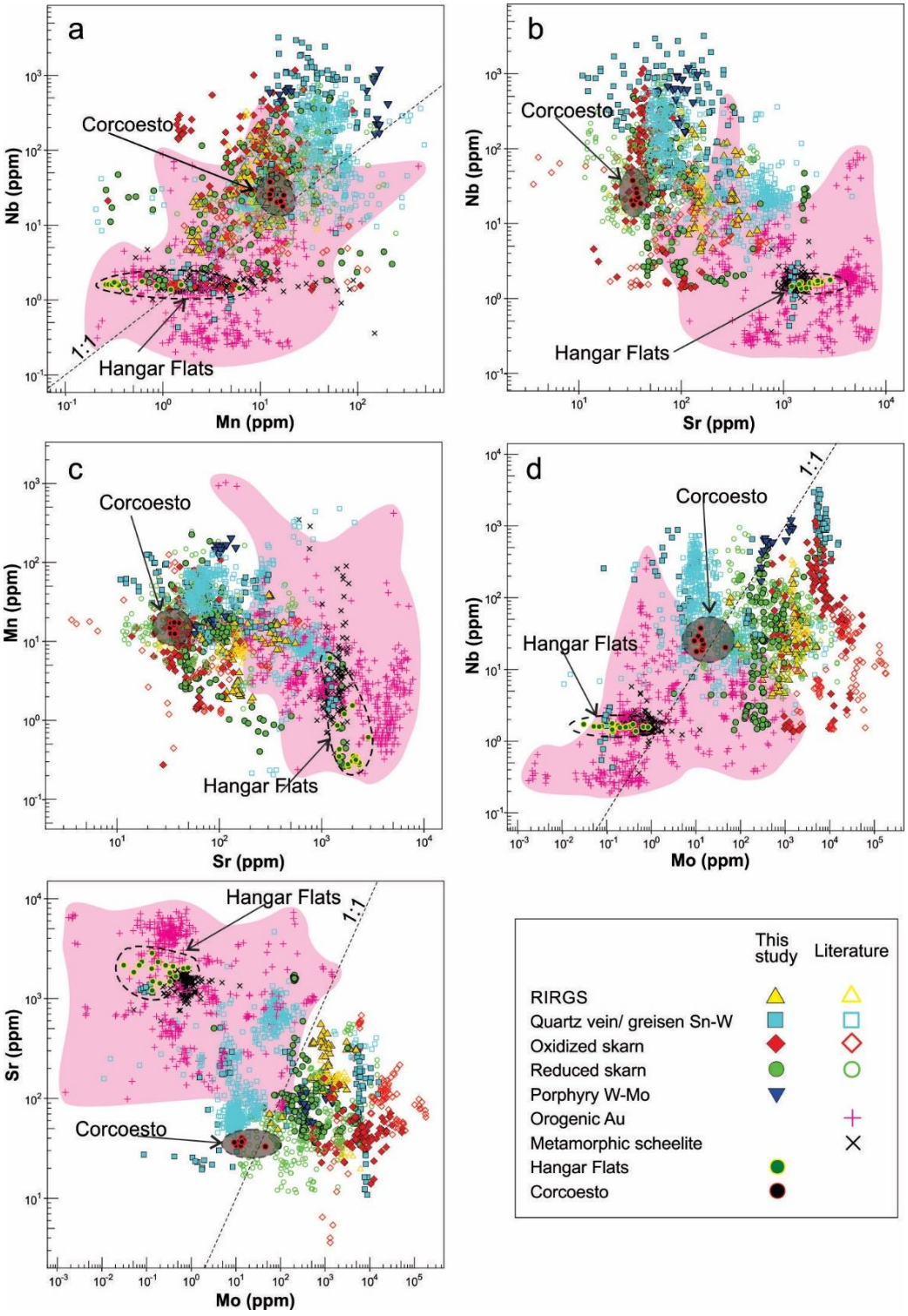

Figure 2.6 Binary plots of minor and trace elements composition scheelite. a. Mn versus Nb, b. Sr versus Nb, c. Sr versus Mn, d. Mo versus Nb, and e. Mo versus Sr. Data from this study and literature (Scanlan et al. 2018; de Bronac de Vazelhes 2019; Li et al. 2021; Palmer 2021; Sciuba et al. 2020; Miranda et al. 2022; Pasava unpubl.).

Few chemical differences exist between Hangar Flats and Corcoesto scheelite. Molybdenum, Nb, Y, As, Pb, Mn, Ti and ΣREE contents are relatively higher in Corcoesto (<45.8 ppm of Mo, <37.6 ppm of Nb, <950 ppm of Y, <14 ppm of As, <0.7 ppm of Pb, <17.4 ppm of Mn, <5 ppm of Ti, and <1483 ppm of ΣREE) compared to Hangar Flats scheelite (<0.85 ppm of Mo, <1.7 ppm of Nb, <61 ppm of Y, <0.44 ppm of As, <0.57 ppm of Pb, <6.1 ppm of Mn, <1.3 ppm of Ti, and <100 ppm of ΣREE; Fig. 4 and Table 2.2), whereas Sr and U contents are higher in Hangar Flats (1200 to 2855 ppm of Sr, and 0.8 to 11.7 ppm of U) relative to Corcoesto scheelite (32 to 40 ppm of Sr and 0.01 to 2.3 ppm of U). Hangar Flats and Corcoesto scheelite contain similar concentration ranges of Th (from 0.04 to 1.7 ppm), Na (from 7.8 to 65 ppm) and K (2.6 to 51.4 ppm; Fig. 2.4).

Figure 2.6 shows the relationship between few trace elements in scheelite, from this study and literature data (Appendix 2.2B), that are useful to discriminate scheelite from different deposits. Overall, Mn and Nb are positively correlated for most magmatic-hydrothermal scheelite, whereas orogenic Au and metamorphic scheelite show no correlation (Fig. 2.6a). Niobium and Sr display a negative correlation for scheelite from magmatic-hydrothermal deposits (Fig. 2.6b). Similarly, Mn and Sr show a slightly negative correlation among magmatic-hydrothermal scheelite (Fig. 2.6c). Niobium and Mo contents increase from orogenic towards magmatic-hydrothermal scheelite (Fig. 2.6d), whereas the Sr content decreases from orogenic towards magmatic-hydrothermal scheelite (Fig. 2.6e). Hangar Flats scheelite plots in all diagrams with orogenic Au scheelite. In contrast, scheelite from Corcoesto plots more closely with magmatic-hydrothermal scheelite (Fig. 2.6a-e).

2.6.3 REE patterns

Scheelite from magmatic-hydrothermal deposits displays 6 REE patterns: (i) steep and (ii) shallow negative slopes, (iii) flat to slightly concave, (iv) concave, (v) convex, and (vi) positive slope (Fig. 2.7). Appendix 2.1A shows the REE patterns for individual deposit, and when available, the REE patterns for intrusions associated with mineralization. The steep negative slope pattern is characterized by La/Sm and Gd/Lu ratios >7, high La/Lu ratio (>300), negative Eu anomaly and is commonly displayed by scheelite from oxidized skarn deposits (Fig. 2.7a). The shallow negative slope pattern is characterized by La/Sm >0.7, given that some scheelite is slightly depleted in La relative to Sm, Gd/Lu >1, and La/Lu >2 ratios, positive and negative Eu anomalies, and is characteristic of scheelite from RIRGS and oxidized and reduced skarns (Fig. 2.7b).

The flat to slightly concave pattern occurs in scheelite from all deposit types (Fig. 2.7c) and is characterized by La/Sm, Gd/Lu and La/Lu ratios around 1, and with both positive and negative Eu anomalies. Scheelite with this pattern displays slight enrichments in middle REE (Sm-Dy), and in the heavy REE (Ho-Lu; Appendix 2.1A Appendix 2.1A). Few reduced skarn scheelites have ΣREE contents (between 0.8 to 4 ppm) depleted relative to chondrite (Fig. 2.7c). The concave shape pattern is characterized by La/Sm <1, Gd/Lu >1 and La/Lu from around 1 to higher than 10, and positive to negative Eu anomalies. The concave shape is found in scheelite from all deposit types apart from porphyry W-Mo deposits (Fig. 2.7d). The convex REE pattern displays La/Sm >0.7 and Gd/Lu <1 ratios, with positive or negative Eu anomalies, mostly in scheelite from quartz-vein/greisen Sn-W, with a few from reduced and oxidized skarns (Fig. 2.7e).

The positive slope REE patterns are characterized by La/Sm, Gd/Lu and La/Lu ratios <1, predominantly negative Eu anomalies and are mostly in scheelite from quartz veins/greisen-type W-Sn deposit, with few from oxidized skarn and RIRGS (Figs. 2.7f and Appendix 2.1A).

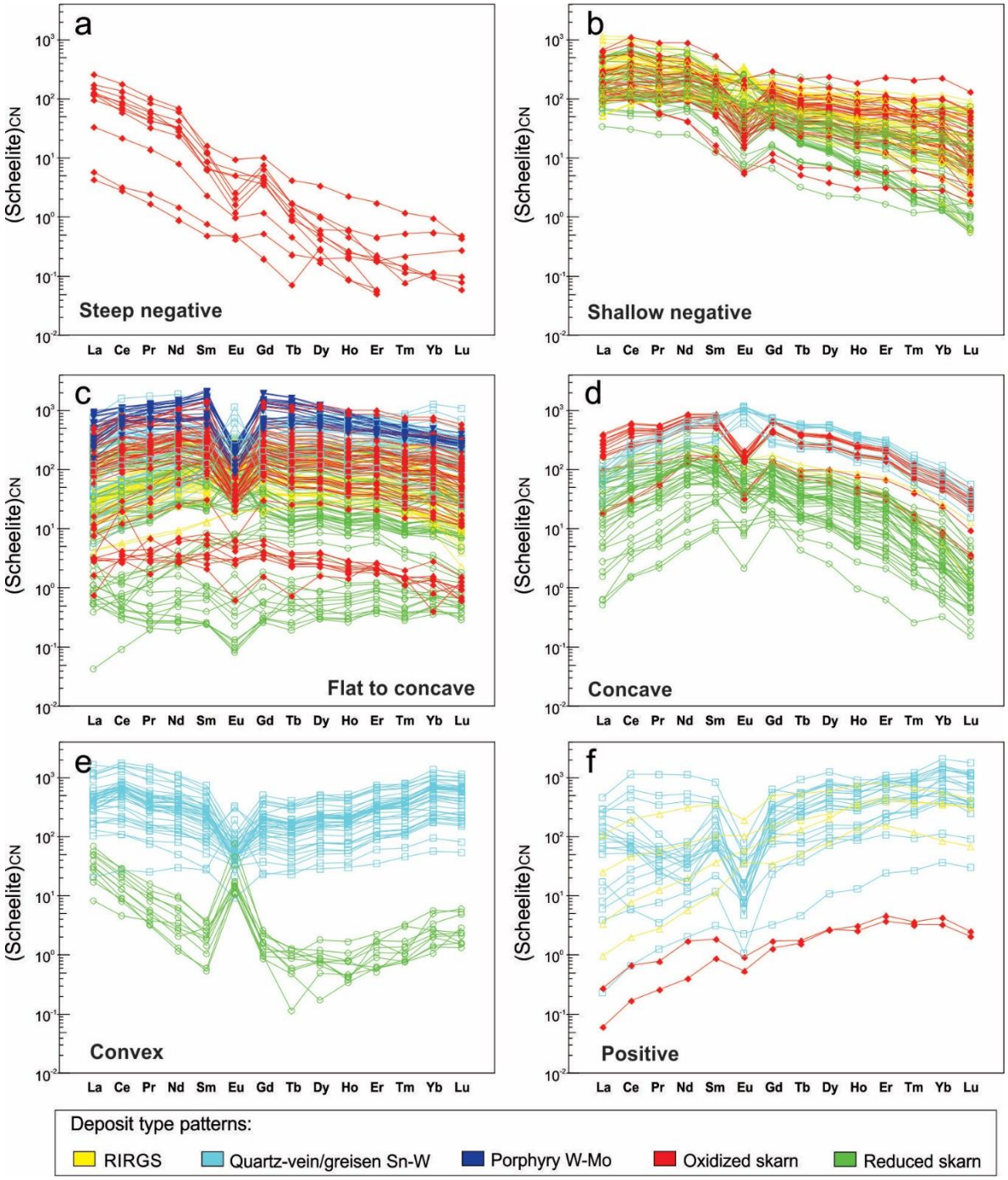

Figure 2.7 Chondrite-normalized REE patterns of scheelite. Chondrite normalized values from McDonough and Sun (1995). a. steep and b. shallow negative slope REE patterns in scheelite with predominantly negative Eu anomaly. c. Flat to slightly concave shape with positive and negative Eu anomalies. Note that few reduced skarn scheelite are depleted in REE and display scheelite/chondrite ratio <1. d. concave REE patterns with predominantly negative Eu anomaly. e. convex shape with both positive and negative Eu anomalies, and f. positive slope with negative Eu anomaly.

2.7 Multivariate statistical analysis of scheelite composition

2.7.1 PLS-DA of scheelite from magmatic-hydrothermal deposits

Figure 2.8 displays PLS-DA results of compositional variation of scheelite from magmatic-hydrothermal deposits: RIRGS, porphyry W-Mo, quartz-veins/greisen Sn-W and oxidized and reduced skarns. The loadings plot of the first and second (qw*1-qw*2) components shows the relationship between the variables (Na, Mg, K, Ti, V, Mn, As, Sr, Y, Nb, Mo, Ta, Pb, Th, U, ΣREE and Europium anomaly) and the groups (Fig. 2.8a), whereas the scores plot displays the distribution of samples in t1-t2 space (Fig. 2.8b). Positive correlations exist between As and V at negative qw*1 and positive qw*2; Pb, Y, Th, U, Ta at positive qw*1 and qw*2; and between Mn and Nb at positive qw*1 and negative qw*2 (Fig. 2.8a).

Figure 2.8a show that oxidized skarn plots at negative qw1 and positive qw2 as result of Mo, V and As contributions. Reduced intrusion related gold system plots close to the origin at negative qw*1 and qw*2. Quartz-vein/greisen Sn-W and porphyry W-Mo plot at positive qw*1 and qw*2 as result of As, U, Pb, Th contributions. Reduced skarn plots at positive qw*1 and negative qw*2 as result of Mn and Eu anomaly contributions.

Scheelite from oxidized skarns and RIRGS plot mostly at negative t1, and scatter through positive and negative t2 due to high As, V and Mo contents (Fig. 2.8b and Appendix 2.2A). Scheelite from porphyry W-Mo plots mostly at positive t1 and t2 as a result of high concentrations of As, Ta, Pb, Th and U (Fig. 2.8b and Appendix 2.2A), whereas few samples scatter at negative t1 (Fig. 2.8b). Quartz vein/greisen Sn-W scheelite plots mostly at positive t1, and spreads through negative and positive t2 due to high As, U, Th, Ta and Pb contents (Appendix 2.2A), except for a group of analyses that plot separately at negative t1 and positive t2 because of high As concentrations (Fig. 2.8b). Scheelite from reduced skarns scatters mostly through negative and positive t1 and negative t2 due to high Nb and Mn concentrations and Eu anomaly, with few analyses in positive t1 and t2 quadrant. The VIP plot (Fig. 2.8c) highlights that V, Mn, As, Mo, U and Eu anomaly are important elements (VIP >1) that contribute the model, whereas Nb, Ta, and Th have a moderate contribution (VIP between 0.8 and 1).

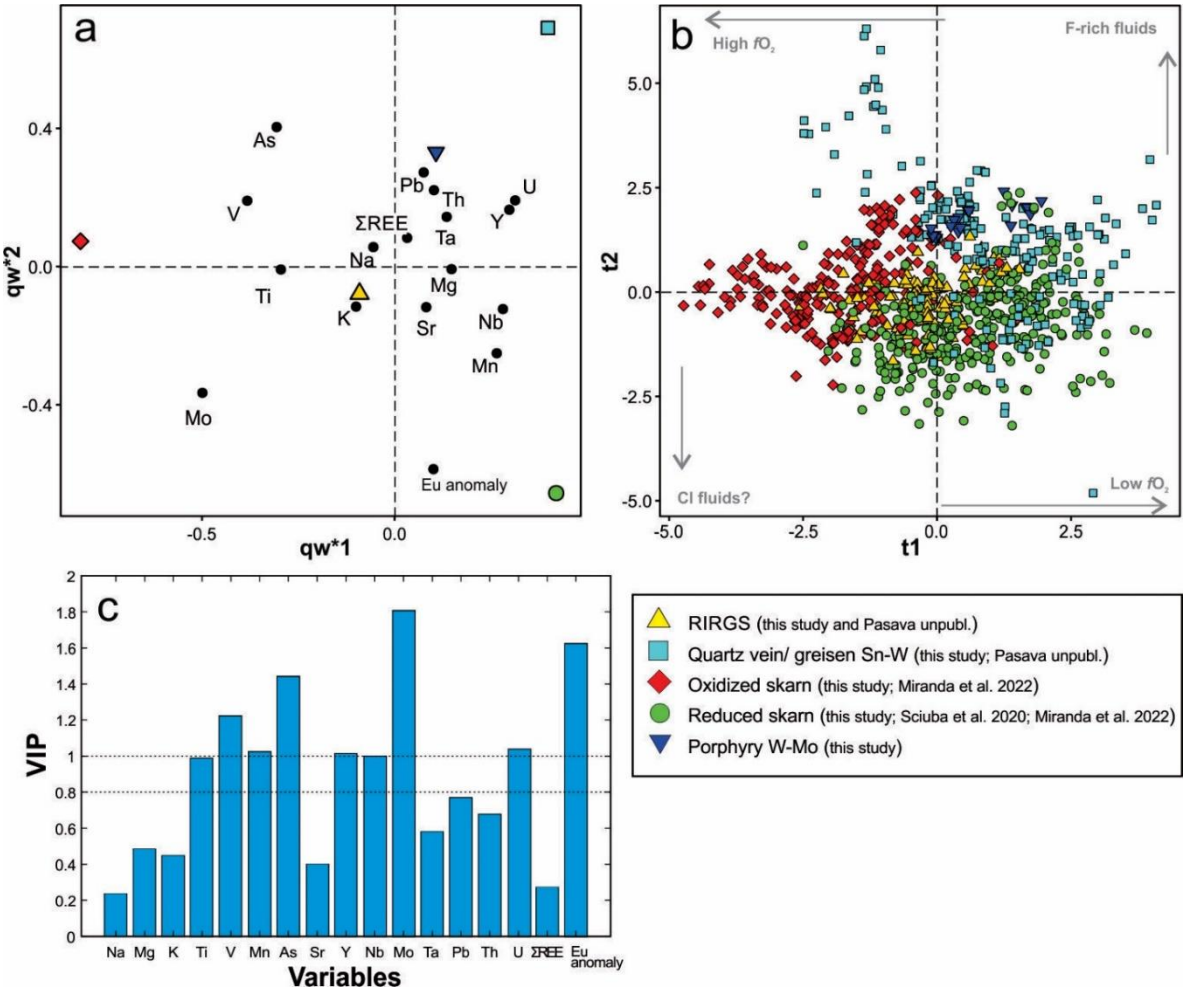

Figure 2.8 Partial least-squares discriminant analysis (PLS-DA) of LA-ICP-MS data for scheelite from magmatic-hydrothermal deposits. a. qw*1–qw*2 (first and second loadings) plot showing the correlations among elemental variables and magmatic-hydrothermal deposit types. b. t1–t2 (first and second scores) plot showing the distribution of scheelite analyses in the latent variable space defined by qw*1–qw*2. c. Variable Importance on Projection (VIP) plot showing the importance of compositional variables in the PLS-DA model.

2.7.2 PLS-DA of scheelite-bearing samples from magmatic-hydrothermal and orogenic settings

Figure 2.9 displays PLS-DA results of compositional variation of scheelite from magmatic-hydrothermal and orogenic settings. The loadings plots of the first and second (qw*1-qw*2; Fig. 2.9a), and first and third (qw*1-qw*3; Fig. 9c) components show the relationship between the variables (Na, Mg, Mn, As, Sr, Y, Nb, Mo, Pb, ΣREE and Europium anomaly) and the groups, whereas the scores plot displays the distribution of samples in t1-

t2 (Fig. 2.9b) and t1-t3 (Fig. 2.9d) spaces. Positive correlations exist between Nb and Mn at positive qw*1 and qw*2, Eu anomaly and Sr at negative qw*1 and qw*2, Na, Y and REE at negative qw*1 and positive qw*2 (Fig. 2.9a), and between As, Pb and ΣREE at negative qw*1 and positive qw*3 (Fig. 2.9c). Additionally, scheelite from Corcoesto and Hangar Flats are plotted in the PLS-DA model to compare their chemical affinity to scheelite from diverse deposit types (Fig. 2.9b and d).

Figure 2.9a shows that reduced and oxidized skarns and RIRGS plot at positive qw*1 and negative qw*2 as result of Mo contribution. Quartz-vein/greisen Sn-W and porphyry W-Mo plot at positive qw*1 and qw*2 as result of Nb, Mn, Y and ΣREE contributions. Metamorphic scheelite and orogenic gold plot at negative qw*1 and qw*2 related to Eu anomaly and Sr contributions. Overall, orogenic Au and metamorphic scheelite are mainly discriminated from quartz-vein/greisen Sn-W, porphyry W-Mo, RIRGS and reduced and oxidized skarns by qw*1, due to negative correlation between Sr with Mo and Mn, whereas oxidized and reduced skarns, and RIRGS are mainly discriminated from porphyry W-Mo and quartz-vein/greisen Sn-W by qw*2.

Figure 2.9b shows significant overlaps between orogenic Au and metamorphic scheelite at negative t1 and positive and negative t2, and between reduced skarns and RIRGS scheelite at positive t1 and negative t2. Few analyses of quartz-vein/greisen Sn-W scheelite spread through all the quadrants, but most of them cluster through negative and positive t1 and positive t2. Porphyry W-Mo scheelite clusters at positive t1 and t2, overlapping with few scheelite from reduced and oxidized skarns and from quartz-vein/greisen Sn-W. Oxidized skarn scheelite plots mostly at positive t1 and negative t2 due to high Mo concentrations, with few analyses at positive t2 as result of high Nb and Mn contents. Corcoesto scheelite plots at positive t1 and t2, overlapping with the cluster of quartz-vein/greisen Sn-W scheelite. Hangar Flats scheelite plots mostly at negative t1 and t2, which coincide with the orogenic Au field and metamorphic scheelite.

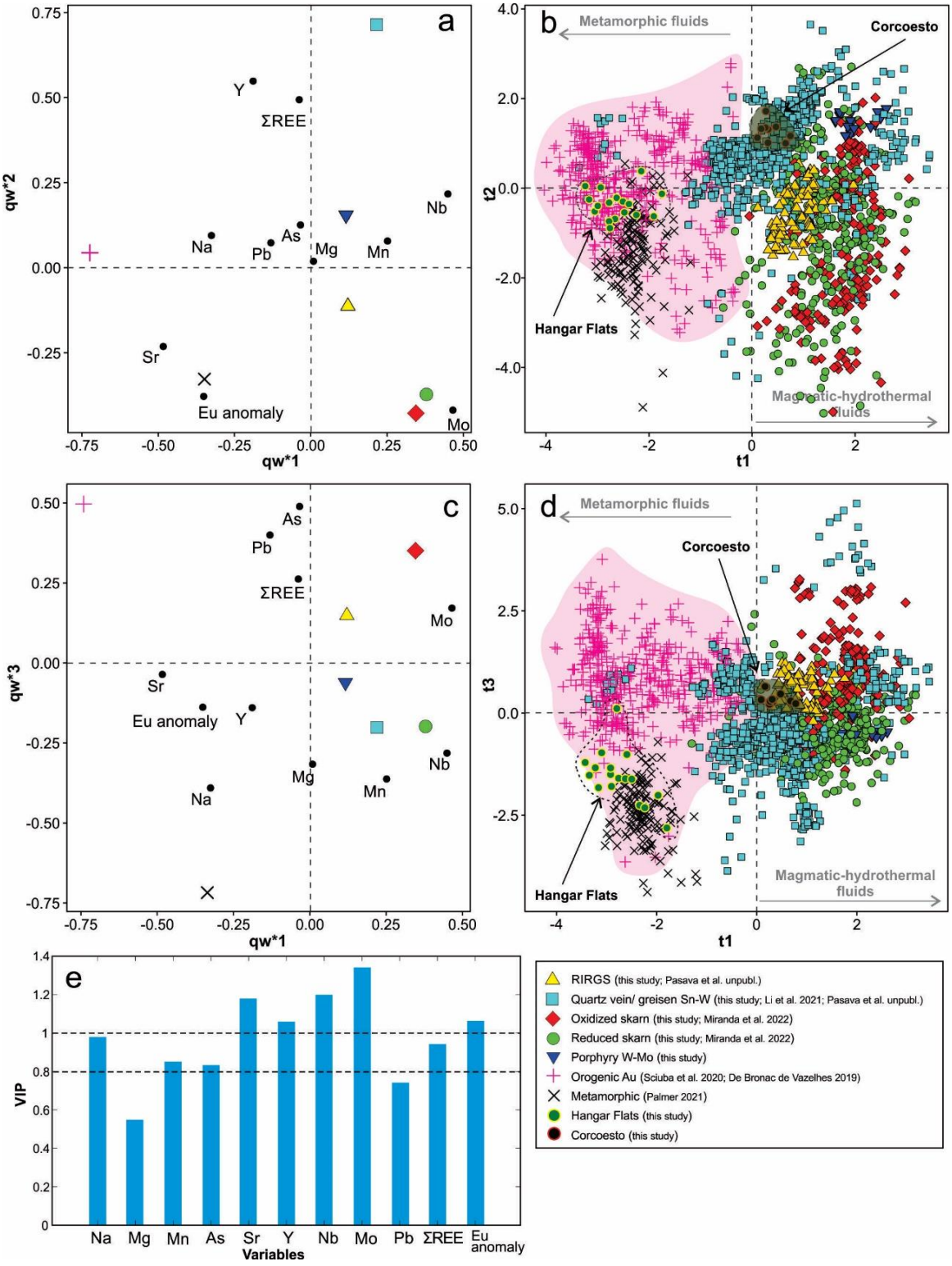

Figure 2.9 Partial least-squares discriminant analysis (PLS-DA) of LA-ICP-MS data for scheelite from orogenic settings and magmatic-hydrothermal deposits. a. qw*1–qw*2 (first and second loadings) and c. qw*1–qw*3 (first and third loadings) plots show the correlations among elemental variables

and orogenic settings and magmatic-hydrothermal deposit types. b. t1–t2 (first and second scores) and d. t1–t3 (first and third scores) plots show the distribution of scheelite analyses in the latent variable space defined by qw*1–qw*2 and qw*1–qw*3, respectively. e. Variable Importance on Projection (VIP) plot showing the importance of compositional variables in the PLS-DA model.

In the qw*1-qw*3 plot (Fig. 2.9c), metamorphic scheelite plots at negative qw*1 and qw*3 as result of Eu anomaly, Na and Mg correlations, whereas orogenic Au plot at positive qw*3 due to correlations among Pb, As and ΣREE. Porphyry W-Mo, reduced skarn and quartz-vein/greisen plot at negative qw*3, whereas oxidized skarn and RIRGS plot at positive qw*3. In the space t1-t3 (Fig. 2.9d), scheelite from all magmatic-hydrothermal deposits overlap each other mostly at positive t1 and positive and negative t3. In contrast, metamorphic scheelite clusters at negative t1 and t3 as result of high Mg and Na contents, whereas orogenic Au scheelite plot mostly at negative t1 and positive t3 with few analysis at negative t3 (Fig. 2.9d). Similar to t1-t2 space, in t1-t3 space Corcoesto scheelite plots closely to scheelite from magmatic-hydrothermal deposits, whereas Hangar Flats scheelite plots between the clusters of metamorphic and orogenic Au scheelite. Overall, Sr, Y, Nb, Mo and Eu anomaly are the most important for the discrimination (VIP>1), followed by Na, Mn, As and ΣREE, with moderate importance (VIP>0.8) (Fig. 2.9e).

2.7.3 Random Forest

Random forest classifier was performed using only scheelite-bearing deposit types (i.e., RIRGS, reduced and oxidized skarns, quartz vein/greisen Sn-W, porphyry W-Mo and orogenic Au deposits) (Appendices 2.5B-2.6B). Metamorphic scheelite was not used in the classifier since it is not a type of deposit, and because all analyses are from the same site (Boanerges Peak). However, it was used as blind data. Therefore, using 70% of the untransformed data to train the RF classifier, 11 variables and 6 deposit classes, RF classifier yields an overall prediction accuracy of 97%. Testing data outcome is summarized in the Table 2.3 and the variable importance shown in the figure 2.10.

Table 2.3 Confusion matrix of the Random Forest model testing data.

		Predicted							
		RIRGS	Porphyry W-Mo	Quartz-vein/ Greisen W-Sn	Oxidized skarn	Reduced skarn	Orogenic gold	Sum	% correctly classified
Reference	RIRGS	**33**		1		3		37	89.2
	Porphyry W-Mo		**6**					6	100.0
	Quartz-vein/Greisen W-Sn			**223**		1	4	228	97.8
	Oxidized skarn	1			**63**	1		65	96.9
	Reduced skarn				2	**101**		103	98.1
	Orogenic gold			1			**137**	138	99.3
								Accuracy	**97%**

Molybdenum, Nb, Sr, Y, Pb and As have the highest mean decrease Gini score followed by Mn, Na and ΣREE. Europium anomaly and Mg display the lowest scores (Fig. 2.10). The confusion matrix (Table 2.3) shows accuracies higher than 89% for all deposit types, where 89.2% of RIRGS, 100% of porphyry W-Mo, 97.8% of quartz-veins/greisen Sn-W, 96.9% of oxidized skarns, 98.1% of reduced skarns and 99.3% of orogenic Au of the test data were correctly classified. The highest misclassified prediction was for RIRGS, where approximately 8% of the test data were classified as reduced skarn, and 3% as quartz-veins/greisen Sn-W. All other analyses misclassifications are below 3% (Table 2.3).

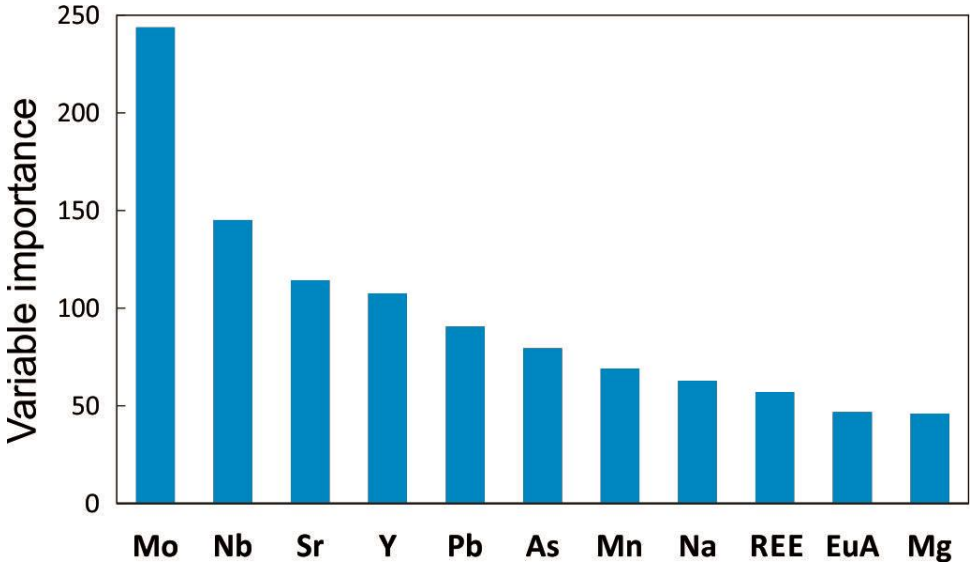

Figure 2.10 Bar plot showing the variable importance for the RF classification model.

Figure 2.11 and tables 2.4 and 2.5 show the prediction results for the scheelite from Hangar Flats and Corcoesto and for blind data, which includes scheelite from orogenic Au (Cave 2016; Cave et al. 2017; Liu et al. 2021) and W greisen and oxidized skarn deposits (Huang et al. 2022), and metamorphic scheelite (Cave et al. 2017; Palmer 2021) (Appendix 2.3B). All scheelite analyses (100%) from Hangar Flats, Majiaxao and Paradise were correctly predicted as orogenic Au (Tables 2.4 and 2.5). Approximately 98% of scheelite from The Ovens were correctly predicted as orogenic Au and 2% misclassified as RIRGS, whereas ~63% of the ones from Mt. Judah scheelite were correctly classified as orogenic Au and 37% misclassified as RIRGS and reduced skarn (Table 2.4; Fig. 2.11). Scheelite from Xiadian displays the smallest percentage of correct predictions, where nearly only 11% of scheelite analyses were classified as orogenic Au, and 89% were misclassified as quartz-vein/greisen Sn-W (Table 2.4; Fig. 2.11). On the other hand, scheelite from Corcoesto was

predicted mostly as quartz-vein/greisen Sn-W (77%) and as reduced skarn (23%) instead of orogenic Au (Fig. 2.11).

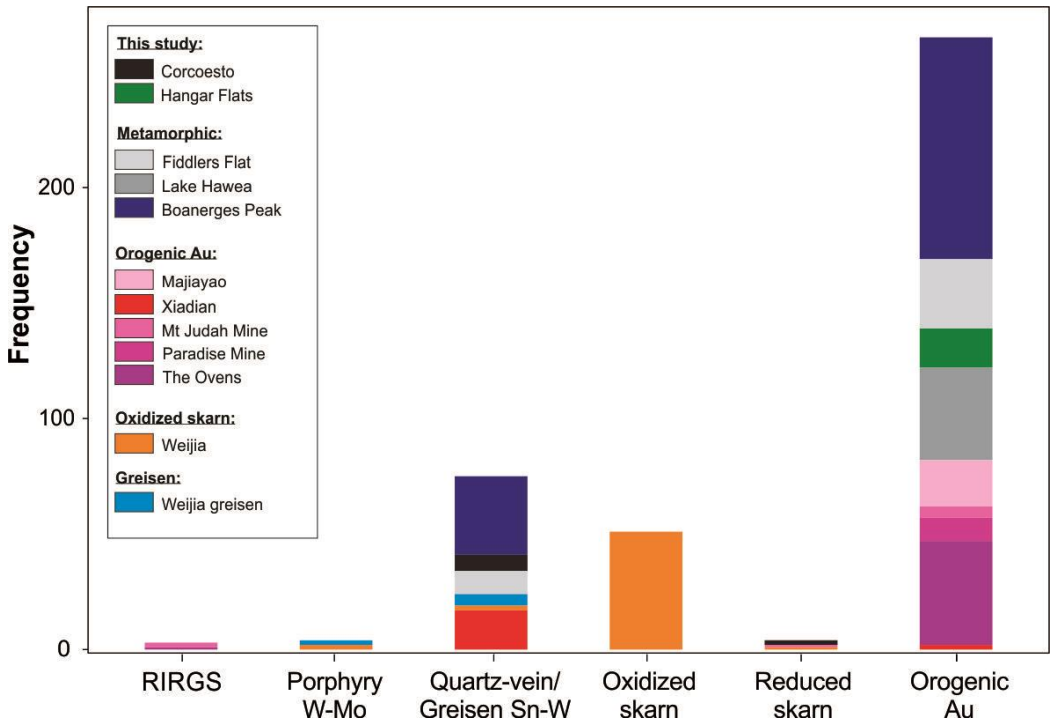

Figure 2.11 Histogram of the predicted classification frequencies of RF on Hangar Flats, Corcoesto, orogenic gold and skarn deposits and metamorphic scheelite. (References in Appendix 2.2B).

In Weijia greisen- and skarn-type W deposit, 71.4% of scheelite hosted in quartz-vein/greisen were correctly classified whereas the 28.6% remaining were misclassified as porphyry W-Mo (Table 2.4; Fig. 2.11). Yet for those scheelite hosted in skarns, ~91% were correctly classified as oxidized skarns and ~9% as porphyry W-Mo, quartz-vein/greisen Sn-W and reduced skarn (Fig. 2.11; Table 2.4). Seventy-five percent of Fiddlers Flat, 100% Lake Hawea and 73% of Boanerges Peak metamorphic scheelite were predicted as orogenic Au (Table 2.5). The remaining data was predicted as quartz-vein/greisen Sn-W (Fig. 2.11).

2.8 Discussion

2.8.1 Trace element incorporation and REE patterns

Trace element composition of scheelite depends on fluid and host rock compositions, temperature, pressure, fO_2, pH, crystallographic control and the partition coefficients

between fluid, scheelite, and co-precipitating minerals (Ghaderi et al. 1999; Brugger et al. 2002; Song et al. 2014; Sciuba et al. 2020). Scheelite ($CaWO_4$) forms a complete solid solution with powellite ($CaMoO_4$), where Mo^{6+} replaces W^{6+} at moderate to high fO_2 (Hsu and Galli 1973; Hsu 1977; Tyson et al. 1988). Niobium^{5+}, Ta^{5+}, As^{5+} and V^{5+} are substitute for W^{6+} following the substitution described below, whereas divalent cations (Sr^{2+}, Eu^{2+}, Mn^{2+}, Pb^{2+} and Mg^{2+}) are readily incorporated into Ca-site due their similarities to Ca^{2+}.

Additionally, scheelite contains significant amounts of ΣREE^{3+} and Y^{3+} that are substitute for Ca^{2+} through three main mechanisms (Nassau 1963; Burt 1989; Ghaderi et al. 1999):

(1) $2Ca^{2+} = Na^{+} + (REE,Y)^{3+}$

(2) $W^{6+} + Ca^{2+} = (Nb,Ta,As,V)^{5+} + (REE,Y)^{3+}$

(3) $3Ca^{2+} = 2(REE,Y)^{3+} + \square Ca$, where $\square Ca$ is a vacancy site.

Gadheri et al. (1999) suggested that the different mechanisms of ΣREE-Y substitution would lead to distinct REE patterns in scheelite. In equation (1) for example, Na provides charge balance to maintain crystal neutrality and Na content should be equal to that of ΣREE and Y. As result, because of Ca-site size restrictions, the MREE would be preferentially incorporated into scheelite, resulting thus in a concave REE pattern. Brugger et al. (2002) questioned this statement and showed that even at low Na content, a simple positive correlation between Na and REE-Y, should be necessary to explain the REE-Y incorporation. Our results show that although Na content is lower than that of ΣREE-Eu+Y (Fig. 2.5a), their positive correlation suggests that REE-Y are partially incorporated by Na charge balance. In addition, we did not notice a direct relation between the concave REE pattern and the Na concentration of scheelite predicted if only equation (1) accounts for the REE content of scheelite.

The correlation between Nb+Ta versus ΣREE-Eu+Y (Fig. 2.5b) supports that REE-Y incorporation is also partially governed by equation (2), because scheelite from all deposit types but RIRGS show strong positive correlation between Nb-Ta and ΣREE-Y (r^2= 0.75 and 0.92; Fig. 2.5b). Additionally, given that few scheelite contain higher ΣREE-Y contents relative to Nb-Ta, at least part of the REE-Y substitution should be controlled by equation (3).

Figure in Appendix 2.1A shows that scheelite from Mawchi, Felbertal, Obří důl, Dublin Gulch and Čelina deposits display shallow negative slope and flat to concave REE patterns that are similar to that of the felsic intrusions related to the mineralization, suggesting that the exsolved mineralizing fluid REE patterns is controlled by the chemistry of the ore-related intrusions and reflected by the REE concentration of scheelite grains. This supports that scheelite REE patterns are, at least for some case, directly controlled by fluid chemistry regardless of the substitution mechanism controlling the REE incorporation in scheelite.

Table 2.4 Proportions of RF classification model predictions for scheelite from orogenic Au deposits and W greisen and skarn. The overall accuracy counts the predictions of orogenic Au and Weijia deposits.

Name	Deposit type	% Correct	Number correctly classified	Number misclassified	Number of analysis
Majiaxao	Orogenic Au	100	20	0	20
Xidian	Orogenic Au	10.5	2	17	19
Mt. Judah	Orogenic Au-W	62.5	5	3	8
Paradise	Orogenic Au	100	10	0	10
The Ovens	Orogenic Au	97.8	45	1	46
	Total Orogenic Au	**74.2**			
Weijia	Quartz-vein/Greisen	71.4	5	2	7
	Oxidized skarn	91.1	51	5	56
	Overall accuracy	**78.9**			

More fractionated REE patterns such as steep negative slope (Obří důl; Appendix 2.1A), positive (Felbertal; Appendix 2.1A) and convex shapes (Traversella; Appendix 2.1A) or those that differ from the REE pattern of the magmatic source (Nui Phao and Northern Dancer; Appendix 2.1A) suggest that the fluid REE pattern do not always reflect the one of its magmatic source and that other processes (i.e., co-precipitation of other mineral phase, type of ligands, salinity) affect the REE pattern of formed scheelite (Haas et al. 1995; Brugger et al. 2000; Migdisov et al. 2016; Miranda et al. 2022).

Miranda et al. (2022) showed that steep negative slope REE pattern is strongly associated with prograde scheelite from oxidized skarns. This has been interpreted as the

high-salinity fluids involved in the formation of the prograde scheelite as high Cl concentration favor the transport of LREE over HREE in mineralizing fluid (Haas et al. 1995; Migdisov et al. 2016). Although there is no available information about fluid salinity of the oxidized skarns studied here, we suggest that the similar HREE depletion observed in scheelite from oxidized skarns can result of the same mechanism.

Additionally, Miranda et al. (2022) also pointed out that shallow negative slope REE pattern with a marked depletion between Dy-Lu results from clinopyroxene co-precipitation, which leads to a depletion of Dy-Lu in the fluid. Brugger et al. (2000) emphasized that the occurrence of MREE-depleted/convex REE pattern in scheelite would be explained by scheelite precipitation itself in a closed-system, which preferentially incorporates MREE over LREE and HREE (Li et al. 2018; Poulin et al. 2018). A similar argument is presented by Cave et al. (2017) for scheelite from quartz-vein and metasedimentary rocks in the Otago Schist, which display positive slope REE pattern (Palmer 2021). Therefore, the occurrence of fractionated REE patterns such as convex shape and positive slope REE patterns likely results from the precipitation of REE-bearing minerals, during the evolution of hydrothermal systems.

2.8.2 Eu anomaly

Similar to REE patterns, the Eu anomaly in scheelite is often interpreted as inherited from the mineralizing fluid and reflects the fluids source (Ghaderi et al. 1999; Song et al. 2014). Magmatic-derived fluids commonly display negative Eu anomaly as a result of plagioclase crystallization (Banks et al. 1994; Barker et al. 2004). As shown in Appendix 2.1A, scheelite displays similar Eu anomaly, as well as REE patterns, to that of the related intrusion (Mawchi, Felbertal, Obří důl, Traversella, Dublin Gulch, Čelina and Northern Dancer), suggesting that in part, scheelite Eu anomaly is inherited from the fluid source. However, few scheelite from reduced skarns, RIRGS and quartz-vein/greisen yield weak to strong positive Eu anomalies (Figs. 2.5c and Appendix 2.1A), implying that factors such as temperature, pH, and fO_2 of the hydrothermal fluids, as well as the breakdown of Ca-bearing minerals during fluid-rock interaction control Eu^{2+}/Eu^{3+} ratio of the fluids, and consequently in scheelite (Bau 1991; Ghaderi et al. 1999; Brugger et al. 2000; 2008; Song et al. 2014; Sun and Chen, 2017; Sun et al., 2019; Wu et al., 2019; Yuan et al., 2019).

Accurately estimating which factor influenced most of the changes in Eu anomalies is challenging given that we do not have detailed information about fluid composition of the studied samples. However, correlations among Eu anomaly, Sr and Mo, and the REE patterns may suggest that fluid-rock interaction and fO_2 have a control on the Eu anomaly (Brugger et al. 2000,2008; Song et al. 2014). Previous studies have shown that the breakdown of Ca-bearing minerals, such as plagioclase to form mica during fluid-rock interaction, releases Eu and Sr into the fluid (Sverjensky 1984; Yuan et al. 2019). So, a progressive increase of Sr contents coupled with smaller of the negative Eu anomalies in scheelite may be a result of the progressive breakdown of plagioclase. The positive relationship between Eu anomaly and Sr in scheelite from quartz-vein/greisen Sn-W deposits in which feldspath-destructive phyllic alteration supports this hypothesis (Fig. 2.5c). On the other hand the same does not occur in few scheelite from reduced skarns and RIRGS (Fig. 2.5c).

Table 2.5 Proportions of RF classification model predictions for scheelite from Corcoesto, Hangar Flats, Fiddlers Flat, Lake Hawea and Boanerges Peak.

Name	Deposit type	% Correct	Number correctly classified	Number misclassified	Number of analysis
Corcoesto	Orogenic Au	0	0	9	9
Hangar Flats	Orogenic Au	100	17	0	17
Fiddlers Flat	Metamorphic	75*	30	10	40
Lake Hawea	Metamorphic	100*	40	0	40
Boanerges Peak	Metamorphic	73.8*	96	34	130
Overal prediction for metamorphic scheelite only		**83**			

*percentage predicted as orogenic Au

Molybdenum content in scheelite is often used as a proxy of fO_2 (Hsu and Galli 1973; Hsu 1977). Under reduced conditions Mo occurs as Mo^{4+} and is not compatible in the scheelite structure, thus forming molybdenite, whereas under more oxidized conditions Mo occurs as Mo^{6+} and substitutes for W^{6+}. As result, low Mo concentrations in scheelite reflects reduced conditions, whereas high Mo content reflects more oxidized conditions (Song et al. 2014; Poulin et al. 2018; Miranda et al. 2022). Therefore, the combination of both Eu anomaly and Mo can provide clues about the redox conditions in the scheelite-related mineralizing systems. Figure 2.5d shows decreasing Mo content with increasing positive Eu

anomalies in scheelite from RIRGS and for few reduced skarns, which might suggest that reduced condition favor positive Eu anomalies in scheelite. Additionally, few scheelite from quartz-vein/greisen Sn-W deposits with positive Eu anomalies contains very low contents of Mo (<10 ppm), suggesting low fO_2 in the fluids as well.

2.8.3 Chemical variation in scheelite from distinct magmatic-hydrothermal deposit types

Figure 2.8 shows that despite overlaps, scheelite composition varies as function of the magmatic-hydrothermal deposit types and that V, Mn, As, Nb, Mo, Ta, Th, U and Eu anomaly are the most important variables for discrimination (Fig. 2.8c). This suggests that hydrothermal processes and physico-chemical conditions of the mineralizing fluids typical of the different deposits type control the incorporation of V, Mn, As, Nb, Mo, Ta, Th and U in scheelite. On the other hand, Na, Mg, K, Ti, Sr and REE are apparently less important variables for deposit type discrimination (Fig. 2.8c), suggesting that the occurrence of these elements in scheelite was controlled by similar parameters in the different deposit types. Given that in all deposits scheelite precipitated from magmatic-related fluids, those elements are probably reflecting the source of the fluids instead of variation and physico-chemical conditions triggering scheelite precipitation.

Tungsten mineralization is typically associated with fractionated felsic magmas that form under slightly oxidized to reduced fO_2 conditions (Newberry and Swanson 1986; Candela 1992; Wood and Samson 2000). Miranda et al. (2022) showed that scheelite from oxidized skarns distinguished from that of reduced skarns based on high Mo, As and V concentrations as a result of oxidized magmatic-derived fluids. In contrast, scheelite from reduced skarns is characterized by low Mo, As and V, and high Mn and Nb contents due to reduced conditions of the ore-related intrusions. Thus, the chemical signature of scheelite seems to have a potential to trace the oxygen fugacity of the ore-related intrusions. In fact, the PLS-DA results show that oxidized skarns have high Mo, As and V concentrations (Fig. 2.8a), implying that scheelite was formed under high fO_2. In contrast, quartz-vein/greisen Sn-W and reduced skarns plot at the right side of the diagram as a result of high Mn and Nb contents, indicating low fO_2, which agrees with the oxidation state of the ore-related intrusions (references in Tables 2.1 and Appendix 2.2B). Therefore, qw*1 separates scheelite-bearing deposit types as a function of the oxidation state of their ore-related intrusions. Additionally, RIRGS and porphyry W-Mo deposits plot between these two end-

members, suggesting thus intermediate fO_2 conditions of the source intrusion relative to reduced and oxidized skarns related intrusions.

Additionally, porphyry W-Mo and quartz-vein/greisen Sn-W are characterized by high Th, U, Ta, Y and Pb contents, which discriminate them from oxidized skarns and RIRGS (Figs. 2.4, 2.8, and Appendix 2.2A). The high concentrations of Th, U, Ta, Y and Pb in scheelite is likely related to the high content of fluorine in the mineralizing fluids common in quartz-vein/greisen Sn-W deposits (Pollard et al. 1987; Breiter et al. 2017; Song et al. 2019; Pan et al. 2019; Wang et al. 2021). It has been demonstrated that fluorine increases the solubility of REE, Y and HSFE in magma (Keppler 1993; Agangi et al. 2010). As a result, REE-, Y- and HSFE-rich fluids exsolved from those intrusions can precipitate minerals that having high REE, Y, Pb, Nb, Ta, U and Th concentrations, such as scheelite. The occurrence of abundant fluorite in scheelite-bearing samples from porphyry W-Mo and quartz-vein/greisen Sn-W deposits support this hypothesis (Table 2.1).

2.8.4 Chemical variations in scheelite from distinct fluid sources: magmatic vs metamorphic

Orogenic Au deposits and metamorphic scheelite are characterized by low Mo, Nb and Mn, high Sr and Na contents, with commonly positive Eu anomalies (Fig. 2.6 and 2.9). In contrast, scheelite from magmatic-hydrothermal settings have higher Mo, Nb and Mn, lower Sr and Na contents, and both negative and positive Eu anomalies (Figs. 2.6 and 2.9). The distinct contents of these elements in scheelite are mainly a function of fluid source (magmatic vs metamorphic) and of the physico-chemical conditions inherent to each deposit type, supporting thus the use of scheelite composition as a fluid-source tracker (Fig. 2.9). It is noteworthy to point that although RIRGS and orogenic Au deposits share several similar features such as low salinity, CO_2-rich and reduced fluids and anomalous Te, W and Bi signature (Baker 2002; Goldfarb et al. 2005; Hart 2007), our results show that scheelite associated with RIRGS is chemically distinct to those from orogenic Au deposits characterized by the higher Mo, Nb and Mn contents (Fig. 2.9b), consistent with the distinct fluid sources for both deposit types.

The low Mo content (<100 ppm) and characteristic positive Eu anomaly displayed by scheelite from orogenic settings (Fig. 2.12a) support a relatively reduced metamorphic-derived fluids relative to magmatic-derived fluids, which are more oxidized (Song et al. 2014;

Poulin et al. 2018; Sciuba et al. 2020). The high Sr content in metamorphic and orogenic Au scheelite results from the release of Sr during the breakdown of Ca-bearing minerals hosted in metasediments and/or mafic-ultramafic volcanic rocks (Paterson and Rankin 1979; Kempe et al. 2001), whereas the low concentrations of Nb and Mn are in function of their low concentration in the host rocks (Sciuba et al. 2019). In contrast, the low concentration of Sr in magmatic-hydrothermal scheelite reflect the low content of Sr from exsolved magmatic-derived fluids that are depleted in Sr due to plagioclase crystallization during differentiation of their source magmas (Miller and Mittlefehldt 1984), whereas Nb and Mn have an incompatible behavior relative to Sr, thus becoming enriched in the magma during fractional crystallization, and consequently become concentrated in the mineralizing fluid compared to metamorphic fluids (Fig. 2.6a-c; Miller and Stoddard 1981; Shae and Chappell 1999; Picolli and Cadela 2002; Seo et al. 2020). As a result, scheelite from magmatic-hydrothermal settings contains higher Nb and Mn contents relative to those from orogenic settings (Figs. 2.6a, d-e and 2.9).

Additionally, Figs. 2.9c-d highlight that metamorphic scheelite contains low ΣREE, As and Pb contents relative to those associated with gold mineralization, thus allowing their discrimination as show Figs. 2.12c-d. Palmer et al. (2022) pointed out that the low ΣREE, Pb and As contents in metamorphic scheelite from the Otago schist is likely related to local host rock compositions which are poor in these elements, and/or to the low metamorphic conditions (sub- to low-greenschist facies), which do not allow the release these elements from their host minerals (Cave et al. 2017). Moreover, Sr isotopic ratios reveal that scheelite that is not associated with gold displays a heterogeneous isotopic signature that arises from local variations of the host rocks and small amounts of fluid flow. On the other hand, scheelite that formed temporally and spatially associated with gold displays a homogeneous signature, which results from fluids derived from a distal source with long fluid flow pathway (Scanlan et al. 2018; Palmer et al. 2022).

In summary, metamorphic grade conditions, host rock composition and the transport of fluids along variable pathways are essentials factors controlling gold mineralization in orogenic settings, which are recorded in scheelite chemistry (Cave et al. 2017; Scanlan et al. 2018; Sciuba et al. 2020; Palmer 2021). The compatibility of Sr and Eu during felsic magma crystallization and the abundance of Mo, Nb and Mn either due to fO_2 or incompatible behavior of these elements during magma crystallization contribute to discriminate scheelite from distinct mineral deposit types (Figs. 2.6, 2.8, 2.9 and 2.12).

2.9 Implications for mineral exploration

Previous studies have attempted to use scheelite chemistry to differentiate deposit types through binary diagrams or multivariate methods (Song et al. 2014; Poulin et al. 2018; Sciuba et al. 2020; Miranda et al. 2022). Binary diagrams have become less effective especially for those scheelite that form under similar hydrothermal conditions (i.e., RIRGS vs reduced skarns; Fig. 2.6). Alternatively, the combination of several variables with supervised classification methods have shown great improvement in the results, allowing a better discrimination among different scheelite-bearing deposits (Figs. 2.8 and 2.9), even with limited literature data (Sciuba et al. 2020). Our results show that, although PLS-DA is useful for discrimination and to understand the correlation between variables and samples, there are still overlaps between scheelite from magmatic-hydrothermal and orogenic settings (Figs. 2.8 and 2.9).

Recent studies show that the RF classifier is an effective tool for mineral deposit discrimination and prediction (O'Brien et al. 2015; Gregory et al. 2019; Liu and Beaudoin 2021; Bédard et al. 2022; Caraballo et al. 2022; Nathwani et al. 2022). The high overall accuracy of testing data prediction (97%) proves the efficiency of the RF classifier to predict mineral deposit types based in scheelite composition.

Scheelite from Corcoesto Au deposit has similar contents of Mo, Mn and Nb to that of worldwide orogenic Au deposits (Fig. 2.6), but its low Sr content made it classified as quartz-vein/greisen Sn-W and as reduced skarn in both PLS-DA and RF models, since Sr is an important element for discrimination of scheelite between orogenic gold and magmatic-hydrothermal deposits (Figs. 2.9 and 2.10). Similar to Variscan Au deposits in Western Europe (Castromil, Limarinho and Penedono), the Corcoesto Au deposit is shear-hosted, developed along strike-slip fault systems linked to late stages of the Variscan orogeny (Boiron et al. 2003; Vallance et al. 2003; Fuertes-Fuente et al. 2016; Neiva et al. 2019) and are sometimes associated with greisenisation of the host rocks, a characteristic of quartz-vein/greisen Sn-W deposits (Vallance et al. 2003). In addition, in these deposits Au deposition is linked to mixing between ascending metamorphic fluid with shallow meteoric water (Boiron et al., 2003), and thus the low Sr content of the scheelite may be caused by this input of Sr-poor meteoric water. More studies are needed to confirm this hypothesis. Therefore, these atypical features can partly explain the misclassification of scheelite from Corcoesto Au deposit as reduced skarn or veinz quartz/greisen Sn-W deposits by our PLS-

DA and RF models. It is noteworthy that orogenic gold, reduced skarn and vein quartz/greisen Sn-W deposits formed from more reduced fluids, perhaps providing another explanation for the misclassification of Corcoesto.

Hangar Flats scheelite displays chemical similarities to that from orogenic settings (Figs. 2.9b,d) and is predicted as belong to orogenic Au deposit (Fig. 2.11), agreeing with the findings of Wintzer et al. (2022), who showed that the W mineralization is no related to magmatic-hydrothermal fluids. Moreover, our results also show that Hangar Flats scheelite has low Pb, As and REE contents as does metamorphic scheelite (Figs. 2.4, 2.6, 2.9 and 2.12c). Given the similarity between metamorphic scheelite and Hangar Flats scheelite and considering that the W (57 Ma) or W-Sb (45 Ma) mineralisation postdates the Au mineralization (68-57 Ma) at Hangar Flats (Wintzer et al. 2022), our results may suggest that Hangar Flats scheelite from the first W mineralization formed from the similar types of metamorphic fluids as the Otago metamorphic scheelite (Figs. 2.9 and 2.12).

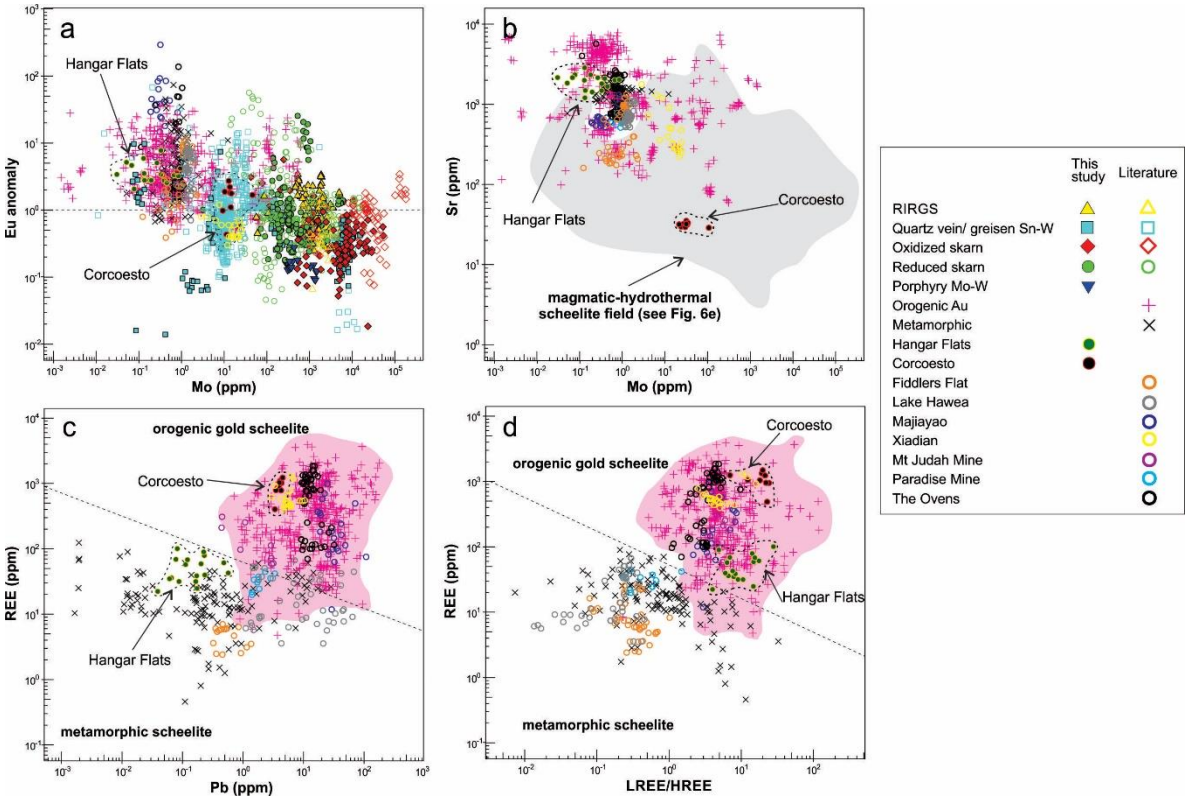

Figure 2.12 Binary plot showing in a. Mo versus Eu anomaly and b. Mo versus Sr for scheelite from magmatic-hydrothermal and orogenic settings, and in c. Pb versus REE and d. LREE/HREE versus REE for scheelite from orogenic settings only (orogenic gold and metamorphic scheelite). Data from this study and literature, references in Appendix 2.2B and 2.3B.

Most of scheelite analysis from Majiaxao, Mt. Judah, Paradise and The Ovens orogenic Au deposits and Weija skarn-type were correctly classified (Table 2.4; Fig. 2.11). In contrast, ~11% of Xiadian scheelite were predicted as orogenic Au, agreeing with literature classification (Li et al. 2021), whereas most of analyses (89%) were classified as quartz-vein/greisen Sn-W. As show in Figure 2.12a-b, Xiadian scheelite displays intermediate Mo and Sr contents relative to orogenic gold and magmatic-hydrothermal deposits, with mostly negative Eu anomalies, which make it more similar to scheelite from quartz-vein/greisen Sn-W. According to the authors, the Sr and Pb isotope signatures of scheelite and galena, respectively, at Xiadian revealed mixed reservoir sources originated from the nearby granite and metasediments (Li et al. 2021), which may explain classification as quartz-vein/greisen Sn-W and part of orogenic Au deposits.

Although the RF model does not contain metamorphic scheelite in the classification, the prediction of metamorphic scheelite as orogenic Au type enhances the effectiveness of the RF model to predict scheelite from different geological settings and fluid source (Table 2.5; Fig. 2.11). Moreover, the relation between REE and Pb or LREE/HREE are useful to discriminate orogenic gold scheelite from metamorphic scheelite (Figs. 2.12c,d). Although metamorphic scheelite does not occur associated with gold (Cave et al. 2017; Scanlan et al. 2018; Palmer 2021), the occurrence of this type of scheelite in glacial, aeolian and stream sediments provide evidence of metamorphic terrains that may contains resources of W as is the case of Otago schist, New Zealand (e.g., Glenorchy, Mutch 1969; Palmer 2021).

2.10 Conclusion

Our study highlights that scheelite composition varies following source of hydrothermal fluids and deposit types, supporting its use as a mineral deposit type discriminator and its application to mineral exploration targeting. Texturally, scheelite varies from fine- to coarse-grained regardless the deposit type. Scheelite from RIRGS is predominantly homogenous under CL images, whereas in the others deposits it varies from homogenous to zoned. Trace element compositions reveal that scheelite display 6 REE patterns with predominantly negative Eu anomaly, which result from different magma composition, salinity and co-genetic REE-bearing minerals. Few scheelite display positive Eu anomalies that is likely due to fluid-rock interaction, and changes in pH, fO_2 and temperature. The PLS-DA highlights that scheelite from magmatic-hydrothermal deposits vary in composition as a result of fluid fO2 and composition. The low Sr and Eu content of

magmatic-related scheelite due to the compatible behavior of these elements during felsic magma fractionation, and the relative high abundance of Mo, Nb and Mn in magmatic-related scheelite allow to discriminate them from scheelite form by metamorphic fluids in orogenic settings. Metamorphic scheelite with no temporal association with Au contains lower REE, As and Pb contents and LREE/HREE ratio relative to that associated with Au that is likely related to local source for hydrothermal fluids, host rock compositions and low metamorphic grade. Based on the concentrations of Na, Mg, Mn, As, Sr, Y, Nb, Mo, Pb, REE and Eu anomalies in scheelite, a Random Forest classifier yields an overall accuracy of 97%. Predictions from literature data show the effectiveness of the Random Forest scheelite model in predicting mineral deposit types and geological settings, supporting its application as an effective tool for mineral exploration.

2.11 Acknowledgments

This research was supported by the Natural Sciences and Engineering Research Council (NSERC) of Canada, Agnico Eagle Mines Ltd., and Ministère de l'Énergie et des Ressources Naturelles du Québec. It is also a contribution to the RENS project (TAČR SS02030023). We would like to thank David Poole (Kinross Gold Corporation), Lara Lewis (Yukon Geological Survey), Khin Zaw (University of Tasmania), Niki Wintzer (USGS), Christopher Dail (Midas Gold Corporation), Franco Pirajno, Olivier Rabeau (Universite Laval), Karsten Aupers (Wolfram Bergbau und Hütten AG) and František Veselovský (Czech Geological Survey) for providing some of the samples, and Marc Choquette (Université Laval), Dany Savard and Audrey Lavoie (Université du Quebec à Chicoutimi) for their assistance with EPMA and LA-ICP-MS analyses.

2.12 References

Allegro, G.L., 1987. The Gilmore Dome tungsten mineralization, Fairbanks mining district, Alaska: University of Alaska Fairbanks, M.S. thesis, 150 p., illust., maps, 7 folded maps.

Agangi, A., Kamenetsky, V. S., McPhie, J., 2010. The role of fluorine in the concentration and transport of lithophile trace elements in felsic magmas: Insights from the Gawler Range Volcanics, South Australia, Chemical Geology 273, 314-325. https://doi.org/10.1016/j.chemgeo.2010.03.008.

Andersson, S., Wagner, T., Jonsson, E., Fusswinkel, T., Whitehouse, M., 2019. Apatite as a tracer of the source, chemistry and evolution of ore-forming fluids: The case of the Olserum-Djupedal REE-

phosphate mineralisation, SE Sweden, Geochimica et Cosmochimica Acta, 255, 163-187 https://doi.org/10.1016/j.gca.2019.04.014.

Auwera, J.V., and Andre, L., 1991. Trace elements (REE) and isotopes (O, C, Sr) to characterize the metasmatic fluids sources: evidence from the skarn deposit (Fe, W, Cu) of Traversella (Ivrea, Italy). Contrib Mineral Petrol, 106:325-339.

Baker, T., 2002. Emplacement depth and carbon dioxide-rich fuid inclusions in intrusion-related gold deposits: Economic Geology, 97, p. 1111–1117.

Baker, T., Achterberg, E.V., Ryan, C.G., Lang, J.R., 2004. Composition and evolution of ore fluids in a magmatic-hydrothermal skarn deposit. Geology 32(2):117–120

Ball, C.W., 1954. The Emerald, Feeney and Dodger tungsten ore-bodies, Salmo, British Columbia, Canada. Economic Geology, 49, 625–638.

Ballard, J.R., Palin, M.J., Campbell, I.H., 2002. Relative oxidation states of magmas inferred from Ce(IV)/Ce(III) in zircon: application to porphyry copper deposits of northern Chile. Contrib Mineral Petrol 144, 347–364. https://doi.org/10.1007/s00410-002-0402-5.

Banks, D.A., Yardley, B.W.D., Campbell, A.R., Jarvis, K.E., 1994. REE composition of an aqueous magmatic fluid: A fluid inclusion study from the Capitan Pluton, New Mexico, U.S.A., Chemical Geology, 113, 259-272, https://doi.org/10.1016/0009-2541(94)90070-1.

Barnes, S. J., Mansur, E. T., Pagé, P., 2022. Differences in composition of chromites from low-Ti and high-Ti picrites of the Emeishan Large Igneous Province and comparison with chromites of the UG-2 platinum-deposit of the Bushveld complex. Lithos, 412, 106613.

Bau, M., 1991. Rare earth element mobility during hydrothermal and metamorphic fluid-rock interaction and the significance of the oxidation state of europium. Chem Geol 93:219–230

Bédard, É., De Bronac de Vazelhes, V., Beaudoin, G., 2022. Performance of predictive supervised classification models of trace elements in magnetite for mineral exploration. Journal of Geochemical Exploration 236:106959. doi: doi.org/10.1016/j.gexplo.2022.106959.

Belousova, E.A., Griffin, W.L., O'Reilly, Y., Fisher, N.I., 2002. Apatite as an indicator mineral for mineral exploration: trace-element compositions and their relationship to host rock type. Journal of Geochemical Exploration, 76, 45-69, https://doi.org/10.1016/S0375-6742(02)00204-2

Bulm, J.D., 1985. A petrologic and Rb–Sr isotopic study of intrusive rocks near Fairbanks, Alaska. Canadian Journal of Earth Sciences, 22, 1314-1321.

Boiron, M.C., Cathelineau, M., Banks, D., Yardley, B., Noronha, F., Miller, F.M., 1996. P–T–X conditions of fluid penetration in the basement during retrograde metamorphism and uplift: a multidisciplinary investigation of bulk and individual fluid inclusion chemistry from NW Iberian quartz veins. Geochim. Cosmochim. Acta, 60, pp. 43-57

Boiron, M.C., Cathelineau, M., Banks, D.A., Fourcade, S., Vallance, J., 2003. Mixing of metamorphic and surficial fluids during the uplift of the Hercynian upper crust: consequences for gold deposition, Chemical Geology, Volume 194, Issues 1–3, Pages 119-141, https://doi.org/10.1016/S0009-2541(02)00274-7

Breiman, L., 2001. Random Forests. Machine Learning 45, 5–32 2001. https://doi.org/10.1023/A:1010933404324

Breiter, K., Ďurišová, J., Hrstka, T., Korbelová, Z., Vaňková, M. H., Galiová, M. V., Kanický, V., Rambousek, P., Knésl, I., Dobeš, P., Dosbaba, M., 2017. Assessment of magmatic vs. metasomatic processes in rare-metal granites: A case study of the Cínovec/Zinnwald Sn–W–Li deposit, Central Europe. – Lithos 292-293: 198-217. DOI 10.1016/j.lithos.2017.08.015

Breiter, K, Korbelová, Z., Chládek, Š., Uher, P., Knesl, I., Rambousek, P., Honig, S., Šešulka, V., 2017. Diversity of Ti–Sn–W–Nb–Ta oxide minerals in the classic granite-related magmatic–hydrothermal Cínovec/Zinnwald Sn–W–Li deposit (Czech Republic). *European Journal of Mineralogy,* 29 (4): 727–738. doi: https://doi.org/10.1127/ejm/2017/0029-2650

Brugger , J., Lahaye, Y., Costa, S., Lambert, D., Bateman, R., 2000. Inhomogeneous distribution of REE in scheelite and dynamics of Archaean hydrothermal systems (Mt Charlotte and Drysdale gold deposits, Western Australia). Contrib Mineral Petrol 139:251–264.

Brugger, J., Etschmann, B., Pownceby, M., Liu, W., Grundler, P., Brewe, D., 2008. Oxidation state of europium in scheelite: tracking fluid–rock interaction in gold deposits. Chem Geol 257:26–33.

Brugger, J., Giere, R., Grobety, B., Uspensky, E., 1998. Scheelite-powellite and paraniite-(Y) from the Fe-Mn deposit at Fianel, Eastern Swiss Alps. Am Mineral 83:1100–1110.

Burt, D., 1989. Compositional and phase relations among rare earth elements. Rev Mineral 21:259–307.

Candela, P.A., 1992. Controls on ore metal ratios in granite related ore systems: An experimental and computational approach: Royal Society of Edinburgh Transactions, Earth Sciences, 83, 317–326. doi:10.1017/S0263593300007999.

Caraballo, E., Dare, S. Beaudoin, G., 2022. Variation of trace elements in chalcopyrite from worldwide Ni-Cu sulfide and Reef-type PGE deposits: implications for mineral exploration. Miner Deposita. https://doi.org/10.1007/s00126-021-01091-y

Cave, B.J., 2016. Source of scheelite in the turbidite-hosted orogenic au deposits of Otago, New Zealand: an integrated metamorphic source model explaining the presence or absence of scheelite in turbidite-hosted orongenic au deposits, PhD thesis, University of Tasmania.

Cave, B.J., Pitcairn, I.K., Craw, D., Large, R.R., Thompson, J.M., Johnson, S.C., 2017. A metamorphic mineral source for tungsten in the turbidite-hosted orogenic gold deposits of the Otago Schist, New Zealand. Miner Deposita 52, 515–537. https://doi.org/10.1007/s00126-016-0677-5

Cepedal, A., Fuertes-Fuente, M., Martin-Izard, A., Boixet, L., 2014. Tellurides, sulfides and sulfosalts in the mineral paragenesis of the Corcoesto orogenic gold deposit, NW Spain. Conference: IMA 2014 At: Sudafrica Volume: Abstract Volume ISBN: 978-0-620-60082-8, p 14.

Cooke, D.R., Baker, M., Hollings, P., Sweet, G., Chang, Z., Danyushevsky, L., Gilbert, S., Zhou, T., White, N.C., Gemmell, J.B., Inglis, S., 2014. New Advances in Detecting the Distal Geochemical Footprints of Porphyry Systems—Epidote Mineral Chemistry as a Tool for Vectoring and Fertility Assessments, Building Exploration Capability for the 21st Century, Karen D. Kelley, Howard C. Golden.

Darbyshire, D.P.F., Pitfield, P.E.J., Campbell, S.D.G., 1996. Late Archean and Early Proterozoic gold-tungsten mineralization in the Zimbabwe Archean craton: Rb-Sr and Sm-Nd isotope constraints. *Geology*, 24 (1): 19–22. doi: https://doi.org/10.1130/0091-7613(1996)024<0019:LAAEPG>2.3.CO;2

Dare, S.A.S, Barnes, S.J., Beaudoin, G., 2012. Variation in trace element content of magnetite crystallized from a fractionating sulfide liquid, Sudbury, Canada: Implications for provenance discrimination, Geochimica et Cosmochimica Acta, 88, 27-50, https://doi.org/10.1016/j.gca.2012.04.032.

Dare, S.A.S, Barnes, S.J., Beaudoin, G., 2014. Trace elements in magnetite as petrogenetic indicators. Miner Deposita 49, 785–796.

de Bronac de Vazelhes, V., Beaudoin, G., McMartin, I., Côté-Mantha, O., Boulianne-Verschelden, N., 2021. Assessment of the Amaruq gold deposit signature in glacial sediments using multivariate geochemical data analysis and indicator minerals. J Geochem Explor 228:106800

Dubru, M., Vander Auwera, J., Van Marcke De Lummen, G., and Verkaeren, J., 1988. Distribution of scheelite in magnesian skarns at Traversella (Piemontese Alps, Italy) and Costabonne (Eastern

Pyrenees, France): Nature of the associated magmatism and influence of fluid composition. In Mineral Deposits within the European Community (J. Boissonnas & P. Omenetto, eds.). Society for Geology Applied to Mineral Deposits, Special Publication 6, Springer-Verlag, Berlin, Germany (117–134).

Dupuis, C., Beaudoin, G., 2011. Discriminant diagrams for iron oxide trace element fingerprinting of mineral deposit types. Miner Deposita 46, 319–335. https://doi.org/10.1007/s00126-011-0334-y

Elongo, V., Falck, H., Rasmussen, K.L., Robbins, L.J., Creaser, R.A., Luo, Y., Pearson, D.G., Sarkar, C., Adlakha, E., Palmer, M.C., Scott, J.M., Hickey, K., Konhauser, K., Lecumberri-Sanchez, P., 2022. Ancient roots of tungsten in western North America. *Geology*, 50 (7): 791–795. doi: https://doi.org/10.1130/G49801.1

Eriksson, L., Johansson, E., Kettaneh-Wold, N., Wold, S., 2001. Multi- and megavariate data analysis, principles and applications. UMETRICS, Umea, 425 p

Fuertes-Fuente, M., Cepedal, A., Lima, A., Dória, A., Ribeiro, M.A., Guedes, A., 2016. The Au-bearing vein system of the Limarinho deposit (northern Portugal): Genetic constraints from Bi-chalcogenides and Bi–Pb–Ag sulfosalts, fluid inclusions and stable isotopes. Ore Geol. Reviews, 72: 213-231 https://doi.org/10.1016/j.oregeorev.2015.07.009

Gaspar, M., Knaack, C., Meinert, L., Moretti, R., 2008. REE in skarn systems: a LA-ICP-MS study of garnets. Geochim Cosmochim Acta 72:185–205. https://doi.org/10.1016/j.gca.2007.09.033

George, L., Cook, N., Ciobanu, C., Wade, B., 2015. Trace and minor elements in galena: a reconnaissance LA-ICP-MS study. Am Mineral 100:548–569.

George, L., Cook, N., Crowe, B., Ciobanu, C., 2018. Trace elements in hydrothermal chalcopyrite. Mineral Mag 82(1):59–88.

Ghaderi, M., Palin, J., Campbell, I., Sylvester, P., 1999. Rare earth element systematics in scheelite from hydrothermal gold deposits in the Kalgoorlie-Norseman region, Western Australia. Econ Geol 94:423–437.

Gillerman, V.S., Schmitz, M.D., Benowitz, J.A., Layer, P.W., 2019. Geology and temporal evolution of alteration and Au-Sb-W mineralization, Stibnite mining district, Idaho: Idaho Geological Survey Bulletin 31, 149 p.

Goldfarb, R.G., Baker, T., Dubé, B., Groves, D.I., Hart, C.J.R., Gosselin, P., 2005. Distribution, Character, and Genesis of Gold Deposits in Metamorphic Terran, One Hundredth Anniversary Volume, Jeffrey W. Hedenquist, John F. H. Thompson, Richard J. Goldfarb, Jeremy P. Richards.

Gregory, D.D., Cracknell, M.J., Large, R.R., McGoldrick, P., Kuhn, S., Maslennikov, V.V., Baker, M.J., Fox, N., Belousov, I., Figueroa, M.C., Steadman, J.A., Fabris, A.J., Lyons, T.W., 2019. Distinguishing ore deposit type and barren sedimentary pyrite using laser ablation-inductively coupled plasma-mass spectrometry trace element data and statistical analysis of large data sets. Econ Geol 114(4):771–786.

Grzela, D., Beaudoin, G., Bedard, E., 2019. Tourmaline, scheelite, and magnetite compositions from orogenic gold deposits and glacial sediments of the Val-d'Or district (Quebec, Canada): implications to mineral exploration. J Geochem Explor 206:106355.

Guo, Z., Li, J., Xu, X., Song, Z., Dong, X., Tian, J., Yang, Y., She, H., Xiang, A., Kang, Y., 2016. Sm/Nd dating and REE composition of scheelite for the Honghuaerji scheelite deposit, Inner Mongolia, Northeast China. Lithos 261:307–321.

Haas, J., Shock, E.L., Sassani, D., 1995. Rare earth elements in hydrothermal systems: estimates of standard partial molal thermodynamic properties of aqueous complexes of the rare earth elements at high. Geochim Cosmochim Acta 59:4329–4350.

Hart, C., 2007. Reduced Intrusion-Related Gold Systems. In W D Goodfellow, Mineral Deposits of Canada: a synthesis of major deposittypes, district metallogeny, the evolution of geological provinces, and exploration methods (pp 95–112) Geological Association of Canada, Mineral Deposits Division.

Hart, C.J.R., Baker, T., Burke, M.J., 2000. New exploration concepts for country-rock-hosted intrusion-related gold systems: Tintina Gold Belt in Yukon. In The Tintina Gold Belt: Concepts, Exploration, and Discoveries. British Columbia and Yukon Chamber of Mines Special Volume 2, 145–71.

Hart, C.J.R., McCoy, D.T., Goldfarb, R.J., Smith, M., Roberts, P., Hulstein, R., Bakke, A.A., Bundtzen, T.K., 2002. Geology, exploration and discovery in the Tintina Gold Province. In Goldfarb R. J. & Neilson, R. (eds) Geology, Exploration and Discovery in the Tintina Gold Province, Alaska and Yukon. Society of Economic Geologists Special, 9, 241–74

Hsu, L., 1977. Effects of oxygen and sulfur fugacities on the scheelite tungstenite and powellite-molybdenite stability relations. Econ Geol 72:664–670

Hsu, L.C. and Galli, P.E., 1973, Origin of the scheelite-powellite series of minerals. Economic Geology, 68, 681–696.

Huang, X-D., Lu, J-J., Zhang, R-Q., Sizaret, S., Ma, D-S., Wang, R-C., Zhu, X., He, Z-Y., 2022. Garnet and scheelite chemistry of the Weijia tungsten deposit, South China: Implications for fluid evolution

and W skarn mineralization in F-rich ore system, Ore Geology Reviews, Volume 142, 104729, https://doi.org/10.1016/j.oregeorev.2022.104729.

Huang, X-W., Sappin A-A., Boutroy, E., Beaudoin, G., Makvandi, S., 2019. Trace Element Composition of Igneous and Hydrothermal Magnetite from Porphyry Deposits: Relationship to Deposit Subtypes and Magmatic Affinity. *Economic Geology*; 114 (5): 917–952. doi: https://doi.org/10.5382/econgeo.4648

Jochum, K.P., Nohl, U., Herwig, K., Lammel, E., Stoll, B., Hofmann, A.W., 2005. GeoReM: a new geochemical database for reference materials and isotopic standards. Geostand Geoanal Res 29:333–338

Kempe, U., Belyatsky, B., Krymsky, R. Kremenetsky, A.A., Ivanov, P.A., 2001. Sm–Nd and Sr isotope systematics of scheelite from the giant Au(–W) deposit Muruntau (Uzbekistan): implications for the age and sources of Au mineralization. Min Dep 36, 379–392. https://doi.org/10.1007/s001260100156

Kent, A.J.R., Campbell, I.H., McCulloch, M.T., 1995. Sm-Nd systematics of hydrothermal scheelite from the Mount Charlotte Mine, Kalgoorlie, Western Australia; an isotopic link between gold mineralization and komatiites. *Economic Geology*; 90 (8): 2329–2335. doi: https://doi.org/10.2113/gsecongeo.90.8.2329

Keppler, H., 1993. Influence of fluorine on the enrichment of high field strength trace elements in granitic rocks. Contr. Mineral. and Petrol. 114, 479–488. https://doi.org/10.1007/BF00321752

Kozlik, M., Gerdes, A., Raith, J.G., 2016a. Strontium isotope systematics of scheelite and apatite from the Felbertal tungsten deposit, Austria – results of in-situ LA-MC-ICP-MS analysis. Miner Petrol 110, 11–27. https://doi.org/10.1007/s00710-015-0416-0

Kozlik, M., Raith, J.G., Gerdes, A., 2016b. U–Pb, Lu–Hf and trace element characteristics of zircon from the Felbertal scheelite deposit (Austria): New constraints on timing and source of W mineralization. Chemical Geology, 421, 112-126, https://doi.org/10.1016/j.chemgeo.2015.11.018.

Lang, J.R., Baker, T., 2001. Intrusion-related gold systems: the present level of understanding. Min Dep 36, 477–489. https://doi.org/10.1007/s001260100184

Li, W., Xie, G-Q., Mao, J-W., Zhang, H-C., 2021. Mineralogy, fluid inclusion and isotope signatures: Implications for the genesis of the Early Paleozoic Yangjiashan scheelite-quartz vein deposit, South China, Ore Geology Reviews, 134, 104136, https://doi.org/10.1016/j.oregeorev.2021.104136.

Li, X-Y., Gao, J-F., Zhang, R-Q., Lu, J-J., Chen, W-H., Wu, J-W., 2018. Origin of the Muguayuan veinlet-disseminated tungsten deposit, South China: Constraints from in-situ trace element analyses of scheelite. Ore Geology Reviews, 99, 180-194, https://doi.org/10.1016/j.oregeorev.2018.06.005.

Liu, H., Beaudoin, G., 2021. Geochemical signatures in native gold derived from Au-bearing ore deposits. Ore Geology Reviews, 132, 104066, doi: https://doi.org/10.1016/j.oregeorev.2021.104066

Liu, Z., Hollings, P., Mao, X., Lawley, C.J.M., Yang, B., Tang, L., 2021. Metal remobilization from country rocks into the Jiaodong-type orogenic gold systems, Eastern China: New constraints from scheelite and galena isotope results at the Xiadian and Majiayao gold deposits. Ore Geology Reviews 134:104126.

Makvandi, S., Beaudoin, G., McClenaghan, B., Quirt, D., Ledru, P., 2019. PCA of Fe-oxides MLA data as an advanced tool in provenance discrimination and indicator mineral exploration: Case study from bedrock and till from the Kiggavik U deposits area (Nunavut, Canada). Journal of Geochemical Exploration, 197: 199-211. doi.org/10.1016/j.gexplo.2018.11.013

Maloof, T.L., Baker, T. & Thompson, J.F., 2001. The Dublin Gulch intrusion-hosted gold deposit, Tombstone plutonic suite, Yukon Territory, Canada. Min Dep 36, 583–593. https://doi.org/10.1007/s001260100190

Maneglia, N., Beaudoin, G., Simard, M., 2017. Indicator minerals of the Meliadine orogenic gold deposits, Nunavut (Canada), and application to till surveys. Geochem Explor Environ Anal 18:241–251

Mansur, E.T., Barnes, S.J., Duran, C.J., Sluzhenikin, S.F., 2020. Distribution of chalcophile and platinum-group elements among pyrrhotite, pentlandite, chalcopyrite and cubanite from the Noril'sk-Talnakh ores: Implications for the formation of platinum-group minerals. Mineralium Deposita, 55(6), 1215-1232.

Mansur, E.T., Barnes, S-J., Duran, C., 2021. An overview of chalcophile element contents of pyrrhotite, pentlandite, chalcopyrite, and pyrite from magmatic Ni-Cu-PGE sulfide deposits. Mineral Deposita 56:179–204

Mao, M., Rukhlov, A., Rowins, S., Spence, J., Coogan, L., 2016. Apatite trace element compositions: a robust new tool for mineral exploration. Econ Geol 111:1187–1222

Mair, J.L., Goldfarb, R.J., Johnson, C.A., Hart, C.J.R., Marsh, E.E., 2006. Geochemical constraints on the genesis of the Scheelite dome intrusion-related gold deposit, Tombstone gold belt, Yukon, Canada. Economic Geology, 101, 523-553.

McClenaghan, M., Parkhill, M., Pronk, A., Seaman, A., McCurdy, M., Leybourne, M., 2017. Indicator mineral and geochemical signatures associated with the Sisson W-Mo deposit, New Brunswick,Canada. Geochem Explor Environ Anal 17:297–313

Migdisov, A., Williams-Jones, A.E., Brugger, J., Caporuscio, F., 2016. Hydrothermal transport, deposition, and fractionation of REE: experimental data and thermodynamic calculations. Chem Geol 439:13–42

Mihalynuk, M.G., and Heaman, L.M., 2002. Age of mineralizated porphyry at the Logtung deposit W-Mo-Bi-Be (beryl, aqua- marine), northwest BC; in Geological Fieldwork, BC Ministry of Energy and Mines, 35-39

Miller, C.F., Mittlefehldt, D.W., 1984. Extreme fractionation in felsic magma chambers: a product of liquid-state diffusion or fractional crystallization? Earth and Planetary Science Letters, 68, 151-158, https://doi.org/10.1016/0012-821X(84)90147-X.

Miller, C.F., and Stoddard, E.F., 1981. The Role of Manganese in the Paragenesis of Magmatic Garnet: An Example from the Old Woman-Piute Range, California. Journal of Geology, 89, 770-772.

Miranda, A.C.R., Beaudoin, G., Rottier, B., 2022. Scheelite chemistry from skarn systems: implications for ore-forming processes and mineral exploration. Miner Deposita. https://doi.org/10.1007/s00126-022-01118-y

Mutch, A.R., 1969. The scheelite resources of the Glenorchy district, west Otago. New Zealand Geological Survey report 40

Myint, A.Z., Yonezu, K., Boyce, A.J., Selby, D., Scherstén, A., Tindell, T., Watanabe, K., Swe, Y.M., 2018. Stable isotope and geochronological study of the Mawchi Sn-W deposit, Myanmar: Implications for timing of mineralization and ore genesis. Ore Geology Reviews, 95, 663-679, https://doi.org/10.1016/j.oregeorev.2018.03.014

Nassau, K., 1963. Calcium tungstate—IV: the theory of coupled substitution. J of Physics and Chemistry of Solids 24:1511–2151

Nathwani, C.L., Wilkinson, J.J., Fry, G., Armstrong, R.N., Smith, D.J., Ihlenfeld, C., 2022. Machine learning for geochemical exploration: classifying metallogenic fertility in arc magmas and insights into porphyry copper deposit formation. Miner Deposita 57, 1143–1166.

Newberry, R., Swanson, S., 1986. Scheelite Skarn Granitoids: An evaluation of the roles of magmatic source and process. Ore Geol Rev 1:57-81

Neiva, A.M.R., Moura, A., Leal Gomes, C.A., Pereira, M.F., Corfu, F., 2019. The granite-hosted Variscan gold deposit from Santo António mine in the Iberian Massif (Penedono, NW Portugal): constraints from mineral chemistry, fluid inclusions, sulfur and noble gases isotopes. J Iber Geol 45, 443–469. https://doi.org/10.1007/s41513-019-00103-1

Nguyen, T.H., Nevolko, P.A., Pham, T.D., Svetlitskaya, T.V., Tran, T.H., Shelepaev, R.A., Fominykh, P.A., Pham, N.C., 2020. Age and genesis of the W-Bi-Cu-F (Au) Nui Phao deposit, Northeast Vietnam: Constrains from U-Pb and Ar-Ar geochronology, fluid inclusions study, S-O isotope systematic and scheelite geochemistry, Ore Geology Reviews, 123, 103578. https://doi.org/10.1016/j.oregeorev.2020.103578

Noble, S.R, Spooner, E.T.C., Harris, F.R., 1984. The Logtung large tonnage, low-grade W (scheelite)-Mo porphyry deposit, south-central Yukon Territory. *Economic Geology* 79(5):848–868. doi: https://doi.org/10.2113/gsecongeo.79.5.848

O'Brien, J., Spry, P., Teale, G., Jackson, S., Koenig, A., 2015. Gahnite composition as a means to fingerprint metamorphosed massive sulfide and non-sulfide zinc deposits. J Geochem Explor 159:48–61

Palarea-Albaladejo, J., Martin-Fernandez, J.A., 2013. Values below detection limit in compositional chemical data. Anal Chim Acta 764:32–43

Palarea-Albaladejo, J., Martin-Fernandez, J.A, 2015. zCompositions-R package for multivariate imputation of left-censored data under a compositional approach. Chemometr Intell Lab Syst 143:85–96

Palmer, M.C., 2021. Geochemical characterisation of scheelite from New Zealand (Thesis, Doctor of Philosophy). University of Otago. Retrieved from http://hdl.handle.net/10523/12254

Palmer, M.C., Scanlan, E.J., Scott, J.M., Farmer, L., Pickering, D., Wilson, V.J., Oelze, M., Craw, D., le Roux, P.J., Luo, Y., Graham, D.G., Reid, M.R., Stirling, C.H., 2022. Distinct scheelite REE geochemistry and 87Sr/86Sr isotopes in proximally- and distally-sourced metamorphogenic hydrothermal systems, Otago Schist, New Zealand, Ore Geology Reviews, 144, 104800. https://doi.org/10.1016/j.oregeorev.2022.104800

Pan, J.Y., Ni, P., Wang, R.C., 2019. Comparison of fluid processes in coexisting wolframite and quartz from a giant vein-type tungsten deposit, South China: insights from detailed petrography and LA-ICP-MS analysis of fluid inclusions Am. Miner., 104, pp. 1092-1116

Pašava, J., Svojtka, M., Veselovský, F., Ďurišová, J., Ackerman, L., Pour, O., Drábek, M., Halodová, P., Haluzová, E., 2016. Laser ablation ICPMS study of trace element chemistry in molybdenite coupled with scanning electron microscopy (SEM) — An important tool for identification of different types of mineralization, Ore Geology Reviews, 72, 874-895, https://doi.org/10.1016/j.oregeorev.2015.09.007

Paterson C.J., and Rankin, P.C., 1979. Trace element distribution in the schist surrounding a quartz-scheelite lode, Glenorchy, New Zealand, New Zealand Journal of Geology and Geophysics, 22:3, 329-338, DOI: 10.1080/00288306.1979.10424102

Paterson, C.J., and Peter C. Rankin, P.C., 1979 Trace element distribution in the schist surrounding a quartz-scheelite lode, Glenorchy, New Zealand, New Zealand Journal of Geology and Geophysics, 22:3, 329-338, DOI: 10.1080/00288306.1979.10424102

Paton, C., Hellstrom, J., Paul, B., Woodhead, J., and Hergt, J., 2011, Iolite: freeware for the visualization and processing of mass spectrometric data: Journal of Analytical Atomic Spectrometry, 26, p. 2508–2518. https:// doi. org/ 10. 1039/ c1ja1 0172b

Piccoli, P.M., Candela, P.A., 2002. Apatite in Igneous Systems. *Reviews in Mineralogy and Geochemistry*; 48 (1): 255–292. doi: https://doi.org/10.2138/rmg.2002.48.6

Pirajno, F., and Bentley, P.N., 1985. Greisen-related scheelite, gold and sulphide mineralisation at Kirwans Hili and Bateman Creek, Reefton district, Westland, New Zealand. New Zealand Journal of Geology and Geophysics, 28, 97-109.

Pollard, P.J., Pichavant, M., Charoy, B., 1987. Contrasting evolution of fluorine- and boron-rich tin systems. Mineral. Deposita 22, 315–321. https://doi.org/10.1007/BF00204525

Porter, J., McNaughtona, N., Evansa, N., McDonald, J., 2020. Rutile as a pathfinder for metals exploration. Ore Geol Rev 120:03406

Poulin, R., Kontak, D., McDonald, A., McClenaghan, M. 2018. Assessing scheelite as an ore-deposit discriminator using its trace element and REE chemistry. Can Mineral 56:265–302 R Core Team 2021. R: a language and environment for statistical computing. R Foundation for Statistical Computing, Vienna, Austria. URL https:// www.R- proje ct. org/.

Raith, J.G., Gerdes, A., Cornell, D.H., 2011. In situ U–Pb dating of scheelite: constraints on the age and genesis of the Felbertal tungsten deposit. Mineral. Mag. 75, 1690.

Rottier, B., and Casanova, V., 2020. Trace element composition of quartz from porphyry systems: a tracer of the mineralizing fluid evolution. Miner Deposita 55:843-862

Scanlan, E.J., Scott, J.M., Wilson, V.J., Stirling, G.H., Reid, M.R., Le Roux, P.J., 2018. In Situ $^{87}Sr/^{86}Sr$ of Scheelite and Calcite Reveals Proximal and Distal Fluid-Rock Interaction During Orogenic W-Au Mineralization, Otago Schist, New Zealand. *Economic Geology*; 113 (7): 1571–1586. doi: https://doi.org/10.5382/econgeo.2018.4603

Sciuba, M., Beaudoin, G., Grzela, D., Makvandi, S., 2020. Trace element composition of scheelite in orogenic gold deposits. Miner Deposita 55:1149-1172

Sciuba, M., Beaudoin, G., Makvandi, S., 2021. Chemical composition of tourmaline in orogenic gold deposits. Mineralium Deposita 56, 537-560

Seo, J.H., Yoo, B.C., Yang, YS., Lee, J.H., Jang, J., Shin, D., 2020. Scheelite geochemistry of the Sangdong W-Mo deposit and W prospects in the southern Taebaeksan metallogenic region, Korea. Geosci J 24, 701–721. https://doi.org/10.1007/s12303-020-0005-z

Sha, L-K., and Bruce W Chappell, B. W., 1999. Apatite chemical composition, determined by electron microprobe and laser-ablation inductively coupled plasma mass spectrometry, as a probe into granite petrogenesis. Geochimica et Cosmochimica Acta, 63, 3861-3881. https://doi.org/10.1016/S0016-7037(99)00210-0.

Štemprok, M., and Mašková, A., 1992. Scheelite mineralization of the Bohemian Massif. Zbl. Geol. Palaont. Teil (1/2): 117-129.

Song, G., Qin, K., Li, G., Evans, N., Chen, L., 2014. Scheelite elemental and isotopic signatures: Implications for the genesis of skarn-type W-Mo deposits in the Chizhou area, Anhui Province Eastern China. Am Mineral 99:303–317

Stekhoven, D.J., Bühlmann, P., 2012. MissForest—non-parametric missing value imputation for mixed-type data, *Bioinformatics*, 28, 112–118, https://doi.org/10.1093/bioinformatics/btr597

Sun, G., Zeng, Q., Zhou, J-X., 2022. Machine learning coupled with mineral geochemistry reveals the origin of ore deposits, Ore Geology Reviews, 142, 104753

Sun, K., Chen, B., 2017. Trace elements and Sr-Nd isotopes of scheelite:Implications for the W-Cu-Mo polymetallic mineralization of the Shimensi Deposit, south China. Am Mineral 102:1114–1128

Sun, K., Chen, B., Deng, J., 2019. Ore genesis of the Zhuxi supergiant W-Cu skarn polymetallic deposit, South China: evidence from scheelite geochemistry. Ore Geol Rev 107:14–29

Sverjensky, D., 1984. Europium redox equilibria in aqueous solution. Earth Planet Sci Lett 67:70–78

Thompson, J., Sillitoe, R., Baker, T., Lang, J.R., Mortensen, J.K., 1999. Intrusion-related gold deposits associated with tungsten-tin provinces. Mineral. Deposita 34, 323–334. https://doi.org/10.1007/s001260050207

Tyson, R.M., Hemphill, W.R., Theisen, A.R., 1988. Effect of the W:Mo ratio on the shift of excitation and emission spectra in the scheelite-powellite series. *American Mineralogist* 73 (9-10): 1145–1154.

Uspensky, E., Brugger, J., Graeser, S., 1998. REE geochemistry systematics of scheelite from the Alps using luminescence spectroscopy: from global regularities to facies control. Schweiz Mineral Petrogr Mitt 78:33–56

Vallance, J., Cathelineau, M., Boiron, M.C., Fourcade, S., Shepherd, T.J., Naden, J., 2003. Fluid–rock interactions and the role of late Hercynian aplite intrusion in the genesis of the Castromil gold deposit, northern Portugal. Chemical Geology, 194, 201-224. https://doi.org/10.1016/S0009-2541(02)00278-4

Veselovský, F., Ackerman, L., Pašava, J., Žák, K., Haluzová, E., Creaser, R.A., Dobeš, P., Erban, V., Tasler, R., 2018. Multiphase formation of the Obří důl polymetallic skarn deposit, West Sudetes, Bohemian Massif: Geochemistry and Re–Os dating of sulfide mineralization. Miner Deposita 53, 665–682. https://doi.org/10.1007/s00126-017-0766-0

Voicu, G.M., Bardoux, M., Stevenson, R., Jebrak, M., 2001 Nd and Sr isotope study of hydrothermal scheelite and host rocks at Omai, Guiana Shield: implications for ore fluid source and flow path during the formation of orogenic gold deposits Mineralium Deposita 35: 302-314

Wade, C.E., Payne, J.L., Barovich, K., Gilbert, S., Wade, B.P., Crowley, J.L., Reid, A., Jagodzinski, E.A., 2022. Zircon trace element geochemistry as an indicator of magma fertility in iron oxide copper-gold provinces. *Economic Geology*; 117 (3): 703–718. doi: https://doi.org/10.5382/econgeo.4886

Wang, X-S., Williams-Jones, A.E., Hu, R-Z., Shang, L-B., Bi, X-W., 2021. The role of fluorine in granite-related hydrothermal tungsten ore genesis: Results of experiments and modeling, Geochimica et Cosmochimica Acta, 292, 170-187, https://doi.org/10.1016/j.gca.2020.09.032.

Webster, J., Thomas, R., Förster, H.J., Seltmann, R., Tappen, C., 2004. Geochemical evolution of halogen-enriched granite magmas and mineralizing fluids of the Zinnwald tin-tungsten mining district, Erzgebirge, Germany. Miner Deposita 39, 452–472. https://doi.org/10.1007/s00126-004-0423-2

Wilkinson, J.J., Chang, Z., Cooke, D.R., Baker, M.J., Wilkinson, C.C., Inglis, S., Chen, H., Gemmell, J.B., 2015. The chlorite proximitor: A new tool for detecting porphyry ore deposits, Journal of Geochemical Exploration, Volume 152, Pages 10-26

Wintzer, N.E., Schmitz, M.D., Gillerman, V.S., Vervoort, J.D., 2022. U-Pb Scheelite Ages of Tungsten and Antimony Mineralization in the Stibnite-Yellow Pine District, Central Idaho. *Economic Geology*; doi: https://doi.org/10.5382/econgeo.4953

Wood, S.A., and Samson, I.M., 2000. The Hydrothermal Geochemistry of Tungsten in Granitoid Environments: I. Relative Solubilities of Ferberite and Scheelite as a Function of T, P, pH, and mNaCl. Economic geology Vol. 95. pp 143-182.

Wu, S., Mao, J., Ireland, T., Zaho, Z., Yao, F., Yang, Y., Sun, W., 2019. Comparative geochemical study of scheelite from the Shizhuyuan and Xianglushan tungsten skarn deposits, South China: implications for scheelite mineralization. Ore Geol Rev 109:448–464

Xu, J., Ciobanu, C., Cook, N.C., Slattery, A., 2019. Crystals from the powellite-scheelite series at the nanoscale: a case study from the Zhibula Cu skarn, Gangdese Belt. Tibet Minerals 9:340

Yuan, L., Chi, G., Wang, M., Li, Z., Xu, D., Deng, T., Geng, J., Hu, M., Zhang, L., 2019. Characteristics of REEs and trace elements in scheelite from the Zhuxi W deposit, South China: implications for the ore forming conditions and processes. Ore Geol Rev 109:585–597

Žáček V., 2008. Cu-skarn v Kotli v Krkonoších (Česká republika). - Bull. mineral.-petrolog. Odd. Nár. Muz. (Praha) 16/2, 230-237. ISSN: 1211-0329

Zhang, Q., Zhao, K.D., Li, W-Q., Palmer, M.R., Jiang, S-Y., Jaing, H., Zhang, W., Zhang, D., Hussian, A., 2022. Timing and tectonic setting of tin mineralization in southern Myanmar: constraints from cassiterite and wolframite U–Pb ages. Miner Deposita 57, 977–999. https://doi.org/10.1007/s00126-021-01083-y

Zhao, L., Zhang, Y., Shao, Y., Li, H., Shah, S.A., Zhou, W., 2021. Using garnet geochemistry discriminating different skarn mineralization systems: Perspective from Huangshaping W-Mo-Sn-Cu polymetallic deposit, South China, Ore Geology Reviews, Volume 138.

Zhao, W., Zhou, M-F., Williams-Jones, A., Zhao, Z., 2018. Constraints on the uptake of REE by scheelite in the Baoshan tungsten skarn deposit, South China. Chem Geol 477:123–136

Chapter 3 - Prediction of metal endowment in orogenic Au deposits based on scheelite trace element composition and Random Forest classifier

Ana Carolina R. Miranda[1,2], Georges Beaudoin[1,2] and Bertrand Rottier[1,2]

[1]Département de Géologie et Génie Géologique, Université Laval, Québec, Canada

[2]Centre de recherche sur la géologie et l'ingénierie de ressources minérales (E4m), Université Laval, Québec, Canada

3.1 Résumé

L'association spatiale et temporelle de la scheelite avec l'or dans certains gisements orogéniques d'or permet d'utiliser la scheelite comme un minéral indicateur utile pour l'exploration. Dans cet article, la composition en éléments traces de la scheelite de 23 gisements d'or orogéniques distribués dans le monde, dont la dotation en Au est comprise entre 1,4 T et 777 T, a été compilée et évaluée à l'aide d'un classificateur Random Forest (RF) afin de déterminer si la composition de la scheelite peut être utilisée pour prédire la teneur en Au d'un gisement d'or orogénique. Les gisements d'Au contenant de la scheelite ont été classés en trois classes de taille : <100 T, 100-300 T et >300 T Au. En utilisant 13 éléments (Mg, V, Mn, As, Sr, Y, Nb, Mo, Ba, Pb, U, ΣREE et anomalie Eu) comme variables prédictives, les résultats de la RF donnent une précision globale de 94%, avec 87% pour les classes <100 T, 97,9% pour 100-300 T et 95,6% pour >300 T Au. La performance et l'efficacité du modèle RF ont été évaluées à l'aide de la technique de validation croisée décuple, qui donne une excellente précision de classification (>90%), et par des tests avec des données de littérature sur la scheelite provenant de 5 gisements orogéniques d'Au. Les prédictions effectuées sur les données de la littérature montrent que les ensembles de données contenant les 13 variables prédicteurs, ou les variables prédicteurs manquantes de faible importance pour le modèle, telles que V, Ba et U, donnent des précisions comprises entre 70% et 100%. En revanche, les ensembles de données où une ou plusieurs variables importantes sont manquantes, telles que As, Mn et Nb, montrent une diminution significative de la précision de prédiction (<50%). Les résultats suggèrent que le modèle de classification RF basé sur la composition chimique de la scheelite peut être utilisé pour évaluer la dotation en Au des gisements d'Au orogéniques.

Mots clés: scheelite, élément trace, gisements d'Au orogéniques, fertilité, forêt aléatoire

3.2 Abstract

The spatial and temporal association of scheelite with Au in some orogenic Au deposits enables the use of scheelite as a useful indicator mineral for exploration. Here, scheelite trace elements composition from 23 orogenic Au deposits with endowment between 1.4 T and 777 T Au, distributed worldwide, were compiled and evaluated using Random Forest (RF) classifier to assess whether scheelite composition can be used to predict the Au endowment of an orogenic Au deposit. Scheelite-bearing Au deposits were classified in three size classes: <100 T, 100-300 T and >300 T Au. Using 13 elements (Mg, V, Mn, As, Sr, Y, Nb, Mo, Ba, Pb, U, ΣREE and Eu anomaly) as predictor variables, the RF results yield an overall accuracy of 94%, with 87% for <100 T, 97.9% for 100-300 T and 95.6% for >300 T Au for classes. The performance and effectiveness of the RF model were evaluated using tenfold cross-validation technique, which yields excellent classification accuracy (>90%), and by testing with literature scheelite data from 5 orogenic Au deposits/showing. Predictions performed on literature data show that datasets containing all 13 predictor variables, or missing predictor variables with low importance for the model, such as V, Ba and U, yield accuracies between 70% and 100%. In contrast, datasets where one or more important variables are missing, such as As, Mn and Nb, show a significant decrease in prediction accuracy (<50%). The results suggest that RF classification model based on scheelite chemical composition can be used to assess the Au endowment of orogenic Au deposits.

Keywords: scheelite, trace element, orogenic Au deposits, fertility, random forest

3.3 Introduction

Previous studies have investigated the effectiveness of Random Forest (RF) over other machine learning classifier algorithms such as Support Vector Machine, Artificial Neural Network, Naïve Bayes, Logistic Regression and simple statistic analysis, in solving problems of classification and prediction applied to mineral deposits (Cracknell and Reading 2014; Rodriguez-Galiano et al. 2015; Bédard et al. 2022; Nathwani et al. 2022). Such approach has been applied to large datasets to optimize and improve models for discrimination of mineral deposits based on mineral chemistry (Gregory et al. 2019; Bédard et al. 2022), and to target new mineral deposits based on whole-rock geochemistry

(Dmitrijeva et al. 2022; Nathwani et al. 2022; Zou et al. 2022). More specifically, some contributions have successfully used RF classifier to predict the fertility of mineral deposits based on whole-rock geochemistry and mineral trace element composition (O'Brien et al. 2015; Gregory et al. 2019; Zou et al. 2022).

Scheelite is a common mineral in magmatic-hydrothermal deposits (Noble et al. 1984; Hart 2007; Song et al. 2014; Poulin et al. 2018; Miranda et al. 2022), and is often found associated with Au in orogenic Au deposits (Groves et al. 1998; Craw et al. 2015; Sciuba et al. 2020). Its composition has been widely used to constrain the fluid source (Kent et al. 1995; Voicu et al. 2001; Scanlan et al. 2018; Elongo et al. 2022), age (Bell et al. 1989; Anglin et al. 1996; Darbyshire et al. 1996; Wintzer et al. 2022) and as a proxy for physico-chemical conditions in several geological settings (Brugger et al. 2008; Song et al. 2014; Kozlik et al. 2016; Zhao et al. 2018), in addition to discriminate different types of deposits (Kempe and Oberthur 1997; Song et al. 2014; Poulin et al. 2018; Sciuba et al. 2020; Miranda et al. 2022). This is possible because the scheelite crystal lattice accommodates key trace elements (Mo, As, Nb, Sr, Na, Mn, ΣREE), for which abundance is controlled by physico-chemical parameters, composition of the fluids and coprecipitated minerals (Hsu and Galli 1973; Tyson et al. 1988; Raimbault et al. 1993; Brugger et al. 2008; Zhao et al. 2018; Sciuba et al. 2020; Miranda et al. 2022).

Orogenic Au deposits represent for 75% of the world's Au production (Goldfarb et al. 2001; Phillips 2013; Craw et al. 2015). Giant orogenic Au provinces/deposits occur at all geological ages except the Mesoproterozoic, and are unevenly spread over different continents (Goldfarb et al. 2005; Groves et al. 2016). An important question for orogenic gold and other types of deposits is whether it is possible to assess metal endowment of a given deposit using mineral or whole-rock chemistry. Several studies have successfully shown the performance of trace elements in few minerals such as garnet (Gurney 1984; Grütter et al. 2004), apatite (Pan et al. 2016), biotite (Azadbakht et al. 2020) and zircon (Ballard et al. 2002; Wade et al. 2022), as useful to assess fertility for ore systems and metallogenetic provinces. However, none of these studies have attempted to test scheelite potential as an indicator for fertility or Au endowment in orogenic Au deposits.

In this contribution, the trace element composition of scheelite from several well-studied orogenic Au deposits with known Au endowment were compiled. This data was assessed using a RF classifier machine learning algorithm to evaluate whether the trace

element composition of scheelite can be used to predict the Au endowment of orogenic Au deposits. High predictions accuracies obtained by RF classification model suggest it is efficient to assess the Au endowment of orogenic gold deposits.

3.4 Data sources and deposit size classification

Laser ablation-ICP-MS scheelite trace element chemistry from orogenic Au deposits and showings from literature was compiled. Dataset 1 consists of 23 well-studied orogenic Au deposits with known Au endowment, from which 319 in situ scheelite analyses with a set of 16 trace elements and 14 rare earth elements (REE) and with more than 70% values above the detection limit (Appendix 3.1B). Dataset 2 comprises 248 in situ scheelite analyses from 4 Au deposits/showings and from scheelite recovered from till samples down ice of the Amaruq gold deposit (Canada; De Bronac de Vazelhes 2019). This second dataset was used to assess the effectiveness of the RF classification model (Tables 3.1, 3.2 and Appendix 3.2B; Fig. 3.1).

Both datasets include scheelite analyses from the Macraes Au mine, New Zealand. This is because Macraes scheelite in Dataset 2 from Cave et al. (2017) and Pickering (2018) have a smaller set of analysed elements relative to that of Sciuba et al. (2020) included in Dataset 1 and used in the RF classifier (Table 3.2). This is done to assess the effectiveness of the RF model and to avoid any plausible bias created by the imputation from missing elements in scheelite from Cave et al. (2017) and Pickering (2018) if they had been included in Dataset 1.

All scheelite analyses from Dataset 1 were obtained under similar analytical conditions at the LabMaTer, Universite du Quebec a Chicoutimi (UQAC), Canada, (De Bronac de Vazelhes 2019; Sciuba et al. 2020). This is important as it brings consistency in Dataset 1 used to build the RF model. As shown in Table 3.1, the Au deposits vary from small (<70 T) to world-class sized (>70 T) and giant deposits (>500 T) according to Goldfarb et al. (2005). Additionally, the selected deposits in Dataset 1 provides a representative range of geological settings, which englobes Au deposits hosted in different host rocks, metamorphic facies, and having mineralization ages ranging from Archean to Phanerozoic (De Bronac de Vazelhes 2019; Sciuba et al. 2020; Table 3.1).

The Au resources for each deposit (Au endowment) is based on past production, reserves (proven + probable) and resources (measured + indicated) taken from Gosselin and Dube (2005) and company reports that are NI-43-101 or JORC compliant to increase consistency in the compiled gold endowment values. Hence, the deposits are classified in <100 T (≈ 3Moz), between 100-300 T and >300 T (≈ 10Moz) of Au (Table 3.1), which is similar to the classification proposed by Goldfarb et al. (2005). It is noteworthy that some deposits are still under development or production, and the actual resources may increase in the future. In addition, deposits with Au endowment within 5% of the superior limit of a class were moved to the larger class, given the likelihood of future expansion of reserves/resources. This is the case of Lamaque-Sigma Au deposit, which has 296 T Au but was assigned to the >300 T class.

The Au endowment classes yield balanced and similar representation both in terms of analyses and deposits. The <100 T class contains 77 analyses from 8 deposits where scheelite is hosted mainly in mafic-ultramafic and minor felsic-intermediary rocks, and upper greenschist to lower amphibolite, and few middle greenschist metamorphic facies (Sciuba et al. 2020; Table 3.1). The mineralization age is mostly Archean. The 100-300 T class contains 164 analyses from 8 deposits, where scheelite is hosted in sedimentary, felsic-intermediary and mafic-ultramafic rocks. Metamorphic facies of the deposits are mainly characterized by lower and middle greenschist and the mineralization age is predominantly Archean (Table 3.1). The >300 T class contains 78 scheelite analyses from 7 deposits where scheelite is hosted in sedimentary, felsic-intermediate and mafic-ultramafic rocks. The deposits metamorphic facies are mostly lower and middle greenschist facies, and mineralization age are Archean to Phanerozoic (Table 3.1).

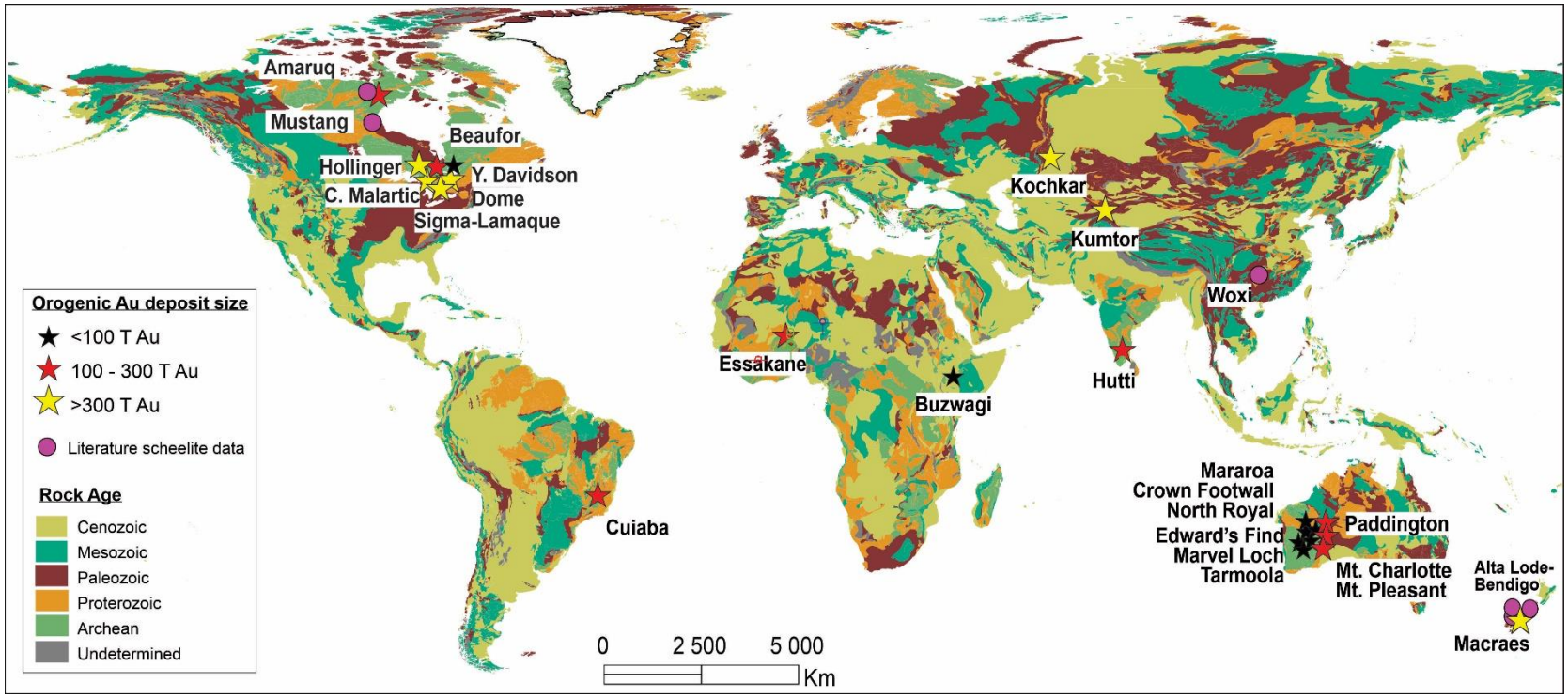

Figure 3.1. Distribution of scheelite-bearing orogenic gold deposits used for the Random Forest model and its testing.

Table 3.1. Summary of characteristics of the orogenic gold deposits used in the Random Forest model.

Deposit name	Country	Major host rock	Metamorphic grade	Mineralization period*	Resources (T)	Number of analysis
Endowment class <100 T						
Edward's Find	Australia	mafic	mid-amphibolite	(Archean)	**1.4**	6
Beaufor	Canada	felsic	greenschist	Archean	**32**	23
Marvel Loch	Australia	komatiites	mid-amphibolite	(Archean)	**35**	11
Mararoa	Australia	mafic-ultramafic	upper greenschist to lower amphibolite	Archean	**37**	6
Buzwagi	Tanzania	felsic	greenschist	(Archean)	**38**	1
Crown Footwall	Australia	mafic-ultramafic	upper greenschist to lower amphibolite	Archean	**41**	10
North Royal	Australia	mafic-ultramafic	upper greenschist to lower amphibolite	Archean	**60**	8
Tarmoola	Australia	komatiites	greenschist	Archean	**85**	12
Endowment class 100-300 T						
Amaruq	Canada	mafic	greenschist	(Archean)	**142**	52
Hutti	India	mafic	amphibolite	Archean	**120**	26
Mt Pleasant	Australia	mafic	lower greenschist	(Archean)	**139**	8
Young Davidson	Canada	felsic	greenschist	Archean	**198**	8
Paddington	Australia	mafic	lower greenschist	(Archean)	**207**	30
Mt Charlotte	Australia	mafic	greenschist	Archean	**209**	15
Essakane	Burkina faso	sedimentary	lower greenschist	Proterozoic	**210**	21
Cuiaba	Brazil	sedimentary (BIF)	greenschist	Archean	**237**	4
Endowment class >300 T						
Sigma-Lamaque	Canada	intermediate	lower greenschist	Archean	**296**	18
Macraes	New Zealand	sedimentary	greenschist	Mesozoic	**313**	19
Malartic	Canada	sedimentary	greenschist	Archean	**373**	5
Kochkar	Russia	intermediate	upper greenschist to lower amphibolite	Paleozoic	**380**	19

Deposit name	Country	Major host rock	Metamorphic grade	Mineralization period*	Resources (T)	Number of analysis
Endowment class >300 T						
Dome	Canada	mafic	greenschist	Archean	**423**	10
Kumtor	Kyrgyzstan	sedimentary	lower greenschist	Paleozoic	**663**	4
Hollinger	Canada	mafic	greenschist	Archean	**777**	3

* In brackets: Ages assumed according to regional geology

Table 3.2. Summary of the literature scheelite-bearing orogenic gold deposits used to test the Random Forest model.

Deposit name	Country	Major host rock	Metamorphic grade	Mineralization period	Total Au (T)	Number of analysis	Missing elements	Reference
Mustang	Canada	Mafic	greenschist	Proterozoic	showing	4	-	Maneglia et al. (2018)
Amaruq till	Canada	Mafic	greenschist	Archean	142	23	-	De Bronac de Vazelles (2019)
Woxi	China	Sedimentary	greenschist	Paleozoic	>50	18	-	Liu (2021); Goldfarb et al. (2019)
Alta Lode - Bendigo	New Zealand	Sedimentary	greenschist	Mesozoic/ Cretaceous	30-150	71	V, Ba, U	Palmer (2021)
Macraes	New Zealand	Sedimentary	greenschist	Mesozoic/ Cretaceous	313	99	V, Ba	Pickering (2018)
Macraes	New Zealand	Sedimentary	greenschist	Mesozoic/ Cretaceous	313	33	As, V, Nb	Cave et al. (2017)

3.5 Methodology

3.5.1 Data preprocessing

Scheelite data preprocessing and the RF classifier were conducted using Rstudio v4.04 software (R Core Team 2021). The preprocessing consists of imputation of values below detection limit (i.e., left-censored data) and missing data (i.e., elements that were not analysed). Missing data imputation was applied only on Dataset 2. Appendix 3.1A summarizes step by step from data compilation to RF predictions.

Left censored data were imputed using log-ratio Expectation-Maximisation (lrEM) algorithm from the R package zCompositions (Palarea-Albaladejo and Martín-Fernández 2015). The lrEM algorithm replaces left-censored values by expected values conditional to the information provided by the compositional dataset (Palarea-Albaladejo and Martín-Fernández 2015).

After establishing which predictor variables are essential for RF model, the imputation of missing data of the blind dataset was conducted using missForest package in R (Stekhoven and Buehlmann 2012). The missForest algorithm consists of building a random forest for each variable based on the input dataset, which is further used to predict the missing data. In this study, Dataset 1 (Table 3.1) was used to impute the missing values of Dataset 2 (Table 3.2).

3.5.2 Random Forest

Random Forest is a supervised machine learning algorithm (Breiman 2001) used to solve classification problems. In mineral deposit geology, RF classifier has been applied to classify deposit types, predict their occurrence from detrital minerals (Gregory et al. 2019; Bédard et al. 2022; Miranda et al. sub.), and assess fertility of mineral deposits (O'Brien et al. 2015; Gregory et al. 2019; Zou et al. 2022). The RF algorithm consists of a large number of decision trees (i.e., forest) that operate as an ensemble. Each tree is individually built from a random sampling subset with replacement (bootstrapping) from the training data and from randomly selected predictor variables. The number (N) of predictor variables in each tree is set to be equal to the square root of the total variables of the training data (Breiman 2001). The predictor variables and their values define each split (nodes) of the tree. Each decision

tree searches through all candidates the optimal split that maximizes the purity of the resulting tree.

Mean decrease Gini is a measure used to show the importance of each variable in the model. The higher the mean decrease Gini score, the higher importance of the variable in the model. The outcome of RF classifier is visualized through a confusion matrix, which is built with the testing data and records predictions of the classifier. The overall accuracy, which is the ratio of the sum of the observations correctly predicted to total of observations, is used to evaluate the RF classifier.

We used the Random Forest classifier from the Caret package in R, for which 70% of the dataset was used to train the RF classifier (training set) and the remaining 30% to test (testing set). The optimal configuration of model parameters was trained by a grid search procedure and validated by tenfold cross-validation technique and scheelite literature data (Dataset 2). After performing the RF classifier with different sets of elements, the best accuracy result was achieved using 13 predictors: Mg, V, Mn, As, Sr, Y, Nb, Mo, Ba, Pb, U, ΣREE and Eu anomaly.

3.6 Results

3.6.1 Scheelite trace element composition

Figure 3.2 displays box plots of the chemical composition of scheelite forming the training data (224 analyses) used in the RF classifier, whereas the Table 3.3 shows the statistic summary of the elements illustrated in Figure 3.2. In general, Sr, Mo, Y, Mg and Mn are the most abundant elements in scheelite with contents up to 7,300 ppm, followed by Nb, Pb and As with contents <360 ppm. Barium, U and V are less abundant elements (Fig. 3.2). The ΣREE ranges between 5.8 and 3,902 ppm. The europium anomaly is predominantly positive for all three classes, varying from 0.45 to 36 (Fig. 3.3a). As illustrated by Figure 3.2, there are increasing median concentration of Mg, Pb and Ba from low to high gold endowment, albeit with large data range overlap, whereas other elements do not display systematic trends of the median value with gold endowment classes.

Figures 3.3b-d show binary plots of As, Mo, Sr, Pb and Mn. In general, there is no correlation between As and Mo, and between Mn and Sr (Figs. 3.3b,c). Strontium and Pb display a general weak positive correlation (Fig. 3.3d). In all three plots, the three classes largely overlap.

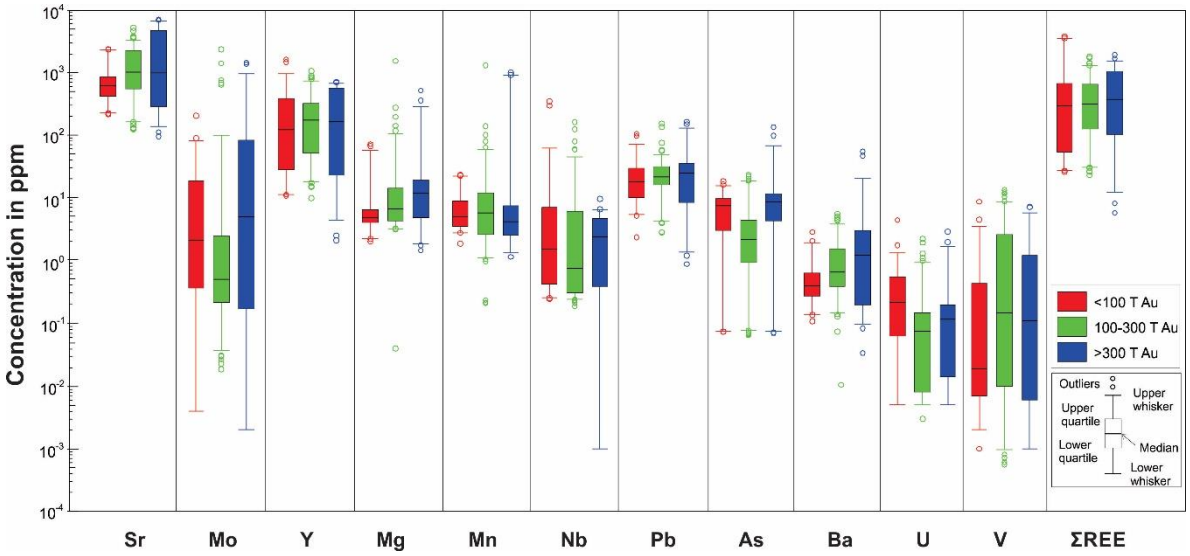

Figure 3.2. Box and whisker diagram of trace elements concentrations in scheelite used in training dataset for the RF classification model.

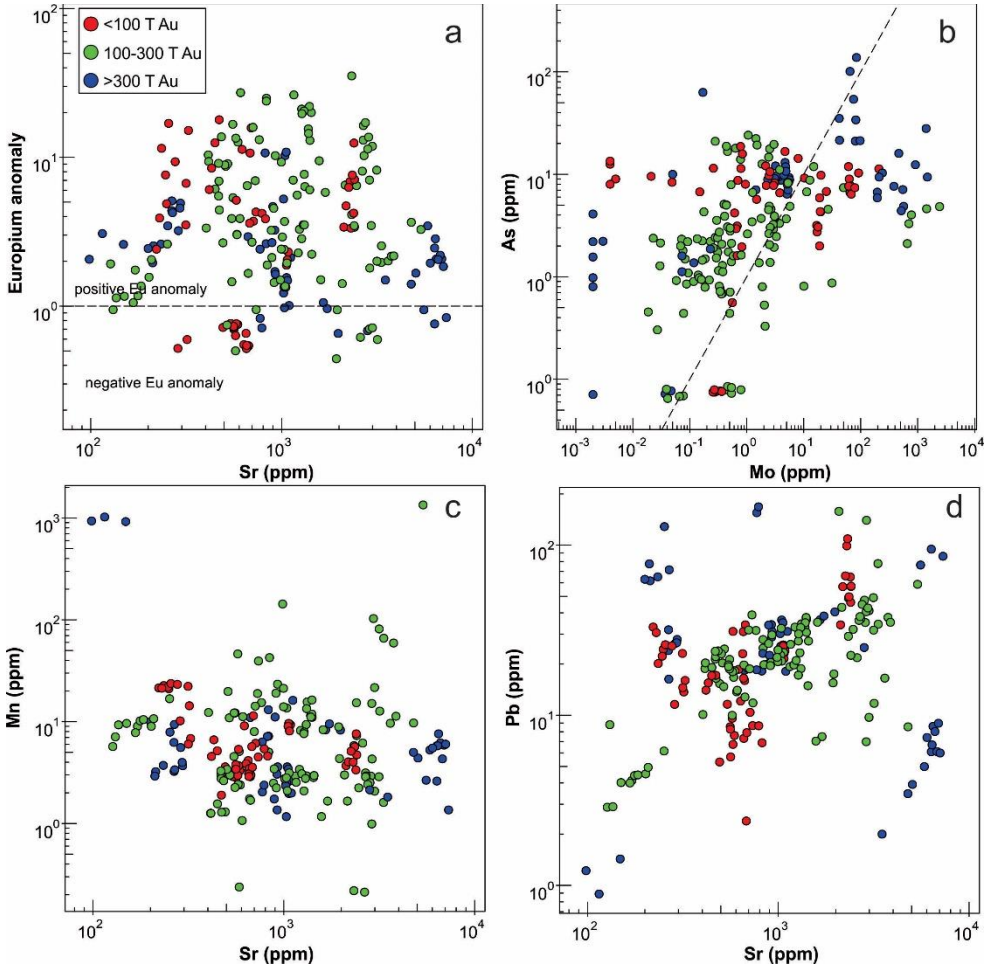

Figure 3.3. Binary plot showing the correlation between Sr and Eu anomaly (a), Mo and As (b), Sr and Mn (c), and Sr and Pb (d) of the training Dataset 1 for the RF classification model.

Table 3.3. Summary of statistics of training data (n=224) used in the Random Forest endowment model.

Deposit endowment (Au)		Mg (ppm)	V (ppm)	Mn (ppm)	As (ppm)	Sr (ppm)	Y (ppm)	Nb (ppm)	Mo (ppm)	Ba (ppm)	Pb (ppm)	U (ppm)	REE (ppm)	Eu anomaly
<100 T	*n*	*54*	*54*	*54*	*54*	*54*	*54*	*54*	*54*	*54*	*54*	*54*	*54*	*54*
	Min	2.06	0.005	1.9	0.07	221	11.11	0.24	0.004	0.109	2.39	0.001	26.95	0.52
	Max	74	4.54	23.7	18.7	2,410	1,680	359	209	2.91	109	8.9	3,901	17.9
	Mean	11.76	0.39	7.8	7.18	852.3	265	17.08	18.43	0.65	24.77	0.64	643.66	4.90
	Median	4.94	0.22	5.15	7.68	643	127	1.6	2.17	0.41	18.61	0.02	305.01	3.66
100-300 T	*n*	*115*	*115*	*115*	*115*	*115*	*115*	*115*	*115*	*115*	*115*	*115*	*115*	*115*
	Min	0.04	0.003	0.21	0.06	127	10.13	0.19	0.02	0.01	2.88	<DL	23.58	0.44
	Max	1,577	2.26	1,344	24.1	5,370	1,090	167.1	2,430	5.72	158	13.53	1,852.6	35.25
	Mean	34.40	0.18	23.12	4.20	1,418	235	9.24	55.06	1.12	26.25	1.89	444.46	6.95
	Median	6.85	0.075	5.82	2.21	1,043	181	0.78	0.51	0.66	22	0.15	326	3.71
>300 T	*n*	*55*	*55*	*55*	*55*	*55*	*55*	*55*	*55*	*55*	*55*	*55*	*55*	*55*
	Min	1.47	0.005	1.17	0.07	98.3	2.14	0.001	0.002	0.034	0.89	0.001	5.88	0.66
	Max	530	2.96	1,022	138	7,300	729	9.8	1,482	56	168	7.3	1,978	10.85
	Mean	39.54	0.31	57.12	14.94	2,224	274.8	2.80	141.5	3.93	34.92	0.93	599.48	2.78
	Median	12.1	0.119	4.31	8.84	1,025	166	2.4	5.07	1.24	25.5	0.112	381	2.12

3.6.2 Random Forest model and predictions

The RF model of scheelite trace elements composition yields an overall accuracy of 94% for the 3 Au endowment classes (Fig. 3.4). The confusion matrix of the testing data shows individual accuracies of 97.9% for 100-300 T Au, 95.6% for >300 T, and 86.9% for <100 T Au (Table 3.4). Figure 3.4 shows that As, Sr and Mo have the highest importance for the RF classifier, followed by Pb, Mn, Nb, Y, Eu anomaly, Ba, ΣREE and V, whereas U and Mg are the least important.

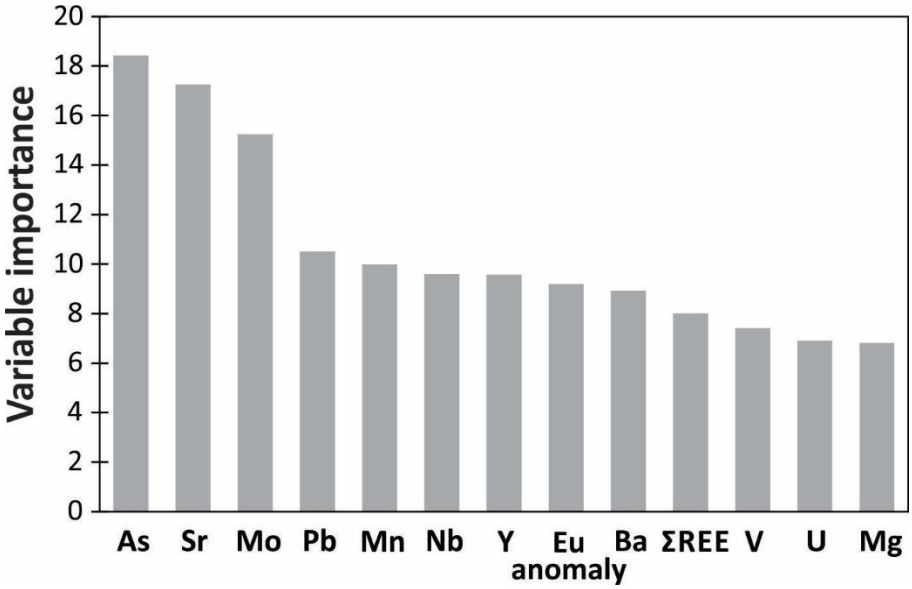

Figure 3.4. Bar plot showing the variable importance for the RF classification model.

The performance for the RF model was assessed using tenfold cross validation, which yields an accuracy of 93%, and by testing the RF classifier using literature scheelite from orogenic Au deposits with different gold endowments, from small to worldclass Au deposits (Table 3.2; Fig. 3.5). Figures 3.5a-b display the results for scheelite of three locations that contain the 13 elements used in RF model, whereas Figure 3.5c shows the predictions for scheelite analyses missing important elements that were imputed (Table 3.2).

All scheelite analyses from the Mustang (showing) are predicted to belong to the <100 T Au endowment class (Fig. 3.5a). The Woxi deposit is estimated to be >50 T Au (Goldfarb et al. 2019), and our results show that 72% of Woxi scheelite are correctly predicted to belonging to the <100 T Au class, whereas 18% are predicted as part of the >300 T Au class (Fig. 3.5a).

Alta Lode-Bendigo (New Zealand) is an exploration project with resources estimates between 30-150 T Au (Santa Barbara mining report 2021). At Alta-Bendigo, V, Ba and U, elements with lower gini values (Fig. 3.4) were not analyzed (Palmer 2021). Most analyses of scheelite from Alta Lode-Bendigo (70%), are predicted to the 100-300T Au class, whereas 24% and 3% are predicted in >300 T and <100 T Au class, respectively. Scheelite analyses from the 314 T Au Macraes deposit (Pickering 2018), for which low gini value V and Ba contents were not measured, are mostly (70%) predicted to belong the >300 T Au class, whereas 30% are predicted to the 100-300 T Au class. Macraes deposit scheelite analyses reported by Cave et al. (2017), which lack values for important predictors (As, Nb and V), are predicted as 39% to the >300 T Au, 39% to the 100-300 T and 21% as <100 T Au classes (Table 3.5; Fig. 3.5b).

Table 3.4 Confusion matrix of the testing data.

		Prediction				
		<100T	100-300T	>300T	Total	% correct
Reference	<100T	20	3		23	86.96%
	100-300T		48	1	49	97.96%
	>300T		1	22	23	95.65%

3.7 Discussion

3.7.1 Performance of the RF classification model

According to Sciuba et al. (2020), scheelite trace element contents in orogenic Au deposits vary as a function of host rock composition and metamorphic facies as result of fluid-rock exchange during fluid flow to gold deposition site. As shown in Table 3.1, the three Au endowment classes comprise at least two of the three major groups of host rock compositions (sedimentary, felsic/intermediate and mafic/ultramafic) and metamorphic facies (lower greenschist, middle greenschist and upper greenschist to lower amphibolite). This suggests that the Au endowment is independent on composition and metamorphic facies of the host rocks, unlike the scheelite trace element composition.

As shown in Figures 3.2 and 3.3, scheelite composition is overall similar for the 3 gold endowment classes, with large overlap in the range of compositional values. There is an increase in the median value of moderately important Pb and Ba, and lower importance

Mg (Fig. 3.4) with increasing gold endowment. Using the most important elements for the RF model, As, Sr, Mo, Pb and Mn, binary plots do not discriminate scheelite from different Au endowment classes (Figs. 3.3b-d). Unlikely binary plots, the RF classification model shows strong performance and the ability to discriminate scheelite from the three classes of gold endowment, yielding an overall accuracy of 94%. The result of tenfold cross validation shows a high prediction accuracy (93%), which proves the ability of RF classifier to effectively distinguish scheelite from deposit with different Au endowments (Table 3.4). This is because unlike simple statistical methods, the RF classifier makes use of all predictor variables to find chemical similarities or differences between the observations (Breiman 2001), even for a dataset with overlapping chemical compositional ranges between the classes (Fig. 3.2; Table 3.3).

Caraballo et al. (subm.) showed that the accuracy of prediction is affected by missing elements, even imputed, especially for those with high importance for the RF classification model. According to the variable importance measure, As, Sr and Mo are the most important elements for RF classification, followed by Pb, Mn, Nb, Y, Eu anomaly and Ba, whereas ΣREE, V, U and Mg are the less important elements (Fig. 3.4). Classification predictions in tests where the dataset is complete yield higher accuracy results (>70%), as is the case of Mustang (100%) and Woxi (72%) scheelite predictions (Fig. 3.5a). Similar high accuracy predictions (70%) were obtained for Macraes data reported by Pickering (2018) and Alta Lode-Bendigo scheelite (73%), which are missing lower importance elements V and Ba, and V, Ba and U, respectively (Figs. 3.4 and 3.5b). In contrast, predictions in which elements with high to moderate importance are missing, e.g. As and Nb for Macraes (Cave et al. 2017), the accuracy decreases drastically (<50%; Table 3.4). Thus, the prediction accuracy is significantly affected depending on the degree of variable importance and how many variables are missing. This may explain the notable difference between the prediction accuracy for Macraes scheelite reported by Cave et al. (2017) and by Pickering (2018) (Fig. 3.5b Table 3.5).

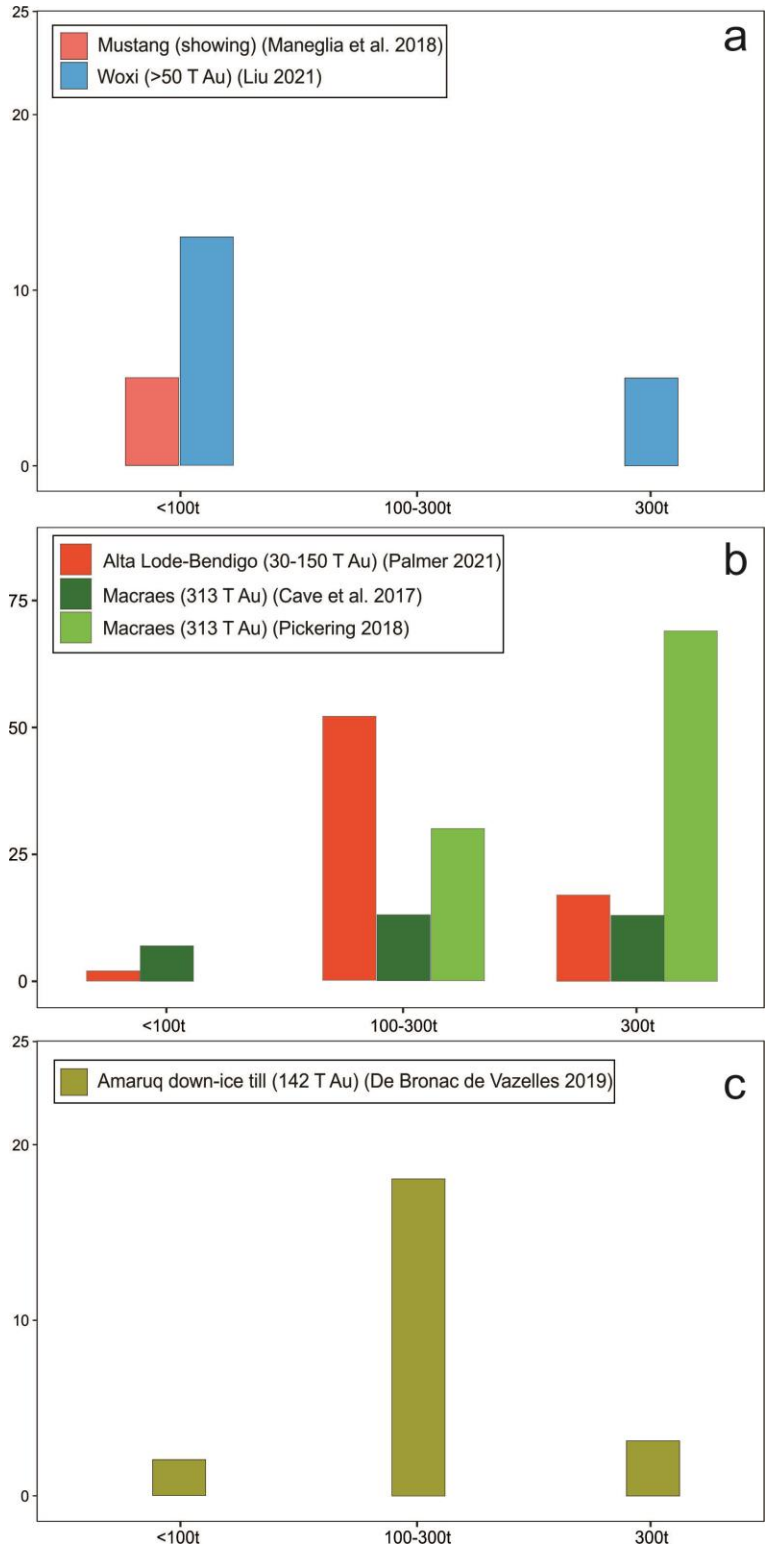

Figure 3.5. Histogram of the predicted classification frequencies of Random Forest classification model. In a-c, predictions performed with complete dataset, and in b, predictions performed with a dataset containing imputed missing elements.

The performance of the RF model on external data confirms its ability to predict scheelite-bearing orogenic Au deposits of different sizes, which makes it a potential tool to assess the Au endowment of orogenic Au deposits. For instance, similar contributions have successfully demonstrated that the combination of RF classifier and mineral chemistry can be used to assess the fertility of metamorphosed VMS using gahnite (O'Brien et al. 2015), and of Cu porphyry deposits using zircon and chlorite (Zou et al. 2022; Li et al. 2022). These studies, combined with our results suggest that RF classifier could be applied to other indicator minerals such as rutile, tourmaline, apatite, etc., to evaluate whether they can be able to assess the fertility/metal endowment of orogenic Au deposits. This creates an opportunity for combining different approaches for mineral targeting.

Table 3.5. Summary of RF predictions for literature data.

Deposit name	Missing elements	Number of analysis	<100 T	100-300 T	>300 T
Mustang	-	4	100%		
Woxi	-	18	72%		28%
Alta Lode - Bendigo	V, Ba, U	71	3%	73%	24%
Macraes (Pickering 2018)	V, Ba	99		30%	70%
Macraes (Cave et al. 2017)	As, V, Nb	33	21%	39%	39%
Till	-				
Amaruq down-ice		23	9%	78%	13%

3.7.2 Applications and limitations of the RF model

The high accuracy predictions obtained by RF classification model using scheelite chemistry enhances its capacity as a potential tool for Au endowment targeting of orogenic Au deposits. However, the use of this model on scheelite from other types of deposits such as skarns, greisen and intrusion-related gold deposit is not recommended because the RF model was trained specifically to predict Au endowment from scheelite-bearing orogenic Au deposits.

Some studies have shown that scheelite from orogenic Au deposits differ of that from magmatic-hydrothermal deposits mainly due their high Sr, and low Mo, Nb, and Mn contents and predominantly positive Eu anomaly (Poulin et al. 2018; Sciuba et al. 2020; Miranda et al. 2022). These studies have proposed discriminate diagrams and PLS-DA models to

discriminate scheelite from different types of deposits. Recent, chapter 2 of this thesis shows that the RF classifier can effectively assess the source of scheelite from 6 deposit types using 11 trace element predictors (Mo, Nb, Sr, Y, Pb, As, Mn, Na, REE, Eu anomaly and Mg). Therefore, the source of scheelite must be assessed before using the RF endowment classification model.

Amaruq is a producing mine with a current 142 T Au endowment that provides an example for testing recognition of the source of scheelite in overburden sediments and to apply the gold endowment classifier to mineral exploration. De Bronac de Vazelhes (2019) and Mendizabal (2022) showed that most scheelite recovered from till samples collected down-ice from the Amaruq deposit has a chemical composition similar to that of the deposit, suggesting that those were sourced from the Amaruq deposit. In contrast, scheelite up-ice from the deposit is exotic to the Amaruq deposit (Mendizabal 2022). We used the RF model to classify deposit types proposed in Chap. 2 and the prediction results confirm that Amaruq down-ice till scheelite has the signature of orogenic Au deposits. Thus, we applied the gold endowment RF model and 78% of scheelite analyses are predicted to belong to the 100-300 T Au class, consistent with the known gold endowment (142 T Au) for the Amaruq deposit (Fig. 3.5c; Table 3.5). This result demonstrates the use of the RF gold endowment model to assess the mineral potential of the source of orogenic gold-derived detrital scheelite.

3.8 Conclusion

This study demonstrates the efficiency of RF classifier model over simple statistical method using scheelite trace elements composition to assess the Au endowment of orogenic Au deposits. The RF classification model yields an overall accuracy of 94%, with individual accuracies of ~87% for <100 T Au, ~98% for 100-300 T Au and 95.6% for >300 T Au. The results reveal that predictions on literature data with a complete set of elements or lacking elements that are less important for the model yields higher accuracy classification (>70%), whereas scheelite composition data missing important elements yields lower accuracy (<40%). Additionally, our results reveal that the Au endowment is independent of composition and metamorphic facies of the deposit host rocks. The RF classification model shows that all 13 predictor elements As, Sr, Mo, Nb, Y, Eu anomaly, Ba, ΣREE, V, U and Mg, in decreasing order of importance as predictors, are essential for accurate predictions of scheelite from orogenic Au deposits.

3.9 Acknowledgments

This research was supported by the Natural Sciences and Engineering Research Council (NSERC) of Canada, Agnico Eagle Mines Ltd., and Ministère de l'Énergie et des Ressources Naturelles du Québec.

3.10 References

Anglin CD, Jonasson IR, Franklin JM (1996) Sm-Nd dating of scheelite and tourmaline: implications for the genesis of Archean gold deposits, Val d'Or, Canada. Econ Geol 91:1372-1382.

Azadbakht, Z., Lentz, D.R., McFarlane, C.R.M., Whalen, J.B., 2020. Using magmatic biotite chemistry to differentiate barren and mineralized Silurian–Devonian granitoids of New Brunswick, Canada. Contrib Mineral Petrol 175:69. doi: https://doi.org/10.1007/s00410-020-01703-2

Ballard, J.R., Palin, J.M., Campbell, I.H., 2002. Relative oxidation states of magmas inferred from Ce"IV"/Ce"III" in zircon: application to porphyry copper deposits of northern Chile. Contrib Mineral Petrol 144: 347-364

Bédard, É, De Bronac de Vazelhes, V., Beaudoin, G., 2022. Performance of predictive supervised classification models of trace elements in magnetite for mineral exploration. J Geochem Explor 236:106959. doi: doi.org/10.1016/j.gexplo.2022.106959.

Bell, K., Anglin, C.D., Franklin, J.M., 1989. Sm-Nd and Rb-Sr isotope systematics of scheelites: Possible implications for the age and genesis of vein-hosted gold deposits. *Geology* 17 (6): 500–504. doi: https://doi.org/10.1130/0091-7613(1989)017<0500:SNARSI>2.3.CO;2

Breiman, L., 2001. Random Forests. Machine Learning 45: 5-32. doi: https://doi.org/10.1023/A:1010933404324

Brugger, J., Etschmann, B., Pownceby, M., Liu, W., Grundler, P., Brewe, D., 2008. Oxidation state of europium in scheelite: tracking fluid–rock interaction in gold deposits. Chem Geol 257:26–33.

Cave, B.J., Pitcairn, I.K., Craw, D., Large, R.R., Thompson, J.M., Johnson, S.C., 2017. A metamorphic mineral source for tungsten in the turbidite-hosted orogenic gold deposits of the Otago Schist, New Zealand. Miner Deposita 52: 515-537. doi: https://doi.org/10.1007/s00126-016-0677-5

Cracknell, M.J., and Reading, A.M., 2014. Geological mapping using remote sensing data: A comparison of five machine learning algorithms, their response to variations in the spatial distribution of training data and the use of explicit spatial information. Computers & Geosciences, 63: 22-33. doi: https://doi.org/10.1016/j.cageo.2013.10.008

Darbyshire, D.P.F., Pitfield, P.E.J., Campbell, S.D.G., 1996. Late Archean and Early Proterozoic gold-tungsten mineralization in the Zimbabwe Archean craton: Rb-Sr and Sm-Nd isotope constraints. *Geology*, 24 (1): 19–22. doi: https://doi.org/10.1130/0091-7613(1996)024<0019:LAAEPG>2.3.CO;2

De Bronac de Vazelhes V., 2019. Étude de la dispersion d'un gisement d'or dans les sédiments glaciaires: Le cas d'Amaruq (Nunavut, Canada). M.Sc. thesis, Université Laval, 213p.

Dmitrijeva, M., Ciobanu, C.L., Ehrig, K., Cook, N.J., Verdugo-Ihl, M.R., Metcalfe, A.V., Kamenetsky, V.S., McPhie, J., Carew, M., 2022. Geochemical Data Analysis of Iron Oxide Copper-Gold Mineralization, Wirrda Well Prospect, South Australia. Econ Geol 117(4): 853–874. doi: https://doi.org/10.5382/econgeo.4904

Elongo, V., Falck, H., Rasmussen, K.L., Robbins, L.J., Creaser, R.A., Luo, Y., Pearson, D.G., Sarkar, C., Adlakha, E., Palmer, M.C., Scott, J.M., Hickey, K., Konhauser, K., Lecumberri-Sanchez, P., 2022. Ancient roots of tungsten in western North America. *Geology*, 50 (7): 791–795. doi: https://doi.org/10.1130/G49801.1

Ghaderi, M., Palin, J., Campbell, I., Sylvester, P., 1999. Rare earth element systematics in scheelite from hydrothermal gold deposits in the Kalgoorlie-Norseman region, Western Australia. Econ Geol 94:423–437.

Goldfarb, R.J., Baker, T., Dubé, B., Groves, D.I., Hart, C.J.R., Gosselin, P., 2005. Distribution, Character, and Genesis of Gold Deposits in Metamorphic Terran, One Hundredth Anniversary Volume, Jeffrey W. Hedenquist, John F. H. Thompson, Richard J. Goldfarb, Jeremy P. Richards.

Goldfarb, R.J., Groves, D.I., Gardoll, S., 2001. Orogenic gold and geologic time: a global synthesis. Ore Geol Rev, 18: 1-75

Goldfarb, R.J., Qiu, K.F., Deng, J., Chen, Y.J., Yang, L.Q., 2019. Orogenic gold deposits of China. Society of Economic Geologists Special Publication, 22: 263-324.

Gosselin, P., and Dubé, B., 2005. Gold deposits of the world: Distribution, geological parameters and gold content: Geological Survey of Canada. Open File 4895, 271 p. (CD-ROM).

Gregory, D.D., Cracknell, M.J., Large, R.R., McGoldrick, P., Kuhn, S., Maslennikov, V.V., Baker, M.J., Fox, N., Belousov, I., Figueroa, M.C., Steadman, J.A., Fabris, A.J., Lyons, T.W., 2019. Distinguishing ore deposit type and barren sedimentary pyrite using laser ablation-inductively coupled plasma-mass spectrometry trace element data and statistical analysis of large data sets. Econ Geol 114(4): 771–786.

Groves, D.I., Goldfarb, R.J., Gebre-Mariam, M., Hagemann, S.G., Robert, F., 1998. Orogenic gold deposits: A proposed classification in the context of their crustal distribution and relationship to other gold deposit types. Ore Geol Rev 13, 7-27, doi: https://doi.org/10.1016/S0169-1368(97)00012-7.

Groves, D.I., Goldfarb, R.J., Santosh, M., 2016.The conjunction of factors that lead to the formation of giant gold provinces and deposits in non-arc settings. Geoscience Frontiers, 7 (3): 303-314

Grütter, H.S., Gurney, J.J., Menzies, A.H., Winter, F., 2004. An updated classification scheme for mantle-derived garnet, for use by diamond explorers. Lithos, 77: 841-857. doi: https://doi.org/10.1016/j.lithos.2004.04.012

Grzela, D., Beaudoin, G., Bedard, E., 2019. Tourmaline, scheelite, and magnetite compositions from orogenic gold deposits and glacial sediments of the Val-d'Or district (Quebec, Canada): implications to mineral exploration. J Geochem Explor 206:106355.

Guo, Z., Li, J., Xu, X., Song, Z., Dong, X., Tian, J., Yang, Y., She, H., Xiang, A., Kang, Y., 2016. Sm/Nd dating and REE composition of scheelite for the Honghuaerji scheelite deposit, Inner Mongolia, Northeast China. Lithos 261: 307–321.

Gurney, J.J., 1984. A correlation between garnets and diamonds. In: Glover, J.E., Harris, P.G. (Eds.), Kimberlite occurrence and origins: a Basis for Conceptual Models in Exploration. Geology Department and University Extension, University of Western Australia, Publication 8 143–166.

Hart, C., 2007. Reduced Intrusion-Related Gold Systems. In W D Goodfellow, Mineral Deposits of Canada: a synthesis of major deposittypes, district metallogeny, the evolution of geological provinces, and exploration methods (pp 95–112) Geological Association of Canada, Mineral Deposits Division.

Hsu, L.C. and Galli, P.E., 1973, Origin of the scheelite-powellite series of minerals. Economic Geology, 68, 681–696.

Kempe, U., and Oberthür, T., 1997. Physical and geochemical characteristics of scheelite from gold deposits; a reconnaissance study. Proceedings of the ... Biennial SGA (Society for Geology Applied to Mineral Deposits) Meeting, Vol. 4, p.209-212.

Kent, A.J.R., Campbell, I.H., McCulloch, M.T., 1995. Sm-Nd systematics of hydrothermal scheelite from the Mount Charlotte Mine, Kalgoorlie, Western Australia; an isotopic link between gold mineralization and komatiites. *Economic Geology*; 90 (8): 2329–2335. doi: https://doi.org/10.2113/gsecongeo.90.8.2329

Kozlik, M., Gerdes, A., Raith, J.G., 2016. Strontium isotope systematics of scheelite and apatite from the Felbertal tungsten deposit, Austria – results of in-situ LA-MC-ICP-MS analysis. Miner Petrol 110, 11–27. https://doi.org/10.1007/s00710-015-0416-0

Li, C., Shen, P., Zhao, Y., Li, P., Zhang, L., Pan, H., 2022. Mineral chemistry of chlorite in different geologic environments and its implications for porphyry Cu ± Au ± Mo deposits. Ore Geol Rev 149: 105112. doi: https://doi.org/10.1016/j.oregeorev.2022.105112

Liu, K., 2021. The Genesis of the Wolfram Camp tungsten-molybdenum deposit, Queensland, Australia, and the geochemistry of tungsten ore minerals. PhD thesis, Colorado School of Mines.

Maneglia, N., Beaudoin, G., Simard, M., 2017. Indicator minerals of the Meliadine orogenic gold deposits, Nunavut (Canada), and application to till surveys. Geochem Explor Environ Anal 18: 241–251

Mendizabal, A 2022. Étude de la composition des minéraux indicateurs et de la géochimie du till en aval d'un gisement d'or: Le cas d'Amaruq (Nunavut, Canada). M.Sc. thesis, Université Laval, 196p.

Miranda, A.C.R., Beaudoin, G., Rottier, B., 2022. Scheelite chemistry from skarn systems: implications for ore-forming processes and mineral exploration. Miner Deposita 57: 1469–1497 doi: https://doi.org/10.1007/s00126-022-01118-y

Nathwani, C.L., Wilkinson, J.J., Fry, G., Armstrong, R.N., Smith, D.J., Ihlenfeld, C., 2022. Machine learning for geochemical exploration: classifying metallogenic fertility in arc magmas and insights into porphyry copper deposit formation. Miner Deposita 57: 1143–1166. doi:https://doi.org/10.1007/s00126-021-01086-9

Noble, S.R, Spooner, E.T.C., Harris, F.R., 1984. The Logtung large tonnage, low-grade W (scheelite)-Mo porphyry deposit, south-central Yukon Territory. Econ Geol 79(5): 848-868. doi: https://doi.org/10.2113/gsecongeo.79.5.848

O'Brien, J., Spry, P., Teale, G., Jackson, S., Koenig, A., 2015. Gahnite composition as a means to fingerprint metamorphosed massive sulfide and non-sulfide zinc deposits. J Geochem Explor 159:48–61

Palarea-Albaladejo, J., Martin-Fernandez, J.A, 2015. zCompositions-R package for multivariate imputation of left-censored data under a compositional approach. Chemometr Intell Lab Syst 143:85–96

Palmer, M.C., 2021. Geochemical characterisation of scheelite from New Zealand (Thesis, Doctor of Philosophy). University of Otago. Retrieved from http://hdl.handle.net/10523/12254

Palmer, M.C., Scanlan, E.J., Scott, J.M., Farmer, L., Pickering, D., Wilson, V.J., Oelze, M., Craw, D., le Roux, P.J., Luo, Y., Graham, D.G., Reid, M.R., Stirling, C.H., 2022. Distinct scheelite REE geochemistry and 87Sr/86Sr isotopes in proximally- and distally-sourced metamorphogenic hydrothermal systems, Otago Schist, New Zealand, Ore Geol Rev , 144, 104800. doi: https://doi.org/10.1016/j.oregeorev.2022.104800

Pan, L.C., Hu, R.Z., Wang, X.S., Bi, X.W., Zhu, J.J., Li, C., 2016. Apatite trace element and halogen compositions as petrogenetic-metallogenic indicators: Examples from four granite plutons in the Sanjiang region, SW China. Lithos, 254–255, 118-130. https://doi.org/10.1016/j.lithos.2016.03.010

Phillips G.N., 2013. Australian and global setting for gold in 2013, in Proceedings world gold 2013, Brisbane, Australia, 26–29 September, 2013. Aust Inst Min Metall. 15–21.

Pickering, D.J., 2018. Geochemical and grain size characterisation of scheelite at Golden Point, Macraes Mine, New Zealand, University of Otago, 124 pp.

Poulin, R., Kontak, D., McDonald, A., McClenaghan, M. 2018. Assessing scheelite as an ore-deposit discriminator using its trace element and REE chemistry. Can Mineral 56: 265–302

R Core Team 2021. R: a language and environment for statistical computing. R Foundation for Statistical Computing, Vienna, Austria. URL https:// www.R- proje ct. org/.

Raimbault, L., Baumer, A., Dubru, M., Benkerrou, C., Croze, V., Zahm, A., 1993. REE fractionation between scheelite and apatite in hydrothermal conditions. *American Mineralogist* 78 (11-12): 1275–1285.

Rodriguez-Galiano, V., Sanchez-Castillo, M., Chica-Olmo, M., Chica-Rivas, M., 2015. Machine learning predictive models for mineral prospectivity: An evaluation of neural networks, random forest, regression trees and support vector machines. Ore Geol Rev 71: 804-818. doi:https://doi.org/10.1016/j.oregeorev.2015.01.001

Scanlan, E.J., Scott, J.M., Wilson, V.J., Stirling, G.H., Reid, M.R., Le Roux, P.J., 2018. In Situ $^{87}Sr/^{86}Sr$ of Scheelite and Calcite Reveals Proximal and Distal Fluid-Rock Interaction During Orogenic W-Au Mineralization, Otago Schist, New Zealand. Econ Geol 113(7): 1571-1586. doi: https://doi.org/10.5382/econgeo.2018.4603

Sciuba, M., Beaudoin, G., Grzela, D., Makvandi, S., 2020. Trace element composition of scheelite in orogenic gold deposits. Miner Deposita 55: 1149-1172

Song, G., Qin, K., Li, G., Evans, N., Chen, L., 2014. Scheelite elemental and isotopic signatures: Implications for the genesis of skarn-type W-Mo deposits in the Chizhou area, Anhui Province Eastern China. Am Mineral 99: 303–317

Stekhoven, D.J., Bühlmann, P., 2012. MissForest—non-parametric missing value imputation for mixed-type data, *Bioinformatics,* 28: 112–118, https://doi.org/10.1093/bioinformatics/btr597

Tyson, R.M., Hemphill, W.R., Theisen, A.R., 1988. Effect of the W:Mo ratio on the shift of excitation and emission spectra in the scheelite-powellite series. *American Mineralogist* 73 (9-10): 1145–1154.

Voicu, G.M., Bardoux, M., Stevenson, R., Jebrak, M., 2001 Nd and Sr isotope study of hydrothermal scheelite and host rocks at Omai, Guiana Shield: implications for ore fluid source and flow path during the formation of orogenic gold deposits Mineralium Deposita 35: 302-314

Wade, C.E., Payne, J.L., Barovich, K., Gilbert, S., Wade, B.P., Crowley, J.L., Reid, A., Jagodzinski, E.A., 2022. Zircon trace element geochemistry as an indicator of magma fertility in iron oxide copper-gold provinces. *Economic Geology*; 117 (3): 703–718. doi: https://doi.org/10.5382/econgeo.4886

Wintzer, N.E., Schmitz, M.D., Gillerman, V.S., Vervoort, J.D., 2022. U-Pb Scheelite Ages of Tungsten and Antimony Mineralization in the Stibnite-Yellow Pine District, Central Idaho. *Economic Geology*; doi: https://doi.org/10.5382/econgeo.4953

Zhao, W., Zhou, M-F., Williams-Jones, A., Zhao, Z., 2018. Constraints on the uptake of REE by scheelite in the Baoshan tungsten skarn deposit, South China. Chem Geol 477:123–136

Zou, S., Chen, X., Brzozowski, M.J., Leng, C.B., Xu, D., 2022. Application of Machine Learning to Characterizing Magma Fertility in Porphyry Cu Deposits. JGR: Solid Earth, 127: 1-17.

Chapter - 4 In situ Sm-Nd analysis in scheelite from magmatic-hydrothermal deposits

4.1 Introduction

This chapter presents the preliminary results of *in-situ* Sm-Nd isotope analysis in scheelite from W-Mo porphyry, W skarns and Reduced Intrusion Related Gold Systems (RIRGS) deposits. Because the results are incomplete, as a result of instrument breakdown during COVID, no interpretation is provided.

4.2 Selected samples

Dublin Gulch, Fort Knox, Scheelite Dome, Mactung, Cantung and Lened scheelite-bearing deposits are located in the Tombstone-Tungsten Belt, in Yukon (Canada) and Alaska (USA) (Fig. 4.1). Dublin Gulch, Fort Knox and Scheelite Dome RIRGS deposits are associated with mid-Cretaceous Mayo plutonic suite (95-92 Ma), intruded into metasediments of the Selwyn Basin (Hart et al. 2004; Hart 2007). The Mayo suite is characterized by biotite-hornblende granodiorite intrusions, metaluminous and moderately reduced. Based on petrological and geochemical data, the magmas that formed the Mayo suite were derived from the melting of the continental crust with a minor mantle contribution. Whole rock εNd values for Mayo suite varies from -8.3 to -12.5 (Farmer et al. 2000; Lang 2000).

Mactung, Cantung and Lened tungsten skarns deposits are associated with a mid-Cretaceous Tungsten plutonic suite (97-94 Ma), intruded in the Paleozoic carbonates of the Selwyn Basin in the Tombstone-Tungsten Belt (Hart et al. 2004). The Tungsten plutonic suite comprises peraluminous monzonite, ilmenite-dominant, and with biotite as the dominant mafic mineral. Whole rock εNd signature of the intrusions belonging to the Tungsten suite ranges from -13 to -15 (Lang 2000). In the three deposits investigated (Mactung, Cantung and Lened), scheelite is hosted in Lower to Middle Cambrian carbonate rocks (Selwyn Basin) that were altered ore-bearing calc-silicate skarn rocks. The skarns have different mineralogical assemblage/facies. At Mactung scheelite is hosted mainly in pyroxene skarn, where pyrrhotite is abundant (Dick and Hodgson 1982; Elongo et al. 2020). At Cantung, scheelite from two different orebodies, Open Pit and E Zone, were analyzed (Mathieson and Clark 1984; Bowman et al. 1985). In both cases scheelite occurs in

amphibole and pyrrhotite skarns. At Lened, scheelite is hosted by biotite-pyrrhotite skarn (Elongo et al. 2020).

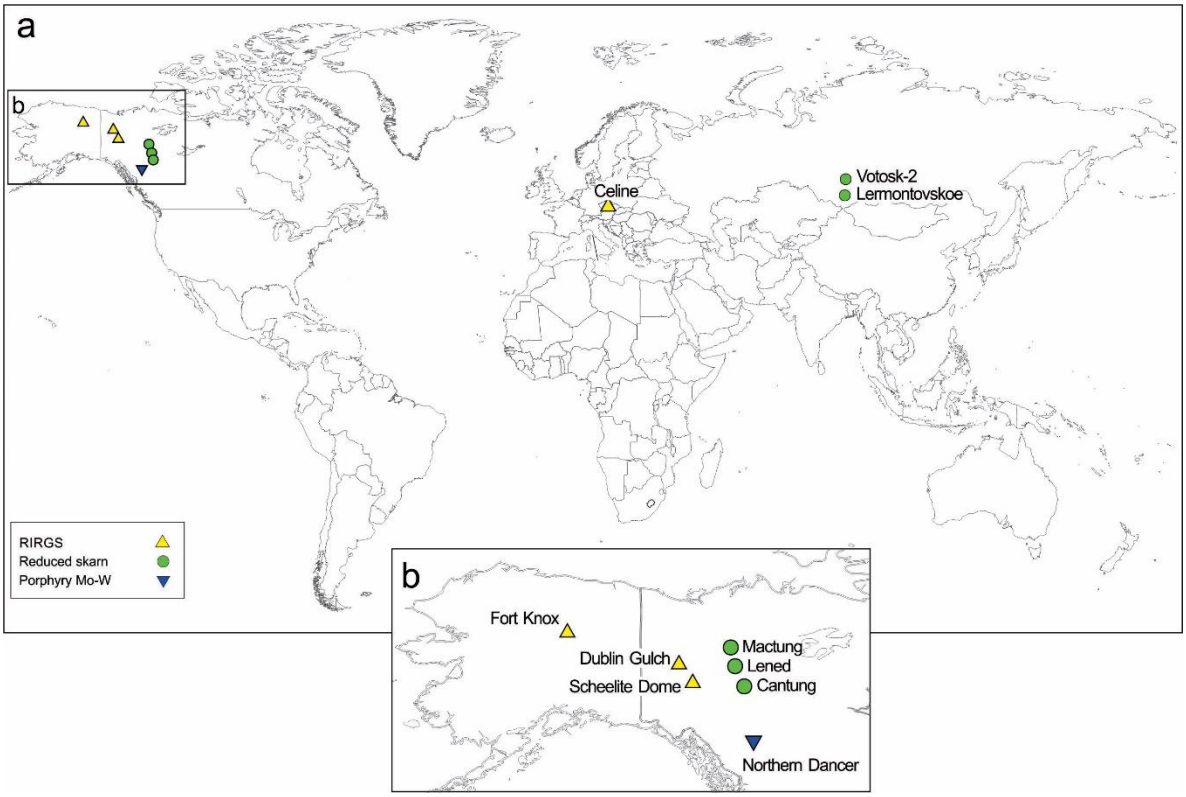

Figure 4.1. Location of the scheelite-bearing samples (a). In (b), samples located in the Tombstone-Tunsgten Belt.

Northern Dancer is a W-Mo porphyry deposit (118 Ma) located in the south central Yukon Territory (Fig. 4.1). The deposit is associated with several felsic porphyritic phases, intruded in graphitic quartzite and calcareous shales. Scheelite occurs in quartz veins crosscutting these metasediments (Noble et al. 1984; Mihalynuk and Heaman 2002). There is no available information about the magma source that formed the Northern Dancer porphyry deposit.

Lermontovskoe and Vostok- 2 deposits are located in the Central Sikhote-Alin Gold-Tungsten Belt, Russia (Fig. 4.1). Lermontovskoe is a tungsten skarn deposit that differs from Cantung, Mactung and Lened due to W-Au-As-Bi-Te-Sb signature. This metal association suggests a close affinity with RIRGS (Soloviev et al. 2015; Soloviev et al. 2017). The deposit is associated with an intrusion that is part of the ilmenite-series, high-K peraluminous granitoid (granodiorite to granite) suite. The melt forming these rocks shows a mixed crustal

and mantellic signature (Soloviev et al. 2017). Scheelite is disseminated in amphibole-biotite skarn. There is no isotopic information of the granites.

Vostok- 2 (W-Au) deposit is classified as a transition between W-dominant and Au-dominant intrusion-related deposits. Scheelite is hosted in exoskarns and quartz veins in the country rocks. Vostok-2 deposit is related to ilmenite-series, high-K calc-alkaline granodiorite intrusion. Whole rock εNd signature for Vostok-2 intrusion range from -3.1 to -5.

Celine is interpreted as a RIRGS deposit located in the central part of the Bohemian Massif, in the Variscan Belt (Zachariáš et al. 2014). The deposit is hosted by the Sazava intrusion (354 Ma), which is composed mainly of metaluminous calc-alkaline biotite-amphibole tonalite (Zachariáš et al. 2014). The Nd initial isotopic data of Sazava tonalite vary from 0.46 to -0.07 (Janoušek et al. 1995). The table 4.1 shows a summary of the main characteristics of the samples analyzed in this study.

Table 4.1 Summary of the main characteristics of the studied samples.

Name	Deposit type	Host Rock	Province	Age (Ma)
Celine	RIRGS	Qz vein in amphibolite	Bohemian Massif	354
Dublin Gulch	RIRGS	Intrusion hosted	Tombstone-Tungsten belt	93
Fort Knox	RIRGS	Intrusion hosted	Tombstone-Tungsten belt	92
Lened	Skarn	Biotite-pyrrhotite skarn	Tombstone-Tungsten belt	96
Lermontovskoe	Skarn	Pyrrhotite skarn	Central Sikhote Alin	112
Northern Dancer	W-Mo porphyry	Pyrite-scheelite-vein	-	118
Mactung	Skarn	Pyroxene skarn	Tombstone-Tungsten belt	96
Scheelite Dome	RIRGS	Pyroxene skarn	Tombstone-Tungsten belt	92.5
Votosk-2	Skarn	Pyrrotite skarn	Central Sikhote Alin	102
Cantung (E Zone)	Skarn	Amphibole skarn	Tombstone-Tungsten belt	96
Cantung (open pit)	Skarn	Pyrrotite skarn	Tombstone-Tungsten belt	96

4.3 Methodology

Scheelite crystals containing >100 ppm Nd were selected. In addition to Nd content, we selected samples from deposits that have known mineralization ages in order to calculate

the εNd. Therefore, a total of 12 scheelite-bearing samples comprising 6 skarns, 4 RIRGS, and 1 W-Mo porphyry deposits were selected for the *in situ* Sm-Nd analysis (Table 4.1).

Simultaneous Sm-Nd isotope and trace element (Sm and Nd) measurements in scheelite were carried out in the Arctic Resources Laboratory at the University of Alberta (Luo et al., 2019) during one analytical session in October 2019. The scheelite samples were ablated using the laser ablation split stream (LASS) technique described by Yuan et al., (2008), Xie et al. (2008), and Fisher et al. (2014). The samples were ablated using a 193 nm Resolution Excimer ArF laser equipped with a Laurin-technic S-155 two-volume ablation cell. Analyses were performed using a laser fluence of 6 J/cm2 and a repetition rate of 10 Hz. Analysis time consisted of 60 seconds of background followed by 70 seconds of ablation and then 40 seconds of sample washout. The carrier gas is a mixture of ~1.6 L/min Ar and 14 ml/min N_2, which entered tangentially from the top of the S-155 ablation cell funnel and ~800 ml/min He entering from the side of the cell. This yielded a pressure in the ablation cell of ~7.5 KPa. The ablated sample aerosol, He, N_2 and Ar mixture was then split after the laser cell using a Y-piece, diverting the ablation product to a Thermo Neptune Plus using multiple Faraday detectors with 10^{11} Ω amplifiers operating in static collection mode (for Sm-Nd) and a Thermo Element-XR 2 mass spectrometer using a single secondary electron multiplier detector in peak hopping mode (for trace elements). The length of tubing was equalized such that the ablated sample aerosol arrives simultaneously at both mass spectrometers. Calibration was performed using NIST SRM 612 in conjunction with internal standardization using isotope ^{43}Ca. The results of the measurements of secondary standards (e.g., NIST614) agree with the reference values within relative uncertainties of typically 5–10% or better at the 95% confidence level.

4.4 Preliminary results

A total of 83 Sm-Nd isotopes analysis were carried out in 12 scheelite-bearing samples (Appendix 4.1A). The table 4.2 shows the summary of the measurements of $^{147}Sm/^{144}Nd$ and $^{143}Nd/^{144}Nd$ ratios, and εNd calculated at the time t of each analysed sample. The isoplotR online (Vermeesch 2018) was used to calculate the isochron but it was not possible to obtain a geologically meaningful age as a result of narrow ranges $^{143}Nd/^{144}Nd_0$ in all samples (Table 4.2).

Table 4.2. Summary Sm-Nd isotope LASS-ICPMS analyses of scheelite crystals

Name	**$^{147}Sm/^{144}Nd_0$**	**$^{143}Nd/^{144}Nd_0$**	**Age Ma (t)**	**εNd_t**
Celine	0.11317 - 0.1332	0.512553 - 0.512393	354	-1.22 to 1.52
Dublin Gulch	0.08446 - 0.09227	0.512042 - 0.512122	93	-10.31 to -8.71
Fort Knox	0.08979 - 0.13509	0.512144 - 0.51231	92	-8.52 to -5.64
Lened	0.08945 - 0.20302	0.511622 - 0.51172	96	-19.16 to -17.51
Lermontovskoe	0.1033 - 0.18429	0.512432 - 0.512573	112	-2.96 to -0.95
Northern Dancer	0.24037 - 0.27308	0.512447 - 0.51249	118	-4.5 to -4
Mactung	0.0995 - 0.11128	0.512079 - 0.512182	96	-9.6 to -7.67
Scheelite Dome	0.16972 - 0.17223	0.511392 - 0.511536	92.5	-23.95 to -21.17
Votosk-2	0.04942 - 0.12439	0.512207 - 0.512503	102	-6.68 to -1.29
Cantung (E Zone)	0.1181 - 0.21643	0.511723 - 0.511932	96	-17.04 to -13.86
Cantung (open pit)	0.2046 - 0.4873	0.511876 - 0.51211	96	-15.37 to -12.44

The εNd_t was calculated using CHUR $^{143}Nd/^{144}Nd_0 = 0.512638$, $^{147}Sm/^{144}Nd_0 = 0.1960$ (Bouvier et al., 2008) and the following formula: $\varepsilon Nd_t = ([^{143}Nd/^{144}Nd]sample_t - [^{143}Nd/^{144}Nd]CHUR_t / [^{143}Nd/^{144}Nd]CHUR_t * 10000)$. Age corrected values calculated using the following formula: $^{143}Nd/^{144}Nd_t = {}^{143}Nd/^{144}Nd_0 - {}^{147}Sm/^{144}Nd_0 (e^{\lambda t} - 1)$, where $^{143}Nd/^{144}Nd_0$ and $^{147}Sm/^{144}Nd_0$ are the measured values, $\lambda = 0.00654$ Ga (White, 2015) and t = sample age.

Scheelite from Scheelite Dome deposit displays strong negative εNd values (-23.95 to -21.17) relative to that of Fort Knox and Dublin Gulch (-8.52 to -5.64 and -10.31 to -8.7, respectively) (Fig. 4.2). The the εNd scheelite signature Fort Knox and Dublin Gulch are relatively similar to that of the respective intrusions related to the deposits (Fig. 4.2).

Mactung scheelite displays less negative εNd values (from -9.6 to -7.67) relative to Cantung and Lened tungsten skarn deposits of the same suite (from -15.37 to -12.44 for Open Pit, from -17.04 to -13.86 for E Zone, and from -19.16 to -17.51 for Lened; Fig. 4.3), and differ from εNd values of the Tungsten plutonic suite (from -13 to -15). Cantung scheelite has εNd values very similar to that of Tungsten plutonic suite (Fig. 4.3), whereas Lened scheelite displays relatively more negative εNd (Fig. 4.3).

Scheelite from Vostok-2 displays similar εNd to that of the Vostok-2 intrusion, as well as scheelite from Celine deposit (Fig. 4.4). There are no εNd data of local lithologies for Northern Dancer nor Lermontovskoe (Fig. 4.3).

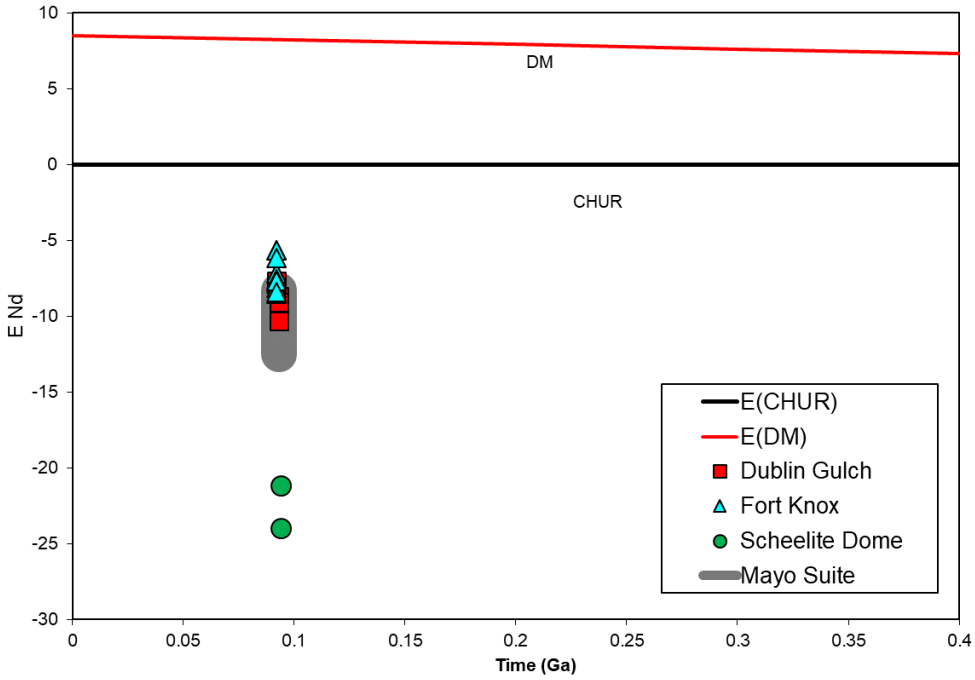

Figure 4.2 εNd at time of formation (t) for scheelite from Dublin Gulch, Fort Knox and Scheelite Dome, and Mayo suite in the Tombstone-Tunsgten belt.

Although these are preliminary outcomes, our results show that scheelite related to magmatic-hydrothermal deposits display similar εNd to that of the related intrusions. This suggests that *in situ* Sm-Nd isotopes analysis in scheelite can be used as a tracer of source materials. The next steps consist of: new analyses will be performed in scheelite associated with orogenic Au deposits; and a compilation of Sm-Nd data of the regional geology in each province to identify the likely source of scheelite.

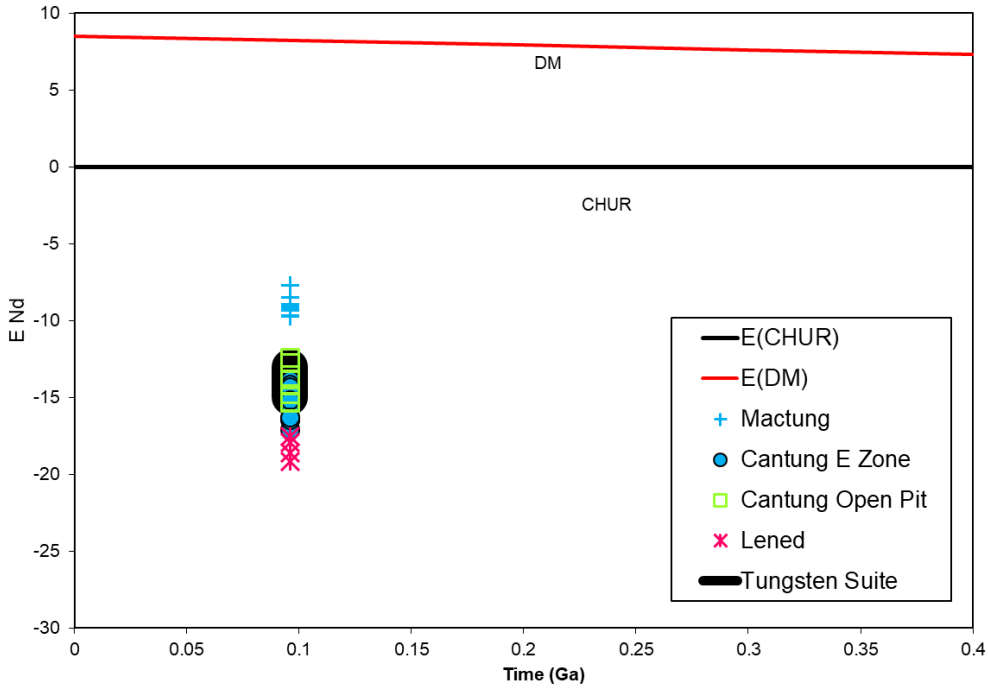

Figure 4.3 εNd at time of formation (t) for scheelite from tungsten skarns (Mactung, Cantung and Lened) of the Tombstone-Tungsten Belt, and for local lithology (Tungsten suite).

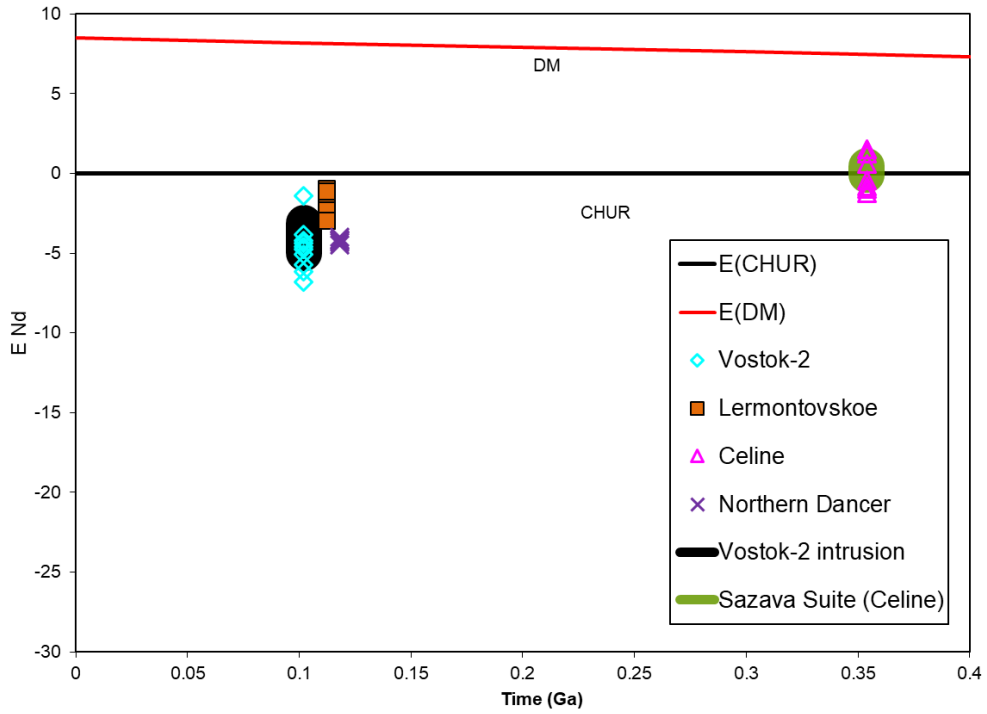

Figure 4.4 εNd at time of formation (t) for scheelite from Vostok-2, Lermontovskoe, Celine and Northern Dancer, for local litologies for Vostok-2 and Celine intrusions.

4.5 References

Bowman, J. Covert, J. J., Clark, A. H. & Mathieson, G. A. 1985. The CanTung E zone scheelite skarn orebody, Tungsten, NorthwestTerritories: oxygen, hydrogen, and carbon isotope studies. Economic Geology 80, 1872–95.

Dick, L., and Hodgson, C., 1982. The MacTung W-Cu(Zn) contact metasomatic and related deposits of the northeastern Canadian Cordillera. Econ Geol 77:845-867

Elongo, V., Lecumberri-Sanchez, P., Legros, H., Falck, H., Adlakha, E., Roy-Garand, A., 2020. Paragenetic constraints on the Cantung, Mactung and Lened tungsten skarn deposits, Canada: Implications for grade distribution. Ore Geology Reviews, 125, 103677. https://doi.org/10.1016/j.oregeorev.2020.103677.

Farmer, G.L., Mueller, S., Marsh, E., Goldfarb, R.J., and Hart, C.J.R., 2000, Isotopic evidence on sources of Au-related mid-Cretaceous Tombstone Plutonic Suite granitic rocks, Clear Creek district, Yukon [abs.]: Geological Society of America, Cordilleran Section Abstracts with Programs A-13.

Fisher, C.M., Vervoort, J.D., DuFrane, S.A., 2014. Accurate Hf isotope determinations of complex zircons using the “laser ablation split stream” method. Geochem. Geophys. Geosyst. 15, 121–139.

Hart, C., 2007. Reduced Intrusion-Related Gold Systems. In W D Goodfellow, Mineral Deposits of Canada: a synthesis of major deposittypes, district metallogeny, the evolution of geological provinces, and exploration methods (pp 95–112) Geological Association of Canada, Mineral Deposits Division.

Hart, C.J.R, Mair, J.L., Goldfarb, R.J., Groves, D.I., 2004. Source and redox controls on metallogenic variations in intrusion related ore systems, TombstoneTungsten Belt, Yukon Territory, Canada. Transactions of the Royal Society of Edinburgh: Earth Sciences, 95, pp 339356 doi:10.1017/S0263593300001115

Lang, J. R. 2000. Regional and system-scale controls on the formation of copper and/or gold magmatic-hydrothermal mineralization. Final Technical Report, Mineral Deposit Research Unit 115 pp.

Luo, Y., Pearson, D.G., Scott, J., Palmer, M.C., Fisher, C.M., Sarkar, C., Vezinet, A., Lecumberri-Sanchez, P., 2019. Simultaneous in situ analysis of Sm-Nd isotopes and trace elements in scheelite by laser ablation split stream ICP-MS: challenges and emerging approaches. In: 2019 North America Laser Ablation Workshop, Austin, p. 34.

Mathieson G, Clark A (1984) The Cantung E Zone Scheelite Skarn Orebody, Tungsten Northwest Territories: A Revised Genetic Model. Econ Geol 79:883-901

Mihalynuk, M.G., and Heaman, L.M., 2002. Age of mineralizated porphyry at the Logtung deposit W-Mo-Bi-Be (beryl, aqua- marine), northwest BC; in Geological Fieldwork, BC Ministry of Energy and Mines, 35-39

Noble, S.R, Spooner, E.T.C., Harris, F.R., 1984. The Logtung large tonnage, low-grade W (scheelite)-Mo porphyry deposit, south-central Yukon Territory. *Economic Geology* 79(5):848–868. doi: https://doi.org/10.2113/gsecongeo.79.5.848

Soloviev S, Kryazhev S, Dvurechenskaya S (2017) Geology, mineralization, stable isotope, and fluid inclusion characteristics of the Vostok-2 reduced W-Cu skarn and Au-W-Bi-As stockwork deposit, Sikhote-Alin, Russia. Ore Geol Rev 86:338–365

Soloviev S, Kryazhev SG, Dvurechenskaya SS (2015) Geology, mineralization, and fluid inclusion characteristics of the Lermontovskoe reduced-type tungsten (±Cu, Au, Bi) skarn deposit, Sikhote-Alin, Russia. Ore Geol Rev 89:15-39

Vermeesch, P., 2018, IsoplotR: a free and open toolbox for geochronology. Geoscience Frontiers, v.9, p.1479-1493, doi: 10.1016/j.gsf.2018.04.001.

Xie, L., Zhang, Y., Zhang, H., Sun, J., Wu, F., 2008. In situ simultaneous determination of trace elements, U-Pb and Lu-Hf isotopes in zircon and baddeleyite. Chin. Sci. Bull. 53, 1565–1573.

Yuan, H.-L., Gao, S., Dai, M.-N., Zong, C.-L., Günther, D., Fontaine, G.H., Liu, X.-M., Diwu, C., 2008. Simultaneous determinations of U–Pb age, Hf isotopes and trace element compositions of zircon by excimer laser-ablation quadrupole and multiple-collector ICP-MS. Chem. Geol. 247, 100–118.

Zachariáš, J., Morávek, P., Gadas, P., Pertoldová, J., 2014. The Mokrsko-West gold deposit, Bohemian Massif, Czech Republic: Mineralogy, deposit setting and classification. Ore Geol Rev 58:238–263.

Discussion

Several studies have shown the use of scheelite recovered from till and stream sediments to target tungsten and gold deposits (Averill 2001; Maneglia et al. 2017; McClenaghan et al. 2017; De Bronac de Vazelhes et al. 2021). Additionally, several discrimination diagrams based on scheelite composition, using both simple and multivariate approaches, have been proposed to discriminate scheelite from orogenic Au to that from magmatic-hydrothermal deposits (Song et al. 2014; Poulin et al. 2018; Sciuba et al. 2020). However, the lack of understanding in the distribution of trace elements in scheelite in diverse magmatic-hydrothermal deposits has limited the application of scheelite in mineral exploration as a robust tool to predict deposit types.

The results of this study show that scheelite trace element composition from magmatic-hydrothermal deposits varies following different redox conditions, magma composition and magmatic-hydrothermal deposit types. This suggests that trace element composition of scheelite can be used to differenciate different deposit types and to track the evolution of magmatic-hydrothermal systems.

Cathodoluminescence images and compositional maps performed by microprobe and LA-ICP-MS, respectively, show that scheelite from oxidized and reduced skarns, quartz-vein/greisen Sn-W and porphyry W-Mo display complex zoning textures (Fig. 2.3), which are mainly controlled by Mo and Nb contents (Figs. 1.7 and 1.8). In contrast, scheelite from RIRGS is texturally homogeneous (Fig. 2.3).

The PLS-DA results show that oxidized and reduced skarns scheelite are chemically different. Oxidized skarns scheelite display higher Mo, V, As and Ti, and lower Nb, Ta, HREE contents relative to reduced skarns scheelite (Fig. 1.11). Such differences are likely a result of salinity and composition of the fluid, fO_2 and co-precipitated minerals (i.e., garnet and clinopyroxene) ((Hsu 1977; Testemale et al. 2004; James-Smith et al. 2010; Brugger et al. 2016). Scheelite from RIRGS displays similar composition to scheelite from oxidized and reduced skarns, which may suggest similar conditions of formation between oxidized and reduced skarn deposits (Figs. 2.6 and 2.8).

Porphyry W-Mo and quartz-vein/greisen Sn-W are characterized by high Th, U, Ta, Y and Pb contents, which differ from RIRGS and oxidized skarns scheelite (Fig. 2.8). The high concentrations of Th, U, Ta, Y and Pb in scheelite is likely related to the high content of fluorine in the mineralizing fluids common in quartz-vein/greisen Sn-W deposits (Pollard

et al. 1987; Breiter et al. 2017; Song et al. 2019; Pan et al. 2019; Wang et al. 2021). It has been demonstrated that fluorine increases the solubility of REE, Y and HSFE in a magma (Keppler 1993; Agangi et al. 2010). As a result, REE-, Y- and HSFE-rich fluids exsolved from those intrusions can precipitate minerals having high REE, Y, Pb, Nb, Ta, U and Th concentrations, such as scheelite. The occurrence of abundant fluorite in scheelite-bearing samples from porphyry W-Mo and quartzvein/greisen Sn-W deposits support this hypothesis.

The PLS-DA results show that orogenic Au deposits and metamorphic scheelite are characterized by low Mo, Nb and Mn, high Sr and Na contents, with commonly positive Eu anomalies (Fig. 2.6 and 2.9). In contrast, scheelite from magmatic-hydrothermal settings have higher Mo, Nb and Mn, lower Sr and Na contents, and both negative and positive Eu anomalies (Figs. 2.6 and 2.9). The distinct contents of these elements in scheelite are mainly a function of fluid source (magmatic vs metamorphic) and of the physico-chemical conditions inherent to each deposit type, supporting thus the use of scheelite composition as a fluid-source tracker (Fig. 2.9). It is noteworthy to point that although RIRGS and orogenic Au deposits share several similar features such as low salinity, CO_2-rich and reduced fluids, and anomalous Te, W and Bi signature (Baker 2002; Goldfarb et al. 2005; Hart 2007), our results show that scheelite associated with RIRGS is chemically distinct to those from orogenic Au deposits characterized by the higher Mo, Nb and Mn contents (Fig. 2.9b), consistent with the distinct fluid sources for both deposit types.

The low Mo content (<100 ppm) and characteristic positive Eu anomaly displayed by scheelite from orogenic settings (Fig. 2.12a) support a relatively reduced metamorphic derived fluids relative to magmatic-derived fluids, which are more oxidized (Song et al. 2014; Poulin et al. 2018; Sciuba et al. 2020). The high Sr content in metamorphic and orogenic Au scheelite results from the release of Sr during the breakdown of Ca-bearing minerals hosted in metasediments and/or mafic-ultramafic volcanic rocks (Paterson and Rankin 1979; Kempe et al. 2001), whereas the low concentrations of Nb and Mn are in function of their low concentration in the host rocks (Sciuba et al. 2020). In contrast, the low concentration of Sr in magmatic-hydrothermal scheelite reflect the low content of Sr from exsolved magmatic-derived fluids that are depleted in Sr due to plagioclase crystallization during differentiation of their source magmas (Miller and Mittlefehldt 1984), whereas Nb and Mn have an incompatible behavior relative to Sr, thus becoming enriched in the magma during fractional crystallization, and consequently become concentrated in the mineralizing fluid

compared to metamorphic fluids (Fig. 2.6a-c; Miller and Stoddard 1981; Shae and Chappell 1999; Picolli and Cadela 2002; Seo et al. 2020). As a result, scheelite from magmatic-hydrothermal settings contains higher Nb and Mn contents relative to those from orogenic settings (Figs. 2.6a, d-e and 2.9).

Additionally, Figs. 2.9c-d highlight that metamorphic scheelite contains low ΣREE, As and Pb contents relative to those associated with gold mineralization, thus allowing their discrimination as shown in Figs. 2.12c-d. Palmer et al. (2022) pointed out that the low ΣREE, Pb and As contents in metamorphic scheelite from the Otago schist is likely related to local host rocks composition, which are poor in these elements, and/or to the low metamorphic conditions (sub- to low-greenschist facies), which do not allow the release these elements from their host minerals (Cave et al. 2017). Moreover, Sr isotopic ratios reveal that scheelite that is not associated with gold displays a heterogeneous isotopic signature that arises from local variations of the host rocks and small amounts of fluid flow. On the other hand, scheelite that formed temporally and spatially associated with gold displays a homogeneous signature, which results from fluids derived from a distal source with long fluid flow pathway (Scanlan et al. 2018; Palmer et al. 2022).

Recent studies show that the RF classifier is an effective tool for mineral deposit discrimination and prediction (O'Brien et al. 2015; Gregory et al. 2019; Liu and Beaudoin 2021; Bédard et al. 2022; Caraballo et al. 2022; Nathwani et al. 2022). The high overall accuracy of testing data prediction (97%) proves the efficiency of the RF classifier to predict mineral deposit types based in scheelite composition (Table 2.3).

The outcomes of this work also show that the metal endowment of an orogenic Au deposit is reflected in scheelite trace element composition. Using a RF classifier, the high prediction accuracy of the testing and external scheelite datasets (94% and >70%, respectively) (Tables 3.4-3.5) show the strong performance and the ability to discriminate scheelite from small (<100T Au), world-class (100-300T Au) and giant orogenic Au deposits (>300T Au). Such abiltity is related to the fact that RF classifier makes use of all predictor variables (As, Sr, Mo, Pb, Mn, Nb, Y, Eu anomaly, Ba, ΣREE, V, U and Mg) to find chemical similarities or differences between the observations (Breiman 2001), even for a dataset with continuous element compositional ranges between the classes.

Moerover, this study highlights the successful application of RF deposit type and endownment models in scheelite recovered from till sediments. Till samples collected up- and down-ice Amaruq orogenic Au deposit, northern Canada, were tested in both RF models

to predict the source and the metal endowment. The predictions results confirmed that most of down-ice deposit till scheelite has the signature of scheelite from orogenic Au deposits, and that 78% were predicted as 100-300T (Fig. 3.5; Table 3.5). These findings agree with de Bronac de Vazelhes (2019) and Mendizabal (2022), where the Amaruq deposit is identified the main source of scheelite, and the metal endowment of 142 T of Au. Therefore, these results support the application of RF deposit type and endownment models in detrital scheelite.

Conclusion

This PhD research aimed to use the trace element composition of scheelite combined with machine learning approach as an effective and robust tool not only to target scheelite-bearing deposits in covered terrains, but also to assess the fertility of scheelite-bearing orogenic Au deposits. This study shows detailed petrographic observations and textural and chemical characterization of scheelite from magmatic-hydrothermal deposits. This new data combined with literature compositional data of scheelite from orogenic Au deposits aimed to find chemical criteria that could allow discriminating scheelite from different deposit types and geological settings.

The results presented in this study demonstrate that scheelite trace element composition from skarn-type deposits varies following the redox state of the skarn system (i.e., reduced and oxidized), intrusion composition and metal content. Such chemical variation is only registered by elements which incorporation in scheelite crystal structure depends on oxygen fugacity, salinity, and fluid composition. These findings support that scheelite chemical composition is strongly dependent on source, composition, and physical-chemical conditions of fluid, which therefore enhances its use as an effective tool for mineral exploration.

The PLS-DA results show that scheelite from magmatic-hydrothermal deposits are chemically distinct to that of orogenic settings due to higher contents of Mo, Mn and Nb, and lower concentrations of Sr, together with predominantly negative Eu anomalies, strongly related to the nature and source of the fluid. Moreover, metamorphic scheelite can be discriminated from that of orogenic Au deposits by their lower Pb, As and REE contents and LREE/HREE ratios, which are related to local host rock composition and metamorphic grade. Additionally, PLS-DA results demonstrate that scheelite composition varies for different magmatic-hydrothermal deposits (i.e., oxidized and reduced skarns, porphyry W-Mo, RIRGS, quartz-vein/greisen Sn-W), and that such compositional variation can be explained by the difference in fO_2 and composition of mineralizing fluids exsolved from the ore-related intrusions. The RF prediction accuracy of the testing and external scheelite datasets prove the ability of trace element composition of scheelite to be used as an efficient tool to predict the source of detrital scheelite, helping thus to orientate strategies in mineral exploration surveys.

Finally, this contribution supports that the RF model based on 13 trace elements in scheelite (As, Sr, Mo, Nb, Y, Eu anomaly, Ba, ΣREE, V, U and Mg) from 23 orogenic Au deposits, classified in three gold endowment classes, can be effectively used to assess the fertility of scheelite-bearing orogenic Au deposits. The high prediction accuracy of the testing and external scheelite datasets demonstrate the effectiveness of the RF classifier algorithm to predict the Au endowment scheelite-bearing orogenic Au deposits. Moreover, these results support the use of RF models as a complementary tool to the decision-making process for the development of exploration targets in known orogenic Au disctricts.

References

Agangi, A., Kamenetsky, V. S., McPhie, J., 2010. The role of fluorine in the concentration and transport of lithophile trace elements in felsic magmas: Insights from the Gawler Range Volcanics, South Australia, Chemical Geology 273, 314-325. https://doi.org/10.1016/j.chemgeo.2010.03.008.

Aitchison, J., 1986. The Statistical Analysis of Compositional Data. (C a Hall, Ed) London.

Allegro, G.L., 1987. The Gilmore Dome tungsten mineralization, Fairbanks mining district, Alaska: University of Alaska Fairbanks, M.S. thesis, 150 p., illust., maps, 7 folded maps.

Andersson, S., Wagner, T., Jonsson, E., Fusswinkel, T., Whitehouse, M., 2019. Apatite as a tracer of the source, chemistry and evolution of ore-forming fluids: The case of the Olserum-Djupedal REE-phosphate mineralisation, SE Sweden, Geochimica et Cosmochimica Acta, 255, 163-187 https://doi.org/10.1016/j.gca.2019.04.014.

Anglin, C.D., Jonasson, I.R., Franklin, J.M. 1996. Sm-Nd dating of scheelite and tourmaline: implications for the genesis of Archean gold deposits, Val d'Or, Canada. Econ Geol 91:1372-1382.

Auwera, J.V., and Andre, L., 1991. Trace elements (REE) and isotopes (O, C, Sr) to characterize the metasmatic fluids sources: evidence from the skarn deposit (Fe, W, Cu) of Traversella (Ivrea, Italy). Contrib Mineral Petrol, 106:325-339.

Averill, S. A., 2001. The application of heavy indicator mineralogy in mineral exploration with emphasis on base metal indicators in glaciated metamorphic and plutonic terrains. Geological Society, London, Special Publications, 185:69-81.

Ayers, J.C., Watson, E.B., 1993. Rutile Solubility and Mobility in Supercritical Fluids. Contrib Mineral Petrol 114:321–330

Azadbakht, Z., Lentz, D.R., McFarlane, C.R.M., Whalen, J.B., 2020. Using magmatic biotite chemistry to differentiate barren and mineralized Silurian–Devonian granitoids of New Brunswick, Canada. Contrib Mineral Petrol 175:69. doi: https://doi.org/10.1007/s00410-020-01703-2

Baker, J.M., Wilkinson, J.J., Wilkinson, C.C., Cooke, D.R., Ireland, T., 2020. Epidote Trace Element Chemistry as an Exploration Tool in the Collahuasi District, Northern Chile. Econ Geol 115(4): 749–770

Baker, T., 2002. Emplacement depth and carbon dioxide-rich fuid inclusions in intrusion-related gold deposits: Economic Geology, 97, p. 1111–1117.

Baker, T., Achterberg, E.V., Ryan, C.G., Lang, J.R., 2004. Composition and evolution of ore fluids in a magmatic-hydrothermal skarn deposit. Geology 32(2):117–120

Ball, C.W., 1954. The Emerald, Feeney and Dodger tungsten ore-bodies, Salmo, British Columbia, Canada. Economic Geology, 49, 625–638.

Ballard, J.R., Palin, M.J., Campbell, I.H., 2002. Relative oxidation states of magmas inferred from Ce(IV)/Ce(III) in zircon: application to porphyry copper deposits of northern Chile. Contrib Mineral Petrol 144, 347–364. https://doi.org/10.1007/s00410-002-0402-5.

Banks, D.A., Yardley, B.W.D., Campbell, A.R., Jarvis, K.E., 1994. REE composition of an aqueous magmatic fluid: A fluid inclusion study from the Capitan Pluton, New Mexico, U.S.A., Chemical Geology, 113, 259-272, https://doi.org/10.1016/0009-2541(94)90070-1.

Barnes, S.-J., Mansur, E. T., Pagé, P., 2022. Differences in composition of chromites from low-Ti and high-Ti picrites of the Emeishan Large Igneous Province and comparison with chromites of the UG-2 platinum-deposit of the Bushveld complex. Lithos, 412, 106613.

Bau, M., 1991. Rare earth element mobility during hydrothermal and metamorphic fluid-rock interaction and the significance of the oxidation state of europium. Chem Geol 93:219–230

Bédard, É., De Bronac de Vazelhes, V., Beaudoin, G., 2022. Performance of predictive supervised classification models of trace elements in magnetite for mineral exploration. J Geochem Explor 236:106959. doi: doi.org/10.1016/j.gexplo.2022.106959.

Bell, K., Anglin, C.D., and Franklin, J.M., 1989. Sm-Nd and Rb-Sr isotope systematics of scheelites: Possible implications for the age and genesis of vein-hosted gold deposits. Geology, 17:500-509.

Belousova, E.A., Griffin, W.L., O'Reilly, Y., Fisher, N.I., 2002. Apatite as an indicator mineral for mineral exploration: trace-element compositions and their relationship to host rock type. Journal of Geochemical Exploration, 76, 45-69, https://doi.org/10.1016/S0375-6742(02)00204-2

Boiron, M.C., Cathelineau, M., Banks, D., Yardley, B., Noronha, F., Miller, F.M., 1996. P–T–X conditions of fluid penetration in the basement during retrograde metamorphism and uplift: a multidisciplinary investigation of bulk and individual fluid inclusion chemistry from NW Iberian quartz veins. Geochim. Cosmochim. Acta, 60, pp. 43-57

Boiron, M.C., Cathelineau, M., Banks, D.A., Fourcade, S., Vallance, J., 2003. Mixing of metamorphic and surficial fluids during the uplift of the Hercynian upper crust: consequences for gold deposition, Chemical Geology, Volume 194, Issues 1–3, Pages 119-141, https://doi.org/10.1016/S0009-2541(02)00274-7

Boutroy, E., Dare, S., Beaudoin, G., Barnes, S-J., Lightfoot, P., 2014. Magnetite composition in Ni-Cu-PGE deposits worldwide and its application to mineral exploration. J Geochem Explor 145:64-81

Bowman, J. Covert, J. J., Clark, A. H. & Mathieson, G. A. 1985. The CanTung E zone scheelite skarn orebody, Tungsten, NorthwestTerritories: oxygen, hydrogen, and carbon isotope studies. Economic Geology 80, 1872–95.

Breiman, L., 2001. Random Forests. Machine Learning 45: 5-32. doi: https://doi.org/10.1023/A:1010933404324

Breiter, K, Korbelová, Z., Chládek, Š., Uher, P., Knesl, I., Rambousek, P., Honig, S., Šešulka, V., 2017. Diversity of Ti–Sn–W–Nb–Ta oxide minerals in the classic granite-related magmatic–hydrothermal Cínovec/Zinnwald Sn–W–Li deposit (Czech Republic). *European Journal of Mineralogy,* 29 (4): 727–738. doi: https://doi.org/10.1127/ejm/2017/0029-2650

Breiter, K., Ďurišová, J., Hrstka, T., Korbelová, Z., Vaňková, M. H., Galiová, M. V., Kanický, V., Rambousek, P., Knésl, I., Dobeš, P., Dosbaba, M., 2017. Assessment of magmatic vs. metasomatic processes in rare-metal granites: A case study of the Cínovec/Zinnwald Sn–W–Li deposit, Central Europe. – Lithos 292-293: 198-217. DOI 10.1016/j.lithos.2017.08.015

Bromiley, G.D., 2021. Do concentrations of Mn, Eu and Ce in apatite reliably record oxygen fugacity in magmas? Lithos 384-385:105900

Brown, I., and Nesbitt, B., 1987. Gold-copper-bismuth mineralization in hedenbergitic skarn, Tombstone Mountains, Yukon. Can J Earth Sci 24:2362-2372

Brown, V.S., Baker, T., Stephens, J.R., 2002. Ray Gulch tungsten skarn, Dublin Gulch, central Yukon: Gold-tungsten relationships in intrusion-related ore systems and implications for gold exploration. In: Yukon Exploration and Geology 2001, DS Emond, LH Weston and LL Lewis (eds), Exploration and Geological Services Division, Yukon Region, Indian and Northern Affairs Canada, p 259-268

Brugger, J., Etschmann, B., Pownceby, M., Liu, W., Grundler, P., Brewe, D., 2008. Oxidation state of europium in scheelite: tracking fluid–rock interaction in gold deposits. Chem Geol 257:26–33.

Brugger, J., Giere, R., Grobety, B., Uspensky, E., 1998. Scheelite-powellite and paraniite-(Y) from the Fe-Mn deposit at Fianel, Eastern Swiss Alps. Am Mineral 83:1100–1110.

Brugger, J., Lahaye, Y., Costa, S., Lambert, D., Bateman, R., 2000. Inhomogeneous distribution of REE in scheelite and dynamics of Archaean hydrothermal systems (Mt Charlotte and Drysdale gold deposits, Western Australia). Contrib Mineral Petrol 139:251–264.

Brugger, J., Liu, W., Etschmann, B., Mei, Y., Sherman, D.M., Testemal, D., 2016. A review of the coordination chemistry of hydrothermal systems, or do coordination changes make ore deposits? Chem Geol 447:219-253

Bulm, J.D., 1985. A petrologic and Rb–Sr isotopic study of intrusive rocks near Fairbanks, Alaska. Canadian Journal of Earth Sciences, 22, 1314-1321.

Burt, D., 1989. Compositional and phase relations among rare earth elements. Rev Mineral 21:259–307.

Candela, P.A., 1992. Controls on ore metal ratios in granite related ore systems: An experimental and computational approach: Royal Society of Edinburgh Transactions, Earth Sciences, 83, 317–326. doi:10.1017/S0263593300007999.

Caraballo, E., Dare, S. Beaudoin, G., 2022. Variation of trace elements in chalcopyrite from worldwide Ni-Cu sulfide and Reef-type PGE deposits: implications for mineral exploration. Miner Deposita. https://doi.org/10.1007/s00126-021-01091-y

Cave, B.J., 2016. Source of scheelite in the turbidite-hosted orogenic au deposits of Otago, New Zealand: an integrated metamorphic source model explaining the presence or absence of scheelite in turbidite-hosted orongenic au deposits, PhD thesis, University of Tasmania.

Cave, B.J., Pitcairn, I.K., Craw, D., Large, R.R., Thompson, J.M., Johnson, S.C., 2017. A metamorphic mineral source for tungsten in the turbidite-hosted orogenic gold deposits of the Otago Schist, New Zealand. Miner Deposita 52, 515–537. https://doi.org/10.1007/s00126-016-0677-5

Cepedal, A., Fuertes-Fuente, M., Martin-Izard, A., Boixet, L., 2014. Tellurides, sulfides and sulfosalts in the mineral paragenesis of the Corcoesto orogenic gold deposit, NW Spain. Conference: IMA 2014 At: Sudafrica Volume: Abstract Volume ISBN: 978-0-620-60082-8, p 14.

Chang, Z., Shu, Q., Meinert, L., 2019. Skarn deposits of China. In: Chang, Zhaoshan, and Goldfard, Richard J (ed) Mineral Deposits of China. Special Publications of the Society of Economic Geologists, 22 Society of Economic Geologists, Littleton, CO, USA, pp 189-234

Choi, W., Park, C., Song, Y., 2020. Multistage W-mineralization and magmatic-hydrothermal fluid evolution: Microtextural and geochemical footprints in scheelite from the Weondong W-skarn deposit, South Korea. Ore Geol Rev 116:103219

Cook, N., Ciobanu, C.L., George, L., Zhu, Z-Y., Wade, B., Ehrig, K., 2016. Trace Element Analysis of Minerals in Magmatic-Hydrothermal Ores by Laser Ablation Inductively-Coupled Plasma Mass Spectrometry: Approaches and Opportunities. Minerals 6(4):111

Cooke, D.R., Baker, M., Hollings, P., Sweet, G., Chang, Z., Danyushevsky, L., Gilbert, S., Zhou, T., White, N.C., Gemmell, J.B., Inglis, S., 2014. New Advances in Detecting the Distal Geochemical Footprints of Porphyry Systems—Epidote Mineral Chemistry as a Tool for Vectoring and Fertility Assessments, Building Exploration Capability for the 21st Century, Karen D. Kelley, Howard C. Golden.

Cooke, D.R., Wilkinson, J.J., Baker, M., Agnew, P., Phillips, J., Chang, Z., Chen, H., Wilkinson, C.C., Inglis, S., Hollings, P., Zhang, L., Gemmell, B., White, N.C., Danyushevsky, L., Martin, H., 2020. Using mineral chemistry to aid exploration: A case study from the Resolution porphyry Cu-Mo deposit, Arizona. Eco Geol 115(4):813-840

Cracknell, M.J., and Reading, A.M., 2014. Geological mapping using remote sensing data: A comparison of five machine learning algorithms, their response to variations in the spatial distribution of training data and the use of explicit spatial information. Computers & Geosciences, 63: 22-33. doi: https://doi.org/10.1016/j.cageo.2013.10.008

Craw, D., Mortensen, J., MacKenzie, D., Pitcairn, I., 2015. Contrasting geochemistry of orogenic gold deposits in Yukon, Canada and Otago, New Zealand. *Geochemistry: Exploration, Environment, Analysis* 15 (2-3): 150–166. doi: https://doi.org/10.1144/geochem2013-262

Darbyshire, D.P.F., Pitfield, P.E.J., Campbell, S.D.G., 1996. Late Archean and Early Proterozoic gold-tungsten mineralization in the Zimbabwe Archean craton: Rb-Sr and Sm-Nd isotope constraints. *Geology*, 24 (1): 19–22. doi: https://doi.org/10.1130/0091-7613(1996)024<0019:LAAEPG>2.3.CO;2

Dare, S.A.S, Barnes, S.J., Beaudoin, G., 2012. Variation in trace element content of magnetite crystallized from a fractionating sulfide liquid, Sudbury, Canada: Implications for provenance discrimination, Geochimica et Cosmochimica Acta, 88, 27-50, https://doi.org/10.1016/j.gca.2012.04.032.

Dare, S.A.S, Barnes, S.J., Beaudoin, G., 2014. Trace elements in magnetite as petrogenetic indicators. Miner Deposita 49, 785–796.

De Bronac de Vazelhes V., 2019. Étude de la dispersion d'un gisement d'or dans les sédiments glaciaires: Le cas d'Amaruq (Nunavut, Canada). M.Sc. thesis, Université Laval, 213p.

De Bronac de Vazelhes, V., Beaudoin, G., McMartin, I., Côté-Mantha, O., Boulianne-Verschelden, N., 2021. Assessment of the Amaruq gold deposit signature in glacial sediments using multivariate geochemical data analysis and indicator minerals. J Geochem Explor 228:106800

Dick, L., and Hodgson, C., 1982. The MacTung W-Cu(Zn) contact metasomatic and related deposits of the northeastern Canadian Cordillera. Econ Geol 77:845-867

Dmitrijeva, M., Ciobanu, C.L., Ehrig, K., Cook, N.J., Verdugo-Ihl, M.R., Metcalfe, A.V., Kamenetsky, V.S., McPhie, J., Carew, M., 2022. Geochemical Data Analysis of Iron Oxide Copper-Gold Mineralization, Wirrda Well Prospect, South Australia. Econ Geol 117(4): 853–874. doi: https://doi.org/10.5382/econgeo.4904

Dostal, J., Kontak, D., Chatterjee, A., 2009. Trace element geochemistry of scheelite and rutile from metaturbidite-hosted quartz vein gold deposits, Meguma Terrane, Nova Scotia, Canada: genetic implications. Mineral Petrol 97:95–109

Drake, M.J., Weill, D.F., 1975. Partition of Sr, Ba, Ca, Y, Eu^{2+}, Eu^{3+}, and other REE between plagioclase feldspar and magmatic liquid: an experimental study. Geochim Cosmochim Acta 39:689-712

Dubru, M., Vander Auwera, J., Van Marcke De Lummen, G., and Verkaeren, J., 1988. Distribution of scheelite in magnesian skarns at Traversella (Piemontese Alps, Italy) and Costabonne (Eastern Pyrenees, France): Nature of the associated magmatism and influence of fluid composition. In Mineral Deposits within the European Community (J. Boissonnas & P. Omenetto, eds.). Society for Geology Applied to Mineral Deposits, Special Publication 6, Springer-Verlag, Berlin, Germany (117–134).

Dupuis, C., Beaudoin, G., 2011. Discriminant diagrams for iron oxide trace element fingerprinting of mineral deposit types. Miner Deposita 46, 319–335. https://doi.org/10.1007/s00126-011-0334-y

Duran, C., Barnes, S-J., Corkerybc, J., 2016. Trace element distribution in primary sulfides and Fe–Ti oxides from the sulfide-rich pods of the Lac des Iles Pd deposits, Western Ontario, Canada:

Constraints on processes controlling the composition of the ore and the use of pentlandite compositions. J Geochem Explor 166:45-63

Duran, C., Dubé-Loubert, H., Page, P., Barnes, S-J., Roy, M., Savard, D., Cave, B.J., Arguin, J-P., Mansur, E., 2019. Applications of trace element chemistry of pyrite and chalcopyrite in glacial sediments to mineral exploration targeting: Example from the Churchill Province, northern Quebec, Canada. J Geochem Explor 196:105-130

Einaudi, M., Burt, D., 1982. Introduction, terminology, classification, and composition of skarn deposits. Econ Geol, 77(4):745-754

Einaudi, M., Meinert, L., Newberry, R., 1981. Skarn deposits. Econ Geol 75:317-391

Elongo, V., Falck, H., Rasmussen, K.L., Robbins, L.J., Creaser, R.A., Luo, Y., Pearson, D.G., Sarkar, C., Adlakha, E., Palmer, M.C., Scott, J.M., Hickey, K., Konhauser, K., Lecumberri-Sanchez, P., 2022. Ancient roots of tungsten in western North America. *Geology*, 50 (7): 791–795. doi: https://doi.org/10.1130/G49801.1

Elongo, V., Lecumberri-Sanchez, P., Legros, H., Falck, H., Adlakha, E., Roy-Garand, A., 2020. Paragenetic constraints on the Cantung, Mactung and Lened tungsten skarn deposits, Canada: Implications for grade distribution. Ore Geology Reviews, 125, 103677. https://doi.org/10.1016/j.oregeorev.2020.103677.

Eppinger, R.G., et al., 2011. Exploration case study using indicator minerals in till at the giant Pebble porphyry Cu-Au-Mo deposit, southwest Alaska, USA, in Indicator mineral methods in mineral exploration: Workshop in the 25th International Applied Geochemistry Symposium 2011, 22-26 August 2011 Rovaniemi, Finland p 41-48 https://pubs.er.usgs.gov/publication/70156777

Eriksson, L., Johansson, E., Kettaneh-Wold, N., Wold, S., 2001. Multi- and megavariate data analysis, principles and applications. UMETRICS, Umea, 425 p

Farmer, G.L., Mueller, S., Marsh, E., Goldfarb, R.J., and Hart, C.J.R., 2000. Isotopic evidence on sources of Au-related mid-Cretaceous Tombstone Plutonic Suite granitic rocks, Clear Creek district, Yukon [abs.]: Geological Society of America, Cordilleran Section Abstracts with Programs A-13.

Fisher, C.M., Vervoort, J.D., DuFrane, S.A., 2014. Accurate Hf isotope determinations of complex zircons using the “laser ablation split stream” method. Geochem. Geophys. Geosyst. 15, 121–139.

Fu, Y., Sun, X., Zhou, H., Lin, H., Jiang, L., Yang, T., 2017. In-situ LA-ICP-MS trace elements analysis of scheelites from the giant Beiya gold-polymetallic deposit in Yunnan Province, Southwest China and its metallogenic implications. Ore Geol Rev 80:828–837

Fuertes-Fuente, M., Cepedal, A., Lima, A., Dória, A., Ribeiro, M.A., Guedes, A., 2016. The Au-bearing vein system of the Limarinho deposit (northern Portugal): Genetic constraints from Bi-chalcogenides and Bi–Pb–Ag sulfosalts, fluid inclusions and stable isotopes. Ore Geol. Reviews, 72: 213-231 https://doi.org/10.1016/j.oregeorev.2015.07.009

Gaspar, M., Knaack, C., Meinert, L., Moretti, R., 2008. REE in skarn systems: a LA-ICP-MS study of garnets. Geochim Cosmochim Acta 72:185–205. https://doi.org/10.1016/j.gca.2007.09.033

George, L., Cook, N., Ciobanu, C., Wade, B., 2015. Trace and minor elements in galena: a reconnaissance LA-ICP-MS study. Am Mineral 100:548–569.

George, L., Cook, N., Crowe, B., Ciobanu, C., 2018. Trace elements in hydrothermal chalcopyrite. Mineral Mag 82(1):59–88.

Ghaderi, M., Palin, J., Campbell, I., Sylvester, P., 1999. Rare earth element systematics in scheelite from hydrothermal gold deposits in the Kalgoorlie-Norseman region, Western Australia. Econ Geol 94:423–437.

Gillerman, V.S., Schmitz, M.D., Benowitz, J.A., Layer, P.W., 2019. Geology and temporal evolution of alteration and Au-Sb-W mineralization, Stibnite mining district, Idaho: Idaho Geological Survey Bulletin 31, 149 p.

Goldfarb, R.G., Baker, T., Dubé, B., Groves, D.I., Hart, C.J.R., Gosselin, P., 2005. Distribution, Character, and Genesis of Gold Deposits in Metamorphic Terran, One Hundredth Anniversary Volume, Jeffrey W. Hedenquist, John F. H. Thompson, Richard J. Goldfarb, Jeremy P. Richards.

Goldfarb, R.J., Groves, D.I., Gardoll, S., 2001. Orogenic gold and geologic time: a global synthesis. Ore Geol Rev, 18: 1-75

Goldfarb, R.J., Qiu, K.F., Deng, J., Chen, Y.J., Yang, L.Q., 2019. Orogenic gold deposits of China. Society of Economic Geologists Special Publication, 22: 263-324.

Gosselin, P., and Dubé, B., 2005. Gold deposits of the world: Distribution, geological parameters and gold content: Geological Survey of Canada. Open File 4895, 271 p. (CD-ROM).

Gregory, D.D., Cracknell, M.J., Large, R.R., McGoldrick, P., Kuhn, S., Maslennikov, V.V., Baker, M.J., Fox, N., Belousov, I., Figueroa, M.C., Steadman, J.A., Fabris, A.J., Lyons, T.W., 2019. Distinguishing ore deposit type and barren sedimentary pyrite using laser ablation-inductively coupled plasma-mass spectrometry trace element data and statistical analysis of large data sets. Econ Geol 114(4): 771–786.

Groves, D.I., Goldfarb, R.J., Gebre-Mariam, M., Hagemann, S.G., Robert, F., 1998. Orogenic gold deposits: A proposed classification in the context of their crustal distribution and relationship to other gold deposit types. Ore Geol Rev 13, 7-27, doi: https://doi.org/10.1016/S0169-1368(97)00012-7.

Groves, D.I., Goldfarb, R.J., Santosh, M., 2016.The conjunction of factors that lead to the formation of giant gold provinces and deposits in non-arc settings. Geoscience Frontiers, 7 (3): 303-314

Grütter, H.S., Gurney, J.J., Menzies, A.H., Winter, F., 2004. An updated classification scheme for mantle-derived garnet, for use by diamond explorers. Lithos, 77: 841-857. doi: https://doi.org/10.1016/j.lithos.2004.04.012

Grzela, D., Beaudoin, G., Bedard, E., 2019. Tourmaline, scheelite, and magnetite compositions from orogenic gold deposits and glacial sediments of the Val-d'Or district (Quebec, Canada): implications to mineral exploration. J Geochem Explor 206:106355.

Guo, Z., Li, J., Xu, X., Song, Z., Dong, X., Tian, J., Yang, Y., She, H., Xiang, A., Kang, Y., 2016. Sm/Nd dating and REE composition of scheelite for the Honghuaerji scheelite deposit, Inner Mongolia, Northeast China. Lithos 261: 307–321.

Gurney, J.J., 1984. A correlation between garnets and diamonds. In: Glover, J.E., Harris, P.G. (Eds.), Kimberlite occurrence and origins: a Basis for Conceptual Models in Exploration. Geology Department and University Extension, University of Western Australia, Publication 8 143–166.

Gurney, J.J., Zweistra, P., 1995. The interpretation of the major element compositions of mantle minerals in diamond exploration. J Geochem Explor 53:293-309

Haas, J., Shock, E.L., Sassani, D., 1995. Rare earth elements in hydrothermal systems: estimates of standard partial molal thermodynamic properties of aqueous complexes of the rare earth elements at high. Geochim Cosmochim Acta 59:4329–4350.

Han, J., Chen, H., Hing, C., Hollings, P., Chu, G., Zang, L., Sun, S., 2020. Texture and geochemistry of multi-stage hydrothermal scheelite in the Tongshankou porphyry-skarn Cu-Mo(-W) deposit, eastern China: Implications for ore-forming process and fluid metasomatism. Am Mineral 105:945–954

Hart, C., 2007. Reduced Intrusion-Related Gold Systems. In W D Goodfellow, Mineral Deposits of Canada: a synthesis of major deposittypes, district metallogeny, the evolution of geological provinces, and exploration methods (pp 95–112) Geological Association of Canada, Mineral Deposits Division.

Hart, C.J.R, Mair, J.L., Goldfarb, R.J., Groves, D.I., 2004. Source and redox controls on metallogenic variations in intrusionrelated ore systems, TombstoneTungsten Belt, Yukon Territory, Canada. Transactions of the Royal Society of Edinburgh: Earth Sciences, 95, pp 339356 doi:10.1017/S0263593300001115

Hart, C.J.R., and Goldfarb, R.J., 2005. Distinguishing intrusion-related from orogenic gold systems: Proceedings of the 2005 New Zealand Minerals Conference, Auckland, November 13–16, 125–133.

Hart, C.J.R., Baker, T., Burke, M.J., 2000. New exploration concepts for country-rock-hosted intrusion-related gold systems: Tintina Gold Belt in Yukon. In The Tintina Gold Belt: Concepts, Exploration, and Discoveries. British Columbia and Yukon Chamber of Mines Special Volume 2, 145–71.

Hart, C.J.R., McCoy, D.T., Goldfarb, R.J., Smith, M., Roberts, P., Hulstein, R., Bakke, A.A., Bundtzen, T.K., 2002. Geology, exploration and discovery in the Tintina Gold Province. In Goldfarb R. J. & Neilson, R. (eds) Geology, Exploration and Discovery in the Tintina Gold Province, Alaska and Yukon. Society of Economic Geologists Special, 9, 241–74

Hsu, L., 1977. Effects of oxygen and sulfur fugacities on the scheelite tungstenite and powellite-molybdenite stability relations. Econ Geol 72:664–670

Hsu, L.C. and Galli, P.E., 1973. Origin of the scheelite-powellite series of minerals. Economic Geology, 68, 681–696.

Huang, X-D., Lu, J-J., Zhang, R-Q., Sizaret, S., Ma, D-S., Wang, R-C., Zhu, X., He, Z-Y., 2022. Garnet and scheelite chemistry of the Weijia tungsten deposit, South China: Implications for fluid evolution

and W skarn mineralization in F-rich ore system, Ore Geology Reviews, Volume 142, 104729, https://doi.org/10.1016/j.oregeorev.2022.104729.

Huang, X-W., Boutroy, E., Makvandi, S., Beaudoin, G., Corriveau, L., De Toni, A., 2019. Trace element composition of iron oxides from IOCG and IOA deposits: Relationship to hydrothermal alteration and deposit subtypes. Mineral Deposita 54:525-552

Huang, X-W., Sappin A-A., Boutroy, E., Beaudoin, G., Makvandi, S., 2019. Trace Element Composition of Igneous and Hydrothermal Magnetite from Porphyry Deposits: Relationship to Deposit Subtypes and Magmatic Affinity. *Economic Geology*; 114 (5): 917–952. doi: https://doi.org/10.5382/econgeo.4648

Ishihara, S., 1981. The magnetite-series and ilmenite-series granitic rocks. Min Geol 27:293-305

Ismail, R., Ciobanu, C.L., Cook, N.J., Teale, G.S., Giles, D., Mumm, A.S., Wade, B., 2014. Rare earths and other trace elements in minerals from skarn assemblages, Hillside iron oxide–copper–gold deposit, Yorke Peninsula, South Australia. Lithos 184:456-477

James-Smith, J., Cauzid, J., Testemale, D., Liu, W., Hazemann, J., Proux, O., Etschmann, B., Philippot, P., Banks, D., Williams, P., Brugger, J., 2010. Arsenic speciation in fluid inclusions using micro-beam X-ray absorption spectroscopy. Am Mineral 95(7):921–932

Jochum, K.P., Nohl, U., Herwig, K., Lammel, E., Stoll, B., Hofmann, A.W., 2005. GeoReM: a new geochemical database for reference materials and isotopic standards. Geostand Geoanal Res 29:333–338

Kelley,K.D. et al. 2011 Porphyry Cu indicator minerals in till as an exploration tool: example from the giant Pebble porphyry Cu-Au-Mo deposit, Alaska, USA, Geochemistry: Exploration, Environment, Analysis, 11(4):321 http://dx.doi.org/10.1144/1467-7873/10-IM-041

Kempe, U., and Oberthür, T., 1997. Physical and geochemical characteristics of scheelite from gold deposits; a reconnaissance study. Proceedings of the ... Biennial SGA (Society for Geology Applied to Mineral Deposits) Meeting, Vol. 4, p.209-212.

Kempe, U., Belyatsky, B., Krymsky, R. Kremenetsky, A.A., Ivanov, P.A., 2001. Sm–Nd and Sr isotope systematics of scheelite from the giant Au(–W) deposit Muruntau (Uzbekistan): implications for the age and sources of Au mineralization. Min Dep 36, 379–392. https://doi.org/10.1007/s001260100156

Kent, A.J.R., Campbell, I.H., McCulloch, M.T., 1995. Sm-Nd systematics of hydrothermal scheelite from the Mount Charlotte Mine, Kalgoorlie, Western Australia; an isotopic link between gold mineralization and komatiites. *Economic Geology*; 90 (8): 2329–2335. doi: https://doi.org/10.2113/gsecongeo.90.8.2329

Keppler, H., 1993. Influence of fluorine on the enrichment of high field strength trace elements in granitic rocks. Contr. Mineral. and Petrol. 114, 479–488. https://doi.org/10.1007/BF00321752

Kozlik, M., Gerdes, A., Raith, J.G., 2016a. Strontium isotope systematics of scheelite and apatite from the Felbertal tungsten deposit, Austria – results of in-situ LA-MC-ICP-MS analysis. Miner Petrol 110, 11–27. https://doi.org/10.1007/s00710-015-0416-0

Kozlik, M., Raith, J.G., Gerdes, A., 2016b. U–Pb, Lu–Hf and trace element characteristics of zircon from the Felbertal scheelite deposit (Austria): New constraints on timing and source of W mineralization. Chemical Geology, 421, 112-126, https://doi.org/10.1016/j.chemgeo.2015.11.018.

Kwak, T., and Tan T., 1981. The geochemistry of zoning in the skarn minerals at the King Island Dolphin mine. Econ Geol 76:468–497

Lang, J. R. 2000. Regional and system-scale controls on the formation of copper and/or gold magmatic-hydrothermal mineralization. Final Technical Report, Mineral Deposit Research Unit 115 pp.

Lang, J.R., and Baker, T., 2001. Intrusion-related gold systems: the present level of understanding. Min Dep 36, 477–489. https://doi.org/10.1007/s001260100184

Li, J., Li, X., Xiao, R., 2019. Multiple-stage tungsten mineralization in the Silurian Jiepai W skarn deposit, South China: Insights from cathodoluminescence images, trace elements, and fluid inclusions of scheelite. J Asian Earth Sci 181:103898

Li, C., Shen, P., Zhao, Y., Li, P., Zhang, L., Pan, H., 2022. Mineral chemistry of chlorite in different geologic environments and its implications for porphyry Cu ± Au ± Mo deposits. Ore Geol Rev 149: 105112. doi: https://doi.org/10.1016/j.oregeorev.2022.105112

Li, W., Xie, G-Q., Mao, J-W., Zhang, H-C., 2021. Mineralogy, fluid inclusion and isotope signatures: Implications for the genesis of the Early Paleozoic Yangjiashan scheelite-quartz vein deposit, South China, Ore Geology Reviews, 134, 104136, https://doi.org/10.1016/j.oregeorev.2021.104136.

Li, X-Y., Gao, J-F., Zhang, R-Q., Lu, J-J., Chen, W-H., Wu, J-W., 2018. Origin of the Muguayuan veinlet-disseminated tungsten deposit, South China: Constraints from in-situ trace element analyses of scheelite. Ore Geology Reviews, 99, 180-194, https://doi.org/10.1016/j.oregeorev.2018.06.005.

Liu, J., Li, W., Zhu, X., Li, C., Zhou, Q., Yang, F., 2020. Origin and evolution of ore-forming fluids of the Larong W-(Mo) deposit, eastern Tibet: Constraints from fluid inclusions, H-O isotopes, and scheelite geochemistry. Ore Geol Rev 124:103620

Liu, H., Beaudoin, G., 2021. Geochemical signatures in native gold derived from Au-bearing ore deposits. Ore Geology Reviews, 132, 104066, doi: https://doi.org/10.1016/j.oregeorev.2021.104066

Liu, K., 2021. The Genesis of the Wolfram Camp tungsten-molybdenum deposit, Queensland, Australia, and the geochemistry of tungsten ore minerals. PhD thesis, Colorado School of Mines.

Liu, Z., Hollings, P., Mao, X., Lawley, C.J.M., Yang, B., Tang, L., 2021. Metal remobilization from country rocks into the Jiaodong-type orogenic gold systems, Eastern China: New constraints from scheelite and galena isotope results at the Xiadian and Majiayao gold deposits. Ore Geology Reviews 134:104126.

Lu ,H-Z., Liu, Y., Wang, C., Xu, Y., Li, H., 2003. Mineralization and Fluid Inclusion Study of the Shizhuyuan W-Sn-Bi-Mo-F Skarn Deposit, Hunan Province, China. Econ Geol 98:955–974

Luo, Y., Pearson, D.G., Scott, J., Palmer, M.C., Fisher, C.M., Sarkar, C., Vezinet, A., Lecumberri-Sanchez, P., 2019. Simultaneous in situ analysis of Sm-Nd isotopes and trace elements in scheelite

by laser ablation split stream ICP-MS: challenges and emerging approaches. In: 2019 North America Laser Ablation Workshop, Austin, p. 34.

Mair, J.L., Goldfarb, R.J., Johnson, C.A., Hart, C.J.R., Marsh, E.E., 2006. Geochemical constraints on the genesis of the Scheelite dome intrusion-related gold deposit, Tombstone gold belt, Yukon, Canada. Economic Geology, 101, 523-553.

Makvandi, S., Ghasemzadeh-Barvarz, M., Beaudion, G., Grunsky, E., McClenaghan, M., Duchesne, C., 2016a. Principal Component Analysis of magnetite composition from volcanogenic massive sulfide deposits: Case studies from the Izok Lake (Nunavut, Canada) and Halfmile Lake (New Brunswick, Canada) deposits. Ore Geol Rev 72:60-85

Makvandi, S., Ghasemzadeh-Barvarz, M., Beaudion, G., Grunsky, E.C., McClenaghan, M.B., Duchesne, C., 2016b. Partial Least Squares Discriminant Analysis of trace element compositions of magnetite from various VMS deposit subtypes: Application to mineral exploration. Ore Geol Rev 78:388-408

Makvandi, S., Huang, X., Beaudoin, G., Quirt, D., Ledru, P., Fayek, M., 2020. Trace element signatures in hematite and goethite associated with the Kiggavik-Andrew Lake structural trend U deposits (Nuvanut, Canada). Mineral Deposita 56:509-535

Makvandi, S., Beaudoin, G., McClenaghan, B., Quirt, D., Ledru, P., 2019. PCA of Fe-oxides MLA data as an advanced tool in provenance discrimination and indicator mineral exploration: Case study from bedrock and till from the Kiggavik U deposits area (Nunavut, Canada). Journal of Geochemical Exploration, 197: 199-211. doi.org/10.1016/j.gexplo.2018.11.013

Maloof, T.L., Baker, T. & Thompson, J.F., 2001. The Dublin Gulch intrusion-hosted gold deposit, Tombstone plutonic suite, Yukon Territory, Canada. Min Dep 36, 583–593. https://doi.org/10.1007/s001260100190

Maneglia, N., Beaudoin, G., Simard, M., 2017. Indicator minerals of the Meliadine orogenic gold deposits, Nunavut (Canada), and application to till surveys. Geochem Explor Environ Anal 18: 241–251

Mansur, E.T., Barnes, S.J., Duran, C.J., Sluzhenikin, S.F., 2020. Distribution of chalcophile and platinum-group elements among pyrrhotite, pentlandite, chalcopyrite and cubanite from the Noril'sk-Talnakh ores: Implications for the formation of platinum-group minerals. Mineralium Deposita, 55(6), 1215-1232.

Mansur, E.T., Barnes, S-J., Duran, C., 2021. An overview of chalcophile element contents of pyrrhotite, pentlandite, chalcopyrite, and pyrite from magmatic Ni-Cu-PGE sulfide deposits. Mineral Deposita 56:179–204

Mao, M., Rukhlov, A., Rowins, S., Spence, J., Coogan, L., 2016. Apatite trace element compositions: a robust new tool for mineral exploration. Econ Geol 111:1187–1222

Mathieson, G., and Clark, A., 1984. The Cantung E Zone Scheelite Skarn Orebody, Tungsten Northwest Territories: A Revised Genetic Model. Econ Geol 79:883-901

McClenaghan, M. B., 2005. Indicator mineral methods in mineral exploration, geochemistry: Exploration, Environment, Analysis, 5(3):233-245.

McClenaghan, M. B., and Cabri, L. J., 2011. Review of gold and platinum group element (PGE) indicator minerals methods for surficial sediment sampling, Geochemistry: Exploration, Environment, Analysis, 11(4):251-263.

McClenaghan, M. B., and Kjarsgaard, B. A., 2007. Indicator mineral and surficial geochemical exploration methods for kimberlite in glaciated terrain; Examples from Canada, p. 983-1006, in Goodfellow, W. D., ed., Mineral Deposits of Canada: A Synthesis of Major Deposit-Types, District Metallogeny, the Evolution of Geological Provinces, and Exploration Methods, Vol. Special Publication No. 5, Geological Association of Canada, Mineral Deposits Division.

McClenaghan, M., Parkhill, M., Pronk, A., Seaman, A., McCurdy, M., Leybourne, M., 2017. Indicator mineral and geochemical signatures associated with the Sisson W-Mo deposit, New Brunswick,Canada. Geochem Explor Environ Anal 17:297–313

McClenaghan, M.B. and Kjarsgaard, B.A. 2001. Indicator mineral and geochemical methods for diamond exploration in glaciated terrain in Canada. In: MCCLENAGHAN, M.B., BOBROWSKY, P.T., Hall, G.E.M., and Cook, S.J. (eds) Drift Exploration in Glaciated Terrain. Special Publication, 185. Geological Society, London, 83–123.

McDonough, W.F., Sun, S.S., 1995. The composition of the earth. Chem Geol 120:223–253

Meinert, L., 1997. Application of Skarn Deposit Zonation Models to Mineral Exploration. Explor Mining Geol 6(2):185-208

Meinert, L., Dipple, G., Nicolescu, S., 2005. World skarn deposits. In J Hedenquist, J Thompson, R Goldfarb, and J Richards. Econ Geol 100th Anniversary Volume, pp 299–336, Littleton, CO: Society of Economic Geologists

Mendizabal, A., 2022. Étude de la composition des minéraux indicateurs et de la géochimie du till en aval d'un gisement d'or : Le cas d'Amaruq (Nunavut, Canada). M.Sc. thesis, Université Laval, 196p.

Migdisov, A., Williams-Jones, A.E., Brugger, J., Caporuscio, F., 2016. Hydrothermal transport, deposition, and fractionation of REE: experimental data and thermodynamic calculations. Chem Geol 439:13–42

Mihalynuk, M.G., and Heaman, L.M., 2002. Age of mineralizated porphyry at the Logtung deposit W-Mo-Bi-Be (beryl, aqua- marine), northwest BC; in Geological Fieldwork, BC Ministry of Energy and Mines, 35-39

Miller, C.F., and Stoddard, E.F., 1981. The Role of Manganese in the Paragenesis of Magmatic Garnet: An Example from the Old Woman-Piute Range, California. Journal of Geology, 89, 770-772.

Miller, C.F., Mittlefehldt, D.W., 1984. Extreme fractionation in felsic magma chambers: a product of liquid-state diffusion or fractional crystallization? Earth and Planetary Science Letters, 68, 151-158, https://doi.org/10.1016/0012-821X(84)90147-X.

Miranda, A.C.R., Beaudoin, G., Rottier, B., 2022. Scheelite chemistry from skarn systems: implications for ore-forming processes and mineral exploration. Miner Deposita 57: 1469–1497 doi: https://doi.org/10.1007/s00126-022-01118-y

Mutch, A.R., 1969. The scheelite resources of the Glenorchy district, west Otago. New Zealand Geological Survey report 40

Myint, A.Z., Yonezu, K., Boyce, A.J., Selby, D., Scherstén, A., Tindell, T., Watanabe, K., Swe, Y.M., 2018. Stable isotope and geochronological study of the Mawchi Sn-W deposit, Myanmar: Implications for timing of mineralization and ore genesis. Ore Geology Reviews, 95, 663-679, https://doi.org/10.1016/j.oregeorev.2018.03.014

Nassau, K., 1963. Calcium tungstate—IV: the theory of coupled substitution. J of Physics and Chemistry of Solids 24:1511–2151

Nathwani, C.L., Wilkinson, J.J., Fry, G., Armstrong, R.N., Smith, D.J., Ihlenfeld, C., 2022. Machine learning for geochemical exploration: classifying metallogenic fertility in arc magmas and insights into porphyry copper deposit formation. Miner Deposita 57: 1143–1166. doi:https://doi.org/10.1007/s00126-021-01086-9

Neiva, A.M.R., Moura, A., Leal Gomes, C.A., Pereira, M.F., Corfu, F., 2019. The granite-hosted Variscan gold deposit from Santo António mine in the Iberian Massif (Penedono, NW Portugal): constraints from mineral chemistry, fluid inclusions, sulfur and noble gases isotopes. J Iber Geol 45, 443–469. https://doi.org/10.1007/s41513-019-00103-1

Newberry, R., 1982. Tungsten-bearing skarns of the Sierra Nevada I The Pine Creek Mine, California. Econ Geol 77:823-844

Newberry, R., 1983. The formation of subcalcic garnet in scheelite-bearing skarns. Can Mineral 21:529-544

Newberry, R., Swanson, S., 1986. Scheelite Skarn Granitoids: An evaluation of the roles of magmatic source and process. Ore Geol Rev 1:57-81

Nguyen, T.H., Nevolko, P.A., Pham, T.D., Svetlitskaya, T.V., Tran, T.H., Shelepaev, R.A., Fominykh, P.A., Pham, N.C., 2020. Age and genesis of the W-Bi-Cu-F (Au) Nui Phao deposit, Northeast Vietnam: Constrains from U-Pb and Ar-Ar geochronology, fluid inclusions study, S-O isotope systematic and scheelite geochemistry, Ore Geology Reviews, 123, 103578. https://doi.org/10.1016/j.oregeorev.2020.103578

Noble, S.R, Spooner, E.T.C., Harris, F.R., 1984. The Logtung large tonnage, low-grade W (scheelite)-Mo porphyry deposit, south-central Yukon Territory. *Economic Geology* 79(5):848–868. doi: https://doi.org/10.2113/gsecongeo.79.5.848

O'Brien, J., Spry, P., Teale, G., Jackson, S., Koenig, A., 2015. Gahnite composition as a means to fingerprint metamorphosed massive sulfide and non-sulfide zinc deposits. J Geochem Explor 159:48–61

Palarea-Albaladejo, J., Martin-Fernandez, J.A, 2015. zCompositions-R package for multivariate imputation of left-censored data under a compositional approach. Chemometr Intell Lab Syst 143:85–96

Palarea-Albaladejo, J., Martin-Fernandez, J.A., 2013. Values below detection limit in compositional chemical data. Anal Chim Acta 764:32–43

Palmer, M.C., 2021. Geochemical characterisation of scheelite from New Zealand (Thesis, Doctor of Philosophy). University of Otago. Retrieved from http://hdl.handle.net/10523/12254

Palmer, M.C., Scanlan, E.J., Scott, J.M., Farmer, L., Pickering, D., Wilson, V.J., Oelze, M., Craw, D., le Roux, P.J., Luo, Y., Graham, D.G., Reid, M.R., Stirling, C.H., 2022. Distinct scheelite REE geochemistry and 87Sr/86Sr isotopes in proximally- and distally-sourced metamorphogenic hydrothermal systems, Otago Schist, New Zealand, Ore Geol Rev , 144, 104800. doi: https://doi.org/10.1016/j.oregeorev.2022.104800

Pan, J.Y., Ni, P., Wang, R.C., 2019. Comparison of fluid processes in coexisting wolframite and quartz from a giant vein-type tungsten deposit, South China: insights from detailed petrography and LA-ICP-MS analysis of fluid inclusions Am. Miner., 104, pp. 1092-1116

Pan, L.C., Hu, R.Z., Wang, X.S., Bi, X.W., Zhu, J.J., Li, C., 2016. Apatite trace element and halogen compositions as petrogenetic-metallogenic indicators: Examples from four granite plutons in the Sanjiang region, SW China. Lithos, 254–255, 118-130. https://doi.org/10.1016/j.lithos.2016.03.010

Pan, X., Hou, Z., Zhao, M., Li, Y., Ouyang, Y., Wei, J., Yang, Y., 2020. Fluid inclusion and stable isotope constraints on the genesis of the worldclass Zhuxi W(Cu) skarn deposit in South China. J Asian Earth Sci 190:104192

Pašava, J., Svojtka, M., Veselovský, F., Ďurišová, J., Ackerman, L., Pour, O., Drábek, M., Halodová, P., Haluzová, E., 2016. Laser ablation ICPMS study of trace element chemistry in molybdenite coupled with scanning electron microscopy (SEM) — An important tool for identification of different types of mineralization, Ore Geology Reviews, 72, 874-895, https://doi.org/10.1016/j.oregeorev.2015.09.007

Paterson, C.J., and Peter C. Rankin, P.C., 1979. Trace element distribution in the schist surrounding a quartz-scheelite lode, Glenorchy, New Zealand, New Zealand Journal of Geology and Geophysics, 22:3, 329-338, DOI: 10.1080/00288306.1979.10424102

Paton, C., Hellstrom, J., Paul, B., Woodhead, J., and Hergt, J., 2011, Iolite: freeware for the visualization and processing of mass spectrometric data: Journal of Analytical Atomic Spectrometry, 26, p. 2508–2518. https:// doi. org/ 10. 1039/ c1ja1 0172b

Phillips, G.N., 2013. Australian and global setting for gold in 2013, in Proceedings world gold 2013, Brisbane, Australia, 26–29 September, 2013. Aust Inst Min Metall. 15–21.

Piccoli, P.M., Candela, P.A., 2002. Apatite in Igneous Systems. *Reviews in Mineralogy and Geochemistry*; 48 (1): 255–292. doi: https://doi.org/10.2138/rmg.2002.48.6

Pickering, D.J., 2018. Geochemical and grain size characterisation of scheelite at Golden Point, Macraes Mine, New Zealand, University of Otago, 124 pp.

Pirajno, F., 1992. Greisen systems, Hydrothermal Mineral Deposits. Springer, pp. 280-324.

Pirajno, F., and Bentley, P.N., 1985. Greisen-related scheelite, gold and sulphide mineralisation at Kirwans Hili and Bateman Creek, Reefton district, Westland, New Zealand. New Zealand Journal of Geology and Geophysics, 28, 97-109.

Plotinskayaa, O., Baksheevb, I., Minervina, E.A., 2018. REE Distribution in Scheelite from the Yubileinoe Porphyry Gold Deposit, South Urals: Evidence from LA-ICP-MS Data. Geol Ore Depos 60(4):355–364

Poitrenaud, T., Poujoi, M., Augier, R., Marcoux, E., 2019. The polyphase evolution of a late Variscan W/Au deposit (Salau, French Pyrenees): insights from REE and U/Pb LA-ICP-MS analyses. Mineral Deposita 55:1127–1147

Pollard, P.J., Pichavant, M., Charoy, B., 1987. Contrasting evolution of fluorine- and boron-rich tin systems. Mineral. Deposita 22, 315–321. https://doi.org/10.1007/BF00204525

Porter, J., McNaughtona, N., Evansa, N., McDonald, J., 2020. Rutile as a pathfinder for metals exploration. Ore Geol Rev 120:03406

Porter, J.P., 2013. Source, emplacement and evolution of the Morgan Creel Pluton, Sierra Nevada Batholith, California, USA PhD thesis, Salt Lake City, USA, The University of Utah, 201 p.

Poulin, R., Kontak, D., McDonald, A., McClenaghan, M. 2018. Assessing scheelite as an ore-deposit discriminator using its trace element and REE chemistry. Can Mineral 56: 265–302

Purtov VK, KoteVnikova AL (1993) Solubility of Titanium In Chloride And Fluoride Hydrothermal Solutions. Intern Geol Rev 35:3279-287

R Core Team 2021. R: a language and environment for statistical computing. R Foundation for Statistical Computing, Vienna, Austria. URL https:// www.R- proje ct. org/.

Raimbault, L., Baumer, A., Dubru, M., Benkerrou, C., Croze, V., Zahm, A., 1993. REE fractionation between scheelite and apatite in hydrothermal conditions. *American Mineralogist* 78 (11-12): 1275–1285.

Raith, J.G., Gerdes, A., Cornell, D.H., 2011. In situ U–Pb dating of scheelite: constraints on the age and genesis of the Felbertal tungsten deposit. Mineral. Mag. 75, 1690.

Reed, B.L. 1986. Descriptive model of Sn greisen deposits; & Mineral Deposit Models, (ed.) D.P. Cox and D.F. Singer; United States Geological Survey, Bulletin 1693, p. 70.

Roberts, S., Palmer, M., Waller, L., 2006. Sm-Nd and REE characteristics of tourmaline and scheelite from the Bjorkdal gold deposit, northern Sweden: Evidence of an intrusion-related gold deposit? Econ Geol 101(7):1415-1425

Rodriguez-Galiano, V., Sanchez-Castillo, M., Chica-Olmo, M., Chica-Rivas, M., 2015. Machine learning predictive models for mineral prospectivity: An evaluation of neural networks, random forest, regression trees and support vector machines. Ore Geol Rev 71: 804-818. doi:https://doi.org/10.1016/j.oregeorev.2015.01.001

Rottier, B., and Casanova, V., 2020. Trace element composition of quartz from porphyry systems: a tracer of the mineralizing fluid evolution. Miner Deposita 55:843-862

Scanlan, E.J., Scott, J.M., Wilson, V.J., Stirling, G.H., Reid, M.R., Le Roux, P.J., 2018. In Situ $^{87}Sr/^{86}Sr$ of Scheelite and Calcite Reveals Proximal and Distal Fluid-Rock Interaction During Orogenic W-Au Mineralization, Otago Schist, New Zealand. Econ Geol 113(7): 1571-1586. doi: https://doi.org/10.5382/econgeo.2018.4603

Sciuba, M., Beaudoin, G., Grzela, D., Makvandi, S., 2020. Trace element composition of scheelite in orogenic gold deposits. Miner Deposita 55: 1149-1172

Sciuba, M., Beaudoin, G., Makvandi, S., 2021. Chemical composition of tourmaline in orogenic gold deposits. Mineralium Deposita 56, 537-560

Seo, J.H., Yoo, B.C., Yang, YS., Lee, J.H., Jang, J., Shin, D., 2020. Scheelite geochemistry of the Sangdong W-Mo deposit and W prospects in the southern Taebaeksan metallogenic region, Korea. Geosci J 24, 701–721. https://doi.org/10.1007/s12303-020-0005-z

Sha, L-K., and Bruce W Chappell, B. W., 1999. Apatite chemical composition, determined by electron microprobe and laser-ablation inductively coupled plasma mass spectrometry, as a probe into granite petrogenesis. Geochimica et Cosmochimica Acta, 63, 3861-3881. https://doi.org/10.1016/S0016-7037(99)00210-0.

Shannon, R.D., 1976. Revised effective ionic radii and systematic studies of interatomic distances in halides and chalcogenides. Acta Cryst A 32:751–767

Shu, Q., Chang, Z., Lai, Y., Hu, X., Wu, H., Zhang, Y., Wang, P., Zhai, D., Zhang, C., 2019. Zircon trace elements and magma fertility: insights from porphyry (-skarn) Mo deposits in NE China. Miner Deposita 54:645–656

Sinclair, W.D., 1986. Molybdenum, tungsten and tin deposits and associated granitoid intrusions in the northern Canadian Cordillera and adjacent parts of Alaska; in Morin, J.A., Mineral Deposits of Northern Cordillera: The Canadian Institute of Mining and Metallurgy, Special Volume 37, p. 216-233

Singoyi, B., and Zaw, K., 2001. A petrological and fluid inclusion study of magnetite–scheelite skarn mineralization at Kara, Northwestern Tasmania: implications for ore genesis. Chem Geol 173:239–253

Soloviev, S., 2015. Geology, mineralization, and fluid inclusion characteristics of the Kumbel oxidized W-Cu-Mo skarn and Au-W stockwork deposit, Tien-Shan, Kyrgyzstan. Mineral Deposita 50:187–220

Soloviev, S., Kryazhev, S., Dvurechenskaya, S., 2017. Geology, mineralization, stable isotope, and fluid inclusion characteristics of the Vostok-2 reduced W-Cu skarn and Au-W-Bi-As stockwork deposit, Sikhote-Alin, Russia. Ore Geol Rev 86:338–365

Soloviev, S., Kryazhev, S.G., Dvurechenskaya, S.S., 2015. Geology, mineralization, and fluid inclusion characteristics of the Lermontovskoe reduced-type tungsten (±Cu, Au, Bi) skarn deposit, Sikhote-Alin, Russia. Ore Geol Rev 89:15-39

Song, G., Cook, N.J., Li, G., Qin, K., Ciobanu, C.L., Yang, Y., Xu, Y., 2019. Scheelite geochemistry in porphyry-skarn W-Mo systems: A case study from the Gaojiabang Deposit, East China. Ore Geol Rev 113:103084

Song, G., Qin, K., Li, G., Evans, N., Chen, L., 2014. Scheelite elemental and isotopic signatures: Implications for the genesis of skarn-type W-Mo deposits in the Chizhou area, Anhui Province Eastern China. Am Mineral 99: 303–317

Souza Neto, J.A., Legrand, J.M., Volfinger, M., Pascal, M-L., Sonnet, P., 2008. W–Au skarns in the Neo-Proterozoic Seridó Mobile Belt, Borborema Province in northeastern Brazil: an overview with emphasis on the Bonfim deposit. Miner Deposita 43:185-205

Stekhoven, D.J., Bühlmann, P., 2012. MissForest—non-parametric missing value imputation for mixed-type data, *Bioinformatics*, 28, 112–118, https://doi.org/10.1093/bioinformatics/btr597

Štemprok, M., and Mašková, A., 1992. Scheelite mineral of the Bohemian Massif. Zbl. Geol. Palaont. Teil (1/2): 117-129.

Su, Q., Mao, J., Wu, S., Zhang, Z., Xu, S., 2018. Geochronology and geochemistry of the granitoids and re-forming age in the Xiaoyao tungsten polymetallic skarn deposit in the Jiangnan Massif tungsten belt China: Implications for their petrogenesis, geodynamic setting, and mineralization. Lithos 29:365–381

Su, Q., Mao, J., Sun, J., Zhao, L., Xu, S., 2020. Geochemistry and Origin of Scheelites from the Xiaoyao Tungsten Skarn Deposit in the Jiangnan Tungsten Belt, SE China. Minerals 10:271

Sun, G., Zeng, Q., Zhou, J-X., 2022. Machine learning coupled with mineral geochemistry reveals the origin of ore deposits, Ore Geology Reviews, 142, 104753

Sun, K., Chen, B., 2017. Trace elements and Sr-Nd isotopes of scheelite:Implications for the W-Cu-Mo polymetallic mineralization of the Shimensi Deposit, south China. Am Mineral 102:1114–1128

Sun, K., Chen, B., Deng, J., 2019. Ore genesis of the Zhuxi supergiant W-Cu skarn polymetallic deposit, South China: evidence from scheelite geochemistry. Ore Geol Rev 107:14–29

Sverjensky, D., 1984. Europium redox equilibria in aqueous solution. Earth Planet Sci Lett 67:70–78

Sylvester, P.J., Jackson, S.E., 2016. A brief history of laser ablation inductively coupled plasma mass spectrometry (LA–ICP–MS). Elements 12(5):307-310

Taylor, R.G. 1979. Geology of Tin Deposits, Elsevier, Amsterdam, 544 p.

Testemale, D., Hazemann, J.L., Pokrovski, G.S., Joly, Y., Roux, J., Argoud, R., Geaymond, O., 2004. Structural and electronic evolution of the As(OH)3 molecule in high temperature aqueous solutions: an X-ray absorption investigation. J Chem Phys 121(18):8973–8982

Thompson, J., Sillitoe, R., Baker, T., Lang, J.R., Mortensen, J.K., 1999. Intrusion-related gold deposits associated with tungsten-tin provinces. Mineral. Deposita 34, 323–334. https://doi.org/10.1007/s001260050207

Tian, Y., Etschmann, B., Mei, Y., Grundler, P.V., Testemale, D., Hazemann, J-L., Elliott, P., Ngothai, Y., Brugger, J., 2014. Speciation and thermodynamic properties of manganese(II) chloride complexes in hydrothermal fluids: in situ XAS study. Geochim Cosmochim Acta 129:77–95

Tischendorf, G., 1977. Geochemical and petrographic characteristics of silicic magmatic rocks associated with rare-element mineralisation. In M. Stemprok, L. Burnol and G. Tischendorf (eds.) Metallization associated with acid magmatism (Geo. Surv. Prague) 2:41-96.

Toverud, O., 1984. Dispersal of tungsten in glacial drift and humus in Bergslagen, southern central Sweden. Journal of Geochemical Exploration, 21:261–272.

Tyson, R.M., Hemphill, W.R., Theisen, A.R., 1988. Effect of the W:Mo ratio on the shift of excitation and emission spectra in the scheelite-powellite series. *American Mineralogist* 73 (9-10): 1145–1154.

Uspensky, E., Brugger, J., Graeser, S., 1998. REE geochemistry systematics of scheelite from the Alps using luminescence spectroscopy: from global regularities to facies control. Schweiz Mineral Petrogr Mitt 78:33–56

Vallance, J., Cathelineau, M., Boiron, M.C., Fourcade, S., Shepherd, T.J., Naden, J., 2003. Fluid–rock interactions and the role of late Hercynian aplite intrusion in the genesis of the Castromil gold deposit, northern Portugal. Chemical Geology, 194, 201-224. https://doi.org/10.1016/S0009-2541(02)00278-4

Vermeesch, P., 2018, IsoplotR: a free and open toolbox for geochronology. Geoscience Frontiers, v.9, p.1479-1493, doi: 10.1016/j.gsf.2018.04.001.

Veselovský, F., Ackerman, L., Pašava, J., Žák, K., Haluzová, E., Creaser, R.A., Dobeš, P., Erban, V., Tasler, R., 2018. Multiphase formation of the Obří důl polymetallic skarn deposit, West Sudetes, Bohemian Massif: Geochemistry and Re–Os dating of sulfide mineralization. Miner Deposita 53, 665–682. https://doi.org/10.1007/s00126-017-0766-0

Voicu, G.M., Bardoux, M., Stevenson, R., Jebrak, M., 2001 Nd and Sr isotope study of hydrothermal scheelite and host rocks at Omai, Guiana Shield: implications for ore fluid source and flow path during the formation of orogenic gold deposits Mineralium Deposita 35: 302-314

Wade, C.E., Payne, J.L., Barovich, K., Gilbert, S., Wade, B.P., Crowley, J.L., Reid, A., Jagodzinski, E.A., 2022. Zircon trace element geochemistry as an indicator of magma fertility in iron oxide copper-gold provinces. *Economic Geology*; 117 (3): 703–718. doi: https://doi.org/10.5382/econgeo.4886

Wang, X-S., Williams-Jones, A.E., Hu, R-Z., Shang, L-B., Bi, X-W., 2021. The role of fluorine in granite-related hydrothermal tungsten ore genesis: Results of experiments and modeling, Geochimica et Cosmochimica Acta, 292, 170-187, https://doi.org/10.1016/j.gca.2020.09.032.

Webster, J., Thomas, R., Förster, H.J., Seltmann, R., Tappen, C., 2004. Geochemical evolution of halogen-enriched granite magmas and mineralizing fluids of the Zinnwald tin-tungsten mining district, Erzgebirge, Germany. Miner Deposita 39, 452–472. https://doi.org/10.1007/s00126-004-0423-2

Wilkinson, J.J., Baker, M., Cooke, D., Wilkinson, C., 2020. Exploration targeting in porphyry Cu systems using propylitic mineral chemistry. Econ Geol 115:771–791

Wilkinson, J.J., Chang, Z., Cooke, D.R., Baker, M.J., Wilkinson, C.C., Inglis, S., Chen, H., Gemmell, J.B., 2015. The chlorite proximitor: A new tool for detecting porphyry ore deposits, Journal of Geochemical Exploration, Volume 152, Pages 10-26

Willden, C.R., and Hotz, P.E., 1955. A gold-scheelite-cinnabar placer in Humboldt County, Nevada. *Economic Geology*; 50 (7): 661–668. doi: https://doi.org/10.2113/gsecongeo.50.7.661

Wintzer, N.E., 2019. Geology, Geochronology, and Geochemistry of the Stibnite-Yellow Pine Gold-Antimony-Tungsten Mining Area, Idaho. PhD thesis, Pullman, USA Washington State University 297p

Wintzer, N.E., Schmitz, M.D., Gillerman, V.S., Vervoort, J.D., 2022. U-Pb Scheelite Ages of Tungsten and Antimony Mineralization in the Stibnite-Yellow Pine District, Central Idaho. *Economic Geology*; doi: https://doi.org/10.5382/econgeo.4953

Wood, S.A., and Samson, I.M., 2000. The Hydrothermal Geochemistry of Tungsten in Granitoid Environments: I. Relative Solubilities of Ferberite and Scheelite as a Function of T, P, pH, and mNaCl. Economic geology Vol. 95. pp 143-182.

Wu, S., Mao, J., Ireland, T., Zaho, Z., Yao, F., Yang, Y., Sun, W., 2019. Comparative geochemical study of scheelite from the Shizhuyuan and Xianglushan tungsten skarn deposits, South China: implications for scheelite mineralization. Ore Geol Rev 109:448–464

Xie, L., Zhang, Y., Zhang, H., Sun, J., Wu, F., 2008. In situ simultaneous determination of trace elements, U-Pb and Lu-Hf isotopes in zircon and baddeleyite. Chin. Sci. Bull. 53, 1565–1573.

Xu, J., Ciobanu, C., Cook, N.C., Slattery, A., 2019. Crystals from the powellite-scheelite series at the nanoscale: a case study from the Zhibula Cu skarn, Gangdese Belt. Tibet Minerals 9:340

Yuan, H.-L., Gao, S., Dai, M.-N., Zong, C.-L., Günther, D., Fontaine, G.H., Liu, X.-M., Diwu, C., 2008. Simultaneous determinations of U–Pb age, Hf isotopes and trace element compositions of zircon by excimer laser-ablation quadrupole and multiple-collector ICP-MS. Chem. Geol. 247, 100–118.

Yuan, L., Chi, G., Wang, M., Li, Z., Xu, D., Deng, T., Geng, J., Hu, M., Zhang, L., 2019. Characteristics of REEs and trace elements in scheelite from the Zhuxi W deposit, South China: implications for the ore forming conditions and processes. Ore Geol Rev 109:585–597

Žáček V., 2008. Cu-skarn v Kotli v Krkonoších (Česká republika). - Bull. mineral.-petrolog. Odd. Nár. Muz. (Praha) 16/2, 230-237. ISSN: 1211-0329

Zachariáš, J., Morávek, P., Gadas, P., Pertoldová, J., 2014. The Mokrsko-West gold deposit, Bohemian Massif, Czech Republic: Mineralogy, deposit setting and classification. Ore Geol Rev 58:238–263.

Zang, Z., Xie, G., Mao, J., Liu, W., Olin, P., Li, W., 2019. Sm-Nd Dating and In-Situ LA-ICP-MS Trace Element Analyses of Scheelite from the Longshan Sb-Au Deposit, Xiangzhong Metallogenic Province, South China. Minerals 9:87

Zaw, K., and Singoyi, B., 2000. Formation of Magnetite-Scheelite Skarn Mineralization at Kara, Northwestern Tasmania: Evidence from Mineral Chemistry and Stable Isotopes. Econ Geol 95:1215–1230

Zhang, Q., Zhang, R.Q., Gao, J.F., Lu, J.J., Wu, J.W., 2018. In-situ LA-ICP-MS trace element analyses of scheelite and wolframite: Constraints on the genesis of veinlet-disseminated and vein-type tungsten deposits, South China. Ore Geol Rev 99:166-179

Zhang, Q., Zhao, K.D., Li, W-Q., Palmer, M.R., Jiang, S-Y., Jaing, H., Zhang, W., Zhang, D., Hussian, A., 2022. Timing and tectonic setting of tin mineralization in southern Myanmar: constraints from cassiterite and wolframite U–Pb ages. Miner Deposita 57, 977–999. https://doi.org/10.1007/s00126-021-01083-y

Zhao, L., Zhang, Y., Shao, Y., Li, H., Shah, S.A., Zhou, W., 2021. Using garnet geochemistry discriminating different skarn mineralization systems: Perspective from Huangshaping W-Mo-Sn-Cu polymetallic deposit, South China, Ore Geology Reviews, Volume 138.

Zhao, W., Zhou, M-F., Williams-Jones, A., Zhao, Z., 2018. Constraints on the uptake of REE by scheelite in the Baoshan tungsten skarn deposit, South China. Chem Geol 477:123–136

Zheng, W., Tang, J., Zhong, K., Ying, L., Leng, Q., Ding, S., Lin, B., 2016. Geology of the Jiama porphyry copper–polymetallic system, Lhasa Region, China. Ore Geol Rev 74:151–169

Zou, S., Chen, X., Brzozowski, M.J., Leng, C.B., Xu, D., 2022. Application of Machine Learning to Characterizing Magma Fertility in Porphyry Cu Deposits. JGR: Solid Earth, 127: 1-17.

Appendices

Electronic Supplementary Materials associated with the Chapter 1

Appendix 1.1A. Binary plots of trace elements composition scheelite. a. K versus ΣREE-Eu+Y, and b. Na+Nb+Ta+As+V versus ΣREE-Eu+Y. Literature data from: Song et al. (2014), Fu et al. (2016), Guo et al. (2016), Ding et al. (2018), Zhao et al. (2018), Li et al. (2019), Wu et al. (2019), Yuan et al. (2019), Xu et al. (2019), Chen et al. (2020), Seo et al. (2020), Song et al. (2020) and Su et al. (2020).

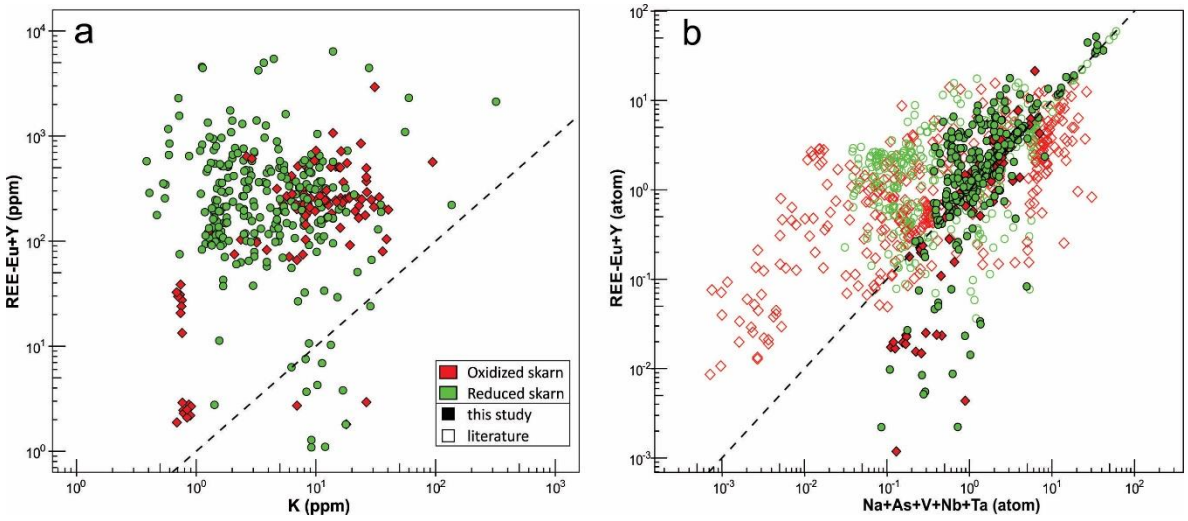

Appendix 1.2A Cathodoluminescence image (grey scale) and LA-ICP-MS multi-element maps (white-violet scale) showing zoned scheelite grain from garnet facies, King Island. The concentrations of the elements in the LA-ICP-MS maps are semi-quantitative. The white lines show the limit of the grain.

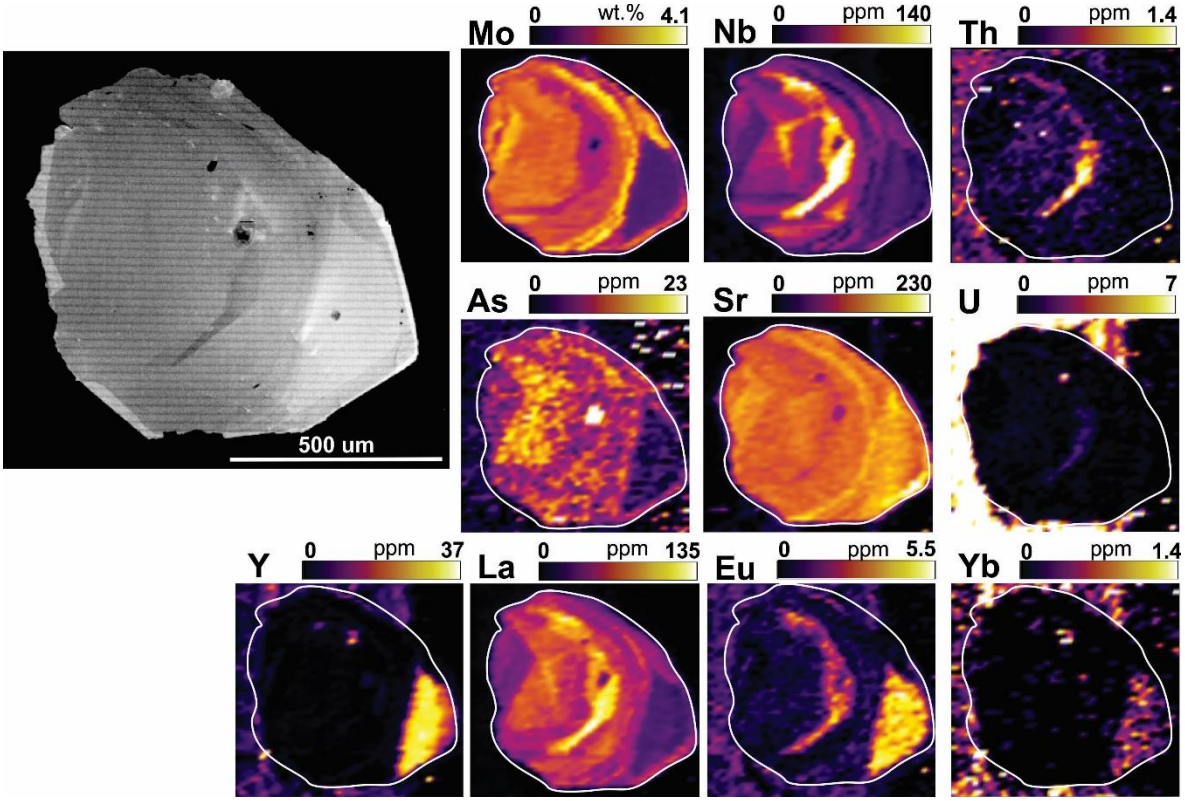

Appendix 1.3A Box and whisker diagram of LREE and HREE in garnet and clinopyroxene from reduced and oxidized skarns.

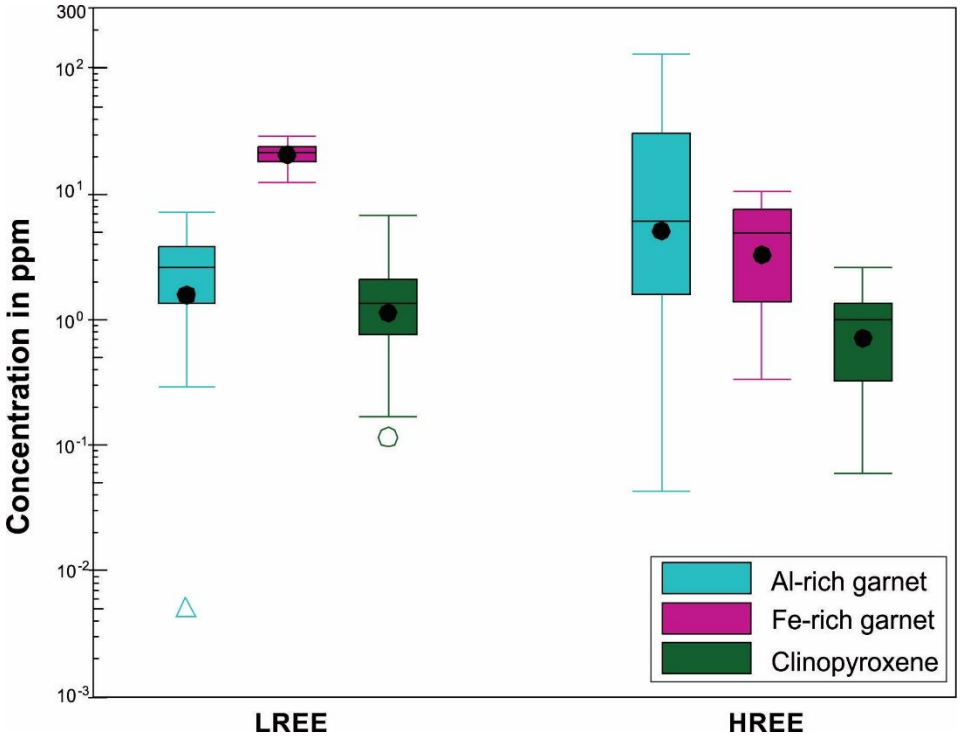

Appendix 1.4A Chondrite-normalized REE patterns of scheelite, garnet and clinopyroxene from some representative deposits where they coexist. Chondrite normalized values from McDonough and Sun (1995).

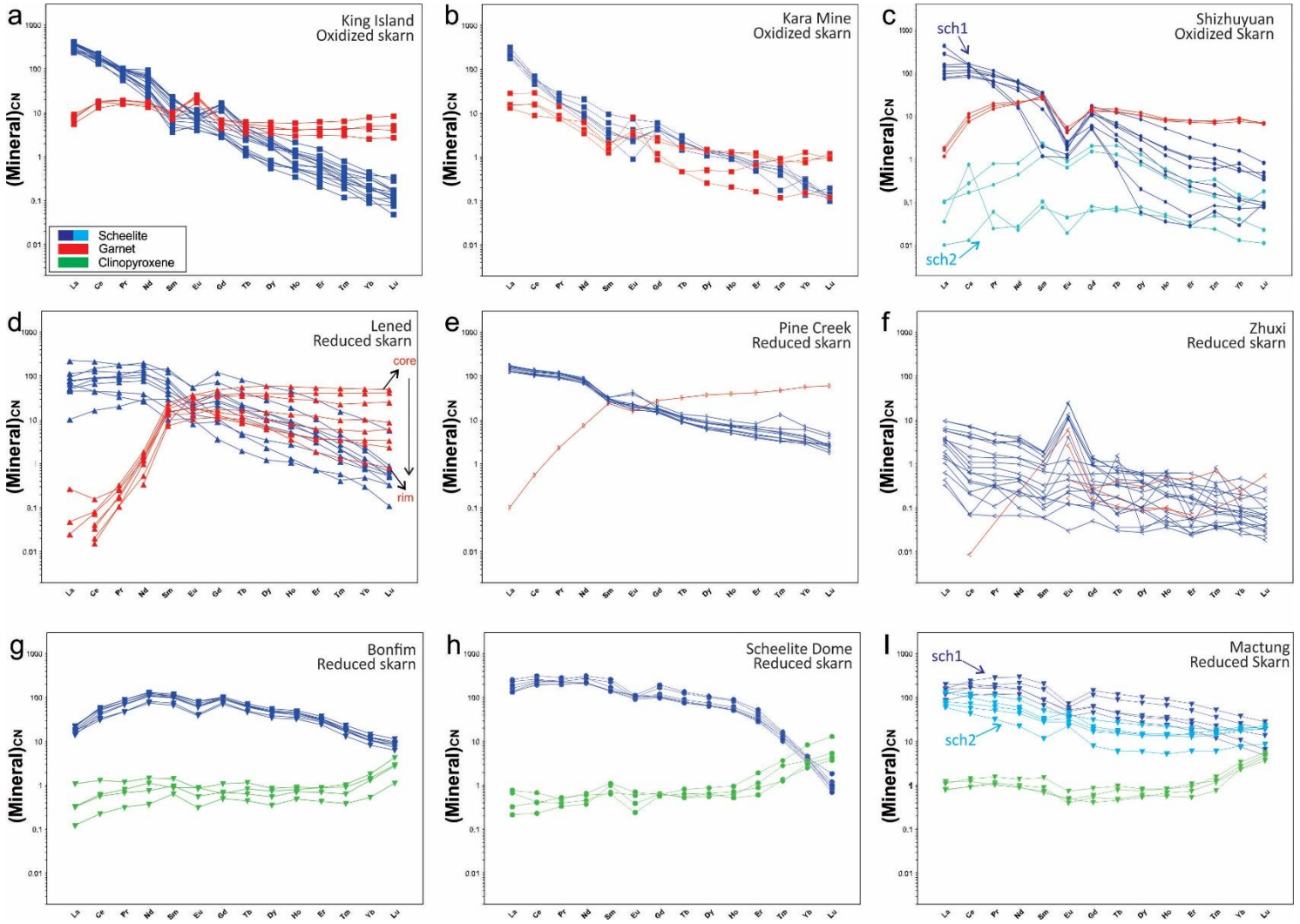

Appendix 1.5A On the left, cathodoluminescence image of scheelite (Mactung). On the right, REE patterns of different spots along the crystal showing the change in the REE patterns with the progress of scheelite crystallization. Chondrite normalized values from McDonough and Sun (1995).

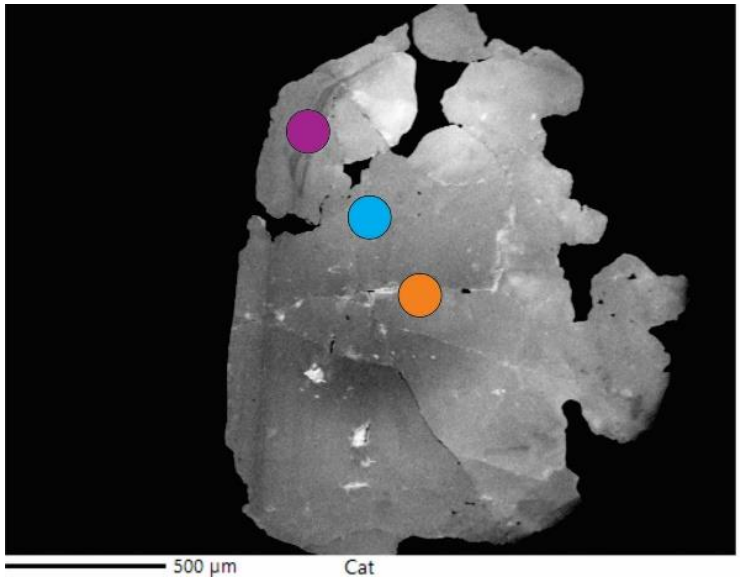

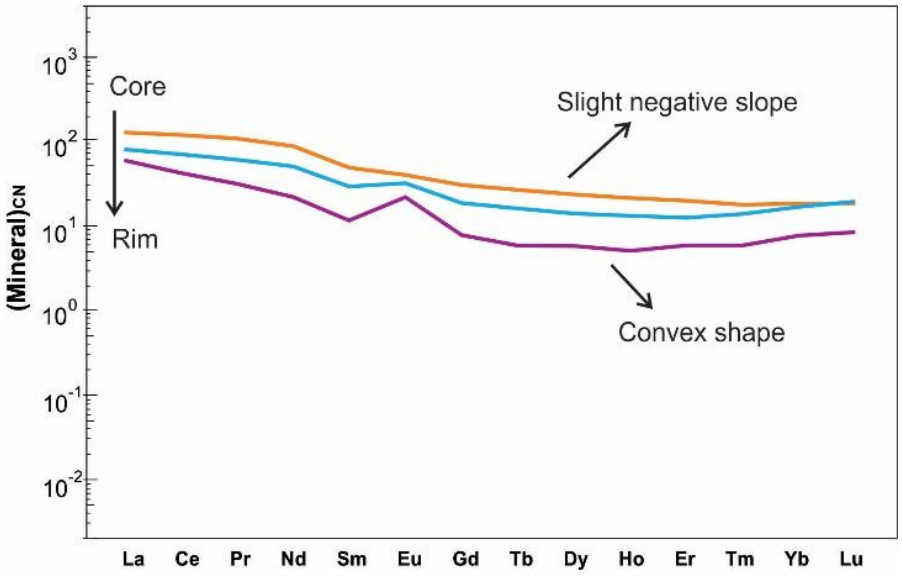

Appendix 1.1B Garnet, clinopyroxene and scheelite major elements.

Mineral	ID_SAMPLE	DEPOSIT	Na2O	Y2O3	Al2O3	MgO	SiO2	CaO	TiO2	Cr2O3	ZnO	FeO
Garnet	KR65-1-4	Kara	0.015	<DL	2.823	0.036	35.19	32.946	<DL	<DL	0.021	25.791
Garnet	KR65-1-5	Kara	0.010	<DL	2.885	0.048	35.21	32.712	<DL	<DL	0.020	25.668
Garnet	Kr65 1	Kara	0.004	<DL	2.581	0.024	32.856	33.191	<DL	<DL	<DL	28.781
Garnet	Kr65 2	Kara	<DL	<DL	3.259	0.043	32.726	33.228	0.016	<DL	0.008	27.814
Garnet	Kr65 3	Kara	<DL	<DL	2.705	0.037	33.367	33.279	<DL	0.020	<DL	28.481
Garnet	Kr65 4	Kara	0.032	<DL	2.987	0.033	33.030	33.399	<DL	0.065	0.004	28.162
Garnet	Kr65 5	Kara	0.027	<DL	1.784	0.018	32.748	31.366	0.144	0.026	<DL	30.863
Garnet	Kr65 6	Kara	0.009	<DL	3.628	0.038	33.731	33.565	0.011	<DL	<DL	27.081
Garnet	Kr65 7	Kara	0.006	<DL	2.466	0.043	33.332	33.306	0.027	0.007	<DL	28.651
Garnet	DM-Grenat 1	King Island	0.024	<DL	3.079	0.038	33.523	32.467	0.118	<DL	<DL	28.361
Garnet	DM-Grenat 2	King Island	0.021	<DL	2.149	0.035	33.492	32.366	0.112	<DL	<DL	29.179
Garnet	DM-Grenat 3	King Island	0.02	<DL	2.996	0.037	33.697	32.515	0.266	<DL	<DL	28.053
Garnet	DM-Grenat 4	King Island	0.01	<DL	2.383	0.067	33.674	32.699	0.367	<DL	<DL	29.265
Garnet	XY199 c1	Xiaoyao	0.035	0.001	4.246	0.029	34.743	34.188	0.016	0.007	<DL	26.435
Garnet	XY199 c2	Xiaoyao	0.026	<DL	2.674	0.018	34.826	33.669	0.064	<DL	<DL	28.630
Garnet	XY199 c3	Xiaoyao	<DL	<DL	4.336	0.061	35.354	34.626	0.130	0.013	<DL	25.835
Garnet	XY199 c4	Xiaoyao	0.027	<DL	1.496	0.015	33.124	33.559	0.011	<DL	0.051	29.978
Garnet	XY199 c5	Xiaoyao	<DL	<DL	5.518	0.025	34.166	34.092	0.076	0.013	<DL	25.077
Garnet	XY199 c6	Xiaoyao	0.017	<DL	5.503	0.071	34.616	34.442	0.460	0.003	0.008	23.836
Garnet	XY199 c7	Xiaoyao	0.003	<DL	4.427	0.063	33.894	34.188	0.442	0.046	0.013	25.831
Garnet	XY199 c8	Xiaoyao	0.023	0.008	3.673	0.044	33.672	33.986	0.005	0.023	0.028	27.573
Garnet	XY199 c9	Xiaoyao	0.011	<DL	6.834	0.057	33.673	34.660	0.260	<DL	<DL	22.744
Garnet	CA16B 6	Pine Creek	0.022	<DL	15.609	0.063	35.443	32.560	0.329	<DL	<DL	11.579
Garnet	CA16B 7	Pine Creek	0.031	0.037	15.215	0.029	35.010	32.567	0.488	0.007	<DL	11.563
Garnet	CA16B 8	Pine Creek	0.001	0.009	15.689	0.038	35.713	32.326	0.110	<DL	0.030	11.747
Garnet	CA16B 9	Pine Creek	<DL	<DL	15.039	0.041	35.681	32.488	0.290	<DL	<DL	12.143
Garnet	SY18A 1	Shizuyuan	0.015	0.002	6.546	0.187	32.881	31.992	<DL	0.016	<DL	22.778
Garnet	SY18A 2	Shizuyuan	<DL	<DL	6.066	0.112	32.547	31.408	0.011	<DL	<DL	24.446
Garnet	SY18A 3	Shizuyuan	0.021	<DL	6.456	0.089	33.286	31.500	0.016	<DL	0.001	23.891

Appendix 1.1B (continued)

Mineral	ID_SAMPLE	DEPOSIT	Na2O	Y2O3	Al2O3	MgO	SiO2	CaO	TiO2	Cr2O3	ZnO	FeO
Garnet	SY18A 4	Shizuyuan	0.017	<DL	6.624	0.096	32.722	31.148	0.011	<DL	<DL	23.812
Garnet	SY18A 5	Shizuyuan	0.021	<DL	4.790	0.103	33.485	33.062	0.032	0.020	<DL	25.129
Garnet	SY18A 6	Shizuyuan	0.005	<DL	4.978	0.059	33.206	33.423	0.022	<DL	<DL	25.101
Garnet	SY18A 7	Shizuyuan	0.026	<DL	5.880	0.158	33.289	32.426	<DL	0.036	0.053	23.641
Garnet	SY18A 8	Shizuyuan	<DL	<DL	4.966	0.107	33.993	33.525	0.011	<DL	0.024	24.776
Garnet	776 1	Jiama	0.029	<DL	0.080	0.028	33.057	32.977	<DL	<DL	<DL	32.166
Garnet	776 2	Jiama	<DL	<DL	0.029	0.010	33.384	32.868	<DL	<DL	<DL	32.399
Garnet	776 3	Jiama	0.029	<DL	0.036	0.037	33.172	33.196	0.016	0.039	<DL	32.205
Garnet	776 4	Jiama	0.003	<DL	1.732	0.026	34.046	34.106	<DL	0.091	0.010	29.196
Garnet	776 5	Jiama	<DL	<DL	0.206	0.032	32.823	33.063	0.027	0.100	<DL	32.039
Garnet	776 6	Jiama	0.011	<DL	0.342	0.030	32.995	33.206	0.016	<DL	0.002	31.345
Garnet	776 7	Jiama	0.037	<DL	0.258	0.057	34.518	33.059	0.011	0.058	0.061	31.590
Garnet	776 8	Jiama	<DL	<DL	0.166	0.041	33.889	33.416	0.027	0.010	0.004	31.841
Garnet	SL8A 1	Salau	0.011	<DL	19.471	0.059	35.808	23.536	2.111	<DL	0.035	14.631
Garnet	SL8A 2	Salau	<DL	<DL	20.122	0.090	35.649	20.155	0.236	<DL	0.085	18.409
Garnet	SL8A 3	Salau	0.035	<DL	20.100	0.105	35.892	20.342	0.257	0.013	<DL	18.183
Garnet	SL8A 4	Salau	0.036	<DL	19.724	0.065	37.439	35.170	0.290	0.045	0.013	6.683
Garnet	SL8A 5	Salau	0.014	<DL	20.724	0.061	35.342	23.578	0.227	<DL	<DL	14.484
Garnet	DHPC 1	Lened	0.013	0.012	20.026	0.049	36.165	24.783	0.347	0.047	0.068	10.271
Garnet	DHPC 2	Lened	0.003	<DL	19.013	0.022	37.332	27.468	0.480	<DL	<DL	11.823
Garnet	DHPC 3	Lened	0.011	<DL	20.132	0.048	35.971	25.417	0.288	<DL	<DL	10.685
Garnet	DHPC 4	Lened	0.023	0.001	20.413	0.060	36.229	23.044	0.097	0.073	<DL	14.640
Garnet	LENED 1	Lened	<DL	<DL	20.444	0.118	36.180	19.983	0.240	0.023	<DL	14.908
Garnet	LENED 2	Lened	0.007	<DL	20.187	0.074	36.768	21.967	0.113	0.003	0.012	13.393
Garnet	LENED 3	Lened	<DL	<DL	20.454	0.128	35.076	19.219	0.207	0.003	<DL	15.136
Garnet	LENED 4	Lened	<DL	0.019	20.319	0.102	34.774	17.274	0.085	<DL	<DL	18.476
Garnet	LENED 5	Lened	0.009	<DL	20.260	0.116	36.188	20.421	0.294	0.033	<DL	14.201
Garnet	LENED 6	Lened	0.006	0.015	20.007	0.154	35.377	15.768	0.247	0.026	0.025	18.839

Appendix 1.1B (continued)

Mineral	ID_SAMPLE	DEPOSIT	Na2O	Y2O3	Al2O3	MgO	SiO2	CaO	TiO2	Cr2O3	ZnO	FeO
Garnet	LENED 7	Lened	<DL	<DL	20.176	0.107	36.112	19.977	0.208	0.023	<DL	14.722
Garnet	LENED 8	Lened	0.003	0.046	20.366	0.118	36.062	20.210	0.181	0.073	<DL	14.348
Garnet	CEZ-Gr 1	Cantung	0.024	0.009	21.155	0.360	36.719	16.756	0.185	0.016	<DL	11.738
Garnet	CEZ-Gr 2	Cantung	0.018	<DL	20.618	0.261	35.697	17.414	0.122	<DL	<DL	10.845
Garnet	CEZ-Gr 3	Cantung	0.013	<DL	21.267	0.328	35.285	16.110	0.211	<DL	0.042	12.098
Garnet	CEZ-Gr 4	Cantung	0.021	<DL	21.386	0.373	36.164	15.617	0.137	0.049	0.024	12.105
Garnet	CEZ-Gr 5	Cantung	<DL	<DL	21.066	0.293	35.757	16.558	0.211	0.033	0.004	11.407
Garnet	CEZ-Gr 6	Cantung	<DL	<DL	20.888	0.198	34.772	19.001	0.149	<DL	0.014	12.061
Garnet	Mt-Gr 1	Mactung	0.029	<DL	20.169	0.033	35.416	26.740	0.533	0.007	<DL	7.611
Garnet	Mt-Gr 2	Mactung	0.002	<DL	19.971	0.038	35.093	34.432	0.701	0.021	<DL	5.258
Garnet	Mt-Gr 3	Mactung	0.027	<DL	19.709	0.037	35.015	34.040	0.654	0.014	<DL	5.444
Garnet	Mt-Gr 4	Mactung	0.021	<DL	19.869	0.027	34.744	34.794	0.717	0.024	0.012	5.274
Garnet	Mt-Gr 5	Mactung	0.015	<DL	19.634	0.022	34.027	34.198	1.026	0.096	<DL	5.241
Garnet	Mt-Gr 6	Mactung	0.020	<DL	19.553	0.024	34.392	34.339	0.911	0.206	<DL	5.223
Garnet	M2B2B 1	Mactung	0.025	<DL	20.216	0.037	34.536	25.600	0.364	0.054	<DL	14.004
Garnet	M2B2B 2	Mactung	0.009	0.014	20.158	0.020	36.568	25.117	0.228	0.003	0.008	14.280
Garnet	M2B2B 3	Mactung	0.007	0.001	20.179	0.019	35.384	25.552	0.201	<DL	<DL	14.432
Garnet	M2B2B 4	Mactung	0.014	<DL	19.693	0.029	36.573	31.032	0.304	<DL	<DL	9.027
Garnet	ZX-25B	Zhuxi	<DL	<DL	19.542	<DL	38.091	34.336	<DL	<DL	<DL	5.238
Garnet	ZX-25B	Zhuxi	0.010	<DL	20.914	0.019	37.996	35.076	0.006	0.017	0.017	3.654
Garnet	ZX-25B	Zhuxi	0.009	<DL	20.205	0.019	36.868	34.891	<DL	<DL	<DL	4.141
Garnet	ZX-25B	Zhuxi	0.021	<DL	19.698	0.011	37.333	34.067	0.006	0.010	<DL	5.078
Garnet	ZX-25B	Zhuxi	0.005	<DL	20.481	0.012	38.044	34.918	<DL	0.017	0.005	3.768
Garnet	ZX-25B	Zhuxi	0.087	<DL	19.059	0.483	36.172	35.481	0.039	<DL	0.033	4.001
Garnet	ZX-25B	Zhuxi	0.011	<DL	19.501	0.010	37.611	34.065	<DL	<DL	0.005	4.964
Garnet	ZX-25B	Zhuxi	0.018	<DL	19.628	0.012	38.267	34.022	<DL	<DL	<DL	5.347
Garnet	ZX-25B	Zhuxi	0.019	<DL	21.003	0.046	37.348	35.095	<DL	0.017	<DL	3.030

Appendix 1.1B (continued)

Mineral	ID_SAMPLE	DEPOSIT	MnO	ZrO2	P2O5	K2O	Total
Garnet	KR65-1-4	Kara	0.564	0.062	0.022	0.003	97.474
Garnet	KR65-1-5	Kara	0.627	0.002	<DL	0.010	97.193
Garnet	Kr65 1	Kara	0.584	<DL	0.003	0.013	98.037
Garnet	Kr65 2	Kara	0.591	<DL	0.027	<DL	97.712
Garnet	Kr65 3	Kara	0.593	0.048	<DL	0.002	98.533
Garnet	Kr65 4	Kara	0.604	0.019	0.012	0.018	98.368
Garnet	Kr65 5	Kara	1.344	0.046	0.003	0.005	98.374
Garnet	Kr65 6	Kara	0.631	0.059	0.037	0.002	98.792
Garnet	Kr65 7	Kara	0.576	<DL	0.010	0.008	98.431
Garnet	DM-Grenat 1	King Island	1.076	0.076	0.027	0.002	97.791
Garnet	DM-Grenat 2	King Island	0.692	<DL	<DL	<DL	98.046
Garnet	DM-Grenat 3	King Island	0.856	0.032	<DL	<DL	98.473
Garnet	DM-Grenat 4	King Island	0.649	0.012	0.026	<DL	99.153
Garnet	XY199 c1	Xiaoyao	0.450	0.008	<DL	0.002	100.160
Garnet	XY199 c2	Xiaoyao	0.524	<DL	<DL	0.001	100.433
Garnet	XY199 c3	Xiaoyao	0.322	0.010	0.015	<DL	100.701
Garnet	XY199 c4	Xiaoyao	0.371	0.010	<DL	<DL	98.643
Garnet	XY199 c5	Xiaoyao	0.543	<DL	<DL	0.008	99.519
Garnet	XY199 c6	Xiaoyao	0.356	0.080	0.011	0.002	99.405
Garnet	XY199 c7	Xiaoyao	0.329	<DL	0.012	<DL	99.248
Garnet	XY199 c8	Xiaoyao	0.396	0.016	0.004	0.004	99.454
Garnet	XY199 c9	Xiaoyao	0.388	<DL	0.001	<DL	98.629
Garnet	CA16B 6	Pine Creek	3.887	0.098	0.008	<DL	99.598
Garnet	CA16B 7	Pine Creek	3.719	<DL	<DL	<DL	98.666
Garnet	CA16B 8	Pine Creek	3.862	0.069	0.015	<DL	99.608
Garnet	CA16B 9	Pine Creek	3.898	<DL	<DL	<DL	99.580
Garnet	SY18A 1	Shizuyuan	2.267	0.096	<DL	<DL	96.781
Garnet	SY18A 2	Shizuyuan	2.374	0.057	<DL	<DL	97.022
Garnet	SY18A 3	Shizuyuan	2.625	0.024	0.036	<DL	97.946
Garnet	SY18A 4	Shizuyuan	2.713	0.035	0.014	<DL	97.191
Garnet	SY18A 5	Shizuyuan	1.392	<DL	<DL	<DL	98.033
Garnet	SY18A 6	Shizuyuan	1.141	0.024	0.023	<DL	97.981
Garnet	SY18A 7	Shizuyuan	2.348	0.002	0.030	0.001	97.890
Garnet	SY18A 8	Shizuyuan	1.154	0.052	0.018	<DL	98.626
Garnet	776 1	Jiama	0.522	0.005	0.026	<DL	98.888
Garnet	776 2	Jiama	0.533	0.018	0.015	<DL	99.257
Garnet	776 3	Jiama	0.479	<DL	<DL	<DL	99.209
Garnet	776 4	Jiama	0.296	0.017	<DL	<DL	99.523
Garnet	776 5	Jiama	0.525	<DL	<DL	<DL	98.816
Garnet	776 6	Jiama	0.492	0.080	<DL	<DL	98.519
Garnet	776 7	Jiama	0.538	<DL	0.011	<DL	100.197
Garnet	776 8	Jiama	0.407	0.081	0.020	0.007	99.908

Appendix 1.1B (continued)

Mineral	ID_SAMPLE	DEPOSIT	MnO	ZrO2	P2O5	K2O	Total
Garnet	SL8A 1	Salau	3.947	0.050	0.011	0.001	99.670
Garnet	SL8A 2	Salau	5.395	0.001	0.049	0.001	100.192
Garnet	SL8A 3	Salau	5.336	0.075	<DL	0.001	100.338
Garnet	SL8A 4	Salau	0.489	<DL	<DL	0.016	99.970
Garnet	SL8A 5	Salau	5.000	0.004	0.014	0.007	99.456
Garnet	DHPC 1	Lened	7.515	<DL	<DL	0.001	99.297
Garnet	DHPC 2	Lened	4.483	<DL	<DL	<DL	100.623
Garnet	DHPC 3	Lened	6.434	0.020	0.033	<DL	99.038
Garnet	DHPC 4	Lened	5.433	0.089	0.004	0.025	100.131
Garnet	LENED 1	Lened	9.180	0.002	<DL	0.005	101.084
Garnet	LENED 2	Lened	8.491	0.001	<DL	<DL	101.015
Garnet	LENED 3	Lened	9.399	<DL	0.033	<DL	99.657
Garnet	LENED 4	Lened	8.934	<DL	0.006	<DL	99.988
Garnet	LENED 5	Lened	9.071	0.021	0.017	<DL	100.630
Garnet	LENED 6	Lened	9.922	0.032	0.003	<DL	100.422
Garnet	LENED 7	Lened	9.377	0.038	0.014	<DL	100.755
Garnet	LENED 8	Lened	9.194	<DL	0.010	<DL	100.611
Garnet	CEZ-Gr 1	Cantung	14.082	0.055	<DL	0.004	101.104
Garnet	CEZ-Gr 2	Cantung	13.732	0.028	<DL	0.049	98.783
Garnet	CEZ-Gr 3	Cantung	14.465	<DL	0.006	<DL	99.825
Garnet	CEZ-Gr 4	Cantung	15.240	<DL	<DL	0.002	101.118
Garnet	CEZ-Gr 5	Cantung	14.634	0.062	<DL	<DL	100.025
Garnet	CEZ-Gr 6	Cantung	12.413	<DL	0.007	0.001	99.504
Garnet	Mt-Gr 1	Mactung	7.801	0.025	<DL	0.001	98.365
Garnet	Mt-Gr 2	Mactung	1.913	0.027	0.025	0.010	97.491
Garnet	Mt-Gr 3	Mactung	3.069	0.009	0.034	0.023	98.074
Garnet	Mt-Gr 4	Mactung	2.022	0.044	<DL	<DL	97.547
Garnet	Mt-Gr 5	Mactung	2.607	0.113	0.003	0.019	97.001
Garnet	Mt-Gr 6	Mactung	1.966	0.040	<DL	0.002	96.678
Garnet	M2B2B 1	Mactung	3.074	<DL	<DL	<DL	97.911
Garnet	M2B2B 2	Mactung	3.241	<DL	<DL	<DL	99.647
Garnet	M2B2B 3	Mactung	2.916	0.061	0.004	0.007	98.763
Garnet	M2B2B 4	Mactung	2.108	0.027	0.001	<DL	98.807
Garnet	ZX-25B	Zhuxi	2.190	0.032	0.020	<DL	99.449
Garnet	ZX-25B	Zhuxi	1.867	<DL	<DL	<DL	99.576
Garnet	ZX-25B	Zhuxi	2.336	0.040	0.036	0.002	98.547
Garnet	ZX-25B	Zhuxi	2.684	0.016	<DL	<DL	98.925
Garnet	ZX-25B	Zhuxi	2.443	<DL	<DL	0.005	99.697
Garnet	ZX-25B	Zhuxi	1.029	<DL	0.011	0.002	96.396
Garnet	ZX-25B	Zhuxi	2.704	<DL	0.004	0.012	98.885
Garnet	ZX-25B	Zhuxi	2.755	0.035	0.005	<DL	100.089
Garnet	ZX-25B	Zhuxi	2.226	0.054	0.014	<DL	98.854

Appendix 1.1B (continued)

Mineral	ID_SAMPLE	DEPOSIT	Na2O	Al2O3	MgO	SiO2	CaO	TiO2	Cr2O3	FeO	MnO
Clinopyroxene	CA16B 1	Pine Creek	0.141	0.207	7.170	50.940	23.278	<DL	<DL	12.653	3.981
Clinopyroxene	CA16B 2	Pine Creek	0.200	0.231	7.289	50.794	23.117	<DL	<DL	13.053	3.939
Clinopyroxene	CA16B 3	Pine Creek	0.161	0.225	6.809	50.492	23.035	<DL	0.045	13.713	4.155
Clinopyroxene	CA16B 4	Pine Creek	0.177	0.297	7.603	50.827	23.248	0.022	0.022	13.747	3.693
Clinopyroxene	CA16B 5	Pine Creek	0.270	0.391	6.563	50.277	22.774	0.072	<DL	14.206	3.974
Clinopyroxene	MT161 1	Mactung	0.185	1.060	9.496	50.966	23.118	0.088	<DL	13.221	0.607
Clinopyroxene	MT161 2	Mactung	0.206	0.941	9.529	51.291	23.115	0.219	<DL	13.267	0.537
Clinopyroxene	MT161 3	Mactung	0.128	0.429	10.225	51.912	23.510	0.103	0.009	12.588	0.564
Clinopyroxene	MT161 4	Mactung	0.169	0.919	9.440	51.178	22.729	0.263	<DL	13.393	0.573
Clinopyroxene	MT231 1	Mactung	0.039	0.145	5.114	50.232	23.370	<DL	<DL	19.303	1.212
Clinopyroxene	MT231 2	Mactung	0.075	0.151	5.272	50.417	23.716	<DL	<DL	18.538	1.293
Clinopyroxene	MT231 3	Mactung	0.058	0.158	5.015	49.803	23.306	0.068	0.017	19.317	1.243
Clinopyroxene	MT231 4	Mactung	0.050	0.288	3.697	49.378	22.789	0.082	<DL	21.398	1.104
Clinopyroxene	MT231 5	Mactung	0.101	0.830	8.917	51.259	23.214	0.014	<DL	13.924	0.771
Clinopyroxene	MT231 6	Mactung	0.128	0.720	9.138	51.089	23.274	0.035	0.009	13.850	0.763
Clinopyroxene	DPCH 4	Lened	0.052	0.165	3.604	49.464	22.893	<DL	<DL	19.900	2.581
Clinopyroxene	DPCH 5	Lened	0.053	0.216	3.006	49.312	22.656	<DL	<DL	21.371	1.782
Clinopyroxene	BF2 1	Bonfim	0.086	0.171	13.398	53.486	24.636	<DL	0.077	7.216	0.779
Clinopyroxene	BF2 2	Bonfim	0.089	0.227	13.517	53.414	24.596	0.052	<DL	6.778	0.792
Clinopyroxene	BF2 3	Bonfim	0.154	0.816	12.919	52.914	24.362	0.007	<DL	7.144	0.802
Clinopyroxene	BF2 4	Bonfim	0.071	0.343	14.388	53.627	24.920	0.015	<DL	5.740	0.551
Clinopyroxene	BF2 5	Bonfim	0.096	0.220	13.630	53.287	24.675	0.066	0.023	6.603	0.736
Clinopyroxene	SD-212-1	Scheelite Dome	0.070	0.266	1.505	48.604	23.052	0.021	0.013	24.803	1.064
Clinopyroxene	SD-212-2	Scheelite Dome	0.071	0.265	1.343	48.429	23.235	0.086	<DL	25.441	0.921
Clinopyroxene	SD-212-3	Scheelite Dome	0.076	0.239	1.401	48.543	23.016	<DL	0.061	25.148	1.039
Clinopyroxene	SD-212-4	Scheelite Dome	0.065	0.165	1.518	48.550	22.458	0.036	<DL	26.717	0.897
Clinopyroxene	SD-212-5	Scheelite Dome	0.095	0.298	1.497	48.474	23.050	0.071	0.017	25.950	0.939
Clinopyroxene	SD-212-6	Scheelite Dome	0.123	0.333	2.170	48.804	22.874	0.050	0.004	23.966	1.968
Clinopyroxene	SD-212-7	Scheelite Dome	0.088	0.221	1.743	48.595	22.851	0.007	0.017	24.662	1.649
Clinopyroxene	SD-212-8	Scheelite Dome	0.033	0.017	1.800	49.144	23.366	<DL	0.022	23.125	2.298
Clinopyroxene	SD-212-9	Scheelite Dome	0.097	0.294	1.577	48.388	23.180	<DL	0.022	24.410	1.246
Clinopyroxene	SD-212-10	Scheelite Dome	0.036	0.069	1.583	49.055	23.642	0.036	0.022	22.867	2.513

Appendix 1.1B (continued)

Mineral	ID_SAMPLE	DEPOSIT	K2O	NiO	Total
Clinopyroxene	CA16B 1	Pine Creek	<DL	<DL	98.370
Clinopyroxene	CA16B 2	Pine Creek	<DL	0.008	98.631
Clinopyroxene	CA16B 3	Pine Creek	0.009	<DL	98.644
Clinopyroxene	CA16B 4	Pine Creek	0.005	0.016	99.657
Clinopyroxene	CA16B 5	Pine Creek	<DL	<DL	98.528
Clinopyroxene	MT161 1	Mactung	0.005	<DL	98.745
Clinopyroxene	MT161 2	Mactung	0.008	<DL	99.114
Clinopyroxene	MT161 3	Mactung	0.009	<DL	99.476
Clinopyroxene	MT161 4	Mactung	0.014	0.025	98.702
Clinopyroxene	MT231 1	Mactung	0.013	<DL	99.428
Clinopyroxene	MT231 2	Mactung	<DL	0.014	99.476
Clinopyroxene	MT231 3	Mactung	<DL	<DL	98.985
Clinopyroxene	MT231 4	Mactung	<DL	<DL	98.786
Clinopyroxene	MT231 5	Mactung	0.006	<DL	99.035
Clinopyroxene	MT231 6	Mactung	0.007	<DL	99.012
Clinopyroxene	DPCH 4	Lened	<DL	0.026	98.686
Clinopyroxene	DPCH 5	Lened	<DL	0.019	98.414
Clinopyroxene	BF2 1	Bonfim	<DL	<DL	99.849
Clinopyroxene	BF2 2	Bonfim	<DL	0.038	99.504
Clinopyroxene	BF2 3	Bonfim	0.001	0.001	99.121
Clinopyroxene	BF2 4	Bonfim	0.011	0.021	99.686
Clinopyroxene	BF2 5	Bonfim	0.006	<DL	99.342
Clinopyroxene	SD-212-1	Scheelite Dome	0.008	<DL	99.406
Clinopyroxene	SD-212-2	Scheelite Dome	0.012	0.010	99.812
Clinopyroxene	SD-212-3	Scheelite Dome	0.007	<DL	99.530
Clinopyroxene	SD-212-4	Scheelite Dome	<DL	<DL	100.406
Clinopyroxene	SD-212-5	Scheelite Dome	0.007	0.017	100.417
Clinopyroxene	SD-212-6	Scheelite Dome	0.001	<DL	100.293
Clinopyroxene	SD-212-7	Scheelite Dome	<DL	<DL	99.834
Clinopyroxene	SD-212-8	Scheelite Dome	<DL	<DL	99.805
Clinopyroxene	SD-212-9	Scheelite Dome	0.011	<DL	99.226
Clinopyroxene	SD-212-10	Scheelite Dome	0.010	<DL	99.833

Appendix 1.1B (continued)

Mineral	ID	Name	CaO	WO3	Total	Na (ppm)	Fe (ppm)	Y (ppm)	Mo (ppm)	Sr (ppm)
Scheelite	2420-776B c1-1	Jiama	20.84	65.18	86.02	0.0055	0.0056	<DL	8.576	<DL
Scheelite	2420-776B c1-2	Jiama	20.60	66.22	86.82	0.0076	0.0026	<DL	9.3791	<DL
Scheelite	2420-776B c1-3	Jiama	19.69	76.13	95.82	0.007	0.0044	<DL	2.9629	<DL
Scheelite	2420-776B c2-1	Jiama	20.57	66.20	86.77	0.0067	<DL	<DL	10.153	<DL
Scheelite	2420-776B c2-2	Jiama	20.57	46.75	67.32	0.0089	0.0041	<DL	21.7232	<DL
Scheelite	2420-848C 1	Jiama	19.00	81.43	100.43	0.0133	0.0036	<DL	0.0908	<DL
Scheelite	2420-848C 2	Jiama	18.90	81.65	100.55	0.0178	0.0025	<DL	0.3708	<DL
Scheelite	2420-848C 3	Jiama	18.86	81.62	100.48	0.0279	0.0027	<DL	0.1052	<DL
Scheelite	DMGr-1 a	King Island	19.30	78.28	97.59	0.0125	0.0135	<DL	1.4655	<DL
Scheelite	DMGr-1 b	King Island	19.26	78.48	97.74	0.0126	0.0027	<DL	0.9297	<DL
Scheelite	DMGr-1 c	King Island	19.34	76.99	96.33	0.0099	0.0191	<DL	2.2113	<DL
Scheelite	DMGr-1 d	King Island	19.08	79.58	98.66	0.0069	0.0719	<DL	0.9486	<DL
Scheelite	DM-Px 1	King Island	19.08	78.74	97.82	0.0148	0.0013	<DL	0.5864	<DL
Scheelite	DM-Px 2	King Island	19.31	77.38	96.69	0.0125	0.0027	<DL	1.2978	<DL
Scheelite	DM-Px 3	King Island	19.27	78.93	98.20	0.01	0.0054	<DL	0.7233	<DL
Scheelite	DM-Px 4	King Island	19.38	77.99	97.36	0.0116	0.0048	<DL	1.388	<DL
Scheelite	DM-Px 5	King Island	19.21	79.30	98.51	0.0131	<DL	<DL	0.6392	<DL
Scheelite	DM-Px 6	King Island	19.32	78.44	97.76	0.0104	0.0002	<DL	1.1781	<DL
Scheelite	DM-Px 7	King Island	19.38	78.42	97.79	0.012	0.0106	<DL	0.5543	<DL
Scheelite	KU001 C1-1	Kumbel	19.60	78.38	97.97	0.0045	0.0093	<DL	0.8308	<DL
Scheelite	KU001 C1-2	Kumbel	19.54	78.31	97.84	0.0043	<DL	<DL	0.8841	<DL
Scheelite	KU001 C1-3	Kumbel	19.46	78.31	97.77	0.0039	0.0015	<DL	0.8639	<DL
Scheelite	KU001 C2-1	Kumbel	19.58	78.26	97.84	0.0038	0.0004	<DL	0.8099	<DL
Scheelite	KU001 C2-2	Kumbel	19.58	77.86	97.43	0.0019	0.0003	<DL	0.8139	<DL
Scheelite	KU001 C2-3	Kumbel	19.59	78.79	98.38	0.0045	0.0033	<DL	0.8245	<DL
Scheelite	KU001 C2-4	Kumbel	19.58	78.25	97.83	0.0043	0.0003	<DL	0.8583	<DL
Scheelite	CN1 C1-1	Brejui	19.36	79.10	98.46	0.0043	<DL	<DL	0.5001	0.0201
Scheelite	CN1 C1-2	Brejui	19.39	78.75	98.14	0.0095	<DL	<DL	0.4793	0.0215
Scheelite	CN1 C1-3	Brejui	19.29	79.28	98.57	0.0073	0.0034	<DL	0.4697	0.0279
Scheelite	CN1 C1-4	Brejui	19.37	78.80	98.17	0.0088	<DL	<DL	0.4653	0.0372
Scheelite	CN1 C2-1	Brejui	19.38	79.65	99.03	0.0068	0.0021	<DL	0.4241	0.0076
Scheelite	CN1 C2-2	Brejui	19.35	79.55	98.90	0.0074	<DL	<DL	0.4364	0.0337
Scheelite	CN1 C2-3	Brejui	19.35	79.45	98.80	0.005	0.0017	<DL	0.4604	0.0175
Scheelite	CN1 C2-4	Brejui	19.46	79.32	98.77	0.0062	0.0039	<DL	0.462	0.0413
Scheelite	CN2 C1-1	Brejui	19.33	79.51	98.84	0.0001	<DL	<DL	0.4316	<DL
Scheelite	CN2 C1-2	Brejui	19.34	78.96	98.30	0.0015	<DL	<DL	0.452	<DL

Appendix 1.1B (continued).

Mineral	ID	Name	CaO	WO3	Total	Na (ppm)	Fe (ppm)	Y (ppm)	Mo (ppm)	Sr (ppm)
Scheelite	CN2 C1-3	Brejui	19.32	79.58	98.89	0.0007	<DL	<DL	0.4453	<DL
Scheelite	CN2 C1-4	Brejui	19.38	79.13	98.51	0.0037	<DL	<DL	0.4397	<DL
Scheelite	KR65-1 1	Kara	19.50	76.94	96.43	0.011	0.38	<DL	2.143	<DL
Scheelite	KR65-1 2	Kara	20.07	70.49	90.57	0.007	0.046	<DL	5.328	0.008
Scheelite	KR65-1 3	Kara	18.93	80.19	99.12	0.008	0.449	<DL	0.014	<DL
Scheelite	KR65-2 1	Kara	20.15	70.39	90.53	0.012	0.032	<DL	5.876	0.013
Scheelite	KR65-2 2	Kara	19.60	77.21	96.81	0.014	0.139	<DL	2.202	<DL
Scheelite	Kr66-1 1	Kara	18.82	81.20	100.03	0.0133	<DL	<DL	0.0233	<DL
Scheelite	Kr66-1 2	Kara	19.09	81.12	100.21	0.0079	<DL	<DL	0.0926	<DL
Scheelite	Kr66-1 3	Kara	19.35	77.39	96.74	0.0067	<DL	<DL	1.9697	0.0043
Scheelite	Kr66-2 1	Kara	19.06	80.75	99.81	0.0157	<DL	<DL	0.0904	<DL
Scheelite	Kr66-2 2	Kara	19.46	76.97	96.43	0.014	0.0017	<DL	1.8856	<DL
Scheelite	Kr66-2 3	Kara	19.38	77.84	97.22	0.0093	0.0018	<DL	1.5932	<DL
Scheelite	KR98A-1 1	Kara	18.90	77.63	96.52	0.0062	0.2334	<DL	1.0032	<DL
Scheelite	KR98C-1 1	Kara	19.12	80.93	100.04	0.0067	0.0002	<DL	0.0468	<DL
Scheelite	KR98C-1 2	Kara	19.67	76.98	96.65	0.0022	0.0082	<DL	2.2152	<DL
Scheelite	KR98C-1 3	Kara	19.20	81.37	100.57	0.0084	0.0144	<DL	0.1118	<DL
Scheelite	KR98C-2 1	Kara	19.20	80.31	99.51	0.0149	0.0071	<DL	0.1153	<DL
Scheelite	KR98C-2 2	Kara	19.26	81.16	100.42	0.0053	0.0433	<DL	0.0867	<DL
Scheelite	KR98C-2 3	Kara	19.24	81.14	100.37	0.004	0.0794	<DL	0.0987	<DL
Scheelite	XY199 1	Xiaoyao	19.98	70.82	90.80	0.0056	0.0031	<DL	5.3922	<DL
Scheelite	XY199 3	Xiaoyao	20.06	71.01	91.07	0.0091	0.0034	<DL	5.8119	<DL
Scheelite	XY199 2	Xiaoyao	19.15	78.91	98.06	0.0066	<DL	<DL	1.194	<DL
Scheelite	SZY18A 1	Shizhuyuan	19.55	76.89	96.44	0.0032	<DL	<DL	2.1853	<DL
Scheelite	SZY18A 2	Shizhuyuan	19.23	81.27	100.50	0.0053	0.018	<DL	0.2267	<DL
Scheelite	SZY18B 1	Shizhuyuan	19.27	80.94	100.21	0.0053	<DL	<DL	0.1008	<DL
Scheelite	SZY18B 2	Shizhuyuan	18.92	81.37	100.29	0.0097	0.0031	<DL	0.0667	<DL
Scheelite	SZY18B 3	Shizhuyuan	19.04	81.64	100.68	0.0067	<DL	<DL	0.0937	<DL
Scheelite	ZX25B c2-1	Zhuxi	19.37	80.59	99.95	0.0036	<DL	<DL	0.0768	<DL
Scheelite	ZX25B c2-2	Zhuxi	19.67	80.90	100.57	0.0044	0.0058	<DL	0.0919	<DL
Scheelite	ZX25B c2-3	Zhuxi	19.13	80.31	99.44	0.004	0.0016	<DL	0.0773	<DL
Scheelite	SL1223 c3-1	Salau	18.98	81.67	100.65	0.0057	0.0054	<DL	<DL	<DL
Scheelite	SL1223 c3-2	Salau	18.71	81.33	100.04	0.0413	0.0084	0.1657	0.003	<DL
Scheelite	SL1223 c3-3	Salau	18.95	81.57	100.52	0.0038	0.0072	<DL	<DL	<DL
Scheelite	SL1223 c5-1	Salau	19.00	81.42	100.42	0.0069	0.003	0.0001	0.0009	<DL
Scheelite	SL1223 c5-2	Salau	19.03	81.70	100.73	0.0071	0.0029	<DL	<DL	<DL

Appendix 1.1B (continued).

Mineral	ID	Name	CaO	WO3	Total	Na (ppm)	Fe (ppm)	Y (ppm)	Mo (ppm)	Sr (ppm)
Scheelite	SL1223 c6-1	Salau	19.03	81.70	100.72	0.0069	0.0027	<DL	<DL	<DL
Scheelite	SL1223 c6-2	Salau	18.99	81.64	100.63	0.0034	0.0026	<DL	<DL	0.0056
Scheelite	SL1223 c6-3	Salau	19.05	81.29	100.34	0.0042	0.0008	<DL	0.0051	<DL
Scheelite	SL8A c1-1	Salau	18.69	81.06	99.74	0.0091	0.0015	<DL	0.0116	<DL
Scheelite	SL8A c1-2	Salau	18.73	81.14	99.86	0.0172	0.0089	<DL	0.0133	<DL
Scheelite	CA16B C1-1	Pine Creek	18.93	81.12	100.05	0.0059	0.0432	<DL	0.2	0.0007
Scheelite	CA16B C1-2	Pine Creek	19.09	81.23	100.32	0.007	0.0073	<DL	0.2135	0.0212
Scheelite	CA16B C1-3	Pine Creek	18.98	81.40	100.38	0.006	0.0171	<DL	0.2406	<DL
Scheelite	RG196 C1-1	Ray Gulch	19.28	79.99	99.26	0.0089	<DL	<DL	0.0608	0.0033
Scheelite	RG196 C1-2	Ray Gulch	19.15	80.29	99.45	0.016	0.0007	<DL	0.07	<DL
Scheelite	RG196 C1-3	Ray Gulch	19.15	80.37	99.51	0.0058	0.0205	<DL	0.0653	0.0201
Scheelite	RG196 C1-4	Ray Gulch	19.18	81.25	100.43	0.0125	0.0032	<DL	0.0637	0.0301
Scheelite	RG196 C1-5	Ray Gulch	19.12	80.53	99.65	0.0085	<DL	<DL	0.0665	0.0033
Scheelite	RG196 C2-1	Ray Gulch	19.20	80.14	99.34	0.0076	0.0078	<DL	0.0696	0.0294
Scheelite	RG196 C2-2	Ray Gulch	19.23	80.28	99.51	0.0104	0.0007	<DL	0.0658	0.0258
Scheelite	RG196 C2-3	Ray Gulch	19.12	80.56	99.68	0.0103	0.0037	<DL	0.1015	0.0081
Scheelite	RG196 C2-4	Ray Gulch	19.21	79.69	98.90	0.0089	0.0005	<DL	0.1188	0.0053
Scheelite	RG196 C2-5	Ray Gulch	19.19	80.81	100.00	0.0102	0.0204	<DL	0.0672	0.0295
Scheelite	DPHB c3 1	Lened	19.22	79.12	98.34	0.0041	0.0749	<DL	0.2857	<DL
Scheelite	DPHB c3 2	Lened	19.21	79.40	98.61	0.0051	0.0056	<DL	0.3479	<DL
Scheelite	DPHB c3 3	Lened	19.16	79.21	98.37	0.0079	0.0033	<DL	0.3886	<DL
Scheelite	DPHB c3 4	Lened	19.21	78.65	97.86	0.0015	0.0025	<DL	0.3814	<DL
Scheelite	DPHB c3 5	Lened	19.29	79.38	98.67	0.0015	0.0267	<DL	0.0091	<DL
Scheelite	LBT-C1 1	Lened	19.20	80.68	99.87	0.0065	0.0435	<DL	0.0052	<DL
Scheelite	LBT-C1 2	Lened	19.27	80.75	100.02	0.0078	0.0176	<DL	0.0046	<DL
Scheelite	LBT-C1 3	Lened	19.21	80.20	99.40	0.001	0.0101	<DL	0.0089	<DL
Scheelite	LBT-C1 4	Lened	19.23	80.49	99.72	0.0044	0.0092	<DL	0.0189	<DL
Scheelite	LBT-C1 5	Lened	19.24	80.18	99.43	0.0047	0.0322	<DL	0.0231	<DL
Scheelite	CEZ-GR C1b 1	Cantung	19.39	79.79	99.17	0.0051	<DL	<DL	0.127	<DL
Scheelite	CEZ-GR C1b 2	Cantung	19.50	78.72	98.22	0.0053	0.0032	<DL	0.8196	<DL
Scheelite	CEZ-GR C1b 3	Cantung	19.38	79.77	99.16	0.0037	0.0025	<DL	0.1495	<DL
Scheelite	CEZ-GR C1b 4	Cantung	19.51	79.53	99.04	0.0058	<DL	<DL	0.5257	<DL
Scheelite	CEZ-Bt2 C4 1	Cantung	19.10	80.14	99.24	0.0015	<DL	<DL	0.0554	<DL
Scheelite	CEZ-Bt2 C4 2	Cantung	19.09	80.90	99.98	0.0029	0.0034	<DL	0.0572	<DL
Scheelite	CEZ-Bt2 C4 3	Cantung	19.07	80.56	99.63	0.0056	0.0028	<DL	0.0339	<DL
Scheelite	CEZ-Bt2 C4 4	Cantung	19.03	80.65	99.68	0.0096	0.0257	<DL	0.0248	<DL

Appendix 1.1B (continued).

Mineral	ID	Name	CaO	WO3	Total	Na (ppm)	Fe (ppm)	Y (ppm)	Mo (ppm)	Sr (ppm)
Scheelite	CEZ-Bt2 C4 5	Cantung	18.92	80.68	99.60	0.0119	0.0133	0.014	0.0163	<DL
Scheelite	CEZ-Bt2 C4 6	Cantung	19.15	80.48	99.63	0.0025	0.0041	<DL	<DL	<DL
Scheelite	CEZ-Po2 C1 1	Cantung	19.19	80.80	100.00	0.0044	0.0256	0.0081	<DL	<DL
Scheelite	CEZ-Po2 C1 2	Cantung	19.16	80.77	99.93	0.0106	0.0333	0.0277	<DL	<DL
Scheelite	CEZ-Po2 C1 3	Cantung	19.23	80.60	99.83	0.0032	<DL	<DL	<DL	<DL
Scheelite	CEZ-Po2 C1 4	Cantung	19.25	80.85	100.10	0.0053	0.0115	<DL	<DL	<DL
Scheelite	CEZ-Po2 C2 5	Cantung	19.14	80.66	99.80	0.0071	0.0093	0.0055	<DL	<DL
Scheelite	CEZ-Po2 C2 7	Cantung	19.08	80.93	100.02	0.0044	0.0048	<DL	0.0106	<DL
Scheelite	MT09B-C2 3	Mactung	19.23	79.22	98.45	0.007	0.0002	<DL	0.093	<DL
Scheelite	MT09B-C1 1	Mactung	19.10	80.12	99.22	0.0057	0.0737	<DL	0.0211	<DL
Scheelite	MT09B-C1 2	Mactung	19.13	79.25	98.38	0.0107	<DL	<DL	0.0228	<DL
Scheelite	MT09B-C1 3	Mactung	19.11	79.68	98.79	0.0152	0.0006	<DL	0.0453	<DL
Scheelite	MT09B-C1 4	Mactung	19.17	79.10	98.27	0.0128	0.0052	<DL	0.0321	<DL
Scheelite	MT09B-C1 5	Mactung	19.16	78.86	98.02	0.0131	<DL	<DL	0.0351	<DL
Scheelite	MT231-C2 1	Mactung	19.22	79.93	99.15	0.0049	<DL	<DL	0.0122	<DL
Scheelite	MT231-C2 2	Mactung	19.10	79.26	98.36	0.0035	0.0018	<DL	0.0112	<DL
Scheelite	MT231-C2 3	Mactung	19.21	79.78	98.99	0.0041	0.001	<DL	0.0148	<DL
Scheelite	MT231-C2 4	Mactung	19.12	79.52	98.64	0.0054	0.0016	<DL	0.0348	<DL
Scheelite	MT231-C4 1	Mactung	19.03	79.51	98.54	0.0168	0.0004	0.0018	0.0077	<DL
Scheelite	M2B-2A C2 3	Mactung	19.11	80.55	99.65	0.0027	0.0035	<DL	0.1812	<DL
Scheelite	M2B-2A C2 4	Mactung	19.31	80.26	99.57	0.0046	0.0075	<DL	0.1667	<DL
Scheelite	M2B-2A C2c 1	Mactung	19.13	80.42	99.55	0.0024	0.0052	<DL	0.1111	<DL
Scheelite	M2B-2A C2c 2	Mactung	19.26	80.41	99.66	0.0025	<DL	<DL	0.1574	0.0009
Scheelite	M2B-2A C2c 3	Mactung	19.20	80.43	99.63	0.0062	0.0055	<DL	0.1615	<DL
Scheelite	M2B-2A C2c 4	Mactung	19.30	80.42	99.71	0.004	<DL	<DL	0.176	<DL
Scheelite	BF-1 1	Bonfim	19.10	81.08	100.18	0.012	0.003	<DL	0.064	<DL
Scheelite	BF-1 2	Bonfim	19.16	80.52	99.68	0.012	<DL	<DL	0.06	0.005
Scheelite	V75 c1-2	Vostok-2	19.15	81.02	100.18	0.0005	<DL	<DL	<DL	<DL
Scheelite	V75 c1-3	Vostok-2	19.07	81.07	100.14	0.0039	0.0107	0.0366	0.0074	<DL
Scheelite	V75 c1-4	Vostok-2	19.10	81.51	100.61	<DL	0.0117	<DL	<DL	<DL
Scheelite	V75 c2a-1	Vostok-2	19.09	80.61	99.70	0.0078	0.0143	0.0221	<DL	<DL
Scheelite	V75 c2a-2	Vostok-2	19.06	80.73	99.78	0.0022	0.0004	0.0573	<DL	<DL
Scheelite	V75 c2a-3	Vostok-2	19.06	80.86	99.92	<DL	<DL	<DL	0.0105	<DL
Scheelite	V75 c2a-4	Vostok-2	19.10	80.50	99.60	0.006	0.0055	<DL	0.0118	<DL
Scheelite	V75 c2a-5	Vostok-2	19.05	81.18	100.23	0.033	0.0004	0.0083	0.0155	<DL
Scheelite	V75 c2a-6	Vostok-2	19.19	80.81	100.00	0.0028	0.0031	<DL	0.0098	<DL

Appendix 1.1B (continued).

Mineral	ID	Name	CaO	WO3	Total	Na (ppm)	Fe (ppm)	Y (ppm)	Mo (ppm)	Sr (ppm)
Scheelite	V63 c2-2	Vostok-2	19.12	80.95	100.07	0.0039	<DL	0.0168	0.0109	<DL
Scheelite	V63 c2-4	Vostok-2	19.11	80.72	99.83	0.0057	0.0055	<DL	0.0168	<DL
Scheelite	L28 c1-1	Lermontovskoe	19.08	80.36	99.44	0.0069	0.0954	<DL	<DL	<DL
Scheelite	L28 c1-2	Lermontovskoe	19.06	80.27	99.33	0.0068	0.0114	<DL	<DL	<DL
Scheelite	L28 c1-3	Lermontovskoe	18.96	80.19	99.14	0.0048	0.0159	0.0334	<DL	0.0094
Scheelite	L28 c2-1	Lermontovskoe	19.06	79.91	98.97	0.0082	0.0056	0.0005	0.0039	<DL
Scheelite	L28 c3-2	Lermontovskoe	18.97	80.19	99.16	0.0048	0.006	0.0041	<DL	<DL
Scheelite	L811 c2-1	Lermontovskoe	19.05	80.51	99.56	0.0067	0.0037	<DL	<DL	<DL
Scheelite	L811 c2-2	Lermontovskoe	19.10	80.05	99.15	0.0032	0.0016	<DL	<DL	<DL
Scheelite	L811 c2-4	Lermontovskoe	19.05	80.02	99.07	0.0085	0.0077	<DL	0.0075	<DL
Scheelite	L811 c2-5	Lermontovskoe	19.04	80.99	100.02	0.0038	0.0322	0.0457	<DL	<DL
Scheelite	L811 c2-6	Lermontovskoe	18.98	80.34	99.32	0.0067	<DL	0.0081	<DL	<DL
Scheelite	L811 c1-4	Lermontovskoe	19.08	80.83	99.91	0.0075	0.0029	<DL	<DL	<DL
Scheelite	SD212 C2 1	Scheelite Dome	19.26	80.43	99.68	0.0056	0.0578	<DL	0.0286	<DL
Scheelite	SD212 C2 3	Scheelite Dome	19.24	79.93	99.17	0.0075	0.0064	<DL	0.1067	<DL
Scheelite	SD212 C2b 1	Scheelite Dome	19.12	79.86	98.97	0.0044	0.1804	<DL	0.1829	<DL
Scheelite	SD212 C2b 2	Scheelite Dome	19.09	79.99	99.08	0.0081	0.0151	<DL	0.1107	0.0114
Scheelite	SD212 C2b 3	Scheelite Dome	18.95	79.69	98.64	0.0055	0.0031	0.0014	0.104	<DL
Scheelite	SD212 C2b 4	Scheelite Dome	19.57	78.90	98.46	0.0054	0.0002	<DL	0.109	<DL
Scheelite	SD212 C2b 5	Scheelite Dome	19.08	80.18	99.26	0.0082	0.0172	<DL	0.126	<DL

Appendix 1.2B Detailed laser setting specifications.

Laser make, model and type	RESOlution M-50 Excimer
Laser wavelength	193 nm
Laser pulse duration	5 ns
Laser energy density	3 J cm-2
Laser repetition rate	15 Hz
Laser spot diameter	33 to 55 µm (spot); 19 to 25 µm (line)
Ablation cell	S-155 (Laurin Technic)
He carrier gas flow	350 ml/min
N2 additional gas	2 ml/min
Gas blank acquisition time	30 s
ICP-MS model and type	7900 Agilent quadrupole
Ar plasma gas flow	14 L/min
Ar auxiliary gas flow	0.0 L/min
Ar makeup gas flow	0.0 L/min
Injector	3.0 mm i.d., quartz
Torch depth/*z*-position	-0.4 mm
RF power	1550 W
Cone	Ni-Pt
m/z monitores (amu)	11, 23, 24, 39, 44, 49, 51, 55, 57, 59, 61, 63, 66, 75, 85, 88, 89, 93, 95, 137, 139, 140, 141, 146, 147, 153, 157, 159, 163, 165, 166, 169, 172, 175, 181, 182, 183, 208, 209, 232, 238.
Dwell time (ti)	5.00 ms
Quad. settling time (τ)	1.90 ms
Total sweep time (T_n)	400 ms

Appendix 1.3B Analyses of reference materials used to monitor the data quality.

Element	B11	Na23	Mg24	K39	Ti49	V51	Mn55	Co59	Ni60	As75	Sr88	Y89	Nb93
GSD-1 g Working value	50	26709	21709	25300	7431.7	44	220	40	58	27	69.4	42	42
Stdev	20	1483.8	241.2	300	359.6	2	20	2	4	8	0.7	2	3
Average GSD-1 g	71	27949	22485	26780	7123	43	228	42	61	37	69	39	37
Stdev (n= 25)	6	1120	2254	887	104	1	11	5	2	3	5	3	3
RSD* (%)	9%	4%	10%	3%	1%	3%	5%	13%	3%	9%	8%	8%	9%
GSE-1 g Working value	330	28934	21106	21800	450	440	590	380	440	260	447	410	420
Stdev	120	1484	181	200	42	20	20	20	30	90	5	30	40
Average GSE-1g	416	29774	21296	23984	416	422	642	392	467	340	443	398	384
Stdev (n= 25)	16	1060	1684	993	8	10	16	13	20	41	19	11	11
RSD (%)	4%	4%	8%	4%	2%	2%	2%	3%	4%	12%	4%	3%	3%
Gprobe6-A Working value	n.d	15506	51318	1577	7012	238	1255	46.9	145.7	n.d	166.6	19.33	4.16
Stdev	n.d	1335	6935	166	1319	27.1	93	3.51	18.9	n.d	26.1	1.78	0.41
Average Gprobe6-A		16431	53166	1815	6436	255	1324	50	163		163	17	3
Stdev (n= 25)		1175	5970	221	55	5	43	2	11		12	2	0.3
RSD (%)		7%	11%	12%	1%	2%	3%	4%	7%		7%	9%	8%
NIST-612 Working value	35	103858	77	66.3	44	39	38	35	38.8	37	78.4	38	40
Stdev	6	-	60	0.8	10	8	2	4	0.2	14	0.2	4	6
Average NIST-612	41	101657	62	68	39.8	37.6	40.4	35.9	39.4	32.7	75.0	35.5	32.7
Stdev (n= 25)	8	1471	2	8	1.3	1.0	2.2	1.6	1.3	1.2	6.3	3.3	3.1
RSD (%)	19%	1%	4%	12%	3%	3%	5%	5%	3%	4%	8%	9%	10%

Appendix 1.3B (continued)

Element	Mo95	Ba137	La139	Ce140	Pr141	Nd146	Sm147	Eu153	Gd157	Tb159	Dy163	Ho165	Er166
GSD-1 g Working value	39	67	39.1	41.4	45	44.7	47.8	41	50.7	47	51.2	49	40.1
Stdev	3	1	0.4	0.4	1	0.5	0.5	2	0.5	2	0.5	2	0.4
Average GSD-1 g	39	68	39	39	41	44	47	40	48	45	50	47	37
Stdev (n= 25)	3	3	4	4	4	1	1	3	1	4	1	4	1
RSD* (%)	8%	4%	9%	10%	10%	2%	2%	7%	2%	9%	2%	9%	3%
GSE-1 g Working value	390	427	392	414	460	453	488	410	514	480	524	501	595
Stdev	30	5	4	4	10	5	5	20	6	20	6	8	6
Average GSE-1g	393	423	405	411	450	452	491	413	511	501	521	515	571
Stdev (n= 25)	15	12	9	9	12	14	13	14	15	15	15	14	21
RSD (%)	4%	3%	2%	2%	3%	3%	3%	3%	3%	3%	3%	3%	4%
Gprobe6-A Working value	n.d	173	5.2	12	1.69	8.4	2.36	0.98	2.87	0.51	3.3	0.72	2.1
Stdev	n.d	25.62	0.56	0.7	0.12	0.98	0.31	0.13	0.46	0.06	0.46	0.09	0.34
Average Gprobe6-A		167	5	10.9	1.50	8.08	2.29	0.99	2.94	0.48	3.18	0.67	1.94
Stdev (n= 25)		3	0.5	1	0.15	0.38	0.11	0.11	0.13	0.05	0.11	0.08	0.09
RSD (%)		2%	10%	10%	10%	5%	5%	11%	4%	10%	4%	12%	5%
NIST-612 Working value	38	39.7	35.8	38.7	37.2	35.9	38.1	35	36.7	36	36	38	38
Stdev	4	0.8	0.8	0.8	1.8	0.8	0.8	2	0.8	6	0.8	2	1.8
Average NIST-612	37.1	38.2	34.9	35.2	33.7	35.9	38.1	35.2	38.4	35.2	35.5	35.4	35.6
Stdev (n= 25)	2.8	1.1	3.7	3.8	3.8	0.8	0.9	2.7	0.8	3.7	0.8	3.7	1.8
RSD (%)	8%	3%	11%	11%	11%	2%	2%	8%	2%	10%	2%	10%	5%

Appendix 1.3B (continued)

Element	Tm169	Yb172	Lu175	Ta181	Pb208	Bi209	Th232	U238
GSD-1 g Working value	49	50.9	51.5	40	50	35	41	41
Stdev	2	0.5	0.5	4	2	4	2	2
Average GSD-1 g	45	50	48	39	49	31	39	40
Stdev (n= 25)	4	1	4	3	3	3	5	4
RSD* (%)	9%	2%	8%	9%	7%	10%	13%	9%
GSE-1 g Working value	500	520	518	390	378	320	380	420
Stdev	20	5	6	40	12	30	20	30
Average GSE-1g	504	521	526	425	384	316	378	419
Stdev (n= 25)	14	16	16	14	17	16	11	13
RSD (%)	3%	3%	3%	3%	4%	5%	3%	3%
Gprobe6-A Working value	0.31	2.06	0.32	0.28	3.28	n.d.	0.33	0.29
Stdev	0.05	0.33	0.04	0.03	0.78	n.d.	0.04	0.06
Average Gprobe6-A	0.27	2.00	0.29	0.23	3.72		0.31	0.31
Stdev (n= 25)	0.03	0.08	0.03	0.04	0.28		0.07	0.04
RSD (%)	12%	4%	10%	18%	8%		22%	13%
NIST-612 Working value	38	39.2	36.9	40	38.57	30	37.79	37.38
Stdev	2	0.8	0.8	4	0.2	12	0.08	0.08
Average NIST-612	33.3	38.7	33.9	34.9	37.1	29.7	35.1	34.5
Stdev (n= 25)	3.6	0.8	3.4	3.9	1.9	3.1	3.5	3.5
RSD (%)	11%	2%	10%	11%	5%	10%	10%	10%

Appendix 1.4B Trace elements analyses of scheelite.

Source_file	Deposit_name	Skarn_type	B (ppm)	Na (ppm)	Mg (ppm)	K (ppm)	Ti (ppm)	V (ppm)	Mn (ppm)	Co (ppm)	Ni (ppm)
Min DL			0.134	0.261	0.008	0.485	0.067	0.003	0.143	0.003	0.034
Max DL			1.888	2.902	0.492	5.948	0.858	0.097	1.864	0.047	0.367
BF2-1.d	Bonfim	Reduced skarn	0.848	26.660	3.642	11.120	<DL	0.252	12.705	0.110	<DL
BF2-2.d	Bonfim	Reduced skarn	<DL	28.370	3.545	7.367	0.792	0.164	14.595	0.132	<DL
BF2-3.d	Bonfim	Reduced skarn	0.542	14.387	3.336	7.923	0.667	0.343	11.315	0.131	<DL
BF2-4.d	Bonfim	Reduced skarn	0.626	13.372	3.614	10.425	<DL	0.360	9.271	0.104	<DL
BF2-L1.d	Bonfim	Reduced skarn	0.556	32.804	4.476	15.012	<DL	0.199	15.457	0.129	0.209
BF2-L1.d	Bonfim	Reduced skarn	<DL	25.159	3.809	15.568	0.612	0.295	14.178	0.097	0.139
BF2-L2.d	Bonfim	Reduced skarn	<DL	28.745	3.670	16.402	0.431	0.168	13.844	0.115	<DL
BF2-L2.d	Bonfim	Reduced skarn	0.626	29.051	4.337	17.931	0.500	0.277	12.927	0.106	<DL
CN1-L1.d	Brejui	Oxidized skarn	1.070	10.981	25.187	<DL	1.960	0.368	15.596	0.227	<DL
CN1-L2.d	Brejui	Oxidized skarn	0.570	3.642	23.852	<DL	1.724	0.670	18.181	0.197	0.185
CN1-L2.d	Brejui	Oxidized skarn	0.639	3.767	23.755	<DL	1.932	0.655	17.820	0.232	0.253
CN1-L3.d	Brejui	Oxidized skarn	0.599	3.684	22.838	<DL	1.988	0.619	18.126	0.204	0.183
CN1-L4.d	Brejui	Oxidized skarn	0.959	4.337	23.477	<DL	1.710	0.173	14.345	0.193	0.188
CN1-L5.d	Brejui	Oxidized skarn	1.126	2.655	22.462	<DL	1.404	0.179	13.247	0.210	0.215
CN1-L6.d	Brejui	Oxidized skarn	0.792	9.035	17.584	<DL	1.640	0.252	19.293	0.182	0.227
CN1-L7.d	Brejui	Oxidized skarn	9.174	13.344	23.991	<DL	1.654	0.156	16.763	0.193	0.254
CN2-L1.d	Brejui	Oxidized skarn	0.667	1.390	14.734	<DL	1.348	0.092	4.865	0.195	0.203
CN2-L1.d	Brejui	Oxidized skarn	0.612	1.473	14.887	<DL	1.279	0.076	4.823	0.195	0.183
CN2-L2.d	Brejui	Oxidized skarn	0.723	0.973	13.803	<DL	1.460	0.075	4.518	0.193	0.570
CN2-L2.d	Brejui	Oxidized skarn	0.528	1.404	14.067	<DL	1.293	0.067	4.490	0.177	0.209
CN2-L3.d	Brejui	Oxidized skarn	0.598	4.712	14.859	<DL	1.237	0.066	5.036	0.182	0.206
CN2-L4.d	Brejui	Oxidized skarn	0.431	2.780	15.193	<DL	1.543	0.067	4.761	0.197	0.128
CN2-L5.d	Brejui	Oxidized skarn	0.495	8.618	13.914	6.950	1.098	0.071	4.954	0.172	0.215
CN2-L6.d	Brejui	Oxidized skarn	0.473	<DL	13.733	<DL	1.265	0.044	4.893	0.174	0.243
CN2-L6.d	Brejui	Oxidized skarn	0.570	0.765	13.664	<DL	1.418	0.054	4.823	0.152	0.164
CN2-L7.d	Brejui	Oxidized skarn	0.410	<DL	15.415	<DL	1.390	0.074	5.226	0.170	0.170

Appendix 1.4B (continued)

Source_file	Deposit_name	Skarn_type	B (ppm)	Na (ppm)	Mg (ppm)	K (ppm)	Ti (ppm)	V (ppm)	Mn (ppm)	Co (ppm)	Ni (ppm)
CEZ-1.d	Cantung (E Zone)	Reduced skarn	0.820	10.189	9.174	<DL	1.751	0.110	127.880	0.177	0.186
CEZ-1.d	Cantung (E Zone)	Reduced skarn	0.598	6.672	4.531	<DL	<DL	<DL	31.942	0.154	<DL
cez-bt2-0.d	Cantung (E Zone)	Reduced skarn	0.820	44.619	10.703	4.948	0.214	0.012	31.845	0.058	0.070
cez-bt2-c1.d	Cantung (E Zone)	Reduced skarn	1.154	12.371	10.425	3.475	<DL	<DL	25.868	0.050	0.107
cez-bt2-c1.d	Cantung (E Zone)	Reduced skarn	1.279	37.530	6.950	5.588	0.239	<DL	26.619	0.075	0.122
cez-bt2-c1b.d	Cantung (E Zone)	Reduced skarn	0.612	34.750	6.380	2.530	0.214	<DL	28.217	0.046	0.071
cez-bt2-c2.d	Cantung (E Zone)	Reduced skarn	1.126	51.986	4.712	5.171	0.215	0.015	35.515	0.059	0.079
cez-bt2-c3b.d	Cantung (E Zone)	Reduced skarn	0.820	29.746	5.852	5.435	0.438	<DL	16.305	0.079	0.076
cez-bt2-c3b.d	Cantung (E Zone)	Reduced skarn	1.126	44.897	50.040	5.421	0.189	0.017	34.889	0.067	0.075
cez-bt2-c4.d	Cantung (E Zone)	Reduced skarn	0.542	64.913	5.435	<DL	0.249	0.030	34.416	0.061	0.065
cez-bt2-c4.d	Cantung (E Zone)	Reduced skarn	0.514	37.113	3.920	1.849	0.238	0.016	29.593	0.054	0.140
cez-gr-c1.d	Cantung (E Zone)	Reduced skarn	0.945	9.730	7.020	2.572	1.237	0.022	24.242	0.079	0.131
cez-gr-c1b.d	Cantung (E Zone)	Reduced skarn	1.404	9.869	5.546	<DL	0.612	<DL	35.306	0.050	<DL
cez-gr-c1b.d	Cantung (E Zone)	Reduced skarn	1.251	10.717	3.809	<DL	1.084	0.036	18.001	0.068	0.100
cez-gr-c1b.d	Cantung (E Zone)	Reduced skarn	<DL	7.548	4.003	<DL	0.834	<DL	20.642	0.089	0.090
cez-gr-c1c.d	Cantung (E Zone)	Reduced skarn	0.723	7.047	6.116	4.448	1.362	0.115	47.260	0.054	0.092
cez-gr-c2.d	Cantung (E Zone)	Reduced skarn	7.784	25.020	4.893	8.757	2.321	0.088	34.194	0.039	0.100
cez-gr-c2a.d	Cantung (E Zone)	Reduced skarn	<DL	4.573	4.253	<DL	0.584	0.028	23.825	0.039	<DL
cez-gr-c2a.d	Cantung (E Zone)	Reduced skarn	<DL	5.518	4.573	<DL	0.626	<DL	23.352	0.054	<DL
cez-gr-c3.d	Cantung (E Zone)	Reduced skarn	1.418	6.672	5.560	<DL	0.751	0.022	21.003	0.070	0.060
cez-gr-c3.d	Cantung (E Zone)	Reduced skarn	1.501	9.174	7.367	4.865	1.168	0.035	20.572	0.095	0.792
cez-po1-c1b.d	Cantung (E Zone)	Reduced skarn	0.723	5.324	5.921	<DL	0.206	0.011	33.694	0.051	0.085
cez-po1-c1b.d	Cantung (E Zone)	Reduced skarn	0.681	2.530	4.865	1.682	0.172	<DL	36.501	0.056	0.053
cez-po1-c2.d	Cantung (E Zone)	Reduced skarn	0.778	28.495	8.465	7.784	0.154	0.040	38.503	0.049	0.070
cez-po1-c2.d	Cantung (E Zone)	Reduced skarn	1.515	13.205	11.815	6.255	0.222	0.032	41.978	0.039	0.068
cez-po1-c3.d	Cantung (E Zone)	Reduced skarn	0.862	4.281	33.221	3.892	0.278	0.025	36.557	0.053	<DL
cez-po1-c3.d	Cantung (E Zone)	Reduced skarn	3.336	20.850	17.514	22.240	0.238	0.017	35.306	0.054	0.115
cez-po1-c3a.d	Cantung (E Zone)	Reduced skarn	0.973	4.670	36.140	3.197	0.142	0.022	51.569	0.053	0.064
cez-po1-c3a.d	Cantung (E Zone)	Reduced skarn	0.890	2.724	4.323	2.989	0.234	<DL	12.927	0.043	0.067

Appendix 1.4B (continued)

Source_file	Deposit_name	Skarn_type	B (ppm)	Na (ppm)	Mg (ppm)	K (ppm)	Ti (ppm)	V (ppm)	Mn (ppm)	Co (ppm)	Ni (ppm)
cez-po1-c5.d	Cantung (E Zone)	Reduced skarn	0.834	7.339	11.815	3.058	<DL	<DL	34.166	0.075	0.101
cez-po1-c5.d	Cantung (E Zone)	Reduced skarn	2.085	6.436	5.699	4.587	0.197	<DL	37.113	0.042	0.096
cez-po1-c6.d	Cantung (E Zone)	Reduced skarn	1.209	19.043	27.105	11.676	0.152	0.095	43.229	0.064	0.138
cez-po1-c6.d	Cantung (E Zone)	Reduced skarn	2.196	14.595	27.522	11.732	0.143	<DL	246.030	0.074	0.186
cez-po1-c6.d	Cantung (E Zone)	Reduced skarn	0.834	10.981	4.712	10.425	0.131	<DL	22.518	0.039	0.115
cez-po1-c6b.d	Cantung (E Zone)	Reduced skarn	0.848	13.344	4.712	10.161	0.158	<DL	13.956	0.052	0.228
cez-po1-c6b.d	Cantung (E Zone)	Reduced skarn	1.195	18.765	7.784	10.981	0.612	0.022	21.267	0.054	0.238
cop-poA-c1-1.d	Cantung (Open Pit)	Reduced skarn	1.321	378.080	4.865	<DL	0.403	0.125	29.899	0.072	<DL
cop-poA-c1-3.d	Cantung (Open Pit)	Reduced skarn	5.143	724.190	21.545	27.800	6.158	0.801	137.610	0.065	<DL
cop-poA-c2-1.d	Cantung (Open Pit)	Reduced skarn	1.307	661.640	3.086	<DL	1.321	0.334	37.252	0.096	<DL
cop-poA-c3-1.d	Cantung (Open Pit)	Reduced skarn	1.390	641.207	4.323	3.308	1.251	0.403	37.030	0.068	<DL
cop-poA-c3-3.d	Cantung (Open Pit)	Reduced skarn	1.932	639.400	3.364	<DL	1.501	0.510	26.535	0.056	0.115
cop-poA-c4-1.d	Cantung (Open Pit)	Reduced skarn	1.557	701.950	4.017	3.670	1.307	0.302	41.005	0.086	0.138
cop-poA-c5-1.d	Cantung (Open Pit)	Reduced skarn	1.654	707.510	6.116	13.900	0.709	0.242	73.531	0.074	0.121
cop-poA-c5-2.d	Cantung (Open Pit)	Reduced skarn	1.182	542.100	3.419	4.448	0.904	0.240	44.202	0.076	<DL
cop-poB-c8-1.d	Cantung (Open Pit)	Reduced skarn	1.877	76.033	15.804	3.725	<DL	0.079	41.478	0.074	0.145
cop-poB-c5-1.d	Cantung (Open Pit)	Reduced skarn	2.127	194.600	5.087	3.197	0.626	0.039	44.758	0.049	0.140
cop-poB-c5-2.d	Cantung (Open Pit)	Reduced skarn	1.793	173.194	4.865	2.002	0.723	0.132	35.584	0.054	0.107
cop-poB-c7-1.d	Cantung (Open Pit)	Reduced skarn	2.683	166.800	70.890	6.811	1.015	0.150	40.588	0.081	<DL
cop-poB-c7-2.d	Cantung (Open Pit)	Reduced skarn	2.071	75.060	38.920	3.892	0.709	0.199	43.090	0.051	<DL
cop-poB-c3-1.d	Cantung (Open Pit)	Reduced skarn	1.446	110.088	5.268	2.488	0.500	0.085	39.087	0.053	<DL
cop-poB-c3-2.d	Cantung (Open Pit)	Reduced skarn	0.917	103.277	4.740	<DL	<DL	0.265	39.212	0.051	0.153
cop-poB-c3-3.d	Cantung (Open Pit)	Reduced skarn	1.404	50.318	59.770	<DL	0.431	0.152	37.669	0.067	0.070
cop-sc-c3-1.d	Cantung (Open Pit)	Reduced skarn	1.056	19.029	3.016	<DL	0.348	0.025	52.125	0.044	<DL
cop-sc-c1a-1.d	Cantung (Open Pit)	Reduced skarn	1.460	49.484	7.826	<DL	0.431	0.065	13.010	0.065	<DL
cop-sc2-c2.d	Cantung (Open Pit)	Reduced skarn	1.487	15.846	6.060	<DL	0.653	0.057	17.361	0.085	<DL
cop-sc2-c4.d	Cantung (Open Pit)	Reduced skarn	3.239	74.782	8.048	18.348	0.917	0.045	43.229	0.062	0.181
cop-sc2-c2-2.d	Cantung (Open Pit)	Reduced skarn	1.877	44.202	75.060	59.770	169.580	0.806	26.966	0.074	<DL
cop-poB-c5b.d	Cantung (Open Pit)	Reduced skarn	2.697	157.070	18.209	319.700	4.170	0.238	41.422	0.077	0.556

Appendix 1.4B (continued)

Source_file	Deposit_name	Skarn_type	B (ppm)	Na (ppm)	Mg (ppm)	K (ppm)	Ti (ppm)	V (ppm)	Mn (ppm)	Co (ppm)	Ni (ppm)
cop-qz-c4.d	Cantung (Open Pit)	Reduced skarn	0.945	72.141	4.782	3.823	0.556	0.189	32.095	0.061	0.079
cop-qz-c4b.d	Cantung (Open Pit)	Reduced skarn	1.501	119.123	12.788	10.286	0.862	0.126	29.204	0.060	0.079
cop-po-sq1.d	Cantung (Open Pit)	Reduced skarn	0.945	97.995	33.360	55.600	2.502	0.284	25.479	0.065	0.192
cop-po-sq2.d	Cantung (Open Pit)	Reduced skarn	1.098	146.645	3.375	5.588	0.271	0.168	43.535	0.047	0.086
cop-sc-sq3.d	Cantung (Open Pit)	Reduced skarn	1.432	50.596	4.351	1.251	0.145	0.183	29.510	0.044	0.060
2420-776A-2.d	Jiama	Oxidized skarn	1.960	56.851	4.170	8.340	15.846	15.499	4.893	0.228	4.587
2420-776A-3.d	Jiama	Oxidized skarn	1.890	39.615	3.781	7.923	12.232	4.434	6.144	0.234	0.709
2420-776A-4.d	Jiama	Oxidized skarn	1.821	27.647	3.739	9.035	18.765	4.823	4.782	0.229	0.172
2420-776A-5.d	Jiama	Oxidized skarn	1.932	44.480	4.518	4.726	18.167	7.172	4.309	0.375	0.249
2420-776B-1.d	Jiama	Oxidized skarn	2.419	68.944	3.767	7.089	14.526	5.032	4.462	9.730	3.753
2420-776B-2.d	Jiama	Oxidized skarn	2.836	51.430	4.114	26.410	18.070	7.742	4.379	0.261	0.211
2420-776B-3.d	Jiama	Oxidized skarn	2.433	49.484	116.760	6.255	18.209	5.115	15.290	0.528	0.445
2420-776B-4.d	Jiama	Oxidized skarn	2.335	27.939	6.116	10.842	16.152	5.991	11.120	0.229	0.221
2420-776B-5.d	Jiama	Oxidized skarn	2.280	46.092	3.670	6.255	14.359	9.730	4.101	0.361	1.668
2420-848C-1.d	Jiama	Oxidized skarn	5.226	30.052	52.403	22.935	2.168	0.737	100.080	0.466	1.001
2420-848C-2.d	Jiama	Oxidized skarn	5.699	42.673	134.830	29.051	2.099	0.250	125.517	0.240	70.890
2420-848C-3.d	Jiama	Oxidized skarn	4.948	72.280	19.182	26.410	2.071	0.124	78.396	0.229	0.185
2420-848C-4.d	Jiama	Oxidized skarn	6.950	85.763	28.495	18.209	1.585	0.096	92.713	0.245	0.375
JIAMA-1.d	Jiama	Oxidized skarn	23.366	9.216	6.283	2.085	7.506	1.251	43.924	0.199	23.630
JIAMA-3.d	Jiama	Oxidized skarn	24.742	10.786	48.650	3.892	5.213	3.336	80.064	0.448	0.249
JIAMA-4.d	Jiama	Oxidized skarn	24.019	9.466	13.997	7.784	3.892	1.257	80.898	0.203	0.751
JIAMA-5.d	Jiama	Oxidized skarn	22.796	8.840	8.813	6.950	1.821	0.575	48.094	0.179	0.238
JIAMA-6.d	Jiama	Oxidized skarn	23.463	27.800	12.788	5.977	5.171	0.667	78.674	0.417	0.217
KR65-1.d	Kara	Oxidized skarn	2.968	6.874	6.464	1.599	4.643	0.206	8.069	0.262	0.209
KR65-2.d	Kara	Oxidized skarn	2.711	4.295	9.730	3.197	5.240	0.227	8.618	0.220	0.270
KR65-3.d	Kara	Oxidized skarn	3.225	9.452	3.197	<DL	4.045	0.186	7.520	0.304	0.149
KR65-4.d	Kara	Oxidized skarn	4.295	16.680	9.174	36.140	6.311	0.204	7.339	0.278	0.275
KR65-5.d	Kara	Oxidized skarn	3.670	7.923	12.510	2.363	4.698	0.481	9.118	0.234	0.256
KR65-6.d	Kara	Oxidized skarn	3.982	12.302	10.842	19.252	5.504	0.343	8.229	0.256	0.265

Appendix 1.4B (continued)

Source_file	Deposit_name	Skarn_type	B (ppm)	Na (ppm)	Mg (ppm)	K (ppm)	Ti (ppm)	V (ppm)	Mn (ppm)	Co (ppm)	Ni (ppm)
KR66-0.d	Kara	Oxidized skarn	0.556	27.522	4.114	16.124	1.626	1.147	16.444	0.114	<DL
KR66-C1-1a.d	Kara	Oxidized skarn	0.653	31.275	5.435	26.688	2.280	0.890	13.358	0.291	<DL
KR66-C1-2a.d	Kara	Oxidized skarn	7.923	30.163	4.726	36.279	1.918	0.986	11.843	0.359	<DL
KR66-C3-1a.d	Kara	Oxidized skarn	0.570	33.499	4.476	21.823	2.210	1.390	15.790	0.100	<DL
KR66-C3-1a.d	Kara	Oxidized skarn	0.542	29.885	4.198	17.514	1.918	0.981	15.304	0.121	<DL
KR66-C3-2a.d	Kara	Oxidized skarn	<DL	31.831	4.406	24.186	1.612	1.808	17.041	0.118	<DL
KR66-C3-2a.d	Kara	Oxidized skarn	<DL	33.777	5.101	33.777	2.488	1.355	18.265	0.115	0.222
KR66-C3-2b.d	Kara	Oxidized skarn	0.598	30.858	4.128	19.043	1.835	1.441	16.569	0.104	0.195
KR66-C3-2b.d	Kara	Oxidized skarn	0.834	31.136	4.295	19.043	1.863	1.444	16.569	0.118	0.161
KR98A-C1-1.d	Kara	Oxidized skarn	8.340	29.190	79.230	16.958	4.170	0.033	33.360	3.614	33.360
KR98A-C1-2.d	Kara	Oxidized skarn	6.130	33.638	88.265	26.410	1.654	0.050	25.854	0.243	55.600
KR98A-C2-1.d	Kara	Oxidized skarn	6.074	16.013	28.217	16.263	1.571	0.043	16.680	0.200	9.730
KR98B-C2-1.d	Kara	Oxidized skarn	5.546	6.491	33.694	40.310	1.487	<DL	7.673	0.207	4.031
KR98C-1-1.d	Kara	Oxidized skarn	8.451	34.611	126.490	94.520	41.422	0.320	17.792	0.737	0.152
KR98C-1-2.d	Kara	Oxidized skarn	7.200	130.660	31.720	30.997	2.141	0.067	18.765	0.193	0.500
KR98C-2-1.d	Kara	Oxidized skarn	7.089	71.863	48.372	13.900	2.196	<DL	13.539	0.306	0.240
DMGr-0a.d	King Island	Oxidized skarn	0.445	17.667	4.490	7.937	1.988	1.266	16.708	0.133	0.200
DMGr-0b.d	King Island	Oxidized skarn	0.598	21.420	3.906	11.815	2.558	0.869	14.484	0.152	0.142
DMGr-0c.d	King Island	Oxidized skarn	0.751	15.304	6.672	12.232	2.238	0.876	14.400	0.143	<DL
DMGr-C1b.d	King Island	Oxidized skarn	<DL	16.958	4.309	12.705	2.613	1.165	14.498	0.165	<DL
DMGr-C1c.d	King Island	Oxidized skarn	0.639	22.504	4.253	12.246	2.474	1.496	14.817	0.177	0.170
DMGr-c1e.d	King Island	Oxidized skarn	<DL	15.207	4.629	11.871	2.488	1.237	12.246	0.147	0.210
DMGr-C2.d	King Island	Oxidized skarn	0.598	18.807	4.643	10.161	2.794	1.422	13.275	0.239	0.224
DMGr-c3a.d	King Island	Oxidized skarn	0.500	15.026	8.479	13.483	2.836	1.657	17.292	0.171	0.125
DM-PX-10.d	King Island	Oxidized skarn	15.707	17.709	2.544	5.699	2.947	3.531	18.487	0.189	0.178
DM-PX-3.d	King Island	Oxidized skarn	17.931	6.338	7.228	6.950	2.683	1.208	18.765	0.431	0.389
DM-PX-4.d	King Island	Oxidized skarn	16.611	12.524	5.699	5.282	2.655	1.611	15.846	1.390	0.264
DM-PX-5.d	King Island	Oxidized skarn	19.182	19.085	23.630	6.811	2.544	1.918	15.971	0.179	<DL
DM-PX-6.d	King Island	Oxidized skarn	14.373	23.213	2.585	5.699	4.448	1.733	17.472	0.188	<DL

Appendix 1.4B (continued)

Source_file	Deposit_name	Skarn_type	B (ppm)	Na (ppm)	Mg (ppm)	K (ppm)	Ti (ppm)	V (ppm)	Mn (ppm)	Co (ppm)	Ni (ppm)
DM-PX-7.d	King Island	Oxidized skarn	16.458	43.090	2.933	7.923	1.932	1.904	19.043	0.873	0.288
DM-PX-8.d	King Island	Oxidized skarn	17.097	21.253	3.155	6.338	2.085	2.641	19.460	0.190	0.239
DM-PX-9.d	King Island	Oxidized skarn	16.096	14.873	2.877	5.282	2.613	1.642	14.873	0.420	0.389
Ku01-L1.d	Kumbel	Oxidized skarn	1.084	12.232	3.878	14.706	1.793	<DL	1.376	0.154	0.188
Ku01-L2.d	Kumbel	Oxidized skarn	1.015	10.091	4.045	15.526	1.501	<DL	1.289	0.158	0.232
Ku01-L3.d	Kumbel	Oxidized skarn	1.084	8.576	3.711	14.595	1.154	<DL	1.390	0.156	0.306
Ku01-L3.d	Kumbel	Oxidized skarn	1.209	10.175	3.447	16.124	1.307	<DL	1.293	0.163	0.228
Ku01-L4.d	Kumbel	Oxidized skarn	0.987	11.454	3.504	17.097	1.446	<DL	1.307	0.154	0.147
Ku01-L5.d	Kumbel	Oxidized skarn	0.806	14.039	3.489	16.680	1.585	<DL	1.515	0.145	<DL
Ku01-L5.d	Kumbel	Oxidized skarn	1.209	10.147	3.531	14.873	1.251	<DL	1.487	0.153	<DL
Ku01-L6.d	Kumbel	Oxidized skarn	1.112	15.568	3.711	15.985	1.043	<DL	1.348	0.157	0.304
Ku01-L6.d	Kumbel	Oxidized skarn	0.570	12.510	3.670	13.344	1.501	<DL	1.223	0.170	0.264
DPHB-C1.d	Lened	Reduced skarn	<DL	5.421	4.142	<DL	1.237	<DL	51.430	0.047	<DL
DPHB-C1a.d	Lened	Reduced skarn	1.321	25.993	2.585	<DL	<DL	<DL	11.690	0.058	<DL
DPHB-C2.d	Lened	Reduced skarn	<DL	16.402	2.836	<DL	1.084	0.117	7.854	0.051	<DL
DPHB-C2a.d	Lened	Reduced skarn	1.779	9.174	3.197	<DL	14.595	0.075	60.187	0.042	<DL
DPHB-C2b.d	Lened	Reduced skarn	1.821	18.348	2.850	<DL	<DL	<DL	15.846	0.057	<DL
DPHB-C2c.d	Lened	Reduced skarn	0.959	<DL	2.961	<DL	<DL	<DL	9.800	0.033	<DL
DPHB-C3.d	Lened	Reduced skarn	1.460	9.341	2.433	<DL	0.681	<DL	9.271	0.039	<DL
DPHB-C3a.d	Lened	Reduced skarn	1.529	15.429	2.349	<DL	0.751	0.079	11.718	0.075	<DL
DPHB-C3b.d	Lened	Reduced skarn	1.182	11.857	2.711	<DL	0.778	<DL	13.483	0.044	<DL
DPHB-C3c.d	Lened	Reduced skarn	3.753	8.479	2.877	5.282	0.639	<DL	9.327	0.029	0.104
LBt-C1.d	Lened	Reduced skarn	0.709	17.375	14.595	10.703	<DL	<DL	17.375	0.044	<DL
LBt-C1a.d	Lened	Reduced skarn	<DL	6.019	3.767	8.062	<DL	<DL	16.277	0.025	<DL
LBt-C2.d	Lened	Reduced skarn	0.848	6.186	3.739	7.923	0.709	<DL	15.540	0.043	0.231
LBt-C3.d	Lened	Reduced skarn	<DL	10.286	6.811	<DL	<DL	0.021	14.539	0.034	0.178
LBt-C4.d	Lened	Reduced skarn	<DL	4.754	5.226	4.726	<DL	0.029	15.777	0.052	<DL
LBt-C4a.d	Lened	Reduced skarn	1.168	4.865	4.128	<DL	<DL	<DL	14.887	0.049	<DL
LBt-C5.d	Lened	Reduced skarn	<DL	9.980	5.199	<DL	<DL	0.070	20.628	0.042	0.113

Appendix 1.4B (continued)

Source_file	Deposit_name	Skarn_type	B (ppm)	Na (ppm)	Mg (ppm)	K (ppm)	Ti (ppm)	V (ppm)	Mn (ppm)	Co (ppm)	Ni (ppm)
LBt-C5a.d	Lened	Reduced skarn	1.446	2.516	4.142	<DL	<DL	<DL	18.070	0.042	<DL
LBt-C5b.d	Lened	Reduced skarn	<DL	3.809	4.809	<DL	<DL	<DL	19.613	0.067	<DL
LCSA-C1.d	Lened	Reduced skarn	<DL	17.028	36.140	13.900	0.792	0.042	30.441	0.028	<DL
LCSA-C1a.d	Lened	Reduced skarn	3.475	15.012	13.344	4.726	0.876	0.088	27.105	0.032	<DL
LCSA-C1a.d	Lened	Reduced skarn	1.404	17.792	119.540	11.120	0.528	0.079	37.530	0.040	<DL
LCSA-C1a.d	Lened	Reduced skarn	0.973	10.912	17.236	<DL	0.500	0.043	27.091	0.046	<DL
LCSA-C2a.d	Lened	Reduced skarn	1.182	11.607	19.460	<DL	<DL	0.093	43.924	0.068	<DL
LCSA-C2c.d	Lened	Reduced skarn	1.126	9.313	19.460	<DL	0.820	0.096	41.005	0.035	<DL
LCSB-C1.d	Lened	Reduced skarn	1.946	20.433	7.367	<DL	<DL	0.075	21.962	0.047	<DL
LCSB-C1.d	Lened	Reduced skarn	<DL	11.120	15.012	<DL	0.556	0.232	61.160	0.070	0.181
LCSB-C1a.d	Lened	Reduced skarn	<DL	11.398	7.867	5.421	1.015	0.079	25.590	0.065	0.210
LCSB-C4.d	Lened	Reduced skarn	1.251	18.001	10.564	6.672	0.500	0.061	21.823	0.035	0.185
LCSB-C5.d	Lened	Reduced skarn	0.862	23.561	6.672	10.564	0.639	0.043	18.696	0.033	0.192
LCSB-C5.d	Lened	Reduced skarn	<DL	17.028	3.378	8.618	0.431	<DL	17.959	0.026	0.122
LOP2A-C1.d	Lened	Reduced skarn	<DL	6.436	2.877	<DL	4.865	0.626	164.020	0.057	<DL
LOP2A-C2.d	Lened	Reduced skarn	1.154	6.797	3.767	<DL	<DL	<DL	16.027	0.056	<DL
LOP2A-C2a.d	Lened	Reduced skarn	1.682	7.701	3.280	<DL	<DL	<DL	14.289	0.068	<DL
LOP2A-C2b.d	Lened	Reduced skarn	0.959	11.217	3.350	<DL	0.806	0.067	16.597	0.049	<DL
LOP2A-C2c.d	Lened	Reduced skarn	3.058	4.170	2.947	<DL	0.917	0.043	28.634	0.042	<DL
LOP2A-C3.d	Lened	Reduced skarn	1.974	8.924	4.420	<DL	<DL	0.053	27.077	0.053	<DL
LOP2A-C3a.d	Lened	Reduced skarn	1.585	7.770	3.823	<DL	1.182	0.174	37.530	0.042	<DL
LOP2A-C3b.d	Lened	Reduced skarn	<DL	5.727	2.905	<DL	<DL	<DL	23.936	0.036	<DL
LOP2A-C3c.d	Lened	Reduced skarn	1.195	3.948	3.795	<DL	9.869	0.574	184.870	0.040	<DL
LOP2B-C1.d	Lened	Reduced skarn	0.723	12.788	7.228	11.676	0.751	0.056	13.483	0.056	<DL
LOP2B-C2.d	Lened	Reduced skarn	0.959	21.406	5.074	13.900	<DL	0.050	14.303	0.039	<DL
LOP2B-C2a.d	Lened	Reduced skarn	1.682	11.134	4.337	5.004	0.639	0.032	21.267	0.186	0.278
LOP2B-C2a.d	Lened	Reduced skarn	<DL	20.016	6.672	7.923	0.904	0.044	15.248	0.039	<DL
LOP2B-C2b.d	Lened	Reduced skarn	0.834	19.599	4.406	4.587	0.334	0.029	16.374	0.046	<DL
L14-C1.d	Lermontovskoe	Reduced skarn	0.695	7.145	4.490	3.002	0.473	<DL	11.315	0.192	0.192

Appendix 1.4B (continued)

Source_file	Deposit_name	Skarn_type	B (ppm)	Na (ppm)	Mg (ppm)	K (ppm)	Ti (ppm)	V (ppm)	Mn (ppm)	Co (ppm)	Ni (ppm)
L14-C1.d	Lermontovskoe	Reduced skarn	0.598	9.035	4.156	1.849	<DL	<DL	15.499	0.178	0.225
L14-C2A.d	Lermontovskoe	Reduced skarn	0.528	13.775	3.767	1.446	0.667	0.026	12.010	0.195	0.202
L14-C2B.d	Lermontovskoe	Reduced skarn	0.612	12.024	3.735	1.223	0.542	0.024	17.319	0.202	0.142
L18-C2A.d	Lermontovskoe	Reduced skarn	0.514	25.298	13.066	2.002	0.945	0.027	26.271	0.177	0.235
L18-C2c.d	Lermontovskoe	Reduced skarn	0.862	16.819	34.750	4.073	0.528	0.033	13.010	0.204	0.140
L18-C3.d	Lermontovskoe	Reduced skarn	0.485	12.788	8.062	1.251	0.712	0.057	15.054	0.177	0.257
L18-C4A.d	Lermontovskoe	Reduced skarn	0.737	26.688	17.931	2.016	0.639	0.035	26.688	0.178	0.147
L18-L1.d	Lermontovskoe	Reduced skarn	0.765	36.835	51.430	4.865	1.209	0.108	13.511	0.196	0.183
L18-L2.d	Lermontovskoe	Reduced skarn	0.445	12.927	58.380	2.113	0.890	0.051	13.344	0.172	0.257
L28-.d	Lermontovskoe	Reduced skarn	0.530	21.990	3.293	<DL	0.863	0.054	14.609	0.185	0.238
L28-C1A-.d	Lermontovskoe	Reduced skarn	0.528	8.743	3.809	<DL	0.904	<DL	15.485	0.186	0.225
L28-C1A-1.d	Lermontovskoe	Reduced skarn	0.904	13.344	3.953	<DL	0.890	0.031	9.341	0.190	0.247
L28-C3A.d	Lermontovskoe	Reduced skarn	0.773	13.761	3.406	<DL	0.987	<DL	26.827	0.214	0.249
L28-C3B.d	Lermontovskoe	Reduced skarn	0.973	5.741	3.472	<DL	1.001	<DL	16.972	0.213	0.232
L28-.d	Lermontovskoe	Reduced skarn	3.753	23.630	7.089	3.058	1.195	0.053	12.135	0.227	0.157
L30-L1.d	Lermontovskoe	Reduced skarn	0.542	21.684	5.087	1.404	2.780	0.092	51.291	0.164	0.295
L30-L2.d	Lermontovskoe	Reduced skarn	0.528	18.765	55.600	20.850	0.945	0.121	38.503	0.285	1.251
L43-C1A.d	Lermontovskoe	Reduced skarn	0.500	9.341	4.615	4.226	0.695	<DL	15.818	0.193	0.329
L43-C1B.d	Lermontovskoe	Reduced skarn	0.487	10.703	21.406	5.393	0.542	0.195	9.313	0.183	0.289
L43-C1c.d	Lermontovskoe	Reduced skarn	1.112	11.398	4.782	3.684	0.667	<DL	13.622	0.186	0.232
L811-C2A-.d	Lermontovskoe	Reduced skarn	0.820	39.337	38.920	1.849	0.834	0.023	29.329	0.196	0.236
L811-C2A-.d	Lermontovskoe	Reduced skarn	0.778	11.996	4.518	1.390	0.667	0.022	10.481	0.197	0.238
L811-C2B-.d	Lermontovskoe	Reduced skarn	0.820	15.151	65.330	34.750	5.143	0.106	38.642	0.204	0.209
L811-C2B-.d	Lermontovskoe	Reduced skarn	0.820	54.905	5.560	1.626	0.737	<DL	46.885	0.188	0.172
L811-.d	Lermontovskoe	Reduced skarn	0.751	19.321	3.697	3.044	0.584	<DL	13.427	0.185	0.353
m2a1-c1.d	Mactung	Reduced skarn	<DL	10.133	3.239	4.726	0.417	<DL	8.159	0.044	<DL
m2a1-c1a.d	Mactung	Reduced skarn	<DL	7.673	3.392	7.784	0.514	<DL	8.215	0.033	<DL
m2a1-c3.d	Mactung	Reduced skarn	<DL	8.896	3.447	<DL	0.445	<DL	9.619	0.049	<DL

Appendix 1.4B (continued)

Source_file	Deposit_name	Skarn_type	B (ppm)	Na (ppm)	Mg (ppm)	K (ppm)	Ti (ppm)	V (ppm)	Mn (ppm)	Co (ppm)	Ni (ppm)
m2b-2a-c1.d	Mactung	Reduced skarn	1.043	10.369	5.282	5.699	0.292	<DL	134.830	0.061	<DL
m2b-2a-c1b.d	Mactung	Reduced skarn	<DL	10.439	3.684	7.645	0.361	<DL	7.311	0.042	<DL
m2b-2a-c1c.d	Mactung	Reduced skarn	0.806	10.161	4.323	<DL	0.348	<DL	10.495	0.038	<DL
m2b-2a-c3.d	Mactung	Reduced skarn	<DL	7.409	4.712	4.170	0.375	2.780	9.841	0.037	<DL
m2b-2a-c3a.d	Mactung	Reduced skarn	0.792	7.200	3.809	<DL	0.653	<DL	9.786	0.023	0.067
m3d2-c1.d	Mactung	Reduced skarn	<DL	5.449	6.936	7.089	<DL	<DL	15.860	0.026	<DL
m3d2-c2.d	Mactung	Reduced skarn	<DL	8.187	8.451	6.255	<DL	<DL	19.140	0.038	<DL
m3d2-c3.d	Mactung	Reduced skarn	0.959	7.826	8.326	3.892	<DL	<DL	20.572	0.047	<DL
m3d-qz-c3.d	Mactung	Reduced skarn	1.807	7.645	13.650	8.896	0.375	0.028	148.452	0.033	<DL
m3d-qz-c3a.d	Mactung	Reduced skarn	0.723	3.169	14.373	6.672	0.320	<DL	123.571	0.042	<DL
mt09b-0.d	Mactung	Reduced skarn	1.279	32.526	41.700	5.977	0.306	0.135	22.379	0.047	0.133
mt09b-0.d	Mactung	Reduced skarn	<DL	37.252	4.059	<DL	<DL	0.139	13.136	0.044	<DL
mt09b-0a.d	Mactung	Reduced skarn	<DL	24.673	5.060	3.892	0.281	0.086	16.207	0.039	0.093
mt09b-c1.d	Mactung	Reduced skarn	<DL	39.615	4.420	2.780	0.306	0.117	13.233	0.040	<DL
mt09b-c4.d	Mactung	Reduced skarn	<DL	25.854	4.087	<DL	0.320	0.133	14.790	0.067	<DL
mt09b-c4.d	Mactung	Reduced skarn	<DL	21.434	3.850	3.892	<DL	0.114	15.429	0.024	<DL
mt09b-c4a.d	Mactung	Reduced skarn	<DL	14.456	5.032	5.004	0.375	0.125	15.665	0.050	<DL
mt09b-c4a.d	Mactung	Reduced skarn	1.029	22.796	3.934	7.784	<DL	0.140	19.460	0.043	<DL
MT161-0.d	Mactung	Reduced skarn	0.765	11.537	5.074	8.757	0.431	0.096	17.278	0.051	0.145
MT161-0.d	Mactung	Reduced skarn	0.959	22.657	31.275	35.028	1.487	0.778	24.881	0.049	0.126
MT161-0a.d	Mactung	Reduced skarn	<DL	11.579	5.324	6.394	0.236	0.070	18.626	0.040	<DL
MT161-0a.d	Mactung	Reduced skarn	<DL	16.680	3.753	10.286	0.250	0.128	21.170	0.049	<DL
MT161-0b.d	Mactung	Reduced skarn	<DL	11.815	3.545	<DL	<DL	0.096	24.978	0.031	0.136
MT161-0b.d	Mactung	Reduced skarn	0.723	5.046	3.823	<DL	<DL	0.079	28.509	0.049	0.100
MT161-c2.d	Mactung	Reduced skarn	1.668	31.275	44.480	136.220	3.753	0.103	33.638	0.063	0.500
MT161-c2.d	Mactung	Reduced skarn	1.056	20.016	26.271	33.082	1.877	0.158	41.978	0.092	0.306
MT161-c6.d	Mactung	Reduced skarn	0.959	24.158	6.811	7.228	<DL	0.093	15.221	0.043	<DL
MT161-c6a.d	Mactung	Reduced skarn	0.778	19.738	5.171	2.641	0.348	0.143	12.635	0.054	<DL

Appendix 1.4B (continued)

Source_file	Deposit_name	Skarn_type	B (ppm)	Na (ppm)	Mg (ppm)	K (ppm)	Ti (ppm)	V (ppm)	Mn (ppm)	Co (ppm)	Ni (ppm)
MT161-c6b.d	Mactung	Reduced skarn	0.765	14.317	8.618	<DL	0.306	0.060	37.530	0.029	0.104
MT161-c6b.d	Mactung	Reduced skarn	<DL	7.728	4.156	4.726	<DL	0.133	28.161	0.038	0.099
MT231-0.d	Mactung	Reduced skarn	0.765	64.357	7.645	11.398	0.431	0.224	15.262	0.039	0.106
MT231-c1.d	Mactung	Reduced skarn	<DL	28.217	13.066	3.336	0.403	0.250	10.078	0.043	0.111
MT231-c1a.d	Mactung	Reduced skarn	0.598	46.426	5.630	5.143	0.348	0.157	10.189	0.046	0.075
MT231-c1b.d	Mactung	Reduced skarn	<DL	25.993	9.869	8.618	0.473	0.124	11.551	0.050	0.206
MT231-c2.d	Mactung	Reduced skarn	<DL	3.823	6.811	3.058	0.389	0.044	16.305	0.054	<DL
MT231-c2.d	Mactung	Reduced skarn	<DL	4.448	4.782	3.058	<DL	0.028	18.056	0.033	<DL
MT231-c2a.d	Mactung	Reduced skarn	0.653	11.148	11.815	4.865	<DL	0.067	25.284	0.043	<DL
MT231-c4.d	Mactung	Reduced skarn	1.390	29.190	5.741	7.923	<DL	0.154	12.149	0.042	<DL
MT231-c4.d	Mactung	Reduced skarn	1.904	8.535	7.020	10.981	0.181	0.092	12.302	0.051	0.161
MT231-c4a.d	Mactung	Reduced skarn	0.681	38.781	11.815	12.093	0.361	0.120	11.509	0.035	0.153
MT231-c5.d	Mactung	Reduced skarn	<DL	11.398	8.284	12.649	0.709	0.135	13.747	0.053	0.236
MT231-c5a.d	Mactung	Reduced skarn	<DL	5.421	4.935	4.031	<DL	0.051	13.108	0.036	0.108
MT-Po1-1.d	Mactung	Reduced skarn	2.697	3.711	19.043	<DL	0.848	<DL	46.245	25.020	9.730
MT-Po1-2.d	Mactung	Reduced skarn	2.335	3.642	11.843	<DL	1.321	0.033	86.875	0.225	0.150
MT-Po1-3.d	Mactung	Reduced skarn	2.419	2.335	14.234	8.062	0.973	<DL	79.925	0.202	0.204
MT-Po1-5.d	Mactung	Reduced skarn	2.196	4.587	15.888	15.151	1.321	<DL	54.141	0.681	0.186
MT-Po1-6.d	Mactung	Reduced skarn	3.044	1.710	14.414	28.495	1.251	<DL	57.129	3.058	0.253
MARN-C1a.d	Marn	Reduced skarn	0.695	7.325	3.684	8.340	0.848	<DL	2.975	0.156	0.181
MARN-C1b.d	Marn	Reduced skarn	1.626	18.070	3.656	17.653	0.848	<DL	4.531	0.106	<DL
MARN-C1c.d	Marn	Reduced skarn	0.820	7.353	3.906	9.174	0.584	<DL	3.364	0.115	0.192
MARN-C1d.d	Marn	Reduced skarn	<DL	8.646	3.558	6.811	<DL	<DL	2.961	0.125	0.135
MARN-C1e.d	Marn	Reduced skarn	1.182	7.728	4.045	8.896	0.973	<DL	3.628	0.167	<DL
MARN-C2a.d	Marn	Reduced skarn	6.255	21.684	4.545	9.869	0.612	0.259	15.151	0.096	<DL
MARN-C2c.d	Marn	Reduced skarn	0.806	7.909	3.864	8.618	0.570	0.067	2.433	0.100	<DL
MARN-C2d.d	Marn	Reduced skarn	0.639	8.674	3.906	9.035	0.584	0.100	1.404	0.125	0.427
MARN-C2e.d	Marn	Reduced skarn	0.612	11.773	3.934	11.120	0.639	<DL	3.002	0.113	<DL

Appendix 1.4B (continued)

Source_file	Deposit_name	Skarn_type	B (ppm)	Na (ppm)	Mg (ppm)	K (ppm)	Ti (ppm)	V (ppm)	Mn (ppm)	Co (ppm)	Ni (ppm)
MARN-C3b.d	Marn	Reduced skarn	0.987	12.413	3.906	8.757	1.029	0.076	2.724	0.133	<DL
CA16B-1.d	Pine Creek	Reduced skarn	4.073	28.217	18.320	<DL	1.890	0.092	30.483	0.459	0.265
CA16B-10.d	Pine Creek	Reduced skarn	4.031	5.602	20.433	5.699	1.404	0.603	26.466	1.001	1.251
CA16B-2.d	Pine Creek	Reduced skarn	4.643	5.949	18.195	2.502	2.641	0.065	29.538	6.950	20.850
CA16B-3.d	Pine Creek	Reduced skarn	4.017	6.352	37.530	<DL	3.892	0.057	34.472	0.277	0.417
CA16B-4.d	Pine Creek	Reduced skarn	3.864	46.704	19.585	2.502	1.571	0.068	28.537	0.247	0.136
CA16B-5.d	Pine Creek	Reduced skarn	3.378	6.241	17.264	5.560	2.280	0.264	27.828	0.246	0.268
CA16B-6.d	Pine Creek	Reduced skarn	4.545	6.811	43.090	<DL	1.863	0.197	41.005	0.245	0.264
CA16B-7.d	Pine Creek	Reduced skarn	7.854	5.963	53.376	2.919	1.279	0.146	52.681	0.361	0.306
CA16B-8.d	Pine Creek	Reduced skarn	3.030	4.629	18.765	<DL	1.863	0.082	24.951	0.231	9.730
RG196-1.d	Ray Gulch	Reduced skarn	5.282	60.882	3.795	10.008	0.556	0.200	10.856	0.093	0.181
RG196-2.d	Ray Gulch	Reduced skarn	1.390	73.253	3.975	9.174	0.820	0.179	16.305	0.103	<DL
RG196-3.d	Ray Gulch	Reduced skarn	<DL	54.627	3.628	10.703	<DL	0.261	10.314	0.095	<DL
RG196-4.d	Ray Gulch	Reduced skarn	0.834	52.959	3.642	13.900	<DL	0.196	13.316	0.110	<DL
RG196-5.d	Ray Gulch	Reduced skarn	0.612	33.944	3.684	9.174	<DL	0.229	10.050	0.124	<DL
RG196-6.d	Ray Gulch	Reduced skarn	0.917	46.148	15.151	8.896	0.667	0.260	14.678	0.160	0.153
RG196-7.d	Ray Gulch	Reduced skarn	0.639	39.615	47.955	10.703	1.029	0.481	23.491	0.737	0.178
RG196-8.d	Ray Gulch	Reduced skarn	<DL	36.766	6.881	8.896	0.890	0.204	15.638	0.125	<DL
RG196-9.d	Ray Gulch	Reduced skarn	<DL	54.488	3.711	8.062	0.931	0.168	12.552	0.126	<DL
SL1223-C2-1.d	Salau	Reduced skarn	6.394	38.920	4.712	<DL	1.585	0.057	52.820	0.848	0.584
SL1223-C2-2.d	Salau	Reduced skarn	3.823	44.480	4.142	<DL	1.237	<DL	45.453	0.278	0.245
SL1223-C3-2.d	Salau	Reduced skarn	3.739	10.703	5.004	<DL	1.904	0.024	12.566	0.334	0.598
SL1223-C4-1.d	Salau	Reduced skarn	3.558	10.411	3.739	<DL	0.931	<DL	11.162	0.188	18.070
SL1223-C4-2.d	Salau	Reduced skarn	4.045	11.815	4.879	<DL	1.154	0.033	18.487	0.177	4.448
SL1223-C4-3.d	Salau	Reduced skarn	3.739	40.310	4.476	13.900	1.543	0.031	14.039	0.183	0.204
SL1223-C5-1.d	Salau	Reduced skarn	4.059	9.744	4.045	<DL	1.612	0.028	20.628	0.292	0.445
SL1223-C5-2.d	Salau	Reduced skarn	4.712	13.970	3.586	<DL	1.376	<DL	16.472	0.172	0.260
SL8A-1.d	Salau	Reduced skarn	4.684	7.867	3.948	<DL	1.668	<DL	9.035	0.214	3.892

Appendix 1.4B (continued)

Source_file	Deposit_name	Skarn_type	B (ppm)	Na (ppm)	Mg (ppm)	K (ppm)	Ti (ppm)	V (ppm)	Mn (ppm)	Co (ppm)	Ni (ppm)
SL8A-3.d	Salau	Reduced skarn	3.823	9.118	4.365	3.058	1.307	<DL	6.408	0.156	0.225
SL8A-4.d	Salau	Reduced skarn	4.101	55.600	44.480	<DL	0.931	<DL	13.900	0.185	0.250
SL8A-5.d	Salau	Reduced skarn	3.836	20.850	3.975	<DL	1.307	<DL	5.782	0.224	0.183
SL8A-7.d	Salau	Reduced skarn	3.475	80.620	4.309	29.190	1.668	<DL	9.813	0.206	0.213
SD212-C1c.d	Scheelite Dome	Reduced skarn	<DL	10.342	2.252	<DL	<DL	<DL	7.576	0.054	<DL
SD212-C1c1.d	Scheelite Dome	Reduced skarn	<DL	11.815	2.294	<DL	0.834	<DL	6.269	0.029	<DL
SD212-C2a.d	Scheelite Dome	Reduced skarn	<DL	16.402	2.307	<DL	0.890	<DL	7.075	0.047	<DL
SD212-C2b.d	Scheelite Dome	Reduced skarn	<DL	7.089	7.812	<DL	0.973	<DL	7.200	<DL	<DL
SD212-C2e.d	Scheelite Dome	Reduced skarn	<DL	36.835	2.641	<DL	<DL	<DL	9.035	0.039	<DL
SD212-C2f.d	Scheelite Dome	Reduced skarn	<DL	27.661	2.335	<DL	<DL	<DL	7.979	0.044	<DL
SD212-C2g.d	Scheelite Dome	Reduced skarn	<DL	7.923	2.168	<DL	<DL	<DL	4.712	<DL	<DL
SY18A-1.d	Shizhuyuan	Oxidized skarn	2.794	33.360	38.725	15.985	3.572	<DL	20.850	0.243	13.900
SY18A-2.d	Shizhuyuan	Oxidized skarn	2.085	35.584	25.020	38.920	4.128	<DL	12.510	0.299	2.780
SY18A-3.d	Shizhuyuan	Oxidized skarn	3.962	76.450	35.028	21.267	5.240	<DL	12.705	0.271	0.165
SY18A-4.d	Shizhuyuan	Oxidized skarn	3.614	8.340	28.648	8.201	4.059	<DL	16.958	0.848	0.973
SY18A-5.d	Shizhuyuan	Oxidized skarn	2.683	14.456	32.345	8.201	4.796	<DL	18.987	0.259	3.892
SZY18B-1.d	Shizhuyuan	Oxidized skarn	4.267	11.815	65.191	22.796	6.241	<DL	20.989	1.571	0.431
SZY18B-C1-1.d	Shizhuyuan	Oxidized skarn	4.392	5.282	8.201	17.931	1.473	0.068	1.195	0.667	0.278
SZY18B-C1-2.d	Shizhuyuan	Oxidized skarn	3.767	8.618	7.311	26.410	1.293	<DL	0.445	0.334	0.239
SZY18B-C1-3.d	Shizhuyuan	Oxidized skarn	4.226	15.290	5.602	21.684	1.515	<DL	1.654	1.140	1.946
SZY18B-C1-4.d	Shizhuyuan	Oxidized skarn	4.003	2.224	5.463	15.429	2.016	<DL	2.641	5.838	18.070
SZY18C-1.d	Shizhuyuan	Oxidized skarn	5.324	29.190	4.448	30.580	10.564	1.323	4.684	9.730	8.757
SZY18C-2.d	Shizhuyuan	Oxidized skarn	5.685	72.280	10.286	25.854	5.532	0.724	5.393	0.232	0.612
SZY18C-3.d	Shizhuyuan	Oxidized skarn	4.545	108.976	13.344	23.769	3.864	15.971	4.476	4.031	20.850
V67-C2A.d	Vostok-2	Reduced skarn	0.865	22.101	5.518	1.626	0.831	0.053	40.338	0.284	0.256
V67-C4A.d	Vostok-2	Reduced skarn	0.904	9.244	7.645	3.406	0.778	0.039	34.778	0.297	0.288
V67-C4B.d	Vostok-2	Reduced skarn	0.890	10.703	3.948	1.890	0.723	0.100	16.346	0.281	0.250
V67-C4C.d	Vostok-2	Reduced skarn	0.748	9.591	4.309	2.863	0.904	0.032	50.596	0.278	0.263
V74-C1.d	Vostok-2	Reduced skarn	0.867	28.634	4.712	2.752	0.890	0.055	30.719	0.278	1.807

Appendix 1.4B (continued)

Source_file	Deposit_name	Skarn_type	B (ppm)	Na (ppm)	Mg (ppm)	K (ppm)	Ti (ppm)	V (ppm)	Mn (ppm)	Co (ppm)	Ni (ppm)
V74-C1A.d	Vostok-2	Reduced skarn	1.197	30.858	4.045	1.960	1.070	0.110	19.794	0.226	0.265
V74-C2A.d	Vostok-2	Reduced skarn	0.987	19.224	4.406	1.293	0.840	0.072	27.786	0.806	0.288
V74-C2B.d	Vostok-2	Reduced skarn	1.626	38.920	3.942	2.433	0.852	0.186	23.922	0.345	0.303
V74-C2C.d	Vostok-2	Reduced skarn	1.390	37.947	4.657	2.224	0.827	0.056	26.354	0.488	0.278
V75-C1.d	Vostok-2	Reduced skarn	0.933	4.184	3.542	<DL	1.724	0.021	10.203	0.393	0.378
V75-C3.d	Vostok-2	Reduced skarn	1.029	5.741	7.089	2.502	1.366	0.040	11.801	0.359	0.384
V75-C4.d	Vostok-2	Reduced skarn	0.813	4.587	3.453	<DL	1.154	0.034	12.913	0.284	0.291
V75-C5.d	Vostok-2	Reduced skarn	1.293	48.928	3.684	<DL	1.209	0.040	35.723	0.342	0.299
V75-C5.d	Vostok-2	Reduced skarn	0.890	4.837	4.295	2.752	1.182	0.023	12.552	0.320	0.342
V75-C5.d	Vostok-2	Reduced skarn	1.668	21.823	291.900	5.004	1.724	0.234	63.940	0.346	0.282
V75-C5.d	Vostok-2	Reduced skarn	1.195	11.676	111.200	13.900	1.557	0.122	28.634	0.325	0.282
V75-C5.d	Vostok-2	Reduced skarn	0.973	24.603	3.294	<DL	0.876	0.101	24.464	0.350	0.334
V75-C5B.d	Vostok-2	Reduced skarn	0.941	12.232	4.643	7.367	0.917	0.053	14.831	0.277	0.227
V75-C6B.d	Vostok-2	Reduced skarn	1.017	10.536	102.860	8.479	1.070	0.113	19.738	0.293	0.310
V75-C7.d	Vostok-2	Reduced skarn	1.084	7.353	8.757	1.279	1.710	0.056	16.541	0.342	0.414
XY199-1.d	Xiaoyao	Oxidized skarn	2.433	27.383	7.784	8.757	6.575	0.295	3.280	0.243	0.167
XY199-2.d	Xiaoyao	Oxidized skarn	2.766	35.862	4.184	8.201	8.020	0.334	3.517	8.618	5.421
XY199-3.d	Xiaoyao	Oxidized skarn	2.572	39.337	3.308	8.896	5.894	1.026	3.628	0.221	9.730
XY199-4.d	Xiaoyao	Oxidized skarn	3.934	148.730	3.280	9.730	4.420	8.562	3.948	0.253	37.530
XY199-5.d	Xiaoyao	Oxidized skarn	4.031	98.690	3.697	10.008	2.933	11.162	6.672	11.120	0.317
XY199-6.d	Xiaoyao	Oxidized skarn	3.684	16.624	3.503	12.232	5.602	3.044	5.574	0.264	2.780
XY199-7.d	Xiaoyao	Oxidized skarn	2.488	24.603	3.517	9.869	5.588	1.404	3.975	0.252	3.058
XY199-8.d	Xiaoyao	Oxidized skarn	2.989	90.072	4.323	2.641	3.308	9.883	4.156	0.243	0.265
XY199-9.d	Xiaoyao	Oxidized skarn	2.933	66.581	3.211	2.919	3.642	9.216	3.294	6.811	1.390
ZX25B-1-1.d	Zhuxi	Reduced skarn	4.101	3.670	7.325	9.174	1.098	<DL	5.546	0.249	0.231
ZX25B-1-2.d	Zhuxi	Reduced skarn	3.461	12.510	19.460	11.954	1.668	<DL	5.074	0.257	56.990
ZX25B-2.d	Zhuxi	Reduced skarn	3.030	0.931	16.819	15.151	1.404	<DL	5.324	0.234	0.253
ZX25B-3.d	Zhuxi	Reduced skarn	2.516	<DL	8.201	29.190	1.251	<DL	4.392	0.653	43.090

Appendix 1.4B (continued)

Source_file	Deposit_name	Skarn_type	B (ppm)	Na (ppm)	Mg (ppm)	K (ppm)	Ti (ppm)	V (ppm)	Mn (ppm)	Co (ppm)	Ni (ppm)
ZX25B-4.d	Zhuxi	Reduced skarn	7.784	18.487	13.177	10.286	1.223	<DL	6.033	0.254	0.250
ZX25B-5.d	Zhuxi	Reduced skarn	5.282	10.981	9.452	<DL	0.904	<DL	5.296	0.253	0.222
ZX25B-6.d	Zhuxi	Reduced skarn	6.450	17.792	11.857	16.819	1.043	<DL	6.491	0.231	0.268
ZX25B-7.d	Zhuxi	Reduced skarn	3.169	4.490	11.537	14.873	1.515	<DL	5.282	0.234	0.183
ZX25B-8.d	Zhuxi	Reduced skarn	2.697	20.850	9.730	17.792	1.473	<DL	5.741	0.247	0.229
ZX25B-9.d	Zhuxi	Reduced skarn	7.367	13.761	33.360	18.070	1.932	0.036	5.504	0.361	0.246
ZX28-1.d	Zhuxi	Reduced skarn	17.514	1.001	12.232	8.340	1.279	<DL	7.645	0.210	5.004
ZX28-2.d	Zhuxi	Reduced skarn	23.630	7.367	13.511	8.201	1.168	0.039	9.994	0.246	0.172
ZX28-3.d	Zhuxi	Reduced skarn	29.190	1.668	16.930	6.255	0.973	0.031	20.294	0.292	50.040
ZX28-4.d	Zhuxi	Reduced skarn	15.638	3.128	23.630	13.344	1.084	0.042	16.263	0.190	0.222
ZX28-5.d	Zhuxi	Reduced skarn	16.569	1.321	10.147	9.174	2.641	0.021	5.226	0.177	6.394
ZX28-6.d	Zhuxi	Reduced skarn	15.346	11.120	19.349	8.757	1.279	0.021	14.873	0.192	11.120
ZX28-7.d	Zhuxi	Reduced skarn	19.043	6.394	31.233	11.259	1.098	0.029	66.998	0.203	0.235

Appendix 1.4B (continued)

Source_file	As (ppm)	Sr (ppm)	Y (ppm)	Nb (ppm)	Mo (ppm)	Ba (ppm)	La (ppm)	Ce (ppm)	Pr (ppm)	Nd (ppm)	Sm (ppm)	Eu (ppm)
Min DL	0.034	0.001	0.001	0.001	0.005	0.009	0.001	0.001	0.001	0.004	0.003	0.001
Max DL	0.835	0.077	0.016	0.072	0.665	0.093	0.187	0.675	0.054	0.129	0.317	0.044
BF2-1.d	0.820	176.113	47.677	20.920	736.7	<DL	5.477	33.388	7.631	56.295	15.832	3.795
BF2-2.d	0.784	184.870	50.735	22.171	764.5	0.067	5.268	36.529	8.535	59.770	16.958	4.198
BF2-3.d	0.780	178.615	33.555	19.516	743.7	<DL	4.142	20.405	4.476	35.334	10.258	2.259
BF2-4.d	0.865	181.951	36.891	19.988	774.2	<DL	3.628	19.001	4.601	37.808	11.468	2.396
BF2-L1.d	0.687	192.932	61.299	23.074	832.6	0.125	5.032	34.611	8.507	60.882	18.362	4.740
BF2-L1.d	0.820	185.426	50.457	22.740	807.6	0.146	4.003	26.883	6.714	51.013	15.248	3.781
BF2-L2.d	0.737	186.538	53.237	23.241	817.3	0.120	4.392	31.192	7.520	55.461	17.250	4.698
BF2-L2.d	0.806	183.758	46.287	23.005	828.4	0.160	3.378	24.617	6.491	50.457	14.956	3.489
CN1-L1.d	1.839	678.876	3.406	5.543	6483.0	0.388	2.655	10.453	1.881	11.092	3.631	0.883

Appendix 1.4B (continued)

Source_file	As (ppm)	Sr (ppm)	Y (ppm)	Nb (ppm)	Mo (ppm)	Ba (ppm)	La (ppm)	Ce (ppm)	Pr (ppm)	Nd (ppm)	Sm (ppm)	Eu (ppm)
CN1-L2.d	1.447	601.314	2.245	5.902	6213.3	0.527	1.828	8.020	1.558	9.674	3.303	0.771
CN1-L2.d	1.294	569.761	2.022	5.782	6185.5	0.379	1.628	7.284	1.400	8.646	2.797	0.657
CN1-L3.d	1.398	593.252	2.345	5.731	6302.3	0.428	1.900	7.937	1.444	9.007	2.940	0.688
CN1-L4.d	1.750	578.101	3.008	4.929	5790.7	0.357	2.542	9.424	1.607	9.202	2.694	0.617
CN1-L5.d	1.325	548.077	3.198	4.495	5731.0	0.257	1.820	6.320	1.058	6.047	1.999	0.452
CN1-L6.d	0.626	505.265	4.176	4.164	5979.8	0.468	0.728	2.288	0.370	2.252	0.731	0.183
CN1-L7.d	1.668	563.228	3.109	4.657	5796.3	0.518	1.525	5.288	0.878	5.021	1.621	0.411
CN2-L1.d	2.071	289.815	1.137	7.325	5184.7	0.214	0.072	0.346	0.057	0.399	0.111	0.012
CN2-L1.d	1.974	288.008	1.070	7.311	4963.7	0.235	0.077	0.329	0.057	0.359	0.129	0.017
CN2-L2.d	2.405	300.240	0.663	7.242	5486.3	0.149	0.101	0.442	0.077	0.488	0.147	0.020
CN2-L2.d	2.196	303.298	0.744	6.992	5496.1	0.156	0.084	0.366	0.060	0.420	0.120	0.021
CN2-L3.d	2.239	251.034	1.245	5.396	4452.2	0.180	0.087	0.379	0.065	0.422	0.132	0.019
CN2-L4.d	1.836	305.939	0.631	7.032	5842.2	0.249	0.071	0.289	0.051	0.289	0.114	0.015
CN2-L5.d	1.975	262.988	1.144	5.493	4852.5	0.191	0.082	0.358	0.062	0.403	0.125	0.017
CN2-L6.d	2.016	289.676	0.559	5.855	5465.5	0.157	0.099	0.436	0.070	0.438	0.149	0.024
CN2-L6.d	1.863	289.398	0.589	6.019	5379.3	0.154	0.079	0.353	0.065	0.442	0.121	0.015
CN2-L7.d	1.596	303.576	0.656	7.252	5405.7	0.235	0.104	0.463	0.076	0.510	0.153	0.021
CEZ-1.d	0.373	58.769	62.133	62.689	49.9	0.046	50.596	69.222	7.103	34.194	18.626	39.337
CEZ-1.d	0.277	44.341	38.642	26.827	98.7	0.036	4.045	14.595	2.544	14.762	4.323	1.918
cez-bt2-0.d	0.916	33.457	49.262	114.675	551.3	0.110	52.959	188.067	26.313	114.119	22.032	2.321
cez-bt2-c1.d	0.612	47.816	21.656	37.391	115.8	0.078	13.539	36.974	5.310	26.188	8.034	4.045
cez-bt2-c1.d	0.821	36.682	64.913	116.482	565.7	0.139	36.835	132.050	19.821	91.462	22.393	2.227
cez-bt2-c1b.d	0.566	40.852	40.310	84.373	520.0	0.118	41.909	138.305	19.238	78.535	15.749	2.364
cez-bt2-c2.d	0.813	40.407	72.141	97.856	538.3	0.100	57.129	182.507	24.853	97.161	21.823	2.355
cez-bt2-c3b.d	2.252	12.983	133.162	218.230	1932.1	0.140	37.405	131.633	18.348	93.825	25.576	1.213
cez-bt2-c3b.d	1.112	40.032	80.481	122.876	526.8	0.209	48.928	151.371	20.933	88.404	21.823	2.022
cez-bt2-c4.d	0.904	47.399	175.140	166.522	537.9	0.113	39.476	134.274	21.601	108.559	33.777	2.516
cez-bt2-c4.d	0.717	35.056	94.520	152.900	703.3	0.063	41.144	146.506	22.226	104.667	26.132	2.612

Appendix 1.4B (continued)

Source_file	As (ppm)	Sr (ppm)	Y (ppm)	Nb (ppm)	Mo (ppm)	Ba (ppm)	La (ppm)	Ce (ppm)	Pr (ppm)	Nd (ppm)	Sm (ppm)	Eu (ppm)
cez-gr-c1.d	0.837	64.496	18.487	50.179	5629.5	0.270	8.521	27.550	4.985	30.594	8.771	1.683
cez-gr-c1b.d	0.514	84.234	11.954	53.237	4962.3	0.178	10.453	30.719	5.087	30.302	7.659	2.002
cez-gr-c1b.d	0.709	50.040	31.136	49.623	7839.6	0.093	4.220	18.390	4.323	35.084	12.816	2.787
cez-gr-c1b.d	0.570	76.172	22.713	54.488	6407.9	0.147	7.506	24.881	4.601	31.025	10.217	2.252
cez-gr-c1c.d	0.784	63.523	23.783	54.488	6394.0	0.196	7.979	26.285	4.837	32.748	10.467	1.897
cez-gr-c2.d	0.648	86.597	5.046	38.642	7797.9	0.114	11.787	33.430	5.143	26.744	4.351	0.904
cez-gr-c2a.d	0.542	99.802	5.379	48.094	6046.5	0.089	13.983	40.032	6.144	29.468	4.865	0.751
cez-gr-c2a.d	0.431	66.859	9.730	48.928	3461.1	0.164	10.925	35.306	6.269	34.472	6.742	1.140
cez-gr-c3.d	0.723	67.971	6.325	28.773	3683.5	0.089	7.145	24.325	4.462	27.856	5.824	1.123
cez-gr-c3.d	0.959	64.079	9.285	34.347	6630.3	0.156	10.397	30.997	5.004	27.244	6.603	1.086
cez-po1-c1b.d	0.300	39.323	1.990	14.567	149.1	0.042	10.425	21.684	4.156	26.215	6.311	23.435
cez-po1-c1b.d	0.311	31.497	0.848	76.172	134.0	0.042	6.783	14.275	2.448	13.789	2.989	7.395
cez-po1-c2.d	0.475	70.014	71.863	92.018	44.1	0.117	83.956	79.647	4.518	9.966	5.504	69.083
cez-po1-c2.d	0.268	57.963	44.480	76.311	63.1	0.035	79.230	70.890	4.031	11.620	4.323	63.523
cez-po1-c3.d	0.195	41.422	3.809	25.437	61.3	0.049	10.147	19.738	2.724	13.080	3.975	10.870
cez-po1-c3.d	0.484	62.411	3.280	16.541	303.0	0.113	6.255	16.430	2.836	15.832	3.294	2.280
cez-po1-c3a.d	0.245	39.476	1.418	15.193	104.7	<DL	16.819	36.696	6.088	32.665	4.921	10.536
cez-po1-c3a.d	0.541	62.828	1.932	11.315	436.5	0.031	7.242	13.247	1.726	8.854	2.363	1.439
cez-po1-c5.d	0.334	38.503	3.809	23.769	71.3	0.078	17.514	28.801	3.836	18.570	3.392	23.074
cez-po1-c5.d	0.605	45.509	2.905	10.425	509.9	0.081	20.572	41.422	5.282	21.684	3.058	2.467
cez-po1-c6.d	0.371	47.677	164.020	122.320	53.7	0.047	13.344	27.383	4.128	20.794	7.784	7.353
cez-po1-c6.d	0.541	53.793	5.810	7.784	515.6	0.225	7.840	10.078	1.094	4.809	1.098	1.918
cez-po1-c6.d	0.373	48.372	1.321	11.996	211.3	0.053	12.927	39.198	7.047	39.615	6.742	6.241
cez-po1-c6b.d	0.461	64.496	2.446	12.232	382.3	0.060	10.286	27.939	4.712	26.549	4.476	4.351
cez-po1-c6b.d	0.439	63.523	7.103	26.827	289.1	0.039	8.340	27.939	5.365	33.360	8.590	3.364
cop-poA-c1-1.d	2.919	61.716	807.590	183.341	97.3	0.050	74.643	338.048	66.303	355.701	113.285	5.199
cop-poA-c1-3.d	8.799	69.778	1441.430	949.370	94.9	1.418	141.780	642.180	133.718	838.170	246.169	3.864
cop-poA-c2-1.d	7.534	63.662	982.730	440.213	112.6	0.046	227.960	1000.800	189.874	1082.810	287.730	6.603

Appendix 1.4B (continued)

Source_file	As (ppm)	Sr (ppm)	Y (ppm)	Nb (ppm)	Mo (ppm)	Ba (ppm)	La (ppm)	Ce (ppm)	Pr (ppm)	Nd (ppm)	Sm (ppm)	Eu (ppm)
cop-poA-c3-1.d	6.283	61.855	1093.930	488.446	86.9	0.021	190.569	875.700	169.163	907.670	223.095	6.603
cop-poA-c3-3.d	5.421	65.330	1606.840	661.640	71.3	0.145	110.644	571.290	123.154	757.550	224.902	7.979
cop-poA-c4-1.d	4.907	69.361	1883.450	455.920	52.7	<DL	165.410	740.870	133.718	700.560	197.936	14.970
cop-poA-c5-1.d	6.283	70.334	1979.360	314.140	30.7	0.521	274.664	1131.460	201.133	1038.330	323.175	24.172
cop-poA-c5-2.d	5.171	69.500	1807.000	313.306	54.9	0.218	198.770	839.560	154.290	842.340	279.390	16.068
cop-poB-c8-1.d	1.279	61.855	308.024	222.400	23.8	0.111	93.686	183.063	25.117	119.123	36.001	4.531
cop-poB-c5-1.d	1.612	63.106	503.180	295.236	61.6	0.018	40.171	164.854	33.082	196.824	82.983	2.683
cop-poB-c5-2.d	1.321	60.882	626.890	448.970	87.8	0.056	24.645	103.694	21.948	140.112	65.747	4.504
cop-poB-c7-1.d	0.626	46.565	111.061	83.539	61.9	0.122	9.841	30.580	5.894	35.723	13.622	8.048
cop-poB-c7-2.d	0.931	50.457	164.437	162.074	79.6	0.035	24.756	63.384	11.009	60.743	20.836	11.593
cop-poB-c3-1.d	1.223	62.967	303.993	186.677	90.6	0.125	13.692	65.608	15.457	108.698	44.897	3.739
cop-poB-c3-2.d	1.418	59.770	797.860	771.450	126.4	0.047	16.972	72.558	16.360	107.586	60.882	3.586
cop-poB-c3-3.d	0.810	55.725	232.964	176.113	201.3	<DL	16.319	60.326	11.481	63.940	26.758	3.350
cop-sc-c3-1.d	0.417	56.156	85.485	38.211	48.8	0.051	229.350	351.670	26.493	66.303	10.314	31.122
cop-sc-c1a-1.d	0.500	27.925	137.749	21.684	138.0	0.036	13.302	38.503	5.282	25.548	10.300	5.977
cop-sc2-c2.d	0.695	53.932	60.743	42.395	174.2	0.044	18.765	39.615	5.616	30.302	11.398	3.809
cop-sc2-c4.d	0.767	64.844	114.814	58.519	47.5	0.107	119.818	289.120	30.997	88.126	14.831	14.081
cop-sc2-c2-2.d	2.127	40.115	397.540	103.972	106.6	0.190	386.420	778.400	89.377	337.770	67.137	16.652
cop-poB-c5b.d	2.057	59.047	934.080	731.140	151.5	1.585	80.620	194.600	31.970	183.480	92.574	6.074
cop-qz-c4.d	1.170	69.361	461.480	202.940	95.2	0.158	81.454	230.740	32.248	140.668	45.314	11.815
cop-qz-c4b.d	1.460	69.875	358.620	112.173	112.5	0.425	61.438	209.890	32.804	142.336	40.032	10.147
cop-po-sq1.d	1.001	70.195	455.920	219.620	85.3	0.459	28.773	104.250	19.043	110.644	51.152	5.491
cop-po-sq2.d	1.411	68.263	599.090	240.470	57.8	0.142	48.233	226.987	44.063	226.570	78.396	10.105
cop-sc-sq3.d	1.161	70.890	625.500	174.167	70.8	0.093	26.271	111.756	21.962	129.131	55.183	7.895
2420-776A-2.d	20.391	85.068	25.145	21.628	129409.0	0.060	174.306	223.373	18.918	44.480	4.601	5.713
2420-776A-3.d	8.604	86.458	12.176	10.981	101470.0	0.096	96.605	154.012	12.899	35.167	4.545	2.435
2420-776A-4.d	12.997	76.033	6.992	8.938	175974.0	0.122	93.269	121.625	8.354	18.404	2.085	1.476
2420-776A-5.d	20.113	69.778	14.317	11.454	177503.0	0.164	102.860	140.390	11.634	31.358	3.461	2.155

Appendix 1.4B (continued)

Source_file	As (ppm)	Sr (ppm)	Y (ppm)	Nb (ppm)	Mo (ppm)	Ba (ppm)	La (ppm)	Ce (ppm)	Pr (ppm)	Nd (ppm)	Sm (ppm)	Eu (ppm)
2420-776B-1.d	8.896	98.412	12.107	13.191	126629.0	0.072	191.264	226.431	21.267	48.372	4.657	4.615
2420-776B-2.d	16.902	64.913	21.489	8.729	181117.0	0.104	122.598	161.240	12.760	34.041	4.420	2.337
2420-776B-3.d	14.220	91.740	12.288	12.051	146923.0	0.026	114.536	189.457	15.151	40.310	4.434	2.516
2420-776B-4.d	13.580	79.369	10.508	13.066	141363.0	0.088	87.709	124.683	9.772	24.798	3.030	1.797
2420-776B-5.d	21.128	78.396	24.089	17.041	131077.0	0.114	127.741	180.978	16.875	46.607	5.185	3.985
2420-848C-1.d	3.517	36.877	18.890	2.647	1861.2	0.157	54.182	87.848	8.382	25.937	3.628	1.316
2420-848C-2.d	20.850	32.123	24.728	2.544	2183.7	0.389	55.322	98.690	9.661	31.553	4.406	1.625
2420-848C-3.d	3.016	36.557	39.337	1.735	2258.8	0.113	86.736	164.854	16.889	55.044	7.617	2.492
2420-848C-4.d	4.740	32.331	42.951	1.426	1962.7	0.542	115.231	244.223	24.589	76.450	10.064	3.767
JIAMA-1.d	6.033	57.963	1.974	4.309	55044.0	0.361	25.437	34.611	2.252	6.769	0.778	0.235
JIAMA-3.d	2.933	57.129	5.032	9.980	8201.0	0.190	23.505	33.068	2.717	10.411	1.397	0.569
JIAMA-4.d	1.098	63.523	5.101	9.549	2207.3	0.348	17.764	29.343	2.680	11.162	1.765	0.606
JIAMA-5.d	4.170	60.048	4.142	4.601	1820.9	0.122	18.543	26.771	2.175	7.951	1.209	0.455
JIAMA-6.d	5.463	59.214	2.627	4.907	39337.0	0.129	21.406	32.665	2.210	7.562	0.809	0.221
KR65-1.d	19.995	162.769	1.370	5.588	30044.9	0.158	59.812	38.559	2.203	6.519	0.931	0.241
KR65-2.d	16.638	174.584	1.621	8.840	35723.0	0.095	44.424	35.028	2.669	9.730	1.446	0.431
KR65-3.d	23.352	150.954	1.119	2.335	24366.7	0.222	75.199	42.089	1.738	3.308	0.417	0.051
KR65-4.d	16.750	217.118	1.460	13.455	47260.0	0.209	41.839	28.092	1.624	4.657	0.639	0.129
KR65-5.d	18.821	177.781	1.599	7.492	33443.4	0.092	56.851	36.766	1.781	4.226	0.517	0.150
KR65-6.d	17.785	197.450	1.529	10.474	40351.7	0.150	49.345	32.429	1.702	4.441	0.578	0.140
KR66-0.d	8.201	118.984	0.260	49.832	17430.6	0.195	86.458	133.162	10.495	25.006	1.175	0.360
KR66-C1-1a.d	12.635	118.845	0.460	62.550	25339.7	0.389	95.771	150.954	12.343	29.899	1.571	0.341
KR66-C1-2a.d	8.840	105.362	0.409	36.835	20085.5	0.284	65.330	106.891	9.063	24.742	1.307	0.356
KR66-C3-1a.d	6.742	97.300	0.399	40.588	20224.5	0.182	84.651	134.830	11.537	30.858	1.710	0.523
KR66-C3-1a.d	8.868	105.918	0.293	46.231	21906.4	0.154	83.400	128.297	10.606	26.938	1.334	0.349
KR66-C3-2a.d	6.519	94.520	0.480	37.850	19084.7	0.164	78.952	125.100	11.064	31.261	1.863	0.584
KR66-C3-2a.d	7.659	101.609	0.370	42.673	23060.1	0.124	86.875	132.050	11.009	28.620	1.668	0.439
KR66-C3-2b.d	7.742	98.690	0.441	40.838	22476.3	0.174	89.794	133.301	10.912	28.523	1.625	0.442

Appendix 1.4B (continued)

Source_file	As (ppm)	Sr (ppm)	Y (ppm)	Nb (ppm)	Mo (ppm)	Ba (ppm)	La (ppm)	Ce (ppm)	Pr (ppm)	Nd (ppm)	Sm (ppm)	Eu (ppm)
KR66-C3-2b.d	9.313	97.717	0.626	41.561	20071.6	0.161	86.597	127.880	10.689	27.008	1.682	0.485
KR98A-C1-1.d	2.572	11.634	30.719	58.519	1815.3	<DL	51.986	148.591	18.487	67.276	15.401	2.961
KR98A-C1-2.d	7.089	23.324	36.696	75.338	1581.8	<DL	69.500	206.137	26.271	96.327	20.683	2.836
KR98A-C2-1.d	7.367	4.017	102.304	76.589	1292.7	<DL	86.041	240.609	32.318	133.023	33.638	8.423
KR98B-C2-1.d	2.099	17.597	21.392	52.264	3272.1	0.038	22.143	69.639	10.133	43.785	10.606	0.901
KR98C-1-1.d	3.545	5.393	46.843	47.969	1494.3	0.079	81.037	218.230	27.939	115.370	25.576	2.947
KR98C-1-2.d	12.496	3.596	196.407	33.499	1299.7	<DL	477.465	1207.910	144.282	576.850	118.845	8.924
KR98C-2-1.d	5.282	6.477	46.287	63.662	870.1	0.584	164.020	486.500	59.631	215.311	38.781	2.569
DMGr-0a.d	7.881	119.123	0.466	44.897	18070.0	0.118	86.180	112.868	7.450	15.916	1.005	0.350
DMGr-0b.d	15.332	125.239	0.723	29.468	25478.7	0.163	92.435	123.293	6.992	11.537	0.563	0.293
DMGr-0c.d	5.838	151.232	1.446	28.634	20335.7	0.128	62.967	78.952	5.977	15.151	1.237	0.612
DMGr-C1b.d	6.950	122.181	0.621	48.789	20961.2	0.142	83.956	109.254	7.659	17.278	1.087	0.450
DMGr-C1c.d	6.811	114.814	1.643	43.660	22309.5	0.227	89.488	118.984	9.021	22.226	1.858	0.563
DMGr-c1e.d	10.203	138.722	0.806	68.110	21836.9	0.100	97.578	123.710	7.576	14.470	0.898	0.234
DMGr-C2.d	11.468	134.135	1.654	46.426	25423.1	0.140	95.493	122.876	7.965	17.028	1.284	0.398
DMGr-c3a.d	8.354	140.807	0.699	35.626	26535.1	0.278	75.686	90.072	5.143	9.744	0.720	0.239
DM-PX-10.d	9.688	158.877	16.360	31.831	18542.6	0.236	67.832	99.385	9.674	44.341	7.979	3.058
DM-PX-3.d	11.982	91.184	0.945	27.883	17555.7	0.253	56.156	95.076	8.771	33.902	3.225	0.502
DM-PX-4.d	9.160	83.400	1.365	33.902	18459.2	0.113	64.079	107.169	9.633	36.557	3.531	0.521
DM-PX-5.d	9.271	90.350	0.947	35.028	15442.9	0.215	72.280	109.532	8.952	27.341	2.113	0.417
DM-PX-6.d	10.814	98.968	1.277	49.762	12732.4	0.167	86.180	134.691	9.827	29.468	2.488	0.349
DM-PX-7.d	9.188	96.188	1.434	50.318	12690.7	0.114	94.937	136.081	9.035	30.580	3.392	0.461
DM-PX-8.d	9.813	91.045	1.639	56.990	11662.1	0.090	94.659	134.552	9.257	31.609	3.572	0.480
DM-PX-9.d	8.145	102.721	2.552	34.347	16276.9	0.209	61.299	96.883	7.965	27.453	2.808	0.676
Ku01-L1.d	100.914	104.111	0.172	1.508	11481.4	0.190	122.320	300.935	28.606	57.907	1.295	0.328
Ku01-L2.d	99.246	103.138	0.270	1.473	12232.0	0.158	120.652	295.514	28.537	58.658	1.375	0.332
Ku01-L3.d	87.987	71.724	0.052	1.626	10605.7	0.171	50.360	138.027	15.526	39.017	1.059	0.353

Appendix 1.4B (continued)

Source_file	As (ppm)	Sr (ppm)	Y (ppm)	Nb (ppm)	Mo (ppm)	Ba (ppm)	La (ppm)	Ce (ppm)	Pr (ppm)	Nd (ppm)	Sm (ppm)	Eu (ppm)
Ku01-L3.d	84.790	71.168	0.054	1.700	10522.3	0.157	48.455	135.942	15.332	39.976	1.166	0.345
Ku01-L4.d	85.763	71.377	0.058	1.642	10522.3	0.152	48.344	134.552	15.234	39.281	1.134	0.332
Ku01-L5.d	82.566	70.751	0.122	1.604	11064.4	0.167	46.134	130.243	14.956	38.906	1.200	0.425
Ku01-L5.d	82.983	70.612	0.045	1.722	10633.5	0.161	47.677	132.745	15.054	39.115	1.038	0.321
Ku01-L6.d	92.296	103.555	0.147	1.478	10897.6	0.179	117.733	293.846	28.259	59.075	1.195	0.322
Ku01-L6.d	102.860	103.555	0.115	1.521	11300.7	0.174	124.405	299.267	28.203	54.252	1.125	0.246
DPHB-C1.d	1.154	91.879	1.423	15.290	4878.9	3.892	15.443	27.453	3.176	12.385	1.557	0.606
DPHB-C1a.d	1.223	57.324	20.405	51.847	3315.2	1.043	22.032	91.184	16.458	93.547	18.779	3.279
DPHB-C2.d	1.293	48.372	53.932	102.999	3651.5	1.432	12.482	51.388	9.633	66.303	22.171	3.128
DPHB-C2a.d	1.029	55.322	13.330	44.758	4031.0	1.946	18.167	56.156	9.105	50.179	11.579	1.289
DPHB-C2b.d	1.237	62.828	11.259	23.338	4475.8	1.974	52.820	130.660	17.514	81.315	13.066	1.437
DPHB-C2c.d	0.309	27.661	1.575	15.985	746.4	0.820	2.446	10.105	1.917	13.427	4.587	0.763
DPHB-C3.d	1.307	64.635	6.102	22.212	4578.7	1.446	11.926	40.977	6.964	36.418	6.060	0.929
DPHB-C3a.d	1.515	66.859	9.132	57.824	4177.0	2.933	27.272	78.118	11.384	55.878	9.118	1.112
DPHB-C3b.d	1.362	67.554	7.951	31.136	4139.4	1.960	17.834	55.044	8.423	42.812	7.145	1.273
DPHB-C3c.d	1.168	95.354	2.982	18.835	4083.8	2.071	10.675	27.216	4.044	18.265	2.738	0.473
LBt-C1.d	2.460	39.087	42.673	35.028	332.3	0.095	52.681	129.270	19.043	82.149	14.345	4.684
LBt-C1a.d	1.168	37.739	86.736	46.565	337.4	0.264	67.276	183.480	28.495	136.637	26.271	6.922
LBt-C2.d	0.820	37.947	39.476	28.551	374.3	0.122	57.129	151.510	22.518	105.501	17.542	5.352
LBt-C3.d	1.626	40.352	38.086	36.001	418.4	0.210	80.064	200.160	27.939	122.459	19.307	6.769
LBt-C4.d	1.529	37.044	83.539	38.225	390.2	0.164	132.606	328.040	46.287	205.442	33.527	7.506
LBt-C4a.d	1.988	39.198	42.951	79.091	461.5	0.068	123.432	289.120	39.754	170.970	27.800	5.921
LBt-C5.d	0.667	45.258	208.500	88.960	163.6	<DL	17.931	70.751	15.346	90.906	32.443	7.909
LBt-C5a.d	1.376	40.102	187.094	32.735	337.4	<DL	53.098	153.456	27.647	155.958	37.113	9.494
LBt-C5b.d	0.487	39.281	59.909	52.264	266.6	<DL	10.689	32.999	6.227	34.152	10.064	5.101
LCSA-C1.d	0.751	46.565	4.935	30.997	2532.6	0.471	15.846	57.268	9.897	57.546	10.425	1.116
LCSA-C1a.d	0.751	61.577	15.471	49.206	2946.8	0.751	11.579	42.395	8.034	49.762	10.953	1.330
LCSA-C1a.d	0.876	58.102	13.344	43.368	2585.4	0.695	10.314	40.449	7.965	49.206	10.244	1.236

Appendix 1.4B (continued)

Source_file	As (ppm)	Sr (ppm)	Y (ppm)	Nb (ppm)	Mo (ppm)	Ba (ppm)	La (ppm)	Ce (ppm)	Pr (ppm)	Nd (ppm)	Sm (ppm)	Eu (ppm)
LCSA-C1a.d	0.612	72.085	8.674	33.638	1986.3	0.378	10.314	42.117	8.479	53.654	11.551	1.608
LCSA-C2a.d	0.389	75.199	26.855	86.458	1305.2	0.245	24.033	71.029	10.369	47.955	9.035	1.904
LCSA-C2c.d	0.528	65.330	35.000	118.984	1287.1	0.327	24.534	71.863	11.190	54.627	12.163	1.818
LCSB-C1.d	0.384	60.187	36.140	76.172	1132.9	0.204	18.487	58.797	9.980	50.596	11.620	1.977
LCSB-C1.d	0.695	86.736	18.487	81.593	1854.3	0.431	22.935	59.492	8.062	37.947	6.950	0.967
LCSB-C1a.d	0.431	78.257	26.368	92.435	1880.7	0.520	23.185	63.481	9.230	42.200	9.021	1.319
LCSB-C4.d	0.626	72.975	24.047	78.952	1984.9	0.227	28.690	72.836	10.369	48.094	10.175	1.108
LCSB-C5.d	0.574	88.404	37.391	69.361	2009.9	0.186	22.059	66.581	10.745	53.515	12.427	1.646
LCSB-C5.d	0.439	88.543	25.646	80.898	1508.2	0.260	28.161	81.593	11.662	50.596	9.271	1.412
LOP2A-C1.d	0.459	176.530	2.627	32.526	746.4	0.125	5.407	24.881	6.199	52.681	17.472	4.712
LOP2A-C2.d	0.681	34.291	14.859	22.546	1939.1	0.056	7.047	44.772	10.286	69.361	16.096	6.630
LOP2A-C2a.d	0.584	36.237	7.270	15.999	1991.9	0.046	6.060	26.229	5.393	31.873	8.590	2.731
LOP2A-C2b.d	1.182	62.967	13.469	16.624	2570.1	0.071	6.227	27.091	5.282	31.345	10.078	2.371
LOP2A-C2c.d	0.542	47.677	2.028	95.771	1688.9	0.157	11.996	46.968	9.383	52.403	8.604	3.503
LOP2A-C3.d	0.876	68.527	12.149	12.413	1362.2	0.200	4.935	17.319	3.428	24.937	11.634	2.238
LOP2A-C3a.d	0.473	114.814	1.712	20.739	1096.7	0.157	4.531	18.084	4.045	29.677	8.368	2.000
LOP2A-C3b.d	0.653	158.043	4.240	84.512	824.3	0.181	14.526	61.577	12.830	88.126	24.506	5.004
LOP2A-C3c.d	0.417	97.856	2.238	34.750	1406.7	0.142	7.951	26.730	5.199	35.445	9.966	2.384
LOP2B-C1.d	0.834	37.530	7.311	14.484	2253.2	0.264	7.450	30.719	6.158	37.669	9.396	1.835
LOP2B-C2.d	0.669	33.527	12.732	7.423	2404.7	1.404	6.811	43.785	9.591	57.546	13.386	6.894
LOP2B-C2a.d	0.848	31.553	10.342	7.965	2399.1	0.103	4.545	27.800	6.158	38.642	9.758	5.727
LOP2B-C2a.d	0.695	27.661	11.759	7.951	2243.5	0.334	10.356	46.982	8.924	49.206	12.566	5.504
LOP2B-C2b.d	0.635	40.727	12.969	12.649	2137.8	0.118	8.535	40.032	7.881	44.341	11.843	4.587
L14-C1.d	1.362	17.014	85.902	10.703	14.6	0.217	29.468	22.101	8.535	42.673	9.202	10.286
L14-C1.d	0.752	21.420	90.628	12.468	14.2	0.195	117.594	87.570	14.665	44.480	7.020	42.812
L14-C2A.d	0.979	21.740	125.100	36.001	12.9	0.106	14.345	11.523	5.588	31.136	8.173	1.592
L14-C2B.d	1.043	22.101	175.557	142.753	12.6	0.133	88.821	61.855	14.275	45.870	7.284	17.792
L18-C2A.d	1.112	22.532	269.660	38.781	31.1	0.277	47.538	28.453	17.750	100.775	24.186	3.642

Appendix 1.4B (continued)

Source_file	As (ppm)	Sr (ppm)	Y (ppm)	Nb (ppm)	Mo (ppm)	Ba (ppm)	La (ppm)	Ce (ppm)	Pr (ppm)	Nd (ppm)	Sm (ppm)	Eu (ppm)
L18-C2c.d	1.182	32.943	196.824	18.487	31.0	0.524	52.264	32.679	17.500	90.350	18.042	4.365
L18-C3.d	0.876	20.544	196.268	14.887	34.7	0.375	58.936	34.611	17.542	87.848	16.750	5.199
L18-C4A.d	1.137	22.727	232.825	19.404	27.1	0.196	72.419	42.812	26.118	148.174	30.580	4.846
L18-L1.d	1.738	24.631	314.140	38.364	29.7	0.361	62.272	33.777	23.074	135.247	32.804	3.419
L18-L2.d	1.738	14.553	373.910	135.247	117.3	0.060	44.758	20.572	20.294	129.131	30.441	1.408
L28-.d	0.439	16.652	348.890	78.813	21.0	0.038	28.898	18.042	7.325	38.406	11.815	4.768
L28-C1A-.d	0.327	17.500	124.822	30.163	16.4	0.081	21.990	17.361	6.325	31.136	6.978	4.559
L28-C1A-1.d	1.444	13.010	379.748	174.723	104.7	0.117	15.943	7.033	8.729	61.577	21.350	0.877
L28-C3A.d	0.343	25.493	129.548	22.240	19.3	0.107	58.241	41.005	11.148	44.758	8.882	12.788
L28-C3B.d	0.178	19.210	129.965	11.815	15.1	0.078	99.524	50.318	7.298	18.195	3.086	28.036
L28-.d	1.140	12.065	418.390	98.690	84.8	0.168	19.043	7.228	8.062	54.905	19.321	0.883
L30-L1.d	0.596	21.698	56.990	51.569	357.2	0.104	37.808	43.785	7.020	26.924	5.032	0.815
L30-L2.d	0.574	24.047	23.630	243.250	1848.7	0.171	102.999	70.056	14.067	50.874	5.365	1.030
L43-C1A.d	0.334	20.920	184.314	11.245	14.4	0.057	78.952	55.600	12.441	47.135	9.466	19.863
L43-C1B.d	0.384	20.155	123.710	23.630	23.8	0.473	9.188	6.450	3.322	19.516	5.449	2.280
L43-C1c.d	0.366	22.198	138.861	10.133	16.8	0.193	64.079	54.766	11.092	37.252	6.589	11.481
L811-C2A-.d	0.767	28.120	193.210	57.824	25.3	0.172	71.029	38.920	20.989	98.412	17.514	3.322
L811-C2A-.d	1.890	11.801	562.950	66.164	148.6	0.126	15.971	9.299	10.870	87.292	29.941	0.646
L811-C2B-.d	0.316	30.983	73.531	11.954	14.8	0.259	50.735	26.827	7.576	28.356	4.809	13.261
L811-C2B-.d	1.238	34.792	276.610	32.943	9.8	0.147	190.708	91.184	48.650	204.747	29.468	7.006
L811-.d	2.433	11.440	325.260	41.144	224.6	0.053	55.183	23.630	22.198	134.691	26.785	0.751
m2a1-c1.d	0.881	37.808	6.811	19.599	2472.8	0.167	10.981	48.650	9.939	61.716	11.203	2.032
m2a1-c1a.d	0.737	37.739	6.019	26.271	2490.9	0.235	18.209	64.635	11.996	67.554	10.995	2.028
m2a1-c3.d	0.445	39.170	31.470	13.080	1531.8	0.147	0.863	8.966	2.933	29.315	12.454	2.245
m2b-2a-c1.d	0.653	36.835	53.376	212.670	1761.1	0.350	51.291	133.301	17.931	80.620	16.430	3.128
m2b-2a-c1b.d	0.820	40.574	15.026	68.666	2178.1	0.284	24.853	76.450	10.717	48.511	8.284	2.880
m2b-2a-c1c.d	0.713	34.986	48.928	159.155	1794.5	0.224	41.422	120.652	17.014	78.118	15.721	3.639
m2b-2a-c3.d	0.385	49.067	9.674	101.887	1847.3	0.193	42.673	92.991	10.453	38.642	5.630	2.113

Appendix 1.4B (continued)

Source_file	As (ppm)	Sr (ppm)	Y (ppm)	Nb (ppm)	Mo (ppm)	Ba (ppm)	La (ppm)	Ce (ppm)	Pr (ppm)	Nd (ppm)	Sm (ppm)	Eu (ppm)
m2b-2a-c3a.d	0.602	39.309	10.258	114.397	2368.6	0.221	45.870	107.308	12.844	50.179	7.840	2.095
m3d2-c1.d	0.179	136.081	1.779	4.003	336.4	0.550	9.994	9.702	0.853	2.752	0.598	0.200
m3d2-c2.d	<DL	91.601	4.657	5.491	348.9	0.260	7.728	18.251	2.697	14.039	3.086	0.489
m3d2-c3.d	0.293	52.820	4.740	5.963	199.6	0.541	5.894	17.333	3.265	20.433	4.684	0.948
m3d-qz-c3.d	0.140	47.260	20.113	186.260	29.1	0.493	32.804	47.955	4.045	10.147	1.390	1.416
m3d-qz-c3a.d	<DL	54.071	25.576	173.750	72.1	0.563	18.251	30.302	3.002	10.745	2.238	0.999
mt09b-0.d	0.441	13.886	45.453	75.060	421.2	0.368	38.503	111.200	16.166	75.199	13.733	1.283
mt09b-0.d	0.723	12.454	74.226	157.904	493.5	0.236	47.816	167.356	25.715	122.459	21.962	2.228
mt09b-0a.d	0.496	12.107	45.453	121.903	582.8	0.329	40.908	119.262	17.834	84.234	14.261	1.569
mt09b-c1.d	0.708	14.637	72.836	142.892	526.4	0.413	40.171	143.448	23.324	116.899	21.225	2.132
mt09b-c4.d	0.487	14.595	48.233	123.293	551.8	0.464	41.978	118.428	17.973	83.261	14.428	1.364
mt09b-c4.d	0.477	19.516	38.781	98.829	639.4	0.466	36.140	103.694	14.817	68.110	11.898	0.981
mt09b-c4a.d	0.528	15.262	81.315	311.360	478.2	0.531	84.512	194.878	26.410	115.370	20.294	1.226
mt09b-c4a.d	0.778	12.427	80.064	167.912	518.6	0.377	53.793	187.650	28.495	129.826	23.352	2.327
MT161-0.d	0.236	31.414	37.947	103.972	295.2	0.338	33.499	74.643	8.827	28.356	6.352	5.852
MT161-0.d	0.431	61.021	30.719	88.404	295.1	1.070	29.468	68.944	8.479	27.939	5.296	3.128
MT161-0a.d	0.203	28.148	28.912	46.982	273.7	0.279	24.325	45.592	5.087	16.235	3.753	8.104
MT161-0a.d	0.252	38.503	52.681	159.989	351.7	0.322	55.044	132.884	16.041	52.403	10.759	2.780
MT161-0b.d	0.206	32.012	33.360	140.390	260.2	0.215	32.248	69.222	7.645	24.186	5.254	2.989
MT161-0b.d	0.145	30.399	19.168	137.610	286.6	0.263	15.735	28.189	3.179	10.592	2.585	5.671
MT161-c2.d	0.806	37.669	43.229	91.740	296.1	0.612	40.588	64.635	7.367	27.383	6.700	12.649
MT161-c2.d	0.695	37.544	24.325	127.880	272.2	0.834	32.526	38.503	3.531	10.981	2.711	10.536
MT161-c6.d	0.374	33.638	47.357	111.617	369.5	0.206	53.376	127.324	14.678	45.036	8.576	2.922
MT161-c6a.d	0.418	35.584	54.210	121.764	313.7	0.267	51.291	101.748	11.968	42.673	10.217	6.644
MT161-c6b.d	0.314	25.103	35.834	51.291	355.0	0.295	16.444	42.256	5.935	23.547	5.908	2.474
MT161-c6b.d	0.254	31.289	24.825	112.451	283.4	0.341	61.994	65.330	4.976	12.482	2.683	16.082
MT231-0.d	0.851	47.260	105.084	121.764	285.5	0.505	37.947	148.452	26.938	138.305	31.414	4.267
MT231-c1.d	0.481	80.481	53.376	107.030	293.3	0.432	47.955	121.486	17.375	74.782	13.803	2.822

Appendix 1.4B (continued)

Source_file	As (ppm)	Sr (ppm)	Y (ppm)	Nb (ppm)	Mo (ppm)	Ba (ppm)	La (ppm)	Ce (ppm)	Pr (ppm)	Nd (ppm)	Sm (ppm)	Eu (ppm)
MT231-c1a.d	0.614	89.655	74.643	88.543	404.5	0.395	27.800	103.416	18.487	99.941	23.352	3.419
MT231-c1b.d	0.373	90.767	31.456	43.368	468.4	0.432	20.572	70.473	11.454	54.071	10.175	2.152
MT231-c2.d	0.238	31.553	30.441	195.990	262.7	1.404	30.302	72.975	10.286	41.144	7.506	2.321
MT231-c2.d	0.150	22.518	9.841	80.064	258.5	0.709	14.178	25.993	2.989	10.286	1.779	1.272
MT231-c2a.d	<DL	30.997	22.101	57.963	390.6	0.364	19.071	43.090	5.782	23.630	4.490	1.860
MT231-c4.d	0.556	74.921	34.639	48.928	138.4	0.366	45.592	96.605	11.662	41.839	7.450	5.338
MT231-c4.d	0.379	124.266	28.592	35.862	515.7	0.503	9.730	35.723	7.325	43.924	9.966	2.377
MT231-c4a.d	0.545	104.111	44.897	53.932	444.8	0.506	36.557	101.609	15.610	73.114	13.330	3.029
MT231-c5.d	0.363	56.295	23.852	85.346	400.3	1.201	30.302	59.075	7.103	27.244	5.032	2.627
MT231-c5a.d	0.284	24.700	21.823	78.813	314.7	1.390	16.680	34.611	4.712	19.738	4.156	1.557
MT-Po1-1.d	<DL	62.411	7.617	25.229	32.1	0.278	14.081	22.991	2.323	7.520	1.336	1.384
MT-Po1-2.d	<DL	63.245	0.691	443.410	27.9	0.057	3.809	5.185	0.378	0.739	0.108	0.942
MT-Po1-3.d	<DL	50.624	2.289	54.071	45.6	0.063	12.204	12.913	0.956	2.405	0.371	5.560
MT-Po1-5.d	<DL	56.156	1.668	49.762	38.2	0.192	10.689	12.385	0.945	2.377	0.289	5.671
MT-Po1-6.d	<DL	53.932	1.715	19.543	47.3	0.147	7.993	10.050	0.856	2.266	0.271	4.017
MARN-C1a.d	3.267	195.712	100.914	21.962	454.5	0.029	20.475	65.886	11.746	67.554	20.058	4.379
MARN-C1b.d	2.905	203.496	106.474	22.268	493.7	0.149	17.931	53.932	9.549	56.156	16.611	4.698
MARN-C1c.d	2.613	198.214	103.694	22.184	489.3	0.042	16.722	51.847	9.633	55.044	16.402	4.768
MARN-C1d.d	3.072	201.272	108.559	19.265	484.7	0.054	22.115	71.307	12.441	70.890	19.404	4.948
MARN-C1e.d	2.822	202.801	103.555	21.031	475.5	0.065	17.736	55.211	10.008	58.102	17.153	4.768
MARN-C2a.d	14.984	160.962	106.335	59.214	522.1	0.074	13.997	46.454	9.105	55.878	16.944	4.851
MARN-C2c.d	4.754	172.499	130.521	19.279	604.7	<DL	21.851	81.176	15.818	98.690	30.163	8.145
MARN-C2d.d	5.324	171.248	151.927	14.192	564.3	0.036	25.951	94.798	19.029	121.764	37.891	8.813
MARN-C2e.d	3.280	180.144	87.014	15.721	618.6	<DL	19.029	70.195	13.831	87.709	25.437	5.463
MARN-C3b.d	4.490	165.688	153.873	13.608	523.6	0.039	18.473	69.639	14.400	91.740	30.650	8.423
CA16B-1.d	3.100	513.605	11.454	93.547	3864.2	0.609	39.879	80.064	10.425	37.099	4.629	2.374
CA16B-10.d	11.120	486.917	7.033	65.678	3071.9	0.549	29.718	62.661	8.493	30.427	3.711	0.959
CA16B-2.d	3.128	558.085	6.269	75.894	3441.6	0.794	36.599	74.921	10.147	36.418	3.850	1.265

Appendix 1.4B (continued)

Source_file	As (ppm)	Sr (ppm)	Y (ppm)	Nb (ppm)	Mo (ppm)	Ba (ppm)	La (ppm)	Ce (ppm)	Pr (ppm)	Nd (ppm)	Sm (ppm)	Eu (ppm)
CA16B-3.d	18.070	519.304	6.394	73.809	3326.3	0.413	34.861	72.280	9.577	34.681	3.572	1.184
CA16B-4.d	9.174	475.380	12.969	102.582	3204.0	0.335	38.128	80.342	10.634	37.947	4.712	2.071
CA16B-5.d	4.309	547.660	6.825	87.709	4307.6	0.653	39.268	81.176	10.939	40.171	4.448	0.908
CA16B-6.d	26.410	478.716	8.771	74.643	3283.2	0.695	32.735	66.025	8.799	33.346	4.281	1.059
CA16B-7.d	2.780	440.352	8.437	73.392	3644.6	0.491	29.982	64.107	8.757	32.762	4.170	1.045
CA16B-8.d	2.099	462.870	9.021	70.473	2788.3	0.530	29.107	60.187	8.076	31.386	4.462	1.213
RG196-1.d	3.962	140.807	47.955	103.416	713.1	0.484	107.169	252.841	27.188	96.327	14.887	2.141
RG196-2.d	1.877	106.335	42.214	112.173	679.7	0.270	147.757	301.630	29.593	100.914	14.595	2.188
RG196-3.d	3.197	164.020	88.265	174.862	835.4	0.277	93.269	246.169	30.163	112.312	19.682	2.460
RG196-4.d	3.155	122.320	77.145	128.575	852.1	0.316	83.122	207.527	25.062	102.860	19.974	2.017
RG196-5.d	3.920	165.410	75.060	136.359	1060.6	0.314	48.428	139.973	18.960	87.292	19.988	1.689
RG196-6.d	4.017	141.085	78.813	138.305	975.8	0.384	72.975	186.816	23.449	98.134	20.544	1.871
RG196-7.d	3.670	148.591	68.110	149.981	961.9	0.492	70.056	184.314	22.157	91.740	18.209	1.868
RG196-8.d	2.349	115.787	66.581	125.100	1280.2	0.322	64.357	159.433	18.821	79.508	17.208	1.682
RG196-9.d	2.655	123.849	86.319	144.838	970.2	0.304	85.485	209.890	24.951	102.443	20.920	2.238
SL1223-C2-1.d	2.585	34.486	307.746	97.161	19.8	<DL	280.641	553.220	72.558	303.993	62.828	13.261
SL1223-C2-2.d	0.848	40.588	87.709	45.453	29.5	0.292	242.694	307.190	27.856	84.373	11.746	19.863
SL1223-C3-2.d	3.753	39.921	36.043	17.292	66.3	0.126	1.501	6.825	1.960	13.970	6.144	1.314
SL1223-C4-1.d	0.890	34.111	67.832	35.445	81.5	0.570	1.372	5.671	1.282	9.313	3.489	1.298
SL1223-C4-2.d	1.529	28.551	140.390	41.283	83.4	0.111	69.500	150.120	20.572	77.840	18.070	2.905
SL1223-C4-3.d	2.502	35.014	181.951	113.285	85.8	0.445	4.434	20.266	4.504	29.134	10.328	3.392
SL1223-C5-1.d	1.098	44.925	120.513	112.729	74.6	0.221	4.212	12.552	2.250	13.539	5.185	2.077
SL1223-C5-2.d	<DL	35.890	80.342	41.130	82.1	0.161	1.596	6.269	1.334	9.466	4.101	1.485
SL8A-1.d	1.154	23.700	15.040	14.845	200.2	0.379	1.523	12.677	4.021	38.892	12.371	4.012
SL8A-3.d	1.432	23.630	18.723	9.466	199.0	0.641	2.084	14.442	4.351	38.767	12.260	3.169
SL8A-4.d	1.710	23.922	13.316	17.792	200.2	0.945	1.893	14.081	4.139	35.362	10.606	3.030
SL8A-5.d	1.460	29.162	7.006	16.402	180.4	0.507	4.337	25.242	5.963	40.546	8.660	2.353
SL8A-7.d	1.473	37.377	4.504	8.757	202.5	3.892	2.078	13.052	3.525	29.121	7.061	1.572

Appendix 1.4B (continued)

Source_file	As (ppm)	Sr (ppm)	Y (ppm)	Nb (ppm)	Mo (ppm)	Ba (ppm)	La (ppm)	Ce (ppm)	Pr (ppm)	Nd (ppm)	Sm (ppm)	Eu (ppm)
SD212-C1c.d	5.643	96.883	104.111	299.128	1559.6	0.235	38.461	136.776	22.087	124.266	34.792	5.838
SD212-C1c1.d	3.711	101.887	116.065	131.216	1545.7	0.100	32.109	139.695	24.395	146.784	39.615	6.533
SD212-C2a.d	3.836	104.389	88.126	282.587	1474.8	0.197	60.604	191.264	26.980	128.436	26.160	6.005
SD212-C2b.d	2.446	98.412	69.361	329.152	1409.5	0.085	55.183	161.657	21.267	98.551	21.198	5.324
SD212-C2e.d	3.169	102.999	74.921	140.112	1460.9	0.110	32.109	118.150	18.835	99.802	22.310	5.643
SD212-C2f.d	3.253	100.914	72.280	131.911	1380.3	0.128	31.692	124.266	19.113	100.636	22.365	6.547
SD212-C2g.d	2.210	96.883	71.724	115.231	1434.5	<DL	44.786	152.344	21.434	103.138	21.754	6.311
SY18A-1.d	5.213	56.156	0.644	52.959	25895.7	0.032	22.435	64.079	8.132	30.441	5.352	0.110
SY18A-2.d	6.116	42.812	1.304	28.912	19112.5	0.653	17.681	49.762	6.102	21.573	4.156	0.129
SY18A-3.d	12.885	43.368	2.752	53.098	32248.0	0.032	37.196	101.192	10.925	29.510	4.128	0.097
SY18A-4.d	14.817	77.423	1.038	42.534	26354.4	0.061	26.730	71.863	8.173	27.147	4.643	0.140
SY18A-5.d	6.227	51.152	0.439	32.179	37543.9	0.064	18.793	55.183	6.338	18.570	2.210	0.149
SZY18B-1.d	23.769	58.936	1.209	33.416	44688.5	0.044	33.360	84.929	9.077	27.995	5.338	0.260
SZY18B-C1-1.d	0.723	32.220	0.642	1.629	1348.3	<DL	0.025	0.103	0.024	0.206	0.185	0.037
SZY18B-C1-2.d	<DL	35.709	0.995	1.511	1346.9	<DL	0.024	0.170	0.075	0.373	0.357	0.052
SZY18B-C1-3.d	8.618	31.150	0.043	9.813	1683.3	0.068	0.008	0.459	<DL	0.013	0.016	<DL
SZY18B-C1-4.d	0.890	20.225	0.060	1.686	1299.7	<DL	<DL	0.008	0.006	<DL	<DL	<DL
SZY18C-1.d	9.369	50.457	0.051	3.767	42951.0	0.292	101.192	97.022	4.657	7.270	0.178	0.064
SZY18C-2.d	9.244	55.739	0.120	6.088	39045.1	0.488	66.720	94.103	5.546	8.340	0.304	0.074
SZY18C-3.d	11.092	110.227	70.612	29.496	28133.6	0.143	97.578	282.309	48.692	236.717	42.395	6.005
V67-C2A.d	0.930	22.004	76.450	66.025	126.6	0.125	76.033	53.237	10.814	41.422	8.201	2.363
V67-C4A.d	1.043	17.292	37.947	28.356	101.7	0.160	68.805	25.298	5.588	17.500	2.321	3.128
V67-C4B.d	1.279	12.218	131.633	76.033	209.8	0.078	59.214	25.854	8.451	36.488	6.811	1.918
V67-C4C.d	1.696	24.130	31.136	68.388	103.3	0.171	31.275	10.856	2.850	11.412	2.113	2.947
V74-C1.d	1.387	21.392	107.447	86.597	176.5	0.135	34.750	84.234	14.456	67.276	16.263	1.066
V74-C1A.d	1.687	63.245	472.600	56.156	88.4	0.153	104.806	162.769	30.858	134.691	28.717	9.855
V74-C2A.d	1.126	52.959	162.908	34.903	70.3	0.139	177.642	372.520	39.379	122.320	18.612	14.220
V74-C2B.d	1.917	30.552	567.120	58.380	77.7	0.146	126.073	194.600	37.391	161.935	32.860	7.715

Appendix 1.4B (continued)

Source_file	As (ppm)	Sr (ppm)	Y (ppm)	Nb (ppm)	Mo (ppm)	Ba (ppm)	La (ppm)	Ce (ppm)	Pr (ppm)	Nd (ppm)	Sm (ppm)	Eu (ppm)
V74-C2C.d	1.147	44.869	119.401	30.914	63.5	0.165	126.351	255.760	27.939	86.041	13.261	10.369
V75-C1.d	1.347	17.917	135.108	21.656	168.1	0.113	31.970	15.707	8.243	45.731	9.633	2.730
V75-C3.d	2.182	17.875	90.906	29.746	171.8	0.085	45.731	21.267	10.759	56.573	10.244	3.072
V75-C4.d	0.733	18.946	95.910	14.901	136.1	0.088	9.591	7.089	3.461	21.684	6.825	2.460
V75-C5.d	1.849	50.318	382.250	48.789	6.5	0.085	98.690	232.130	45.870	205.720	40.866	7.770
V75-C5.d	0.667	19.919	35.306	15.749	102.9	0.124	3.614	4.309	1.182	6.811	2.252	1.736
V75-C5.d	1.034	25.520	129.548	35.167	77.6	0.320	13.580	10.189	5.699	36.418	10.800	2.822
V75-C5.d	0.528	21.350	49.206	14.053	107.7	0.097	5.171	5.602	2.043	12.079	3.989	2.150
V75-C5.d	1.056	27.939	437.850	68.666	14.7	0.074	39.059	69.500	17.375	94.659	27.939	4.156
V75-C5B.d	0.947	22.907	162.630	21.823	132.7	0.126	16.263	26.966	7.506	42.673	11.676	2.961
V75-C6B.d	0.927	21.128	152.900	19.321	138.3	0.195	9.591	6.950	3.531	23.491	7.603	2.794
V75-C7.d	1.154	23.157	76.172	19.001	115.2	0.132	5.949	4.476	2.196	14.484	4.657	2.148
XY199-1.d	11.537	47.580	0.117	1.542	62550.0	0.375	91.045	87.987	4.087	7.589	0.379	0.033
XY199-2.d	18.209	55.461	0.140	2.730	57893.5	2.433	76.450	82.288	4.574	9.549	0.571	0.070
XY199-3.d	10.898	55.989	0.300	12.566	55002.3	0.418	80.342	102.026	6.894	17.292	1.098	0.161
XY199-4.d	16.819	103.416	46.982	20.322	32261.9	0.227	106.891	230.462	29.357	111.895	16.805	7.298
XY199-5.d	35.723	130.243	60.882	29.343	17903.2	0.252	130.243	277.722	33.499	142.197	24.297	4.879
XY199-6.d	51.013	110.505	7.687	31.928	40588.0	0.806	75.616	140.251	15.040	49.901	5.630	1.355
XY199-7.d	9.035	61.855	0.200	12.885	40198.8	0.316	76.450	94.242	6.269	13.817	0.655	0.125
XY199-8.d	8.604	122.181	52.820	14.526	22476.3	0.427	120.652	248.532	30.052	123.154	19.543	5.949
XY199-9.d	34.055	125.100	37.669	15.387	18278.5	0.249	118.984	255.760	29.885	116.204	16.722	4.740
ZX25B-1-1.d	3.614	56.156	0.185	5.046	1150.9	<DL	0.357	0.246	0.029	0.183	0.017	0.012
ZX25B-1-2.d	<DL	55.878	0.227	7.131	1103.7	<DL	0.441	0.222	0.026	0.103	0.022	0.061
ZX25B-2.d	<DL	30.121	0.110	22.657	950.8	<DL	0.240	0.132	0.031	0.086	0.025	0.007
ZX25B-3.d	<DL	78.952	0.041	5.727	1014.7	0.057	0.099	0.040	0.029	0.043	<DL	<DL
ZX25B-4.d	1.946	57.824	0.998	47.816	1237.1	0.057	0.872	0.887	0.129	0.639	0.142	0.072
ZX25B-5.d	0.931	54.210	0.915	36.140	1124.5	<DL	0.749	0.491	0.078	0.271	0.049	0.025
ZX25B-6.d	1.932	58.658	1.161	52.125	1189.8	0.046	0.923	0.656	0.100	0.457	0.100	0.032

Appendix 1.4B (continued)

Source_file	As (ppm)	Sr (ppm)	Y (ppm)	Nb (ppm)	Mo (ppm)	Ba (ppm)	La (ppm)	Ce (ppm)	Pr (ppm)	Nd (ppm)	Sm (ppm)	Eu (ppm)
ZX25B-7.d	1.946	73.809	0.135	4.921	1005.0	<DL	0.145	0.124	0.010	0.111	<DL	0.013
ZX25B-8.d	1.348	55.155	0.371	8.882	1145.4	<DL	0.642	0.381	0.051	0.213	0.025	0.017
ZX25B-9.d	0.765	71.724	0.074	10.036	1130.1	0.039	0.074	0.041	0.006	0.029	<DL	0.007
ZX28-1.d	0.240	43.757	0.242	11.885	393.4	<DL	0.826	1.472	0.153	0.627	0.114	0.651
ZX28-2.d	0.404	31.011	0.373	8.451	621.3	<DL	1.555	3.119	0.313	1.482	0.282	0.791
ZX28-3.d	1.265	46.440	0.424	26.549	613.0	<DL	1.365	2.502	0.324	1.165	0.171	0.630
ZX28-4.d	0.389	30.775	0.574	9.313	495.5	0.051	2.335	4.379	0.456	1.703	0.289	1.461
ZX28-5.d	0.464	41.075	0.185	3.975	847.9	<DL	0.317	0.385	0.038	0.207	0.033	0.239
ZX28-6.d	0.286	42.353	0.555	10.647	448.4	0.024	2.305	4.490	0.464	1.932	0.293	1.483
ZX28-7.d	0.487	42.520	0.359	12.302	615.8	0.500	1.373	2.669	0.278	1.612	0.227	0.677

Appendix 1.4B (continued)

Source_file	Gd (ppm)	Tb (ppm)	Dy (ppm)	Ho (ppm)	Er (ppm)	Tm (ppm)	Yb (ppm)	Lu (ppm)	Ta (ppm)	Pb (ppm)	Bi (ppm)	Th (ppm)	U (ppm)
Min DL	0.005	0.001	0.002	0.001	0.002	0.001	0.002	0.001	0.000	0.002	0.001	0.001	0.001
Max DL	0.089	0.034	0.066	0.034	0.046	0.013	0.034	0.012	0.014	0.105	0.024	0.021	0.009
BF2-1.d	19.168	2.344	11.732	2.483	5.365	0.475	2.127	0.247	0.304	3.137	0.053	<DL	0.011
BF2-2.d	19.947	2.462	12.288	2.449	5.032	0.463	1.814	0.214	0.299	2.902	0.033	<DL	0.004
BF2-3.d	14.595	1.769	8.771	1.858	4.045	0.336	1.421	0.161	0.285	3.378	0.028	<DL	0.004
BF2-4.d	16.013	1.861	9.813	2.022	4.643	0.428	1.738	0.220	0.307	3.253	0.030	<DL	0.007
BF2-L1.d	21.489	2.749	14.331	2.843	6.311	0.599	2.516	0.295	0.293	3.447	0.657	<DL	0.007
BF2-L1.d	20.072	2.382	12.357	2.505	5.435	0.517	2.071	0.229	0.311	3.697	0.354	0.008	0.004
BF2-L2.d	20.238	2.489	13.010	2.616	5.574	0.517	2.141	0.229	0.318	3.350	0.464	<DL	0.006
BF2-L2.d	18.904	2.305	11.662	2.295	4.935	0.432	1.856	0.186	0.325	4.198	0.384	<DL	0.008
CN1-L1.d	3.193	0.346	1.382	0.178	0.267	0.018	0.073	0.008	0.337	9.466	0.252	0.004	0.011
CN1-L2.d	2.706	0.258	0.952	0.110	0.185	0.016	0.076	0.010	0.325	12.816	0.406	0.022	0.008
CN1-L2.d	2.295	0.219	0.780	0.095	0.170	0.014	0.085	0.008	0.318	11.759	0.416	0.009	0.009

Appendix 1.4B (continued)

Source_file	Gd (ppm)	Tb (ppm)	Dy (ppm)	Ho (ppm)	Er (ppm)	Tm (ppm)	Yb (ppm)	Lu (ppm)	Ta (ppm)	Pb (ppm)	Bi (ppm)	Th (ppm)	U (ppm)
CN1-L3.d	2.553	0.254	0.944	0.118	0.174	0.016	0.075	0.009	0.331	11.551	0.389	0.016	0.007
CN1-L4.d	2.295	0.258	1.087	0.147	0.242	0.018	0.060	0.006	0.328	6.199	0.174	0.011	0.014
CN1-L5.d	1.772	0.222	1.030	0.146	0.249	0.022	0.091	0.009	0.318	5.630	0.186	0.016	0.018
CN1-L6.d	0.935	0.160	0.955	0.170	0.356	0.035	0.172	0.022	0.305	9.508	0.495	0.015	0.025
CN1-L7.d	1.612	0.200	0.942	0.140	0.243	0.021	0.088	0.008	0.306	6.922	0.325	0.015	0.025
CN2-L1.d	0.153	0.024	0.186	0.055	0.122	0.020	0.092	0.009	0.306	6.422	0.057	0.011	0.007
CN2-L1.d	0.163	0.026	0.190	0.048	0.139	0.015	0.068	0.009	0.336	6.825	0.063	<DL	0.007
CN2-L2.d	0.215	0.029	0.160	0.028	0.065	0.007	0.034	0.003	0.316	6.311	0.059	<DL	0.002
CN2-L2.d	0.150	0.030	0.165	0.032	0.085	0.008	0.037	0.004	0.321	6.422	0.060	<DL	<DL
CN2-L3.d	0.176	0.028	0.172	0.036	0.097	0.010	0.046	0.005	0.322	6.311	0.049	<DL	0.002
CN2-L4.d	0.145	0.021	0.125	0.025	0.072	0.008	0.037	0.004	0.296	6.450	0.051	<DL	0.002
CN2-L5.d	0.165	0.027	0.165	0.035	0.091	0.011	0.048	0.005	0.289	6.227	0.051	<DL	<DL
CN2-L6.d	0.149	0.022	0.152	0.024	0.064	0.006	0.024	0.003	0.286	6.422	0.049	0.012	0.002
CN2-L6.d	0.152	0.028	0.158	0.024	0.056	0.006	0.023	0.002	0.307	6.380	0.043	<DL	<DL
CN2-L7.d	0.178	0.031	0.170	0.033	0.075	0.007	0.030	0.002	0.304	6.589	0.053	0.007	0.002
CEZ-1.d	16.972	2.057	9.369	1.446	3.962	0.642	5.004	0.592	0.790	5.727	0.068	0.876	2.433
CEZ-1.d	3.280	0.570	3.656	0.667	2.446	0.432	3.600	0.430	0.474	3.239	0.046	<DL	0.018
cez-bt2-0.d	17.319	2.448	12.969	2.403	5.699	0.681	3.211	0.324	0.703	2.513	0.282	0.321	0.381
cez-bt2-c1.d	7.659	1.138	6.074	1.045	2.270	0.252	1.058	0.097	0.290	3.030	0.027	0.008	0.060
cez-bt2-c1.d	19.432	2.962	16.319	3.005	7.159	0.858	3.828	0.323	1.251	2.474	0.167	0.069	0.289
cez-bt2-c1b.d	11.495	1.807	10.147	1.877	4.601	0.621	3.322	0.403	0.428	3.044	0.030	0.167	0.188
cez-bt2-c2.d	17.792	3.002	17.792	3.350	8.340	1.098	5.977	0.682	0.538	2.628	0.075	0.167	0.144
cez-bt2-c3b.d	34.277	5.274	30.914	5.970	10.300	0.574	1.169	0.056	2.854	1.376	0.303	0.152	0.525
cez-bt2-c3b.d	19.043	3.253	18.904	3.697	9.174	1.195	6.102	0.639	0.877	2.724	0.096	0.131	0.195
cez-bt2-c4.d	36.974	6.783	41.839	8.340	21.128	2.655	13.344	1.473	1.546	2.555	0.046	0.066	0.199
cez-bt2-c4.d	25.020	3.989	22.796	4.434	10.578	1.195	5.310	0.496	1.863	2.106	0.020	0.172	0.580
cez-gr-c1.d	9.313	1.123	5.546	0.999	1.960	0.153	0.446	0.025	0.278	12.232	0.431	0.023	0.073
cez-gr-c1b.d	7.242	0.731	3.628	0.648	1.182	0.085	0.320	0.022	0.317	5.310	0.026	0.040	0.111
cez-gr-c1b.d	15.916	1.921	9.841	1.856	3.503	0.260	0.626	0.053	0.438	1.886	0.019	0.013	0.062
cez-gr-c1b.d	12.065	1.422	7.047	1.300	2.394	0.172	0.502	0.029	0.316	2.544	0.025	0.015	0.083
cez-gr-c1c.d	12.163	1.454	7.228	1.361	2.572	0.195	0.600	0.042	0.318	2.622	0.022	0.015	0.075
cez-gr-c2.d	2.794	0.309	1.340	0.213	0.439	0.046	0.128	0.013	0.200	1.724	0.027	0.026	0.056

Appendix 1.4B (continued)

Source_file	Gd (ppm)	Tb (ppm)	Dy (ppm)	Ho (ppm)	Er (ppm)	Tm (ppm)	Yb (ppm)	Lu (ppm)	Ta (ppm)	Pb (ppm)	Bi (ppm)	Th (ppm)	U (ppm)
cez-gr-c2a.d	3.211	0.336	1.430	0.243	0.457	0.043	0.131	0.008	0.313	2.002	0.023	0.022	0.073
cez-gr-c2a.d	5.449	0.575	2.627	0.514	0.904	0.095	0.250	0.021	0.332	1.946	0.022	0.022	0.063
cez-gr-c3.d	3.962	0.409	1.821	0.307	0.524	0.037	0.110	0.004	0.210	2.655	0.017	0.018	0.051
cez-gr-c3.d	5.532	0.585	2.599	0.434	0.752	0.053	0.138	0.005	0.175	3.350	0.067	0.018	0.041
cez-po1-c1b.d	3.100	0.249	0.733	0.070	0.095	0.010	0.041	0.004	0.111	3.597	0.098	0.265	1.897
cez-po1-c1b.d	1.162	0.093	0.286	0.033	0.042	0.005	0.027	0.002	0.206	3.558	0.066	0.199	0.959
cez-po1-c2.d	7.061	1.102	5.810	1.013	3.169	0.930	12.941	2.316	0.826	7.270	0.202	4.087	13.900
cez-po1-c2.d	4.531	0.662	3.406	0.588	1.835	0.653	10.286	1.946	0.712	6.575	0.322	3.322	12.788
cez-po1-c3.d	2.474	0.277	0.862	0.103	0.161	0.013	0.110	0.013	0.126	3.308	0.044	0.028	0.089
cez-po1-c3.d	1.529	0.132	0.566	0.103	0.236	0.035	0.222	0.018	0.138	2.711	0.075	0.010	0.085
cez-po1-c3a.d	1.001	0.058	0.199	0.029	0.078	0.012	0.114	0.017	0.123	3.489	0.088	0.023	0.186
cez-po1-c3a.d	1.460	0.120	0.456	0.068	0.121	0.009	0.030	0.002	0.127	1.621	0.052	0.004	0.023
cez-po1-c5.d	1.446	0.152	0.681	0.111	0.246	0.033	0.211	0.018	0.154	4.698	0.132	0.424	0.723
cez-po1-c5.d	1.877	0.181	0.774	0.113	0.200	0.014	0.065	0.003	0.163	1.904	0.076	0.013	0.019
cez-po1-c6.d	13.066	2.905	20.850	4.448	13.344	2.182	14.873	1.863	1.404	4.392	0.046	0.057	0.085
cez-po1-c6.d	1.041	0.168	0.927	0.189	0.414	0.043	0.186	0.017	0.119	2.224	0.063	0.004	0.029
cez-po1-c6.d	2.155	0.139	0.487	0.058	0.097	0.005	0.018	0.002	0.106	2.321	0.034	0.015	0.146
cez-po1-c6b.d	1.626	0.131	0.512	0.084	0.167	0.018	0.082	0.008	0.130	1.815	0.050	0.008	0.092
cez-po1-c6b.d	7.117	0.687	2.655	0.366	0.578	0.044	0.154	0.016	0.114	2.669	0.061	0.040	0.120
cop-poA-c1-1.d	116.482	22.838	154.012	33.721	96.605	14.526	88.821	11.134	2.430	5.032	0.010	0.493	0.317
cop-poA-c1-3.d	263.822	43.368	280.919	61.299	172.638	25.117	144.004	15.957	13.678	5.630	0.051	3.614	1.529
cop-poA-c2-1.d	257.289	36.557	202.662	39.629	107.586	17.111	111.617	13.525	8.145	5.213	0.010	2.134	0.552
cop-poA-c3-1.d	195.017	31.414	195.017	41.631	124.544	20.447	130.938	15.401	8.312	5.032	0.013	2.620	0.674
cop-poA-c3-3.d	244.362	44.341	302.047	67.832	194.739	28.148	157.070	16.847	10.064	5.310	0.008	2.841	1.093
cop-poA-c4-1.d	224.068	44.480	319.978	77.006	230.462	34.750	204.052	22.740	6.839	5.866	0.051	6.589	1.394
cop-poA-c5-1.d	334.017	63.940	423.672	88.543	246.586	36.946	222.261	24.186	3.437	9.438	0.043	5.254	2.082
cop-poA-c5-2.d	296.070	56.851	380.860	80.342	233.520	34.472	204.330	22.101	5.185	6.366	0.028	6.477	1.140
cop-poB-c8-1.d	41.909	8.590	60.604	13.191	37.210	5.226	29.649	3.536	7.061	8.465	0.033	0.059	0.263
cop-poB-c5-1.d	102.721	19.613	125.100	24.978	61.438	7.603	39.337	4.351	11.954	5.685	0.032	0.174	0.164
cop-poB-c5-2.d	93.964	19.432	133.996	28.217	75.477	9.994	52.820	5.713	12.955	5.880	0.008	0.345	0.457
cop-poB-c7-1.d	17.236	3.114	20.711	4.392	12.093	1.724	11.162	1.418	1.084	4.823	0.019	0.806	1.362
cop-poB-c7-2.d	23.811	4.504	29.051	6.311	17.445	2.558	15.804	2.022	3.753	6.519	0.071	4.559	9.730

Appendix 1.4B (continued)

Source_file	Gd (ppm)	Tb (ppm)	Dy (ppm)	Ho (ppm)	Er (ppm)	Tm (ppm)	Yb (ppm)	Lu (ppm)	Ta (ppm)	Pb (ppm)	Bi (ppm)	Th (ppm)	U (ppm)
cop-poB-c3-1.d	55.322	9.855	62.411	12.816	33.902	4.593	26.063	3.102	4.559	5.921	0.008	0.667	1.724
cop-poB-c3-2.d	96.049	21.545	158.599	34.194	92.713	12.468	64.635	6.477	18.209	3.906	0.009	0.057	0.311
cop-poB-c3-3.d	31.011	6.088	41.283	8.646	23.505	3.267	18.557	1.985	1.863	3.016	0.015	0.067	0.229
cop-sc-c3-1.d	8.173	1.471	10.230	2.298	7.728	1.897	22.393	3.850	0.626	6.199	0.106	7.033	2.496
cop-sc-c1a-1.d	21.128	4.240	28.912	6.464	15.665	1.751	7.492	0.817	0.172	3.350	0.015	0.556	0.445
cop-sc2-c2.d	14.456	2.321	13.761	2.822	6.783	0.737	3.614	0.378	0.336	2.452	0.026	0.334	0.070
cop-sc2-c4.d	10.383	1.988	14.261	3.002	10.356	2.377	21.740	3.141	0.922	5.470	0.737	1.557	0.602
cop-sc2-c2-2.d	69.500	11.746	72.280	15.471	40.866	5.463	32.248	4.420	0.302	3.082	0.071	25.715	3.753
cop-poB-c5b.d	134.691	28.217	196.963	42.117	111.339	14.261	71.446	7.270	20.989	13.622	1.321	0.268	1.098
cop-qz-c4.d	54.488	10.967	76.450	16.819	47.955	7.353	47.955	6.005	3.128	4.406	0.047	2.099	1.237
cop-qz-c4b.d	37.669	7.867	55.183	11.815	36.140	6.241	42.534	5.407	1.348	4.459	0.034	0.475	0.518
cop-po-sq1.d	78.535	15.707	104.250	22.657	55.878	6.867	34.889	4.073	3.308	4.212	0.038	0.348	0.200
cop-po-sq2.d	82.705	17.000	113.702	23.769	67.693	10.773	69.222	8.660	3.823	5.057	0.024	0.542	0.514
cop-sc-sq3.d	76.172	16.055	113.980	26.410	72.697	9.841	52.403	6.060	2.057	4.212	0.027	0.011	0.154
2420-776A-2.d	5.630	0.635	3.823	0.881	2.526	0.396	2.405	0.288	0.438	8.020	0.417	2.961	2.677
2420-776A-3.d	4.267	0.488	2.673	0.513	1.482	0.218	1.480	0.210	0.481	5.921	0.031	0.108	0.050
2420-776A-4.d	2.405	0.232	1.254	0.267	0.710	0.110	0.630	0.072	0.303	5.894	0.026	0.082	0.060
2420-776A-5.d	4.156	0.432	2.613	0.563	1.461	0.204	0.992	0.108	0.324	4.337	0.047	0.388	0.163
2420-776B-1.d	4.907	0.461	2.433	0.499	1.336	0.231	1.403	0.232	0.435	6.561	0.071	1.365	0.224
2420-776B-2.d	5.393	0.628	3.656	0.767	2.000	0.252	1.372	0.142	0.324	5.657	0.028	0.257	0.145
2420-776B-3.d	4.698	0.489	2.641	0.516	1.539	0.210	1.334	0.210	0.385	5.546	0.024	0.542	0.320
2420-776B-4.d	3.141	0.338	1.978	0.402	1.144	0.175	0.995	0.116	0.382	5.101	0.017	0.139	0.167
2420-776B-5.d	6.074	0.705	4.017	0.872	2.367	0.324	1.717	0.186	0.430	5.560	0.153	1.151	0.720
2420-848C-1.d	3.225	0.452	3.275	0.851	3.246	0.680	6.033	0.915	0.557	34.750	11.398	44.091	41.700
2420-848C-2.d	3.836	0.594	4.142	1.062	4.073	0.831	7.548	1.191	0.592	40.310	9.118	26.827	31.275
2420-848C-3.d	6.241	0.920	6.491	1.676	6.227	1.287	11.468	1.775	0.580	52.820	23.185	54.627	77.562
2420-848C-4.d	8.271	1.123	7.423	1.724	6.172	1.262	11.620	1.861	0.531	34.333	5.935	88.126	11.009
JIAMA-1.d	0.827	0.064	0.434	0.089	0.364	0.065	0.995	0.152	0.271	10.508	1.473	1.668	7.589
JIAMA-3.d	1.290	0.147	1.177	0.211	0.904	0.168	2.196	0.324	0.396	10.425	1.180	5.852	5.240
JIAMA-4.d	1.404	0.150	1.202	0.218	0.938	0.167	2.249	0.332	0.395	13.970	1.654	4.059	5.532
JIAMA-5.d	1.138	0.112	0.934	0.170	0.706	0.137	1.806	0.282	0.325	12.927	1.473	3.962	10.217
JIAMA-6.d	0.891	0.074	0.578	0.104	0.466	0.100	1.182	0.190	0.286	11.718	1.093	1.932	2.127

Appendix 1.4B (continued)

Source_file	Gd (ppm)	Tb (ppm)	Dy (ppm)	Ho (ppm)	Er (ppm)	Tm (ppm)	Yb (ppm)	Lu (ppm)	Ta (ppm)	Pb (ppm)	Bi (ppm)	Th (ppm)	U (ppm)
KR65-1.d	1.058	0.084	0.325	0.058	0.101	0.013	0.044	0.003	0.798	4.344	0.095	0.078	0.063
KR65-2.d	1.251	0.113	0.375	0.066	0.124	0.022	0.033	0.003	0.983	3.406	0.100	0.044	0.078
KR65-3.d	0.866	0.054	0.274	0.050	0.079	0.004	0.054	0.003	0.613	5.282	0.089	0.111	0.049
KR65-4.d	0.897	0.081	0.356	0.050	0.099	0.010	0.023	0.005	1.190	3.684	0.090	0.057	0.256
KR65-5.d	0.869	0.088	0.339	0.068	0.118	0.015	0.053	0.003	0.866	4.587	0.195	0.060	0.089
KR65-6.d	0.883	0.084	0.348	0.059	0.108	0.013	0.038	0.004	1.028	4.135	0.142	0.058	0.172
KR66-0.d	0.585	0.032	0.099	0.013	0.016	<DL	0.008	0.002	0.374	9.021	0.063	0.063	0.051
KR66-C1-1a.d	0.784	0.046	0.138	0.018	0.024	0.002	0.010	0.002	0.368	25.020	28.495	0.065	0.088
KR66-C1-2a.d	0.701	0.036	0.107	0.018	0.018	0.003	0.008	<DL	0.328	55.600	59.770	0.033	0.124
KR66-C3-1a.d	0.713	0.046	0.172	0.012	0.022	<DL	<DL	<DL	0.324	10.091	0.111	0.083	0.067
KR66-C3-1a.d	0.656	0.036	0.125	0.014	0.020	<DL	<DL	<DL	0.320	9.021	0.092	0.106	0.057
KR66-C3-2a.d	0.917	0.056	0.174	0.020	0.041	0.004	0.009	<DL	0.285	11.078	0.129	0.113	0.081
KR66-C3-2a.d	0.749	0.039	0.110	0.018	0.022	<DL	0.011	<DL	0.271	11.037	0.178	0.032	0.059
KR66-C3-2b.d	0.752	0.050	0.167	0.019	0.029	<DL	<DL	0.002	0.295	10.078	0.114	0.061	0.074
KR66-C3-2b.d	0.876	0.054	0.204	0.027	0.042	<DL	0.018	0.002	0.310	10.328	0.182	0.100	0.138
KR98A-C1-1.d	12.302	1.646	8.368	1.429	3.328	0.435	2.905	0.220	1.671	0.651	1.390	0.056	0.015
KR98A-C1-2.d	15.971	2.038	10.828	1.769	4.101	0.569	3.503	0.329	2.052	0.904	0.010	0.057	0.556
KR98A-C2-1.d	33.221	4.670	24.339	4.559	10.898	1.510	8.938	0.830	1.685	1.668	0.011	0.041	0.063
KR98B-C2-1.d	8.298	1.093	5.699	1.036	2.537	0.361	2.252	0.211	1.266	0.354	0.012	0.023	0.008
KR98C-1-1.d	21.267	2.738	13.692	2.316	5.477	0.755	4.545	0.460	0.981	1.334	0.040	0.243	0.060
KR98C-1-2.d	101.192	11.509	54.210	8.618	17.806	1.943	9.605	0.880	0.716	1.154	0.019	0.584	0.268
KR98C-2-1.d	28.412	3.275	15.248	2.388	5.018	0.559	2.655	0.192	1.790	1.087	0.026	0.061	0.023
DMGr-0a.d	0.730	0.046	0.139	0.020	0.034	0.003	0.019	<DL	0.348	7.937	0.061	0.097	0.069
DMGr-0b.d	0.598	0.040	0.160	0.031	0.062	0.005	0.020	0.003	0.282	8.076	0.056	0.095	0.104
DMGr-0c.d	0.751	0.090	0.404	0.067	0.126	0.010	0.031	0.003	0.293	7.478	0.032	0.050	0.058
DMGr-C1b.d	0.753	0.057	0.207	0.028	0.047	0.005	0.015	0.002	0.363	7.756	0.065	0.117	0.074
DMGr-C1c.d	1.305	0.126	0.471	0.070	0.122	0.011	0.037	0.003	0.313	7.798	0.090	0.116	0.108
DMGr-c1e.d	0.614	0.046	0.188	0.032	0.072	0.008	0.033	0.004	0.467	6.491	0.089	0.152	0.106
DMGr-C2.d	1.195	0.099	0.436	0.079	0.172	0.015	0.065	0.009	0.354	8.173	0.083	0.163	0.149
DMGr-c3a.d	0.581	0.050	0.188	0.030	0.059	0.007	0.030	0.003	0.297	9.049	0.221	0.079	0.080
DM-PX-10.d	9.591	0.947	5.449	0.799	1.904	0.145	0.673	0.054	0.487	8.104	0.018	0.106	0.054
DM-PX-3.d	2.280	0.124	0.411	0.040	0.092	0.006	0.035	0.003	0.427	9.716	0.057	0.041	<DL

Appendix 1.4B (continued)

Source_file	Gd (ppm)	Tb (ppm)	Dy (ppm)	Ho (ppm)	Er (ppm)	Tm (ppm)	Yb (ppm)	Lu (ppm)	Ta (ppm)	Pb (ppm)	Bi (ppm)	Th (ppm)	U (ppm)
DM-PX-4.d	3.086	0.172	0.575	0.057	0.107	0.009	0.054	0.004	0.445	10.425	0.036	0.038	0.046
DM-PX-5.d	2.349	0.116	0.450	0.036	0.099	0.007	0.021	0.002	0.510	9.188	0.361	0.056	0.016
DM-PX-6.d	2.919	0.145	0.537	0.065	0.103	0.008	0.033	0.003	0.596	9.035	<DL	0.108	0.013
DM-PX-7.d	3.406	0.171	0.578	0.068	0.133	0.011	0.054	0.004	0.470	11.760	21.406	0.089	0.044
DM-PX-8.d	3.419	0.172	0.649	0.069	0.150	0.014	0.064	0.004	0.481	9.021	0.167	0.126	0.047
DM-PX-9.d	2.989	0.203	0.867	0.120	0.247	0.020	0.076	0.007	0.482	21.962	2.641	0.070	0.079
Ku01-L1.d	0.997	0.044	0.089	0.007	0.011	<DL	<DL	<DL	0.247	1.711	0.045	0.095	0.050
Ku01-L2.d	0.937	0.043	0.095	0.011	0.019	<DL	<DL	<DL	0.253	1.529	0.041	0.100	0.049
Ku01-L3.d	0.537	0.023	0.027	0.003	0.008	<DL	<DL	<DL	0.270	1.188	0.038	0.106	0.026
Ku01-L3.d	0.466	0.022	0.032	0.003	<DL	<DL	<DL	<DL	0.265	1.230	0.036	0.100	0.029
Ku01-L4.d	0.489	0.019	0.038	0.003	0.006	<DL	<DL	<DL	0.259	1.250	0.031	0.088	0.030
Ku01-L5.d	0.589	0.028	0.063	0.008	0.009	<DL	<DL	<DL	0.271	1.501	0.029	0.086	0.030
Ku01-L5.d	0.507	0.017	0.038	<DL	<DL	<DL	<DL	<DL	0.256	1.158	0.032	0.110	0.035
Ku01-L6.d	0.833	0.039	0.090	0.009	0.009	<DL	<DL	<DL	0.257	1.333	0.037	0.089	0.045
Ku01-L6.d	0.923	0.033	0.056	0.008	0.008	0.002	<DL	<DL	0.263	1.793	0.040	0.098	0.047
DPHB-C1.d	0.751	0.074	0.311	0.061	0.124	0.011	0.082	0.008	0.209	1.555	0.051	<DL	0.015
DPHB-C1a.d	15.026	1.605	7.270	1.079	1.746	0.120	0.349	0.019	0.070	1.468	0.096	0.416	0.250
DPHB-C2.d	24.520	3.098	15.095	2.569	4.809	0.400	1.738	0.149	0.152	1.650	0.239	0.238	1.252
DPHB-C2a.d	7.881	0.785	3.753	0.482	1.012	0.093	0.409	0.023	0.168	1.500	0.108	0.022	0.099
DPHB-C2b.d	8.910	0.862	3.684	0.546	0.949	0.070	0.229	0.013	0.111	1.312	0.053	0.072	0.092
DPHB-C2c.d	2.224	0.171	0.592	0.075	0.118	0.015	0.051	0.003	0.078	0.927	0.008	<DL	0.021
DPHB-C3.d	4.406	0.442	1.890	0.300	0.514	0.038	0.139	0.008	0.145	1.002	0.061	0.032	0.018
DPHB-C3a.d	5.782	0.677	2.738	0.464	0.739	0.054	0.185	0.017	0.182	1.301	0.031	<DL	0.026
DPHB-C3b.d	5.296	0.612	2.572	0.402	0.770	0.055	0.158	0.015	0.120	1.236	0.024	0.025	0.031
DPHB-C3c.d	1.863	0.186	0.883	0.157	0.318	0.029	0.129	0.013	0.118	1.348	0.040	0.019	0.014
LBt-C1.d	12.788	1.637	8.354	1.503	3.183	0.350	1.654	0.140	0.103	1.073	2.766	0.031	0.133
LBt-C1a.d	23.491	3.058	15.804	2.975	6.630	0.696	3.086	0.206	0.157	1.040	0.133	0.113	0.203
LBt-C2.d	15.193	1.765	8.604	1.430	2.669	0.246	1.015	0.057	0.120	1.052	0.043	0.027	0.070
LBt-C3.d	15.582	1.820	8.882	1.327	1.940	0.150	0.505	0.033	0.118	1.065	0.044	0.036	0.356
LBt-C4.d	28.787	3.418	17.417	2.958	4.768	0.332	1.112	0.061	0.171	0.981	4.726	0.406	0.292
LBt-C4a.d	23.074	2.697	12.607	1.640	1.724	0.081	0.156	0.009	0.311	1.013	0.053	0.133	0.310
LBt-C5.d	34.667	5.435	33.555	6.922	18.723	2.773	16.194	1.501	0.250	1.553	0.013	0.026	0.104

Appendix 1.4B (continued)

Source_file	Gd (ppm)	Tb (ppm)	Dy (ppm)	Ho (ppm)	Er (ppm)	Tm (ppm)	Yb (ppm)	Lu (ppm)	Ta (ppm)	Pb (ppm)	Bi (ppm)	Th (ppm)	U (ppm)
LBt-C5a.d	41.811	5.717	32.304	6.533	15.123	1.649	6.436	0.357	0.200	1.264	0.023	0.146	0.278
LBt-C5b.d	11.607	1.685	9.980	2.036	5.157	0.637	3.350	0.271	0.105	1.290	0.011	0.023	0.040
LCSA-C1.d	5.477	0.443	1.365	0.200	0.339	0.029	0.090	0.009	0.095	1.557	0.047	0.010	0.022
LCSA-C1a.d	8.799	0.920	4.073	0.730	1.557	0.158	0.703	0.058	0.138	2.349	0.051	0.012	0.085
LCSA-C1a.d	7.589	0.760	3.364	0.614	1.209	0.139	0.653	0.053	0.126	2.377	0.057	0.018	0.081
LCSA-C1a.d	8.187	0.687	2.641	0.402	0.692	0.071	0.352	0.033	0.089	1.864	0.008	0.011	0.054
LCSA-C2a.d	7.840	0.994	5.630	1.072	2.711	0.320	1.515	0.133	0.247	1.679	0.029	0.012	0.160
LCSA-C2c.d	11.162	1.365	7.603	1.372	3.392	0.410	1.960	0.152	0.338	1.838	0.019	0.019	0.243
LCSB-C1.d	10.620	1.436	7.756	1.544	3.697	0.443	2.043	0.182	0.286	1.412	0.026	0.033	0.403
LCSB-C1.d	5.713	0.708	3.836	0.702	1.738	0.186	0.848	0.067	0.140	1.626	0.092	0.043	0.147
LCSB-C1a.d	7.381	1.008	5.365	1.023	2.503	0.272	1.241	0.095	0.159	1.295	0.047	0.030	0.176
LCSB-C4.d	9.118	1.091	5.504	0.999	2.141	0.209	0.637	0.054	0.122	1.052	0.028	0.020	0.092
LCSB-C5.d	11.037	1.498	8.298	1.572	3.697	0.374	1.532	0.115	0.161	1.337	0.039	0.014	0.149
LCSB-C5.d	6.644	0.897	4.879	0.916	2.335	0.284	1.120	0.076	0.207	1.319	0.051	0.039	0.209
LOP2A-C1.d	5.963	0.403	1.084	0.131	0.186	0.021	0.047	0.008	0.042	2.085	0.014	0.016	0.131
LOP2A-C2.d	14.651	1.562	6.491	0.917	1.333	0.073	0.190	0.012	0.034	1.711	0.057	0.026	0.076
LOP2A-C2a.d	8.132	0.834	3.183	0.385	0.531	0.036	0.101	0.011	0.039	1.532	0.024	0.013	0.021
LOP2A-C2b.d	10.578	1.180	5.393	0.776	1.264	0.091	0.307	0.029	0.038	1.607	<DL	<DL	0.012
LOP2A-C2c.d	2.961	0.211	0.734	0.089	0.131	0.011	0.043	<DL	0.117	2.342	0.114	0.037	0.778
LOP2A-C3.d	11.801	1.186	4.434	0.671	1.070	0.077	0.327	0.035	0.037	1.714	0.022	0.023	0.095
LOP2A-C3a.d	3.044	0.189	0.639	0.089	0.129	0.011	0.075	0.007	0.058	1.749	0.020	0.013	0.040
LOP2A-C3b.d	8.312	0.560	1.587	0.189	0.268	0.017	0.072	0.008	0.107	2.380	0.033	0.033	0.537
LOP2A-C3c.d	4.184	0.281	0.919	0.101	0.174	0.018	0.060	0.004	0.070	1.863	0.029	0.021	0.145
LOP2B-C1.d	7.339	0.733	3.141	0.381	0.556	0.036	0.093	0.013	0.037	1.807	0.047	0.009	0.017
LOP2B-C2.d	12.385	1.394	5.671	0.724	0.998	0.060	0.129	0.011	0.033	1.927	0.213	0.006	0.029
LOP2B-C2a.d	9.591	1.097	4.462	0.577	0.798	0.043	0.124	0.006	0.032	2.822	3.197	0.007	0.019
LOP2B-C2a.d	11.509	1.297	5.491	0.655	0.944	0.064	0.171	0.012	0.035	1.779	0.114	0.007	0.018
LOP2B-C2b.d	11.245	1.302	5.199	0.681	1.013	0.062	0.195	0.017	0.036	1.674	0.046	<DL	0.023
L14-C1.d	12.093	1.710	10.981	2.419	6.241	0.765	4.643	0.626	0.413	2.113	0.103	0.542	3.058
L14-C1.d	6.811	1.182	8.243	1.890	6.394	1.265	12.204	2.029	0.667	2.419	0.072	6.060	8.382
L14-C2A.d	12.079	2.016	14.109	3.280	9.383	1.247	7.423	0.954	1.182	2.017	0.022	0.071	0.049
L14-C2B.d	8.882	1.529	11.968	3.058	10.912	2.294	21.545	3.336	3.392	2.919	0.038	4.893	4.782

Appendix 1.4B (continued)

Source_file	Gd (ppm)	Tb (ppm)	Dy (ppm)	Ho (ppm)	Er (ppm)	Tm (ppm)	Yb (ppm)	Lu (ppm)	Ta (ppm)	Pb (ppm)	Bi (ppm)	Th (ppm)	U (ppm)
L18-C2A.d	36.140	5.268	35.028	8.020	20.433	2.572	14.387	1.917	0.940	2.975	0.031	0.367	0.145
L18-C2c.d	23.491	3.267	21.406	5.074	14.081	1.861	10.800	1.416	0.541	3.141	0.048	0.373	0.150
L18-C3.d	20.767	2.944	20.044	4.768	13.831	1.954	11.885	1.522	0.470	1.886	0.031	0.783	0.570
L18-C4A.d	37.530	4.796	29.190	6.408	16.958	2.242	13.302	1.826	0.612	2.558	0.029	0.646	0.286
L18-L1.d	46.704	6.658	42.117	9.160	23.491	2.877	15.638	2.043	0.862	3.169	0.036	0.384	0.193
L18-L2.d	51.569	7.298	48.511	11.162	22.893	1.860	6.783	0.573	0.848	1.140	0.020	0.095	0.076
L28-.d	20.892	4.073	33.082	8.479	26.132	3.809	23.269	2.904	1.441	1.847	0.029	0.175	0.099
L28-C1A-.d	9.466	1.654	12.593	3.100	9.299	1.347	8.354	1.033	0.717	2.633	0.027	0.080	0.061
L28-C1A-1.d	42.423	6.894	49.887	12.107	32.040	3.670	17.736	1.793	0.496	1.265	0.027	0.022	0.142
L28-C3A.d	10.689	1.821	13.469	3.211	9.688	1.478	10.356	1.428	0.630	2.794	0.079	1.529	1.863
L28-C3B.d	4.448	0.865	7.617	2.127	8.215	1.790	17.486	2.890	0.443	2.196	0.040	1.758	2.691
L28-.d	39.337	6.436	46.982	11.773	32.526	4.114	23.491	2.850	0.416	0.997	0.025	0.018	0.071
L30-L1.d	5.880	0.849	5.352	1.187	3.016	0.403	2.307	0.327	0.716	2.808	0.026	0.243	0.196
L30-L2.d	4.226	0.475	2.405	0.467	1.126	0.160	0.848	0.103	2.043	4.726	0.334	0.517	1.307
L43-C1A.d	12.649	2.209	17.041	4.434	14.053	2.184	15.749	2.292	0.541	2.277	0.060	1.974	1.197
L43-C1B.d	9.661	1.696	12.677	3.239	9.174	1.237	7.325	0.904	0.360	1.539	0.061	0.025	0.029
L43-C1c.d	8.521	1.478	11.746	3.072	9.897	1.668	12.580	1.877	0.392	1.956	0.057	0.603	0.403
L811-C2A-.d	20.850	3.183	21.962	5.365	14.929	1.988	11.732	1.487	1.751	2.933	0.052	0.231	0.086
L811-C2A-.d	63.801	9.702	69.500	17.292	42.965	4.087	14.512	0.981	1.051	1.029	0.261	<DL	0.022
L811-C2B-.d	5.630	0.945	6.978	1.682	5.240	0.892	7.589	1.371	0.435	3.447	0.197	4.809	11.273
L811-C2B-.d	30.024	4.490	31.275	7.186	20.433	3.044	19.641	2.601	0.712	3.962	0.062	0.487	0.204
L811-.d	44.480	5.894	38.920	9.077	18.932	1.212	3.072	0.157	0.541	0.685	0.043	0.012	0.013
m2a1-c1.d	6.922	0.656	2.683	0.382	0.613	0.047	0.121	0.007	0.123	2.267	0.018	0.013	0.043
m2a1-c1a.d	6.616	0.594	2.238	0.328	0.535	0.036	0.097	0.005	0.125	2.369	0.019	0.019	0.046
m2a1-c3.d	17.097	2.239	11.481	2.056	3.836	0.272	0.744	0.045	0.086	2.794	0.015	0.015	0.041
m2b-2a-c1.d	15.693	2.291	12.635	2.446	4.976	0.381	0.945	0.041	0.449	3.531	0.042	2.307	1.626
m2b-2a-c1b.d	6.561	0.812	3.962	0.670	1.158	0.078	0.160	0.006	0.129	2.975	0.020	0.316	0.384
m2b-2a-c1c.d	14.470	2.135	12.079	2.381	4.768	0.373	0.927	0.043	0.253	3.697	0.028	1.307	0.998
m2b-2a-c3.d	3.684	0.455	2.104	0.374	0.767	0.066	0.210	0.012	0.152	3.100	0.023	0.364	0.441
m2b-2a-c3a.d	5.491	0.600	2.659	0.389	0.712	0.056	0.138	0.009	0.166	3.050	0.022	0.249	0.313
m3d2-c1.d	0.407	0.055	0.279	0.053	0.124	0.016	0.114	0.014	0.075	2.149	0.112	<DL	0.013
m3d2-c2.d	2.363	0.299	1.339	0.263	0.556	0.062	0.285	0.036	0.069	1.865	0.104	<DL	0.018

Appendix 1.4B (continued)

Source_file	Gd (ppm)	Tb (ppm)	Dy (ppm)	Ho (ppm)	Er (ppm)	Tm (ppm)	Yb (ppm)	Lu (ppm)	Ta (ppm)	Pb (ppm)	Bi (ppm)	Th (ppm)	U (ppm)
m3d2-c3.d	3.364	0.418	1.886	0.309	0.637	0.066	0.322	0.041	0.098	2.480	0.425	0.070	0.043
m3d-qz-c3.d	1.125	0.263	2.312	0.705	2.463	0.481	4.003	0.592	0.910	13.233	0.973	2.057	29.885
m3d-qz-c3a.d	2.280	0.474	3.600	0.927	3.364	0.610	4.768	0.692	0.710	12.093	0.905	2.850	22.518
mt09b-0.d	12.635	1.658	8.924	1.796	4.573	0.548	2.989	0.393	0.125	3.002	0.037	0.639	0.292
mt09b-0.d	19.488	2.585	14.623	3.072	7.756	0.912	5.324	0.699	0.146	3.336	0.043	4.128	2.252
mt09b-0a.d	12.746	1.647	8.952	1.801	4.308	0.455	1.992	0.208	0.153	2.758	0.039	1.334	1.208
mt09b-c1.d	19.974	2.635	14.748	3.030	7.339	0.834	4.017	0.482	0.173	3.753	0.061	2.391	1.793
mt09b-c4.d	13.094	1.753	9.369	1.917	4.629	0.531	2.641	0.292	0.161	3.461	0.040	0.592	0.555
mt09b-c4.d	10.689	1.453	7.728	1.521	3.572	0.381	1.920	0.202	0.135	2.794	0.034	0.431	0.304
mt09b-c4a.d	18.904	2.572	14.734	3.169	7.937	1.030	5.991	0.816	0.388	3.836	0.058	2.947	2.377
mt09b-c4a.d	20.308	2.808	15.429	3.197	8.145	0.960	5.282	0.630	0.168	3.406	0.042	3.934	2.182
MT161-0.d	4.351	0.949	6.102	1.209	3.711	0.742	6.158	0.872	7.172	8.187	0.074	2.016	3.030
MT161-0.d	3.823	0.720	4.712	0.959	2.891	0.555	4.448	0.612	4.156	6.783	0.022	0.389	0.945
MT161-0a.d	2.808	0.559	3.906	0.756	2.433	0.538	5.463	0.833	2.877	8.173	0.150	3.072	7.228
MT161-0a.d	7.381	1.514	9.897	1.807	5.379	0.926	6.992	0.847	8.729	7.784	0.022	0.352	0.542
MT161-0b.d	3.572	0.792	5.379	1.029	3.169	0.641	5.185	0.695	10.842	9.118	0.053	0.792	1.529
MT161-0b.d	1.988	0.407	2.708	0.532	1.690	0.370	3.475	0.509	10.703	9.939	0.132	2.766	6.728
MT161-c2.d	5.852	1.152	7.492	1.472	4.365	0.906	8.326	1.487	3.280	15.012	0.250	1.738	6.186
MT161-c2.d	2.502	0.531	3.558	0.694	2.168	0.537	5.602	1.036	4.128	17.625	0.478	3.072	18.209
MT161-c6.d	5.741	1.147	7.617	1.542	4.684	0.876	6.533	0.845	3.528	7.965	0.037	0.278	0.499
MT161-c6a.d	8.271	1.585	10.342	1.974	5.741	1.084	9.299	1.473	4.059	7.951	0.054	1.710	5.699
MT161-c6b.d	4.948	0.974	6.589	1.332	3.850	0.677	5.115	0.790	1.118	6.700	0.044	0.158	0.459
MT161-c6b.d	2.043	0.436	2.891	0.612	2.057	0.595	7.784	1.478	2.669	10.786	0.409	7.548	31.275
MT231-0.d	30.024	4.462	25.854	5.060	11.885	1.329	6.366	0.714	1.807	4.073	0.031	0.824	0.784
MT231-c1.d	12.663	1.706	9.772	2.002	4.962	0.578	2.947	0.353	0.350	3.128	0.040	0.653	0.792
MT231-c1a.d	23.491	3.364	19.321	3.767	8.479	0.904	4.309	0.470	1.362	3.137	0.031	0.681	0.806
MT231-c1b.d	9.424	1.236	6.797	1.329	2.961	0.304	1.268	0.124	0.152	2.847	0.065	0.046	0.084
MT231-c2.d	6.255	1.001	5.977	1.209	3.294	0.455	3.128	0.470	3.906	6.283	0.083	0.449	2.711
MT231-c2.d	1.599	0.220	1.473	0.288	0.977	0.150	1.307	0.214	0.425	5.004	0.099	0.371	0.606
MT231-c2a.d	3.836	0.602	3.572	0.746	2.071	0.354	2.863	0.493	0.246	4.587	0.092	0.487	0.994
MT231-c4.d	6.589	0.933	5.574	1.162	3.684	0.621	4.879	0.856	0.324	3.600	0.033	0.177	0.400
MT231-c4.d	9.800	1.261	6.783	1.365	3.002	0.282	1.140	0.116	0.142	2.585	0.034	0.065	0.104

Appendix 1.4B (continued)

Source_file	Gd (ppm)	Tb (ppm)	Dy (ppm)	Ho (ppm)	Er (ppm)	Tm (ppm)	Yb (ppm)	Lu (ppm)	Ta (ppm)	Pb (ppm)	Bi (ppm)	Th (ppm)	U (ppm)
MT231-c4a.d	12.816	1.657	8.924	1.815	4.101	0.418	1.863	0.165	0.171	2.947	0.033	0.181	0.235
MT231-c5.d	4.476	0.660	3.753	0.810	2.306	0.368	3.100	0.580	0.525	5.032	0.099	0.560	0.841
MT231-c5a.d	3.406	0.557	3.392	0.755	2.460	0.446	3.558	0.500	0.713	5.226	0.076	0.271	0.666
MT-Po1-1.d	1.309	0.175	1.051	0.217	0.670	0.103	0.751	0.110	0.542	6.853	0.270	0.385	2.613
MT-Po1-2.d	0.081	0.012	0.071	0.015	0.053	0.013	0.111	0.024	2.540	10.745	0.386	0.406	10.495
MT-Po1-3.d	0.300	0.054	0.238	0.051	0.163	0.034	0.350	0.065	0.655	6.797	1.136	2.075	58.658
MT-Po1-5.d	0.325	0.034	0.188	0.042	0.120	0.024	0.167	0.032	0.710	7.186	0.834	1.808	46.843
MT-Po1-6.d	0.254	0.042	0.209	0.039	0.104	0.018	0.161	0.022	0.493	6.658	0.455	0.869	21.128
MARN-C1a.d	25.187	3.194	17.514	3.711	8.243	0.776	3.183	0.295	0.286	1.298	0.010	<DL	0.032
MARN-C1b.d	22.796	3.241	17.625	3.685	8.118	0.795	3.072	0.285	0.325	1.821	0.009	<DL	0.035
MARN-C1c.d	22.810	3.080	17.542	3.778	8.118	0.748	2.808	0.277	0.318	1.376	0.013	<DL	0.040
MARN-C1d.d	24.937	3.386	17.917	3.892	8.479	0.838	3.322	0.341	0.281	1.315	<DL	0.019	0.046
MARN-C1e.d	22.601	3.100	17.278	3.681	8.090	0.758	2.766	0.295	0.320	2.474	0.030	<DL	0.031
MARN-C2a.d	24.339	3.446	18.320	3.807	8.159	0.717	2.335	0.161	0.316	3.753	<DL	<DL	0.071
MARN-C2c.d	38.920	5.143	26.827	5.268	10.647	0.935	3.711	0.300	0.257	1.333	0.016	<DL	0.043
MARN-C2d.d	47.955	5.908	30.663	6.047	12.746	1.125	4.170	0.367	0.249	1.309	0.016	0.020	0.032
MARN-C2e.d	30.163	3.684	18.292	3.586	7.353	0.645	2.530	0.228	0.238	1.540	0.018	<DL	0.021
MARN-C3b.d	40.352	5.296	28.717	5.727	12.329	1.113	3.989	0.309	0.254	1.304	0.014	<DL	0.026
CA16B-1.d	3.600	0.407	2.196	0.396	1.073	0.146	0.920	0.094	1.365	13.136	3.823	0.320	6.811
CA16B-10.d	2.850	0.304	1.480	0.296	0.662	0.087	0.448	0.067	1.165	12.719	14.359	0.206	6.533
CA16B-2.d	3.030	0.321	1.526	0.263	0.580	0.075	0.443	0.041	1.380	9.202	0.139	0.107	0.125
CA16B-3.d	2.766	0.313	1.384	0.256	0.603	0.076	0.491	0.056	1.300	10.369	0.111	0.057	0.120
CA16B-4.d	4.184	0.474	2.822	0.487	1.230	0.306	1.084	0.108	1.379	9.661	0.361	0.220	5.004
CA16B-5.d	3.016	0.307	1.622	0.303	0.720	0.088	0.499	0.047	1.510	14.734	11.259	0.138	0.352
CA16B-6.d	3.517	0.396	1.975	0.370	0.927	0.125	0.677	0.060	1.337	15.290	8.062	0.165	2.433
CA16B-7.d	3.225	0.366	1.959	0.361	0.842	0.109	0.564	0.058	1.307	11.092	6.533	0.149	5.143
CA16B-8.d	3.406	0.386	2.003	0.381	0.979	0.115	0.626	0.060	1.194	10.731	0.236	0.236	12.510
RG196-1.d	12.343	1.589	9.230	1.897	5.060	0.681	4.240	0.600	0.438	4.601	0.011	0.024	0.035
RG196-2.d	11.690	1.479	7.826	1.642	4.267	0.609	4.101	0.534	0.395	10.453	0.013	0.195	0.133
RG196-3.d	18.682	2.566	14.234	3.336	9.563	1.576	10.759	1.307	0.325	4.601	<DL	0.143	0.186
RG196-4.d	17.417	2.426	13.664	2.950	8.326	1.205	6.700	0.637	0.313	5.935	0.008	0.058	0.067
RG196-5.d	19.947	2.805	15.360	3.136	8.104	1.051	5.254	0.609	0.607	4.059	0.013	0.027	0.059

Appendix 1.4B (continued)

Source_file	Gd (ppm)	Tb (ppm)	Dy (ppm)	Ho (ppm)	Er (ppm)	Tm (ppm)	Yb (ppm)	Lu (ppm)	Ta (ppm)	Pb (ppm)	Bi (ppm)	Th (ppm)	U (ppm)
RG196-6.d	19.446	2.717	15.054	3.168	8.660	1.208	6.325	0.659	0.363	6.005	0.013	0.129	0.087
RG196-7.d	15.526	2.235	12.218	2.566	7.061	0.970	5.741	0.669	0.335	5.296	<DL	0.067	0.097
RG196-8.d	16.138	2.364	12.885	2.655	6.881	0.906	5.296	0.542	0.348	5.393	0.006	0.107	0.120
RG196-9.d	18.195	2.684	15.054	3.280	9.383	1.357	8.132	0.954	0.414	6.241	0.016	0.145	0.097
SL1223-C2-1.d	64.357	9.174	49.345	8.993	20.141	2.274	11.787	1.411	1.204	4.448	0.093	2.766	1.968
SL1223-C2-2.d	12.496	1.528	8.827	1.726	4.740	0.801	6.477	1.052	0.709	4.309	0.147	5.324	6.130
SL1223-C3-2.d	9.077	1.380	7.325	1.384	2.870	0.252	1.012	0.103	0.414	1.849	6.366	0.017	<DL
SL1223-C4-1.d	6.380	1.227	8.535	2.116	5.421	0.641	2.641	0.202	0.442	1.216	0.125	<DL	0.004
SL1223-C4-2.d	20.294	3.155	18.765	3.823	9.424	1.108	6.158	0.820	0.434	1.703	0.026	0.051	0.075
SL1223-C4-3.d	17.653	3.194	22.615	5.546	14.623	1.647	7.145	0.584	0.406	1.211	0.417	<DL	0.037
SL1223-C5-1.d	9.563	1.850	14.331	3.610	10.133	1.225	5.643	0.562	0.404	2.029	0.029	0.018	0.031
SL1223-C5-2.d	7.840	1.465	10.689	2.563	6.783	0.760	3.100	0.257	0.393	1.724	0.389	0.015	<DL
SL8A-1.d	13.372	1.384	6.144	0.983	1.387	0.063	0.103	<DL	0.550	0.710	0.010	0.039	0.973
SL8A-3.d	15.068	1.657	7.659	1.322	2.020	0.108	0.221	0.014	0.475	0.713	0.012	0.035	0.051
SL8A-4.d	11.815	1.297	5.671	0.935	1.403	0.070	0.110	<DL	0.527	0.945	2.224	0.027	3.058
SL8A-5.d	5.491	0.520	2.057	0.348	0.510	0.033	0.082	<DL	0.584	0.667	0.570	0.028	0.005
SL8A-7.d	4.559	0.346	1.414	0.189	0.361	0.021	0.081	0.015	0.427	1.084	0.834	0.024	0.004
SD212-C1c.d	34.945	4.712	25.354	4.726	7.228	0.395	0.702	0.021	0.320	5.101	0.037	3.892	6.172
SD212-C1c1.d	39.476	5.087	27.383	5.074	8.674	0.421	0.796	0.030	0.164	5.546	<DL	0.791	2.289
SD212-C2a.d	24.283	3.382	19.126	3.475	6.060	0.370	0.737	0.047	0.202	5.324	0.038	2.141	4.392
SD212-C2b.d	20.155	2.827	16.624	2.947	4.698	0.259	0.541	0.023	0.342	5.616	<DL	1.013	1.911
SD212-C2e.d	21.809	3.037	16.666	3.139	5.352	0.328	0.612	0.026	0.133	4.823	0.033	0.571	1.555
SD212-C2f.d	21.615	2.979	16.166	2.933	5.143	0.329	0.702	0.026	0.139	5.185	<DL	0.727	1.625
SD212-C2g.d	20.947	2.822	16.207	2.905	4.921	0.288	0.567	0.018	0.136	5.115	0.021	0.495	1.383
SY18A-1.d	2.182	0.138	0.418	0.031	0.050	0.006	0.019	0.002	0.837	4.670	0.257	0.113	0.099
SY18A-2.d	2.349	0.259	0.867	0.099	0.177	0.020	0.090	0.012	0.728	5.935	0.417	0.054	0.709
SY18A-3.d	3.503	0.455	2.141	0.293	0.527	0.054	0.268	0.021	0.835	1.960	0.473	0.138	0.022
SY18A-4.d	2.488	0.213	0.719	0.070	0.110	0.015	0.135	0.010	0.784	10.286	1.877	0.096	0.165
SY18A-5.d	1.229	0.104	0.222	0.024	0.039	0.004	0.021	0.003	0.692	10.008	1.209	0.074	0.070
SZY18B-1.d	2.794	0.228	0.852	0.106	0.188	0.026	0.100	0.009	0.637	25.298	8.340	0.099	0.195
SZY18B-C1-1.d	0.311	0.048	0.190	0.022	0.030	0.003	<DL	0.005	0.548	0.556	0.023	<DL	0.042
SZY18B-C1-2.d	0.418	0.077	0.328	0.034	0.047	0.009	0.025	<DL	0.582	0.765	0.017	0.010	0.019

Appendix 1.4B (continued)

Source_file	Gd (ppm)	Tb (ppm)	Dy (ppm)	Ho (ppm)	Er (ppm)	Tm (ppm)	Yb (ppm)	Lu (ppm)	Ta (ppm)	Pb (ppm)	Bi (ppm)	Th (ppm)	U (ppm)
SZY18B-C1-3.d	0.017	0.002	0.020	0.003	0.006	<DL	<DL	<DL	0.557	1.251	0.016	0.009	<DL
SZY18B-C1-4.d	<DL	0.003	0.013	<DL	0.004	<DL	<DL	<DL	0.559	0.473	0.008	<DL	0.014
SZY18C-1.d	1.030	0.026	0.015	<DL	0.005	<DL	<DL	0.002	0.570	2.363	0.029	0.054	0.017
SZY18C-2.d	1.095	0.031	0.051	0.006	0.008	0.083	<DL	0.002	0.531	1.967	0.035	0.033	0.019
SZY18C-3.d	37.252	4.031	18.431	3.062	5.699	0.525	2.053	0.213	0.976	2.573	0.031	0.128	0.106
V67-C2A.d	7.576	1.307	8.298	1.751	4.976	0.774	5.699	0.865	1.133	3.289	0.841	0.443	6.533
V67-C4A.d	2.335	0.348	2.377	0.571	1.835	0.320	2.697	0.442	0.592	3.169	0.033	0.398	6.950
V67-C4B.d	8.493	1.250	8.257	2.038	6.102	0.838	5.004	0.587	0.680	2.071	0.032	0.039	3.948
V67-C4C.d	2.724	0.377	2.377	0.542	1.460	0.171	0.927	0.119	1.270	4.337	0.890	0.334	9.522
V74-C1.d	16.124	2.572	15.985	3.225	8.187	1.056	5.963	0.673	1.293	2.627	0.870	0.101	0.256
V74-C1A.d	32.095	5.477	39.476	9.313	28.745	4.504	29.663	3.878	0.556	2.460	0.164	0.196	0.856
V74-C2A.d	14.581	2.580	18.515	4.253	14.470	2.762	22.629	3.236	0.657	2.396	0.213	1.739	0.414
V74-C2B.d	35.501	6.255	45.967	10.995	35.181	5.727	39.295	5.393	0.559	2.641	0.424	0.109	0.450
V74-C2C.d	10.675	1.863	13.316	3.016	9.994	1.842	14.651	2.082	0.616	2.502	0.243	1.126	0.293
V75-C1.d	15.207	2.016	12.246	2.683	5.921	0.541	2.196	0.199	0.245	2.042	0.099	0.007	0.052
V75-C3.d	14.136	1.756	10.036	1.854	3.002	0.195	0.778	0.083	0.270	1.209	0.152	0.017	0.285
V75-C4.d	10.898	1.487	9.188	1.974	4.907	0.553	3.030	0.402	0.262	1.761	0.170	<DL	0.057
V75-C5.d	42.256	6.700	44.063	9.674	26.827	3.753	24.603	3.253	0.872	6.422	1.307	0.079	0.063
V75-C5.d	3.684	0.524	3.044	0.657	1.655	0.221	1.432	0.202	0.243	1.974	0.220	0.006	0.010
V75-C5.d	16.722	2.155	12.274	2.572	6.144	0.716	4.184	0.566	0.247	2.224	2.919	0.005	0.185
V75-C5.d	5.699	0.792	4.796	0.963	2.488	0.318	1.904	0.256	0.264	1.890	0.145	<DL	0.017
V75-C5.d	42.951	6.908	45.592	10.328	27.383	3.558	21.406	3.128	0.656	3.128	0.057	0.018	0.061
V75-C5B.d	17.653	2.572	15.985	3.628	9.341	1.154	6.755	0.917	0.331	2.099	0.681	0.017	0.036
V75-C6B.d	13.316	1.968	12.732	3.058	8.257	1.013	5.616	0.660	0.263	1.877	1.168	0.007	0.041
V75-C7.d	7.881	1.111	6.742	1.494	3.823	0.471	2.822	0.375	0.250	2.294	0.820	<DL	0.016
XY199-1.d	1.037	0.030	0.047	0.005	<DL	<DL	<DL	<DL	0.541	3.475	0.029	0.020	0.017
XY199-2.d	0.981	0.028	0.051	0.007	0.006	<DL	<DL	<DL	0.575	113.980	6.533	0.016	0.031
XY199-3.d	1.426	0.058	0.107	0.015	0.018	<DL	0.028	0.003	0.678	3.670	0.043	0.021	0.033
XY199-4.d	15.804	1.963	10.773	2.152	5.226	0.651	3.517	0.487	0.673	2.836	0.024	0.154	0.097
XY199-5.d	24.631	2.983	14.887	2.881	6.311	0.632	3.141	0.406	0.860	3.322	0.389	0.067	0.037

Appendix 1.4B (continued)

Source_file	Gd (ppm)	Tb (ppm)	Dy (ppm)	Ho (ppm)	Er (ppm)	Tm (ppm)	Yb (ppm)	Lu (ppm)	Ta (ppm)	Pb (ppm)	Bi (ppm)	Th (ppm)	U (ppm)
XY199-6.d	5.296	0.442	2.085	0.364	0.666	0.081	0.320	0.046	0.819	2.850	0.018	0.038	0.196
XY199-7.d	1.234	0.046	0.076	0.013	0.013	<DL	<DL	<DL	0.720	2.690	0.029	0.027	0.250
XY199-8.d	18.737	2.242	11.732	2.243	5.463	0.613	2.961	0.384	0.664	4.490	0.612	0.122	0.046
XY199-9.d	16.027	1.828	8.840	1.710	3.850	0.425	2.099	0.257	0.651	3.336	0.149	0.046	0.042
ZX25B-1-1.d	0.024	0.006	0.024	0.002	0.009	<DL	<DL	<DL	0.681	1.578	0.667	<DL	0.195
ZX25B-1-2.d	0.025	0.003	0.020	<DL	0.006	<DL	<DL	<DL	0.689	1.668	0.053	<DL	0.040
ZX25B-2.d	0.021	0.057	<DL	0.003	<DL	<DL	<DL	<DL	0.676	1.222	0.076	<DL	0.006
ZX25B-3.d	<DL	<DL	<DL	<DL	<DL	<DL	<DL	<DL	0.681	2.502	0.068	<DL	<DL
ZX25B-4.d	0.190	0.031	0.156	0.035	0.097	0.009	0.076	0.007	0.730	1.454	0.075	0.027	0.086
ZX25B-5.d	0.064	0.012	0.056	0.018	0.044	0.003	0.017	0.002	0.664	1.505	0.058	0.022	0.021
ZX25B-6.d	0.118	0.023	0.138	0.029	0.055	0.007	0.025	0.006	0.746	1.526	0.070	<DL	0.028
ZX25B-7.d	0.051	0.003	0.023	0.031	0.006	0.008	<DL	<DL	0.703	2.502	0.075	0.051	<DL
ZX25B-8.d	0.042	0.006	0.025	0.010	0.019	<DL	<DL	<DL	0.666	1.529	0.077	<DL	<DL
ZX25B-9.d	0.019	<DL	0.008	0.003	<DL	<DL	<DL	<DL	0.682	1.473	0.065	0.009	<DL
ZX28-1.d	0.082	0.011	0.068	0.038	0.013	0.021	0.016	0.002	0.350	2.446	0.032	<DL	0.332
ZX28-2.d	0.231	0.042	0.093	0.010	0.029	0.002	0.014	0.002	0.310	2.054	0.167	0.019	0.108
ZX28-3.d	0.196	0.013	0.097	0.010	0.027	0.003	0.013	0.001	0.328	2.385	0.256	<DL	0.060
ZX28-4.d	0.278	0.026	0.143	0.022	0.044	0.006	0.033	0.004	0.324	2.460	0.093	0.041	0.253
ZX28-5.d	0.046	0.003	0.041	0.004	0.008	0.002	<DL	0.002	0.314	1.765	0.050	0.038	0.005
ZX28-6.d	0.285	0.026	0.156	0.018	0.057	0.004	0.049	0.002	0.342	1.967	0.050	0.070	0.364
ZX28-7.d	0.200	0.016	0.101	0.012	0.026	0.002	0.010	<DL	0.300	2.724	0.170	0.024	0.042

Appendix 1.4B (continued)

Source_file	ΣREE	Eu anomaly	(La/Sm) cn	(Gd/Lu) cn
Min DL				
Max DL				
BF2-1.d	166.358	0.67	0.22	9.58
BF2-2.d	175.925	0.70	0.20	11.52
BF2-3.d	109.831	0.56	0.26	11.19
BF2-4.d	115.640	0.54	0.20	9.01
BF2-L1.d	183.266	0.73	0.18	9.01
BF2-L1.d	153.210	0.66	0.17	10.82
BF2-L2.d	167.328	0.77	0.16	10.91
BF2-L2.d	145.963	0.63	0.15	12.54
CN1-L1.d	36.058	0.78	0.47	49.81
CN1-L2.d	29.468	0.77	0.36	33.89
CN1-L2.d	26.077	0.77	0.38	33.45
CN1-L3.d	28.060	0.75	0.42	34.93
CN1-L4.d	30.199	0.74	0.61	45.35
CN1-L5.d	21.236	0.72	0.59	24.62
CN1-L6.d	9.358	0.68	0.64	5.23
CN1-L7.d	17.998	0.77	0.61	25.15
CN2-L1.d	1.659	0.29	0.42	2.09
CN2-L1.d	1.625	0.36	0.38	2.26
CN2-L2.d	1.817	0.34	0.44	8.33
CN2-L2.d	1.581	0.48	0.45	5.13
CN2-L3.d	1.675	0.26	0.43	4.16
CN2-L4.d	1.266	0.35	0.40	4.54
CN2-L5.d	1.592	0.31	0.42	4.01
CN2-L6.d	1.659	0.49	0.43	6.30
CN2-L6.d	1.523	0.34	0.42	11.23
CN2-L7.d	1.854	0.39	0.44	8.94
CEZ-1.d	259.121	6.64	1.75	3.54
CEZ-1.d	57.268	1.50	0.60	0.94
cez-bt2-0.d	450.865	0.35	1.55	6.60
cez-bt2-c1.d	113.682	1.55	1.09	9.80
cez-bt2-c1.d	358.673	0.32	1.06	7.44
cez-bt2-c1b.d	330.372	0.51	1.72	3.52
cez-bt2-c2.d	443.862	0.35	1.69	3.22
cez-bt2-c3b.d	396.534	0.13	0.94	75.45
cez-bt2-c3b.d	395.490	0.30	1.45	3.68
cez-bt2-c4.d	472.739	0.22	0.75	3.10
cez-bt2-c4.d	417.106	0.31	1.02	6.23
cez-gr-c1.d	101.668	0.57	0.63	46.52
cez-gr-c1b.d	100.078	0.81	0.88	40.76
cez-gr-c1b.d	111.594	0.60	0.21	37.05
cez-gr-c1b.d	105.412	0.62	0.47	50.61
cez-gr-c1c.d	109.827	0.51	0.49	35.69
cez-gr-c2.d	87.639	0.74	1.75	25.61
cez-gr-c2a.d	101.102	0.55	1.86	51.91
cez-gr-c2a.d	105.288	0.56	1.05	32.52
cez-gr-c3.d	77.908	0.68	0.79	113.63
cez-gr-c3.d	91.428	0.53	1.02	136.65
cez-po1-c1b.d	96.527	14.35	1.07	95.04
cez-po1-c1b.d	49.329	10.12	1.47	69.82
cez-po1-c2.d	287.017	33.87	9.85	0.38
cez-po1-c2.d	257.524	43.54	11.83	0.29
cez-po1-c3.d	64.548	9.86	1.65	22.68
cez-po1-c3.d	49.767	2.71	1.23	10.62
cez-po1-c3a.d	109.233	9.81	2.21	7.48
cez-po1-c3a.d	37.136	2.20	1.98	94.04
cez-po1-c5.d	98.085	27.25	3.33	9.89
cez-po1-c5.d	97.712	2.92	4.34	79.46
cez-po1-c6.d	154.318	2.22	1.11	0.87
cez-po1-c6.d	29.823	5.40	4.61	7.59
cez-po1-c6.d	114.730	3.95	1.24	168.05
cez-po1-c6b.d	80.940	4.04	1.48	24.51
cez-po1-c6b.d	98.575	1.28	0.63	56.50

Appendix 1.4B (continued)

Source_file	ΣREE	Eu anomaly	(La/Sm) cn	(Gd/Lu) cn
cop-poA-c1-1.d	1491.317	0.14	0.43	1.29
cop-poA-c1-3.d	3013.006	0.05	0.37	2.04
cop-poA-c2-1.d	3581.752	0.07	0.51	2.35
cop-poA-c3-1.d	3127.208	0.09	0.55	1.57
cop-poA-c3-3.d	2850.904	0.10	0.32	1.79
cop-poA-c4-1.d	3111.001	0.22	0.54	1.22
cop-poA-c5-1.d	4433.085	0.22	0.55	1.71
cop-poA-c5-2.d	3638.964	0.17	0.46	1.66
cop-poB-c8-1.d	661.437	0.36	1.68	1.46
cop-poB-c5-1.d	905.738	0.09	0.31	2.92
cop-poB-c5-2.d	780.263	0.18	0.24	2.03
cop-poB-c7-1.d	175.557	1.61	0.47	1.50
cop-poB-c7-2.d	293.825	1.59	0.77	1.46
cop-poB-c3-1.d	460.154	0.23	0.20	2.20
cop-poB-c3-2.d	764.625	0.14	0.18	1.83
cop-poB-c3-3.d	316.514	0.35	0.39	1.93
cop-sc-c3-1.d	773.293	10.01	14.36	0.26
cop-sc-c1a-1.d	185.382	1.21	0.83	3.20
cop-sc2-c2.d	154.376	0.91	1.06	4.73
cop-sc2-c4.d	624.221	3.29	5.22	0.41
cop-sc2-c2-2.d	1927.749	0.74	3.72	1.94
cop-poB-c5b.d	1195.622	0.17	0.56	2.29
cop-qz-c4.d	810.231	0.73	1.16	1.12
cop-qz-c4b.d	699.504	0.79	0.99	0.86
cop-po-sq1.d	642.208	0.26	0.36	2.38
cop-po-sq2.d	1027.877	0.38	0.40	1.18
cop-sc-sq3.d	725.816	0.37	0.31	1.55
2420-776A-2.d	487.973	3.43	24.46	2.42
2420-776A-3.d	316.995	1.66	13.72	2.51
2420-776A-4.d	250.893	2.01	28.88	4.10
2420-776A-5.d	302.388	1.73	19.19	4.77
2420-776B-1.d	508.106	2.93	26.52	2.61
2420-776B-2.d	351.606	1.46	17.91	4.70
2420-776B-3.d	378.041	1.67	16.68	2.77
2420-776B-4.d	260.078	1.77	18.69	3.34
2420-776B-5.d	397.632	2.17	15.91	4.03
2420-848C-1.d	199.968	1.15	9.64	0.44
2420-848C-2.d	224.534	1.18	8.11	0.40
2420-848C-3.d	369.718	1.07	7.35	0.43
2420-848C-4.d	513.779	1.23	7.39	0.55
JIAMA-1.d	73.072	0.89	21.10	0.67
JIAMA-3.d	78.085	1.27	10.86	0.49
JIAMA-4.d	69.981	1.14	6.50	0.52
JIAMA-5.d	62.390	1.17	9.90	0.50
JIAMA-6.d	68.458	0.79	17.08	0.58
KR65-1.d	109.952	0.74	41.46	41.83
KR65-2.d	95.715	0.96	19.84	48.37
KR65-3.d	124.188	0.26	116.42	35.00
KR65-4.d	78.500	0.52	42.24	22.15
KR65-5.d	101.842	0.68	70.98	42.92
KR65-6.d	90.171	0.60	55.09	29.07
KR66-0.d	257.409	1.18	47.52	44.48
KR66-C1-1a.d	291.902	0.83	39.36	49.79
KR66-C1-2a.d	208.580	1.03	32.28	84.80
KR66-C3-1a.d	265.074	1.23	31.96	115.63
KR66-C3-1a.d	251.776	1.01	40.35	104.51
KR66-C3-2a.d	250.045	1.21	27.36	130.57
KR66-C3-2a.d	261.610	1.04	33.62	79.23
KR66-C3-2b.d	265.615	1.07	35.67	58.66
KR66-C3-2b.d	255.563	1.10	33.24	51.91
KR98A-C1-1.d	335.333	0.64	2.18	6.92
KR98A-C1-2.d	460.861	0.46	2.17	5.99
KR98A-C2-1.d	623.016	0.76	1.65	4.95
KR98B-C2-1.d	178.693	0.28	1.35	4.85
KR98C-1-1.d	522.348	0.38	2.05	5.71

Appendix 1.4B (continued)

Source_file	ΣREE	Eu anomaly	(La/Sm) cn	(Gd/Lu) cn
KR98C-1-2.d	2740.039	0.24	2.59	14.22
KR98C-2-1.d	1024.558	0.23	2.73	18.31
DMGr-0a.d	224.760	1.19	55.36	73.65
DMGr-0b.d	236.032	1.54	106.00	26.57
DMGr-0c.d	166.378	1.80	32.86	29.02
DMGr-C1b.d	220.798	1.44	49.86	47.85
DMGr-C1c.d	244.288	1.05	31.09	48.36
DMGr-c1e.d	245.461	0.91	70.15	18.21
DMGr-C2.d	247.115	0.96	48.00	16.87
DMGr-c3a.d	182.552	1.09	67.86	22.46
DM-PX-10.d	251.830	1.07	5.49	21.87
DM-PX-3.d	200.622	0.54	11.24	106.69
DM-PX-4.d	225.554	0.47	11.72	91.46
DM-PX-5.d	223.714	0.57	22.09	130.55
DM-PX-6.d	266.816	0.39	22.36	129.78
DM-PX-7.d	278.912	0.41	18.07	97.68
DM-PX-8.d	278.671	0.41	17.11	95.02
DM-PX-9.d	201.613	0.71	14.09	51.10
Ku01-L1.d	512.540	0.85	60.96	470.55
Ku01-L2.d	506.173	0.85	56.66	149.21
Ku01-L3.d	244.940	1.28	30.69	94.96
Ku01-L3.d	241.739	1.20	26.82	489.76
Ku01-L4.d	239.434	1.17	27.52	222.90
Ku01-L5.d	232.561	1.37	24.83	240.76
Ku01-L5.d	236.512	1.20	29.64	569.63
Ku01-L6.d	501.410	0.94	63.58	528.96
Ku01-L6.d	508.527	0.72	71.42	225.81
DPHB-C1.d	62.041	1.51	6.40	10.94
DPHB-C1a.d	272.491	0.58	0.76	96.12
DPHB-C2.d	217.482	0.41	0.36	20.38
DPHB-C2a.d	160.913	0.39	1.01	42.47
DPHB-C2b.d	312.075	0.38	2.61	85.19
DPHB-C2c.d	36.496	0.64	0.34	98.88
DPHB-C3.d	111.013	0.52	1.27	64.23
DPHB-C3a.d	193.540	0.44	1.93	41.80
DPHB-C3b.d	142.409	0.61	1.61	44.85
DPHB-C3c.d	66.989	0.60	2.52	17.25
LBt-C1.d	331.782	1.04	2.37	11.26
LBt-C1a.d	505.027	0.83	1.65	14.11
LBt-C2.d	390.530	0.98	2.10	33.19
LBt-C3.d	486.937	1.16	2.68	58.71
LBt-C4.d	812.260	0.72	2.55	58.58
LBt-C4a.d	698.984	0.69	2.87	325.68
LBt-C5.d	355.055	0.72	0.36	2.85
LBt-C5a.d	546.695	0.73	0.92	14.47
LBt-C5b.d	133.954	1.44	0.69	5.29
LCSA-C1.d	160.051	0.41	0.98	74.92
LCSA-C1a.d	141.051	0.40	0.68	18.81
LCSA-C1a.d	133.796	0.41	0.65	17.76
LCSA-C1a.d	140.788	0.48	0.58	30.59
LCSA-C2a.d	184.539	0.68	1.72	7.26
LCSA-C2c.d	203.609	0.47	1.30	9.11
LCSB-C1.d	179.179	0.53	1.03	7.21
LCSB-C1.d	150.151	0.46	2.13	10.58
LCSB-C1a.d	167.325	0.48	1.66	9.65
LCSB-C4.d	191.024	0.34	1.82	21.06
LCSB-C5.d	195.096	0.42	1.15	11.84
LCSB-C5.d	199.846	0.52	1.96	10.86
LOP2A-C1.d	119.196	1.13	0.20	94.69
LOP2A-C2.d	179.423	1.30	0.28	156.96
LOP2A-C2a.d	94.090	0.98	0.46	88.18
LOP2A-C2b.d	102.011	0.70	0.40	45.00
LOP2A-C2c.d	137.036	1.71	0.90	184.29
LOP2A-C3.d	84.092	0.58	0.27	41.15
LOP2A-C3a.d	70.889	0.99	0.35	56.39

Appendix 1.4B (continued)

Source_file	ΣREE	Eu anomaly	(La/Sm) cn	(Gd/Lu) cn
LOP2A-C3b.d	217.583	0.86	0.38	123.19
LOP2A-C3c.d	93.414	0.96	0.52	137.79
LOP2B-C1.d	105.519	0.65	0.51	72.51
LOP2B-C2.d	159.386	1.61	0.33	134.30
LOP2B-C2a.d	109.326	1.79	0.30	198.34
LOP2B-C2a.d	153.680	1.37	0.53	116.30
LOP2B-C2b.d	136.933	1.20	0.47	79.99
L14-C1.d	161.740	2.98	2.07	2.39
L14-C1.d	354.158	18.68	10.81	0.41
L14-C2A.d	122.845	0.49	1.13	1.57
L14-C2B.d	299.420	6.75	7.87	0.33
L18-C2A.d	346.109	0.38	1.27	2.33
L18-C2c.d	296.595	0.65	1.87	2.05
L18-C3.d	298.598	0.85	2.27	1.69
L18-C4A.d	437.201	0.44	1.53	2.54
L18-L1.d	439.282	0.27	1.23	2.83
L18-L2.d	397.252	0.11	0.95	11.13
L28-.d	231.892	0.92	1.58	0.89
L28-C1A-.d	135.194	1.72	2.03	1.13
L28-C1A-1.d	282.060	0.09	0.48	2.92
L28-C3A.d	228.961	4.01	4.23	0.93
L28-C3B.d	251.894	23.12	20.82	0.19
L28-.d	276.951	0.10	0.64	1.71
L30-L1.d	140.704	0.46	4.85	2.22
L30-L2.d	254.200	0.64	12.39	5.08
L43-C1A.d	294.067	5.55	5.38	0.68
L43-C1B.d	92.115	0.95	1.09	1.32
L43-C1c.d	236.096	4.68	6.28	0.56
L811-C2A-.d	331.682	0.53	2.62	1.73
L811-C2A-.d	376.858	0.04	0.34	8.04
L811-C2B-.d	161.891	7.77	6.81	0.51
L811-C2B-.d	690.456	0.71	4.18	1.43
L811-.d	384.981	0.07	1.33	35.00
m2a1-c1.d	155.952	0.66	0.63	125.62
m2a1-c1a.d	185.866	0.67	1.07	154.83
m2a1-c3.d	94.547	0.47	0.04	46.92
m2b-2a-c1.d	342.109	0.59	2.02	47.46
m2b-2a-c1b.d	185.101	1.15	1.94	135.67
m2b-2a-c1c.d	313.741	0.72	1.70	41.91
m2b-2a-c3.d	200.173	1.33	4.89	37.65
m2b-2a-c3a.d	236.189	0.93	3.78	75.11
m3d2-c1.d	25.162	1.17	10.79	3.66
m3d2-c2.d	51.492	0.53	1.62	8.14
m3d2-c3.d	59.600	0.70	0.81	10.21
m3d-qz-c3.d	109.700	3.36	15.24	0.23
m3d-qz-c3a.d	82.252	1.34	5.26	0.41
mt09b-0.d	289.600	0.29	1.81	3.97
mt09b-0.d	441.995	0.32	1.41	3.45
mt09b-0a.d	310.177	0.35	1.85	7.57
mt09b-c1.d	400.260	0.31	1.22	5.12
mt09b-c4.d	311.656	0.30	1.88	5.54
mt09b-c4.d	263.106	0.26	1.96	6.56
mt09b-c4a.d	497.842	0.19	2.69	2.86
mt09b-c4a.d	482.202	0.32	1.49	3.99
MT161-0.d	181.623	3.22	3.40	0.62
MT161-0.d	161.973	2.03	3.59	0.77
MT161-0a.d	120.391	7.32	4.18	0.42
MT161-0a.d	304.652	0.90	3.30	1.08
MT161-0b.d	162.006	1.99	3.96	0.64
MT161-0b.d	77.630	7.36	3.93	0.48
MT161-c2.d	190.374	6.04	3.91	0.49
MT161-c2.d	115.414	12.15	7.75	0.30
MT161-c6.d	280.897	1.20	4.02	0.84
MT161-c6a.d	264.309	2.14	3.24	0.69
MT161-c6b.d	120.838	1.36	1.80	0.77

Appendix 1.4B (continued)

Source_file	ΣREE	Eu anomaly	(La/Sm) cn	(Gd/Lu) cn
MT161-c6b.d	181.444	20.18	14.92	0.17
MT231-0.d	473.017	0.42	0.78	5.19
MT231-c1.d	313.205	0.64	2.24	4.43
MT231-c1a.d	340.519	0.44	0.77	6.18
MT231-c1b.d	192.339	0.66	1.31	9.38
MT231-c2.d	186.323	1.01	2.61	1.65
MT231-c2.d	62.724	2.26	5.14	0.92
MT231-c2a.d	112.462	1.34	2.74	0.96
MT231-c4.d	232.783	2.28	3.95	0.95
MT231-c4.d	132.795	0.73	0.63	10.40
MT231-c4a.d	275.007	0.70	1.77	9.58
MT231-c5.d	147.436	1.66	3.89	0.95
MT231-c5a.d	96.529	1.23	2.59	0.84
MT-Po1-1.d	54.020	3.16	6.81	1.47
MT-Po1-2.d	11.541	29.52	22.68	0.42
MT-Po1-3.d	35.665	49.33	21.23	0.57
MT-Po1-5.d	33.288	56.32	23.87	1.25
MT-Po1-6.d	26.302	46.03	19.04	1.43
MARN-C1a.d	252.199	0.60	0.66	10.56
MARN-C1b.d	218.494	0.74	0.70	9.89
MARN-C1c.d	213.575	0.75	0.66	10.19
MARN-C1d.d	264.217	0.69	0.74	9.05
MARN-C1e.d	221.545	0.74	0.67	9.48
MARN-C2a.d	208.514	0.73	0.53	18.66
MARN-C2c.d	347.596	0.73	0.47	16.02
MARN-C2d.d	417.227	0.63	0.44	16.15
MARN-C2e.d	288.144	0.60	0.48	16.35
MARN-C3b.d	331.158	0.73	0.39	16.16
CA16B-1.d	183.303	1.71	5.56	4.74
CA16B-10.d	142.163	0.87	5.17	5.28
CA16B-2.d	169.479	1.09	6.14	9.23
CA16B-3.d	162.100	1.11	6.30	6.15
CA16B-4.d	184.528	1.40	5.22	4.77
CA16B-5.d	183.512	0.72	5.70	7.91
CA16B-6.d	154.292	0.81	4.94	7.24
CA16B-7.d	148.308	0.84	4.64	6.83
CA16B-8.d	142.386	0.91	4.21	7.04
RG196-1.d	536.193	0.47	4.65	2.54
RG196-2.d	628.823	0.50	6.54	2.71
RG196-3.d	566.078	0.39	3.06	1.77
RG196-4.d	493.885	0.32	2.69	3.38
RG196-5.d	372.594	0.26	1.56	4.05
RG196-6.d	461.025	0.28	2.29	3.65
RG196-7.d	435.330	0.33	2.48	2.87
RG196-8.d	388.676	0.30	2.41	3.68
RG196-9.d	504.963	0.34	2.64	2.36
SL1223-C2-1.d	1453.983	0.63	2.88	5.64
SL1223-C2-2.d	731.368	4.98	13.34	1.47
SL1223-C3-2.d	55.116	0.54	0.16	10.91
SL1223-C4-1.d	49.587	0.83	0.25	3.91
SL1223-C4-2.d	402.554	0.46	2.48	3.06
SL1223-C4-3.d	145.065	0.76	0.28	3.74
SL1223-C5-1.d	86.730	0.89	0.52	2.10
SL1223-C5-2.d	57.707	0.79	0.25	3.77
SL8A-1.d	96.932	0.95	0.08	303.04
SL8A-3.d	103.141	0.71	0.11	135.34
SL8A-4.d	90.412	0.82	0.12	227.78
SL8A-5.d	96.141	0.97	0.32	109.97
SL8A-7.d	63.395	0.79	0.19	37.89
SD212-C1c.d	440.302	0.51	0.71	205.78
SD212-C1c1.d	476.072	0.50	0.52	160.29
SD212-C2a.d	496.929	0.72	1.50	63.51
SD212-C2b.d	411.253	0.78	1.68	107.96
SD212-C2e.d	347.817	0.77	0.93	102.07
SD212-C2f.d	354.510	0.90	0.91	104.46

Appendix 1.4B (continued)

Source_file	ΣREE	Eu anomaly	(La/Sm) cn	(Gd/Lu) cn
SD212-C2g.d	398.440	0.89	1.33	146.67
SY18A-1.d	133.394	0.08	2.71	129.37
SY18A-2.d	103.276	0.12	2.75	23.47
SY18A-3.d	190.311	0.08	5.82	20.63
SY18A-4.d	142.454	0.11	3.72	30.73
SY18A-5.d	102.889	0.25	5.49	60.70
SZY18B-1.d	165.260	0.18	4.03	40.07
SZY18B-C1-1.d	1.189	0.47	0.09	8.39
SZY18B-C1-2.d	1.989	0.41	0.04	20.91
SZY18B-C1-3.d	0.543	0.21	0.34	3.54
SZY18B-C1-4.d	0.034	0.64	0.13	5.63
SZY18C-1.d	211.460	0.36	367.17	53.88
SZY18C-2.d	176.364	0.35	141.49	69.57
SZY18C-3.d	784.962	0.45	1.49	21.65
V67-C2A.d	223.316	0.90	5.99	1.08
V67-C4A.d	133.564	4.06	19.14	0.65
V67-C4B.d	171.304	0.77	5.61	1.79
V67-C4C.d	70.149	3.75	9.56	2.82
V74-C1.d	271.830	0.20	1.38	2.96
V74-C1A.d	624.847	0.99	2.36	1.02
V74-C2A.d	827.719	2.55	6.16	0.56
V74-C2B.d	744.887	0.69	2.48	0.81
V74-C2C.d	577.160	2.58	6.15	0.63
V75-C1.d	155.021	0.69	2.14	9.46
V75-C3.d	179.487	0.78	2.88	20.95
V75-C4.d	83.549	0.87	0.91	3.35
V75-C5.d	792.175	0.57	1.56	1.61
V75-C5.d	31.322	1.83	1.04	2.26
V75-C5.d	124.839	0.64	0.81	3.65
V75-C5.d	48.251	1.38	0.84	2.75
V75-C5.d	413.942	0.37	0.90	1.70
V75-C5B.d	166.049	0.63	0.90	2.38
V75-C6B.d	100.580	0.84	0.81	2.49
V75-C7.d	58.627	1.08	0.82	2.60
XY199-1.d	192.240	0.15	154.89	830.20
XY199-2.d	174.576	0.28	86.39	701.13
XY199-3.d	209.468	0.39	47.23	60.39
XY199-4.d	543.279	1.35	4.11	4.02
XY199-5.d	668.710	0.60	3.46	7.50
XY199-6.d	297.093	0.75	8.67	14.10
XY199-7.d	192.940	0.42	75.38	361.16
XY199-8.d	592.257	0.94	3.99	6.04
XY199-9.d	577.331	0.87	4.59	7.70
ZX25B-1-1.d	0.909	1.88	13.83	4.48
ZX25B-1-2.d	0.930	7.87	12.71	5.85
ZX25B-2.d	0.602	0.87	6.20	6.04
ZX25B-3.d	0.211	0.53	7.44	1.65
ZX25B-4.d	3.342	1.34	3.97	3.53
ZX25B-5.d	1.878	1.35	9.94	4.74
ZX25B-6.d	2.669	0.89	5.95	2.50
ZX25B-7.d	0.524	1.31	6.84	6.56
ZX25B-8.d	1.431	1.62	16.57	4.09
ZX25B-9.d	0.187	1.62	5.50	2.59
ZX28-1.d	4.093	19.61	4.68	4.34
ZX28-2.d	7.964	9.19	3.56	17.24
ZX28-3.d	6.517	10.48	5.15	17.97
ZX28-4.d	11.179	15.54	5.21	9.16
ZX28-5.d	1.326	18.68	6.13	3.40
ZX28-6.d	11.564	15.48	5.07	14.90
ZX28-7.d	7.203	9.51	3.91	27.61

Appendix 1.5B Trace elements analysis of garnet and clinopyroxene.

Source_file	Deposit	Mineral	La (ppm)	Ce (ppm)	Pr (ppm)	Nd (ppm)	Sm (ppm)	Eu (ppm)	Gd (ppm)	Tb (ppm)	Dy (ppm)
Min DL			0.0038	0.0031	0.0023	0.0129	0.0152	0.0045	0.0140	0.0020	0.0106
Max DL			0.0075	0.0072	0.0055	0.0305	0.0400	0.0097	0.0362	0.0054	0.0387
PINE-GRT1.d	Pine Creek	garnet Al-rich	0.020	0.292	0.195	3.133	3.435	0.836	5.245	1.123	8.866
DPHB-GRT1.d	Lened	garnet Al-rich	0.006	0.045	0.024	0.596	2.034	0.797	3.564	0.608	3.870
DPHB-GRT2.d	Lened	garnet Al-rich	<DL	0.012	0.010	0.470	2.214	1.130	2.646	0.337	1.557
DPHB-GRT3.d	Lened	garnet Al-rich	<DL	0.021	0.017	0.697	2.340	1.075	3.114	0.464	2.556
COP-GRT1.d	Cantung (Open Pit)	garnet Al-rich	0.009	0.027	<DL	0.036	0.218	0.323	1.743	0.608	5.471
COP-GRT2.d	Cantung (Open Pit)	garnet Al-rich	0.012	0.032	0.020	0.775	3.744	2.000	16.075	4.681	38.187
COP-GRT3.d	Cantung (Open Pit)	garnet Al-rich	<DL	0.016	0.017	0.355	1.566	0.576	2.243	0.302	1.599
LOP2A-GRT1.d	Lened	garnet Al-rich	0.064	0.095	0.027	0.748	3.043	2.171	7.122	1.322	8.782
LOP2A-GRT2.d	Lened	garnet Al-rich	<DL	<DL	<DL	0.160	1.120	0.614	2.365	0.382	1.743
LOP2A-GRT3.d	Lened	garnet Al-rich	0.011	0.050	0.032	0.885	3.665	2.102	9.792	2.102	14.978
LOP2A-GRT4.d	Lened	garnet Al-rich	<DL	0.010	0.010	0.250	1.300	1.979	2.268	0.319	1.770
LOP2A-GRT5.d	Lened	garnet Al-rich	<DL	0.025	0.016	0.567	2.711	1.588	7.620	1.513	10.248
ZHUXI-GRT-CORE.d	Zhuxi	garnet Al-rich	<DL	0.005	<DL	<DL	<DL	0.384	0.057	0.016	0.079
ZHUXI-GRT-RIM.d	Zhuxi	garnet Al-rich	<DL	<DL	<DL	<DL	<DL	0.010	<DL	<DL	<DL
ZHUXI-GRT1.d	Zhuxi	garnet Al-rich	<DL	<DL	<DL	<DL	<DL	0.166	0.035	0.004	0.022
ZHUXI-GRT2.d	Zhuxi	garnet Al-rich	<DL	<DL	<DL	<DL	<DL	0.028	<DL	<DL	0.027
KR65-GR-C1.d	Kara	garnet Fe-rich	3.506	9.904	0.856	1.943	0.314	0.191	0.479	0.061	0.358
KR65-GR-C2.d	Kara	garnet Fe-rich	4.369	10.493	0.920	3.113	1.094	0.380	1.394	0.249	1.486
KR65-GR-C3.d	Kara	garnet Fe-rich	6.683	17.779	1.377	2.853	0.309	0.219	0.566	0.064	0.375
KR65-GR-B1.d	Kara	garnet Fe-rich	3.664	9.597	0.707	1.580	0.189	0.189	0.248	0.018	0.127
KR65-GR-B2.d	Kara	garnet Fe-rich	3.273	10.304	1.353	5.848	1.172	1.113	1.042	0.155	0.981
KR65-GR-B3.d	Kara	garnet Fe-rich	3.075	5.423	0.710	2.924	0.238	0.474	0.177	0.018	0.066
SY18A-GR-1.d	Shizhuyuan	garnet Fe-rich	0.432	6.858	1.870	10.022	3.856	0.314	2.656	0.485	2.623
SY18A-GR-2.d	Shizhuyuan	garnet Fe-rich	0.388	5.701	1.649	9.260	4.457	0.245	3.210	0.536	3.071
SY18A-GR-3.d	Shizhuyuan	garnet Fe-rich	0.275	4.572	1.416	9.260	4.387	<DL	2.921	0.460	2.667
CEZ-Gt1.d	Cantung (E Zone)	garnet Fe-rich	0.071	0.211	0.073	1.355	0.782	1.808	0.624	0.050	0.219
CEZ-Gt2.d	Cantung (E Zone)	garnet Fe-rich	0.039	0.095	0.035	0.670	0.803	4.041	0.696	0.085	0.416
CEZ-Gt3.d	Cantung (E Zone)	garnet Fe-rich	<DL	0.019	0.018	0.316	0.937	1.158	0.907	0.137	0.671
DM-GrB.d	King Island	garnet Fe-rich	1.720	11.248	1.857	8.134	1.590	1.225	1.406	0.211	1.211
DM-GrC.d	King Island	garnet Fe-rich	2.182	10.667	1.534	6.345	1.116	0.983	0.916	0.130	0.855
DM-GrC1.d	King Island	garnet Fe-rich	1.315	7.995	1.492	7.177	1.357	1.390	1.188	0.173	1.097

Appendix 1.5B (continued)

Source_file	Deposit	Mineral	La (ppm)	Ce (ppm)	Pr (ppm)	Nd (ppm)	Sm (ppm)	Eu (ppm)	Gd (ppm)	Tb (ppm)	Dy (ppm)
DM-GrB2.d	King Island	garnet Fe-rich	1.901	10.900	1.831	7.971	1.520	1.459	1.418	0.231	1.532
PINE-CPX1.d	Pine Creek	clinopyroxene	0.211	0.648	0.125	0.625	0.142	0.023	0.069	0.014	0.036
PINE-CPX2.d	Pine Creek	clinopyroxene	0.267	0.825	0.108	0.386	0.040	0.028	0.021	0.004	0.054
PINE-CPX3.d	Pine Creek	clinopyroxene	0.097	0.340	0.074	0.228	0.031	0.010	0.035	0.003	0.028
PINE-CPX4.d	Pine Creek	clinopyroxene	0.120	0.388	0.068	0.231	0.041	0.011	0.025	0.003	0.031
MT161-CPX1.d	Mactung	clinopyroxene	0.223	0.873	0.142	0.787	0.245	0.086	0.223	0.050	0.388
MT161-CPX2.d	Mactung	clinopyroxene	0.216	0.944	0.182	0.922	0.307	0.094	0.296	0.061	0.436
MT161-CPX3.d	Mactung	clinopyroxene	0.145	0.658	0.119	0.663	0.256	0.067	0.212	0.050	0.359
MT161-CPX4.d	Mactung	clinopyroxene	0.499	1.552	0.256	0.990	0.316	0.114	0.335	0.063	0.443
MT161-CPX5.d	Mactung	clinopyroxene	1.139	3.196	0.435	1.590	0.378	0.212	0.340	0.057	0.340
BONFIM-CPX1.d	Bonfim	clinopyroxene	0.076	0.350	0.065	0.354	0.150	0.032	0.143	0.024	0.139
BONFIM-CPX2.d	Bonfim	clinopyroxene	0.029	0.137	0.030	0.173	0.097	0.018	0.102	0.017	0.090
BONFIM-CPX3.d	Bonfim	clinopyroxene	0.078	0.384	0.077	0.525	0.134	0.051	0.136	0.032	0.190
BONFIM-CPX4.d	Bonfim	clinopyroxene	0.257	0.794	0.114	0.690	0.220	0.049	0.224	0.043	0.218
SD212-CPX1.d	Scheelite Dome	clinopyroxene	0.160	0.256	0.037	0.213	0.107	0.034	0.134	0.020	0.142
SD212-CPX2.d	Scheelite Dome	clinopyroxene	0.051	0.142	0.032	0.173	0.152	0.023	0.132	0.021	0.163
SD212-CPX3.d	Scheelite Dome	clinopyroxene	0.183	0.417	0.046	0.307	0.170	0.041	0.127	0.031	0.223
SD212-CPX4.d	Scheelite Dome	clinopyroxene	0.078	0.249	0.050	0.280	0.097	0.014	0.119	0.024	0.167
COP-CPX1.d	Cantung (Open Pit)	clinopyroxene	0.049	0.090	0.022	0.173	0.037	0.046	0.129	0.013	0.075
COP-CPX2.d	Cantung (Open Pit)	clinopyroxene	0.021	0.049	0.007	0.039	<DL	0.011	0.034	0.004	0.021
COP-CPX3.d	Cantung (Open Pit)	clinopyroxene	0.037	0.096	0.017	0.099	0.024	0.009	0.028	<DL	<DL
COP-CPX4.d	Cantung (Open Pit)	clinopyroxene	0.040	0.080	0.016	0.034	<DL	0.012	0.019	0.003	0.018
COP-CPX5.d	Cantung (Open Pit)	clinopyroxene	0.054	0.155	0.023	0.125	0.047	0.017	0.057	0.007	0.033
M3DE-CPX1.d	Mactung	clinopyroxene	0.158	0.551	0.104	0.521	0.185	0.024	0.218	0.026	0.205
M3DE-CPX2.d	Mactung	clinopyroxene	1.232	2.581	0.345	1.332	0.295	0.052	0.293	0.036	0.248
M3DE-CPX3.d	Mactung	clinopyroxene	0.079	0.350	0.062	0.360	0.135	0.032	0.127	0.034	0.195
M3DE-CPX4.d	Mactung	clinopyroxene	0.167	0.538	0.090	0.401	0.152	0.032	0.153	0.017	0.138
M3DE-CPX5.d	Mactung	clinopyroxene	0.436	1.402	0.231	1.224	0.381	0.075	0.305	0.067	0.408
MT-231-CPX1.d	Mactung	clinopyroxene	0.186	0.568	0.109	0.461	0.137	0.023	0.110	0.018	0.153
MT-231-CPX2.d	Mactung	clinopyroxene	0.290	0.748	0.098	0.428	0.105	0.029	0.083	0.017	0.137
MT-231-CPX3.d	Mactung	clinopyroxene	0.190	0.568	0.101	0.411	0.115	0.028	0.125	0.029	0.193
MT-231-CPX4.d	Mactung	clinopyroxene	0.256	0.881	0.148	0.651	0.235	0.043	0.178	0.037	0.210

Appendix 1.5B (continued)

Source_file	Eu (ppm)	Gd (ppm)	Tb (ppm)	Dy (ppm)	Ho (ppm)	Er (ppm)	Tm (ppm)	Yb (ppm)	Lu (ppm)	ΣREE ppm	ΣLREE ppm	ΣHREE ppm
Min DL	0.0045	0.0140	0.0020	0.0106	0.0020	0.0059	0.0019	0.0094	0.0020			
Max DL	0.0097	0.0362	0.0054	0.0387	0.0039	0.0121	0.0050	0.0209	0.0044			
PINE-GRT1.d	0.836	5.245	1.123	8.866	2.101	6.545	1.128	9.145	1.441	43.507	7.076	35.595
DPHB-GRT1.d	0.797	3.564	0.608	3.870	0.749	2.009	0.254	1.746	0.223	16.525	2.705	13.023
DPHB-GRT2.d	1.130	2.646	0.337	1.557	0.270	0.596	0.091	0.484	0.061	9.878	2.706	6.041
DPHB-GRT3.d	1.075	3.114	0.464	2.556	0.454	1.057	0.151	0.929	0.155	13.029	3.075	8.879
COP-GRT1.d	0.323	1.743	0.608	5.471	1.380	3.970	0.568	4.374	0.607	19.334	0.289	18.722
COP-GRT2.d	2.000	16.075	4.681	38.187	9.410	27.567	3.841	24.969	3.180	134.493	4.584	127.910
COP-GRT3.d	0.576	2.243	0.302	1.599	0.286	0.584	0.064	0.324	0.032	7.965	1.954	5.434
LOP2A-GRT1.d	2.171	7.122	1.322	8.782	1.696	4.605	0.588	4.135	0.644	35.043	3.976	28.895
LOP2A-GRT2.d	0.614	2.365	0.382	1.743	0.205	0.311	0.034	0.178	0.021	7.133	1.281	5.239
LOP2A-GRT3.d	2.102	9.792	2.102	14.978	3.260	9.045	1.326	8.782	1.249	57.278	4.643	50.533
LOP2A-GRT4.d	1.979	2.268	0.319	1.770	0.275	0.635	0.089	0.600	0.087	9.593	1.570	6.044
LOP2A-GRT5.d	1.588	7.620	1.513	10.248	2.213	6.846	1.019	6.943	1.059	42.368	3.319	37.461
ZHUXI-GRT-CORE.d	0.384	0.057	0.016	0.079	0.028	0.079	0.019	0.042	0.015	0.725	0.005	0.335
ZHUXI-GRT-RIM.d	0.010	<DL	<DL	<DL	<DL	<DL	<DL	<DL	<DL	0.010	0.000	0.000
ZHUXI-GRT1.d	0.166	0.035	0.004	0.022	0.006	0.009	<DL	0.031	<DL	0.273	0.000	0.107
ZHUXI-GRT2.d	0.028	<DL	<DL	0.027	0.005	0.012	<DL	<DL	<DL	0.071	0.000	0.044
KR65-GR-C1.d	0.191	0.479	0.061	0.358	0.074	0.179	0.019	0.149	0.024	18.057	16.523	1.343
KR65-GR-C2.d	0.380	1.394	0.249	1.486	0.309	0.865	0.117	0.745	0.097	25.630	19.989	5.261
KR65-GR-C3.d	0.219	0.566	0.064	0.375	0.071	0.205	0.021	0.130	0.031	30.683	29.001	1.463
KR65-GR-B1.d	0.189	0.248	0.018	0.127	0.026	0.111	0.024	0.217	0.024	16.720	15.737	0.794
KR65-GR-B2.d	1.113	1.042	0.155	0.981	0.203	0.750	0.167	1.363	0.162	27.887	21.951	4.823
KR65-GR-B3.d	0.474	0.177	0.018	0.066	0.012	0.027	0.003	0.026	0.003	13.175	12.370	0.331
SY18A-GR-1.d	0.314	2.656	0.485	2.623	0.434	1.180	0.175	1.245	0.171	32.322	23.039	8.969
SY18A-GR-2.d	0.245	3.210	0.536	3.071	0.485	1.291	0.190	1.506	0.169	32.157	21.455	10.457
SY18A-GR-3.d	<DL	2.921	0.460	2.667	0.457	1.291	0.193	1.409	0.178	29.486	19.910	9.576
CEZ-Gt1.d	1.808	0.624	0.050	0.219	0.034	0.091	0.014	0.137	0.019	5.488	2.491	1.188
CEZ-Gt2.d	4.041	0.696	0.085	0.416	0.071	0.194	0.041	0.224	0.031	7.442	1.643	1.758
CEZ-Gt3.d	1.158	0.907	0.137	0.671	0.107	0.270	0.042	0.249	0.043	4.873	1.289	2.426
DM-GrB.d	1.225	1.406	0.211	1.211	0.232	0.713	0.106	0.858	0.129	30.639	24.548	4.866
DM-GrC.d	0.983	0.916	0.130	0.855	0.167	0.509	0.077	0.437	0.069	25.986	21.843	3.160
DM-GrC1.d	1.390	1.188	0.173	1.097	0.239	0.686	0.112	0.727	0.102	25.049	19.336	4.323

Appendix 1.5B (continued)

Source_file	Eu (ppm)	Gd (ppm)	Tb (ppm)	Dy (ppm)	Ho (ppm)	Er (ppm)	Tm (ppm)	Yb (ppm)	Lu (ppm)	ΣREE ppm	ΣLREE ppm	ΣHREE ppm
DM-GrB2.d	1.459	1.418	0.231	1.532	0.330	1.030	0.164	1.332	0.213	31.832	24.123	6.249
PINE-CPX1.d	0.023	0.069	0.014	0.036	0.005	0.015	<DL	0.019	0.008	1.942	1.751	0.167
PINE-CPX2.d	0.028	0.021	0.004	0.054	0.011	0.043	0.011	0.302	0.072	2.172	1.626	0.518
PINE-CPX3.d	0.010	0.035	0.003	0.028	0.007	0.022	0.009	0.102	0.027	1.012	0.770	0.232
PINE-CPX4.d	0.011	0.025	0.003	0.031	0.005	0.014	0.008	0.139	0.048	1.132	0.849	0.272
MT161-CPX1.d	0.086	0.223	0.050	0.388	0.073	0.213	0.055	0.739	0.182	4.277	2.268	1.923
MT161-CPX2.d	0.094	0.296	0.061	0.436	0.093	0.268	0.060	0.790	0.197	4.866	2.571	2.201
MT161-CPX3.d	0.067	0.212	0.050	0.359	0.072	0.203	0.052	0.811	0.223	3.890	1.841	1.982
MT161-CPX4.d	0.114	0.335	0.063	0.443	0.090	0.281	0.067	0.752	0.193	5.951	3.612	2.225
MT161-CPX5.d	0.212	0.340	0.057	0.340	0.082	0.250	0.048	0.550	0.197	8.813	6.737	1.864
BONFIM-CPX1.d	0.032	0.143	0.024	0.139	0.040	0.116	0.016	0.222	0.070	1.797	0.995	0.770
BONFIM-CPX2.d	0.018	0.102	0.017	0.090	0.027	0.072	0.010	0.092	0.029	0.923	0.466	0.439
BONFIM-CPX3.d	0.051	0.136	0.032	0.190	0.046	0.148	0.027	0.308	0.108	2.243	1.198	0.994
BONFIM-CPX4.d	0.049	0.224	0.043	0.218	0.052	0.146	0.023	0.247	0.074	3.152	2.076	1.027
SD212-CPX1.d	0.034	0.134	0.020	0.142	0.034	0.186	0.072	0.625	0.137	2.157	0.773	1.350
SD212-CPX2.d	0.023	0.132	0.021	0.163	0.030	0.101	0.035	0.425	0.095	1.574	0.550	1.002
SD212-CPX3.d	0.041	0.127	0.031	0.223	0.054	0.318	0.094	1.416	0.330	3.756	1.122	2.593
SD212-CPX4.d	0.014	0.119	0.024	0.167	0.041	0.147	0.032	0.521	0.109	1.927	0.754	1.159
COP-CPX1.d	0.046	0.129	0.013	0.075	0.009	0.037	0.005	0.042	0.012	0.738	0.371	0.321
COP-CPX2.d	0.011	0.034	0.004	0.021	0.004	0.009	<DL	<DL	0.004	0.202	0.115	0.075
COP-CPX3.d	0.009	0.028	<DL	<DL	<DL	0.012	<DL	0.022	0.005	0.350	0.274	0.067
COP-CPX4.d	0.012	0.019	0.003	0.018	<DL	<DL	<DL	0.017	0.004	0.242	0.170	0.060
COP-CPX5.d	0.017	0.057	0.007	0.033	0.007	0.018	0.004	0.046	0.007	0.600	0.404	0.179
M3DE-CPX1.d	0.024	0.218	0.026	0.205	0.054	0.158	0.047	0.509	0.117	2.877	1.519	1.334
M3DE-CPX2.d	0.052	0.293	0.036	0.248	0.047	0.150	0.029	0.351	0.099	7.090	5.784	1.254
M3DE-CPX3.d	0.032	0.127	0.034	0.195	0.042	0.128	0.033	0.453	0.096	2.124	0.985	1.107
M3DE-CPX4.d	0.032	0.153	0.017	0.138	0.035	0.103	0.030	0.425	0.097	2.377	1.347	0.998
M3DE-CPX5.d	0.075	0.305	0.067	0.408	0.092	0.330	0.074	0.751	0.128	5.904	3.675	2.155
MT-231-CPX1.d	0.023	0.110	0.018	0.153	0.032	0.088	0.019	0.408	0.112	2.424	1.461	0.941
MT-231-CPX2.d	0.029	0.083	0.017	0.137	0.038	0.122	0.030	0.388	0.093	2.605	1.668	0.908
MT-231-CPX3.d	0.028	0.125	0.029	0.193	0.048	0.157	0.039	0.571	0.144	2.718	1.384	1.306
MT-231-CPX4.d	0.043	0.178	0.037	0.210	0.047	0.181	0.033	0.471	0.128	3.499	2.171	1.284

Appendix 1.6B Trace element scheelite literature data used in PLS-DA model.

Name	Deposit_type	Reference	Sample ID	B ppm	Na ppm	Mg ppm	K ppm	Ti ppm	V ppm
Meliadine	Orogenic gold	Sciuba et al 2020	MELI-01	1.3	44	3.7	350	0.13	0.197
Meliadine	Orogenic gold	Sciuba et al 2020	MELI-01	0.82	106.2	3.1	<DL	<DL	0.45
Meliadine	Orogenic gold	Sciuba et al 2020	MELI-01	<DL	148.3	2.93	11	<DL	0.25
Meliadine	Orogenic gold	Sciuba et al 2020	MELI-01	0.46	49.1	2.58	<DL	0.51	0.364
Meliadine	Orogenic gold	Sciuba et al 2020	MELI-01	0.83	75.9	3.02	<DL	0.71	0.402
Dome	Orogenic gold	Sciuba et al 2020	DOME-02	0.65	189	5.17	3.75	0.3	<DL
Dome	Orogenic gold	Sciuba et al 2020	DOME-02	0.92	213	6.3	6.11	0.53	0.065
Dome	Orogenic gold	Sciuba et al 2020	DOME-02	1.02	212.6	14	4.19	0.31	0.071
Hollinger	Orogenic gold	Sciuba et al 2020	HOLL-01	0.53	13.4	530	2.8	<DL	0.157
Hollinger	Orogenic gold	Sciuba et al 2020	HOLL-01	0.5	4.7	368.2	2.1	0.13	0.093
Hollinger	Orogenic gold	Sciuba et al 2020	HOLL-01	0.35	10.5	197	<DL	<DL	<DL
Young Davidson	Orogenic gold	Sciuba et al 2020	YOUN-01	1.54	165	12.3	23	<DL	2.29
Young Davidson	Orogenic gold	Sciuba et al 2020	YOUN-01	1.17	310	11	64	0.25	1.97
Young Davidson	Orogenic gold	Sciuba et al 2020	YOUN-01	1.37	225	11.4	52	0.26	2.26
Young Davidson	Orogenic gold	Sciuba et al 2020	YOUN-01	1.12	168.5	7.3	81	0.23	1.51
Young Davidson	Orogenic gold	Sciuba et al 2020	YOUN-01	1.08	218	6	53	<DL	1.38
Young Davidson	Orogenic gold	Sciuba et al 2020	YOUN-01	1.08	124	5.3	5.8	0.22	1.11
Young Davidson	Orogenic gold	Sciuba et al 2020	YOUN-01	1.06	166	8.9	50	0.16	1.39
Young Davidson	Orogenic gold	Sciuba et al 2020	YOUN-01	1.19	210	13.7	57	0.48	1.64
Canadian Malartic	Orogenic gold	Sciuba et al 2020	MALA-10	1.19	92	32.6	20.6	2.5	0.468
Canadian Malartic	Orogenic gold	Sciuba et al 2020	MALA-10	0.82	118	20.9	6.4	0.75	1.36
Canadian Malartic	Orogenic gold	Sciuba et al 2020	MALA-10	0.76	128	34	15.7	1.9	1.39
Canadian Malartic	Orogenic gold	Sciuba et al 2020	MALA-10	0.54	85	24.9	11.4	0.58	0.27
Canadian Malartic	Orogenic gold	Sciuba et al 2020	MALA-10	1.15	132	36.8	27.2	2.9	0.348
Beaufor	Orogenic gold	Sciuba et al 2020	96-DP-162	1.7	110.8	5.72	1.8	0.69	0.692
Beaufor	Orogenic gold	Sciuba et al 2020	96-DP-162	1.7	132	4.63	2.5	0.4	0.74
Beaufor	Orogenic gold	Sciuba et al 2020	96-DP-162	1.4	103	5.8	2.94	0.16	0.7
Beaufor	Orogenic gold	Sciuba et al 2020	96-DP-162	<DL	152	3.39	<DL	0.25	0.64
Beaufor	Orogenic gold	Sciuba et al 2020	96-DP-162	<DL	196	3.36	<DL	0.31	0.7
Beaufor	Orogenic gold	Sciuba et al 2020	96-DP-162	<DL	82.2	4.08	<DL	0.24	0.55
Beaufor	Orogenic gold	Sciuba et al 2020	96-DP-162	<DL	97	4.28	<DL	0.1	0.77
Beaufor	Orogenic gold	Sciuba et al 2020	96-DP-162	<DL	82.2	8.2	1.28	0.75	0.62

Appendix 1.6B (continued)

Name	Deposit_type	Reference	Sample ID	B ppm	Na ppm	Mg ppm	K ppm	Ti ppm	V ppm
Beaufor	Orogenic gold	Sciuba et al 2020	96-DP-162	<DL	158	3.33	<DL	<DL	0.7
Beaufor	Orogenic gold	Sciuba et al 2020	96-DP-162	0.28	120	4.32	0.7	0.25	0.621
Beaufor	Orogenic gold	Sciuba et al 2020	96-DP-162	0.65	85.8	3.82	0.97	0.65	0.52
Beaufor	Orogenic gold	Sciuba et al 2020	96-DP-162	0.99	82	4.09	1.36	0.39	0.476
Beaufor	Orogenic gold	Sciuba et al 2020	96-DP-162	0.47	66.8	3.86	1.56	<DL	0.41
Beaufor	Orogenic gold	Sciuba et al 2020	B580-15	<DL	215.9	4.45	1.8	<DL	0.219
Beaufor	Orogenic gold	Sciuba et al 2020	B580-15	<DL	324	4.28	0.99	<DL	0.217
Beaufor	Orogenic gold	Sciuba et al 2020	B580-15	0.37	272	4.55	2.04	<DL	0.201
Beaufor	Orogenic gold	Sciuba et al 2020	B580-15	0.32	160.8	4.95	3.8	0.51	0.096
Beaufor	Orogenic gold	Sciuba et al 2020	B580-15	<DL	362	5.18	1.78	<DL	0.237
Beaufor	Orogenic gold	Sciuba et al 2020	B580-15	<DL	277	5.7	6.1	<DL	0.26
Beaufor	Orogenic gold	Sciuba et al 2020	B580-15	0.25	314	4.44	1.7	<DL	0.254
Beaufor	Orogenic gold	Sciuba et al 2020	B580-15	0.24	310	4.95	2.3	<DL	0.223
Beaufor	Orogenic gold	Sciuba et al 2020	B580-15	0.3	247.9	6	3.7	0.16	0.248
Beaufor	Orogenic gold	Sciuba et al 2020	B580-15	0.46	247	5.81	4.7	0.077	0.281
Sigma	Orogenic gold	Sciuba et al 2020	94-GB-15A	0.84	240.1	2.98	1.43	0.083	0.129
Sigma	Orogenic gold	Sciuba et al 2020	94-GB-15A	1.69	101.7	4.76	1.75	0.073	0.119
Sigma	Orogenic gold	Sciuba et al 2020	94-GB-15A	3.2	172	7	1.38	0.28	0.144
Sigma	Orogenic gold	Sciuba et al 2020	94-GB-15A	1.19	127.2	3.96	2.44	0.17	0.105
Sigma	Orogenic gold	Sciuba et al 2020	94-GB-15A	1.16	275	2.88	2	0.28	0.13
Sigma	Orogenic gold	Sciuba et al 2020	94-GB-15A	1.38	157	3.93	2.05	0.12	0.119
Sigma	Orogenic gold	Sciuba et al 2020	94-GB-15A	39	274	63	3.65	2.4	0.62
Sigma	Orogenic gold	Sciuba et al 2020	SIGM-01	1.26	115.8	6.96	13.5	0.14	0.11
Sigma	Orogenic gold	Sciuba et al 2020	SIGM-01	1.18	245.1	9.52	10.8	0.059	0.16
Sigma	Orogenic gold	Sciuba et al 2020	SIGM-01	1.29	184	8.24	8.8	0.075	0.131
Sigma	Orogenic gold	Sciuba et al 2020	SIGM-01	1.31	289.3	10.64	19	0.116	0.164
Sigma	Orogenic gold	Sciuba et al 2020	SIGM-01	1.44	105.6	15.6	8.1	0.11	0.176
Sigma	Orogenic gold	Sciuba et al 2020	SIGM-01	1.74	300	49.6	78	0.61	0.101
Sigma	Orogenic gold	Sciuba et al 2020	SIGM-01	1.33	151	21.5	9.2	0.13	0.147
Sigma	Orogenic gold	Sciuba et al 2020	SIGM-01	1.34	130.3	7.17	40.7	0.22	0.129
Lamaque	Orogenic gold	Sciuba et al 2020	LAMA-01	1.59	253	19	121	0.44	1.56
Lamaque	Orogenic gold	Sciuba et al 2020	LAMA-01	1.48	204	13.5	114	0.74	1.34

Appendix 1.6B (continued)

Name	Deposit_type	Reference	Sample ID	B ppm	Na ppm	Mg ppm	K ppm	Ti ppm	V ppm
Lamaque	Orogenic gold	Sciuba et al 2020	LAMA-01	1.43	229	23.9	106	1.1	1.487
Cuiaba	Orogenic gold	Sciuba et al 2020	CUIA-03	1.17	16.3	7	1.28	0.58	0.065
Cuiaba	Orogenic gold	Sciuba et al 2020	CUIA-03	2.7	19.2	13	1.69	1.53	0.075
Cuiaba	Orogenic gold	Sciuba et al 2020	CUIA-03	1.29	26.1	4.43	<DL	0.27	<DL
Cuiaba	Orogenic gold	Sciuba et al 2020	CUIA-03	1.75	86	17.3	2.53	2.6	0.095
Essakane	Orogenic gold	Sciuba et al 2020	160277	1.32	73.2	5.99	33.5	0.44	<DL
Essakane	Orogenic gold	Sciuba et al 2020	160277	1.87	79	15.2	31.3	1.55	0.057
Essakane	Orogenic gold	Sciuba et al 2020	160286	6.7	25.4	14.8	8.5	0.6	0.104
Essakane	Orogenic gold	Sciuba et al 2020	160286	19	46	33	8.5	1.7	0.35
Essakane	Orogenic gold	Sciuba et al 2020	160286	3	36	17.8	23.1	2.2	0.105
Essakane	Orogenic gold	Sciuba et al 2020	160304	6.5	34.3	14.6	6.8	0.62	0.073
Essakane	Orogenic gold	Sciuba et al 2020	160304	0.6	26.9	4.39	6.9	0.34	<DL
Essakane	Orogenic gold	Sciuba et al 2020	160304	0.45	23.9	5.2	4.9	0.18	<DL
Essakane	Orogenic gold	Sciuba et al 2020	160304	<DL	88.7	8.1	6.8	<DL	<DL
Essakane	Orogenic gold	Sciuba et al 2020	160304	0.52	85	4.13	5.7	0.2	<DL
Essakane	Orogenic gold	Sciuba et al 2020	160304	0.5	41.9	5.14	6.18	0.18	<DL
Essakane	Orogenic gold	Sciuba et al 2020	160304	0.47	47.4	4.8	6.3	0.1	<DL
Essakane	Orogenic gold	Sciuba et al 2020	160304	<DL	84	4.5	5.7	<DL	<DL
Essakane	Orogenic gold	Sciuba et al 2020	160304	1.5	63	7.2	10.4	0.54	<DL
Essakane	Orogenic gold	Sciuba et al 2020	160304	1.23	65	5.37	5.4	0.19	<DL
Essakane	Orogenic gold	Sciuba et al 2020	160304	0.58	123	4.79	3.8	0.32	<DL
Essakane	Orogenic gold	Sciuba et al 2020	160310	0.55	16.1	9.1	7.5	0.3	<DL
Essakane	Orogenic gold	Sciuba et al 2020	160310	0.38	10.9	5	0.91	<DL	<DL
Essakane	Orogenic gold	Sciuba et al 2020	160310	0.83	31.2	6.85	3.9	0.22	<DL
Essakane	Orogenic gold	Sciuba et al 2020	160310	0.67	20.8	5.86	2.66	0.158	<DL
Essakane	Orogenic gold	Sciuba et al 2020	160310	0.57	15.4	6.5	9.3	0.52	<DL
Buzwagi	Orogenic gold	Sciuba et al 2020	BZWA-01	1.83	52.9	80	1.42	0.31	0.401
Hutti	Orogenic gold	Sciuba et al 2020	HUTT-01	0.25	145.2	4.08	2.2	0.65	<DL
Hutti	Orogenic gold	Sciuba et al 2020	HUTT-01	0.34	108	4.34	4.7	0.74	0.093
Hutti	Orogenic gold	Sciuba et al 2020	HUTT-01	0.29	44.2	3.36	1.23	0.87	0.174
Hutti	Orogenic gold	Sciuba et al 2020	HUTT-01	0.49	180	4.05	15	0.33	<DL
Hutti	Orogenic gold	Sciuba et al 2020	HUTT-01	<DL	47.6	8.6	13	1.1	0.117

Appendix 1.6B (continued)

Name	Deposit_type	Reference	Sample ID	B ppm	Na ppm	Mg ppm	K ppm	Ti ppm	V ppm
Hutti	Orogenic gold	Sciuba et al 2020	HUTT-01	<DL	36.4	3.32	1.9	0.22	<DL
Hutti	Orogenic gold	Sciuba et al 2020	HUTT-01	<DL	41	9.6	3.5	0.59	0.12
Hutti	Orogenic gold	Sciuba et al 2020	HUTT-01	0.6	38.9	6.7	2.4	1.47	0.09
Hutti	Orogenic gold	Sciuba et al 2020	HUTT-01	<DL	42.2	7.2	3.09	0.96	0.099
Hutti	Orogenic gold	Sciuba et al 2020	HUTT-01	0.56	56	19	8.5	4.6	0.148
Hutti	Orogenic gold	Sciuba et al 2020	HUTT-01	0.51	53.4	14	6.7	3.4	0.147
Hutti	Orogenic gold	Sciuba et al 2020	HUTT-01	0.5	50.7	6.4	4.1	2.9	<DL
Hutti	Orogenic gold	Sciuba et al 2020	HUTT-01	0.18	37.7	4.3	3.3	0.32	0.108
Hutti	Orogenic gold	Sciuba et al 2020	HUTT-01	0.59	31	3.31	<DL	0.28	<DL
Hutti	Orogenic gold	Sciuba et al 2020	HUTT-01	0.47	41.8	3.7	<DL	0.63	<DL
Hutti	Orogenic gold	Sciuba et al 2020	HUTT-02	0.38	33.4	6.9	1.56	0.78	0.102
Hutti	Orogenic gold	Sciuba et al 2020	HUTT-02	<DL	40.5	8.3	2.9	1.25	0.23
Hutti	Orogenic gold	Sciuba et al 2020	HUTT-02	0.46	57	8.2	2.17	1.54	0.315
Hutti	Orogenic gold	Sciuba et al 2020	HUTT-02	0.38	44.5	7.32	2.12	0.98	0.174
Hutti	Orogenic gold	Sciuba et al 2020	HUTT-02	0.35	70.8	10.9	3	0.54	<DL
Hutti	Orogenic gold	Sciuba et al 2020	HUTT-04	0.56	19.7	9.5	6.2	0.22	<DL
Hutti	Orogenic gold	Sciuba et al 2020	HUTT-04	0.51	25.5	10	5.1	0.37	0.065
Hutti	Orogenic gold	Sciuba et al 2020	HUTT-04	<DL	56	19.6	8.8	0.7	0.198
Hutti	Orogenic gold	Sciuba et al 2020	HUTT-04	<DL	10.6	6.5	1.2	0.63	<DL
Hutti	Orogenic gold	Sciuba et al 2020	HUTT-04	0.74	24.1	14.5	5.94	0.21	0.091
Hutti	Orogenic gold	Sciuba et al 2020	HUTT-04	0.84	31	15.5	6.7	0.51	0.093
Kochkar	Orogenic gold	Sciuba et al 2020	KOCH-05A	0.73	65	13.5	2.9	7	0.146
Kochkar	Orogenic gold	Sciuba et al 2020	KOCH-05A	0.84	69	19	5.5	0.8	0.14
Kochkar	Orogenic gold	Sciuba et al 2020	KOCH-05A	0.56	52.8	5.94	<DL	<DL	0.127
Kochkar	Orogenic gold	Sciuba et al 2020	KOCH-05A	0.69	40.5	6.78	<DL	0.21	0.29
Kochkar	Orogenic gold	Sciuba et al 2020	KOCH-05A	0.59	56.3	8	0.91	0.14	0.121
Kochkar	Orogenic gold	Sciuba et al 2020	KOCH-05A	0.45	43.5	4.89	<DL	0.1	0.2
Kochkar	Orogenic gold	Sciuba et al 2020	KOCH-05A	0.79	65.3	10.2	2.8	1.1	0.311
Kochkar	Orogenic gold	Sciuba et al 2020	KOCH-05A	<DL	49.2	12.3	1.56	0.42	0.213
Kochkar	Orogenic gold	Sciuba et al 2020	KOCH-06A	0.74	620	127	35.4	0.53	0.118
Kochkar	Orogenic gold	Sciuba et al 2020	KOCH-06A	0.45	380	68	28.5	<DL	<DL
Kochkar	Orogenic gold	Sciuba et al 2020	KOCH-06A	1.06	980	176	54	1.2	0.21

Appendix 1.6B (continued)

Name	Deposit_type	Reference	Sample ID	B ppm	Na ppm	Mg ppm	K ppm	Ti ppm	V ppm
Kochkar	Orogenic gold	Sciuba et al 2020	KOCH-06A	0.42	17.9	5.41	2.8	0.33	<DL
Kochkar	Orogenic gold	Sciuba et al 2020	KOCH-06A	0.47	11.1	5	2.29	0.09	0.127
Kochkar	Orogenic gold	Sciuba et al 2020	KOCH-06A	0.45	7	4.9	1.9	<DL	0.085
Kochkar	Orogenic gold	Sciuba et al 2020	KOCH-06A	0.44	7.5	5.9	1.5	0.1	0.188
Kochkar	Orogenic gold	Sciuba et al 2020	KOCH-06B	1.8	19.5	16.2	2.5	2.6	0.227
Kochkar	Orogenic gold	Sciuba et al 2020	KOCH-06B	1.92	11.7	8.4	<DL	7	<DL
Kochkar	Orogenic gold	Sciuba et al 2020	KOCH-06B	1.66	17.3	9.9	1.7	0.49	0.29
Kochkar	Orogenic gold	Sciuba et al 2020	KOCH-06B	1.5	16.4	11.6	1.3	0.43	0.301
Kumtor	Orogenic gold	Sciuba et al 2020	KUMT-04	1.96	8.4	3.77	<DL	0.2	0.94
Kumtor	Orogenic gold	Sciuba et al 2020	KUMT-04	1.7	33	5.4	1.9	0.34	0.64
Kumtor	Orogenic gold	Sciuba et al 2020	KUMT-04	1.58	12.3	3.46	<DL	0.047	2.96
Kumtor	Orogenic gold	Sciuba et al 2020	KUMT-04	1.87	24.6	4.31	1.43	0.19	1.66
Marvel Loch	Orogenic gold	Sciuba et al 2020	MARV-01	1.43	16.8	4.89	29	0.05	0.238
Marvel Loch	Orogenic gold	Sciuba et al 2020	MARV-01	1.36	13.6	4.81	23.9	0.067	0.597
Marvel Loch	Orogenic gold	Sciuba et al 2020	MARV-01	1.5	99	7.9	200	0.41	0.643
Marvel Loch	Orogenic gold	Sciuba et al 2020	MARV-01	1.24	66.2	5.29	81.5	0.19	0.427
Marvel Loch	Orogenic gold	Sciuba et al 2020	MARV-01	1.12	47.6	9.4	42	0.1	0.171
Marvel Loch	Orogenic gold	Sciuba et al 2020	MARV-01	1.29	232	8.3	129	0.48	0.309
Marvel Loch	Orogenic gold	Sciuba et al 2020	MARV-01	1	125	5.29	58	0.15	0.238
Marvel Loch	Orogenic gold	Sciuba et al 2020	MARV-01	1.06	37	4.65	24.6	0.09	0.22
Marvel Loch	Orogenic gold	Sciuba et al 2020	MARV-01	1.26	84	6.5	53.7	0.1	0.21
Marvel Loch	Orogenic gold	Sciuba et al 2020	MARV-01	2	54.6	5.06	25.2	0.13	0.438
Marvel Loch	Orogenic gold	Sciuba et al 2020	MARV-01	1.44	72	5.92	38	0.065	0.485
Nevoria	Skarn Au	Sciuba et al 2020	NVOR-01	1.89	4.2	2.5	2.9	0.05	0.201
Nevoria	Skarn Au	Sciuba et al 2020	NVOR-01	1.65	6.1	2.35	2.05	0.15	0.232
Nevoria	Skarn Au	Sciuba et al 2020	NVOR-01	1.78	6.3	2.35	2.57	0.45	0.23
Nevoria	Skarn Au	Sciuba et al 2020	NVOR-01	1.86	44	5.83	50	0.14	0.106
Nevoria	Skarn Au	Sciuba et al 2020	NVOR-01	1.45	19.1	6.1	17.6	0.27	0.141
Nevoria	Skarn Au	Sciuba et al 2020	NVOR-01	2.45	15.6	4.71	39	0.27	<DL
Edward's Find	Orogenic gold	Sciuba et al 2020	EDWA-01	1.49	51	6.5	124	2.8	0.963
Edward's Find	Orogenic gold	Sciuba et al 2020	EDWA-01	1.53	6.4	2.62	1.8	0.1	1.21
Edward's Find	Orogenic gold	Sciuba et al 2020	EDWA-01	1.12	8.4	2.33	5.1	<DL	1.03

Appendix 1.6B (continued)

Name	Deposit_type	Reference	Sample ID	B ppm	Na ppm	Mg ppm	K ppm	Ti ppm	V ppm
Edward's Find	Orogenic gold	Sciuba et al 2020	EDWA-01	1.2	7.4	2.34	4.5	<DL	0.57
Edward's Find	Orogenic gold	Sciuba et al 2020	EDWA-01	0.9	11.2	2.06	19	<DL	1.79
Edward's Find	Orogenic gold	Sciuba et al 2020	EDWA-01	1.13	11.8	2.25	1.6	<DL	4.54
Tarmoola	Orogenic gold	Sciuba et al 2020	TARM-01	1.05	199	74	16.6	7.4	0.3
Tarmoola	Orogenic gold	Sciuba et al 2020	TARM-01	1.2	228	64	80	6	0.44
Tarmoola	Orogenic gold	Sciuba et al 2020	TARM-01	1.35	234	69	15.7	5.3	0.46
Tarmoola	Orogenic gold	Sciuba et al 2020	TARM-01	0.98	121	47	10.2	2.7	0.144
Tarmoola	Orogenic gold	Sciuba et al 2020	TARM-01	0.59	133	39	9.8	3.3	0.108
Tarmoola	Orogenic gold	Sciuba et al 2020	TARM-01	0.52	213	49	10.4	2.16	0.213
Tarmoola	Orogenic gold	Sciuba et al 2020	TARM-01	0.87	146	43.9	10.3	2.8	0.146
Tarmoola	Orogenic gold	Sciuba et al 2020	TARM-01	0.6	109	19.5	6.5	0.82	0.062
Tarmoola	Orogenic gold	Sciuba et al 2020	TARM-01	0.42	151	55	15.4	3.9	0.23
Tarmoola	Orogenic gold	Sciuba et al 2020	TARM-01	0.78	113	24.5	7.7	1.76	0.104
Tarmoola	Orogenic gold	Sciuba et al 2020	TARM-01	0.66	108	21.5	6.71	1.26	0.055
Tarmoola	Orogenic gold	Sciuba et al 2020	TARM-01	0.68	156	23.8	8.2	1.65	0.09
Paddington	Orogenic gold	Sciuba et al 2020	PADD-01A	0.97	244	59	12.3	2.6	0.129
Paddington	Orogenic gold	Sciuba et al 2020	PADD-01A	1.24	176	56	13.3	2.13	0.136
Paddington	Orogenic gold	Sciuba et al 2020	PADD-01A	1.44	116	41.7	11.2	1.3	0.129
Paddington	Orogenic gold	Sciuba et al 2020	PADD-01A	1.14	66.1	8.13	71.3	0.4	<DL
Paddington	Orogenic gold	Sciuba et al 2020	PADD-01A	1.14	176	23.8	4.5	0.67	0.068
Paddington	Orogenic gold	Sciuba et al 2020	PADD-01A	1.34	119.8	14.2	1.54	<DL	<DL
Paddington	Orogenic gold	Sciuba et al 2020	PADD-01A	0.87	42.8	10.9	1.85	0.045	<DL
Paddington	Orogenic gold	Sciuba et al 2020	PADD-01A	1.12	132	10.6	1.6	<DL	<DL
Paddington	Orogenic gold	Sciuba et al 2020	PADD-01A	1.05	94	14.6	2.6	0.17	<DL
Paddington	Orogenic gold	Sciuba et al 2020	PADD-01A	0.73	66	14.6	2.4	0.28	<DL
Paddington	Orogenic gold	Sciuba et al 2020	PADD-01A	0.86	54.2	12.3	1.89	0.12	0.054
Paddington	Orogenic gold	Sciuba et al 2020	PADD-01A	1.03	120	16.8	2.9	0.12	<DL
Paddington	Orogenic gold	Sciuba et al 2020	PADD-01A	0.85	71.5	14.7	2.8	0.31	0.049
Paddington	Orogenic gold	Sciuba et al 2020	PADD-01A	1.17	56	5.5	43	2.5	0.049
Paddington	Orogenic gold	Sciuba et al 2020	PADD-01A	1.61	31	4.44	31	0.06	<DL
Paddington	Orogenic gold	Sciuba et al 2020	PADD-01A	0.91	19	3.74	39	0.1	<DL
Paddington	Orogenic gold	Sciuba et al 2020	PADD-01A	1.13	43.6	4.96	43.7	1	0.031

Appendix 1.6B (continued)

Name	Deposit_type	Reference	Sample ID	B ppm	Na ppm	Mg ppm	K ppm	Ti ppm	V ppm
Paddington	Orogenic gold	Sciuba et al 2020	PADD-02B	1.54	35	4.13	74	0.7	<DL
Paddington	Orogenic gold	Sciuba et al 2020	PADD-02B	1.2	28.6	3.68	48	0.19	<DL
Paddington	Orogenic gold	Sciuba et al 2020	PADD-02B	1.21	46.8	3.39	42.9	<DL	<DL
Paddington	Orogenic gold	Sciuba et al 2020	PADD-02B	1.06	17.8	3.57	24.9	<DL	<DL
Paddington	Orogenic gold	Sciuba et al 2020	PADD-02B	1.57	246	7.1	83	<DL	<DL
Paddington	Orogenic gold	Sciuba et al 2020	PADD-02B	1.16	20.2	3.69	17.5	0.1	<DL
Paddington	Orogenic gold	Sciuba et al 2020	PADD-02B	1.31	33.5	3.31	26.9	0.21	<DL
Paddington	Orogenic gold	Sciuba et al 2020	PADD-02B	1.21	75	4.42	48.2	0.127	<DL
Paddington	Orogenic gold	Sciuba et al 2020	PADD-02B	1.35	65	5.03	50.7	2.3	<DL
Paddington	Orogenic gold	Sciuba et al 2020	PADD-02B	1.31	104	4.7	70	0.74	<DL
Paddington	Orogenic gold	Sciuba et al 2020	PADD-02B	1.02	93	4.92	44	0.39	<DL
Paddington	Orogenic gold	Sciuba et al 2020	PADD-02B	1.21	71.9	5.14	52.5	1.5	<DL
Paddington	Orogenic gold	Sciuba et al 2020	PADD-02B	1.04	60	4.39	59	0.38	<DL
Mount Pleasant	Orogenic gold	Sciuba et al 2020	MTPL-01	0.86	265.9	10.7	11.4	<DL	<DL
Mount Pleasant	Orogenic gold	Sciuba et al 2020	MTPL-01	0.99	280	8.3	61.2	<DL	<DL
Mount Pleasant	Orogenic gold	Sciuba et al 2020	MTPL-01	0.83	242	12.2	95	0.49	<DL
Mount Pleasant	Orogenic gold	Sciuba et al 2020	MTPL-01	0.47	135.3	4.67	31.2	0.14	<DL
Mount Pleasant	Orogenic gold	Sciuba et al 2020	MTPL-01	0.67	173	9.6	71	0.78	0.045
Mount Pleasant	Orogenic gold	Sciuba et al 2020	MTPL-01	0.73	361	5.99	76	<DL	<DL
Mount Pleasant	Orogenic gold	Sciuba et al 2020	MTPL-01	0.72	226	7.1	67.6	0.52	0.036
Mount Pleasant	Orogenic gold	Sciuba et al 2020	MTPL-01	0.51	107	4.14	17.1	0.15	<DL
North Royal Norseman	Orogenic gold	Sciuba et al 2020	NORS-01	0.53	12	6.76	12.5	0.064	<DL
North Royal Norseman	Orogenic gold	Sciuba et al 2020	NORS-01	0.52	17	5.98	19.3	0.038	<DL
North Royal Norseman	Orogenic gold	Sciuba et al 2020	NORS-01	0.42	15.4	4.48	8.2	0.32	<DL
North Royal Norseman	Orogenic gold	Sciuba et al 2020	NORS-01	0.3	39	4.47	29.6	<DL	<DL
North Royal Norseman	Orogenic gold	Sciuba et al 2020	NORS-01	0.38	37	3.76	21	<DL	<DL
North Royal Norseman	Orogenic gold	Sciuba et al 2020	NORS-01	0.44	15.7	5.45	3.56	<DL	<DL
North Royal Norseman	Orogenic gold	Sciuba et al 2020	NORS-01	0.8	34.2	6.2	6.8	0.36	<DL
North Royal Norseman	Orogenic gold	Sciuba et al 2020	NORS-01	0.61	27.6	4.93	21.5	0.081	<DL
Crown Footwall Norseman	Orogenic gold	Sciuba et al 2020	NORS-02A	0.89	354	6.6	68	0.33	0.086
Crown Footwall Norseman	Orogenic gold	Sciuba et al 2020	NORS-02A	1.05	328	3.77	15.1	0.17	<DL
Crown Footwall Norseman	Orogenic gold	Sciuba et al 2020	NORS-02A	1.17	379	4.47	32	0.08	<DL

Appendix 1.6B (continued)

Name	Deposit_type	Reference	Sample ID	B ppm	Na ppm	Mg ppm	K ppm	Ti ppm	V ppm
Crown Footwall Norseman	Orogenic gold	Sciuba et al 2020	NORS-02A	1.04	61.1	4.01	30	0.15	<DL
Crown Footwall Norseman	Orogenic gold	Sciuba et al 2020	NORS-02A	0.78	66.7	4.73	43	0.09	<DL
Crown Footwall Norseman	Orogenic gold	Sciuba et al 2020	NORS-02A	0.86	105	5.8	43	0.4	<DL
Crown Footwall Norseman	Orogenic gold	Sciuba et al 2020	NORS-02A	0.93	79.2	4.94	39.8	0.23	<DL
Crown Footwall Norseman	Orogenic gold	Sciuba et al 2020	NORS-02B	0.8	109.9	6.1	76.1	0.42	0.043
Crown Footwall Norseman	Orogenic gold	Sciuba et al 2020	NORS-02B	0.73	55	4.11	28.3	0.31	0.095
Crown Footwall Norseman	Orogenic gold	Sciuba et al 2020	NORS-02B	0.35	39.3	4.3	25.7	0.64	0.161
Mararoa Norseman	Orogenic gold	Sciuba et al 2020	NORS-03	0.69	92	2.93	6.8	0.131	<DL
Mararoa Norseman	Orogenic gold	Sciuba et al 2020	NORS-03	1.18	24.8	3.41	13.7	0.13	0.044
Mararoa Norseman	Orogenic gold	Sciuba et al 2020	NORS-03	0.8	58.9	5	26	0.098	0.221
Mararoa Norseman	Orogenic gold	Sciuba et al 2020	NORS-03	0.82	77.3	3.05	29	0.21	0.277
Mararoa Norseman	Orogenic gold	Sciuba et al 2020	NORS-03	0.83	39.8	2.97	19	0.041	0.065
Mararoa Norseman	Orogenic gold	Sciuba et al 2020	NORS-03	1.07	59	3.74	23.9	0.12	<DL
Mount Charlotte	Orogenic gold	Sciuba et al 2020	MTCH-01A	1.38	34.1	4.41	51	0.12	<DL
Mount Charlotte	Orogenic gold	Sciuba et al 2020	MTCH-01A	1.13	42.8	5.92	84	0.9	<DL
Mount Charlotte	Orogenic gold	Sciuba et al 2020	MTCH-01A	1	164	4.33	22	0.12	0.085
Mount Charlotte	Orogenic gold	Sciuba et al 2020	MTCH-01A	1.09	92	4	20.9	<DL	0.112
Mount Charlotte	Orogenic gold	Sciuba et al 2020	MTCH-01A	1.11	129.8	4.79	32.8	0.14	0.087
Mount Charlotte	Orogenic gold	Sciuba et al 2020	MTCH-01A	0.89	9.4	3.56	13.9	<DL	<DL
Mount Charlotte	Orogenic gold	Sciuba et al 2020	MTCH-01B	1.48	150	6.1	74	0.17	0.126
Mount Charlotte	Orogenic gold	Sciuba et al 2020	MTCH-01B	1.94	217	6.2	66	0.56	0.154
Mount Charlotte	Orogenic gold	Sciuba et al 2020	MTCH-01B	1.59	203	6.4	75	0.96	0.109
Mount Charlotte	Orogenic gold	Sciuba et al 2020	MTCH-01B	1.48	73.4	4.3	46.1	0.24	<DL
Mount Charlotte	Orogenic gold	Sciuba et al 2020	MTCH-01B	1.69	173	7.2	74	0.47	0.112
Mount Charlotte	Orogenic gold	Sciuba et al 2020	MTCH-01B	1.38	82.1	4.18	18.8	0.05	<DL
Mount Charlotte	Orogenic gold	Sciuba et al 2020	MTCH-01B	1.17	75.6	3.92	18	0.069	<DL
Mount Charlotte	Orogenic gold	Sciuba et al 2020	MTCH-01B	1.02	26.2	3.63	16.3	0.06	<DL
Mount Charlotte	Orogenic gold	Sciuba et al 2020	MTCH-01B	1.32	55.5	3.87	18.2	0.13	<DL
Macraes	Orogenic gold	Sciuba et al 2020	MACR-01B	8	28.5	277	1220	79	2.01
Macraes	Orogenic gold	Sciuba et al 2020	MACR-01D	2.03	68.1	16.2	6.9	0.28	<DL
Macraes	Orogenic gold	Sciuba et al 2020	MACR-01D	1.83	49.8	15.4	9.5	2	<DL
Macraes	Orogenic gold	Sciuba et al 2020	MACR-01D	5.4	73	37	13	1.4	0.2

Appendix 1.6B (continued)

Name	Deposit_type	Reference	Sample ID	B ppm	Na ppm	Mg ppm	K ppm	Ti ppm	V ppm
Macraes	Orogenic gold	Sciuba et al 2020	MACR-01D	1.44	37	13.9	6.8	0.39	<DL
Macraes	Orogenic gold	Sciuba et al 2020	MACR-01D	1.61	35.1	12.1	4.43	0.61	0.053
Macraes	Orogenic gold	Sciuba et al 2020	MACR-01D	2.14	53.1	15.9	7.2	0.8	0.044
Macraes	Orogenic gold	Sciuba et al 2020	MACR-01D	1.75	52.7	18.8	7.5	0.58	<DL
Macraes	Orogenic gold	Sciuba et al 2020	MACR-01D	1.43	62.5	17.5	7.6	0.64	<DL
Macraes	Orogenic gold	Sciuba et al 2020	MACR-01D	1.51	79	19.7	10.1	0.36	<DL
Macraes	Orogenic gold	Sciuba et al 2020	MACR-01D	1.27	40.4	11.4	4.88	0.32	<DL
Macraes	Orogenic gold	Sciuba et al 2020	MACR-01D	1.45	68	21.8	10.4	0.73	<DL
Macraes	Orogenic gold	Sciuba et al 2020	MACR-01D	1.52	62.4	18	9.1	0.66	<DL
Macraes	Orogenic gold	Sciuba et al 2020	MACR-01D	1.2	74	57	219	9.9	0.45
Macraes	Orogenic gold	Sciuba et al 2020	MACR-01D	1.4	55	19	8.8	0.83	<DL
Macraes	Orogenic gold	Sciuba et al 2020	MACR-01D	1.6	66	32	14	1.8	<DL
Macraes	Orogenic gold	Sciuba et al 2020	MACR-01D	1.33	56	14.8	3.7	0.08	<DL
Macraes	Orogenic gold	Sciuba et al 2020	MACR-01D	1.01	48.7	17.3	6.6	0.64	<DL
Macraes	Orogenic gold	Sciuba et al 2020	MACR-01D	1.27	55.6	21	22	1.64	<DL
Crusader	IRGS	Sciuba et al 2020	CRUS-01A	0.42	22	8.64	4.2	0.58	0.122
Crusader	IRGS	Sciuba et al 2020	CRUS-01A	0.31	84.9	12.2	5.1	0.37	1.29
Crusader	IRGS	Sciuba et al 2020	CRUS-01A	0.359	38.7	10.1	4.12	0.41	0.347
Crusader	IRGS	Sciuba et al 2020	CRUS-01A	0.33	138.8	14.5	4.18	0.97	2.16
Crusader	IRGS	Sciuba et al 2020	CRUS-01A	<DL	216	15.6	4.85	0.91	5.53
Crusader	IRGS	Sciuba et al 2020	CRUS-01A	0.25	184	15.6	4.22	0.85	3.76
Crusader	IRGS	Sciuba et al 2020	CRUS-01A	<DL	56.5	11	1.65	0.65	1.54
Crusader	IRGS	Sciuba et al 2020	CRUS-01A	<DL	51.2	9	4.4	0.6	0.31
Crusader	IRGS	Sciuba et al 2020	CRUS-01A	0.39	43.2	6.79	3.23	0.64	0.64
Crusader	IRGS	Sciuba et al 2020	CRUS-01A	0.5	37.5	6.68	1.71	0.35	0.56
Crusader	IRGS	Sciuba et al 2020	CRUS-01A	0.35	40.9	7.5	2.15	0.53	0.69
Crusader	IRGS	Sciuba et al 2020	CRUS-01A	0.4	42.9	8.1	2.03	0.69	0.775
Crusader	IRGS	Sciuba et al 2020	CRUS-01A	0.7	159	9.29	2.03	0.72	2.91
Crusader	IRGS	Sciuba et al 2020	CRUS-01A	0.36	50.7	15.3	8	3.8	0.95
Crusader	IRGS	Sciuba et al 2020	CRUS-01A	0.5	100	12.4	5	2.3	1.86
Crusader	IRGS	Sciuba et al 2020	CRUS-01B	1.05	166.1	6.84	2.33	0.38	4.25
Crusader	IRGS	Sciuba et al 2020	CRUS-01B	0.87	15.6	5.65	2.15	0.27	0.166

Appendix 1.6B (continued)

Name	Deposit_type	Reference	Sample ID	B ppm	Na ppm	Mg ppm	K ppm	Ti ppm	V ppm
Crusader	IRGS	Sciuba et al 2020	CRUS-01B	0.95	75	6.32	2.41	0.4	1.59
Crusader	IRGS	Sciuba et al 2020	CRUS-01B	0.66	63.2	7.1	3.78	0.51	1.05
Crusader	IRGS	Sciuba et al 2020	CRUS-01B	0.84	124	6.65	4.48	0.37	2.87
Crusader	IRGS	Sciuba et al 2020	CRUS-01B	0.79	98	6.7	5.11	0.51	2.12
Crusader	IRGS	Sciuba et al 2020	CRUS-01B	0.9	188.7	6.68	1.76	1.8	5.19
Crusader	IRGS	Sciuba et al 2020	CRUS-01B	0.64	227.4	7.8	2.6	0.72	5.15
Crusader	IRGS	Sciuba et al 2020	CRUS-01B	1.08	237	26	6.4	2.2	4.81
Crusader	IRGS	Sciuba et al 2020	CRUS-01B	0.83	216.7	11.8	4.6	1.34	5.12
Crusader	IRGS	Sciuba et al 2020	CRUS-01B	0.48	235	9	1.85	0.31	5.3
Crusader	IRGS	Sciuba et al 2020	CRUS-01B	0.96	76.6	7.61	1.42	0.36	5.33
Crusader	IRGS	Sciuba et al 2020	CRUS-01B	0.77	193	7.91	3.1	0.26	5.18
Crusader	IRGS	Sciuba et al 2020	CRUS-01B	0.77	162	7.53	1.63	0.3	5.26
Amaruq	Orogenic gold	de Bronac de Vazelhes et al 2021	288464-1-1.d	<DL	39.3	20.3	<DL	0.35	0.135
Amaruq	Orogenic gold	de Bronac de Vazelhes et al 2021	288464-1-2.d	<DL	22.9	450	9	1.9	0.156
Amaruq	Orogenic gold	de Bronac de Vazelhes et al 2021	288464-1-3.d	1.78	12.84	19.3	1.18	0.267	0.057
Amaruq	Orogenic gold	de Bronac de Vazelhes et al 2021	288464-1-4.d	2.12	10.45	5.2	<DL	<DL	0.084
Amaruq	Orogenic gold	de Bronac de Vazelhes et al 2021	288464-1-5.d	4.3	15	56	1.43	2.48	0.204
Amaruq	Orogenic gold	de Bronac de Vazelhes et al 2021	288464-1-6.d	1.24	12.4	9	2.08	2.04	0.059
Amaruq	Orogenic gold	de Bronac de Vazelhes et al 2021	288464-1-7.d	1.69	10.42	4.1	1.2	0.191	0.059
Amaruq	Orogenic gold	de Bronac de Vazelhes et al 2021	331805-1-1.d	2.88	14.07	7	<DL	<DL	0.062
Amaruq	Orogenic gold	de Bronac de Vazelhes et al 2021	331805-1-2.d	2.92	22.7	4.48	<DL	<DL	0.0282
Amaruq	Orogenic gold	de Bronac de Vazelhes et al 2021	331806B-1-1.d	3.38	69.1	3.96	1.49	0.29	0.0357
Amaruq	Orogenic gold	de Bronac de Vazelhes et al 2021	331806B-1-2.d	2.9	55.6	13	<DL	<DL	<DL
Amaruq	Orogenic gold	de Bronac de Vazelhes et al 2021	331806B-1-3.d	2.45	46.9	10.7	1.8	0.46	0.05
Amaruq	Orogenic gold	de Bronac de Vazelhes et al 2021	331807-4-1.d	3.12	141.8	23.4	<DL	0.88	0.163
Amaruq	Orogenic gold	de Bronac de Vazelhes et al 2021	331807-4-2.d	2.6	128.7	5.1	<DL	0.5	0.211
Amaruq	Orogenic gold	de Bronac de Vazelhes et al 2021	331807-6-1.d	5.6	118.9	11.3	<DL	0.45	0.143
Amaruq	Orogenic gold	de Bronac de Vazelhes et al 2021	331807-6-2.d	9	133	40	3.3	3.1	0.64
Amaruq	Orogenic gold	de Bronac de Vazelhes et al 2021	331807-6-3.d	5.3	114	9.5	<DL	1.9	0.98
Amaruq	Orogenic gold	de Bronac de Vazelhes et al 2021	331807-6-4.d	<DL	99.7	4.9	<DL	0.85	0.36
Amaruq	Orogenic gold	de Bronac de Vazelhes et al 2021	331807-6-5.d	4.9	89.4	23	<DL	0.24	0.313
Amaruq	Orogenic gold	de Bronac de Vazelhes et al 2021	331807-7-6.d	<DL	123	55	3.9	0.83	0.429

Appendix 1.6B (continued)

Name	Deposit_type	Reference	Sample ID	B ppm	Na ppm	Mg ppm	K ppm	Ti ppm	V ppm
Amaruq	Orogenic gold	de Bronac de Vazelhes et al 2021	331807-7-7.d	<DL	115	6.2	<DL	0.77	0.4
Amaruq	Orogenic gold	de Bronac de Vazelhes et al 2021	331815-2-1.d	<DL	166.1	3.89	1.68	0.69	0.402
Amaruq	Orogenic gold	de Bronac de Vazelhes et al 2021	331815-2-2.d	<DL	138.2	6.6	1.46	0.51	0.353
Amaruq	Orogenic gold	de Bronac de Vazelhes et al 2021	331807-2-3.d	2.08	113	11.1	0.74	0.46	0.244
Amaruq	Orogenic gold	de Bronac de Vazelhes et al 2021	331807-2-4.d	1.8	82	5.4	1.69	0.55	0.186
Amaruq	Orogenic gold	de Bronac de Vazelhes et al 2021	331807-1.d	<DL	154.9	16.5	1.24	0.26	0.463
Amaruq	Orogenic gold	de Bronac de Vazelhes et al 2021	331807-3.d	1.69	83.2	13.7	<DL	0.38	0.19
Amaruq	Orogenic gold	de Bronac de Vazelhes et al 2021	331813-1.d	6.1	263.9	27	<DL	1.9	0.95
Amaruq	Orogenic gold	de Bronac de Vazelhes et al 2021	331813-2.d	5.46	200.1	3.36	<DL	<DL	0.679

Appendix 1.6B (continued)

Sample ID	Mn ppm	As ppm	Sr ppm	Y ppm	Nb ppm	Mo ppm	Ba ppm	La ppm	Ce ppm	Pr ppm	Nd ppm	Sm ppm	Eu ppm	Gd ppm
MELI-01	8.1	320	256	157	53.4	41.8	0.23	0.696	3.99	1.27	15	13.6	5.17	52.2
MELI-01	8.31	<DL	508	258	75.9	9.55	0.34	1.53	10.9	4.39	62	70	16.6	190
MELI-01	10	<DL	437.2	461.8	69.9	85	0.12	0.45	2.89	1.009	13.8	22.9	10.04	131
MELI-01	9.38	<DL	281	185.1	51.5	88	0.31	1.181	5.96	1.66	16.08	13.93	4.85	59.3
MELI-01	10.75	<DL	342	216	81.6	13.74	0.22	1.11	6.9	2.25	29.8	37.5	9.5	118.7
DOME-02	1.36	8.77	923	585	6.56	3.98	0.96	19.7	270	39	353	151.7	91.6	176.4
DOME-02	3.6	9.52	928	710	6.44	3.67	1.36	24.1	155	44.1	388	167	97.2	196
DOME-02	2.41	8.92	1025	480	5.99	3.02	1.91	13.7	97.9	31.2	299.4	150	66.4	182.9
HOLL-01	922	<DL	148.4	2.57	<DL	0.047	0.24	0.334	0.763	0.14	1.03	0.71	0.632	0.769
HOLL-01	935	<DL	98.3	5.38	<DL	0.037	0.46	1.38	3.48	0.611	3.69	1.68	1.174	1.773
HOLL-01	1022	<DL	115.1	11.1	<DL	<DL	0.2	0.158	0.39	0.076	0.423	0.36	0.509	0.69
YOUN-01	2.35	5.71	1828	295	0.448	47	2	37.5	122	19.91	115.3	42	21.3	65.8
YOUN-01	4.3	7.41	2900	433	0.72	50	1.6	44.6	161	27.1	158	56.6	39.9	80.9
YOUN-01	3	6.66	2080	328	0.492	65	1.97	37.6	131.6	23.23	144.7	59.1	33.4	87.7
YOUN-01	1.42	10.4	3520	446	0.837	115	0.23	990	1480	157	650	108	50.6	98
YOUN-01	1.07	7.46	3610	383	0.674	14.8	0.45	93	280	38.4	181	47.2	34.3	54.5
YOUN-01	1.61	6.75	3330	402	0.78	11.3	0.21	77	261	36.8	182	49.9	35.7	61.7

Appendix 1.6B (continued)

Sample ID	Mn ppm	As ppm	Sr ppm	Y ppm	Nb ppm	Mo ppm	Ba ppm	La ppm	Ce ppm	Pr ppm	Nd ppm	Sm ppm	Eu ppm	Gd ppm
YOUN-01	1.47	8.65	3508	412	0.791	54	0.308	430	730	83	360	71	40.9	73.1
YOUN-01	1.99	7.61	3480	418	0.819	11.3	0.31	98.2	306	41.4	202	56.1	39.1	67.7
MALA-10	7.14	36	1846	48.8	1.062	1395	3.15	8.44	38.8	8.36	60.2	16.8	5.27	20.8
MALA-10	8.27	12.4	1980	144	3.96	914	1.41	8.9	34.3	7.8	79.1	48.5	15.6	103.6
MALA-10	9.69	22.6	2083	159.7	2.62	871	1.76	4	20	6.12	75.8	49.4	17.78	109.5
MALA-10	8.3	9.4	1656	34.2	1.49	1482	2.07	13.5	53.1	9.66	60.6	15.8	5.74	17.3
MALA-10	9.51	28	1734	34.3	1.337	1408	2.9	13.3	55.5	10.3	64.7	14.51	4.86	16.3
96-DP-162	1.59	9.68	558	448	6	63.5	0.298	1.99	16.8	5.91	63.2	53.4	23.22	149.9
96-DP-162	2.81	11.9	563	483	6.92	61.1	0.26	3.17	19.8	6.7	70.2	59.4	24.3	167.1
96-DP-162	3.6	9	493	327	4.62	63.1	0.41	2.8	17.2	5.5	55	45.6	18.3	119
96-DP-162	2.89	7.4	541	419	4.11	65.6	0.21	4.8	29	8.9	85	69.6	29.2	177
96-DP-162	3.31	7.7	589	471	4.86	67	0.47	4.6	28.8	8.6	88	71	30	187
96-DP-162	2.97	11.3	574	238	3.7	209	0.35	0.96	8.35	3.28	39.6	38.3	14.7	113
96-DP-162	3.01	6.9	554	397	4.38	61.1	0.17	2.15	16.8	5.82	67.5	61.2	26.4	169
96-DP-162	3.7	7.66	579	393	4.5	61.7	0.48	2.18	17.4	6.1	70	60.1	26.2	163
96-DP-162	3.78	6.4	560	418	4.84	68.3	0.138	4.89	31.6	9.8	96.3	73.8	29.3	190
96-DP-162	3.42	7.4	561	394	4.36	79	0.289	3.18	21.5	7.08	75.1	63.2	26.1	168.3
96-DP-162	4.37	9.1	538	612	6.8	67.1	0.105	2.54	21.1	7.36	82.6	75.2	26.6	208
96-DP-162	4.11	9.95	542	540	5.43	65.8	0.18	2.38	19.4	6.74	76.2	67.8	25.3	191.7
96-DP-162	4.26	11.1	544	348	4.42	61.2	0.21	1.56	14.4	5.46	67	55.9	22.9	152
B580-15	2.88	3.17	667	853	7.84	16.9	0.109	6.1	56.9	22.3	277	261	69.2	568
B580-15	3.36	6.8	660	780	7.27	25	0.27	260	630	110	770	390	88	620
B580-15	2.99	4.3	672	842	7.81	19.8	0.145	71	210	47	420	305	77.2	600
B580-15	4.15	2	651	267.5	3.95	18.99	0.265	5.27	37.6	12.58	131.4	93.4	27.1	167.3
B580-15	3.78	3.43	700	661	8.64	17.97	0.16	10.3	69	23.9	278	242	59.8	509
B580-15	3.26	3.19	653	800	9.72	18.8	0.055	11.5	82	26.3	304	266	69.4	571
B580-15	3.86	2.74	635	576	7.14	17.2	0.28	5.1	44.2	17.5	222	208	56	441
B580-15	3.46	3.06	658	657	7.97	17.87	0.166	8.4	60.6	21.8	258	231	60	490
B580-15	3.07	5.9	654	492	7.05	19	0.4	5.4	38.5	15	188	180	46.2	390
B580-15	2.9	4.33	656	589	7.47	19.5	0.4	5.1	71	16.3	204	194	52.4	422
94-GB-15A	9.39	9.33	267	605	2.45	5.54	0.103	33.1	185.2	38.3	231	80	125.6	100.1
94-GB-15A	3.25	6.64	266.1	521	2.24	5.07	0.177	13.4	72	17.3	120	51.8	102.9	73.5

Appendix 1.6B (continued)

Sample ID	Mn ppm	As ppm	Sr ppm	Y ppm	Nb ppm	Mo ppm	Ba ppm	La ppm	Ce ppm	Pr ppm	Nd ppm	Sm ppm	Eu ppm	Gd ppm
94-GB-15A	6.25	8.45	265.6	630	2.404	5.22	0.108	44	206	41	239	81	129	100
94-GB-15A	3.69	6.41	295.2	606	2.57	5.1	0.034	32.1	177	35.8	213	74.8	135	93.9
94-GB-15A	5.57	8.84	288	664	3.41	5.66	0.147	38	201	42.7	278	108.1	130.7	143
94-GB-15A	3.98	7.05	293.4	636	2.68	5.29	0.084	32.4	181.5	37.2	223.7	79.9	134.6	101.7
94-GB-15A	8.08	13.6	254.1	600	3.12	5.02	0.197	27.9	165.3	38	262	106.5	117.5	138.8
SIGM-01	4	11.42	255.4	624	3.86	4.83	0.098	27.4	185	42.4	290	114.4	107.8	137.7
SIGM-01	3.23	13.05	213	648	4.27	4.71	0.135	32.4	213.6	48.7	334	135.2	124.3	164.8
SIGM-01	3.72	11.86	233.6	608	3.87	4.81	0.141	28.2	187.8	43.2	299	120.1	113.1	145.6
SIGM-01	10.04	9.81	199.9	589.8	4.02	4.48	0.174	18.66	142	37.37	278	124.8	112.3	158.7
SIGM-01	2.92	10.71	211.1	660	4.63	4.88	0.152	42	240	52	375	169	123	219
SIGM-01	7.89	8.32	253.2	551	2.65	5.45	0.28	20.9	148.9	35.8	245	96	121.7	120.1
SIGM-01	5.25	11.3	247.9	646	4.02	5.21	0.226	33	181	41.5	292	124	119.9	165
SIGM-01	3.37	8.01	268.2	533	2.855	5.1	0.124	22.4	149	32.7	209	75.7	117.1	93.8
LAMA-01	2.19	43	812	575	2.26	46.6	0.51	19	145	47	490	330	94	446
LAMA-01	2.04	21.5	772	328	2.02	42.5	0.198	9	77	28.1	300	205	65	281
LAMA-01	2.38	35.1	788	504	2.188	42.1	0.34	13.6	108	36.4	383	311	79.7	373
CUIA-03	5.03	0.85	833	54.9	0.262	0.088	0.265	27.5	34.1	3.09	10	1.85	16.5	2.2
CUIA-03	7.2	1.09	832	42.7	0.246	0.094	0.348	18.6	23.4	2.03	6.58	1.39	12.46	1.83
CUIA-03	15.4	<DL	764	44.1	0.264	0.039	0.42	25.9	36.6	3.48	11.8	2.5	11.41	2.8
CUIA-03	18.9	2.33	728	138	0.274	0.072	0.57	35	84	10.6	43	9.7	24.2	11.6
160277	3.63	1.4	2486	113	0.418	0.71	1.11	17.7	46	6.73	32.6	12.1	25.9	18.4
160277	7.3	18	2406	142	0.487	0.636	0.559	35	81	11.7	59.7	20.6	28.8	32.5
160286	1.79	0.64	2298	54.7	0.304	0.375	0.248	22.1	43.8	5.28	23.7	6.6	24.5	8.2
160286	1.66	1.29	2154	145	0.302	0.374	0.165	36.8	117	17.6	85.1	23.6	55.2	28.4
160286	5.82	1.4	2331	46.7	0.309	0.538	0.44	25.8	34.9	3.27	11.7	3.21	40.5	3.83
160304	2.88	1.04	3152	66	0.262	0.141	0.55	16.3	33.3	4.54	23	7.7	23.2	9.7
160304	3.14	0.79	2680	65.9	0.216	0.185	0.37	16.8	31.6	3.83	17	5.3	24.9	6.4
160304	2.08	0.9	2990	54.2	0.19	0.117	0.95	14.8	29	3.43	15.9	4.6	19.9	5.7
160304	2.24	1.8	2470	250	0.252	0.076	0.53	25.1	87	15.3	79.1	24.5	61	34
160304	2.92	0.93	2860	242	0.29	0.22	0.61	30.7	94	13.7	60.2	15.1	75	18.6
160304	2.94	0.98	2705	109	0.222	0.147	0.45	19.4	45.7	6.4	30.1	8.9	33.8	11.4
160304	1.35	1.66	2340	116	0.202	0.13	0.29	11.5	38.4	6.33	32.4	10.5	32.4	13.3

Appendix 1.6B (continued)

Sample ID	Mn ppm	As ppm	Sr ppm	Y ppm	Nb ppm	Mo ppm	Ba ppm	La ppm	Ce ppm	Pr ppm	Nd ppm	Sm ppm	Eu ppm	Gd ppm
160304	<DL	1.73	2650	207	0.31	0.31	0.35	23.2	76.4	11.4	56	15.6	48.7	21.8
160304	0.99	1.5	2890	138	0.265	0.186	0.39	18.8	55	8.7	45	14.2	37.5	18.7
160304	1.14	1.67	2440	164	0.269	0.15	0.277	16.2	54.3	9.4	50	17.6	40.6	23.1
160304	<DL	2.24	2330	305	0.44	0.166	0.27	23	93	17.5	101	37.1	58.6	51
160310	2.87	0.44	2682	53.3	0.64	0.078	0.204	13.2	34.8	4.8	21.3	5.7	34	7.1
160310	2.52	<DL	2830	87	0.363	0.077	0.075	16.7	52	8	38	10.1	43.1	13.3
160310	2.42	<DL	2752	31	0.403	0.066	0.15	11.24	22.9	2.73	11.6	3.26	20.2	3.99
160310	2.38	<DL	2824	47.7	0.377	0.087	0.121	12.67	31.3	4.3	19.2	5.1	27.4	6.5
160310	3	1.19	3580	37	0.49	<DL	0.05	32	49	4.5	14	3	27.6	2.96
BZWA-01	32.73	4.01	1948	94.4	2.1	142.5	0.48	0.528	6.84	3.98	57.1	40.8	14.8	58.8
HUTT-01	22.3	7.3	344	473	10.22	0.38	0.47	43	166	25.7	125	35.5	41.4	52.3
HUTT-01	16.8	12.6	252	364	11.6	1.85	0.7	14.8	66	11.9	65	22.1	24.1	35.7
HUTT-01	9.01	17.7	171	241	13.1	2.53	0.9	2.27	13.3	3.36	26.1	13	10.28	24.2
HUTT-01	5.7	11.1	127	186	20.8	3.78	0.66	1.78	9.7	2.43	19.1	10.3	8.93	19.1
HUTT-01	9.61	19.6	150	229	24.7	3	1.14	2.03	11.6	3.26	25.8	13.26	7.1	25.4
HUTT-01	14.8	13.3	247	154	1.82	0.38	0.38	6	24	4.68	26.8	9.89	8.42	15.8
HUTT-01	9	21	202	185	2.48	0.28	1.53	1.39	9.31	2.55	18.7	8.78	6.29	16.7
HUTT-01	10.18	22.3	176.6	250	30	1.45	1.15	1.87	11.58	3.14	24.4	12.2	6.7	24.1
HUTT-01	10.48	19.3	183.7	210.2	15.8	1.52	1.05	2.44	13.2	3.35	24.46	11.54	7.09	21.3
HUTT-01	7.1	14.7	131	188	18.7	2.43	1.93	1.57	7.87	2.33	20.5	11.42	4.96	21.8
HUTT-01	9.1	16.3	147	194.2	15.3	1.94	1.58	1.56	9.5	2.91	24.6	12.9	5.83	23.8
HUTT-01	10.7	18.6	178	208	9.32	1.43	1.08	1.57	11.8	3.72	30.4	15	7.01	26.7
HUTT-01	7.8	24.1	167	249	14.1	1.06	1.54	1.58	9.9	2.84	23.6	11.8	5.81	23.2
HUTT-01	9.3	14	136	187	12.2	0.78	0.98	2.05	11.8	3.14	24.3	11.2	5.7	20.5
HUTT-01	10.7	16.7	208	192.6	2.11	0.46	0.83	3.11	18.9	4.65	31.9	12.7	10.85	20.4
HUTT-02	12.3	5.03	403	89.4	1	0.44	0.52	12.5	24.5	2.88	12.3	4.07	5.89	7
HUTT-02	7.7	12.3	239	192	48	4.5	0.52	5.8	19.7	3.95	26	12.1	7.7	25.2
HUTT-02	6.27	17.6	236	208	32	1.47	0.44	7.4	23	4.33	28.1	12.8	7.47	24.6
HUTT-02	9.7	10.4	315	148	13.1	1.18	0.391	9.39	24.7	3.92	22.1	9.2	7.39	16.7
HUTT-02	8.3	1.55	426	156	1.29	0.522	0.65	21.5	47.9	5.17	17.74	4.25	9.82	6
HUTT-04	16.9	17.2	481	31.8	0.239	0.31	1.74	5.05	13.6	2.14	11	3.66	4.85	4.46
HUTT-04	15.9	24.4	477	54	0.27	0.348	1.52	4.97	16.9	3.28	20.9	7.4	8.5	9.8

Appendix 1.6B (continued)

Sample ID	Mn ppm	As ppm	Sr ppm	Y ppm	Nb ppm	Mo ppm	Ba ppm	La ppm	Ce ppm	Pr ppm	Nd ppm	Sm ppm	Eu ppm	Gd ppm
HUTT-04	12.6	63	417	166.3	0.372	0.2	1.52	6.04	35.4	8.77	64.6	24.3	23.6	33.6
HUTT-04	19.8	7.92	510	15.3	0.242	0.53	1.02	3.45	7.37	0.936	4.47	1.13	3.94	1.69
HUTT-04	12.18	18.8	556	35.6	0.28	0.44	1.01	4.37	10.69	1.571	7.79	2.71	5.41	3.52
HUTT-04	19.3	19.1	556	39.3	0.286	0.69	1.3	5.04	13.06	2.06	11.99	4.42	6.48	6.07
KOCH-05A	13.1	54	830	33.7	4.91	75.1	4.4	31	146	25.5	137	25.5	19.6	18.6
KOCH-05A	16.2	101	1115	52.1	6.13	65	3.4	28	149	29.4	168	35.7	22.5	27.2
KOCH-05A	10.98	21.1	667	23.3	4.31	80.7	0.7	31.8	142	23.3	123	20.6	17.3	14.2
KOCH-05A	7.16	21.3	820	14.2	9.8	97.7	1.7	30.8	118	16.7	69.2	10.8	32.8	7.23
KOCH-05A	7.19	35.8	811	17.6	4.94	99.8	37	81	203	25.6	105	16.7	40.7	11.2
KOCH-05A	6.32	138	771	23.2	6.38	84.4	1.26	20.3	89.7	16.2	95	20.7	15.3	17.1
KOCH-05A	11.1	34	900	29	6.7	82.2	56	28.9	127.3	21.8	114.9	22.4	31.1	17.1
KOCH-05A	9.85	27.3	883	22.4	4.74	114	26	22.8	98	16.3	83.6	16.1	33.6	11.8
KOCH-06A	3.6	4.87	1042	5.86	1.97	567	1.88	3.17	7.9	1.12	5.5	1.27	4.34	1.29
KOCH-06A	3.43	4.41	1057	5.67	1.99	516	1.24	2.25	5.65	0.85	4.15	1.18	3.88	0.95
KOCH-06A	3.86	6.8	970	7.99	2.15	619	3.5	5.24	13.3	1.9	9.2	1.96	5.83	2.05
KOCH-06A	2.03	1.81	897	9.6	0.45	334	0.15	8.19	28.2	4.5	21.6	4.96	6.59	4.2
KOCH-06A	2.01	5.51	960	7.39	0.879	428	0.127	4.64	16.6	2.7	13.7	3.29	4.72	2.98
KOCH-06A	2.34	7.1	1024	9.81	1.31	549	0.13	5.36	17	2.66	13.5	3.2	5.52	3.16
KOCH-06A	2.4	6.9	985	5.51	0.93	404	0.17	3.22	12.6	2.08	11.3	2.82	3.96	2.36
KOCH-06B	3.05	16	921	8.6	5.35	467	48	4.52	15.5	2.48	13.4	3.68	4.01	3.83
KOCH-06B	1.74	7.64	891	5.4	4.76	383	13	1.86	7.74	1.45	8.6	2.86	2.56	2.95
KOCH-06B	2.51	16.5	960	9.72	5.59	517	38	5.67	17.5	2.58	13.48	3.38	4.7	3.52
KOCH-06B	2.6	16.6	943	10.14	5.39	509	34	5.77	18.7	2.84	14.9	3.89	4.74	4.16
KUMT-04	1.36	6.7	7300	13.2	0.38	196	0.35	8	20	3.4	17.6	6.6	2.04	8.4
KUMT-04	2.14	10.3	2820	6.1	0.39	240	1.32	40	76	9.6	37.9	6.5	1.31	4.86
KUMT-04	2.61	5.9	6340	2.14	0.385	195.6	1.21	2	3.78	0.85	3.15	1.11	0.298	1.29
KUMT-04	2.66	9.4	5570	5.2	0.413	211	1.12	12.5	26	3.8	16.5	3.8	1.16	3.6
MARV-01	11.56	7.92	684	12.57	0.294	0.034	0.17	4.41	8.9	1.319	7.2	2.17	15.9	2.55
MARV-01	11.44	9.55	693	13.77	0.295	0.021	0.217	4.83	10.31	1.524	8.44	2.83	15.3	3.07
MARV-01	10.96	12.38	668.2	16.83	0.36	0.02	0.406	6.08	15.27	2.347	13.04	4.06	11.97	4.24
MARV-01	9.1	11.47	621	14.02	0.388	0.26	0.36	4.44	11.49	1.852	10.81	3.49	13.32	3.66
MARV-01	9.34	8.22	1084	11.11	0.519	3.1	0.56	5.84	12.1	1.702	10.58	3.63	3.11	4.66

Appendix 1.6B (continued)

Sample ID	Mn ppm	As ppm	Sr ppm	Y ppm	Nb ppm	Mo ppm	Ba ppm	La ppm	Ce ppm	Pr ppm	Nd ppm	Sm ppm	Eu ppm	Gd ppm
MARV-01	9.61	9.8	1061	11.65	0.649	20.1	0.53	6.43	13.11	1.9	12.82	4.35	2.95	5.25
MARV-01	9	10.3	1053	13.06	1.19	92	0.41	6.73	13.76	2.04	12.9	4.38	2.234	5.95
MARV-01	8.1	9.2	1071	13.5	1.21	10.3	0.44	5.79	12.56	1.77	12.31	4.22	3.1	5.07
MARV-01	9.08	8.82	1091	11.92	0.729	20.3	0.456	6.31	12.98	1.835	11.74	3.85	2.97	4.92
MARV-01	9.68	10.47	689	12.48	0.328	0.034	0.248	4.88	11.54	1.719	9.31	2.87	15.46	2.87
MARV-01	9.79	10.02	656	12.52	0.356	0.031	0.198	4.86	11.67	1.796	10.23	3.19	13.78	3.27
NVOR-01	6.04	3.52	83.5	4.95	31.6	11060	0.234	2.13	10.19	2.6	27.01	12.22	4.51	8.59
NVOR-01	6.2	3.05	134.1	8.84	21.83	10690	0.17	3.04	9.42	1.772	15.11	6.3	2.87	5.06
NVOR-01	6.26	3.37	106.4	6.06	25.49	10910	0.302	2.64	9.76	2.142	19.8	8.68	3.64	6.35
NVOR-01	6.6	2.33	212.4	12.5	12.05	14590	0.35	1.035	2.66	0.424	2.55	0.93	0.456	1.68
NVOR-01	10.9	3.58	243	16.9	12.5	14620	0.31	1.237	3.73	0.61	3.98	1.49	0.7	2.68
NVOR-01	6.15	0.85	172.7	4.71	6.74	14670	0.52	0.566	1.26	0.132	0.74	0.221	0.151	0.398
EDWA-01	4.5	8.37	734	25.64	0.337	0.049	1.8	5.21	12.18	1.791	9.08	2.97	4.62	3.64
EDWA-01	5.4	9	790	27	0.329	<DL	0.46	5.22	12.22	1.82	9.84	3.24	4.79	3.73
EDWA-01	6.13	8	712	29.9	0.305	<DL	0.64	6.08	13.85	2.22	11.8	3.56	5.11	4.95
EDWA-01	5.25	6.4	901	25.4	0.24	0.044	0.31	4.63	10.59	1.59	8.87	3	4.58	3.62
EDWA-01	4.6	12.55	823	40	0.34	<DL	0.39	4.75	13.2	2.26	11.67	4.39	6.3	5.66
EDWA-01	5.69	13.45	680	50.8	0.262	<DL	0.24	6.17	18.2	3.01	17.9	7.06	9.1	8.4
TARM-01	5.2	16.7	2286	149.2	1.034	4.7	1.74	34.1	120.3	19.5	101.3	32.4	77.6	36.5
TARM-01	1.6	14.3	2380	235	1.2	10	1.92	32.4	183	36.9	220	76.8	105	85
TARM-01	3.7	14.3	2120	214	1.38	8	1.11	23.6	132	28.3	175	62.3	74.6	72
TARM-01	7.6	6.6	2396	84.4	0.443	3.8	1.22	29.2	78.5	11.08	51.7	15.6	67.7	17.5
TARM-01	4.72	9.7	2410	110.5	0.66	2.46	1.87	25.3	90.1	14.7	75.4	25.3	62	27.9
TARM-01	4.03	7.8	2178	190	1	2.2	0.99	29.6	151	29.3	166	58.2	95.4	65.1
TARM-01	5.66	7.79	2349	116.3	0.632	2.95	1.29	29.2	100.3	16.4	86	28	73.6	31
TARM-01	3.36	5.7	2386	131	1.39	1.49	1.43	22	79.4	14.9	89	34.7	52.3	41.3
TARM-01	5.13	12.1	2250	114.5	1.02	2.15	1.54	25.7	91.3	15.7	85.6	28.1	61.3	31.4
TARM-01	5.85	6.3	2649	99	0.577	2.38	2.18	30.4	78.6	11.7	58.9	20.5	65	23.6
TARM-01	4.7	7.1	2485	122	0.88	2.35	2.43	26.7	83.4	14.7	83	32.2	61.5	37.5
TARM-01	4.01	10.6	2310	210	1.81	2.56	2.91	22.6	108	23.8	161	69	83.8	85
PADD-01A	5.1	5.1	584	442	0.459	0.4	1.87	26.2	133	28.5	193	82	98.7	120
PADD-01A	4.55	5	548	358	0.41	0.437	1.97	34.5	143	26.1	172	61.3	92.4	86.5

Appendix 1.6B (continued)

Sample ID	Mn ppm	As ppm	Sr ppm	Y ppm	Nb ppm	Mo ppm	Ba ppm	La ppm	Ce ppm	Pr ppm	Nd ppm	Sm ppm	Eu ppm	Gd ppm
PADD-01A	3.6	4	594	307	0.559	0.39	1.31	30.4	127.1	24.2	148.6	58.7	65.9	84.8
PADD-01A	1.75	1.45	661	238	0.349	0.166	0.65	38	106	15.8	80	25.6	63.9	35.8
PADD-01A	3.14	3.16	530	429	0.51	0.223	1.03	22.8	122.9	27.2	186	86.3	88.8	129.3
PADD-01A	1.3	2.35	493	308	0.583	0.135	0.22	16.7	89	20.7	155	80	87.4	125
PADD-01A	1.26	1.15	412.9	207	0.336	0.32	0.269	33.7	103.9	14.8	73.8	25.5	102.3	35.6
PADD-01A	1.07	2.21	605	322	0.518	0.23	0.52	22.2	109.6	22.2	142	57	89.6	87.2
PADD-01A	1.29	1.92	472	275	0.445	0.26	0.322	25.4	100.7	18.6	118	51.9	93.5	80
PADD-01A	2.25	1.22	420	192	0.278	0.22	0.066	29.6	87.8	13.1	70.4	26.5	69	34.8
PADD-01A	1.26	1.12	415	272	0.305	0.38	0.219	41	136	19.4	95	31.8	112.2	42.1
PADD-01A	<DL	2.42	584	451	0.529	0.28	0.14	24.3	117	23.5	161	70.3	88.4	113.1
PADD-01A	1.56	1.53	449	291	0.33	0.293	0.187	33.4	116	18.5	103	39.3	94.3	56.3
PADD-01A	1.66	0.94	1696	63.7	0.366	0.16	0.83	4.48	24.5	5.9	41.9	16	33.7	19.6
PADD-01A	1.17	<DL	1575	24.4	0.296	0.041	0.23	1.92	9.7	2.55	20.9	9.27	32.7	12
PADD-01A	1.74	<DL	1622	11.2	0.275	0.117	0.36	1.35	6.45	1.385	8.54	3.24	13.1	3.66
PADD-01A	1.76	0.77	1633	39.4	0.327	0.123	0.64	3.02	16.1	3.89	28	11.1	27.5	13.6
PADD-02B	3.02	<DL	468	18.9	0.28	0.344	0.41	1.6	5.03	0.847	5.11	2.05	4.32	2.82
PADD-02B	2.76	<DL	469.7	32.9	0.303	0.446	0.5	2.7	9	1.62	9.8	3.74	9.4	4.6
PADD-02B	2.99	<DL	522	115	0.307	0.46	1.26	9.8	31.3	5.55	32.2	11.6	37.3	13.6
PADD-02B	2.54	<DL	465	12.87	0.316	0.57	0.33	0.89	3.19	0.622	4.18	1.59	3.9	2.07
PADD-02B	2.48	<DL	505	15.3	0.31	0.61	0.33	1.72	4.21	0.713	4.4	1.78	5.98	1.63
PADD-02B	3.4	<DL	504	17.6	0.283	0.54	0.38	1.35	4.29	0.79	5.71	2.28	6.95	2.48
PADD-02B	2.63	0.71	484	15.73	0.234	0.51	0.42	1.21	3.21	0.557	3.19	1.17	6.36	1.71
PADD-02B	2.89	<DL	493.7	15.72	0.272	0.502	0.403	1.54	3.88	0.651	3.89	1.45	6.42	1.74
PADD-02B	2.83	2	1431	20.5	0.313	0.069	1.96	4.14	12.9	2.31	13.3	5.2	37.5	6.3
PADD-02B	2.93	0.92	1150	58	0.3	0.058	0.69	7.1	24	3.99	22.1	7.2	19.2	9.7
PADD-02B	3.44	2.2	890	136	0.338	0.092	1.92	10.18	51.7	11.5	79	33	25.7	41.5
PADD-02B	2.94	1.49	1315	48	0.306	0.083	1.67	5.87	22.4	4.41	27.6	11	30.9	13.7
PADD-02B	3.28	0.44	467.7	15.63	0.291	0.503	0.259	1.288	3.54	0.666	4.34	1.8	5.95	2.21
MTPL-01	2.05	4.57	1674	710	11.03	0.29	0.363	24.1	196	58.6	506	269	105	354
MTPL-01	3.04	4.74	1246	559	6.12	0.94	0.64	24	183	59	610	292	98.9	369
MTPL-01	4.34	4.3	1958	509	16.82	0.177	0.77	30	210	59	490	257	88	315
MTPL-01	1.61	2.26	1207	374.9	2.29	0.639	0.326	17.7	123.8	32.4	239.4	108.1	65.9	129.5

Appendix 1.6B (continued)

Sample ID	Mn ppm	As ppm	Sr ppm	Y ppm	Nb ppm	Mo ppm	Ba ppm	La ppm	Ce ppm	Pr ppm	Nd ppm	Sm ppm	Eu ppm	Gd ppm
MTPL-01	3.4	1.75	1208	748	1.66	0.476	0.44	61.2	236	36.8	175	50.4	100.4	60
MTPL-01	2.96	3.07	1440	1090	16.8	0.46	0.75	31.2	191	44.4	290	119	99.2	155
MTPL-01	3.08	2.8	1241	812	7	0.513	0.62	71	290	52	284	89	102.6	102
MTPL-01	2.77	1.6	1299	707	1.78	0.581	0.331	44.4	207	38	217	82.6	104.7	99.7
NORS-01	1.9	<DL	471	41	0.284	0.276	0.332	8.2	13	1.44	5.82	1.59	10.49	2.02
NORS-01	5.17	<DL	448	21.6	0.264	0.364	0.65	3.46	5.37	0.67	3.35	1.2	5.8	1.67
NORS-01	3.57	<DL	684	11.6	0.287	0.255	0.44	1.32	3.88	0.73	4.8	1.69	7.1	2.44
NORS-01	5.35	0.77	579	26.2	0.537	0.34	0.52	2.75	6.06	0.902	5.03	2.42	4.92	3.52
NORS-01	4.9	0.59	577	25.4	0.651	0.353	0.217	1.68	4.39	0.642	2.91	0.88	4.23	1.1
NORS-01	6.63	0.69	430	26.6	0.274	0.376	0.55	2.29	5.43	0.78	3.85	1.35	4.28	1.77
NORS-01	4.56	<DL	418	26.1	0.256	0.27	0.68	4.9	8.49	1.08	5.8	1.88	4.53	2.76
NORS-01	6.23	0.33	466	30.4	0.339	0.236	0.66	3.14	6.68	0.935	4.6	1.56	9.02	2.08
NORS-02A	10.19	11.4	286.3	1510	359	0.79	0.139	76	460	115	890	660	120	750
NORS-02A	14.33	8	320	1680	305	0.95	0.218	45	290	77	1050	498	111	650
NORS-02A	16.67	6.8	302.3	858	251	0.76	0.194	21.1	157	46.6	395	324	86.6	383
NORS-02A	21.7	<DL	252.9	91.7	6.57	0.75	0.267	13.07	38.9	5.38	25.2	10.2	39.5	9.1
NORS-02A	22.6	0.56	235	90.7	2.88	0.56	0.32	14.64	42.5	6	26.6	10.8	39.1	9.6
NORS-02A	21.05	3.13	249.7	167	16.6	0.68	0.33	16.34	59.3	10.68	58.5	28.7	46.9	29.6
NORS-02A	21.85	1.61	246.6	123	8.5	0.679	0.276	14.41	47.5	7.63	37.9	17.3	43	16.8
NORS-02B	5.44	1.12	120.8	120.5	0.498	2.86	5.4	15.79	56.3	10.36	60	19.47	53.5	23.8
NORS-02B	6.83	6.74	325	52.4	0.245	0.15	1.42	6.93	21.7	3.65	19.3	5.04	26.9	5.81
NORS-02B	6.02	8.73	316	87.3	0.51	0.7	2.1	3.08	14.9	4.04	30.8	11.02	28.4	15.3
NORS-03	22.22	2.95	314.8	196.2	30.2	0.65	0.394	11.4	59.3	11.13	58.9	28.3	32.99	28.5
NORS-03	23.7	1.96	256	40.2	5.2	0.82	0.289	4.79	15.32	2.46	12.15	5.86	32.1	5.58
NORS-03	21.46	15.8	221	149	37.7	0.84	0.65	3.49	20.1	5.52	43.2	32.9	28.5	39.5
NORS-03	21.31	18.7	229.4	199	24.5	0.78	0.6	5.77	30.6	7.13	46.3	28.2	38.1	31.2
NORS-03	23.24	4.2	277	88.1	20.3	0.611	0.26	4.75	21.86	4.15	22.07	10.88	34.24	11.36
NORS-03	20.59	3.2	285	69.4	11.3	0.71	0.6	5.57	20.3	3.72	21.8	12	34.34	12.5
MTCH-01A	2.54	<DL	1160	52.4	0.264	0.79	0.35	16.42	25.7	2.47	8.62	2.28	21.7	2.79
MTCH-01A	2.09	<DL	1275	58.1	0.274	0.54	0.51	18.4	29	2.9	10.6	3.2	23.1	3.46
MTCH-01A	3.14	2.4	1067	393	0.674	0.307	0.58	15	106	30.4	257	162	112.9	193
MTCH-01A	2.76	2.12	1010	504	0.635	0.54	0.39	15.3	110	30.3	218	112	120.7	143

Appendix 1.6B (continued)

Sample ID	Mn ppm	As ppm	Sr ppm	Y ppm	Nb ppm	Mo ppm	Ba ppm	La ppm	Ce ppm	Pr ppm	Nd ppm	Sm ppm	Eu ppm	Gd ppm
MTCH-01A	2.81	2.08	1031	391	0.614	0.365	0.74	14.4	101	27.7	217	122	105.9	148
MTCH-01A	1.63	<DL	1391	85	0.274	0.574	0.191	20.9	43.9	5.32	22.9	6.83	29.18	7.77
MTCH-01B	2.49	3.56	883	470	0.488	0.297	0.58	21.7	124	28.4	197	92.7	110.6	118
MTCH-01B	2.38	4.5	1281	420	0.598	0.45	0.34	12.3	103	33.4	328	222	120	275
MTCH-01B	2.1	3.9	1043	305	0.72	0.41	1.56	11.1	190	28	281	193	96	241
MTCH-01B	1.69	1.63	669	93.2	0.56	0.8	0.71	5.6	38.9	11.5	98	61	34.9	67
MTCH-01B	2.24	2.99	914	256	0.639	0.511	1.16	9	93	22	212	144	74.9	175
MTCH-01B	2.39	0.68	591	202	0.411	0.36	0.91	22.8	104	13.3	66.3	20.1	87.8	22.2
MTCH-01B	2.42	0.81	576	181	0.377	0.33	0.74	19.2	94	11.6	56.5	16.9	78	18.4
MTCH-01B	2.05	<DL	542	69.5	0.355	0.32	0.48	12.7	33.1	4.07	16.6	3.63	45	4.16
MTCH-01B	2.26	0.72	555	135	0.356	0.341	0.59	16.9	65	8.7	40.6	11.6	66.3	12.6
MACR-01B	4.39	63	5050	182	0.565	0.17	17.1	50.6	132.8	17.37	77.6	19.3	11.1	21.3
MACR-01D	7.6	2.2	6470	145	0.282	<DL	4.54	26.8	55.6	7.18	35.8	11.4	9.4	16.8
MACR-01D	5.88	0.98	6910	73	0.299	<DL	4.4	15.63	26.2	3.38	16.4	5.26	4.39	7.9
MACR-01D	5.8	4.1	6340	208	0.39	<DL	4.9	27.9	66.8	8.9	40	11.6	11.3	17
MACR-01D	1.82	2.22	3500	176	0.65	<DL	3.1	12.8	53	12.9	84	31	18.3	45
MACR-01D	4.31	0.8	6780	74.2	0.357	<DL	1.8	18.2	28.1	3.28	14.3	4.3	3.81	6.5
MACR-01D	6.19	1.56	6620	112.8	0.334	<DL	3.67	21.3	41.4	5.53	28.5	8.8	7.17	12.9
MACR-01D	4.6	1.12	6090	100.4	0.299	0.062	6.13	20.3	37.3	4.44	19.3	5.39	5.46	7.86
MACR-01D	6.01	1.12	7050	166	0.359	0.073	2.51	18.2	47.6	6.24	27.6	7.8	5.8	11.8
MACR-01D	5.8	1.87	6400	250	0.37	0.23	4.1	27.2	91	12.2	53	14.7	16.7	22
MACR-01D	1.22	1.48	2250	536	0.53	0.17	1.46	17.7	137	26.4	131	37.7	80	60.1
MACR-01D	4.31	<DL	5130	115	0.364	0.073	3.76	15.6	35.6	4.7	22	6.34	6.33	9.5
MACR-01D	5.27	1.37	5830	214	0.397	0.118	3	17.5	61.1	9.5	45.3	13.3	18.8	20.6
MACR-01D	2.7	8.2	5160	248	0.42	0.19	9.4	12.9	79.4	16.4	95.6	36.2	21.6	55.5
MACR-01D	5.51	1.6	6020	71.7	0.271	0.073	5.4	13.94	23	2.89	14.3	4.68	3.62	6.9
MACR-01D	5	10	4780	124	0.51	0.05	7.4	14.2	41	6.9	36.1	12.4	7.25	19.9
MACR-01D	3.2	2.22	5000	421	0.54	0.15	2.29	34.9	138	23.5	129	46.8	20.9	66.5
MACR-01D	5.98	2.67	5410	106.2	0.311	0.061	5.77	17.6	32.9	4.07	19	6	4.23	8.9
MACR-01D	4.89	2.78	5540	137	0.356	0.09	5.77	16.6	43.7	6.9	36.5	12.9	7.7	18.9
CRUS-01A	6.88	7.69	115.1	1.8	1.27	68800	1.22	0.0085	0.117	<DL	0.008	<DL	0.028	0.015

Appendix 1.6B (continued)

Sample ID	Mn ppm	As ppm	Sr ppm	Y ppm	Nb ppm	Mo ppm	Ba ppm	La ppm	Ce ppm	Pr ppm	Nd ppm	Sm ppm	Eu ppm	Gd ppm
CRUS-01A	4.55	60.8	115	311	12.6	64500	0.98	0.169	0.61	0.145	1.57	2.1	4.99	8.2
CRUS-01A	6.18	20.3	110.9	79	3.92	63700	1.11	0.052	0.26	0.043	0.48	0.59	1.5	2.53
CRUS-01A	4.92	89.6	153.2	516	18.9	62400	1.26	4.82	11.51	1.82	10.4	5.51	9.83	14.9
CRUS-01A	5.04	224	132.9	1177	64.8	62000	1.34	1.75	5.76	1.29	13.9	16.3	19.2	76.3
CRUS-01A	4.92	159	139.2	854	42.4	61100	1.3	2.78	7.78	1.522	12.4	12	16.1	49.1
CRUS-01A	5.46	84	185.2	291	7	77100	1.19	10.58	33.7	6.7	44.8	24.6	15.3	47
CRUS-01A	6.99	14.2	149	124	2.68	77000	1.85	0.6	1.34	0.206	1.73	1.52	1.37	4.8
CRUS-01A	6.81	23	160.3	133	2.1	76600	1.63	3.27	8.2	1.34	8.2	4.4	3.08	9
CRUS-01A	7.93	23.3	171	109	1.72	76400	1.72	4.62	10	1.48	8.2	4.32	3.3	8.3
CRUS-01A	6.23	38.9	169.6	152	10.7	69500	1.61	5.55	12.4	2.1	14.1	9.2	6.21	23.6
CRUS-01A	6.46	34.6	174	144.5	4.64	74000	1.87	5.72	13.25	2.11	13.4	7.78	5.67	16.4
CRUS-01A	5.4	133	181.6	570	53.3	59100	4.4	14.8	61.7	15	130.9	80.8	40.4	162.5
CRUS-01A	5.39	32.4	170.8	151	1.75	74300	2.7	4.25	10.46	1.67	9.94	5.52	3.3	11.3
CRUS-01A	5.36	80	175.9	344	25.5	67500	3.4	9.1	34.1	7.8	66	40.2	20.3	81
CRUS-01B	4.51	172	116.2	860	48.8	58300	0.76	0.666	2.76	0.745	8.1	10.2	14.39	48
CRUS-01B	6.22	6.18	122.5	15.5	1.5	70200	1.09	0.0273	0.143	0.01	0.147	0.179	0.213	0.74
CRUS-01B	5.57	67	118.6	335	18.4	64300	0.97	0.305	1.2	0.295	3.09	3.8	5.8	17.4
CRUS-01B	5.34	58.6	108.8	260	11.38	60000	0.79	0.127	0.725	0.205	2.42	2.83	5.86	11.57
CRUS-01B	5.52	114.4	115.1	565	28.7	59800	0.72	0.203	0.937	0.257	2.48	4	10.33	20.8
CRUS-01B	5.49	95.8	113.5	507	23.3	60200	0.804	0.214	1.05	0.274	2.68	3.36	8.91	16.4
CRUS-01B	4.9	233	121.2	1018	85.6	60800	0.7	1.85	10.04	2.92	30.85	36	28.84	130.9
CRUS-01B	4.23	231.7	118.5	1137	78.7	59300	0.82	1.5	8.01	2.26	24.1	28.6	27.1	113.2
CRUS-01B	4.6	221.8	125.7	1139	66	63200	0.82	0.784	4.25	1.187	13.6	16.77	20.05	78.4
CRUS-01B	4.7	231.5	119.9	1087	79.5	59900	0.786	1.518	8.24	2.36	25.2	29.8	26.6	115.1
CRUS-01B	5.86	241	120.5	1180	79.9	59500	1.13	1.58	7.84	2.06	21.6	24.2	25	98
CRUS-01B	6.2	229.4	119.7	1074	64	58800	0.79	0.972	6.88	1.954	22.94	27.6	24.22	111.8
CRUS-01B	5.65	244	118.9	1007	82.8	58700	0.65	1.49	8.31	2.38	26.6	31.4	25	123.3
CRUS-01B	5.84	232.2	117.7	1073	68.3	58400	0.8	1.318	7.57	2.127	23.85	27.64	25.27	111.2
288464-1-1.d	7.36	1.6	658	54.7	2.053	49	0.83	4.48	26.86	8.31	72.6	28.8	34.7	36.5
288464-1-2.d	45	1.17	984	40.6	1.93	3.6	2.23	6.67	20.04	4.15	31.5	9.81	14.8	13.9
288464-1-3.d	14.4	1.022	1205	22.68	1.82	3.43	0.995	6.89	13.05	1.935	10	2.95	7.6	3.74
288464-1-4.d	8.63	1.49	1098	25.17	2.27	37.9	1.41	6.44	13.8	2.043	11.28	3.03	6.11	3.98

Appendix 1.6B (continued)

Sample ID	Mn ppm	As ppm	Sr ppm	Y ppm	Nb ppm	Mo ppm	Ba ppm	La ppm	Ce ppm	Pr ppm	Nd ppm	Sm ppm	Eu ppm	Gd ppm
288464-1-5.d	11.4	1.35	1044	32.07	2.85	68.2	1.73	5.96	14.96	2.387	14.99	4.61	6.32	6.27
288464-1-6.d	12.8	1.1	1112	22.3	1.942	7.5	1.1	6	12.5	1.79	9.62	2.76	6.1	3.81
288464-1-7.d	10.59	1.03	1176	20.46	2.086	44.7	0.91	6.44	11.72	1.628	8.55	2.51	5.61	2.98
331805-1-1.d	11.21	0.748	1321	243.4	1.804	1.948	0.125	29.1	56.3	7.3	34.8	13.05	97.1	22.59
331805-1-2.d	10.49	0.773	1306	153.9	1.776	2.022	0.139	16.8	29.1	3.9	20.5	9	107.9	13.7
331806B-1-1.d	8.66	1.26	1310	193.1	2.241	2.19	0.78	46	105.4	14.9	71.8	21.74	102.8	26.16
331806B-1-2.d	7.79	1.09	1269	141.6	1.87	1.46	0.18	38.7	84	11.1	49	13.2	129.5	16.7
331806B-1-3.d	11.1	1.109	1263.9	123.1	1.849	1.83	0.572	41.3	77.5	8.9	39.3	11.07	115.7	12.43
331807-4-1.d	15.1	5.07	1327	407	2.244	2.42	1.019	50.8	122.1	18.9	99.2	33.3	92	49.5
331807-4-2.d	14.6	5.71	922	304	3.65	2.55	1.82	14.71	62.7	13.09	89.9	39.3	27.8	63.4
331807-6-1.d	13.17	3.13	1192	397	2.26	2.06	0.61	14.2	41.4	7.86	53.1	26.7	58.5	51.6
331807-6-2.d	110	8	718	282	11.2	2.71	3.2	8.67	40.9	9.6	75.7	36.3	15.92	62.1
331807-6-3.d	44	8.2	699	280	16.5	2.9	2.6	8.58	44.6	10.6	81.8	40.4	15.8	67
331807-6-4.d	12.2	9.2	713	265	10.8	2.2	2.87	9.9	48.1	11.5	85	35.9	15.2	60.8
331807-6-5.d	68	4.34	887	250	9.9	3.08	1.36	9.8	29.2	5.94	41.9	21.3	37.3	41.8
331807-7-6.d	28.2	6.52	981	296	4.88	2.52	1.6	11.93	43.7	9.72	68.5	32.1	33.4	55.2
331807-7-7.d	21.1	4.7	1012	345	12.1	3.48	1.39	9.59	33.4	7.32	52.8	29.4	37.9	57.2
331815-2-1.d	13.34	8.08	538.8	388	17.23	5.46	1.97	5.61	39.9	12.54	116.2	70.8	24.42	120.1
331815-2-2.d	12.01	5.89	497	325	16.76	5.72	1.67	4.18	31.3	10.24	96	60.4	20.8	105.1
331807-2-3.d	29.7	5.89	876	287	3.78	2.04	1.59	13.43	44.7	9.28	62.5	28.8	44	49.2
331807-2-4.d	14.46	4.75	942	204	4.11	1.45	2.44	123	282	39.8	192	52	103.4	58
331807-1.d	9.52	4.65	1223	440	2.79	2.85	0.63	132	346	50.6	254	83.9	77.6	113.3
331807-3.d	16.3	4.21	996	195	5.9	2.89	1.6	19.9	52.3	8.23	48.4	20.1	81.6	31.3
331813-1.d	14.16	5.28	548	627	15.7	4.83	0.63	19.25	111.3	28.23	214.8	110.7	69	165.8
331813-2.d	9.3	4.75	699	586	6.24	3.67	0.281	51	224	41.8	232.5	78.1	82.5	98.9

Appendix 1.6B (continued)

Sample ID	Tb ppm	Dy ppm	Ho ppm	Er ppm	Tm ppm	Yb ppm	Lu ppm	Ta ppm	Pb ppm	Th ppm	U ppm	ΣREE ppm	Eu anomaly
MELI-01	9.9	59.7	10.9	21.8	2.07	8.32	0.92	0.48	13.5	<DL	0.015	205.536	0.52
MELI-01	28.2	135	20.6	36.4	2.92	11.4	1.09	0.543	16.6	<DL	0.0023	591.03	0.41
MELI-01	27.6	177	32	58.8	4.5	16.2	1.36	0.55	17.4	0.023	0.0019	499.549	0.44
MELI-01	11.17	69.2	12.65	24.8	2.17	8.82	1.005	0.386	16.7	0.0022	0.0058	232.776	0.44
MELI-01	19.6	99.1	16.26	29.11	2.481	10.02	1.027	0.456	13.79	<DL	0.0077	383.358	0.40
DOME-02	25.52	155.4	27.8	66.7	6.82	30.6	2.84	0.0454	28.8	0.0142	0.02	1417.08	1.71
DOME-02	29.7	182	34	81	8.5	39.5	3.6	0.0454	31.06	0.0161	0.0107	1449.7	1.64
DOME-02	26.27	150.9	25.1	54	4.95	19.8	1.61	0.0408	24.6	0.0041	0.0066	1124.13	1.22
HOLL-01	0.1108	0.67	0.089	0.221	0.0313	0.326	0.054	<DL	1.43	<DL	<DL	5.8801	2.60
HOLL-01	0.251	1.25	0.181	0.45	0.05	0.522	0.097	<DL	1.22	<DL	<DL	16.589	2.06
HOLL-01	0.1206	1.14	0.332	1.33	0.216	2.32	0.347	<DL	0.89	<DL	<DL	8.4116	3.07
YOUN-01	11.01	70.1	12.34	27	2.71	13.59	1.302	0.0215	152	0.0033	0.02	561.862	1.24
YOUN-01	12.92	80.9	14.46	35.8	4.22	23.6	2.42	0.0254	140	0.021	0.0215	742.42	1.80
YOUN-01	13.8	81.5	13.53	29.4	3.04	15.5	1.51	0.022	158	0.0115	0.05	675.61	1.42
YOUN-01	12.1	66.9	11.11	25.9	3.14	18.28	1.794	0.0218	93.2	0.184	0.74	3672.824	1.48
YOUN-01	8.48	53.3	9.37	22.75	2.87	16.79	1.66	0.0154	91	0.041	0.034	843.62	2.06
YOUN-01	9.47	60	10.66	25.59	3.14	18.49	1.813	0.0228	77.9	0.0363	1.3	833.263	1.97
YOUN-01	10.08	60.2	10.38	24.69	3.047	17.83	1.761	0.0221	90.2	0.093	0.61	1915.988	1.72
YOUN-01	10.37	64.3	11.12	26.8	3.21	18.41	1.783	0.0257	132.2	0.0377	0.049	946.493	1.94
MALA-10	2.36	12.4	2.02	4.07	0.356	1.5	0.156	0.069	56.4	0.0142	0.0048	181.532	0.86
MALA-10	13.35	68.7	10.2	17.4	1.21	3.98	0.35	0.069	40.5	0.0057	0.004	412.99	0.66
MALA-10	14.18	72.6	10.71	18.41	1.261	4.2	0.354	0.045	41.2	0.0038	0.0056	404.315	0.72
MALA-10	2.07	10.8	1.67	3.3	0.244	1.14	0.113	0.035	36.4	0.04	0.137	195.037	1.06
MALA-10	1.79	8.88	1.42	2.99	0.253	1.119	0.1179	0.059	38.3	0.0139	0.016	196.0399	0.96
96-DP-162	28.91	177	29.31	56.4	4.75	16.82	1.14	0.0444	6.52	0.0342	0.0083	628.75	0.74
96-DP-162	32	196	31.2	57.5	4.73	16.7	1.031	0.0532	5.69	0.0113	0.0138	689.831	0.70
96-DP-162	23.7	138.8	21.7	38.8	3.08	10	0.583	0.043	5.31	0.009	0.0153	500.063	0.72
96-DP-162	32.1	184	28.2	51.6	4.41	16.1	1.06	0.043	11.6	0.0039	0.0022	720.97	0.76
96-DP-162	34.6	200	31.7	58.1	4.67	17	1.107	0.046	7.6	0.0027	0.0064	765.177	0.75
96-DP-162	20.5	113.3	17.3	30.6	2.46	9.4	0.599	0.021	9.6	0.011	0.0066	412.349	0.63
96-DP-162	31.3	174	27.7	50.6	4.04	15.4	1.001	0.035	7.87	0.0054	0.0067	652.911	0.74
96-DP-162	30	170.9	27.03	52	4.15	15.64	1.04	0.041	6.74	0.005	0.0041	645.74	0.76

Appendix 1.6B (continued)

Sample ID	Tb ppm	Dy ppm	Ho ppm	Er ppm	Tm ppm	Yb ppm	Lu ppm	Ta ppm	Pb ppm	Th ppm	U ppm	ΣREE ppm	Eu anomaly
96-DP-162	33.8	193	30.1	53.7	4.21	14.8	0.9	0.032	8.55	0.0009	0.0033	766.2	0.72
96-DP-162	30.5	173.6	27.3	50	4.07	14.93	0.959	0.0375	8.28	0.006	0.0046	665.819	0.73
96-DP-162	40.6	248	39.1	69.4	5.53	18.3	1.011	0.07	15.5	0.0095	0.003	845.341	0.61
96-DP-162	37.1	226	36	63.7	4.92	16.3	0.919	0.0538	14.82	0.0064	0.0033	774.459	0.63
96-DP-162	28	166	25.1	42.6	3.26	10	0.52	0.033	15	0.005	0.0013	594.7	0.71
B580-15	86.6	444	64.5	116	10.03	40.6	3.62	0.059	16	0.0051	0.0108	2025.85	0.53
B580-15	88	412	56.1	95.4	7.64	29.6	2.55	0.0504	7.31	0.015	0.024	3559.29	0.55
B580-15	89.9	446	63.2	112.1	9.53	38.6	3.38	0.065	34	0.0116	0.0141	2492.91	0.54
B580-15	24.71	122.9	17.56	32.4	2.91	12.28	1.103	0.0405	23	0.0033	0.006	688.513	0.66
B580-15	75	366	51.5	90.9	7.12	27.1	2.4	0.071	13.1	0.0022	0.0076	1812.02	0.51
B580-15	85.2	431	62.3	111.5	9.17	37.4	3.35	0.079	25	0.0109	0.0098	2070.12	0.53
B580-15	65.4	318	45	77.9	6.19	23.5	2.09	0.062	12.11	0.0005	0.0071	1531.88	0.55
B580-15	72.2	356	50.8	89.3	7.15	28.1	2.44	0.0648	16.5	0.0048	0.0099	1735.79	0.53
B580-15	57.7	286	40.1	68.9	5.49	20.9	1.81	0.0515	18.6	<DL	0.008	1344	0.52
B580-15	62.4	313	45.1	80.3	6.62	26.8	2.39	0.049	31	0.0052	0.0152	1501.41	0.54
94-GB-15A	16.53	107	18.93	48.9	5.87	30.31	2.683	0.0405	16.3	0.0079	0.0052	1023.523	4.29
94-GB-15A	12.9	87.3	16.3	43.4	5.56	29.9	2.76	0.0359	31.8	0.0105	0.0046	649.02	5.10
94-GB-15A	16.7	107.8	19.2	50	6.13	32.2	2.89	0.0399	24	0.021	0.0064	1074.92	4.38
94-GB-15A	15.8	103.7	18.8	48.9	6.16	33.8	3.04	0.0444	27.9	0.0309	0.0065	991.8	4.92
94-GB-15A	22.9	143	24.9	60.5	6.83	32.9	2.91	0.051	26.4	0.0136	0.0019	1235.44	3.21
94-GB-15A	17	109.9	19.93	51.9	6.5	35.2	3.17	0.0467	26.68	0.0258	0.0055	1034.6	4.56
94-GB-15A	22.13	134	22.64	53.7	5.73	26.9	2.29	0.0484	18.6	0.0115	0.0052	1123.39	2.95
SIGM-01	22.16	134.4	22.48	51.8	5.93	31	2.58	0.047	71.2	0.0128	0.0077	1175.05	2.62
SIGM-01	25.4	151.1	24.8	56.6	6.4	32.6	2.82	0.0589	61.7	0.0148	0.005	1352.72	2.54
SIGM-01	22.7	136	22.5	51.8	5.85	30.3	2.57	0.0523	65.1	0.0134	0.0045	1208.72	2.61
SIGM-01	24.87	145.7	23.75	52.65	5.556	26.54	2.188	0.0475	63	0.0038	0.0038	1153.084	2.44
SIGM-01	32	184	28.6	62	6.5	31.7	2.85	0.0599	77.6	0.0144	0.0046	1567.65	1.95
SIGM-01	18.9	113.9	19.1	44.8	5.12	26.6	2.22	0.0457	128.5	0.0037	0.0079	1019.04	3.46
SIGM-01	25.8	152	25.3	57.2	6.14	30.6	2.54	0.0491	103.8	0.0151	0.0039	1255.98	2.56
SIGM-01	15.11	94.8	16.47	40.6	4.99	27.1	2.33	0.0455	71.6	0.0206	0.0079	901.1	4.25
LAMA-01	59.6	293	40.2	71.3	6.04	24.5	1.94	0.029	179	0.0101	0.016	2067.58	0.75
LAMA-01	35.9	174	24	42.2	3.27	13.5	1.09	0.026	155	0.0064	0.026	1259.06	0.83

Appendix 1.6B (continued)

Sample ID	Tb ppm	Dy ppm	Ho ppm	Er ppm	Tm ppm	Yb ppm	Lu ppm	Ta ppm	Pb ppm	Th ppm	U ppm	ΣREE ppm	Eu anomaly
LAMA-01	50.8	249	34.3	61.3	5.16	21.4	1.72	0.0312	168	0.05	0.13	1728.38	0.71
CUIA-03	0.43	3.55	0.854	3.02	0.52	4	0.547	0.0156	24.82	0.888	4.55	108.161	24.96
CUIA-03	0.345	2.91	0.696	2.49	0.42	3.28	0.454	0.0131	27.85	0.534	4.31	76.885	23.88
CUIA-03	0.468	3.22	0.737	2.38	0.38	2.95	0.371	0.0122	31.5	0.91	3.32	104.996	13.13
CUIA-03	1.97	14.2	3.05	9.1	1.26	7.6	0.83	0.014	38.9	0.86	2.32	256.11	6.96
160277	3.1	20.2	3.78	10.7	1.56	10.6	1.29	0.0769	47.6	0.68	3.2	210.66	5.30
160277	5.23	32.5	6.1	15.9	1.96	12	1.46	0.098	57.1	1.26	4.84	344.45	3.39
160286	1.42	8.8	1.56	4.4	0.65	4.93	0.662	0.0534	48.5	1.102	4.9	156.602	10.17
160286	4.79	29.2	5.12	13.07	1.73	10.45	1.19	0.0521	43.1	0.345	0.84	429.25	6.51
160286	0.71	4.68	0.92	2.96	0.56	5.41	0.808	0.07	48.9	1.02	4.36	139.258	35.25
160304	1.61	10.2	1.87	5.4	0.86	6.84	0.927	0.0201	49.1	1.284	12.38	145.447	8.20
160304	1.12	7.7	1.49	4.68	0.774	6.48	0.879	0.0255	37	0.94	4.5	128.953	13.05
160304	1.04	6.7	1.3	4.4	0.68	5.9	0.83	0.0121	41.2	1.17	10.7	114.18	11.87
160304	6.08	41.3	8.1	23.1	3.11	19.7	2.12	0.0237	32	1.5	5.9	429.51	6.46
160304	3.37	25	5.26	17.7	2.86	19.7	2.36	0.0189	35.1	1.24	6.9	383.55	13.67
160304	2.03	14.2	2.79	8.6	1.32	9.7	1.22	0.0229	36.9	1.11	6.2	195.56	10.26
160304	2.4	16.43	3.09	9.36	1.37	9.2	1.01	0.0203	33.6	0.145	0.98	187.69	8.38
160304	3.8	25.8	5	15.2	2.18	15.4	1.7	0.0145	36.1	1.09	8.7	322.18	8.07
160304	3.2	21.4	4	11.4	1.58	10.8	1.25	0.0201	40.6	1	9	251.53	7.04
160304	4	27.1	4.9	13.6	1.87	11.6	1.3	0.0179	33.2	0.49	3.5	275.57	6.16
160304	8.8	57	10	25.9	3.29	18.2	1.86	0.0174	29.1	0.36	1.8	506.25	4.12
160310	1.21	8.1	1.5	4.32	0.633	4.4	0.513	0.079	38	0.88	6.03	141.576	16.33
160310	2.5	16.6	3.1	8.2	1.12	6.5	0.75	0.0312	47.5	0.93	6.72	219.97	11.37
160310	0.662	4.54	0.84	2.41	0.364	2.81	0.352	0.061	44.8	0.849	7.32	87.898	17.10
160310	1.17	7.9	1.46	4.08	0.58	3.86	0.474	0.0475	46.5	0.882	7.19	125.994	14.54
160310	0.56	3.8	0.85	2.64	0.43	4	0.52	0.076	71.6	1.35	14	145.86	27.98
BZWA-01	8.37	43.2	6.94	13.38	1.182	5.48	0.731	0.0279	34.4	0.038	0.136	262.131	0.92
HUTT-01	11.11	83.4	15.67	38	3.78	16.4	1.413	0.207	8.43	0.86	0.19	658.673	2.93
HUTT-01	7.87	61.7	12.1	31.6	3.42	17.1	1.62	0.278	6.16	0.45	0.95	375.01	2.61
HUTT-01	5.3	41.8	8.3	22	2.54	14.4	1.39	0.326	4.14	0.08	0.109	188.24	1.75
HUTT-01	4.42	34	6.76	17.5	2.02	10.2	1.02	0.62	2.88	0.249	0.6	147.26	1.92
HUTT-01	5.66	44.7	9.43	25.6	3	15.9	1.67	0.576	4.02	0.352	1.8	194.41	1.16

Appendix 1.6B (continued)

Sample ID	Tb ppm	Dy ppm	Ho ppm	Er ppm	Tm ppm	Yb ppm	Lu ppm	Ta ppm	Pb ppm	Th ppm	U ppm	ΣREE ppm	Eu anomaly
HUTT-01	3.24	27.4	5.38	14.5	1.8	10.13	1.23	0.063	5.48	0.58	4.8	159.27	2.05
HUTT-01	3.7	30.3	6.7	19	2.5	15	1.63	0.104	4.52	0.55	4.3	142.55	1.56
HUTT-01	5.32	44.9	9.62	27.1	3.4	19.9	2.11	0.87	4.42	0.294	1.03	196.34	1.17
HUTT-01	4.69	38	8.08	22.3	2.71	15.24	1.636	0.406	4.46	0.51	3.4	176.036	1.37
HUTT-01	4.51	35.5	7.38	18.8	2.1	10.77	1.071	0.446	8.8	0.176	0.39	150.581	0.95
HUTT-01	4.88	37.9	7.86	20.25	2.27	11.71	1.193	0.344	7.2	0.137	0.24	167.163	1.00
HUTT-01	5.45	41.2	8.57	22.5	2.55	13.6	1.39	0.193	5.2	0.071	0.054	191.46	1.06
HUTT-01	5.43	47.1	10.31	29.4	3.5	20.4	2.19	0.35	4	0.126	0.102	197.06	1.05
HUTT-01	4.47	36.8	7.93	21.9	2.47	13.2	1.37	0.39	2.9	0.59	0.97	166.83	1.14
HUTT-01	4.2	33.2	6.67	18.45	2.18	12.58	1.314	0.056	4.94	1.5	5.3	181.104	2.05
HUTT-02	1.48	11.5	2.26	6.01	0.87	6.03	0.786	0.0249	10.1	1.25	8	98.076	3.35
HUTT-02	5.26	39.7	7.1	17.6	1.93	9.76	1.01	1.04	5.5	1.18	3.5	182.81	1.32
HUTT-02	5.33	39.3	7.61	19.8	2.22	12.3	1.36	0.76	8.5	0.51	6.4	195.62	1.27
HUTT-02	3.49	26	4.88	12.6	1.5	8.67	0.974	0.29	8.16	0.98	6.7	151.514	1.80
HUTT-02	1.472	13.28	3.01	10.05	1.571	11.27	1.398	0.033	8.54	0.98	5.07	154.431	5.94
HUTT-04	0.78	5.2	0.92	2.37	0.326	2.2	0.245	0.0196	18.9	0.0026	0.071	56.801	3.67
HUTT-04	1.57	10.3	1.81	4.5	0.51	2.86	0.298	0.0195	17.86	0.01	0.196	93.598	3.05
HUTT-04	5.32	34.6	6.08	14.88	1.54	7.75	0.74	0.021	13.5	0.0131	0.068	267.22	2.52
HUTT-04	0.312	2.09	0.335	0.86	0.123	0.73	0.084	0.0157	20.3	0.023	0.5	27.52	8.70
HUTT-04	0.66	4.85	0.941	2.72	0.399	2.76	0.325	0.0269	21.3	0.031	0.73	48.716	5.35
HUTT-04	0.989	6.56	1.257	3.37	0.462	3.08	0.361	0.0291	25.1	0.025	0.63	65.199	3.82
KOCH-05A	1.9	9.4	1.45	3.35	0.35	1.88	0.243	0.03	23.1	0.068	0.135	421.773	2.63
KOCH-05A	2.9	14.8	2.3	5.33	0.552	3.11	0.36	0.038	31.1	0.0312	0.112	489.152	2.12
KOCH-05A	1.37	6.56	0.97	2.27	0.23	1.19	0.174	0.0206	18.4	0.082	0.152	384.964	2.93
KOCH-05A	0.753	4.1	0.588	1.24	0.125	0.608	0.054	0.0233	18.2	0.296	0.232	292.998	10.69
KOCH-05A	1.1	5.2	0.78	1.63	0.159	0.89	0.096	0.0203	19.8	0.98	0.707	493.055	8.58
KOCH-05A	1.75	8.34	1.19	2.39	0.201	0.954	0.099	0.0324	18.5	0.034	0.045	289.224	2.41
KOCH-05A	1.94	9.4	1.42	3.06	0.295	1.3	0.128	0.0372	22.5	0.286	0.328	381.043	4.67
KOCH-05A	1.37	6.9	1.11	2.24	0.229	1.13	0.124	0.0293	22.3	0.316	0.314	295.303	7.12
KOCH-06A	0.177	1.04	0.174	0.372	0.0351	0.166	0.0142	0.0135	36.3	1.7	7.3	26.5683	10.27
KOCH-06A	0.136	0.98	0.144	0.361	0.039	0.183	0.0122	0.0144	35	0.614	3.62	20.7652	10.85
KOCH-06A	0.267	1.5	0.277	0.53	0.041	0.227	0.0219	0.0144	39.1	3.35	12	42.3439	8.82

Appendix 1.6B (continued)

Sample ID	Tb ppm	Dy ppm	Ho ppm	Er ppm	Tm ppm	Yb ppm	Lu ppm	Ta ppm	Pb ppm	Th ppm	U ppm	ΣREE ppm	Eu anomaly
KOCH-06A	0.524	2.84	0.365	0.66	0.0555	0.099	0.0098	0.0164	28.9	2.38	0.56	82.7933	4.30
KOCH-06A	0.394	2.06	0.295	0.525	0.0369	0.096	0.0058	0.0162	28.21	3.9	1.6	52.0427	4.52
KOCH-06A	0.45	2.64	0.396	0.68	0.049	0.166	0.008	0.0128	30.2	12.6	5.64	54.789	5.24
KOCH-06A	0.328	1.59	0.22	0.435	0.0241	0.057	0.0042	0.018	27	0.549	0.149	40.9983	4.56
KOCH-06B	0.504	2.74	0.398	0.703	0.0512	0.145	0.0067	0.017	34.12	6.7	1.77	51.9679	3.24
KOCH-06B	0.355	1.92	0.271	0.481	0.022	0.133	0.0079	0.0128	33.9	1.62	0.632	31.2099	2.67
KOCH-06B	0.486	2.78	0.433	0.778	0.065	0.124	0.0064	0.0167	34	10.28	2.78	55.5024	4.13
KOCH-06B	0.558	3.08	0.463	0.811	0.068	0.139	0.006	0.0159	33.9	9.84	2.37	60.125	3.58
KUMT-04	1.26	6.59	1.14	2.29	0.194	0.79	0.0846	0.0254	86	9.2	7.2	78.3886	0.84
KUMT-04	0.51	2.4	0.345	0.66	0.074	0.277	0.0133	0.0252	25	49.6	3.09	180.4493	0.68
KUMT-04	0.188	0.92	0.154	0.31	0.029	0.116	0.009	0.0192	94.7	0.684	2.4	14.204	0.76
KUMT-04	0.47	2.34	0.38	0.75	0.07	0.262	0.0245	0.0201	76.4	12.3	3.68	71.6565	0.94
MARV-01	0.326	1.833	0.351	0.736	0.1008	0.55	0.0573	0.0212	19.6	0.034	0.17	46.4031	20.62
MARV-01	0.403	2.37	0.392	0.92	0.1045	0.628	0.0688	0.0221	18.87	0.023	0.22	51.1903	15.78
MARV-01	0.586	3.43	0.578	1.394	0.1659	0.864	0.0967	0.0203	19.49	0.013	0.0042	64.1216	8.75
MARV-01	0.494	2.7	0.469	1.074	0.118	0.649	0.0688	0.0203	18.63	0.0142	0.015	54.6348	11.31
MARV-01	0.595	3.22	0.591	1.349	0.13	0.612	0.086	0.0208	23.94	0.003	0.0023	48.205	2.31
MARV-01	0.606	3.5	0.652	1.48	0.138	0.64	0.105	0.0161	25.5	0.0027	0.0008	53.931	1.88
MARV-01	0.709	3.76	0.728	1.791	0.153	0.71	0.11	0.0183	23.4	0.0072	0.0033	55.955	1.34
MARV-01	0.653	3.76	0.686	1.74	0.177	0.8	0.095	0.0296	21.5	0.007	0.0056	52.731	2.05
MARV-01	0.605	3.32	0.61	1.44	0.1402	0.678	0.0975	0.0205	24.36	0.0031	0.0035	51.4957	2.09
MARV-01	0.399	2.27	0.392	0.921	0.108	0.538	0.0671	0.0235	19.8	0.028	0.45	53.3441	16.29
MARV-01	0.433	2.43	0.402	0.906	0.0969	0.567	0.0618	0.0204	19.2	0.0203	0.0074	53.6927	12.93
NVOR-01	0.648	2.09	0.245	0.369	0.0292	0.128	0.015	0.508	4.34	0.021	0.048	70.7742	1.28
NVOR-01	0.487	2.28	0.386	0.815	0.095	0.514	0.0551	0.331	5.9	0.0108	0.014	48.2041	1.50
NVOR-01	0.517	1.962	0.271	0.53	0.054	0.274	0.0323	0.398	5.46	0.0141	0.0295	56.6523	1.43
NVOR-01	0.296	2.1	0.472	1.41	0.179	1.091	0.138	0.071	5.93	0.0057	0.0089	15.421	1.10
NVOR-01	0.491	3.04	0.74	1.88	0.223	1.22	0.171	0.091	8.12	0.0034	0.0107	22.192	1.06
NVOR-01	0.082	0.664	0.161	0.54	0.0875	0.67	0.111	0.0302	4.75	0.0082	0.0267	5.7835	1.54
EDWA-01	0.663	4.59	0.868	2.161	0.267	1.488	0.1549	0.0203	8.69	0.0083	0.0108	49.6829	4.29
EDWA-01	0.747	4.41	0.875	2.17	0.248	1.51	0.166	0.0143	8.67	<DL	0.008	50.986	4.20
EDWA-01	0.78	5.39	0.94	2.27	0.25	1.599	0.165	0.0147	10.4	<DL	0.0072	58.964	3.72

Appendix 1.6B (continued)

Sample ID	Tb ppm	Dy ppm	Ho ppm	Er ppm	Tm ppm	Yb ppm	Lu ppm	Ta ppm	Pb ppm	Th ppm	U ppm	ΣREE ppm	Eu anomaly
EDWA-01	0.641	4.38	0.811	2.12	0.243	1.37	0.159	0.017	7.57	0.0038	0.0036	46.604	4.24
EDWA-01	0.971	6.69	1.251	3.54	0.458	2.74	0.304	0.024	6.89	0.0031	0.003	64.184	3.86
EDWA-01	1.49	8.87	1.64	3.83	0.518	2.67	0.261	0.0109	2.39	<DL	0.0057	89.119	3.61
TARM-01	5.67	33	4.96	10.38	0.948	4.08	0.274	0.144	99	0.453	1.99	481.012	6.87
TARM-01	12.6	70.4	10	18.3	1.47	4.88	0.307	0.2	26.7	0.089	0.101	857.057	3.95
TARM-01	10.97	61.8	9.24	17.14	1.475	4.7	0.309	0.16	34	0.093	0.124	673.434	3.40
TARM-01	2.74	16.5	2.53	5.41	0.565	2.64	0.197	0.112	46.1	0.352	1.92	301.862	12.48
TARM-01	4.45	25.3	3.87	7.87	0.732	3.07	0.214	0.097	57.4	0.144	0.108	366.206	7.10
TARM-01	9.7	53.5	7.62	14.5	1.206	4.18	0.278	0.075	57	0.071	0.078	685.584	4.72
TARM-01	4.8	27.1	4.04	8.13	0.761	3.07	0.219	0.099	49.7	0.228	0.78	412.62	7.60
TARM-01	6.4	36.5	5.5	10.5	0.91	3.57	0.244	0.052	65	0.53	3.3	397.224	4.22
TARM-01	4.78	27.4	3.94	7.79	0.732	2.74	0.203	0.105	66	0.13	0.15	386.685	6.28
TARM-01	3.72	21.3	3.17	6.8	0.666	3.11	0.227	0.07	85	0.248	1.94	327.693	9.01
TARM-01	5.8	32.8	4.73	9.2	0.84	3.37	0.236	0.064	84.9	0.231	1.02	395.976	5.40
TARM-01	13	71	9.9	17.4	1.384	4.64	0.301	0.062	109	0.26	1.03	670.825	3.34
PADD-01A	19.5	121	20.9	47.3	4.84	22.3	2.13	0.036	18.3	0.058	0.0082	919.37	3.04
PADD-01A	14.4	89.8	15.8	37.1	4.05	20.65	2.04	0.085	19.79	0.127	0.0108	799.64	3.88
PADD-01A	14.4	89.2	15.4	35.8	3.62	17.7	1.59	0.0212	21.42	0.166	0.0075	717.41	2.85
PADD-01A	5.95	40	8.03	21.7	2.9	18.1	2.15	0.0213	19.75	0.056	0.107	463.93	6.45
PADD-01A	20.8	126.1	21.6	50.9	4.7	20.99	1.985	0.023	16.02	0.35	0.147	910.375	2.57
PADD-01A	19.3	113	18.7	38.4	3.4	13.8	1.26	0.0252	15.35	0.079	0.0078	781.66	2.66
PADD-01A	5.92	38.8	7.45	19.6	2.53	14.4	1.72	0.0146	18.82	0.187	0.0169	480.02	10.38
PADD-01A	13.9	87	16.1	37.9	3.69	16.1	1.67	0.0191	13.73	0.104	0.0174	706.16	3.88
PADD-01A	12.7	77.7	13.8	31.4	3.23	15.4	1.633	0.0204	16.49	0.136	0.0137	643.963	4.43
PADD-01A	5.88	37.4	6.75	17.2	2.17	14	1.491	0.025	19.5	0.374	0.0289	416.091	6.95
PADD-01A	7.12	47.3	9	24.6	3.22	19.6	2.19	0.0166	20.3	0.203	0.0186	590.53	9.37
PADD-01A	18.7	119	21.3	49.7	5.08	24	2.32	0.0186	16.7	0.066	0.009	837.7	3.02
PADD-01A	9.4	60.3	11	27.9	3.33	19	2.02	0.09	19.09	0.21	0.0172	593.75	6.13
PADD-01A	3.08	18.5	3.04	6.29	0.584	2.41	0.196	0.0207	7.49	0.072	0.292	180.18	5.81
PADD-01A	1.73	9.67	1.46	2.75	0.239	0.781	0.065	0.0192	7.05	0.03	1.62	105.735	9.48
PADD-01A	0.58	3.42	0.529	0.95	0.102	0.456	0.028	0.0232	6.17	0.0101	0.0321	43.79	11.59
PADD-01A	2.12	12.4	1.99	4	0.371	1.48	0.119	0.0206	7.05	0.0426	0.69	125.69	6.84

Appendix 1.6B (continued)

Sample ID	Tb ppm	Dy ppm	Ho ppm	Er ppm	Tm ppm	Yb ppm	Lu ppm	Ta ppm	Pb ppm	Th ppm	U ppm	ΣREE ppm	Eu anomaly
PADD-02B	0.466	3.36	0.708	1.95	0.273	1.95	0.262	0.0167	21.4	0.0013	0.0049	30.746	5.49
PADD-02B	0.8	5.3	1.13	3.24	0.49	3.79	0.51	0.0202	22.09	0.009	0.0202	56.12	6.92
PADD-02B	2.26	15.3	3.32	10	1.64	13.8	1.99	0.0212	24.52	0.049	0.108	189.66	9.06
PADD-02B	0.354	2.4	0.472	1.36	0.194	1.42	0.168	0.0252	23.3	0.0036	0.0065	22.81	6.57
PADD-02B	0.295	1.96	0.396	1.21	0.209	1.91	0.269	0.025	25.7	0.0055	0.0082	26.682	10.54
PADD-02B	0.373	2.55	0.501	1.46	0.228	1.94	0.297	0.0212	22.95	0.0025	0.0093	31.199	8.89
PADD-02B	0.252	1.88	0.407	1.295	0.214	1.82	0.3	0.0225	23.9	0.0027	0.0045	23.575	13.73
PADD-02B	0.282	1.95	0.418	1.299	0.2163	1.842	0.2911	0.0198	23.83	0.002	0.0074	25.8694	12.34
PADD-02B	0.94	5.5	0.92	1.92	0.219	1.1	0.101	0.023	14.91	0.0157	0.15	92.35	20.00
PADD-02B	1.91	12.6	2.43	5.8	0.67	3.2	0.3	0.0183	19.3	0.0079	0.03	120.2	7.02
PADD-02B	6.8	41.2	7.1	15.7	1.61	7.8	0.77	0.0226	26.4	0.0122	0.055	333.56	2.12
PADD-02B	2.24	13.6	2.35	5.2	0.55	2.71	0.261	0.0203	18.8	0.0216	0.278	142.791	7.69
PADD-02B	0.36	2.23	0.468	1.375	0.2197	1.943	0.303	0.0189	23.77	0.0017	0.0097	26.6927	9.11
MTPL-01	53.7	290.2	46.6	97.9	9.85	44.4	4.29	0.0253	15.63	0.0092	0.0045	2059.64	1.04
MTPL-01	53.6	267	38.8	71.4	6.35	25.1	1.91	0.035	18.23	0.0058	0.0047	2100.06	0.92
MTPL-01	44.7	225	33.6	65.4	6.15	26.4	2.39	0.0242	17.48	0.0118	0.0077	1852.64	0.94
MTPL-01	20.22	116.4	19.54	43.78	4.82	23.85	2.41	0.0182	20.82	0.0045	0.00125	947.82	1.70
MTPL-01	11.6	86.3	18.5	58.5	9.7	69.5	8.97	0.016	19.76	0.191	0.066	982.87	5.57
MTPL-01	30	208	42.3	120	16.7	100.5	11.81	0.039	27.3	0.177	0.044	1459.11	2.23
MTPL-01	18.5	127	25.5	73.6	11	70.4	8.49	0.0224	21	0.28	0.059	1325.09	3.28
MTPL-01	18.3	120.6	23.3	65	9.31	60.8	7.71	0.0178	23.3	0.181	0.285	1098.42	3.52
NORS-01	0.389	2.87	0.64	2.18	0.435	3.84	0.562	0.0102	17.17	0.0039	0.434	53.476	17.89
NORS-01	0.292	2.13	0.441	1.37	0.241	2.05	0.277	0.0138	17.11	<DL	0.462	28.321	12.52
NORS-01	0.38	2.25	0.41	0.95	0.119	0.78	0.097	0.014	7.9	0.0105	0.59	26.946	10.68
NORS-01	0.567	3.5	0.679	1.97	0.335	2.84	0.381	0.0144	31.1	0.0017	0.179	35.874	5.15
NORS-01	0.248	2.02	0.477	1.65	0.323	2.84	0.382	0.0138	29.8	0.0018	0.145	23.772	13.14
NORS-01	0.331	2.56	0.581	1.8	0.302	2.3	0.345	0.011	15.5	0.0047	0.203	27.969	8.46
NORS-01	0.46	3.15	0.641	1.82	0.296	2.43	0.354	0.0137	14.04	0.0052	0.182	38.591	6.07
NORS-01	0.375	2.66	0.553	1.69	0.278	2.06	0.259	0.0127	18.8	0.0044	0.427	35.89	15.31
NORS-02A	101	478	63	118	12	54	4.7	5.4	11.58	0.183	0.065	3901.7	0.52
NORS-02A	95	490	70	151	15.1	78	5.9	4.57	13.7	0.25	0.117	3626	0.60
NORS-02A	53.9	268	36.8	75.4	7.18	33.4	2.6	3.7	17.14	0.077	0.059	1890.58	0.75

Appendix 1.6B (continued)

Sample ID	Tb ppm	Dy ppm	Ho ppm	Er ppm	Tm ppm	Yb ppm	Lu ppm	Ta ppm	Pb ppm	Th ppm	U ppm	ΣREE ppm	Eu anomaly
NORS-02A	1.48	9.48	1.68	4.89	0.862	6.9	0.837	0.063	20	0.189	4.8	167.479	12.28
NORS-02A	1.64	10.1	1.62	4.75	0.837	6.49	0.769	0.0412	20.14	0.046	0.28	175.446	11.49
NORS-02A	4.44	25.9	4.05	10.32	1.55	10.68	1.199	0.14	24.41	0.123	1.28	308.159	4.88
NORS-02A	2.64	15.7	2.57	7.07	1.14	8.58	1.001	0.083	22.25	0.124	2.05	223.241	7.61
NORS-02B	3.8	24.7	4.59	11.42	1.362	7.22	0.75	0.0119	13.93	0.0065	0.0313	293.062	7.59
NORS-02B	0.91	6.38	1.21	3.45	0.475	3.04	0.359	0.0141	16.02	0.0039	0.0105	105.154	15.15
NORS-02B	2.33	14.97	2.86	7.28	0.824	4.11	0.446	0.0137	14.53	0.0034	0.0137	140.36	6.69
NORS-03	4.56	26.55	4.28	11.19	1.601	10.21	0.945	0.468	23.09	0.0246	0.0342	289.856	3.51
NORS-03	0.892	5.42	0.88	2.38	0.386	3.27	0.342	0.052	25.98	0.0388	8.9	91.83	16.91
NORS-03	6.05	32.4	4.99	11.4	1.43	9.3	0.91	0.432	33	0.0181	2.4	239.69	2.41
NORS-03	5.23	31	5.02	13.2	1.9	12.86	1.275	0.264	30.6	0.058	2.75	257.785	3.91
NORS-03	1.833	11.08	1.85	5.26	0.829	5.88	0.632	0.171	25.54	0.048	4.6	136.674	9.34
NORS-03	1.93	10.8	1.69	4.19	0.605	4.35	0.443	0.103	24.81	0.051	4.9	134.238	8.50
MTCH-01A	0.524	3.85	0.845	3.06	0.654	6.87	1.054	0.0155	26.1	0.039	0.327	96.837	26.28
MTCH-01A	0.664	4.76	1	3.54	0.734	7.27	1.065	0.0199	27.32	0.0427	0.389	109.693	21.10
MTCH-01A	28.4	151	23	47.7	4.8	23.6	2.23	0.0161	23.4	0.047	0.0042	1157.03	1.95
MTCH-01A	23.7	144	24.3	60	6.9	36.5	3.52	0.0212	23	0.029	0.0023	1048.22	2.91
MTCH-01A	22.7	126.8	20.2	45	4.89	25.3	2.45	0.0196	22.5	0.0287	0.0041	983.34	2.41
MTCH-01A	1.39	9.9	2.02	6.33	1.08	9.1	1.22	0.0199	26.72	0.0399	0.22	167.84	12.20
MTCH-01B	18	104	17.6	42.5	5.09	27.4	2.8	0.0218	20.07	0.0425	0.0031	909.79	3.23
MTCH-01B	38.2	185	27.3	52.1	4.86	20.8	1.91	0.0272	25	0.0129	0.0022	1423.87	1.48
MTCH-01B	33	156	22	40.8	3.55	14.8	1.31	0.0203	20.8	0.0056	0.0016	1311.56	1.36
MTCH-01B	9	40.9	5.54	10.55	1.025	4.9	0.456	0.0201	12.8	0.0029	<DL	389.271	1.66
MTCH-01B	24.1	116	16.7	32	2.98	13.2	1.2	0.0244	20.4	0.0081	0.0023	936.08	1.44
MTCH-01B	3.94	26.9	5.38	16.14	2.51	17.43	2.1	0.0183	18.25	0.045	0.0039	410.9	12.65
MTCH-01B	3.28	22.6	4.53	13.7	2.2	15.9	1.98	0.0184	18.02	0.044	0.0021	358.79	13.45
MTCH-01B	0.74	5.29	1.27	4.51	0.926	7.77	1.14	0.0218	18.73	0.033	0.0046	140.906	35.29
MTCH-01B	2.21	15.3	3.12	9.8	1.64	12.4	1.61	0.0187	18.71	0.031	0.0036	267.78	16.67
MACR-01B	3.72	25.5	5.01	14.7	2.07	13.9	1.481	0.0211	3.92	2.5	0.67	396.451	1.67
MACR-01D	3	19.7	3.74	10.49	1.61	12.15	1.43	0.0407	8.6	1.71	1	215.1	2.07
MACR-01D	1.38	9.2	1.77	5.03	0.763	6.29	0.783	0.0243	8.97	1.41	1.51	104.376	2.08
MACR-01D	3.21	23.8	4.7	14.2	2.12	14.9	1.59	0.24	6.1	1.38	0.77	248.02	2.46

Appendix 1.6B (continued)

Sample ID	Tb ppm	Dy ppm	Ho ppm	Er ppm	Tm ppm	Yb ppm	Lu ppm	Ta ppm	Pb ppm	Th ppm	U ppm	ΣREE ppm	Eu anomaly
MACR-01D	7.5	47	7.7	15.5	1.47	7.2	0.71	0.039	2	0.93	1.23	344.08	1.50
MACR-01D	1.2	8.8	1.69	4.93	0.826	6.56	0.894	0.0351	6.12	1.58	1.87	103.39	2.20
MACR-01D	2.3	15.6	2.95	8.21	1.23	9.11	1.107	0.046	8.02	1.6	1.35	166.107	2.06
MACR-01D	1.46	11	2.31	7.12	1.126	8.65	1.069	0.041	4.27	0.842	1.197	132.785	2.56
MACR-01D	2.46	19.5	4.18	13.4	2.01	13.8	1.54	0.0361	6	0.432	0.766	181.93	1.84
MACR-01D	4.3	32	6.6	18.6	2.51	14.7	1.46	0.05	6.7	0.368	0.66	316.97	2.83
MACR-01D	10.6	75.7	14.3	34.7	3.33	13.6	0.97	0.029	0.71	0.056	0.053	643.1	5.12
MACR-01D	1.82	13.8	2.78	8.5	1.21	8.3	0.96	0.041	2.96	0.523	1.36	137.44	2.49
MACR-01D	3.9	28.9	5.73	15.9	2.01	12.03	1.24	0.039	4.99	0.373	0.75	255.81	3.46
MACR-01D	10.1	65.5	11.02	24.3	2.35	9.9	0.75	0.029	2.69	0.33	0.243	441.52	1.47
MACR-01D	1.25	8.9	1.73	5.02	0.783	6.67	0.882	0.0336	7.4	0.69	1.73	94.565	1.95
MACR-01D	3.45	25	4.32	11.48	1.37	9.1	0.95	0.091	3.46	0.56	1.92	193.42	1.41
MACR-01D	12.1	80.6	14.5	37.6	4.7	24.5	2.41	0.022	2.94	0.56	0.34	636.01	1.14
MACR-01D	1.71	12.3	2.47	7.74	1.304	10.4	1.21	0.034	6.05	0.85	1.3	129.834	1.77
MACR-01D	3.41	23.2	4.27	11.3	1.49	9.8	1.09	0.0348	5.8	0.668	1.38	197.76	1.51
CRUS-01A	0.0072	0.101	0.066	0.515	0.121	1.27	0.263	0.0225	2.66	<DL	0.0035	2.5197	13.23
CRUS-01A	2.8	37.7	14.4	67.9	11.9	85.4	11.9	0.11	2.39	<DL	0.0008	249.784	3.21
CRUS-01A	0.79	10	3.5	15.8	2.72	20.1	3	0.0487	2.533	<DL	0.0039	61.365	3.20
CRUS-01A	4.96	65.4	23.5	104	16.2	106.9	14.06	0.127	6.21	0.0022	0.0025	393.81	3.12
CRUS-01A	23	235	60.9	182	21.8	123	14.24	0.447	5.32	<DL	0.007	794.44	1.39
CRUS-01A	14.7	155	42.5	140.7	18.31	107.9	13.11	0.321	5.41	0.00136	0.0046	593.902	1.75
CRUS-01A	9.8	71	13.5	38.7	5.05	32	4.74	0.056	6.74	0.0046	0.0107	357.47	1.35
CRUS-01A	1.17	13.2	5.39	28.2	4.55	37.9	8.12	0.028	8.35	0.003	0.0007	110.096	1.42
CRUS-01A	2.09	18.6	5.59	24.9	4.05	32.6	6.7	0.0312	7.64	0.0028	0.0048	132.02	1.46
CRUS-01A	1.96	17	4.47	18.4	3.02	24.8	4.75	0.0348	9.43	0.0101	0.0065	114.62	1.66
CRUS-01A	4.92	36.1	7.52	24	3.48	25.5	4.56	0.114	8.04	0.0044	0.0096	179.24	1.22
CRUS-01A	3.51	27.4	6.35	22.8	3.49	26.87	4.88	0.0597	8.45	0.0064	0.0072	159.63	1.50
CRUS-01A	28.2	181.6	31.4	73	7.64	40.5	4.62	0.628	5.5	0.006	0.0055	873.06	1.06
CRUS-01A	2.62	22.9	6.36	25.8	4.08	31.6	5.83	0.0281	7.55	0.0043	0.0072	145.63	1.25
CRUS-01A	14.4	96	17.9	47.5	5.74	35.8	5.29	0.304	6.63	0.0049	0.0068	481.13	1.07
CRUS-01B	14.7	154	42.3	135.3	17.43	99.4	11.78	0.332	4.22	0.0013	0.0043	559.771	1.65
CRUS-01B	0.196	1.97	0.71	3.8	0.769	7.54	1.66	0.0218	3.21	<DL	0.0036	18.1043	1.54

Appendix 1.6B (continued)

Sample ID	Tb ppm	Dy ppm	Ho ppm	Er ppm	Tm ppm	Yb ppm	Lu ppm	Ta ppm	Pb ppm	Th ppm	U ppm	ΣREE ppm	Eu anomaly
CRUS-01B	5.4	57	15.9	53	7.1	43.2	5.6	0.131	3.77	0.00062	0.0039	219.09	1.83
CRUS-01B	3.39	38.3	12.3	46	6.76	42.4	5.6	0.091	3.22	0.0009	0.0036	178.487	2.70
CRUS-01B	7.64	92	29.2	102.5	13.47	78.4	9.86	0.197	3.3	0.0028	0.0092	372.077	2.80
CRUS-01B	5.83	72.9	23.9	89.7	13	82.9	10.4	0.165	3.25	0.0019	0.0068	331.518	3.02
CRUS-01B	31.3	254.9	53.1	136.6	14.92	79.9	8.69	0.588	3.77	0.00063	0.0057	820.81	1.14
CRUS-01B	30.1	266.8	61.9	170.9	19.71	107.2	12.26	0.568	4.04	0.0008	0.0031	873.64	1.27
CRUS-01B	23	226.6	58.7	177.1	21.19	121.4	14.3	0.511	4.25	<DL	0.0119	777.331	1.41
CRUS-01B	29.48	255.3	57.8	157.3	17.92	97.6	11.06	0.586	4.27	0.001	0.0057	835.278	1.22
CRUS-01B	26.5	248	60.2	173	20.7	115	13.3	0.585	3.14	<DL	0.0046	836.98	1.36
CRUS-01B	29.4	257	58.4	157	17.3	94	10.6	0.49	2.85	0.0031	0.0146	820.066	1.15
CRUS-01B	31.1	257	56.2	149	16.2	84	9.3	0.602	3.64	0.0016	0.0048	821.28	1.07
CRUS-01B	29.09	254.6	58.1	157.1	17.65	94.9	10.69	0.508	2.93	0.0015	0.0104	821.105	1.21
288464-1-1.d	4.05	18.27	2.56	3.9	0.265	0.796	0.0607	0.109	19.24	0.0084	<DL	242.1517	3.27
288464-1-2.d	1.73	9.11	1.55	3.02	0.364	1.62	0.16	0.117	34	0.02	<DL	118.424	3.87
288464-1-3.d	0.555	3.31	0.665	1.641	0.217	1.368	0.162	0.1237	28.28	<DL	0.0523	54.083	6.99
288464-1-4.d	0.612	3.99	0.794	2.02	0.257	1.53	0.167	0.137	35.2	0.0159	<DL	56.053	5.38
288464-1-5.d	0.983	5.94	1.172	2.88	0.354	1.89	0.193	0.154	47	0.0178	0.0082	68.909	3.59
288464-1-6.d	0.559	3.4	0.67	1.8	0.22	1.35	0.151	0.132	34.4	0.0133	0.0246	50.73	5.75
288464-1-7.d	0.451	2.82	0.586	1.506	0.202	1.262	0.138	0.1301	35.3	<DL	0.0323	46.403	6.26
331805-1-1.d	4.85	35.82	8.43	24.7	3.898	27.82	4.018	0.1414	34.74	0.594	4.01	369.776	17.15
331805-1-2.d	2.88	21.5	4.93	15.58	2.54	19.05	2.99	0.1473	32.73	0.531	4.55	270.37	29.65
331806B-1-1.d	4.86	32.28	6.78	19.24	2.995	21.54	3.119	0.154	30.49	1.1	1.569	479.614	13.16
331806B-1-2.d	2.84	20.1	4.33	13.2	2.2	16.1	2.6	0.139	29.2	1.17	2.63	403.57	26.65
331806B-1-3.d	2.28	15.91	3.43	10.81	1.964	16.48	2.801	0.1644	33.53	1.445	3.06	359.875	30.03
331807-4-1.d	9.58	66.1	15.03	41.8	5.93	37.2	4.37	0.1676	28.93	1.114	0.995	645.81	6.92
331807-4-2.d	11.6	70.8	14.4	36.1	4.24	22.4	2.55	0.183	16.8	0.022	0.0141	472.99	1.70
331807-6-1.d	10.8	77.2	18	49.2	6.56	36.4	4.43	0.177	27.9	0.356	6.38	455.95	4.74
331807-6-2.d	12.44	76.7	15.86	38.3	4.21	20.6	2.05	0.192	15.4	0.024	0.073	419.35	1.02
331807-6-3.d	12.34	78.7	15.2	34.9	3.7	17.8	1.72	0.28	18.2	0.064	0.05	433.14	0.92
331807-6-4.d	11.9	70.3	14.5	31.8	3.66	16.8	1.38	0.25	21.9	0.058	0.038	416.74	0.99
331807-6-5.d	8.16	55.9	11.89	30.1	3.68	21.7	2.75	0.256	19.34	0.184	5.6	321.42	3.75
331807-7-6.d	10.44	69.5	14.8	36.5	4.46	22.7	2.69	0.211	23.4	0.235	6.6	415.64	2.41

Appendix 1.6B (continued)

Sample ID	Tb ppm	Dy ppm	Ho ppm	Er ppm	Tm ppm	Yb ppm	Lu ppm	Ta ppm	Pb ppm	Th ppm	U ppm	ΣREE ppm	Eu anomaly
331807-7-7.d	11.7	79.7	17.2	43.3	5.15	27.3	3.21	0.269	19.5	0.259	4	415.17	2.78
331815-2-1.d	20.71	120.4	22.37	47.8	4.79	19.47	1.9	0.311	15.98	<DL	0.008	627.01	0.80
331815-2-2.d	18.06	104.4	18.9	39.9	3.95	15.6	1.41	0.315	14.66	<DL	0.0102	530.24	0.79
331807-2-3.d	9.49	62.8	13.46	34.9	4.48	26.2	3.09	0.2	19.67	0.191	2.03	406.33	3.55
331807-2-4.d	8.5	45.9	7.95	18.8	2.48	13.29	1.49	0.232	21.11	0.474	1.89	948.61	5.73
331807-1.d	18.8	105.1	19.01	45.1	5.95	38.7	5.6	0.199	34.37	2.07	1.09	1295.66	2.43
331807-3.d	6.06	40	8.26	21	2.89	17.3	2.08	0.226	25.3	0.314	4.3	359.42	9.92
331813-1.d	27.92	166.5	32.48	78.7	8.98	46.7	5.13	0.205	20.2	0.051	0.0153	1085.49	1.55
331813-2.d	17.38	112	24.49	68.5	9.26	55.2	7.03	0.212	33.22	0.196	0.03	1102.66	2.87

Electronic Supplementary Materials associated with the chapter 2

Appendix 2.1A Chondrite-normalized REE patterns of scheelite and related intrusions. Chondrite normalized values from McDonough and Sun (1995).

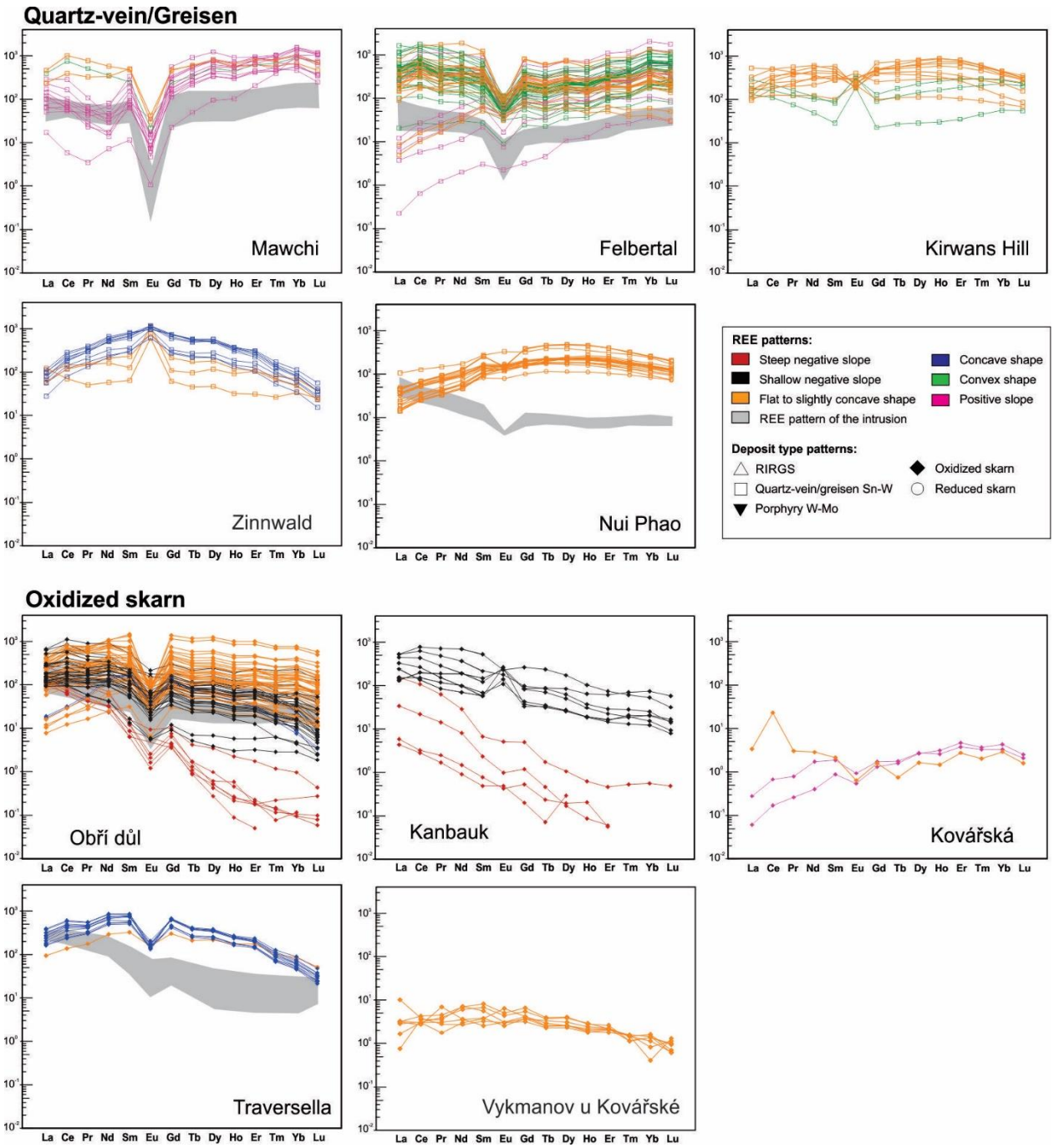

Reduced skarn

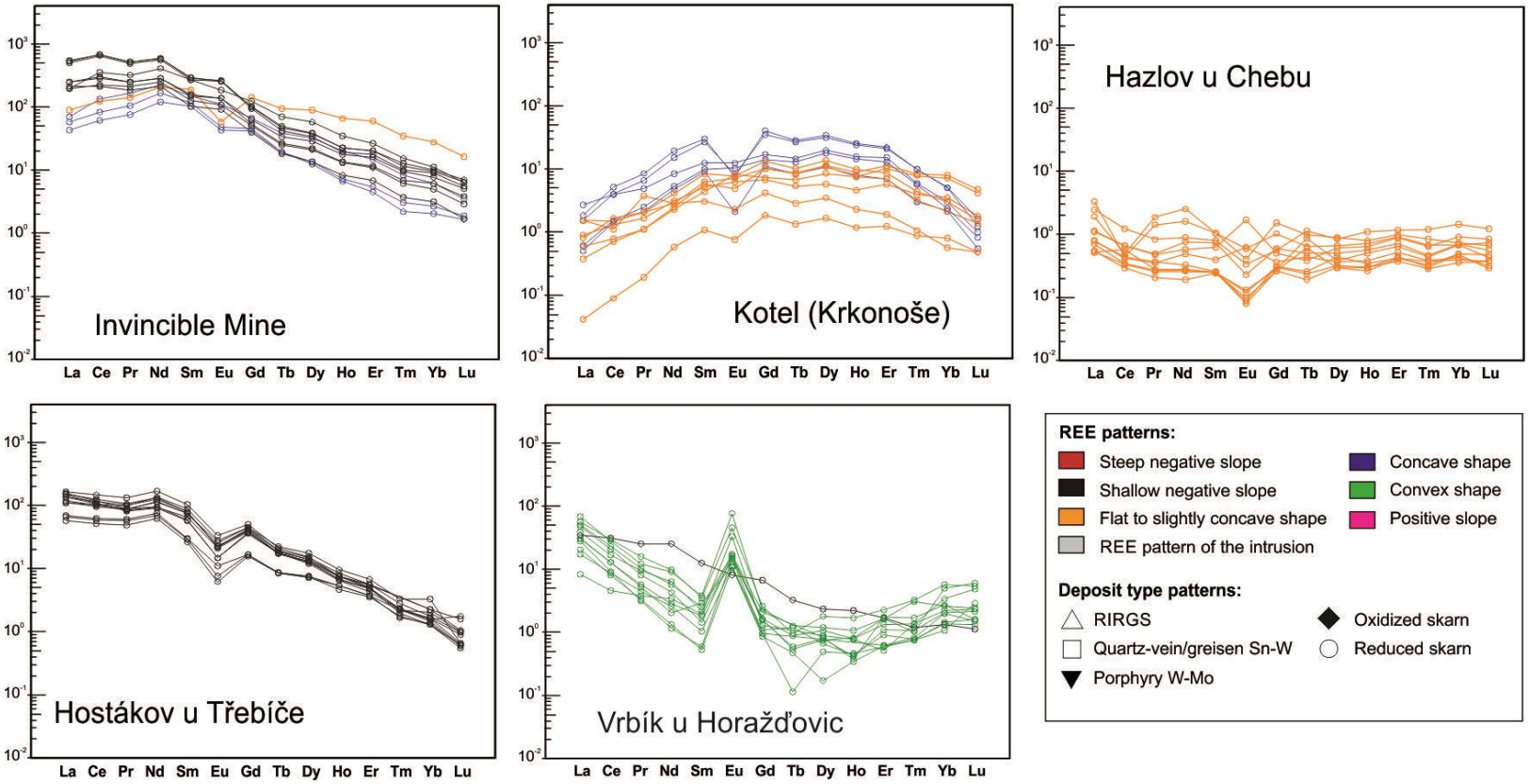

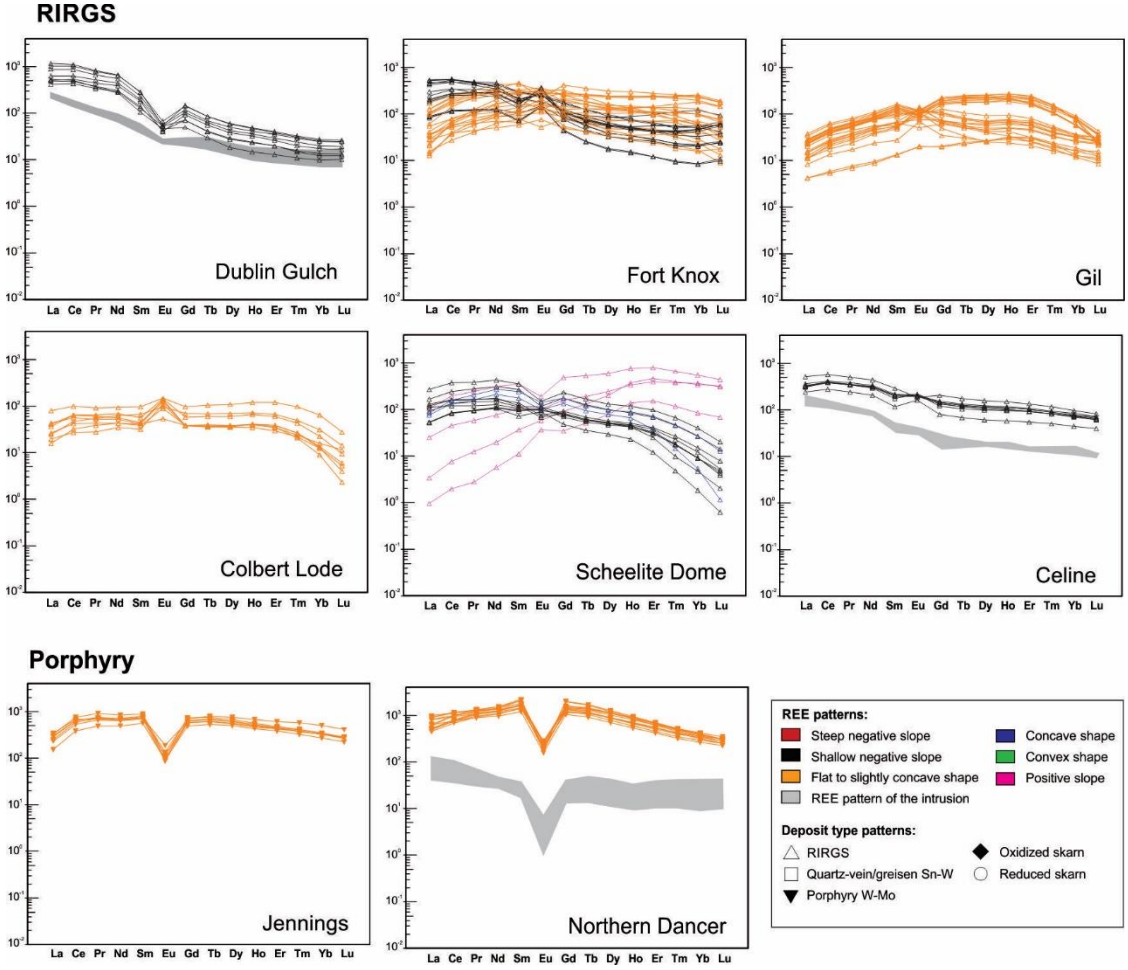
RIRGS
Dublin Gulch
Fort Knox
Gil
Colbert Lode
Scheelite Dome
Celine
Porphyry
Jennings
Northern Dancer
La Ce Pr Nd Sm Eu Gd Tb Dy Ho Er Tm Yb Lu
REE patterns:
Steep negative slope
Shallow negative slope
Flat to slightly concave shape
REE pattern of the intrusion
Concave shape
Convex shape
Positive slope
Deposit type patterns:
RIRGS
Quartz-vein/greisen Sn-W
Porphyry W-Mo
Oxidized skarn
Reduced skarn

Appendix 2.2A Scores contribution plots for each magmatic-hydrothermal deposit of PLS-DA on Fig. 2.8.

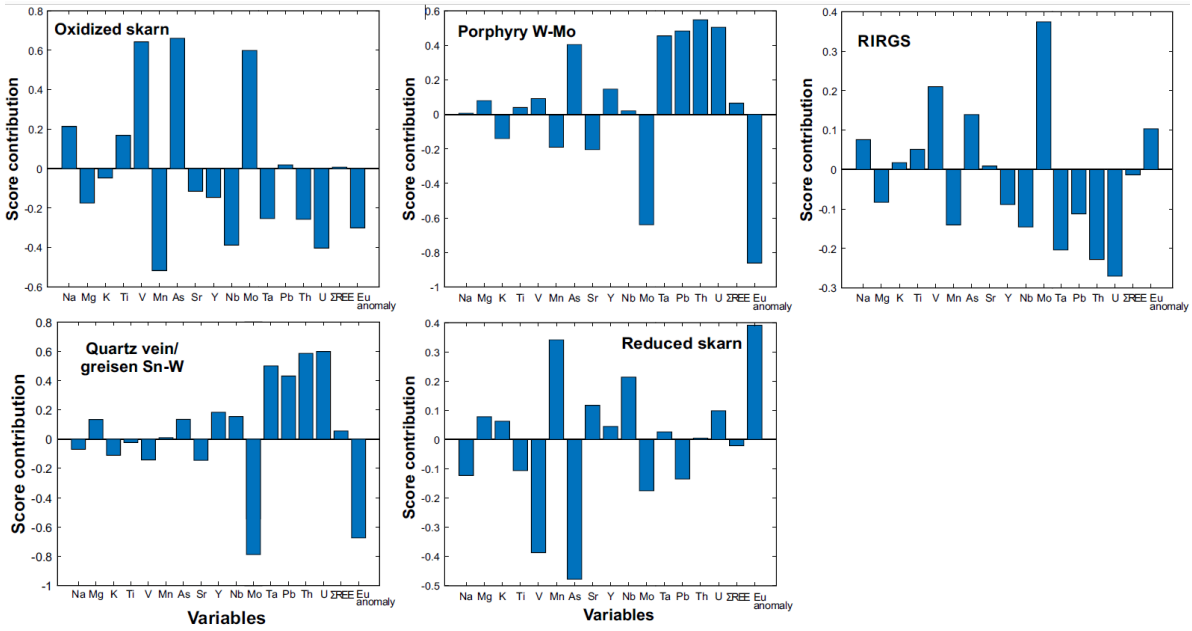

Appendix 2.1B Major and minor EPMA results.

Sample	Deposit name	Deposit type	CaO (%)	WO3 (%)	Total	Na (ppm)	Fe (ppm)	Mo (ppm)	Sr (ppm)
FB-A71-1A	Felbertal	Quartz-vein/greisen Sn-W	19.31	80.25	99.56	0.019	0.002	0.433	0.000
FB-A71-1A	Felbertal	Quartz-vein/greisen Sn-W	19.29	80.16	99.45	0.027	0.000	0.004	0.000
FB-A71-1A	Felbertal	Quartz-vein/greisen Sn-W	19.32	80.94	100.26	0.014	0.000	0.047	0.000
FB-A71-1B	Felbertal	Quartz-vein/greisen Sn-W	19.26	80.50	99.76	0.009	0.054	0.015	0.000
FB-A71-1B	Felbertal	Quartz-vein/greisen Sn-W	19.29	80.17	99.46	0.008	0.002	0.278	0.000
FB-A71-1B	Felbertal	Quartz-vein/greisen Sn-W	19.33	79.80	99.12	0.009	0.009	0.403	0.000
FB-EOZ-1A	Felbertal	Quartz-vein/greisen Sn-W	19.36	80.72	100.08	0.022	0.003	0.167	0.000
FB-EOZ-1A	Felbertal	Quartz-vein/greisen Sn-W	19.48	80.55	100.03	0.007	0.006	0.493	0.000
FB-EOZ-1A	Felbertal	Quartz-vein/greisen Sn-W	19.50	80.00	99.50	0.008	0.000	0.476	0.000
FB-EOZ-1B	Felbertal	Quartz-vein/greisen Sn-W	19.30	80.77	100.08	0.010	0.000	0.083	0.000
FB-EOZ-1B	Felbertal	Quartz-vein/greisen Sn-W	19.33	80.48	99.81	0.005	0.007	0.191	0.000
FB-K7B	Felbertal	Quartz-vein/greisen Sn-W	19.49	80.94	100.43	0.007	0.002	0.002	0.000
FB-K7B	Felbertal	Quartz-vein/greisen Sn-W	19.30	79.93	99.24	0.022	0.014	0.010	0.000
FB-K7A	Felbertal	Quartz-vein/greisen Sn-W	19.41	79.61	99.03	0.004	0.004	0.381	0.000
FB-K7A	Felbertal	Quartz-vein/greisen Sn-W	19.33	80.46	99.79	0.005	0.000	0.060	0.000
FB-K7A	Felbertal	Quartz-vein/greisen Sn-W	19.40	80.68	100.08	0.009	0.013	0.077	0.000
FK11-1	FortKnox	RIRGS	19.14	80.82	99.97	0.009	0.003	0.082	0.000
FK11-1	FortKnox	RIRGS	19.15	80.86	100.00	0.008	0.003	0.098	0.002
FK11-1	FortKnox	RIRGS	19.08	81.14	100.22	0.005	0.000	0.093	0.007
FK12	FortKnox	RIRGS	18.98	81.79	100.78	0.003	0.000	0.052	0.000
FK12	FortKnox	RIRGS	18.91	81.60	100.51	0.007	0.020	0.053	0.000
FK12	FortKnox	RIRGS	19.11	81.16	100.28	0.008	0.000	0.075	0.000
FK13	FortKnox	RIRGS	19.18	79.82	99.00	0.008	0.002	0.072	0.008
FK13	FortKnox	RIRGS	19.00	80.46	99.46	0.007	0.000	0.069	0.000
FK13	FortKnox	RIRGS	19.11	79.86	98.97	0.003	0.003	0.075	0.002
FK15	FortKnox	RIRGS	19.30	79.75	99.05	0.008	0.001	0.204	0.006
FK15	FortKnox	RIRGS	19.35	79.89	99.24	0.010	0.000	0.209	0.000
FK15	FortKnox	RIRGS	19.37	80.11	99.47	0.009	0.002	0.192	0.000

Appendix 2.1B (continued)

Sample	Deposit name	Deposit type	CaO (%)	WO3 (%)	Total	Na (ppm)	Fe (ppm)	Mo (ppm)	Sr (ppm)
FK15	FortKnox	RIRGS	19.37	79.90	99.27	0.011	0.000	0.398	0.010
DG-96	DublinGulch	RIRGS	19.10	79.51	98.71	0.020	0.003	0.066	0.000
DG-96	DublinGulch	RIRGS	19.32	79.85	99.30	0.069	0.020	0.083	0.000
DG-96	DublinGulch	RIRGS	18.99	79.71	98.77	0.031	0.010	0.050	0.000
DG-96	DublinGulch	RIRGS	19.47	79.67	99.23	0.016	0.005	0.057	0.000
DG-96	DublinGulch	RIRGS	19.19	79.10	98.38	0.028	0.004	0.059	0.000
CC57	Corcoesto	Orogenic Au	18.78	81.04	99.82	0.018	0.002	0.000	0.000
CC57	Corcoesto	Orogenic Au	18.97	80.83	99.81	0.006	0.002	0.008	0.000
CC57	Corcoesto	Orogenic Au	18.70	80.64	99.33	0.014	0.000	0.000	0.000
23858	Corcoesto	Orogenic Au	18.89	81.11	100.00	0.004	0.002	0.000	0.000
23858	Corcoesto	Orogenic Au	18.90	80.91	99.81	0.017	0.000	0.000	0.003
23858	Corcoesto	Orogenic Au	18.93	80.18	99.11	0.008	0.000	0.000	0.000
Cel-2	Celine	RIRGS	19.30	80.11	99.62	0.021	0.002	0.136	0.000
Cel-2	Celine	RIRGS	18.82	80.70	99.73	0.021	0.005	0.145	0.000
Cel-2	Celine	RIRGS	18.55	80.88	99.64	0.049	0.001	0.143	0.000
Cel-2	Celine	RIRGS	19.26	80.34	99.83	0.117	0.000	0.148	0.000
Cel-2	Celine	RIRGS	19.31	80.00	99.54	0.009	0.002	0.150	0.000
Cel-2	Celine	RIRGS	19.28	80.36	99.88	0.016	0.000	0.157	0.000
SD-11	SchDome	RIRGS	18.86	80.26	99.12	0.038	0.022	0.000	0.000
SD-12	SchDome	RIRGS	18.95	80.49	99.43	0.030	0.001	0.000	0.013
SD-13	SchDome	RIRGS	19.10	80.35	99.45	0.016	0.011	0.000	0.000
SD-14	SchDome	RIRGS	18.62	80.43	99.05	0.042	0.005	0.000	0.000
SD-15	SchDome	RIRGS	18.73	80.40	99.14	0.009	0.000	0.000	0.000
SD-17	SchDome	RIRGS	18.80	80.36	99.15	0.027	0.053	0.000	0.000
sch11	Hostákov u Třebíče	Oxidized skarn	19.50	80.28	99.78	0.010	0.009	0.056	0.000
sch11	Hostákov u Třebíče	Oxidized skarn	19.58	81.13	100.71	0.005	0.001	0.023	0.000
sch11	Hostákov u Třebíče	Oxidized skarn	19.44	80.36	99.80	0.007	0.001	0.011	0.000
sch11	Hostákov u Třebíče	Oxidized skarn	19.60	80.42	100.01	0.008	0.000	0.015	0.000

Appendix 2.1B (continued)

Sample	Deposit name	Deposit type	CaO (%)	WO3 (%)	Total	Na (ppm)	Fe (ppm)	Mo (ppm)	Sr (ppm)
sch11	Hostákov u Třebíče	Oxidized skarn	19.47	80.97	100.44	0.007	0.001	0.029	0.000
sch11	Hostákov u Třebíče	Oxidized skarn	19.49	80.86	100.35	0.003	0.002	0.022	0.000
sch11	Hostákov u Třebíče	Oxidized skarn	19.45	80.80	100.25	0.007	0.005	0.018	0.000
sch11	Hostákov u Třebíče	Oxidized skarn	19.46	80.16	99.62	0.004	0.003	0.024	0.000
sch16	Kovářská	Oxidized skarn	19.38	79.53	98.92	0.004	0.002	0.027	0.000
sch16	Kovářská	Oxidized skarn	19.44	80.28	99.72	0.046	0.000	0.000	0.000
sch16	Kovářská	Oxidized skarn	19.31	80.65	99.96	0.051	0.000	0.000	0.000
sch16	Kovářská	Oxidized skarn	19.65	80.39	100.04	0.045	0.004	0.000	0.003
sch16	Kovářská	Oxidized skarn	19.59	79.39	98.97	0.052	0.000	0.000	0.000
sch17	Kotel (Krkonoše)	Reduced skarn	19.45	80.01	99.46	0.052	0.001	0.001	0.000
sch17	Kotel (Krkonoše)	Reduced skarn	19.49	79.80	99.29	0.058	0.000	0.000	0.000
sch17	Kotel (Krkonoše)	Reduced skarn	19.51	80.11	99.62	0.069	0.000	0.002	0.010
sch17	Kotel (Krkonoše)	Reduced skarn	19.43	79.96	99.39	0.063	0.002	0.000	0.000
sch17	Kotel (Krkonoše)	Reduced skarn	19.52	79.89	99.42	0.047	0.005	0.000	0.000
sch17	Kotel (Krkonoše)	Reduced skarn	19.51	79.55	99.06	0.042	0.011	0.000	0.013
sch20	Obří důl	Oxidized skarn	19.27	79.17	98.44	0.017	0.026	0.251	0.000
sch20	Obří důl	Oxidized skarn	19.25	79.68	98.93	0.001	0.004	0.006	0.096
sch20	Obří důl	Oxidized skarn	19.38	79.31	98.69	0.000	0.000	0.020	0.000
sch20	Obří důl	Oxidized skarn	19.24	79.82	99.07	0.002	0.005	0.003	0.000
sch20	Obří důl	Oxidized skarn	19.16	79.28	98.44	0.000	0.000	0.013	0.000
sch20	Obří důl	Oxidized skarn	19.11	79.27	98.38	0.006	0.003	0.000	0.000
sch20	Obří důl	Oxidized skarn	19.22	79.76	98.98	0.004	0.028	0.027	0.000
sch20	Obří důl	Oxidized skarn	19.36	79.02	98.39	0.007	0.000	0.000	0.000
sch22	Obří důl	Oxidized skarn	19.33	78.98	98.31	0.003	0.003	0.000	0.000
sch22	Obří důl	Oxidized skarn	19.15	79.85	99.00	0.004	0.002	0.001	0.000
sch22	Obří důl	Oxidized skarn	19.16	79.52	98.68	0.001	0.006	0.000	0.000
sch22	Obří důl	Oxidized skarn	19.44	78.84	98.28	0.033	0.000	0.166	0.000
sch23	Obří důl	Oxidized skarn	19.17	79.24	98.41	0.036	0.000	0.157	0.000

Appendix 2.1B (continued)

Sample	Deposit name	Deposit type	CaO (%)	WO3 (%)	Total	Na (ppm)	Fe (ppm)	Mo (ppm)	Sr (ppm)
sch23	Obří důl	Oxidized skarn	19.22	79.91	99.13	0.039	0.001	0.209	0.000
sch23	Obří důl	Oxidized skarn	19.00	80.32	99.32	0.029	0.002	0.174	0.000
sch23	Obří důl	Oxidized skarn	19.30	80.21	99.50	0.011	0.003	0.000	0.000
sch23	Obří důl	Oxidized skarn	19.15	80.50	99.65	0.006	0.003	0.005	0.000
sch23	Obří důl	Oxidized skarn	19.20	79.68	98.88	0.011	0.000	0.000	0.000
sch23	Obří důl	Oxidized skarn	19.15	80.17	99.33	0.007	0.000	0.007	0.000
sch24	Obří důl	Oxidized skarn	19.39	79.78	99.16	0.027	0.002	0.900	0.000
sch24	Obří důl	Oxidized skarn	19.40	80.21	99.61	0.007	0.004	1.187	0.000
sch24	Obří důl	Oxidized skarn	19.38	80.56	99.95	0.005	0.006	0.354	0.000
sch24	Obří důl	Oxidized skarn	19.36	80.37	99.73	0.004	0.006	0.630	0.000
sch24	Obří důl	Oxidized skarn	19.37	80.37	99.74	0.009	0.015	1.122	0.000
sch25	Obří důl	Oxidized skarn	19.34	79.82	99.16	0.005	0.083	0.000	0.000
sch25	Obří důl	Oxidized skarn	19.37	80.28	99.65	0.011	0.018	0.083	0.007
sch25	Obří důl	Oxidized skarn	19.22	80.45	99.67	0.002	0.004	0.518	0.000
sch25	Obří důl	Oxidized skarn	19.31	80.55	99.85	0.008	0.000	0.477	0.000
sch25	Obří důl	Oxidized skarn	19.45	80.55	100.00	0.003	0.076	0.220	0.000
sch31	Hazlov u Chebu	Reduced skarn	19.25	79.44	98.69	0.010	0.001	0.208	0.000
sch31	Hazlov u Chebu	Reduced skarn	19.19	80.00	99.19	0.013	0.000	0.255	0.000
sch31	Hazlov u Chebu	Reduced skarn	19.31	80.26	99.57	0.021	0.000	0.232	0.000
sch31	Hazlov u Chebu	Reduced skarn	19.21	80.24	99.44	0.021	0.001	0.205	0.000
sch31	Hazlov u Chebu	Reduced skarn	19.30	79.97	99.28	0.037	0.000	0.211	0.000
sch40	Vrbík u Horažďovic	Reduced skarn	19.02	78.96	97.98	0.003	0.006	0.163	0.000
sch40	Vrbík u Horažďovic	Reduced skarn	19.01	79.75	98.77	0.006	0.000	1.361	0.000
sch40	Vrbík u Horažďovic	Reduced skarn	19.28	79.97	99.26	0.004	0.000	0.022	0.000
sch44	Vykmanov	Oxidized skarn	19.70	79.81	99.50	0.009	0.000	0.000	0.000
sch44	Vykmanov	Oxidized skarn	19.42	80.87	100.29	0.013	0.006	0.000	0.000
sch44	Vykmanov	Oxidized skarn	19.38	80.68	100.05	0.027	0.001	0.000	0.000
sch44	Vykmanov	Oxidized skarn	19.45	79.38	98.83	0.013	0.001	0.001	0.000

Appendix 2.1B (continued)

Sample	Deposit name	Deposit type	CaO (%)	WO3 (%)	Total	Na (ppm)	Fe (ppm)	Mo (ppm)	Sr (ppm)
sch44	Vykmanov	Oxidized skarn	19.42	80.44	99.86	0.037	0.002	0.000	0.000
sch44	Vykmanov	Oxidized skarn	19.40	80.47	99.87	0.029	0.000	0.000	0.000
YP5B	YellowPine	Orogenic W-Sb-Au	19.05	80.34	99.40	0.006	0.004	0.000	0.075
YP5B	YellowPine	Orogenic W-Sb-Au	19.10	79.88	98.99	0.009	0.003	0.000	0.045
YP5B	YellowPine	Orogenic W-Sb-Au	19.18	80.48	99.66	0.013	0.001	0.000	0.105
YP5B	YellowPine	Orogenic W-Sb-Au	19.06	80.59	99.66	0.005	0.000	0.000	0.050
YP5A	YellowPine	Orogenic W-Sb-Au	19.06	81.14	100.19	0.004	0.003	0.000	0.141
YP5A	YellowPine	Orogenic W-Sb-Au	19.01	80.86	99.87	0.002	0.000	0.000	0.144
YP5A	YellowPine	Orogenic W-Sb-Au	19.05	81.51	100.57	0.009	0.000	0.003	0.115
YP5A	YellowPine	Orogenic W-Sb-Au	19.21	80.96	100.17	0.003	0.001	0.000	0.118
YP5A	YellowPine	Orogenic W-Sb-Au	19.02	81.10	100.13	0.002	0.007	0.002	0.148
YP5A	YellowPine	Orogenic W-Sb-Au	18.96	80.60	99.56	0.005	0.000	0.000	0.189
YP5A	YellowPine	Orogenic W-Sb-Au	18.95	80.82	99.76	0.009	0.007	0.000	0.168
YP5A	YellowPine	Orogenic W-Sb-Au	18.88	80.29	99.17	0.002	0.005	0.006	0.185
YP5A	YellowPine	Orogenic W-Sb-Au	18.94	80.88	99.81	0.002	0.000	0.000	0.166
YP5A	YellowPine	Orogenic W-Sb-Au	18.98	80.74	99.73	0.008	0.011	0.000	0.192
G22	Gil-Sourdough	RIRGS	18.87	80.49	99.36	0.003	0.000	0.047	0.000
G22	Gil-Sourdough	RIRGS	18.90	80.13	99.03	0.004	0.000	0.067	0.000
G22	Gil-Sourdough	RIRGS	19.11	80.04	99.15	0.004	0.000	0.067	0.000
G22	Gil-Sourdough	RIRGS	18.90	80.23	99.13	0.004	0.000	0.082	0.000
G24	Gil-Sourdough	RIRGS	19.15	80.47	99.62	0.026	0.000	0.051	0.011
G24	Gil-Sourdough	RIRGS	18.98	80.61	99.59	0.015	0.000	0.094	0.000
G24	Gil-Sourdough	RIRGS	19.17	80.45	99.62	0.003	0.000	0.250	0.000
G24	Gil-Sourdough	RIRGS	19.045	80.21	99.25	0.004	0.000	0.187	0.000
G24	Gil-Sourdough	RIRGS	18.902	80.24	99.14	0.016	0.000	0.194	0.000
CL16-1	ColbertLode	RIRGS	19.288	80.79	100.08	0.007	0.000	0.151	0.000
CL16-2	ColbertLode	RIRGS	19.2	81.09	100.29	0.011	0.001	0.144	0.003
CL16-3	ColbertLode	RIRGS	19.238	81.30	100.53	0.006	0.000	0.146	0.000

Appendix 2.2B Summary of scheelite literature data used in the PLS-DA and RF models.

Name	Country	Deposit type	Number of analysis	Reference
Batemans	New Zealand	Quartz-vein/Greisen W-Sn	132	Palmer (2021)
Canaan Downs	New Zealand	Quartz-vein/Greisen W-Sn	204	Palmer (2021)
Cetoraz	Czech Republic	Quartz-vein/Greisen W-Sn	11	Pasava unpubl.
Cinovec	Czech Republic	Quartz-vein/Greisen W-Sn	21	Pasava unpubl.
H. Slavkov, Huber, 1968	Czech Republic	Quartz-vein/Greisen W-Sn	8	Pasava unpubl.
Horní Babákov	Czech Republic	Quartz-vein/Greisen W-Sn	12	Pasava unpubl.
Ovesná Lhota	Czech Republic	Quartz-vein/Greisen W-Sn	9	Pasava unpubl.
Yangjiashan	China	Quartz-vein/Greisen W-Sn	253	Li et al. (2021)
Shizhuyuan	China	Oxidized skarn	13	Miranda et al. (2022)
Kumbel	Kyrgyzstan	Oxidized skarn	9	Miranda et al. (2022)
Xiaoyao	China	Oxidized skarn	9	Miranda et al. (2022)
Brejui	Brazil	Oxidized skarn	18	Miranda et al. (2022)
Kara	Australia	Oxidized skarn	22	Miranda et al. (2022)
King Island	Australia	Oxidized skarn	16	Miranda et al. (2022)
Jiama	China	Oxidized skarn	18	Miranda et al. (2022)
Pine Creek	USA	Reduced skarn	9	Miranda et al. (2022)
Zhuxi	China	Reduced skarn	17	Miranda et al. (2022)
Lened	Canada	Reduced skarn	45	Miranda et al. (2022)
Cantung	Canada	Reduced skarn	63	Miranda et al. (2022)
Mactung	Canada	Reduced skarn	50	Miranda et al. (2022)
Salau	France	Reduced skarn	13	Miranda et al. (2022)
Bonfim	Brazil	Reduced skarn	8	Miranda et al. (2022)
Vostok-2	Russia	Reduced skarn	20	Miranda et al. (2022)
Lermontovskoe	Russia	Reduced skarn	26	Miranda et al. (2022)
Marn	Canada	Reduced skarn	10	Miranda et al. (2022)

Appendix 2.2B (continued)

Name	Country	Deposit type	Number of analysis	Reference
Nevoria	Australia	Reduced skarn	6	Sciuba et al. (2020)
Wolf (Ray Gulch or Mar)	Canada	RIRGS	9	Miranda et al. (2022)
Vacíkov, Petráčkova hora	Czech Republic	RIRGS	23	Pasava unpubl.
Amaruq	Canada	Orogenic Au	29	de Bronac de Vazelhes (2019)
Beaufor	Canada	Orogenic Au	23	Sciuba et al. (2020)
Buzwagi	Tanzania	Orogenic Au	1	Sciuba et al. (2020)
Edward's Find	Australia	Orogenic Au	6	Sciuba et al. (2020)
Marvel Loch	Australia	Orogenic Au	11	Sciuba et al. (2020)
Mt Pleasant	Australia	Orogenic Au	8	Sciuba et al. (2020)
Paddington	Australia	Orogenic Au	30	Sciuba et al. (2020)
Tarmoola	Australia	Orogenic Au	12	Sciuba et al. (2020)
Young Davidson	Canada	Orogenic Au	8	Sciuba et al. (2020)
Lamaque	Canada	Orogenic Au	4	Sciuba et al. (2020)
Sigma	Canada	Orogenic Au	13	Sciuba et al. (2020)
Cuiaba	Brazil	Orogenic Au	4	Sciuba et al. (2020)
Dome	Canada	Orogenic Au	10	Sciuba et al. (2020)
Essakane	Burkina Faso	Orogenic Au	21	Sciuba et al. (2020)
Macraes	New Zeland	Orogenic Au	19	Sciuba et al. (2020)
Canandian Malartic	Canada	Orogenic Au	5	Sciuba et al. (2020)
Hollinger	Canada	Orogenic Au	3	Sciuba et al. (2020)
Kumtor	Russia	Orogenic Au	4	Sciuba et al. (2020)
Hutti	India	Orogenic Au	26	Sciuba et al. (2020)
Mt Charlotte	Australia	Orogenic Au	15	Sciuba et al. (2020)
Kochkar	Kyrgyzstan	Orogenic Au	19	Sciuba et al. (2020)
Mararoa, Norseman district	Australia	Orogenic Au	6	Sciuba et al. (2020)

Appendix 2.2B (continued)

Name	Country	Deposit type	Number of analysis	Reference
Crown Footwall, Norseman district	Australia	Orogenic Au	10	Sciuba et al. (2020)
North Royal, Norseman district	Australia	Orogenic Au	8	Sciuba et al. (2020)
Glenorchy	New Zealand	Orogenic Au-W	34	Palmer (2021)
Barewood	New Zealand	Orogenic Au-W	41	Scanlan et al. (2018)
Alta Lode (Bendigo)	New Zealand	Orogenic Au-W	89	Palmer (2021)
Boanerges Peak*	New Zealand	Metamorphic scheelite	130	Palmer (2021)

*used only in PLS-DA

Appendix 2.3B Summary of scheelite from literature used for RF predictions.

Name	Country	Deposit type	Number of analysis	Reference
Corcoesto	Spain	Orogenic Au	9	This study
Hangar Flats	USA	Orogenic Au	17	This study
Xiadian	China	Orogenic Au	20	Liu et al. (2021)
Majiayao	China	Orogenic Au	19	Liu et al. (2021)
The Ovens	Canada	Orogenic Au	46	Cave 2016
Mt Judah Mine	New Zealand	Orogenic W-Au	8	Cave 2016
Paradise Mine	New Zealand	Metamorphic scheelite	10	Cave 2016
Fiddlers Flat	New Zealand	Metamorphic scheelite	40	Cave et al. (2017)
Lake Hawea	New Zealand	Metamorphic scheelite	40	Cave et al. (2017)
Boanerges Peak	New Zealand	Metamorphic scheelite	130	Palmer (2021)
Weijia	China	Greisen and oxidized skarn	63	Huang et al. (2022)

Appendix 2.4B Minor and trace element composition of scheelite.

Point ID	Deposit name	Deposit type	B (ppm)	Na (ppm)	Mg (ppm)	K (ppm)	Ti (ppm)	V (ppm)	Mn (ppm)
Min DL			0.134	0.261	0.008	0.479	0.067	0.001	0.104
Max DL			2.387	0.779	0.204	2.100	0.554	0.637	0.309
Cel-L1.d	Celine	RIRGS	0.6672	113.98	3.7252	15.8877	0.6672	0.2641	13.7888
Cel-L2.d	Celine	RIRGS	1.0842	117.733	3.4889	13.9695	0.5282	0.28217	14.2753
Cel-L3.d	Celine	RIRGS	0.6672	104.667	3.6835	14.178	0.7923	0.24464	15.5541
Cel-L4.d	Celine	RIRGS	0.7506	169.302	3.5584	11.259	0.8479	0.30441	13.205
Cel-L4.d	Celine	RIRGS	0.4448	69.778	3.2526	11.0366	0.7506	0.28356	13.4413
Cel-L5.d	Celine	RIRGS	0.8896	108.698	3.8225	16.124	0.7784	0.25437	13.7471
Cel-L6.d	Celine	RIRGS	1.2371	99.246	3.8225	15.151	0.6811	0.26688	16.3325
Cel-L7.d	Celine	RIRGS	0.8062	107.169	3.6696	14.5255	0.9174	0.27105	13.4274
CL16-2-C1a.d	Colbert Lode	RIRGS	0.7089	18.6121	5.4905	15.2066	0.7506	0.14456	12.4544
CL16-2-C2b.d	Colbert Lode	RIRGS	1.0981	35.584	5.3237	15.012	0.7228	0.16263	12.4961
CL16-2-C2c.d	Colbert Lode	RIRGS	0.4448	15.2205	5.4766	13.483	0.7784	0.21823	14.4421
CL16-3-1.d	Colbert Lode	RIRGS	0.7784	36.6404	4.9762	10.981	0.6672	0.07645	12.927
CL16-3-2.d	Colbert Lode	RIRGS	0.6672	22.0176	4.448	10.147	0.4587	0.14595	12.1486
CL16-3-3.d	Colbert Lode	RIRGS	0.8618	22.9072	4.4758	20.85	0.973	0.05143	12.2737
CL16-3-4.d	Colbert Lode	RIRGS	0.7645	12.7602	4.6704	13.622	0.7645	0.05282	12.8019
CL16-3-5.d	Colbert Lode	RIRGS	0.7506	9.591	5.4071	14.039	0.6394	<DL	14.0251
CC57-1.d	Corcoesto	Orogenic Au	3.5584	15.0954	71.863	4.448	0.9591	0.04726	14.9147
CC57-2.d	Corcoesto	Orogenic Au	5.56	21.128	80.759	16.958	1.4734	0.04309	17.1526
CC57-3.d	Corcoesto	Orogenic Au	4.587	15.9155	26.688	2.919	0.8618	0.06116	13.0799
CC57-4.d	Corcoesto	Orogenic Au	3.0163	21.6979	62.967	16.402	4.587	0.04865	17.0136
CC57-5.d	Corcoesto	Orogenic Au	2.8773	19.0986	45.1472	11.12	1.2788	0.07645	16.2074
CC57-6.d	Corcoesto	Orogenic Au	4.726	41.561	71.029	19.46	0.9452	0.07784	17.3889
CC57-7.d	Corcoesto	Orogenic Au	2.9051	28.4394	37.947	9.869	1.0425	0.06394	12.6073
CC57-8.d	Corcoesto	Orogenic Au	3.614	53.237	33.638	51.43	0.695	0.14456	12.5795
CC57-9.d	Corcoesto	Orogenic Au	3.5028	64.913	40.31	12.232	2.3352	0.11954	12.5239
DG28-C1a.d	Dublin Gulch	RIRGS	0.6811	149.564	11.815	16.541	1.5707	0.43507	10.5362
DG28-C2b.d	Dublin Gulch	RIRGS	0.6672	195.712	13.205	17.792	1.4039	0.58658	11.1895
DG28-C1c.d	Dublin Gulch	RIRGS	1.0703	181.395	14.456	16.124	1.4039	0.72002	9.2157
DG28-C1c.d	Dublin Gulch	RIRGS	0.7923	97.3	13.344	14.039	1.112	0.50457	7.7979
DG28-C3a.d	Dublin Gulch	RIRGS	0.6116	82.288	35.028	14.734	0.9035	0.39615	12.3432
DG28-C3b.d	Dublin Gulch	RIRGS	0.834	116.621	13.066	20.989	1.4039	0.46426	10.2304
DG28-C3b.d	Dublin Gulch	RIRGS	0.5977	72.558	22.657	14.317	1.0564	0.39337	16.819
DG28-C3c.d	Dublin Gulch	RIRGS	0.8062	82.983	15.012	18.487	1.2232	0.36001	7.8535

Appendix 2.4B (continued)

Point ID	Deposit name	Deposit type	B (ppm)	Na (ppm)	Mg (ppm)	K (ppm)	Ti (ppm)	V (ppm)	Mn (ppm)
FBA711B-SCH2-10.d	Felbertal	Quartz vein/Greisen Sn-W	14.039	68.527	45.731	22.24	2.5159	1.37471	36.0566
FBA711B-SCH2-11.d	Felbertal	Quartz vein/Greisen Sn-W	16.124	23.213	7.228	7.645	1.8348	0.48233	18.4036
FBA711B-SCH2-2.d	Felbertal	Quartz vein/Greisen Sn-W	15.846	57.824	107.447	12.927	2.7661	1.15231	51.3883
FBA711B-SCH2-3.d	Felbertal	Quartz vein/Greisen Sn-W	14.6645	55.878	108.837	13.761	2.9468	1.14397	53.793
FBA711B-SCH2-4.d	Felbertal	Quartz vein/Greisen Sn-W	16.819	50.04	92.296	14.039	2.5993	1.26907	55.878
FBA711B-SCH2-5.d	Felbertal	Quartz vein/Greisen Sn-W	26.41	62.689	77.423	8.757	1.9738	0.89794	48.65
FBA711B-SCH2-6.d	Felbertal	Quartz vein/Greisen Sn-W	13.5664	53.932	109.254	12.093	3.1275	1.36776	56.295
FBA711B-SCH2-7.d	Felbertal	Quartz vein/Greisen Sn-W	24.603	74.643	62.828	22.379	2.363	0.87709	27.9251
FBA711B-SCH2-8.d	Felbertal	Quartz vein/Greisen Sn-W	16.124	81.037	62.55	31.97	2.4325	0.91879	29.607
FBA711B-SCH2-9.d	Felbertal	Quartz vein/Greisen Sn-W	12.0374	50.04	96.466	30.58	2.9468	1.09671	49.8176
FBA711B-SCH3-1.d	Felbertal	Quartz vein/Greisen Sn-W	12.5934	45.036	35.723	8.201	2.4325	1.10227	24.0887
FBA711B-SCH3-2.d	Felbertal	Quartz vein/Greisen Sn-W	11.8011	9.1879	7.923	37.53	2.4881	0.01946	12.3154
FBA712B-SCH2-1.d	Felbertal	Quartz vein/Greisen Sn-W	16.6939	54.627	7.8257	11.676	7.784	1.11339	15.3873
FBA712B-SCH2-2.d	Felbertal	Quartz vein/Greisen Sn-W	13.6915	33.221	6.4079	10.703	1.7792	3.475	14.7896
FBA712B-SCH2-3.d	Felbertal	Quartz vein/Greisen Sn-W	14.1919	43.09	22.518	10.425	16.68	1.3483	38.086
FBA712B-SCH2-4.d	Felbertal	Quartz vein/Greisen Sn-W	15.985	44.5217	16.1379	15.985	2.0016	0.84095	18.4731
FBA712B-SCH2-6.d	Felbertal	Quartz vein/Greisen Sn-W	14.4421	68.249	40.032	10.842	2.2796	1.1398	79.23
FBA712B-SCH2-7.d	Felbertal	Quartz vein/Greisen Sn-W	17.653	82.705	57.546	10.703	3.0719	1.05223	32.665
FBA712B-SCH2-8.d	Felbertal	Quartz vein/Greisen Sn-W	14.595	225.18	117.872	15.985	3.8225	1.61657	46.148
FBA712B-SCH2-9.d	Felbertal	Quartz vein/Greisen Sn-W	14.873	103.972	59.77	13.483	3.6974	1.69163	23.1991
FBA712B-SCH3-1.d	Felbertal	Quartz vein/Greisen Sn-W	20.6137	54.21	3.475	9.73	3.0163	0.06394	11.8845
FBA712B-SCH3-3.d	Felbertal	Quartz vein/Greisen Sn-W	19.0708	67.971	38.7949	7.367	4.7538	1.78059	26.7575
FBA712B-SCH3-4.d	Felbertal	Quartz vein/Greisen Sn-W	19.599	48.65	48.65	9.313	3.5028	0.74365	18.1812
FBA712B-SCH3-5.d	Felbertal	Quartz vein/Greisen Sn-W	17.4445	15.1649	8.896	3.892	1.8626	0.022379	14.5811
FBA712B-SCH3-7.d	Felbertal	Quartz vein/Greisen Sn-W	17.2082	37.252	10.2026	9.313	6.2828	0.95493	15.568
FBA712B-SCH3-8.d	Felbertal	Quartz vein/Greisen Sn-W	16.3742	27.7722	2.8773	13.761	1.5568	0.1251	10.3138
FBA713A-SCH2-1.d	Felbertal	Quartz vein/Greisen Sn-W	10.1053	93.547	40.6714	19.043	5.143	1.96268	26.3405
FBA713A-SCH2-2.d	Felbertal	Quartz vein/Greisen Sn-W	11.676	129.409	63.801	16.68	5.977	2.7383	31.5252
FBA713A-SCH2-3.d	Felbertal	Quartz vein/Greisen Sn-W	9.4381	80.203	42.7703	16.263	3.0024	3.475	25.5204
FBA713A-SCH2-4.d	Felbertal	Quartz vein/Greisen Sn-W	8.9377	79.23	52.959	15.568	3.0997	1.09393	27.0077
FBA713A-SCH2-5.d	Felbertal	Quartz vein/Greisen Sn-W	10.2443	48.511	60.326	16.402	2.9885	1.14258	23.4215
FBA713A-SCH3-1.d	Felbertal	Quartz vein/Greisen Sn-W	10.8976	34.055	13.1077	10.981	1.2649	0.09452	22.24
FBA713A-SCH3-2.d	Felbertal	Quartz vein/Greisen Sn-W	11.676	82.01	47.26	22.24	3.1414	1.46923	33.6241
FBA713A-SCH3-3.d	Felbertal	Quartz vein/Greisen Sn-W	8.8543	35.167	19.3488	10.842	0.9174	0.05699	14.9147
FBA713A-SCH3-4.d	Felbertal	Quartz vein/Greisen Sn-W	9.2296	57.963	37.669	10.842	2.8217	1.946	23.8107

Appendix 2.4B (continued)

Point ID	Deposit name	Deposit type	B (ppm)	Na (ppm)	Mg (ppm)	K (ppm)	Ti (ppm)	V (ppm)	Mn (ppm)
FBA713A-SCH3-5.d	Felbertal	Quartz vein/Greisen Sn-W	9.3964	43.09	35.0558	11.537	2.9607	0.695	17.4445
FBA713A-SCH3-6.d	Felbertal	Quartz vein/Greisen Sn-W	11.398	63.94	49.623	11.815	1.4873	0.55461	30.5522
FBA713A-SCH3-7.d	Felbertal	Quartz vein/Greisen Sn-W	10.703	29.19	27.7027	13.344	0.9035	0.07367	15.4151
FBA713B-SCH2-1.d	Felbertal	Quartz vein/Greisen Sn-W	11.1617	55.6	34.5693	12.093	4.7816	1.21347	22.379
FBA713B-SCH2-2.d	Felbertal	Quartz vein/Greisen Sn-W	11.3285	69.083	43.6877	10.703	4.5036	1.41919	21.0585
FBA713B-SCH2-3.d	Felbertal	Quartz vein/Greisen Sn-W	10.6057	59.214	47.26	10.703	15.846	1.66522	33.082
FBA713B-SCH2-4.d	Felbertal	Quartz vein/Greisen Sn-W	9.6049	36.835	47.26	6.672	2.8773	1.23432	19.182
FBA713B-SCH2-5.d	Felbertal	Quartz vein/Greisen Sn-W	10.6891	20.2384	29.607	11.676	2.4881	0.45453	20.7388
FBEOZ1A-1.d	Felbertal	Quartz vein/Greisen Sn-W	21.4755	11.7177	22.24	152.9	17.375	1.6541	58.4217
FBEOZ1A-2.d	Felbertal	Quartz vein/Greisen Sn-W	27.8	90.489	14.6645	48.928	27.244	2.8773	30.6773
FBEOZ1A-3.d	Felbertal	Quartz vein/Greisen Sn-W	21.823	49.067	53.098	878.48	17.653	1.3622	38.6976
FBEOZ1A-4.d	Felbertal	Quartz vein/Greisen Sn-W	19.7102	9.452	10.1192	16.124	7.784	0.59909	54.4324
FBEOZ1A-5.d	Felbertal	Quartz vein/Greisen Sn-W	22.0454	75.894	18.07	71.724	59.631	2.7105	30.1908
FBEOZ1A-6.d	Felbertal	Quartz vein/Greisen Sn-W	18.6538	12.8575	14.2753	26.827	9.174	1.1676	62.2303
FBEOZ1A-7.d	Felbertal	Quartz vein/Greisen Sn-W	20.3496	36.14	27.522	136.22	14.734	0.71307	34.2496
FBEOZ1B-1.d	Felbertal	Quartz vein/Greisen Sn-W	33.499	20.989	19.599	172.36	21.684	0.85485	27.8556
FBEOZ1B-2.d	Felbertal	Quartz vein/Greisen Sn-W	25.576	20.155	38.642	303.02	35.584	1.4178	38.1833
FBEOZ1B-3.d	Felbertal	Quartz vein/Greisen Sn-W	24.603	59.77	12.3293	29.19	4.9067	1.58321	60.882
FBEOZ1B-4.d	Felbertal	Quartz vein/Greisen Sn-W	26.132	105.64	55.461	486.5	39.476	2.67297	49.067
FBEOZ1B-5.d	Felbertal	Quartz vein/Greisen Sn-W	21.406	33.916	54.488	325.26	41.7	1.6263	42.9371
FBK71A-1.d	Felbertal	Quartz vein/Greisen Sn-W	37.53	33.36	101.47	75.06	20.572	11.259	46.565
FBK71A-2.d	Felbertal	Quartz vein/Greisen Sn-W	22.935	23.0184	10.286	6.394	3.2387	0.9035	13.9556
FBK71A-3.d	Felbertal	Quartz vein/Greisen Sn-W	21.8508	46.009	13.4274	6.811	2.4881	1.14119	15.29
FBK71A-4.d	Felbertal	Quartz vein/Greisen Sn-W	21.823	16.4854	10.4528	2.085	4.6982	2.0711	15.0537
FBK71A-5.d	Felbertal	Quartz vein/Greisen Sn-W	20.7249	59.77	15.429	3.475	2.9885	1.9321	15.1232
FBK71A-6.d	Felbertal	Quartz vein/Greisen Sn-W	21.1002	34.75	6.4635	13.205	3.2526	0.95632	13.205
FBK7A-SCH3-2.d	Felbertal	Quartz vein/Greisen Sn-W	22.379	17.3611	6.1855	<DL	2.2101	0.55739	14.5672
FK11-1-C1a.d	Fort Knox	RIRGS	0.7506	11.2868	4.031	4.587	<DL	0.0973	11.2868
FK11-1-C1b.d	Fort Knox	RIRGS	0.8062	17.931	4.4758	6.255	0.6811	0.26549	17.514
FK11-1-C1c.d	Fort Knox	RIRGS	1.39	32.248	4.2117	8.34	0.7784	0.2641	12.7046
FK11-1-C2a.d	Fort Knox	RIRGS	0.8201	26.7019	3.6001	9.591	0.834	0.15985	9.3825
FK11-1-C2b.d	Fort Knox	RIRGS	<DL	18.487	3.3499	7.923	0.6811	0.21406	10.5501
FK11-1-C2c.d	Fort Knox	RIRGS	1.1954	24.881	4.726	10.703	<DL	0.17653	10.5362
FK11-1-C2d.d	Fort Knox	RIRGS	1.0564	9.1184	3.3499	9.73	1.0147	0.07645	9.9941
FK11-1-C2e.d	Fort Knox	RIRGS	0.9313	30.302	3.6001	8.201	0.8479	0.1529	10.0914

Appendix 2.4B (continued)

Point ID	Deposit name	Deposit type	B (ppm)	Na (ppm)	Mg (ppm)	K (ppm)	Ti (ppm)	V (ppm)	Mn (ppm)
FK11-1-C2f.d	Fort Knox	RIRGS	0.9869	29.051	3.6835	7.645	0.6394	0.10008	9.452
FK11-1-C2g.d	Fort Knox	RIRGS	0.9869	19.5295	3.6001	7.367	0.7645	0.14317	9.3964
FK13-1-L1.d	Fort Knox	RIRGS	1.0008	53.654	5.0457	8.757	1.1815	0.06394	16.263
FK13-1-L1.d	Fort Knox	RIRGS	1.0703	65.191	4.6426	13.2745	0.8896	0.12371	17.2499
FK15-L1.d	Fort Knox	RIRGS	1.0564	27.5915	10.3972	12.1903	0.8479	0.52959	36.279
FK15-L2.d	Fort Knox	RIRGS	0.8062	25.6038	13.8027	11.398	1.1676	0.64496	38.3362
FK15-L2.d	Fort Knox	RIRGS	0.9035	33.221	6.3801	17.236	1.0842	0.63384	36.974
FK15-L3.d	Fort Knox	RIRGS	0.8618	26.8409	12.8575	13.6359	0.973	0.6672	39.1007
FK15-L3.d	Fort Knox	RIRGS	0.7228	33.499	6.811	14.595	0.4865	0.63245	37.8497
FK15-L4.d	Fort Knox	RIRGS	0.8201	29.2456	12.6212	16.5966	0.9452	0.67137	38.4891
FK15-L5.d	Fort Knox	RIRGS	0.7506	27.244	10.8281	10.2165	0.9869	0.66303	38.0999
FK13-1-L2.d	Fort Knox	RIRGS	0.5838	11.8289	6.5469	17.3889	0.5282	0.05143	16.8607
FK13-1-L3.d	Fort Knox	RIRGS	0.5143	10.703	4.8094	16.8607	0.35306	0.039754	15.9016
FK13-1-L4.d	Fort Knox	RIRGS	0.4031	11.7872	4.5036	17.3611	0.4309	0.046704	16.9441
FK13-1-L5.d	Fort Knox	RIRGS	0.6533	14.456	4.7399	17.5279	0.4865	0.05004	16.7078
FK13-1-L6.d	Fort Knox	RIRGS	0.7506	13.0104	4.8094	14.873	0.4309	0.06672	15.9294
FK12-1.d	Fort Knox	RIRGS	4.865	24.742	14.873	45.87	2.502	0.73948	23.63
FK12-2.d	Fort Knox	RIRGS	12.371	47.955	15.985	2.919	1.7236	0.79647	15.6653
FK12-3.d	Fort Knox	RIRGS	4.5175	37.947	14.178	<DL	1.1537	0.4309	16.7217
FK12-4.d	Fort Knox	RIRGS	4.6287	14.8313	9.8829	6.116	1.2927	0.25715	17.0414
FK12-5.d	Fort Knox	RIRGS	4.0588	30.58	11.4953	4.17	2.0155	0.6394	15.3317
FK12-6.d	Fort Knox	RIRGS	4.1839	20.0299	14.2614	<DL	2.0572	2.04191	14.5255
FK12-7.d	Fort Knox	RIRGS	4.8094	27.1884	18.765	6.95	1.9182	1.39417	16.0545
FK12-8.d	Fort Knox	RIRGS	5.1152	10.2721	18.07	<DL	1.8209	1.21069	15.2066
FK12-9.d	Fort Knox	RIRGS	5.3098	12.8297	24.5613	<DL	1.8487	1.32189	17.0414
Gil-C1.d	Gil-Sourdough	RIRGS	<DL	<DL	2.7522	<DL	<DL	<DL	2.5159
G25-C1a.d	Gil-Sourdough	RIRGS	<DL	2.1128	2.6271	<DL	0.5004	0.16958	1.7653
G25-C1b.d	Gil-Sourdough	RIRGS	<DL	2.0155	2.4464	<DL	<DL	0.05838	2.1962
G25-C2b.d	Gil-Sourdough	RIRGS	<DL	<DL	2.641	<DL	<DL	<DL	2.2518
G25-C1c.d	Gil-Sourdough	RIRGS	15.429	5.0179	2.7244	<DL	0.4726	1.1259	4.031
G25-C3a.d	Gil-Sourdough	RIRGS	1.1259	1.9043	2.4603	<DL	<DL	0.0834	2.0155
G25-C3b.d	Gil-Sourdough	RIRGS	<DL	<DL	2.4047	<DL	0.3197	<DL	2.3908
G25-C4.d	Gil-Sourdough	RIRGS	0.8479	<DL	2.5576	<DL	0.2919	0.06255	2.3074
G25-C1a.d	Gil-Sourdough	RIRGS	1.8209	5.0318	11.398	10.2304	0.8618	0.07923	3.1831
G25-C1a.d	Gil-Sourdough	RIRGS	1.3066	6.533	4.8789	10.008	0.8062	0.15985	2.0433

Appendix 2.4B (continued)

Point ID	Deposit name	Deposit type	B (ppm)	Na (ppm)	Mg (ppm)	K (ppm)	Ti (ppm)	V (ppm)	Mn (ppm)
G25-C2a.d	Gil-Sourdough	RIRGS	0.9591	4.9901	4.5314	9.7717	0.6255	0.20294	1.9321
G22-L1.d	Gil-Sourdough	RIRGS	1.0425	4.309	4.3368	6.811	0.5977	0.07506	2.2935
G22-L1.d	Gil-Sourdough	RIRGS	1.1815	10.3138	3.8364	8.7709	1.2371	0.04726	2.3213
G22-L2.d	Gil-Sourdough	RIRGS	1.0981	11.676	3.8503	9.035	1.0703	0.03475	2.5576
G22-L2.d	Gil-Sourdough	RIRGS	1.3205	12.4405	4.5453	10.286	0.6255	0.0556	2.2101
G22-L3.d	Gil-Sourdough	RIRGS	1.1676	11.954	3.9337	12.4266	0.7784	0.05282	2.1545
G23-L1.d	Gil-Sourdough	RIRGS	1.1259	8.3956	4.0866	5.9909	0.9452	<DL	2.78
G23-L1.d	Gil-Sourdough	RIRGS	1.5707	10.2026	4.1005	5.8658	0.7923	0.0417	2.7383
G23-L2.d	Gil-Sourdough	RIRGS	1.7375	9.3686	3.892	7.645	0.7089	<DL	3.1831
G23-L2.d	Gil-Sourdough	RIRGS	1.2371	9.3547	3.8503	7.923	0.7089	<DL	3.0858
G22-L4.d	Gil-Sourdough	RIRGS	0.9452	11.537	27.8	22.657	1.1954	0.09313	1.8348
G23-L3.d	Gil-Sourdough	RIRGS	1.0008	11.2868	4.1283	10.703	0.9313	0.03475	2.3769
G23-L3.d	Gil-Sourdough	RIRGS	0.973	8.2288	5.0318	11.537	0.7784	0.08618	2.3074
SCH31-1.d	Hazlov	Reduced skarn	22.657	2.641	5.9492	7.089	1.8626	<DL	0.26132
SCH31-2.d	Hazlov	Reduced skarn	21.823	30.58	9.313	11.398	1.3344	<DL	0.4448
SCH31-3.d	Hazlov	Reduced skarn	20.2106	10.286	4.9067	8.201	1.4317	<DL	0.29051
SCH31-4.d	Hazlov	Reduced skarn	19.182	0.7784	5.3237	19.46	3.197	<DL	0.5282
SCH31-5.d	Hazlov	Reduced skarn	18.7372	2.224	5.7685	5.143	1.2927	<DL	4.726
SCH31-6.d	Hazlov	Reduced skarn	18.9179	27.522	6.255	13.761	1.5012	1.251	5.143
SCH31-7.d	Hazlov	Reduced skarn	18.3897	84.79	4.4619	15.568	1.5429	0.021128	0.30024
SCH31-8.d	Hazlov	Reduced skarn	19.043	0.7784	4.8233	6.116	1.3344	<DL	0.79091
SCH31-9.d	Hazlov	Reduced skarn	19.599	2.0155	10.842	8.062	1.3344	1.39	0.8062
SCH31-10.d	Hazlov	Reduced skarn	16.6105	11.398	244.64	11.676	1.4873	0.973	2.7105
SCH31-11.d	Hazlov	Reduced skarn	16.5132	1.7514	6.672	9.591	1.3483	<DL	0.3475
SCH11-1.d	Hostákov u Třebíče	Reduced skarn	9.8551	12.51	26.41	10.425	0.973	<DL	9.2435
SCH11-2.d	Hostákov u Třebíče	Reduced skarn	9.3825	19.46	11.259	29.19	0.7784	<DL	11.2868
SCH11-3.d	Hostákov u Třebíče	Reduced skarn	11.676	2.919	3.7669	8.062	3.058	0.03475	10.1887
SCH11-4.d	Hostákov u Třebíče	Reduced skarn	11.1895	2.9468	7.0473	8.34	1.3344	0.024881	6.7971
SCH11-5.d	Hostákov u Třebíče	Reduced skarn	12.1903	4.2673	<DL	10.147	1.3622	0.02502	9.7578
SCH11-6.d	Hostákov u Třebíče	Reduced skarn	11.1061	18.07	<DL	25.02	0.9035	<DL	10.5084
SCH11-7.d	Hostákov u Třebíče	Reduced skarn	14.178	2.5715	7.0612	25.02	1.1954	<DL	8.8821
SCH11-8.d	Hostákov u Třebíče	Reduced skarn	10.8976	3.0024	8.2566	5.421	1.4734	<DL	10.842
SCH11-9.d	Hostákov u Třebíče	Reduced skarn	11.9818	2.0433	7.9369	12.371	1.251	<DL	10.5779
SCH11-10.d	Hostákov u Třebíče	Reduced skarn	11.7455	<DL	19.46	7.645	<DL	<DL	6.1716
SCH11-11.d	Hostákov u Třebíče	Reduced skarn	3.4889	<DL	11.12	11.954	<DL	<DL	6.5191

Appendix 2.4B (continued)

Point ID	Deposit name	Deposit type	B (ppm)	Na (ppm)	Mg (ppm)	K (ppm)	Ti (ppm)	V (ppm)	Mn (ppm)
SCH11-12.d	Hostákov u Třebíče	Reduced skarn	<DL	<DL	7.1029	41.7	2.0016	1.112	6.7832
INV-1-RIM1.d	Invisible Mine	Reduced skarn	2.1267	59.909	27.105	<DL	1.4178	0.8062	1.1398
INV-1-RIM2.d	Invisible Mine	Reduced skarn	2.8356	18.765	2.7105	5.977	<DL	<DL	21.3365
INV-1-RIM3.d	Invisible Mine	Reduced skarn	<DL	30.024	3.1414	2.1545	<DL	<DL	21.7118
INV-1-RIM4.d	Invisible Mine	Reduced skarn	3.2804	42.812	3.9476	1.6402	<DL	<DL	3.9893
INV-1-RIM5.d	Invisible Mine	Reduced skarn	<DL	30.58	9.591	3.6418	2.1962	0.20433	29.4958
INV-1-1.d	Invisible Mine	Reduced skarn	<DL	4.6565	2.3074	<DL	<DL	0.22518	52.5003
INV-1-2.d	Invisible Mine	Reduced skarn	<DL	3.9198	2.3908	<DL	<DL	0.24742	51.5551
INV-1-3.d	Invisible Mine	Reduced skarn	<DL	6.4357	2.4464	0.6533	<DL	0.24325	50.8879
INV-1-4.d	Invisible Mine	Reduced skarn	<DL	6.116	2.2657	<DL	<DL	0.14873	44.202
INV-1-5.d	Invisible Mine	Reduced skarn	<DL	4.2395	2.4464	<DL	0.834	0.13622	38.9756
INV-1-6.d	Invisible Mine	Reduced skarn	8.34	14.595	3.0719	1.39	<DL	0.13483	35.4589
INV-1-7.d	Invisible Mine	Reduced skarn	<DL	27.8	3.0024	1.2788	0.695	0.17097	49.484
M61-1.d	Kanbauk	Oxidized skarn	4.5036	30.163	45.453	15.985	1.4873	0.03058	185.148
M61-2.d	Kanbauk	Oxidized skarn	4.726	54.627	69.917	37.53	1.1676	0.05143	68.666
M61-3.d	Kanbauk	Oxidized skarn	4.2534	82.983	129.27	23.074	1.3483	0.07506	47.955
M61-4.d	Kanbauk	Oxidized skarn	4.309	41.7	45.175	48.65	1.3344	<DL	224.902
M61-5.d	Kanbauk	Oxidized skarn	3.9615	39.9208	60.465	21.406	1.7653	<DL	97.995
M61A-C1-1.d	Kanbauk	Oxidized skarn	3.475	83.122	89.377	83.4	2.502	0.05838	105.779
M61A-C2-1.d	Kanbauk	Oxidized skarn	4.1422	167.495	103.555	7.506	1.1676	0.03058	67.554
M62-1.d	Kanbauk	Oxidized skarn	4.7121	15.29	17.5835	18.209	2.5437	<DL	14.734
M62-2.d	Kanbauk	Oxidized skarn	3.8086	3.1136	21.6006	19.599	2.78	0.0973	11.6621
M62A-1.d	Kanbauk	Oxidized skarn	4.5592	50.04	21.267	51.43	2.3352	0.09174	34.889
M62A-2.d	Kanbauk	Oxidized skarn	4.7538	7.784	29.19	19.599	3.7252	<DL	13.0382
KH61A-1.d	Kirwans Hill	Quartz vein/Greisen Sn-W	2.8912	97.3	32.109	19.321	1.3622	<DL	69.778
KH61A-2.d	Kirwans Hill	Quartz vein/Greisen Sn-W	3.2109	133.44	32.526	34.472	1.6819	<DL	21.962
KH61A-3.d	Kirwans Hill	Quartz vein/Greisen Sn-W	3.475	72.28	30.163	24.047	1.39	<DL	35.723
KH61A-4.d	Kirwans Hill	Quartz vein/Greisen Sn-W	4.2395	30.997	32.7067	31.414	1.3344	<DL	59.353
KH61A-5.d	Kirwans Hill	Quartz vein/Greisen Sn-W	3.9893	103.416	36.0427	26.688	2.1684	0.03892	41.6027
KH61A-6.d	Kirwans Hill	Quartz vein/Greisen Sn-W	3.5028	96.188	64.357	28.078	1.7097	0.1529	58.102
KH61A-7.d	Kirwans Hill	Quartz vein/Greisen Sn-W	3.8781	115.509	23.769	22.24	1.7792	0.04031	58.102
KH61A-8.d	Kirwans Hill	Quartz vein/Greisen Sn-W	5.977	51.43	24.603	32.943	1.9182	<DL	59.5476
KH61A-9.d	Kirwans Hill	Quartz vein/Greisen Sn-W	4.0866	87.014	61.994	24.742	1.5429	<DL	65.052
KH61A-10.d	Kirwans Hill	Quartz vein/Greisen Sn-W	3.6835	80.62	67.554	32.248	1.7236	<DL	55.2803
KH61A-11.d	Kirwans Hill	Quartz vein/Greisen Sn-W	2.7939	58.936	27.5498	24.881	1.0703	<DL	36.4597

Appendix 2.4B (continued)

Point ID	Deposit name	Deposit type	B (ppm)	Na (ppm)	Mg (ppm)	K (ppm)	Ti (ppm)	V (ppm)	Mn (ppm)
KH61A-12.d	Kirwans Hill	Quartz vein/Greisen Sn-W	3.7252	94.659	48.511	25.854	4.448	<DL	47.816
SCH17-1.d	Kotel (Krkonoše)	Reduced skarn	8.7848	2.224	8.479	9.869	12.51	0.3058	0.7228
SCH17-2.d	Kotel (Krkonoše)	Reduced skarn	9.452	1.9043	2.9885	12.788	3.753	0.02085	0.98829
SCH17-3.d	Kotel (Krkonoše)	Reduced skarn	9.0628	13.483	5.421	11.398	3.475	0.000139	0.87848
SCH17-4.d	Kotel (Krkonoše)	Reduced skarn	15.846	1.807	2.7383	17.514	0.9591	<DL	0.6811
SCH17-5.d	Kotel (Krkonoše)	Reduced skarn	9.2574	9.73	3.8781	8.479	0.5699	0.00417	1.0564
SCH17-6.d	Kotel (Krkonoše)	Reduced skarn	10.8837	0.4448	3.0858	14.734	0.9869	<DL	0.8201
SCH17-7.d	Kotel (Krkonoše)	Reduced skarn	8.6736	10.981	3.2665	11.537	1.112	0.007923	0.4031
SCH17-8.d	Kotel (Krkonoše)	Reduced skarn	8.7014	0.7089	11.12	10.147	5.004	0.01529	1.0286
SCH17-9.d	Kotel (Krkonoše)	Reduced skarn	10.981	12.51	3.5584	11.12	1.5012	<DL	1.946
SCH17-10.d	Kotel (Krkonoše)	Reduced skarn	9.1879	1.2232	3.9754	7.367	2.78	<DL	1.0008
SCH17-11.d	Kotel (Krkonoše)	Reduced skarn	10.842	1.6263	11.398	6.255	0.8479	0.009313	0.9174
SCH17-12.d	Kotel (Krkonoše)	Reduced skarn	9.6744	9.313	5.56	15.846	1.7097	0.0278	1.4734
SCH16-2.d	Kovářská	Oxidized skarn	11.537	10.842	7.2002	45.87	1.0981	0.03058	2.78
SCH16-3.d	Kovářská	Oxidized skarn	15.012	1.5151	16.68	44.48	1.7236	4.17	2.1267
SCH16-6.d	Kovářská	Oxidized skarn	9.73	1.7375	11.4675	32.248	1.8904	0.4865	107.03
LT-L1.d	Logtung	Porphyry W-Mo	2.2657	294.68	204.886	14.178	1.1398	12.6768	154.846
LT-L2.d	Logtung	Porphyry W-Mo	3.058	295.931	234.493	13.344	1.4873	12.2181	165.41
LT-L3.d	Logtung	Porphyry W-Mo	2.0294	293.707	234.771	17.097	1.0564	12.4544	166.939
LT-L4.d	Logtung	Porphyry W-Mo	1.6124	270.772	202.384	31.831	1.2649	11.0505	150.815
LT-L5.d	Logtung	Porphyry W-Mo	1.4456	293.012	207.249	9.9802	1.39	11.8567	166.105
LT-L6.d	Logtung	Porphyry W-Mo	1.1398	300.935	211.28	14.734	1.3066	8.9238	203.913
LT-L7.d	Logtung	Porphyry W-Mo	2.2101	361.122	206.971	9.313	1.529	16.124	158.182
LT2-1.d	Logtung	Porphyry W-Mo	5.143	232.964	210.724	8.201	3.753	7.4087	144.282
LT2-2.d	Logtung	Porphyry W-Mo	37.53	218.369	218.647	16.124	5.282	6.6025	153.873
LT2-3.d	Logtung	Porphyry W-Mo	5.2125	201.133	258.957	20.155	4.6565	6.9917	166.522
LT2-4.d	Logtung	Porphyry W-Mo	3.892	230.601	217.813	7.506	4.3785	7.3531	147.201
LT2-5.d	Logtung	Porphyry W-Mo	4.9901	236.3	207.11	18.765	3.1414	5.8519	145.95
LT2-6.d	Logtung	Porphyry W-Mo	3.4333	204.747	191.959	13.622	2.9468	6.672	123.293
MCW3-1-1.d	Machwi	Quartz vein/Greisen Sn-W	8.8126	33.4712	5.6295	17.375	0.7228	<DL	124.266
MCW3-1-2.d	Machwi	Quartz vein/Greisen Sn-W	6.8666	56.573	3.7391	14.873	<DL	<DL	125.795
MCW3-1-3.d	Machwi	Quartz vein/Greisen Sn-W	<DL	32.9986	3.5306	13.066	<DL	<DL	125.239
MCW3-1-4.d	Machwi	Quartz vein/Greisen Sn-W	<DL	83.261	9.313	12.649	<DL	<DL	113.563
MCW3-1-5.d	Machwi	Quartz vein/Greisen Sn-W	<DL	25.298	2.9329	13.066	<DL	0.3475	77.006
MCW3-1.d	Machwi	Quartz vein/Greisen Sn-W	7.9925	27.4108	3.197	10.981	<DL	<DL	97.995

Appendix 2.4B (continued)

Point ID	Deposit name	Deposit type	B (ppm)	Na (ppm)	Mg (ppm)	K (ppm)	Ti (ppm)	V (ppm)	Mn (ppm)
MCW3-2.d	Machwi	Quartz vein/Greisen Sn-W	5.8797	28.6618	3.2109	10.147	<DL	1.39	99.385
MCW3-3.d	Machwi	Quartz vein/Greisen Sn-W	8.1871	28.4394	2.919	3.058	0.6672	0.4448	73.809
MCW3-4.d	Machwi	Quartz vein/Greisen Sn-W	8.7987	20.4052	3.6696	<DL	8.4373	0.05004	7367
MCW3-5.d	Machwi	Quartz vein/Greisen Sn-W	7.2419	51.43	15.29	4.17	0.5004	<DL	93.13
MCW2-D-2.d	Machwi	Quartz vein/Greisen Sn-W	9.2018	45.592	17.4167	12.371	0.8201	<DL	58.241
MCW2-D-4.d	Machwi	Quartz vein/Greisen Sn-W	10.5084	29.9962	8.479	13.066	2.363	2.363	96.744
MCW2-D-5.d	Machwi	Quartz vein/Greisen Sn-W	9.73	66.72	4.9345	14.595	0.8062	0.023213	97.995
MCW2-D-6.d	Machwi	Quartz vein/Greisen Sn-W	8.5624	44.758	19.46	11.259	0.7784	<DL	45.0499
MCW2-D-7.d	Machwi	Quartz vein/Greisen Sn-W	8.9238	7.6172	21.4894	11.12	1.0147	<DL	34.194
NP1-C4-L1.d	Nui Phao	Reduced skarn	0.5282	6.2967	27.1189	18.6955	0.4448	<DL	15.8877
NP1-C4-L2.d	Nui Phao	Reduced skarn	<DL	11.398	27.4247	25.159	0.3892	<DL	15.4568
NP1-C4-L3.d	Nui Phao	Reduced skarn	0.417	9.2435	27.3691	20.155	<DL	<DL	15.1649
NP1-C1-L1.d	Nui Phao	Reduced skarn	<DL	6.6859	25.5204	19.043	0.6255	<DL	15.4707
NP1-C1-L1.d	Nui Phao	Reduced skarn	0.5004	12.371	30.5661	18.904	0.4031	<DL	17.6252
NP1-0.d	Nui Phao	Reduced skarn	<DL	9.452	29.6348	28.356	0.3058	<DL	16.7634
NP1-C2a.d	Nui Phao	Reduced skarn	0.7784	9.3547	27.0216	9.313	0.7645	<DL	15.8599
NP1-C2b.d	Nui Phao	Reduced skarn	0.7089	2.1823	27.2023	9.869	0.6394	<DL	16.0406
NP1-C2c.d	Nui Phao	Reduced skarn	0.7645	2.502	25.8818	8.479	0.5838	<DL	16.2491
NP1-1-L1.d	Nui Phao	Quartz vein/Greisen Sn-W	0.6811	8.757	34.1523	15.0259	0.8896	<DL	10.0636
NP1-1-L2.d	Nui Phao	Quartz vein/Greisen Sn-W	0.8757	9.035	35.3616	15.151	0.4865	<DL	9.7717
NP1-1-L3.d	Nui Phao	Quartz vein/Greisen Sn-W	1.1676	16.124	34.2913	17.792	0.4309	<DL	10.8698
NP1-2-L1.d	Nui Phao	Quartz vein/Greisen Sn-W	0.7784	3.8364	35.4867	19.877	<DL	<DL	10.1609
NP1-2-L1.d	Nui Phao	Quartz vein/Greisen Sn-W	0.7089	10.703	39.198	17.375	<DL	<DL	12.8436
NP1-2-L2.d	Nui Phao	Quartz vein/Greisen Sn-W	0.5421	9.2435	40.171	13.066	0.4726	<DL	13.0104
NP1-2-L2.d	Nui Phao	Quartz vein/Greisen Sn-W	0.7923	6.1438	27.8	12.232	0.3892	<DL	13.2884
NP1-2-L3.d	Nui Phao	Quartz vein/Greisen Sn-W	0.5004	8.9238	41.144	14.873	0.4309	0.0278	13.0382
NP1-2-L3.d	Nui Phao	Quartz vein/Greisen Sn-W	<DL	9.452	32.943	17.097	0.3753	<DL	11.4675
NP1-2-L4.d	Nui Phao	Quartz vein/Greisen Sn-W	0.7367	17.653	18.0005	24.881	0.4587	<DL	20.8083
SCH19-1.d	Obří důl	Oxidized skarn	13.0243	113.98	3.058	10.147	2.502	1.71526	3.2109
SCH19-2.d	Obří důl	Oxidized skarn	14.873	206.276	10.286	9.452	3.0302	1.76252	27.8
SCH19-3.d	Obří důl	Oxidized skarn	13.0382	290.649	2.7939	10.008	2.8078	2.9746	8.5763
SCH19-4.d	Obří důl	Oxidized skarn	12.5378	61.438	10.286	10.564	2.3769	1.34274	6.7415
SCH19-5.d	Obří důl	Oxidized skarn	13.205	138.722	2.9746	12.093	1.7931	3.336	12.0513
SCH19-7.d	Obří důl	Oxidized skarn	13.1355	305.8	2.1823	10.425	2.6549	2.0155	22.796
SCH19-8.d	Obří důl	Oxidized skarn	12.7046	168.19	1.5151	14.456	1.9738	0.02363	17.2221

Appendix 2.4B (continued)

Point ID	Deposit name	Deposit type	B (ppm)	Na (ppm)	Mg (ppm)	K (ppm)	Ti (ppm)	V (ppm)	Mn (ppm)
SCH19-9.d	Obří důl	Oxidized skarn	38.92	174.723	2.8356	12.093	2.2657	1.8209	13.483
SCH20-1.d	Obří důl	Oxidized skarn	9.2991	58.241	2.9468	14.456	1.9877	0.52403	12.0096
SCH20-2.d	Obří důl	Oxidized skarn	10.286	251.59	2.3769	19.321	3.892	3.336	18.07
SCH20-3.d	Obří důl	Oxidized skarn	10.0358	124.127	5.56	13.622	1.5429	0.82288	10.3555
SCH20-4.d	Obří důl	Oxidized skarn	12.927	102.721	2.7939	14.595	2.3769	0.82566	10.6613
SCH20-5.d	Obří důl	Oxidized skarn	8.8126	147.34	3.1553	25.298	2.0155	1.0703	8.7848
SCH20-7.d	Obří důl	Oxidized skarn	7.784	131.355	<DL	10.703	2.1545	1.00914	16.541
SCH20-8.d	Obří důl	Oxidized skarn	9.73	128.297	3.2387	6.116	1.9738	1.5707	10.7169
SCH20-9.d	Obří důl	Oxidized skarn	8.6458	76.589	3.0163	20.155	1.5568	1.251	11.3563
SCH20-10.d	Obří důl	Oxidized skarn	10.842	55.044	2.8912	14.317	1.0147	0.62689	8.6041
SCH20-11.d	Obří důl	Oxidized skarn	9.1601	65.33	8.201	10.425	2.3491	0.70612	12.371
SCH20-12.d	Obří důl	Oxidized skarn	11.537	91.601	7.089	19.46	1.8348	0.72419	11.12
SCH20-13.d	Obří důl	Oxidized skarn	9.2574	73.392	11.12	17.931	1.5985	0.77284	9.2296
SCH21-1.d	Obří důl	Oxidized skarn	15.4429	59.77	4.6704	18.487	4.4202	0.53098	18.9735
SCH21-2.d	Obří důl	Oxidized skarn	16.0684	47.26	3.2248	20.433	5.143	0.34055	14.734
SCH21-3.d	Obří důl	Oxidized skarn	15.7626	51.43	2.4881	14.178	1.807	0.3475	25.02
SCH21-4.d	Obří důl	Oxidized skarn	13.9834	39.615	72.975	23.63	2.6688	0.62133	87.987
SCH21-5.d	Obří důl	Oxidized skarn	12.788	184.87	4.1144	56.99	2.3491	0.51013	45.87
SCH21-6.d	Obří důl	Oxidized skarn	14.6228	33.221	3.4194	12.371	1.7375	0.65052	7.228
SCH21-7.d	Obří důl	Oxidized skarn	15.3873	50.04	2.8217	73.67	3.2665	0.03058	16.402
SCH21-8.d	Obří důl	Oxidized skarn	17.097	34.055	3.0441	14.456	5.838	0.38225	6.5469
SCH22-A1.d	Obří důl	Oxidized skarn	19.599	64.635	7.506	5.56	1.3483	0.36974	14.178
SCH22-A2.d	Obří důl	Oxidized skarn	15.012	49.762	3.1275	10.008	1.2371	0.59353	5.5183
SCH22-A4.d	Obří důl	Oxidized skarn	18.626	72.28	3.0858	10.564	18.07	0.80203	5.7129
SCH22-A5.d	Obří důl	Oxidized skarn	10.9115	42.256	5.56	7.645	1.1259	0.28773	7.3531
SCH22-A6.d	Obří důl	Oxidized skarn	4.2395	102.86	2.5715	6.95	1.39	0.28078	4.8789
SCH22-B1.d	Obří důl	Oxidized skarn	12.3293	24.742	3.4472	11.12	3.0719	<DL	3.0163
SCH22-B2.d	Obří důl	Oxidized skarn	16.2491	22.24	2.6827	25.298	7.089	<DL	3.0441
SCH22-B3.d	Obří důl	Oxidized skarn	13.7888	4.1005	1.9043	9.174	3.6696	0.024186	2.4881
SCH22-B4.d	Obří důl	Oxidized skarn	13.6359	5.977	1.8348	10.286	3.4889	0.03614	3.5584
SCH22-B5.d	Obří důl	Oxidized skarn	13.1077	17.931	4.17	16.958	3.4055	<DL	4.0588
SCH22-B6.d	Obří důl	Oxidized skarn	14.2753	17.792	3.4333	14.595	3.9337	<DL	3.9337
SCH23-B1.d	Obří důl	Oxidized skarn	22.8655	117.594	7.7006	7.645	1.6819	0.71585	38.086
SCH23-B2.d	Obří důl	Oxidized skarn	24.3389	62.55	4.2117	3.475	1.8487	0.60326	17.236
SCH23-B3.d	Obří důl	Oxidized skarn	23.074	79.23	4.1978	13.066	1.9599	0.96466	15.151

Appendix 2.4B (continued)

Point ID	Deposit name	Deposit type	B (ppm)	Na (ppm)	Mg (ppm)	K (ppm)	Ti (ppm)	V (ppm)	Mn (ppm)
SCH23-B4.d	Obří důl	Oxidized skarn	22.6014	55.183	3.6557	<DL	1.1537	0.43229	8.6597
SCH23-B5.d	Obří důl	Oxidized skarn	20.3079	29.051	3.1831	2.78	1.8765	0.30719	11.537
SCH23-C1.d	Obří důl	Oxidized skarn	21.5172	111.2	3.4194	7.089	2.2657	0.95076	10.5223
SCH23-C2.d	Obří důl	Oxidized skarn	21.8508	95.91	3.1553	36.14	1.7375	0.69778	8.5207
SCH23-C3.d	Obří důl	Oxidized skarn	22.0454	70.334	3.058	3.614	2.1962	1.10783	10.5918
SCH23-C4.d	Obří důl	Oxidized skarn	21.128	61.021	4.1144	12.371	1.3205	0.417	9.8273
SCH23-C5.d	Obří důl	Oxidized skarn	20.8361	181.395	3.7113	6.95	2.5576	0.97022	12.8992
SCH24-1.d	Obří důl	Oxidized skarn	11.6204	109.81	3.0163	34.75	<DL	0.94659	9.591
SCH24-2.d	Obří důl	Oxidized skarn	12.2042	56.99	15.29	16.958	3.058	0.5282	30.58
SCH24-3.d	Obří důl	Oxidized skarn	12.6073	87.57	2.8356	25.02	2.1128	0.63106	6.2272
SCH24-4.d	Obří důl	Oxidized skarn	12.6768	32.387	3.0858	11.954	4.1422	0.78535	4.4202
SCH24-5.d	Obří důl	Oxidized skarn	10.7169	51.152	0.9313	14.456	1.9599	0.78118	4.2395
SCH24-6.d	Obří důl	Oxidized skarn	12.2181	28.495	<DL	13.622	2.4186	0.38364	6.4357
SCH24-7.d	Obří důl	Oxidized skarn	13.5664	209.89	7.645	54.21	1.3205	0.46426	10.564
SCH24-1A-R.d	Obří důl	Oxidized skarn	10.3416	79.23	3.2526	5.977	4.031	1.22181	6.2133
SCH24-1A-C.d	Obří důl	Oxidized skarn	9.9246	28.356	2.9885	10.008	1.9321	0.49484	4.6982
SCH24-2A-R.d	Obří důl	Oxidized skarn	10.9393	<DL	3.475	15.012	1.4456	0.05977	<DL
SCH24-2A-R1.d	Obří důl	Oxidized skarn	12.649	264.1	4.1839	48.65	1.3761	0.84929	25.854
SCH25-1.d	Obří důl	Oxidized skarn	12.3988	26.41	3.0441	8.618	1.8626	0.13622	7.2975
SCH25-3.d	Obří důl	Oxidized skarn	12.3849	33.082	2.9329	16.819	1.3066	0.12788	6.4774
SCH25-4.d	Obří důl	Oxidized skarn	13.8305	27.661	2.78	14.873	1.0981	0.08479	12.371
SCH25-5B.d	Obří důl	Oxidized skarn	14.734	65.33	2.9468	20.989	1.0425	0.21406	19.46
SCH25-6B.d	Obří důl	Oxidized skarn	13.8861	16.7217	3.1136	8.618	0.973	0.08062	5.3376
SCH26-1.d	Obří důl	Oxidized skarn	15.1232	23.908	37.808	18.209	2.1128	0.89794	20.85
SCH26-2.d	Obří důl	Oxidized skarn	20.294	116.76	3.1414	58.38	1.9877	0.77979	11.398
SCH26-3.d	Obří důl	Oxidized skarn	13.344	13.3301	3.5584	22.24	2.6688	0.27522	7.8674
SCH26-4.d	Obří důl	Oxidized skarn	12.4683	33.36	7.923	8.618	5.977	0.12232	12.7463
SCH26-5.d	Obří důl	Oxidized skarn	14.0529	47.26	3.9754	52.82	3.3082	0.11259	10.2443
SCH26-6.d	Obří důl	Oxidized skarn	13.6359	16.402	10.286	14.873	1.5846	0.32526	14.039
SCH26-7.d	Obří důl	Oxidized skarn	13.3579	20.711	12.093	16.68	5.4349	0.7089	27.8
SCH26-8.d	Obří důl	Oxidized skarn	13.4552	19.182	12.232	15.985	3.336	0.32109	15.985
SCH27-C1.d	Obří důl	Oxidized skarn	17.514	44.897	3.0302	2.085	2.3908	0.68805	9.9524
SCH27-C2.d	Obří důl	Oxidized skarn	17.7781	22.518	3.197	3.614	2.5159	0.83261	8.3956
SCH27-C3.d	Obří důl	Oxidized skarn	18.7928	69.5	3.3499	11.12	1.8904	1.10088	10.4111
SCH27-4.d	Obří důl	Oxidized skarn	18.6677	31.692	7.4504	6.811	1.3066	0.63801	8.2149

Appendix 2.4B (continued)

Point ID	Deposit name	Deposit type	B (ppm)	Na (ppm)	Mg (ppm)	K (ppm)	Ti (ppm)	V (ppm)	Mn (ppm)
SCH27-5.d	Obří důl	Oxidized skarn	18.9179	109.254	3.2804	11.12	2.2657	0.34055	4.6148
SCH27-6.d	Obří důl	Oxidized skarn	18.6399	45.036	3.2248	19.46	2.2935	<DL	5.8797
SD11-C2.d	Scheelite Dome	RIRGS	1.0842	5.1847	2.5437	<DL	0.6394	0.21545	11.676
SD11-C1b.d	Scheelite Dome	RIRGS	<DL	51.569	3.0997	<DL	0.5838	0.87848	11.4258
SD11-C1c.d	Scheelite Dome	RIRGS	8.757	305.8	8.201	31.97	0.3058	0.60604	40.449
SD11-C1d.d	Scheelite Dome	RIRGS	<DL	40.5324	3.1692	13.205	<DL	0.29885	15.2483
SD28-sch1.d	Scheelite Dome	RIRGS	1.7097	35.445	2.1406	<DL	0.4448	<DL	4.6982
SD28-sch1a.d	Scheelite Dome	RIRGS	2.085	38.92	2.4047	<DL	0.7367	<DL	7.8535
SD28-sch2.d	Scheelite Dome	RIRGS	2.2657	36.279	2.5993	<DL	0.3614	0.03753	7.6311
SD28-sch2a.d	Scheelite Dome	RIRGS	2.641	107.03	2.5437	9.869	0.7367	<DL	6.8527
SD28-sch2b.d	Scheelite Dome	RIRGS	1.4039	15.9433	2.4603	<DL	0.4865	<DL	5.8241
SD28-sch3.d	Scheelite Dome	RIRGS	<DL	40.588	2.2935	<DL	0.417	0.15985	9.5771
SD28-sch3a.d	Scheelite Dome	RIRGS	1.1815	14.2614	2.7244	<DL	0.4031	0.09452	9.1879
SD28-sch3b.d	Scheelite Dome	RIRGS	<DL	30.302	2.3908	<DL	<DL	<DL	7.6033
SD28-sch4.d	Scheelite Dome	RIRGS	<DL	18.348	2.502	<DL	<DL	0.08896	6.2133
SD28-sch4a.d	Scheelite Dome	RIRGS	<DL	40.588	2.4881	<DL	<DL	<DL	7.1307
SD28-sch4b.d	Scheelite Dome	RIRGS	2.1684	61.021	2.2101	<DL	0.6672	0.05977	6.811
ITALY-1.d	Travesella	Oxidized skarn	<DL	1.0981	1.5707	<DL	<DL	0.16958	1.39
ITALY-2.d	Travesella	Oxidized skarn	<DL	4.8233	2.2379	<DL	<DL	0.43924	1.4873
ITALY-3.d	Travesella	Oxidized skarn	<DL	7.923	1.7236	0.695	<DL	0.3892	1.4317
ITALY-4.d	Travesella	Oxidized skarn	<DL	3.753	2.363	<DL	<DL	0.28912	1.4456
ITALY-5.d	Travesella	Oxidized skarn	<DL	3.7113	2.3769	<DL	<DL	0.33638	1.4317
ITALY-6.d	Travesella	Oxidized skarn	<DL	3.7808	1.807	<DL	<DL	0.32109	1.4456
ITALY-7.d	Travesella	Oxidized skarn	<DL	6.2828	1.6541	<DL	<DL	0.43646	1.5846
ITALY-8.d	Travesella	Oxidized skarn	<DL	6.533	1.7653	<DL	<DL	0.43229	1.6402
ITALY-9.d	Travesella	Oxidized skarn	<DL	3.197	1.668	<DL	<DL	0.33916	1.9738
ITALY-10.d	Travesella	Oxidized skarn	<DL	8.1732	1.7375	<DL	<DL	0.13622	1.5846
ITALY-11.d	Travesella	Oxidized skarn	<DL	7.5755	1.8209	<DL	<DL	0.20433	1.946
ITALY-12.d	Travesella	Oxidized skarn	<DL	9.0628	1.8765	<DL	<DL	0.29885	1.6541
TSE-1.d	Jennings	Porphyry W-Mo	17.653	89.655	102.721	9.035	2.641	0.47399	18.2924
TSE-2.d	Jennings	Porphyry W-Mo	38.92	112.59	102.999	48.65	2.3074	0.37669	18.904
TSE-3.d	Jennings	Porphyry W-Mo	19.46	145.394	128.575	24.742	2.5993	0.31692	19.5295
TSE-4.d	Jennings	Porphyry W-Mo	5.4349	98.273	181.256	<DL	1.5568	0.23352	15.6792
TSE-5.d	Jennings	Porphyry W-Mo	10.703	137.054	139.973	22.101	2.919	0.33777	12.5656
TSE-6.d	Jennings	Porphyry W-Mo	55.183	64.496	79.786	14.595	2.1962	0.32665	20.8917

Appendix 2.4B (continued)

Point ID	Deposit name	Deposit type	B (ppm)	Na (ppm)	Mg (ppm)	K (ppm)	Ti (ppm)	V (ppm)	Mn (ppm)
TSE-7.d	Jennings	Porphyry W-Mo	13.205	85.624	88.96	6.811	1.9182	0.27383	16.4298
SCH40-1.d	Vrbík u Horažďovic	Reduced skarn	27.8	12.51	<DL	<DL	1.1676	0.04726	4.2951
SCH40-2.d	Vrbík u Horažďovic	Reduced skarn	12.8575	15.29	3.0719	5.421	0.9591	0.02641	6.4357
SCH40-3.d	Vrbík u Horažďovic	Reduced skarn	12.1903	2.4464	2.8078	5.004	1.2093	0.04726	5.0457
SCH40-4.d	Vrbík u Horažďovic	Reduced skarn	11.4397	1.4595	11.12	6.255	0.7784	0.05004	5.0179
SCH40-5.d	Vrbík u Horažďovic	Reduced skarn	9.174	73.67	6.394	12.788	0.5143	0.05282	5.421
SCH40-6.d	Vrbík u Horažďovic	Reduced skarn	5.282	40.31	2.7105	22.24	<DL	0.05004	4.2812
SCH40-7.d	Vrbík u Horažďovic	Reduced skarn	8.7014	3.4889	2.7105	<DL	<DL	0.07089	4.4341
SCH40-8.d	Vrbík u Horažďovic	Reduced skarn	13.622	19.46	13.066	10.842	2.085	0.05282	11.3285
SCH40-9.d	Vrbík u Horažďovic	Reduced skarn	13.761	15.012	1.3622	10.147	1.0981	0.02363	9.3547
SCH40-10.d	Vrbík u Horažďovic	Reduced skarn	12.649	4.726	22.24	9.174	1.5985	<DL	8.1593
SCH40-11.d	Vrbík u Horažďovic	Reduced skarn	16.68	1.3344	2.3769	18.07	1.1259	0.834	5.5461
SCH40-12.d	Vrbík u Horažďovic	Reduced skarn	11.9262	5.143	36.14	9.73	1.4039	<DL	7.645
SCH44-3.d	Vykmanov	Oxidized skarn	8.896	21.128	94.52	14.178	1.6124	0.26966	5.0735
SCH44-4.d	Vykmanov	Oxidized skarn	10.564	5.004	21.406	38.92	1.0147	0.0973	5.3237
SCH44-5.d	Vykmanov	Oxidized skarn	8.757	69.5	59.77	21.267	1.6402	0.34333	4.6009
SCH44-6.d	Vykmanov	Oxidized skarn	10.425	22.379	92.435	15.29	2.502	0.8201	33.638
SCH44-7.d	Vykmanov	Oxidized skarn	10.147	26.549	24.325	10.703	1.0008	0.139	4.031
SCH44-8.d	Vykmanov	Oxidized skarn	7.784	10.564	127.88	<DL	6.95	6.116	10.008
SCH44-9.d	Vykmanov	Oxidized skarn	9.591	6.95	108.698	82.01	2.6132	0.6394	34.611
YP5B-C3.d	Hangar Flats	Orogenic Au	1.4734	10.3138	185.982	<DL	0.3197	<DL	<DL
YP5A-C5a.d	Hangar Flats	Orogenic Au	1.7514	44.619	11.0366	10.5084	1.0564	<DL	<DL
YP5A-C5b.d	Hangar Flats	Orogenic Au	1.3761	43.646	159.85	14.456	0.5143	0.21267	1.541
YP5A-C5b.d	Hangar Flats	Orogenic Au	1.4178	40.588	6.0326	11.6482	0.695	<DL	<DL
YP5A-C1a.d	Hangar Flats	Orogenic Au	0.7506	27.522	22.935	13.761	0.7784	<DL	<DL
YP5A-C1a.d	Hangar Flats	Orogenic Au	0.8201	22.935	6.2272	11.6621	0.5004	<DL	<DL
YP5A-C1b.d	Hangar Flats	Orogenic Au	1.2649	45.453	8.5624	12.8019	0.7784	<DL	<DL
YP5A-C3a.d	Hangar Flats	Orogenic Au	1.4873	32.387	19.599	36.14	0.4726	<DL	<DL
YP5A-C3a.d	Hangar Flats	Orogenic Au	1.0842	24.047	16.263	36.14	0.6394	<DL	<DL
YP5A-C3b.d	Hangar Flats	Orogenic Au	1.0981	31.136	25.159	11.676	0.3892	<DL	<DL
YP5A-C3b.d	Hangar Flats	Orogenic Au	0.8062	34.75	31.414	12.51	0.6811	<DL	<DL
YP5A-C1c.d	Hangar Flats	Orogenic Au	1.4456	36.557	22.379	12.2598	0.4865	<DL	0.6116
YP5A-C1d.d	Hangar Flats	Orogenic Au	1.4456	62.133	6.8388	13.7749	0.417	<DL	<DL
YP5B-C1a.d	Hangar Flats	Orogenic Au	1.2232	13.6081	150.537	20.433	0.5838	<DL	0.4309
YP5B-C1b.d	Hangar Flats	Orogenic Au	0.834	7.8813	223.79	14.3031	0.5838	<DL	1.2093

Appendix 2.4B (continued)

Point ID	Deposit name	Deposit type	B (ppm)	Na (ppm)	Mg (ppm)	K (ppm)	Ti (ppm)	V (ppm)	Mn (ppm)
YP5B-C3a.d	Hangar Flats	Orogenic Au	1.2371	28.078	139	28.773	0.3892	0.04865	6.116
YP5B-C2a.d	Hangar Flats	Orogenic Au	0.7645	24.047	155.68	29.19	1.3344	<DL	0.8618
ZIV-1.d	Zinnwald	Quartz vein/Greisen Sn-W	<DL	37.947	3.058	0.8618	1.112	<DL	1.4317
ZIV-2.d	Zinnwald	Quartz vein/Greisen Sn-W	<DL	168.19	2.6966	1.112	<DL	<DL	1.8904
ZIV-3.d	Zinnwald	Quartz vein/Greisen Sn-W	1.6541	90.628	2.5854	1.0425	<DL	<DL	3.3638
ZIV-4.d	Zinnwald	Quartz vein/Greisen Sn-W	<DL	218.23	2.9885	1.6819	<DL	<DL	2.6688
ZIV-5.d	Zinnwald	Quartz vein/Greisen Sn-W	<DL	166.8	2.641	1.4039	<DL	<DL	1.3622
ZIV-6.d	Zinnwald	Quartz vein/Greisen Sn-W	<DL	54.7799	1.7792	<DL	<DL	<DL	1.8209
ZIV-7.d	Zinnwald	Quartz vein/Greisen Sn-W	<DL	100.08	2.9329	0.9313	<DL	<DL	5.0318
ZIV-8.d	Zinnwald	Quartz vein/Greisen Sn-W	<DL	140.39	1.7931	0.834	<DL	<DL	1.6541
ZIV-9.d	Zinnwald	Quartz vein/Greisen Sn-W	<DL	90.35	2.9051	<DL	<DL	<DL	4.9345
ZIV-10.d	Zinnwald	Quartz vein/Greisen Sn-W	<DL	99.802	2.5159	<DL	<DL	<DL	4.7121
ZIV-11.d	Zinnwald	Quartz vein/Greisen Sn-W	<DL	59.075	2.5298	<DL	0.695	<DL	3.3082
ZIV-12.d	Zinnwald	Quartz vein/Greisen Sn-W	<DL	78.952	2.1267	<DL	<DL	<DL	1.529

Appendix 2.4B (continued)

Point ID	Co (ppm)	Ni (ppm)	As (ppm)	Sr (ppm)	Y (ppm)	Nb (ppm)	Mo (ppm)	Ba (ppm)	La (ppm)	Ce (ppm)	Pr (ppm)
Min DL	0.003	0.023	0.034	0.001	0.001	0.001	0.005	0.009	0.001	0.001	0.001
Max DL	0.033	0.100	0.129	0.842	0.088	0.479	0.092	0.178	0.203	0.584	0.391
Cel-L1.d	0.154	0.232	3.225	43.966	154.290	61.299	1969.63	0.218	74.504	239.219	33.819
Cel-L2.d	0.143	0.235	3.239	44.327	166.105	61.716	2055.81	0.157	85.485	256.733	35.959
Cel-L3.d	0.139	0.202	3.336	44.661	139.834	58.936	1939.05	0.157	76.867	235.466	32.415
Cel-L4.d	0.140	<DL	4.142	46.009	200.577	61.577	1932.10	0.157	121.347	349.863	47.816
Cel-L4.d	0.132	0.209	3.072	46.065	85.485	48.497	2115.58	0.271	57.685	170.553	22.810
Cel-L5.d	0.131	0.211	3.100	43.855	144.977	60.465	1926.54	0.243	72.697	232.964	33.068
Cel-L6.d	0.132	0.202	2.863	46.079	141.502	59.075	2078.05	0.171	79.786	243.806	33.721
Cel-L7.d	0.154	0.299	2.961	47.399	154.985	63.662	1966.85	0.193	73.948	232.547	32.943
CL16-2-C1a.d	0.111	0.124	1.049	137.749	56.295	16.346	2000.21	0.174	6.199	25.715	4.059
CL16-2-C2b.d	0.110	<DL	1.612	140.668	111.478	23.352	2028.01	0.125	5.824	28.773	5.199
CL16-2-C2c.d	0.129	0.257	4.170	146.506	203.913	102.443	1847.31	0.165	19.043	60.604	8.660

Appendix 2.4B (continued)

Point ID	Co (ppm)	Ni (ppm)	As (ppm)	Sr (ppm)	Y (ppm)	Nb (ppm)	Mo (ppm)	Ba (ppm)	La (ppm)	Ce (ppm)	Pr (ppm)
CL16-3-1.d	0.142	<DL	1.251	138.027	107.725	15.248	1900.13	0.050	8.632	38.920	6.172
CL16-3-2.d	0.100	<DL	1.585	142.753	72.141	26.493	1869.55	0.075	9.508	39.031	5.671
CL16-3-3.d	0.115	<DL	0.834	135.525	62.133	9.285	1919.59	0.047	10.189	34.194	4.907
CL16-3-4.d	0.118	<DL	0.959	133.301	59.353	11.537	1837.58	<DL	4.629	16.680	2.641
CL16-3-5.d	0.115	0.235	0.987	134.691	55.044	13.803	1819.51	<DL	3.753	19.669	3.614
CC57-1.d	0.161	0.115	4.754	32.929	392.675	20.294	45.87	<DL	106.057	378.497	60.465
CC57-2.d	0.220	0.172	5.226	40.185	497.620	18.543	13.61	<DL	136.915	503.180	78.813
CC57-3.d	0.203	0.277	4.226	36.321	134.552	29.107	11.36	0.044	28.912	137.332	28.495
CC57-4.d	0.195	0.264	4.879	33.986	558.780	17.792	10.31	<DL	92.991	378.080	60.604
CC57-5.d	1.529	1.529	5.532	36.098	430.205	20.767	14.30	<DL	112.173	457.310	76.589
CC57-6.d	0.292	0.834	7.103	36.279	950.760	25.076	9.24	<DL	75.755	333.600	62.689
CC57-7.d	0.320	0.202	5.755	37.947	202.662	22.421	14.75	<DL	111.895	354.450	53.654
CC57-8.d	0.229	0.250	14.178	33.596	628.280	37.669	12.83	<DL	139.000	560.170	91.879
CC57-9.d	0.197	0.302	10.759	36.696	347.500	25.687	13.59	0.079	89.099	358.620	58.936
DG28-C1a.d	0.206	0.199	3.308	261.320	54.863	115.231	872.92	0.477	212.392	536.123	63.843
DG28-C2b.d	0.200	0.239	3.558	223.234	65.010	120.096	1182.89	0.366	281.336	683.880	78.952
DG28-C1c.d	0.203	0.293	4.031	279.529	60.465	119.818	1278.80	0.425	247.837	631.060	75.755
DG28-C1c.d	0.199	0.213	4.782	387.115	41.950	88.821	910.45	0.531	122.459	336.380	42.812
DG28-C3a.d	0.207	0.403	2.391	352.504	31.831	82.010	989.68	0.537	118.428	294.680	36.001
DG28-C3b.d	0.174	0.104	3.044	336.797	46.426	92.296	1362.20	0.466	151.371	396.150	49.623
DG28-C3b.d	0.235	0.245	3.461	261.598	21.295	79.508	1010.53	0.621	129.270	311.360	35.445
DG28-C3c.d	0.218	0.149	2.446	365.570	31.553	44.202	3016.30	0.404	101.470	268.270	32.665
FBA711B-SCH2-10.d	0.389	0.185	20.197	235.049	453.140	561.560	5810.20	5.032	393.370	870.140	82.010
FBA711B-SCH2-11.d	0.200	0.120	30.580	333.600	225.458	301.491	6143.80	0.987	39.476	119.540	13.302
FBA711B-SCH2-2.d	0.206	0.136	19.265	178.754	526.810	728.360	6074.30	0.987	71.863	285.089	29.162
FBA711B-SCH2-3.d	0.792	3.336	18.946	286.340	165.410	205.025	5518.30	1.904	79.647	191.820	15.151
FBA711B-SCH2-4.d	0.197	4.448	18.821	199.465	332.210	412.830	6046.50	0.588	102.582	296.070	25.854
FBA711B-SCH2-5.d	0.189	27.800	12.524	186.955	237.551	309.692	5935.30	1.487	38.920	128.158	14.581
FBA711B-SCH2-6.d	0.204	0.264	21.545	328.040	22.907	5.713	2335.20	0.348	0.053	0.393	0.117
FBA711B-SCH2-7.d	0.185	0.224	19.557	163.603	127.046	172.360	6157.70	1.390	24.158	66.998	8.090
FBA711B-SCH2-8.d	0.278	0.157	19.265	203.218	76.311	82.010	1223.20	1.529	4.921	16.402	2.391
FBA711B-SCH2-9.d	0.172	0.188	18.042	14.581	406.158	875.700	8340.00	1.223	69.917	227.960	21.837
FBA711B-SCH3-1.d	0.174	0.164	20.113	22.032	1118.950	1712.480	8173.20	1.348	110.783	529.590	67.971
FBA711B-SCH3-2.d	0.334	0.264	9.452	27.522	647.740	999.410	8020.30	5.671	65.747	275.081	31.859
FBA712B-SCH2-1.d	0.222	0.132	32.804	12.246	253.536	587.970	7714.50	0.238	46.398	117.872	13.344

Appendix 2.4B (continued)

Point ID	Co (ppm)	Ni (ppm)	As (ppm)	Sr (ppm)	Y (ppm)	Nb (ppm)	Mo (ppm)	Ba (ppm)	La (ppm)	Ce (ppm)	Pr (ppm)
FBA712B-SCH2-2.d	0.234	0.147	19.766	26.897	742.260	1277.410	8145.40	3.072	83.261	353.060	40.588
FBA712B-SCH2-3.d	0.195	0.204	20.238	12.302	405.046	882.650	7728.40	0.265	73.948	232.130	21.851
FBA712B-SCH2-4.d	0.189	0.210	24.005	31.289	390.590	668.590	8006.40	1.154	52.264	183.758	19.669
FBA712B-SCH2-6.d	0.213	0.209	21.809	38.642	578.240	781.180	5490.50	2.266	34.333	108.976	15.318
FBA712B-SCH2-7.d	0.204	0.157	22.907	47.260	533.760	906.280	7283.60	3.044	53.654	201.272	23.310
FBA712B-SCH2-8.d	0.417	0.203	32.387	10.828	578.240	946.590	8770.90	0.211	94.520	324.565	32.248
FBA712B-SCH2-9.d	0.220	0.542	39.476	16.305	608.820	1164.820	8854.30	3.211	109.671	373.910	36.557
FBA712B-SCH3-1.d	0.242	0.196	20.113	16.305	533.760	1078.640	7589.40	6.672	83.539	301.352	31.998
FBA712B-SCH3-3.d	0.204	1.251	38.920	161.240	689.440	590.750	125.10	0.057	94.520	264.100	26.688
FBA712B-SCH3-4.d	0.197	0.306	22.198	92.713	1823.680	2738.300	6171.60	0.220	277.583	985.510	115.509
FBA712B-SCH3-5.d	0.204	0.204	23.978	161.796	854.850	1075.860	5629.50	0.203	67.693	317.337	31.484
FBA712B-SCH3-7.d	0.197	0.143	34.472	194.878	447.580	430.900	1570.70	0.145	1.877	11.329	2.572
FBA712B-SCH3-8.d	0.973	0.375	17.959	195.017	1395.560	1946.000	5143.00	0.310	67.971	382.250	46.565
FBA713A-SCH2-1.d	1.251	2.780	25.576	149.147	492.060	447.441	351.67	<DL	2.850	16.624	3.850
FBA713A-SCH2-2.d	0.234	0.136	31.970	165.966	2182.300	3210.900	5782.40	0.468	108.698	690.830	106.752
FBA713A-SCH2-3.d	0.293	0.202	19.293	177.364	696.390	993.850	4823.30	0.542	68.805	319.700	35.139
FBA713A-SCH2-4.d	0.307	0.435	16.430	78.257	707.510	1081.420	6338.40	0.403	123.154	451.750	42.256
FBA713A-SCH2-5.d	0.310	0.322	15.471	111.756	850.680	1092.540	5740.70	0.306	81.037	359.037	34.361
FBA713A-SCH3-1.d	1.112	0.154	9.939	56.990	992.460	1271.850	5156.90	0.135	102.304	507.350	50.874
FBA713A-SCH3-2.d	0.192	0.348	20.808	44.758	1175.940	1531.780	5379.30	0.279	111.756	557.390	57.268
FBA713A-SCH3-3.d	0.335	0.375	4.156	36.418	1499.810	2422.770	5448.80	0.104	286.896	1081.420	142.336
FBA713A-SCH3-4.d	0.232	0.174	17.041	55.600	1848.700	2960.700	4434.10	0.192	182.507	982.730	167.078
FBA713A-SCH3-5.d	1.102	1.140	10.675	58.241	682.490	899.330	5240.30	0.139	140.807	423.950	33.249
FBA713A-SCH3-6.d	0.224	25.020	9.952	74.365	674.150	897.940	5685.10	0.147	98.134	369.323	32.123
FBA713A-SCH3-7.d	0.213	0.236	3.280	46.287	550.440	874.310	6380.10	0.040	112.451	391.285	36.668
FBA713B-SCH2-1.d	0.210	0.167	26.341	49.206	422.560	560.170	6977.80	0.025	82.566	302.047	26.521
FBA713B-SCH2-2.d	0.211	5.977	29.329	47.955	697.780	1034.160	6588.60	<DL	125.100	444.800	39.476
FBA713B-SCH2-3.d	0.202	0.150	29.746	139.834	679.710	879.870	5004.00	0.247	109.254	383.918	32.040
FBA713B-SCH2-4.d	0.158	0.182	18.765	92.157	728.360	896.550	5671.20	0.543	113.563	400.598	33.013
FBA713B-SCH2-5.d	0.190	0.161	12.955	68.527	701.950	900.720	5699.00	0.125	96.605	366.543	29.009
FBEOZ1A-1.d	0.245	0.299	30.858	66.303	849.290	1282.970	5504.40	0.060	120.096	439.240	45.314
FBEOZ1A-2.d	0.459	40.310	40.449	259.235	717.240	1125.900	6630.30	0.236	57.824	283.004	32.359
FBEOZ1A-3.d	0.200	0.297	46.287	258.401	593.530	977.170	5212.50	0.135	109.393	423.950	42.534
FBEOZ1A-4.d	0.250	0.542	19.780	385.030	258.540	246.030	234.91	0.164	0.897	3.531	0.717
FBEOZ1A-5.d	0.500	1.612	64.357	127.046	575.460	973.000	7228.00	0.150	97.578	409.911	43.604

Appendix 2.4B (continued)

Point ID	Co (ppm)	Ni (ppm)	As (ppm)	Sr (ppm)	Y (ppm)	Nb (ppm)	Mo (ppm)	Ba (ppm)	La (ppm)	Ce (ppm)	Pr (ppm)
FBEOZ1A-6.d	0.213	0.172	11.579	134.274	638.010	1068.910	6936.10	0.570	104.250	461.480	51.013
FBEOZ1A-7.d	0.192	27.800	25.298	159.016	654.690	1515.100	8062.00	0.222	78.674	370.991	45.453
FBEOZ1B-1.d	0.178	0.348	47.399	144.560	414.498	682.490	10035.80	0.136	50.179	276.610	33.874
FBEOZ1B-2.d	0.417	0.338	39.476	188.762	203.218	302.742	6727.60	0.242	50.318	121.208	12.204
FBEOZ1B-3.d	0.417	0.253	14.067	293.290	180.700	66.025	126.35	0.402	1.398	6.978	1.653
FBEOZ1B-4.d	0.211	0.331	20.016	131.355	879.870	1296.870	6046.50	0.206	157.626	514.300	47.260
FBEOZ1B-5.d	0.190	0.189	27.383	296.070	112.312	49.484	163.05	0.385	2.043	9.786	2.225
FBK71A-1.d	0.459	2.502	26.132	160.128	305.244	405.880	10633.50	0.417	36.140	223.790	29.468
FBK71A-2.d	0.211	12.510	12.871	201.133	244.640	322.480	10550.10	0.848	21.448	103.833	17.806
FBK71A-3.d	0.204	11.120	31.136	96.188	227.960	383.918	7144.60	0.182	64.774	205.303	19.293
FBK71A-4.d	0.234	0.411	12.093	223.929	82.149	40.727	187.23	0.192	1.162	6.283	1.561
FBK71A-5.d	0.213	0.681	28.356	100.775	1207.910	1879.280	5754.60	0.431	220.732	778.400	89.377
FBK71A-6.d	0.242	0.260	20.155	60.743	1491.470	2358.830	5838.00	0.040	262.988	978.560	129.687
FBK7A-SCH3-2.d	0.218	0.222	11.190	145.672	428.120	585.190	15720.90	0.171	46.148	243.111	29.204
FK11-1-C1a.d	0.126	0.168	1.056	223.234	80.064	18.362	1182.89	0.257	20.572	68.944	11.662
FK11-1-C1b.d	0.140	<DL	1.668	348.056	157.070	20.558	1185.67	0.434	70.890	208.917	28.036
FK11-1-C1c.d	0.090	<DL	2.155	313.306	209.195	27.161	1173.16	0.314	40.032	156.653	26.799
FK11-1-C2a.d	0.096	<DL	1.751	325.677	98.412	20.113	836.78	0.136	3.350	22.018	5.491
FK11-1-C2b.d	0.093	<DL	3.030	386.976	182.229	54.349	781.18	0.110	9.772	48.233	10.759
FK11-1-C2c.d	0.108	<DL	1.835	340.411	150.537	10.828	947.98	0.054	5.254	36.835	9.522
FK11-1-C2d.d	0.104	<DL	0.778	469.125	37.294	7.214	921.57	0.138	8.340	31.762	5.880
FK11-1-C2e.d	0.139	0.232	1.501	441.742	72.280	12.024	1125.90	0.101	8.729	35.362	6.644
FK11-1-C2f.d	0.100	<DL	1.793	553.220	145.394	8.006	797.86	0.231	24.728	118.845	24.645
FK11-1-C2g.d	0.154	0.222	1.334	319.561	57.546	9.994	917.40	0.172	3.697	16.666	3.821
FK13-1-L1.d	0.181	0.171	1.487	365.570	46.106	14.512	810.37	0.199	29.746	132.328	25.493
FK13-1-L1.d	0.213	0.174	2.224	425.062	168.607	46.871	818.71	0.185	29.746	142.197	30.983
FK15-L1.d	0.149	0.236	2.419	305.661	72.141	19.335	2996.84	0.124	56.712	203.357	32.220
FK15-L2.d	0.115	0.120	3.600	308.580	83.400	20.252	4813.57	0.099	123.571	336.380	43.507
FK15-L2.d	0.146	<DL	3.294	319.422	107.725	25.256	3586.20	0.136	107.586	320.534	46.565
FK15-L3.d	0.129	0.128	3.447	307.329	81.871	20.753	4983.15	0.146	123.988	341.245	44.188
FK15-L3.d	0.115	0.195	3.211	312.472	104.250	25.312	3518.09	0.196	100.080	294.263	43.507
FK15-L4.d	0.121	0.171	3.280	309.414	83.817	21.253	5015.12	0.145	127.046	341.662	44.758
FK15-L5.d	0.131	0.133	3.503	305.244	76.728	20.572	4948.40	0.139	111.061	296.904	39.573
FK13-1-L2.d	0.140	0.185	0.777	347.500	22.226	9.786	520.83	0.278	19.599	69.222	11.023
FK13-1-L3.d	0.125	0.213	0.806	351.670	23.074	9.494	511.80	0.240	21.072	72.419	11.620

Appendix 2.4B (continued)

Point ID	Co (ppm)	Ni (ppm)	As (ppm)	Sr (ppm)	Y (ppm)	Nb (ppm)	Mo (ppm)	Ba (ppm)	La (ppm)	Ce (ppm)	Pr (ppm)
FK13-1-L4.d	0.124	0.178	1.182	367.794	48.247	11.370	528.34	0.218	44.007	151.649	23.964
FK13-1-L5.d	0.124	0.118	1.176	366.126	52.556	11.398	548.22	0.224	48.219	169.580	27.216
FK13-1-L6.d	0.142	0.152	1.168	360.427	50.374	11.176	559.06	0.202	46.648	166.800	26.994
FK12-1.d	0.234	0.334	4.462	157.070	387.810	41.283	772.84	0.862	14.317	86.180	22.379
FK12-2.d	1.251	0.945	4.142	140.668	348.890	23.922	1117.56	0.050	4.879	39.212	11.662
FK12-3.d	0.876	0.292	2.474	189.040	169.580	28.120	1085.59	0.081	7.979	41.839	9.813
FK12-4.d	0.334	0.168	1.738	143.448	65.608	22.949	1765.30	0.058	6.505	23.352	4.170
FK12-5.d	0.196	0.157	2.738	131.355	174.445	16.360	1711.09	0.031	3.002	24.200	6.394
FK12-6.d	0.221	0.220	16.472	127.463	223.929	174.584	1434.48	0.175	13.094	48.080	9.230
FK12-7.d	0.417	16.680	7.145	121.903	110.644	23.130	3056.61	0.047	6.783	33.569	7.645
FK12-8.d	0.220	0.295	5.213	137.193	395.455	18.793	1752.79	0.145	24.269	110.922	22.754
FK12-9.d	0.277	1.390	6.033	141.224	420.753	17.125	2503.39	0.076	23.032	102.582	20.211
Gil-C1.d	0.039	0.361	0.778	155.124	102.165	4.240	495.40	0.195	2.652	10.731	2.243
G25-C1a.d	<DL	<DL	1.112	203.496	54.071	4.643	963.27	0.165	3.475	16.152	3.531
G25-C1b.d	0.028	<DL	1.015	163.464	96.049	5.838	725.58	0.129	5.894	25.715	5.254
G25-C2b.d	0.033	<DL	0.709	152.483	108.698	4.851	617.16	0.168	3.531	15.179	3.239
G25-C1c.d	0.075	<DL	2.947	156.375	69.917	6.603	686.66	0.256	2.933	14.526	3.197
G25-C3a.d	0.038	<DL	1.182	163.881	92.157	5.921	707.51	0.129	5.365	24.186	5.087
G25-C3b.d	0.035	<DL	0.931	157.904	33.471	4.879	743.65	0.097	4.726	21.045	4.142
G25-C4.d	0.038	<DL	0.931	152.900	72.836	4.601	526.81	0.182	2.597	13.497	2.877
G25-C1a.d	0.200	0.246	1.279	159.155	87.709	5.504	594.92	0.338	2.697	12.204	2.627
G25-C1a.d	0.117	0.211	1.960	160.406	39.476	20.086	468.43	0.272	1.960	8.229	1.640
G25-C2a.d	0.175	0.153	1.186	211.280	125.795	7.131	1216.25	0.306	5.467	23.408	5.043
G22-L1.d	0.214	0.264	0.737	118.011	44.480	7.075	308.58	0.163	0.994	3.239	0.648
G22-L1.d	0.193	0.158	2.266	142.475	275.359	19.252	892.38	0.177	5.518	25.256	5.256
G22-L2.d	0.220	0.217	2.808	144.699	252.563	23.491	921.57	0.152	5.310	23.561	4.879
G22-L2.d	0.177	0.363	2.766	147.062	305.800	23.672	1011.92	0.229	6.269	27.995	5.838
G22-L3.d	0.179	0.457	2.446	156.375	297.460	17.250	1248.22	0.206	6.742	29.357	6.033
G23-L1.d	0.181	0.181	1.807	142.058	224.485	16.068	789.52	0.132	5.796	25.937	5.463
G23-L1.d	0.158	0.250	2.252	145.116	239.358	19.418	1091.15	0.190	6.394	28.815	5.908
G23-L2.d	0.163	0.265	3.600	151.371	346.666	25.924	981.34	0.129	8.952	38.030	7.659
G23-L2.d	0.171	0.235	3.433	151.510	347.917	26.674	902.11	0.078	8.062	34.945	7.047
G22-L4.d	0.172	0.639	1.946	121.347	42.701	8.410	344.30	2.502	0.994	3.572	0.713
G23-L3.d	0.107	<DL	1.904	147.896	248.393	18.696	1109.22	0.218	6.491	29.704	6.241
G23-L3.d	0.145	<DL	1.265	135.108	39.337	8.674	2582.62	0.285	3.739	17.041	3.642

Appendix 2.4B (continued)

Point ID	Co (ppm)	Ni (ppm)	As (ppm)	Sr (ppm)	Y (ppm)	Nb (ppm)	Mo (ppm)	Ba (ppm)	La (ppm)	Ce (ppm)	Pr (ppm)
SCH31-1.d	0.181	0.210	0.584	1662.440	0.411	29.454	193.21	0.375	0.121	0.348	0.026
SCH31-2.d	0.261	0.174	0.467	1720.820	0.492	23.519	204.19	0.695	0.164	0.209	0.025
SCH31-3.d	0.203	37.530	0.304	1569.310	0.493	11.106	197.66	0.225	0.183	0.265	0.034
SCH31-4.d	0.190	0.167	0.473	1634.640	0.386	23.950	196.69	0.131	0.124	0.200	0.024
SCH31-5.d	0.514	0.186	0.973	1599.890	0.898	28.189	195.99	0.108	0.264	0.396	0.045
SCH31-6.d	0.195	0.284	0.944	1604.060	0.694	25.020	219.62	0.256	0.129	0.175	0.019
SCH31-7.d	0.196	0.156	2.488	1506.760	2.377	17.139	203.36	0.820	0.801	0.295	0.175
SCH31-8.d	0.185	0.209	0.378	1535.950	0.528	16.041	212.11	0.190	0.185	0.253	0.033
SCH31-9.d	0.256	6.255	0.681	1587.380	1.368	28.773	211.28	0.161	0.574	0.741	0.078
SCH31-10.d	0.598	0.375	2.210	1570.700	1.640	20.586	211.70	0.339	0.771	0.261	0.133
SCH31-11.d	0.190	0.203	0.816	1594.330	0.784	47.260	204.19	0.132	0.256	0.400	0.046
SCH11-1.d	0.320	0.271	1.974	48.233	6.352	38.906	2125.31	0.720	13.705	31.831	4.657
SCH11-2.d	0.306	0.335	1.612	50.457	7.576	55.322	2468.64	0.860	16.624	38.670	5.755
SCH11-3.d	0.206	0.278	1.640	47.260	7.172	48.511	2197.59	1.126	15.693	35.959	5.421
SCH11-4.d	0.862	0.183	1.418	41.005	9.244	117.872	592.14	0.538	32.290	72.002	9.716
SCH11-5.d	0.196	37.530	2.405	37.808	7.701	99.802	571.29	0.543	35.904	77.006	10.105
SCH11-6.d	0.334	<DL	1.890	37.238	9.549	92.713	568.51	0.834	25.965	64.079	9.535
SCH11-7.d	0.213	<DL	1.404	39.337	9.091	107.169	594.92	0.336	28.231	61.855	8.507
SCH11-8.d	0.177	<DL	1.557	35.862	8.715	151.371	590.75	0.584	39.337	90.350	12.663
SCH11-9.d	0.199	<DL	1.070	36.279	10.161	108.837	601.87	0.553	32.623	66.164	8.006
SCH11-10.d	0.207	<DL	1.056	41.283	11.231	124.127	657.47	0.662	37.558	72.836	8.396
SCH11-11.d	1.390	<DL	1.334	41.436	10.981	113.007	701.95	0.620	35.292	66.998	7.770
SCH11-12.d	0.206	<DL	1.168	37.947	12.454	108.559	593.53	0.765	26.869	59.214	8.284
INV-1-RIM1.d	0.217	0.156	0.459	504.292	24.325	4.615	3.22	1.696	16.402	82.010	15.624
INV-1-RIM2.d	0.243	0.232	0.563	77.701	8.257	106.752	1914.03	1.321	13.553	50.666	9.994
INV-1-RIM3.d	0.215	0.171	0.480	89.933	8.952	69.361	1840.36	2.891	10.105	37.099	7.159
INV-1-RIM4.d	0.236	0.153	0.873	593.530	38.781	18.487	316.92	3.378	46.009	215.033	30.413
INV-1-RIM5.d	0.247	0.959	0.820	76.867	86.041	195.017	2613.20	3.614	21.170	75.338	13.358
INV-1-1.d	0.179	0.235	1.821	33.916	32.609	495.257	6153.53	0.125	125.378	416.583	49.317
INV-1-2.d	0.224	0.234	1.821	34.013	31.803	502.485	6296.70	0.113	128.158	418.529	49.109
INV-1-3.d	0.240	0.275	1.779	34.625	28.968	466.623	6046.50	0.097	119.262	395.733	46.259
INV-1-4.d	0.220	0.170	0.616	41.436	10.967	355.145	5472.43	0.206	50.346	129.409	17.723
INV-1-5.d	0.214	0.218	1.036	59.353	25.507	601.870	5369.57	0.309	58.658	174.862	23.310
INV-1-6.d	0.227	0.314	0.945	79.647	17.500	360.566	4700.98	0.600	46.662	135.803	19.947
INV-1-7.d	0.293	0.395	1.237	56.295	17.667	174.723	4798.28	0.659	58.241	183.341	23.547

Appendix 2.4B (continued)

Point ID	Co (ppm)	Ni (ppm)	As (ppm)	Sr (ppm)	Y (ppm)	Nb (ppm)	Mo (ppm)	Ba (ppm)	La (ppm)	Ce (ppm)	Pr (ppm)
M61-1.d	0.295	0.268	0.973	80.620	5.699	4.406	42.12	<DL	56.156	81.871	7.951
M61-2.d	0.765	0.261	0.945	61.577	8.840	3.128	248.81	0.104	76.311	161.657	14.456
M61-3.d	0.459	0.178	2.502	107.586	18.098	1.835	77.70	0.236	103.972	261.459	27.105
M61-4.d	0.293	0.279	0.931	53.793	9.035	3.016	344.86	0.076	35.431	92.435	11.092
M61-5.d	26.410	4.865	1.321	46.954	9.271	2.349	208.50	<DL	31.247	120.374	17.625
M61A-C1-1.d	0.334	0.542	2.335	67.832	7.909	4.198	118.15	0.239	123.710	380.860	46.009
M61A-C2-1.d	0.271	0.203	3.795	65.608	15.916	4.448	21.82	0.047	122.598	469.820	67.693
M62-1.d	0.256	0.222	1.821	15.526	0.192	3.125	12357.10	1.251	1.382	1.974	0.235
M62-2.d	0.240	11.120	2.655	13.956	0.031	4.566	10633.50	<DL	1.033	1.724	0.158
M62A-1.d	0.334	0.239	2.363	39.893	0.639	1.508	9660.50	0.033	36.418	65.608	6.005
M62A-2.d	0.210	23.630	1.988	23.588	0.139	1.936	12398.80	<DL	7.937	13.275	1.333
KH61A-1.d	1.112	0.232	2.210	301.769	485.110	46.426	4.92	0.203	125.378	308.580	40.310
KH61A-2.d	4.309	0.214	19.460	510.130	285.784	71.863	4.45	0.500	22.796	107.030	22.101
KH61A-3.d	0.361	0.204	1.154	265.907	154.290	20.892	5.64	0.215	25.576	77.006	11.634
KH61A-4.d	2.085	13.900	1.223	226.848	339.160	31.122	7.02	0.185	68.110	134.552	15.179
KH61A-5.d	0.210	7.089	4.726	181.534	827.050	96.883	6.66	0.121	38.225	119.540	18.765
KH61A-6.d	3.336	0.264	2.585	174.167	840.950	76.867	5.39	0.834	37.391	195.295	41.478
KH61A-7.d	1.390	25.020	2.266	213.365	482.330	70.056	4.38	0.036	52.264	213.643	36.001
KH61A-8.d	0.267	0.222	29.190	293.707	84.929	7.840	8.17	0.342	30.997	66.720	7.159
KH61A-9.d	0.243	0.256	2.752	180.978	785.350	89.655	7.51	0.346	76.450	309.970	52.820
KH61A-10.d	0.247	0.202	2.572	175.140	622.720	53.654	4.87	0.135	28.495	162.352	34.611
KH61A-11.d	0.193	1.251	0.709	237.273	446.190	46.009	5.39	0.695	42.534	99.246	11.773
KH61A-12.d	0.249	0.234	1.779	223.790	661.640	123.849	5.70	0.463	41.005	146.228	24.714
SCH17-1.d	0.183	0.139	3.892	239.775	6.255	1.725	412.83	0.086	0.215	0.799	0.160
SCH17-2.d	0.222	0.239	7.367	176.530	25.548	1.924	257.15	0.139	0.645	2.433	0.467
SCH17-3.d	0.236	0.218	0.951	340.967	32.220	1.997	190.57	0.025	0.438	3.197	0.815
SCH17-4.d	1.390	0.206	1.543	283.560	9.994	2.142	187.65	0.032	0.120	0.890	0.202
SCH17-5.d	0.227	0.473	1.487	250.200	12.315	1.835	365.85	0.050	0.361	0.685	0.361
SCH17-6.d	0.196	0.186	1.487	404.490	30.872	2.075	204.19	0.029	0.363	2.478	0.632
SCH17-7.d	0.185	0.210	0.862	248.393	10.300	1.719	369.74	0.096	0.140	0.480	0.106
SCH17-8.d	0.189	0.252	3.572	124.961	2.155	1.483	233.80	0.046	0.366	0.917	0.200
SCH17-9.d	0.195	0.320	0.409	108.003	1.191	1.432	72.14	0.035	0.010	0.055	0.018
SCH17-10.d	0.185	5.977	0.539	269.660	10.230	1.573	312.61	0.064	0.090	0.435	0.106
SCH17-11.d	0.403	0.200	0.778	191.542	21.809	1.842	218.23	0.050	0.147	0.933	0.238

Appendix 2.4B (continued)

Point ID	Co (ppm)	Ni (ppm)	As (ppm)	Sr (ppm)	Y (ppm)	Nb (ppm)	Mo (ppm)	Ba (ppm)	La (ppm)	Ce (ppm)	Pr (ppm)
SCH17-12.d	0.193	0.192	3.336	208.639	12.441	1.692	310.11	0.111	0.193	1.015	0.200
SCH16-2.d	26.410	0.167	0.306	105.501	4.156	1.675	1014.70	0.514	0.064	0.403	0.072
SCH16-3.d	0.973	0.612	0.653	111.895	4.518	1.501	977.17	0.612	0.014	0.100	0.024
SCH16-6.d	0.613	0.320	0.528	103.416	2.711	1.560	1052.23	1.738	0.784	13.900	0.282
LT-L1.d	0.167	0.278	14.414	98.134	799.250	224.763	287.04	0.115	123.432	485.110	101.609
LT-L2.d	0.177	0.197	13.636	97.161	881.260	213.504	290.79	0.096	119.957	482.330	102.860
LT-L3.d	0.167	0.268	13.719	93.269	879.870	221.427	277.58	0.090	114.258	459.951	98.968
LT-L4.d	0.158	0.359	11.620	108.698	692.220	165.410	288.70	0.389	105.223	417.973	87.292
LT-L5.d	0.158	0.245	12.663	108.281	699.170	170.275	285.65	0.189	117.316	448.970	91.879
LT-L6.d	0.175	0.168	12.149	130.104	767.280	415.610	307.33	0.099	139.834	600.758	126.073
LT-L7.d	0.136	0.167	17.625	99.385	877.090	263.683	292.60	0.085	151.232	581.854	117.733
LT2-1.d	0.207	0.190	17.514	91.184	956.320	939.640	1441.43	0.095	216.423	700.560	121.486
LT2-2.d	15.290	20.850	20.628	144.838	1223.200	979.950	1277.41	0.263	194.878	599.090	111.061
LT2-3.d	3.892	0.218	21.684	117.594	1223.200	1203.740	1364.98	5.352	230.740	699.170	124.266
LT2-4.d	0.306	8.340	16.986	91.740	917.400	911.840	1473.40	1.529	209.612	686.660	119.957
LT2-5.d	0.270	0.236	15.276	102.582	746.430	840.950	1235.71	0.092	185.565	572.680	101.331
LT2-6.d	1.251	1.946	16.819	99.107	668.590	629.670	1045.28	0.054	148.035	464.816	83.539
MCW3-1-1.d	0.218	<DL	1.168	20.642	878.480	302.047	8.48	<DL	68.527	172.499	10.244
MCW3-1-2.d	3.336	0.213	2.029	20.197	971.610	499.010	1.77	<DL	92.435	460.090	48.233
MCW3-1-3.d	0.220	0.228	1.200	19.432	1023.040	329.430	1.74	<DL	54.488	101.609	5.755
MCW3-1-4.d	0.218	58.380	2.752	21.726	946.590	688.050	2.92	<DL	109.949	625.500	73.809
MCW3-1-5.d	0.254	0.234	0.734	25.632	414.637	307.190	1.06	<DL	24.812	54.488	5.032
MCW3-1.d	0.211	0.200	0.467	23.005	640.790	201.828	1.38	<DL	23.408	40.171	2.961
MCW3-2.d	0.185	0.167	0.698	23.477	751.990	233.937	1.22	<DL	33.638	45.453	2.431
MCW3-3.d	0.193	0.257	1.070	24.061	544.880	387.810	1.95	0.153	40.727	63.106	5.630
MCW3-4.d	0.196	0.487	18.487	54.766	411.440	881.260	3.91	0.040	18.960	49.345	4.267
MCW3-5.d	0.185	0.158	0.714	29.357	761.720	314.001	10.43	<DL	28.690	37.530	2.193
MCW2-D-2.d	1.251	0.172	1.001	26.146	946.590	179.866	0.42	0.101	11.926	31.650	4.768
MCW2-D-4.d	0.806	<DL	1.223	30.288	867.360	197.936	4.17	<DL	15.777	34.194	3.936
MCW2-D-5.d	0.218	<DL	2.822	76.728	795.080	867.360	2.36	0.043	56.295	240.470	31.136
MCW2-D-6.d	0.196	0.234	0.774	27.411	920.180	256.733	0.09	0.028	14.762	40.588	6.283
MCW2-D-7.d	0.225	0.220	0.417	162.213	242.972	33.638	1.54	0.082	4.017	3.558	0.328
NP1-C4-L1.d	0.126	0.193	0.377	59.325	254.231	24.478	338.33	0.050	8.479	33.082	6.825
NP1-C4-L2.d	0.122	0.228	0.360	63.801	205.998	26.952	339.02	0.114	3.642	16.819	3.892
NP1-C4-L3.d	0.093	<DL	0.498	66.720	239.775	29.385	302.74	0.106	4.504	20.989	4.837

Appendix 2.4B (continued)

Point ID	Co (ppm)	Ni (ppm)	As (ppm)	Sr (ppm)	Y (ppm)	Nb (ppm)	Mo (ppm)	Ba (ppm)	La (ppm)	Ce (ppm)	Pr (ppm)
NP1-C1-L1.d	0.100	0.158	0.348	62.550	239.358	25.771	331.52	0.081	7.437	30.580	6.477
NP1-C1-L1.d	0.126	0.320	0.820	71.446	146.923	85.902	368.21	0.106	6.019	21.948	4.226
NP1-0.d	0.117	0.135	0.361	56.170	155.402	25.618	320.26	0.070	4.448	16.819	3.753
NP1-C2a.d	0.139	0.178	0.449	57.546	179.171	25.520	307.89	<DL	11.537	37.947	7.131
NP1-C2b.d	0.101	<DL	0.409	57.963	264.656	24.603	317.34	<DL	8.396	34.013	7.325
NP1-C2c.d	0.164	0.193	0.371	59.631	256.316	25.117	308.30	<DL	8.618	33.221	6.603
NP1-1-L1.d	0.156	0.217	0.407	78.035	279.946	49.762	144.00	0.056	3.253	14.817	3.134
NP1-1-L2.d	0.152	0.239	0.306	80.898	289.120	55.461	145.53	0.061	3.350	15.665	3.300
NP1-1-L3.d	0.156	0.231	0.314	74.532	284.116	44.341	134.14	0.093	3.670	15.373	3.132
NP1-2-L1.d	0.140	<DL	0.417	78.396	314.140	51.430	145.12	0.042	5.296	19.919	3.975
NP1-2-L1.d	0.108	<DL	0.638	74.226	421.170	60.743	152.90	0.072	10.745	40.866	8.646
NP1-2-L2.d	0.177	0.165	0.591	76.728	423.950	63.523	152.76	<DL	10.439	40.310	8.493
NP1-2-L2.d	0.146	0.131	0.626	64.635	242.972	30.538	268.55	<DL	10.133	40.449	8.104
NP1-2-L3.d	0.135	0.146	0.613	77.145	428.120	65.608	153.18	0.051	10.773	41.978	8.715
NP1-2-L3.d	0.117	0.243	0.324	75.616	211.280	30.969	215.17	0.022	8.229	31.553	6.283
NP1-2-L4.d	0.143	0.186	0.739	53.084	252.980	12.913	136.36	0.026	24.742	76.311	13.858
SCH19-1.d	0.320	0.142	16.374	47.677	485.110	544.880	5351.50	0.111	60.465	318.310	55.322
SCH19-2.d	0.175	0.088	8.757	43.924	703.340	644.960	5045.70	0.104	84.651	432.290	73.114
SCH19-3.d	0.210	<DL	14.790	40.574	1341.350	1004.970	5087.40	0.264	70.056	380.443	70.195
SCH19-4.d	0.225	<DL	23.825	43.368	299.823	287.035	5212.50	0.139	25.965	135.525	27.828
SCH19-5.d	1.668	11.120	8.576	46.148	298.711	376.690	7089.00	0.061	116.760	435.070	58.658
SCH19-7.d	0.197	0.171	10.536	42.395	1476.180	1167.600	4726.00	<DL	62.272	332.210	63.384
SCH19-8.d	0.204	20.850	8.701	36.696	479.550	437.850	3975.40	0.071	74.087	371.130	62.411
SCH19-9.d	0.403	<DL	10.703	35.445	715.850	587.970	3117.77	0.057	65.052	315.808	51.847
SCH20-1.d	0.195	0.292	5.421	38.114	116.482	89.655	4990.10	0.070	42.951	141.502	20.113
SCH20-2.d	0.243	0.157	7.020	39.851	369.879	298.433	7728.40	<DL	160.684	686.660	86.180
SCH20-3.d	0.178	0.200	4.045	38.767	150.815	153.178	7672.80	<DL	152.483	523.752	52.806
SCH20-4.d	0.200	0.206	3.600	37.613	138.305	127.046	7436.50	0.044	101.470	395.872	44.285
SCH20-5.d	0.178	0.278	5.643	38.656	210.307	183.758	7367.00	0.058	92.713	418.946	52.403
SCH20-7.d	0.222	0.172	12.621	42.937	245.335	236.300	7130.70	0.170	99.385	411.023	51.986
SCH20-8.d	0.389	0.181	9.535	43.507	373.910	471.210	7269.70	0.047	124.683	515.690	66.025
SCH20-9.d	3.336	0.097	4.003	47.399	80.342	78.535	8562.40	0.082	68.388	229.767	25.284
SCH20-10.d	0.150	<DL	7.256	40.519	94.798	110.783	8492.90	0.093	69.361	217.118	22.949
SCH20-11.d	0.118	0.389	17.347	45.036	92.157	146.506	7519.90	0.145	62.550	226.431	26.702
SCH20-12.d	0.190	0.264	5.713	42.395	154.846	170.970	7089.00	0.054	81.732	320.117	37.433

Appendix 2.4B (continued)

Point ID	Co (ppm)	Ni (ppm)	As (ppm)	Sr (ppm)	Y (ppm)	Nb (ppm)	Mo (ppm)	Ba (ppm)	La (ppm)	Ce (ppm)	Pr (ppm)
SCH20-13.d	0.211	0.153	5.032	53.376	154.707	131.772	6185.50	0.028	57.129	229.767	30.358
SCH21-1.d	0.598	0.681	54.905	31.261	52.403	74.226	7742.30	0.268	17.820	61.299	10.300
SCH21-2.d	0.182	0.271	30.580	29.412	25.187	56.851	18389.70	0.267	46.009	108.837	12.844
SCH21-3.d	2.224	0.220	22.101	32.526	48.650	56.295	6741.50	0.165	26.007	74.226	10.717
SCH21-4.d	0.211	0.389	18.431	41.144	181.256	341.940	10981.00	2.780	59.075	183.063	23.561
SCH21-5.d	0.215	0.252	27.661	37.530	95.493	97.856	10452.80	0.542	23.185	73.114	12.496
SCH21-6.d	0.177	0.138	20.516	36.488	78.952	96.744	9507.60	0.054	19.238	71.446	13.052
SCH21-7.d	0.218	2.502	14.345	32.540	3.545	47.538	23338.10	0.626	41.700	83.122	8.159
SCH21-8.d	0.206	0.182	15.790	44.619	47.399	49.206	22684.80	0.181	22.852	68.944	10.203
SCH22-A1.d	0.188	0.156	3.600	39.476	158.321	123.015	515.69	0.056	27.758	129.270	23.630
SCH22-A2.d	0.215	36.140	4.935	32.693	149.286	103.416	991.07	0.240	24.325	92.157	17.792
SCH22-A4.d	0.174	<DL	3.378	30.511	140.390	25.993	692.22	0.459	23.519	106.057	17.709
SCH22-A5.d	0.152	25.020	2.558	31.136	75.477	26.688	1096.71	0.031	24.450	83.678	12.677
SCH22-A6.d	0.210	0.243	2.168	35.139	167.912	30.427	692.22	0.032	35.445	162.352	25.673
SCH22-B1.d	0.247	0.132	19.543	49.623	0.499	32.957	18236.80	0.136	27.995	54.905	5.574
SCH22-B2.d	0.195	0.200	26.368	47.121	0.379	17.875	23365.90	0.136	23.102	40.171	4.073
SCH22-B3.d	0.120	1.946	18.292	66.025	0.289	24.923	27230.10	0.057	28.565	36.835	3.094
SCH22-B4.d	0.013	<DL	64.357	46.996	0.310	2.727	24047.00	0.056	29.663	44.730	4.023
SCH22-B5.d	0.322	<DL	69.361	71.168	0.349	3.989	29009.30	0.125	62.272	109.949	9.827
SCH22-B6.d	0.325	0.279	50.735	65.469	0.117	4.573	28467.20	0.115	31.094	51.152	4.657
SCH23-B1.d	0.207	0.229	10.036	67.137	64.079	57.268	1843.14	0.299	65.330	255.065	31.553
SCH23-B2.d	0.222	1.112	13.205	52.264	181.673	163.881	726.97	0.263	21.281	92.574	18.362
SCH23-B3.d	0.239	0.570	10.550	51.847	320.951	362.790	867.36	0.156	31.303	122.320	23.269
SCH23-B4.d	0.206	0.204	6.561	48.789	63.245	29.343	854.85	0.224	23.060	92.574	16.082
SCH23-B5.d	0.200	0.348	10.578	51.708	62.550	29.468	539.32	0.143	13.928	54.210	10.064
SCH23-C1.d	0.224	0.232	8.229	44.480	269.104	235.605	5212.50	0.265	51.152	216.562	31.775
SCH23-C2.d	0.203	0.259	8.549	44.202	343.886	293.568	522.64	0.125	35.862	159.711	29.426
SCH23-C3.d	0.264	6.533	12.037	50.040	166.105	183.619	8062.00	0.097	57.546	214.755	28.606
SCH23-C4.d	0.129	0.342	7.993	40.838	134.691	66.303	575.46	0.264	31.275	128.158	20.530
SCH23-C5.d	0.060	0.265	10.244	38.920	326.650	344.720	4878.90	0.221	95.771	493.450	74.087
SCH24-1.d	0.186	0.375	13.650	40.449	237.690	181.951	6950.00	0.089	35.584	142.336	24.325
SCH24-2.d	0.214	0.128	18.960	40.727	87.292	121.347	7506.00	0.118	26.591	84.651	13.817
SCH24-3.d	0.267	0.149	13.622	42.256	130.104	195.712	7784.00	0.306	43.646	153.595	23.658
SCH24-4.d	0.202	0.185	30.024	53.098	120.513	173.055	6908.30	0.067	28.384	100.497	17.681
SCH24-5.d	0.195	0.234	20.016	37.141	114.814	128.575	7130.70	0.222	34.291	120.652	19.488

Appendix 2.4B (continued)

Point ID	Co (ppm)	Ni (ppm)	As (ppm)	Sr (ppm)	Y (ppm)	Nb (ppm)	Mo (ppm)	Ba (ppm)	La (ppm)	Ce (ppm)	Pr (ppm)
SCH24-6.d	0.188	6.116	20.669	39.615	41.839	77.145	14164.10	0.236	30.413	86.458	12.232
SCH24-7.d	0.197	0.152	9.939	41.478	107.308	93.130	7658.90	0.114	28.231	92.713	15.679
SCH24-1A-R.d	0.186	0.228	6.728	33.638	271.606	283.282	3594.54	0.068	36.279	158.182	26.257
SCH24-1A-C.d	0.206	0.681	10.481	32.401	56.573	94.659	9340.80	0.097	26.146	80.064	12.107
SCH24-2A-R.d	0.190	0.193	<DL	28.273	29.051	21.128	1762.52	0.028	1.835	7.506	1.571
SCH24-2A-R1.d	0.242	0.135	<DL	32.192	129.270	122.598	4086.60	0.239	23.422	93.825	17.306
SCH25-1.d	0.171	0.225	3.141	28.509	41.005	10.898	942.42	0.195	2.517	12.218	3.128
SCH25-3.d	<DL	0.088	4.740	22.866	53.098	31.275	2738.30	0.044	4.490	19.655	5.630
SCH25-4.d	0.175	<DL	4.434	23.185	47.816	22.379	2621.54	<DL	4.212	17.764	5.101
SCH25-5B.d	0.193	0.158	2.071	22.782	53.376	15.735	825.66	0.056	3.823	17.917	4.823
SCH25-6B.d	0.165	0.193	2.989	34.611	43.229	10.689	1230.15	0.083	2.833	11.996	2.672
SCH26-1.d	0.232	0.114	17.458	56.017	71.446	97.717	9577.10	0.110	21.990	75.755	12.983
SCH26-2.d	0.193	0.182	12.093	36.557	94.659	98.968	7617.20	0.218	29.829	98.829	16.138
SCH26-3.d	0.210	0.206	15.373	64.218	26.758	50.318	18904.00	0.264	22.504	59.770	8.340
SCH26-4.d	0.106	<DL	12.343	50.040	9.619	40.171	53932.00	0.265	38.058	62.133	5.421
SCH26-5.d	<DL	<DL	14.776	53.932	5.171	25.117	31580.80	0.445	32.568	58.241	5.699
SCH26-6.d	<DL	<DL	13.122	50.318	38.503	80.342	16846.80	0.178	23.797	76.172	10.981
SCH26-7.d	0.556	0.179	16.819	45.870	29.871	56.990	52403.00	0.158	37.530	87.153	10.328
SCH26-8.d	0.21406	0.2363	18.07	58.519	41.005	99.663	21030.70	0.2502	34.889	109.949	15.6236
SCH27-C1.d	0.18487	0.26966	6.116	42.4923	66.998	98.968	8131.50	0.3475	74.226	205.164	21.2809
SCH27-C2.d	0.21962	0.28356	14.0946	44.063	36.5987	45.87	15429.00	1.529	21.9203	58.519	8.5902
SCH27-C3.d	0.22657	11.12	19.1125	38.642	73.531	67.693	11231.20	0.10008	66.303	157.626	17.0692
SCH27-4.d	0.20155	1.668	19.5017	51.569	77.006	131.911	6866.60	0.13761	44.063	123.432	17.9727
SCH27-5.d	0.21545	0.21267	6.255	45.87	91.184	67.554	7214.10	0.08757	124.822	354.45	36.0288
SCH27-6.d	0.22657	0.24603	16.7912	54.627	40.727	71.307	10049.70	0.09591	42.951	107.586	13.0382
SD11-C2.d	0.03753	<DL	6.0326	64.913	492.06	19.6824	107.31	0.05421	0.79369	4.6704	1.17455
SD11-C1b.d	0.015568	<DL	4.9067	56.295	1120.34	99.246	60.33	<DL	24.5891	120.096	22.9489
SD11-C1c.d	0.05838	<DL	4.5175	69.5	518.47	84.651	56.71	0.13344	5.9075	27.7861	5.4349
SD11-C1d.d	0.03336	<DL	6.3801	48.8585	189.874	21.9759	86.88	0.11259	0.22657	1.20096	0.26132
SD28-sch1.d	0.03892	<DL	11.2312	109.81	60.604	24.8532	1601.28	0.24742	28.3977	96.327	15.5124
SD28-sch1a.d	0.02919	<DL	3.475	135.525	77.701	153.734	1535.95	0.24464	30.4827	98.412	15.6236
SD28-sch2.d	0.07367	<DL	3.2109	139.139	72.002	46.148	1602.67	0.17931	21.406	80.898	13.7332
SD28-sch2a.d	0.03197	<DL	2.6271	123.988	59.909	43.8128	1695.80	0.7506	12.5656	51.6524	9.2018
SD28-sch2b.d	0.04865	<DL	5.5322	135.525	29.4958	40.3934	2026.62	0.47677	12.6073	50.9018	8.8404
SD28-sch3.d	0.06811	<DL	4.4202	159.989	120.374	212.253	1641.59	0.11815	39.5594	146.645	26.1042

Appendix 2.4B (continued)

Point ID	Co (ppm)	Ni (ppm)	As (ppm)	Sr (ppm)	Y (ppm)	Nb (ppm)	Mo (ppm)	Ba (ppm)	La (ppm)	Ce (ppm)	Pr (ppm)
SD28-sch3a.d	0.02641	<DL	2.7661	145.533	173.333	72.28	1652.71	0.09035	63.106	225.875	36.5153
SD28-sch3b.d	0.03892	<DL	3.7252	108.559	59.631	31.4418	1590.16	0.14595	25.993	73.392	11.3563
SD28-sch4.d	0.0278	<DL	2.4047	122.737	61.021	42.673	1715.26	0.24325	12.2598	49.9149	8.9794
SD28-sch4a.d	0.04309	<DL	6.3523	116.899	83.539	51.7914	892.38	0.23769	17.792	81.037	15.4707
SD28-sch4b.d	0.02641	<DL	3.3221	137.193	113.841	58.936	1581.82	0.12649	19.9882	95.632	19.4322
ITALY-1.d	0.22101	0.25576	134.969	59.214	292.039	221.01	3620.95	0.01668	22.0871	83.678	16.8051
ITALY-2.d	0.2363	0.13622	274.942	59.77	462.036	292.317	3515.31	0.01529	48.6639	218.508	38.0026
ITALY-3.d	0.21684	0.16263	281.475	82.288	442.298	257.984	4172.78	0.03614	55.878	246.447	39.893
ITALY-4.d	0.21684	0.15568	186.538	62.411	250.895	185.009	4197.80	0.04865	43.2012	167.634	31.9978
ITALY-5.d	0.19738	0.15151	178.337	60.882	224.207	146.228	4264.52	0.03058	38.5169	144.282	28.5506
ITALY-6.d	0.2085	0.26549	204.886	60.604	292.317	140.39	4274.25	0.01529	40.2127	150.815	29.3707
ITALY-7.d	0.21962	0.14873	307.329	62.828	424.367	165.966	5120.76	0.03892	62.411	270.494	42.6035
ITALY-8.d	0.26688	0.17236	324.843	64.218	455.086	170.553	5280.61	0.04309	66.442	283.143	43.5765
ITALY-9.d	0.2224	0.29329	309.97	62.689	280.224	257.706	4937.28	0.03753	76.033	292.456	40.4351
ITALY-10.d	0.1946	0.1946	289.954	62.55	401.154	162.491	4675.96	0.04448	74.226	308.024	45.6059
ITALY-11.d	0.23352	0.14456	340.689	64.218	434.514	182.646	4813.57	0.03753	87.987	355.284	51.2215
ITALY-12.d	0.23074	0.21267	362.79	65.747	465.65	198.77	4656.50	0.03753	92.574	370.852	52.959
TSE-1.d	0.25159	20.85	3.9059	82.844	357.23	617.16	403.10	2.9468	67.832	393.37	70.612
TSE-2.d	1.112	37.53	23.63	87.292	394.76	640.79	338.05	2.1823	58.519	361.4	68.388
TSE-3.d	0.3892	0.4587	4.0727	73.948	446.19	679.71	356.95	2.502	77.284	464.26	87.292
TSE-4.d	0.5699	0.2224	4.31	59.492	359.037	558.78	435.07	<DL	70.334	387.949	69.639
TSE-5.d	0.27105	0.21962	3.4194	57.685	511.52	592.14	524.03	0.5977	55.0023	321.507	62.1469
TSE-6.d	0.30441	0.139	3.7391	114.397	415.61	617.16	376.69	6.8944	81.732	412.83	66.303
TSE-7.d	0.23213	0.33777	3.8086	88.682	341.384	454.113	338.05	1.7097	36.418	236.022	46.426
SCH40-1.d	0.22379	0.11954	2.0572	53.515	2.5854	23.8941	1187.06	0.07923	8.1315	18.8762	2.39914
SCH40-2.d	0.19043	0.13761	1.39	47.26	1.03972	20.989	725.58	0.05699	4.0171	5.3515	0.41561
SCH40-3.d	0.17514	0.16402	2.224	47.677	1.73194	60.882	857.63	0.09174	7.3948	7.8813	0.53654
SCH40-4.d	0.17375	0.1668	1.9738	50.318	2.1128	51.013	902.11	0.04448	9.1879	10.2443	0.8896
SCH40-5.d	0.21267	0.23352	3.753	49.623	0.87709	67.415	906.28	0.3475	6.6025	5.5739	0.29746
SCH40-6.d	0.21267	0.8618	2.6827	47.955	2.71884	58.936	936.86	0.2224	11.8289	13.9834	0.96883
SCH40-7.d	0.19182	0.29329	3.0858	51.847	2.4047	79.23	1046.67	0.06672	11.3424	12.6073	0.76172
SCH40-8.d	0.17236	1.946	0.61855	82.705	2.3352	24.2138	526.81	<DL	16.2213	17.2082	1.15092
SCH40-9.d	1.251	25.02	0.27105	73.114	1.26073	7.3948	717.24	<DL	1.94461	2.78	0.35584
SCH40-10.d	0.18209	3.197	1.0286	55.461	4.1005	25.993	714.46	<DL	13.2328	17.931	1.49703
SCH40-11.d	0.2085	0.19321	0.9591	41.561	1.10088	36.279	839.56	0.1529	4.8372	4.8789	0.31275

Appendix 2.4B (continued)

Point ID	Co (ppm)	Ni (ppm)	As (ppm)	Sr (ppm)	Y (ppm)	Nb (ppm)	Mo (ppm)	Ba (ppm)	La (ppm)	Ce (ppm)	Pr (ppm)
SCH40-12.d	0.23769	54.21	0.7089	46.148	1.43031	12.3015	939.64	0.3614	7.0612	7.8396	0.49762
SCH44-3.d	0.21962	<DL	0.8618	124.822	3.614	1.3761	1495.64	0.3892	0.74643	2.5854	0.42395
SCH44-4.d	0.20572	0.2502	<DL	74.643	3.1414	1.59572	2446.40	0.14178	0.17653	2.1267	0.33221
SCH44-5.d	0.19877	0.3892	0.695	107.308	2.6827	1.8626	1251.00	48.65	0.38781	1.807	0.16541
SCH44-6.d	13.9	0.3892	0.6672	99.246	3.1275	1.36915	1552.63	0.4865	0.7645	1.8209	0.2919
SCH44-7.d	<DL	0.1807	0.556	137.332	2.9885	1.43587	2085.00	0.24325	2.363	2.2935	0.26132
SCH44-8.d	<DL	0.2641	1.1815	159.155	2.9051	2.224	949.37	0.556	0.66581	1.8765	0.37252
SCH44-9.d	0.26549	0.139	0.4309	101.192	2.919	1.53734	1237.10	1.0008	0.72697	1.6402	0.6533
YP5B-C3.d	0.02363	<DL	0.20711	1478.96	19.2098	1.63325	0.33	0.4031	2.8912	7.784	0.95771
YP5A-C5a.d	0.18209	0.20016	0.42673	2335.2	18.209	1.62491	0.08	0.50318	16.68	40.171	5.2959
YP5A-C5b.d	0.17792	0.24186	0.43507	2000.21	33.082	1.59294	0.67	1.9738	6.0882	18.487	2.641
YP5A-C5b.d	0.15429	0.19599	0.20016	1837.58	23.074	1.61101	0.05	0.54071	5.6156	12.6907	1.4734
YP5A-C1a.d	0.17931	0.17236	0.2676	2329.64	19.043	1.66105	0.18	0.6255	9.7578	22.379	2.9051
YP5A-C1a.d	0.14734	<DL	0.17236	1808.39	21.406	1.6124	0.33	0.32665	8.2844	12.3154	1.2232
YP5A-C1b.d	0.16263	0.15707	0.26132	1991.87	22.24	1.62213	0.13	0.53654	7.8535	14.4004	1.47757
YP5A-C3a.d	0.17653	<DL	0.16402	2148.94	9.591	1.57626	0.27	0.6394	6.5747	9.452	0.94381
YP5A-C3a.d	0.1807	0.139	0.23908	2032.18	25.854	1.57626	0.85	0.9452	10.842	30.024	3.9754
YP5A-C3b.d	0.12788	0.15846	0.19043	2154.5	17.1943	1.5985	0.07	0.48094	6.1438	10.6891	1.32467
YP5A-C3b.d	0.15707	0.19738	0.17792	2100.29	32.665	1.71665	0.39	0.51708	7.4782	18.904	2.9468
YP5A-C1c.d	0.16124	0.18209	0.23213	2855.06	17.653	1.76947	0.13	0.66025	10.6196	24.881	2.9329
YP5A-C1d.d	0.15151	0.139	0.30163	2157.28	20.85	1.72221	0.03	0.8757	9.9385	26.827	3.5306
YP5B-C1a.d	0.13483	0.25854	0.29468	1487.3	25.576	1.3622	0.14	1.19123	9.2713	12.51	1.2927
YP5B-C1b.d	0.14039	0.17792	0.3058	1666.61	14.595	1.3761	0.45	1.1676	16.402	7.9508	0.51152
YP5B-C3a.d	0.13344	<DL	0.24047	1203.74	61.16	1.44699	0.13	1.0981	12.51	26.271	3.9893
YP5B-C2a.d	0.16541	<DL	0.4031	1421.97	21.962	1.54568	0.20	1.3344	15.429	12.093	1.0008
ZIV-1.d	0.2224	0.20433	0.3058	1138.41	74.643	0.43229	0.13	0.31414	29.19	42.256	4.7816
ZIV-2.d	0.22657	0.16819	2.8495	1252.39	354.45	1.62769	0.10	0.5421	19.182	125.1	30.719
ZIV-3.d	0.23213	0.18626	0.63662	1212.08	257.428	0.54766	0.08	0.78952	22.0315	89.099	14.0529
ZIV-4.d	0.19738	0.22379	1.9877	1245.44	447.997	1.92932	0.10	1.0981	15.8599	108.698	27.7861
ZIV-5.d	0.2224	0.1807	1.8626	1160.65	487.89	1.99187	0.09	0.57824	18.209	116.76	27.661
ZIV-6.d	0.20155	0.2224	2.0572	1380.27	383.084	2.96487	0.12	0.02085	26.6046	175.974	37.6968
ZIV-7.d	0.23769	0.21684	1.2788	1232.93	204.33	0.98273	0.07	2.0155	13.3301	73.948	16.0267
ZIV-8.d	0.20433	0.19182	1.9182	1189.84	490.67	2.60764	0.11	0.1668	24.047	137.61	29.746
ZIV-9.d	0.21545	0.23491	1.5429	1301.04	299.406	1.10505	0.09	1.8626	13.5942	86.18	19.9048
ZIV-10.d	0.2363	0.2363	1.0703	1269.07	183.063	0.77562	0.08	1.1537	14.456	71.724	14.2475

Point ID	Co (ppm)	Ni (ppm)	As (ppm)	Sr (ppm)	Y (ppm)	Nb (ppm)	Mo (ppm)	Ba (ppm)	La (ppm)	Ce (ppm)	Pr (ppm)
ZIV-11.d	0.18209	0.37669	1.3483	1167.6	143.17	1.23571	0.13	2.4325	6.5886	48.233	12.6907
ZIV-12.d	0.18626	0.20989	1.8626	1298.26	460.229	2.31574	0.10	0.05699	23.074	155.541	34.889

Appendix 2.4B (continued)

Point ID	Nd (ppm)	Sm (ppm)	Eu (ppm)	Gd (ppm)	Tb (ppm)	Dy (ppm)	Ho (ppm)	Er (ppm)	Tm (ppm)	Yb (ppm)	Lu (ppm)
Min DL	0.004	0.003	0.0	0.005	0.001	0.002	0.001	0.002	0.001	0.002	0.001
Max DL	0.126	0.479	0.8	0.489	0.293	0.466	0.193	0.227	0.200	0.581	0.233
Cel-L1.d	146.228	31.331	12.5	29.746	4.684	29.246	6.269	17.055	2.281	12.983	1.682
Cel-L2.d	157.765	33.082	11.6	31.692	4.962	30.997	6.575	17.959	2.424	14.220	1.833
Cel-L3.d	136.498	26.883	12.4	24.937	3.934	24.853	5.393	14.901	2.071	12.079	1.603
Cel-L4.d	204.330	44.202	10.8	41.700	6.575	39.893	8.521	22.365	2.961	16.555	2.078
Cel-L4.d	95.910	17.889	9.4	16.583	2.559	15.387	3.267	9.132	1.270	7.534	1.008
Cel-L5.d	143.448	29.482	11.6	27.675	4.351	26.994	5.630	15.373	2.100	11.843	1.529
Cel-L6.d	145.672	30.024	11.4	28.495	4.420	26.966	5.741	15.276	2.116	12.357	1.605
Cel-L7.d	146.923	31.275	11.6	29.496	4.615	28.676	6.186	16.889	2.260	13.275	1.751
CL16-2-C1a.d	19.891	6.297	3.1	7.923	1.390	8.910	1.928	4.907	0.557	2.099	0.133
CL16-2-C2b.d	29.468	10.091	5.6	14.178	2.572	17.514	4.059	11.023	1.265	5.226	0.361
CL16-2-C2c.d	43.229	14.706	8.5	19.669	3.934	27.619	6.742	19.960	2.489	10.967	0.698
CL16-3-1.d	31.331	8.660	8.3	11.857	2.200	14.984	3.739	9.869	1.084	3.795	0.238
CL16-3-2.d	26.563	6.672	7.9	7.784	1.397	9.410	2.285	6.352	0.674	2.155	0.101
CL16-3-3.d	24.144	6.380	7.2	7.965	1.382	9.410	2.232	5.935	0.525	1.526	0.059
CL16-3-4.d	16.138	4.907	6.4	7.603	1.340	9.091	2.284	6.422	0.673	2.280	0.153
CL16-3-5.d	19.933	5.935	5.1	7.993	1.466	9.702	2.217	5.699	0.606	2.669	0.286
CC57-1.d	258.262	55.044	28.1	44.480	6.213	35.820	7.367	22.087	3.674	29.051	4.759
CC57-2.d	324.843	65.330	35.8	52.125	7.270	43.034	8.882	27.244	4.573	35.139	5.908
CC57-3.d	155.402	44.619	5.9	36.279	4.670	23.380	4.101	9.772	1.211	7.061	0.997
CC57-4.d	249.505	51.291	29.2	41.422	6.686	43.507	9.452	30.997	5.532	43.090	6.853
CC57-5.d	327.067	66.581	22.1	52.403	7.172	41.853	8.340	24.867	3.845	27.397	4.233
CC57-6.d	301.630	87.848	27.8	82.844	14.095	90.350	19.293	59.075	9.716	69.500	10.203
CC57-7.d	232.130	48.789	25.7	37.113	5.407	31.970	6.366	17.667	2.572	17.792	2.530
CC57-8.d	375.300	71.724	56.9	51.569	6.950	40.880	8.201	26.563	4.990	42.256	6.881
CC57-9.d	247.420	48.233	31.4	36.140	4.976	28.342	5.574	17.389	2.961	22.129	3.725
DG28-C1a.d	257.428	35.584	3.4	24.436	2.610	12.719	2.350	5.860	0.739	4.214	0.626
DG28-C2b.d	313.723	43.618	3.9	29.899	3.208	15.262	2.812	6.769	0.840	4.740	0.678

Appendix 2.4B (continued)

Point ID	Nd (ppm)	Sm (ppm)	Eu (ppm)	Gd (ppm)	Tb (ppm)	Dy (ppm)	Ho (ppm)	Er (ppm)	Tm (ppm)	Yb (ppm)	Lu (ppm)
DG28-C1c.d	308.858	44.202	3.1	30.413	3.207	15.026	2.717	6.436	0.787	4.379	0.639
DG28-C1c.d	184.036	27.842	2.3	19.182	2.111	9.883	1.871	4.323	0.520	2.961	0.424
DG28-C3a.d	144.004	21.350	2.5	14.748	1.537	7.103	1.340	3.322	0.399	2.363	0.339
DG28-C3b.d	210.307	30.302	3.1	21.309	2.377	10.939	2.064	4.879	0.619	3.419	0.496
DG28-C3b.d	130.660	16.541	2.7	10.495	1.130	4.740	0.848	2.182	0.282	1.685	0.263
DG28-C3c.d	136.220	19.877	3.1	14.734	1.571	7.548	1.389	3.294	0.382	2.099	0.317
FBA711B-SCH2-10.d	284.950	46.982	6.3	43.507	4.809	42.117	8.215	35.028	5.671	57.268	7.409
FBA711B-SCH2-11.d	65.191	14.345	2.1	14.053	2.038	19.933	4.295	19.919	3.322	35.028	4.545
FBA711B-SCH2-2.d	151.093	35.306	4.9	34.611	4.851	46.426	9.577	41.700	6.755	69.917	8.868
FBA711B-SCH2-3.d	61.438	10.717	2.2	11.301	1.404	14.512	3.280	16.499	2.794	30.288	4.101
FBA711B-SCH2-4.d	118.984	22.963	4.3	22.629	2.873	27.439	5.824	26.368	4.281	45.592	5.894
FBA711B-SCH2-5.d	73.114	15.485	2.8	15.665	2.132	20.572	4.392	20.614	3.447	36.140	4.782
FBA711B-SCH2-6.d	0.931	0.467	0.1	0.655	0.170	2.711	0.721	3.948	0.667	6.130	0.753
FBA711B-SCH2-7.d	37.391	7.923	1.8	7.701	1.175	12.913	2.962	14.970	2.665	29.204	3.864
FBA711B-SCH2-8.d	14.039	4.170	0.5	4.962	0.848	9.035	2.071	10.022	1.654	16.124	2.071
FBA711B-SCH2-9.d	105.362	33.847	2.8	31.372	4.796	43.354	7.534	28.717	4.545	45.314	4.948
FBA711B-SCH3-1.d	444.800	165.549	4.0	165.132	22.045	180.005	29.176	94.937	11.634	93.408	9.077
FBA711B-SCH3-2.d	187.650	68.249	3.0	65.330	9.341	81.593	13.678	48.789	6.728	61.716	6.519
FBA712B-SCH2-1.d	64.218	21.142	1.8	19.947	2.940	26.924	4.615	18.404	2.880	30.441	3.461
FBA712B-SCH2-2.d	235.049	83.678	3.2	78.396	11.051	94.520	15.610	55.183	7.548	67.971	7.172
FBA712B-SCH2-3.d	106.196	34.194	2.8	32.373	4.907	44.619	7.756	30.288	4.712	47.538	5.240
FBA712B-SCH2-4.d	106.474	36.766	2.3	35.431	5.282	47.538	8.076	30.566	4.406	43.090	4.615
FBA712B-SCH2-6.d	92.018	41.561	2.6	46.982	7.673	69.222	12.037	44.202	6.436	60.882	6.408
FBA712B-SCH2-7.d	131.494	49.345	3.6	46.565	7.047	62.550	10.814	40.310	5.880	56.434	5.949
FBA712B-SCH2-8.d	165.688	53.793	3.1	49.762	7.478	67.276	11.329	43.229	6.311	62.133	6.700
FBA712B-SCH2-9.d	183.202	56.851	4.2	51.152	7.589	68.249	11.620	43.507	6.464	62.828	6.616
FBA712B-SCH3-1.d	175.696	59.770	3.6	56.017	7.923	69.778	11.593	41.978	5.921	56.712	6.033
FBA712B-SCH3-3.d	127.880	35.723	3.4	40.727	6.450	61.716	12.441	52.820	8.215	82.566	9.730
FBA712B-SCH3-4.d	372.381	74.226	3.2	71.724	11.134	112.034	23.269	110.644	20.405	233.798	29.343
FBA712B-SCH3-5.d	151.232	37.947	2.7	40.171	5.755	57.129	12.163	58.380	10.842	127.463	16.902
FBA712B-SCH3-7.d	19.738	10.105	1.0	15.123	2.961	33.360	7.993	40.129	7.061	77.840	10.105
FBA712B-SCH3-8.d	244.640	63.523	2.7	68.527	11.120	110.783	23.769	109.810	19.877	223.790	30.024
FBA713A-SCH2-1.d	29.816	15.512	2.0	22.421	3.864	39.490	8.701	39.351	6.616	69.917	8.618
FBA713A-SCH2-2.d	515.690	127.602	4.5	128.714	19.043	191.820	40.032	180.700	30.580	350.280	44.897
FBA713A-SCH2-3.d	178.198	45.036	1.9	43.090	6.088	55.044	11.217	50.318	8.813	97.578	12.927

Appendix 2.4B (continued)

Point ID	Nd (ppm)	Sm (ppm)	Eu (ppm)	Gd (ppm)	Tb (ppm)	Dy (ppm)	Ho (ppm)	Er (ppm)	Tm (ppm)	Yb (ppm)	Lu (ppm)
FBA713A-SCH2-4.d	191.542	43.507	2.4	43.563	5.977	54.488	11.009	48.094	8.312	87.987	11.259
FBA713A-SCH2-5.d	148.869	34.055	2.5	35.473	5.393	52.264	11.356	55.044	10.439	118.150	16.068
FBA713A-SCH3-1.d	198.492	35.667	2.7	31.317	5.032	51.430	11.885	59.770	11.593	132.745	18.167
FBA713A-SCH3-2.d	245.474	50.596	3.4	49.484	7.298	71.168	15.888	76.450	14.317	160.545	22.004
FBA713A-SCH3-3.d	493.450	95.076	4.0	86.319	12.538	115.648	25.215	112.312	18.654	189.318	24.714
FBA713A-SCH3-4.d	879.870	187.094	5.1	169.858	22.796	189.040	36.279	144.143	22.379	218.230	27.661
FBA713A-SCH3-5.d	118.289	24.673	2.7	24.464	3.875	39.115	9.244	48.094	9.786	108.559	14.998
FBA713A-SCH3-6.d	138.444	32.637	2.5	31.928	4.921	45.161	10.217	49.484	9.744	111.756	15.985
FBA713A-SCH3-7.d	182.785	43.507	3.0	42.673	6.005	52.125	10.939	46.843	8.354	97.161	14.470
FBA713B-SCH2-1.d	116.343	26.813	2.6	25.965	3.767	33.763	7.159	32.262	6.297	75.616	11.551
FBA713B-SCH2-2.d	177.781	42.395	2.9	43.368	6.227	55.739	12.065	54.210	9.980	109.949	15.207
FBA713B-SCH2-3.d	125.100	26.980	2.6	26.354	4.309	42.395	10.036	51.152	10.161	115.926	16.221
FBA713B-SCH2-4.d	133.162	30.594	2.7	29.885	4.698	45.036	10.230	50.735	10.203	116.482	16.402
FBA713B-SCH2-5.d	102.165	21.337	2.6	21.072	3.506	35.681	8.743	46.982	9.730	111.478	15.777
FBEOZ1A-1.d	239.775	69.778	3.3	74.087	10.731	89.933	18.153	71.724	11.676	119.679	16.458
FBEOZ1A-2.d	181.673	54.905	3.2	57.685	8.757	75.060	15.554	63.801	10.536	109.532	15.137
FBEOZ1A-3.d	203.357	46.982	2.3	46.148	6.408	54.349	11.982	51.152	8.382	83.400	11.565
FBEOZ1A-4.d	5.338	3.294	0.4	6.033	1.377	17.778	5.421	30.024	5.949	63.384	8.743
FBEOZ1A-5.d	222.678	53.376	4.7	50.527	7.159	59.492	12.302	48.483	7.589	73.114	10.453
FBEOZ1A-6.d	270.077	65.330	5.0	62.550	8.479	68.110	13.844	53.098	8.048	76.450	10.842
FBEOZ1A-7.d	261.181	70.890	5.4	68.805	9.480	74.782	14.706	54.627	7.923	68.666	9.494
FBEOZ1B-1.d	190.708	51.152	6.3	49.164	6.589	49.623	9.702	33.791	4.643	38.322	5.032
FBEOZ1B-2.d	55.322	12.635	2.6	13.275	1.831	15.763	3.308	14.762	3.030	39.115	6.658
FBEOZ1B-3.d	15.999	9.813	2.3	17.222	2.851	23.686	4.796	17.695	2.389	18.737	2.291
FBEOZ1B-4.d	193.627	40.171	4.1	38.295	6.172	57.268	13.719	64.357	11.746	120.652	17.584
FBEOZ1B-5.d	18.209	10.286	2.5	16.889	2.572	18.960	3.267	10.814	1.351	10.189	1.261
FBK71A-1.d	171.109	48.511	6.8	46.148	6.352	47.677	9.021	31.219	4.406	37.447	4.823
FBK71A-2.d	112.590	35.028	4.6	34.611	4.851	36.696	7.131	24.742	3.503	30.580	3.962
FBK71A-3.d	85.207	18.543	2.8	17.681	2.513	19.863	4.212	17.194	2.918	33.040	5.477
FBK71A-4.d	13.886	7.965	2.1	14.067	2.109	15.095	2.662	8.410	0.991	6.978	0.796
FBK71A-5.d	383.640	86.875	5.4	81.454	12.079	102.304	23.630	100.914	16.555	158.877	22.796
FBK71A-6.d	514.300	112.451	6.7	103.277	15.304	127.046	29.176	123.015	19.808	182.924	26.229
FBK7A-SCH3-2.d	156.236	41.005	5.8	38.614	5.491	41.867	8.701	32.401	4.768	41.519	5.671
FK11-1-C1a.d	59.075	15.540	8.7	16.346	2.353	13.844	3.054	9.007	1.379	8.674	1.052
FK11-1-C1b.d	118.567	25.090	18.1	22.407	3.447	21.462	4.948	16.110	2.836	20.530	2.370

Appendix 2.4B (continued)

Point ID	Nd (ppm)	Sm (ppm)	Eu (ppm)	Gd (ppm)	Tb (ppm)	Dy (ppm)	Ho (ppm)	Er (ppm)	Tm (ppm)	Yb (ppm)	Lu (ppm)
FK11-1-C1c.d	138.861	38.712	19.0	38.350	5.838	34.111	7.770	22.615	3.486	21.615	2.230
FK11-1-C2a.d	40.616	15.790	8.0	20.461	3.004	17.889	4.017	11.593	1.628	8.173	0.662
FK11-1-C2b.d	76.450	31.136	9.9	44.619	6.922	39.309	8.507	21.823	2.952	16.527	1.667
FK11-1-C2c.d	75.338	31.428	6.9	41.700	5.824	32.387	6.867	17.764	2.307	10.731	0.958
FK11-1-C2d.d	32.470	10.217	8.2	11.120	1.522	8.298	1.540	3.864	0.528	2.822	0.228
FK11-1-C2e.d	40.032	13.858	6.3	17.736	2.509	14.261	2.940	7.715	1.041	4.893	0.449
FK11-1-C2f.d	158.460	50.179	21.1	51.986	6.936	35.862	6.700	15.415	1.956	9.966	0.865
FK11-1-C2g.d	29.134	11.940	3.0	15.902	2.221	12.190	2.624	6.992	0.812	3.989	0.334
FK13-1-L1.d	146.089	31.164	16.2	25.173	2.540	11.190	1.986	4.323	0.459	2.697	0.441
FK13-1-L1.d	200.438	67.137	18.5	67.276	8.535	41.422	7.631	17.250	1.900	9.827	1.373
FK15-L1.d	151.232	32.971	10.4	25.437	3.296	16.207	2.905	7.006	0.890	5.504	0.929
FK15-L2.d	176.113	31.386	15.1	22.532	2.925	15.012	2.863	7.339	1.086	7.826	1.501
FK15-L2.d	214.199	44.897	14.9	37.113	4.657	24.645	4.337	10.620	1.361	9.313	1.660
FK15-L3.d	176.669	31.039	15.6	21.934	2.776	14.484	2.737	7.298	1.045	7.742	1.519
FK15-L3.d	197.658	43.090	13.9	34.319	4.587	22.657	4.017	10.078	1.295	8.827	1.501
FK15-L4.d	176.669	31.122	15.5	21.684	2.843	14.651	2.772	7.311	1.074	7.993	1.519
FK15-L5.d	161.657	28.370	15.1	20.683	2.665	13.747	2.588	6.839	0.998	7.159	1.407
FK13-1-L2.d	53.793	10.689	8.2	8.813	0.942	4.365	0.827	1.968	0.232	1.387	0.249
FK13-1-L3.d	57.129	11.148	8.2	9.202	0.966	4.545	0.870	2.017	0.248	1.453	0.272
FK13-1-L4.d	111.478	19.947	20.3	15.373	1.697	8.354	1.622	4.212	0.532	3.410	0.610
FK13-1-L5.d	130.521	24.047	21.2	18.946	2.052	9.869	1.914	4.694	0.589	3.693	0.645
FK13-1-L6.d	132.189	25.159	20.8	20.155	2.082	9.897	1.924	4.675	0.581	3.558	0.600
FK12-1.d	164.020	71.585	12.6	85.485	13.344	78.118	16.819	46.009	6.505	40.449	4.559
FK12-2.d	94.798	44.758	12.5	58.241	9.800	61.994	13.580	38.642	5.574	32.943	3.628
FK12-3.d	63.940	24.603	8.4	29.607	4.879	30.719	6.491	18.209	2.683	17.014	1.946
FK12-4.d	23.491	8.785	4.4	9.994	1.553	9.396	1.932	5.908	0.959	6.811	0.862
FK12-5.d	44.480	17.625	12.4	21.684	3.962	25.868	5.935	18.014	2.774	16.861	1.847
FK12-6.d	52.125	21.017	9.3	25.270	4.796	31.873	7.395	23.978	4.119	30.608	3.611
FK12-7.d	45.814	17.125	7.3	19.724	3.207	19.432	3.996	11.412	1.817	11.982	1.326
FK12-8.d	133.579	49.067	16.4	55.183	9.522	60.743	13.441	39.754	6.060	38.781	4.476
FK12-9.d	118.289	45.286	18.2	51.708	8.952	57.546	12.482	37.572	6.213	43.590	4.879
Gil-C1.d	17.306	7.367	8.2	14.206	2.350	15.276	3.874	10.786	1.180	5.755	0.794
G25-C1a.d	24.881	10.230	4.3	15.068	2.117	10.731	2.344	5.157	0.552	2.196	0.252
G25-C1b.d	37.989	14.539	6.7	22.157	3.098	17.361	4.049	10.064	1.026	5.435	0.642
G25-C2b.d	23.185	10.286	7.4	19.363	2.918	18.001	4.267	11.662	1.241	6.116	0.765

Appendix 2.4B (continued)

Point ID	Nd (ppm)	Sm (ppm)	Eu (ppm)	Gd (ppm)	Tb (ppm)	Dy (ppm)	Ho (ppm)	Er (ppm)	Tm (ppm)	Yb (ppm)	Lu (ppm)
G25-C1c.d	21.962	8.062	5.1	13.219	1.904	11.329	2.741	7.298	0.823	4.448	0.596
G25-C3a.d	35.473	13.344	6.7	21.615	2.851	16.152	3.713	9.369	1.015	5.324	0.644
G25-C3b.d	26.549	8.465	6.2	10.161	1.247	6.297	1.354	3.433	0.396	2.168	0.281
G25-C4.d	21.350	8.271	5.8	13.956	2.028	12.510	2.868	7.798	0.855	4.212	0.571
G25-C1a.d	18.723	8.006	7.5	14.817	2.341	14.150	3.443	9.091	0.984	5.199	0.684
G25-C1a.d	11.120	4.184	3.9	7.020	1.133	6.700	1.612	4.198	0.491	2.752	0.395
G25-C2a.d	35.570	15.568	5.7	25.673	3.924	23.394	5.365	13.080	1.357	6.074	0.607
G22-L1.d	4.045	1.974	1.2	3.975	0.848	6.547	1.826	5.268	0.609	3.169	0.341
G22-L1.d	36.613	18.501	5.3	35.945	7.197	51.347	12.454	33.388	3.474	13.789	0.891
G22-L2.d	34.472	17.278	4.7	32.248	6.589	46.148	11.551	29.927	3.114	12.760	0.877
G22-L2.d	39.559	20.308	5.6	38.920	8.104	58.519	14.109	36.001	3.823	15.026	1.074
G22-L3.d	40.699	20.238	5.7	39.281	8.090	57.338	13.608	34.430	3.524	13.566	0.941
G23-L1.d	38.003	19.001	5.5	34.986	6.728	45.662	10.550	25.771	2.630	9.605	0.638
G23-L1.d	41.700	20.947	6.2	39.337	7.826	52.264	11.509	27.077	2.690	9.925	0.642
G23-L2.d	51.986	24.812	7.0	45.870	9.174	64.913	15.360	39.226	3.906	12.913	0.631
G23-L2.d	46.982	22.866	6.8	43.021	8.868	63.384	15.360	40.060	3.878	12.441	0.532
G22-L4.d	4.462	2.057	1.1	4.114	0.898	6.755	1.769	4.893	0.559	2.690	0.311
G23-L3.d	44.758	22.643	6.7	42.854	8.590	56.990	12.232	28.259	2.705	9.841	0.701
G23-L3.d	24.242	9.800	2.9	12.635	1.888	10.161	1.903	4.114	0.450	1.970	0.217
SCH31-1.d	0.129	0.038	0.0	0.053	0.007	0.075	0.016	0.072	0.008	0.079	0.007
SCH31-2.d	0.124	0.038	0.0	0.053	0.022	0.074	0.015	0.068	0.008	0.082	0.139
SCH31-3.d	0.150	0.039	0.0	0.063	0.009	0.111	0.019	0.067	0.009	0.065	0.009
SCH31-4.d	0.120	0.038	0.0	0.061	0.009	0.081	0.017	0.060	0.007	0.060	0.009
SCH31-5.d	0.264	0.095	0.1	0.101	0.014	0.153	0.036	0.146	0.016	0.152	0.021
SCH31-6.d	0.088	0.036	0.0	0.057	0.032	0.097	0.028	0.104	0.011	0.114	0.011
SCH31-7.d	1.159	0.156	0.0	0.310	0.036	0.221	0.044	0.160	0.021	0.122	0.017
SCH31-8.d	0.224	0.060	0.0	0.074	0.016	0.092	0.021	0.085	0.010	0.072	0.008
SCH31-9.d	0.413	0.120	0.0	0.114	0.042	0.213	0.061	0.192	0.030	0.243	0.031
SCH31-10.d	0.741	0.157	0.0	0.209	0.023	0.164	0.040	0.147	0.017	0.114	0.018
SCH31-11.d	0.350	0.111	0.0	0.120	0.018	0.126	0.032	0.117	0.012	0.115	0.014
SCH11-1.d	28.995	4.073	0.4	3.197	0.317	1.868	0.264	0.585	0.045	0.220	0.016
SCH11-2.d	35.806	4.643	0.6	3.433	0.325	1.949	0.307	0.617	0.055	0.281	0.017
SCH11-3.d	32.637	4.504	0.4	3.419	0.321	1.839	0.307	0.616	0.043	0.231	0.015
SCH11-4.d	58.936	12.135	1.3	8.813	0.705	3.461	0.430	0.834	0.056	0.342	0.026
SCH11-5.d	61.577	12.260	1.3	8.632	0.662	3.072	0.368	0.721	0.058	0.247	0.015

Appendix 2.4B (continued)

Point ID	Nd (ppm)	Sm (ppm)	Eu (ppm)	Gd (ppm)	Tb (ppm)	Dy (ppm)	Ho (ppm)	Er (ppm)	Tm (ppm)	Yb (ppm)	Lu (ppm)
SCH11-6.d	63.523	13.747	1.6	9.244	0.738	3.795	0.477	0.934	0.072	0.300	0.025
SCH11-7.d	52.403	11.468	1.3	8.090	0.645	3.308	0.378	0.785	0.059	0.277	0.023
SCH11-8.d	78.952	15.999	1.9	10.397	0.788	3.878	0.425	0.808	0.051	0.220	0.014
SCH11-9.d	44.063	10.022	1.2	7.895	0.646	3.239	0.391	0.809	0.059	0.260	0.044
SCH11-10.d	44.480	9.132	0.9	7.659	0.677	3.586	0.436	0.923	<DL	0.379	0.040
SCH11-11.d	42.117	8.771	0.9	7.381	0.659	3.322	0.416	0.920	<DL	0.384	0.027
SCH11-12.d	53.793	11.634	1.5	9.202	0.842	4.462	0.545	1.116	0.085	0.556	0.017
INV-1-RIM1.d	104.250	23.032	6.4	13.580	1.458	8.159	1.147	2.433	0.210	1.034	0.089
INV-1-RIM2.d	77.006	17.695	2.8	9.230	0.717	3.155	0.373	0.741	0.055	0.345	0.042
INV-1-RIM3.d	55.739	15.638	2.5	8.660	0.714	3.419	0.407	0.898	0.078	0.448	0.048
INV-1-RIM4.d	190.708	40.727	10.8	25.507	2.617	14.526	1.953	4.392	0.388	1.881	0.161
INV-1-RIM5.d	95.910	28.620	3.3	28.731	3.522	22.462	3.688	9.897	0.887	4.670	0.414
INV-1-1.d	275.915	44.466	14.9	20.836	1.831	9.716	1.284	3.350	0.327	1.693	0.177
INV-1-2.d	272.440	43.910	15.3	20.475	1.726	9.535	1.268	3.289	0.295	1.604	0.163
INV-1-3.d	259.374	40.741	14.6	19.377	1.572	8.562	1.090	2.905	0.253	1.529	0.139
INV-1-4.d	97.995	15.568	5.3	8.020	0.673	3.392	0.463	1.118	0.095	0.532	0.043
INV-1-5.d	133.996	24.172	8.0	12.885	1.245	7.284	0.999	2.640	0.242	1.302	0.129
INV-1-6.d	115.509	19.349	6.3	10.369	0.934	5.310	0.742	1.804	0.156	0.833	0.073
INV-1-7.d	131.355	22.740	8.0	11.023	0.995	5.504	0.763	1.889	0.174	1.033	0.097
M61-1.d	32.401	8.757	8.0	6.672	1.219	6.825	1.081	2.577	0.521	3.364	0.374
M61-2.d	45.175	8.618	15.3	7.645	1.159	6.505	1.074	2.724	0.467	3.503	0.416
M61-3.d	88.821	18.376	14.9	17.139	3.225	21.086	3.614	9.952	1.767	12.524	1.441
M61-4.d	45.870	10.425	6.3	8.604	1.290	6.519	1.049	2.409	0.332	2.057	0.202
M61-5.d	86.458	22.560	13.4	16.652	2.619	12.691	1.736	3.670	0.478	2.572	0.235
M61A-C1-1.d	170.970	32.526	10.4	20.016	3.128	15.777	2.059	4.740	0.716	4.253	0.357
M61A-C2-1.d	323.870	79.508	13.2	53.098	8.785	43.229	5.782	12.037	1.551	<DL	0.798
M62-1.d	0.688	0.117	0.0	0.107	0.009	0.049	0.011	0.009		<DL	0.005
M62-2.d	0.416	0.074	0.0	0.040	0.003	0.074	<DL	<DL	<DL	<DL	<DL
M62A-1.d	13.414	1.012	0.3	1.015	0.064	0.265	0.035	0.075	0.013	0.093	0.012
M62A-2.d	3.781	0.353	0.1	0.245	0.017	0.043	0.005	0.010	<DL	<DL	0.002
KH61A-1.d	170.831	42.534	23.3	52.125	10.328	73.531	16.944	50.179	7.701	49.623	6.102
KH61A-2.d	146.367	54.071	11.2	81.593	14.456	91.323	18.709	44.619	4.740	20.391	2.195
KH61A-3.d	56.948	15.387	12.5	20.586	4.087	29.051	6.380	17.500	2.382	13.469	1.743
KH61A-4.d	54.488	12.538	18.8	18.723	4.351	37.169	9.383	31.456	5.435	38.920	5.254
KH61A-5.d	102.443	43.646	18.1	101.609	23.825	194.878	49.067	135.386	15.749	76.172	8.020

Appendix 2.4B (continued)

Point ID	Nd (ppm)	Sm (ppm)	Eu (ppm)	Gd (ppm)	Tb (ppm)	Dy (ppm)	Ho (ppm)	Er (ppm)	Tm (ppm)	Yb (ppm)	Lu (ppm)
KH61A-6.d	263.405	89.099	11.9	141.363	28.078	205.720	49.623	131.216	15.429	73.114	8.104
KH61A-7.d	193.071	60.465	14.6	83.400	16.166	111.478	23.561	59.075	7.145	40.171	3.962
KH61A-8.d	23.074	4.420	11.1	4.657	1.001	7.256	1.707	5.796	1.161	9.577	1.372
KH61A-9.d	283.560	74.087	13.6	103.138	20.794	156.097	38.503	111.200	14.428	76.589	8.966
KH61A-10.d	214.199	67.832	10.3	100.358	19.113	139.417	32.943	93.130	11.676	61.438	7.159
KH61A-11.d	47.121	13.956	17.8	26.521	6.658	57.546	14.845	48.650	7.589	47.399	5.935
KH61A-12.d	140.251	48.650	17.2	96.466	20.906	165.132	42.645	119.540	13.803	65.191	7.631
SCH17-1.d	1.460	0.787	0.4	1.391	0.203	1.469	0.263	0.960	0.101	0.602	0.046
SCH17-2.d	3.962	1.932	0.7	3.558	0.552	5.046	0.902	2.537	0.153	0.518	0.025
SCH17-3.d	9.132	4.670	0.4	8.451	1.079	8.882	1.471	3.675	0.253	0.851	0.032
SCH17-4.d	2.266	1.390	0.1	2.307	0.317	2.780	0.449	1.175	0.077	0.373	0.014
SCH17-5.d	1.357	0.974	0.4	2.113	0.324	2.879	0.513	1.870	0.217	1.362	0.123
SCH17-6.d	7.159	4.101	0.5	7.339	1.011	8.006	1.371	3.545	0.257	0.873	0.042
SCH17-7.d	1.074	0.673	0.5	1.501	0.253	2.180	0.435	1.685	0.202	1.237	0.106
SCH17-8.d	1.334	0.471	0.1	0.870	0.107	0.892	0.132	0.318	0.027	0.097	0.012
SCH17-9.d	0.271	0.165	0.0	0.379	0.050	0.423	0.067	0.204	0.023	0.136	0.012
SCH17-10.d	1.172	0.888	0.3	2.113	0.314	2.836	0.425	1.163	0.082	0.361	0.035
SCH17-11.d	2.502	1.529	0.6	2.905	0.488	4.601	0.816	2.174	0.145	0.402	0.021
SCH17-12.d	1.932	1.287	0.4	2.766	0.386	3.545	0.560	1.447	0.112	0.518	0.040
SCH16-2.d	0.778	0.281	0.1	0.959	0.064	0.673	0.142	0.610	0.081	0.548	0.051
SCH16-3.d	0.182	0.131	0.0	0.259	0.057	0.657	0.174	0.748	0.090	0.714	0.063
SCH16-6.d	1.293	0.320	0.0	0.320	0.027	0.406	0.081	0.445	0.050	0.482	0.039
LT-L1.d	581.020	244.362	14.4	280.363	46.926	255.065	45.481	101.470	11.607	59.353	6.978
LT-L2.d	590.750	256.733	14.7	294.958	50.290	276.749	49.081	111.478	12.858	66.025	7.715
LT-L3.d	578.101	255.899	14.7	295.931	50.624	278.417	49.345	111.200	12.816	66.998	7.867
LT-L4.d	497.620	212.253	12.5	237.690	40.713	222.122	39.504	88.821	10.453	54.210	6.311
LT-L5.d	511.520	214.894	12.6	237.134	40.866	223.929	39.476	88.682	10.356	54.071	6.352
LT-L6.d	701.950	314.557	13.5	325.677	54.071	282.309	47.121	103.833	12.371	66.581	7.701
LT-L7.d	664.698	274.247	16.2	308.997	52.167	281.892	50.346	112.451	12.844	66.595	7.687
LT2-1.d	628.280	251.868	10.3	278.695	43.868	224.485	38.559	87.570	10.634	60.465	7.770
LT2-2.d	650.520	322.480	11.2	398.930	61.021	304.410	50.179	107.447	12.232	64.079	7.826
LT2-3.d	711.680	334.990	10.9	406.297	62.550	321.646	53.237	114.675	13.177	71.307	8.632
LT2-4.d	628.280	247.003	10.5	272.301	41.825	217.535	37.044	83.122	10.022	56.712	7.089
LT2-5.d	550.162	221.705	11.8	251.451	38.475	196.824	33.332	74.782	8.827	49.581	6.297
LT2-6.d	449.248	182.507	9.1	211.280	33.652	174.445	30.010	68.388	8.062	44.480	5.616

Appendix 2.4B (continued)

Point ID	Nd (ppm)	Sm (ppm)	Eu (ppm)	Gd (ppm)	Tb (ppm)	Dy (ppm)	Ho (ppm)	Er (ppm)	Tm (ppm)	Yb (ppm)	Lu (ppm)
MCW3-1-1.d	18.835	13.024	2.1	36.835	12.315	141.919	30.219	133.996	24.728	239.914	26.855
MCW3-1-2.d	164.576	37.558	1.3	50.318	12.691	129.548	25.562	103.972	17.000	154.568	17.764
MCW3-1-3.d	13.928	23.005	0.9	63.523	20.141	210.446	39.559	143.726	20.781	161.935	15.846
MCW3-1-4.d	270.772	72.141	1.7	96.605	21.823	188.762	30.997	103.972	14.609	114.536	11.746
MCW3-1-5.d	16.055	9.744	0.5	23.005	7.895	85.346	16.750	67.832	11.301	98.412	9.619
MCW3-1.d	7.923	9.633	0.4	27.439	9.758	112.173	24.047	109.115	21.906	234.771	27.786
MCW3-2.d	6.394	11.301	0.9	35.167	12.315	140.946	30.135	134.691	25.812	264.795	30.719
MCW3-3.d	20.252	14.442	0.6	31.692	10.022	104.945	19.571	74.504	11.634	95.076	9.160
MCW3-4.d	13.483	11.176	0.4	26.424	8.479	87.292	17.153	71.724	13.580	150.259	19.043
MCW3-5.d	8.076	16.291	0.9	42.534	14.706	157.348	31.358	127.046	21.100	182.090	18.112
MCW2-D-2.d	31.831	51.013	0.4	114.536	34.069	313.584	51.152	154.290	17.458	108.837	8.757
MCW2-D-4.d	21.698	27.383	0.9	59.909	19.015	198.214	38.308	153.873	26.730	256.455	28.856
MCW2-D-5.d	158.043	76.450	2.4	95.215	22.935	205.303	35.723	129.409	20.294	173.750	17.792
MCW2-D-6.d	37.655	36.376	0.3	70.612	20.808	198.492	32.874	104.806	12.649	77.701	6.255
MCW2-D-7.d	3.336	1.751	0.1	4.629	1.853	24.117	5.810	34.055	10.078	170.136	26.688
NP1-C4-L1.d	44.563	23.839	8.7	39.976	8.062	54.766	11.871	31.748	4.201	25.048	3.065
NP1-C4-L2.d	28.217	17.375	7.1	31.317	6.616	46.287	10.105	27.147	3.725	22.018	2.697
NP1-C4-L3.d	33.610	20.350	7.7	38.586	8.271	58.936	12.663	33.457	4.379	24.964	2.940
NP1-C1-L1.d	42.395	23.060	8.2	39.337	7.854	52.403	11.509	30.775	3.962	24.130	2.973
NP1-C1-L1.d	25.729	12.343	4.5	20.308	4.253	28.384	6.213	16.958	2.369	13.970	1.800
NP1-0.d	26.549	16.402	9.8	31.553	6.283	41.978	8.910	22.754	2.891	15.568	1.890
NP1-C2a.d	44.619	20.711	8.6	35.445	6.811	45.592	9.772	25.381	3.350	19.543	2.431
NP1-C2b.d	48.511	25.256	9.3	42.673	8.576	57.824	12.774	33.708	4.531	26.174	3.232
NP1-C2c.d	44.202	22.991	8.8	39.226	8.173	55.739	12.176	31.984	4.323	25.229	3.086
NP1-1-L1.d	21.489	14.331	7.6	30.497	7.242	55.878	13.149	35.862	4.601	25.312	3.146
NP1-1-L2.d	22.907	14.790	7.6	30.928	7.256	55.600	13.136	35.654	4.462	24.700	3.030
NP1-1-L3.d	21.295	14.136	6.7	30.955	7.478	58.102	13.580	37.502	4.865	26.938	3.328
NP1-2-L1.d	25.910	16.736	8.1	33.221	8.034	61.716	14.943	41.144	5.268	29.329	3.670
NP1-2-L1.d	56.851	38.225	8.5	76.589	16.889	118.289	25.159	65.330	8.006	43.646	5.171
NP1-2-L2.d	57.963	38.503	8.4	78.674	17.014	118.150	25.159	64.496	7.993	41.839	4.921
NP1-2-L2.d	53.376	24.283	8.7	40.866	8.423	57.407	12.566	32.234	4.142	23.380	2.734
NP1-2-L3.d	58.658	38.642	8.2	77.840	17.083	119.540	25.854	65.052	7.909	42.534	4.990
NP1-2-L3.d	40.171	19.669	7.0	33.916	6.797	45.731	10.022	26.549	3.322	18.334	2.307
NP1-2-L4.d	79.786	40.866	18.8	65.052	14.122	96.466	19.599	51.152	7.103	39.476	4.184
SCH19-1.d	369.740	115.648	4.2	114.258	15.790	108.559	18.682	55.461	6.700	43.090	4.365

Appendix 2.4B (continued)

Point ID	Nd (ppm)	Sm (ppm)	Eu (ppm)	Gd (ppm)	Tb (ppm)	Dy (ppm)	Ho (ppm)	Er (ppm)	Tm (ppm)	Yb (ppm)	Lu (ppm)
SCH19-2.d	487.890	157.765	4.7	155.402	22.268	154.568	26.619	79.508	9.716	63.801	6.742
SCH19-3.d	508.740	208.917	4.8	239.497	37.961	277.722	48.511	144.421	17.736	118.706	12.844
SCH19-4.d	202.106	61.021	2.4	62.272	8.896	62.411	11.329	34.750	4.281	28.398	3.304
SCH19-5.d	336.519	83.956	4.2	79.647	10.397	68.527	11.787	35.084	4.337	29.551	3.230
SCH19-7.d	500.400	226.709	4.4	286.062	44.619	319.700	56.990	167.495	19.863	132.884	14.984
SCH19-8.d	394.760	111.478	5.6	97.022	13.622	94.381	16.388	51.291	6.755	47.399	5.226
SCH19-9.d	330.125	113.980	4.8	120.791	18.779	136.359	24.019	74.365	9.758	71.446	8.368
SCH20-1.d	114.675	28.106	2.2	26.771	3.472	25.090	4.281	13.455	1.701	12.774	1.357
SCH20-2.d	424.784	83.678	12.5	61.994	8.173	61.299	10.703	38.684	5.352	39.198	3.372
SCH20-3.d	222.817	39.490	10.3	36.057	4.177	30.302	5.352	18.445	2.521	17.667	1.628
SCH20-4.d	200.855	36.265	9.2	28.231	3.543	26.354	4.670	16.722	2.325	17.125	1.565
SCH20-5.d	264.656	51.569	8.5	38.475	5.087	37.808	6.728	24.283	3.328	24.520	2.177
SCH20-7.d	275.637	58.797	6.8	47.677	6.102	45.314	7.993	27.494	3.715	26.480	2.456
SCH20-8.d	371.130	84.790	7.5	65.747	8.827	64.774	11.273	39.615	5.463	41.839	4.059
SCH20-9.d	119.540	22.615	3.7	19.877	2.348	16.555	2.823	9.647	1.282	9.716	0.972
SCH20-10.d	109.810	22.518	3.1	20.767	2.777	20.141	3.531	12.037	1.547	11.634	1.183
SCH20-11.d	140.946	28.592	2.9	25.312	3.026	21.698	3.725	11.996	1.526	10.439	1.029
SCH20-12.d	177.503	34.319	5.0	27.369	3.667	28.384	4.976	18.404	2.754	22.574	2.517
SCH20-13.d	169.302	39.059	3.4	33.958	4.406	32.276	5.560	18.126	2.362	17.611	1.782
SCH21-1.d	61.994	14.873	1.5	13.858	1.904	12.107	2.111	6.380	0.770	4.643	0.438
SCH21-2.d	56.295	9.383	1.8	9.007	0.974	6.074	0.913	2.116	0.161	0.745	0.062
SCH21-3.d	58.936	13.608	2.1	14.192	1.806	12.218	2.071	5.379	0.456	1.557	0.065
SCH21-4.d	130.938	37.113	2.6	38.781	5.685	40.588	7.159	19.599	1.867	7.728	0.374
SCH21-5.d	80.898	23.825	1.8	26.827	3.600	25.187	4.295	11.064	1.026	4.003	0.235
SCH21-6.d	79.230	19.974	1.8	18.014	2.488	17.333	3.169	10.036	1.322	9.091	0.835
SCH21-7.d	28.495	2.474	0.5	2.113	0.157	0.873	0.128	0.289	0.030	0.164	0.011
SCH21-8.d	55.183	12.691	1.4	11.857	1.522	10.314	1.817	5.268	0.605	3.545	0.300
SCH22-A1.d	155.402	44.758	1.9	43.507	5.491	36.418	6.311	17.931	2.110	13.886	1.712
SCH22-A2.d	120.513	35.306	5.7	38.781	5.018	34.194	6.199	16.986	1.749	9.730	1.002
SCH22-A4.d	102.304	25.937	5.0	29.649	4.267	30.121	5.824	19.099	2.877	24.089	2.975
SCH22-A5.d	69.917	18.723	2.3	19.766	2.446	16.527	2.989	9.466	1.195	8.354	0.708
SCH22-A6.d	157.487	39.615	5.6	42.117	5.352	36.140	6.491	18.779	2.156	14.442	1.927
SCH22-B1.d	20.238	1.835	0.1	1.341	0.064	0.250	0.026	0.037	0.003	<DL	0.001
SCH22-B2.d	15.234	1.329	<DL	0.884	0.049	0.154	0.033	0.029	0.006	<DL	0.007
SCH22-B3.d	11.120	0.981	<DL	0.727	0.034	0.129	0.015	0.029	0.003	<DL	0.003

Appendix 2.4B (continued)

Point ID	Nd (ppm)	Sm (ppm)	Eu (ppm)	Gd (ppm)	Tb (ppm)	Dy (ppm)	Ho (ppm)	Er (ppm)	Tm (ppm)	Yb (ppm)	Lu (ppm)
SCH22-B4.d	14.762	1.343	0.1	0.944	0.041	0.108	0.012	0.029	0.004	0.016	0.002
SCH22-B5.d	32.554	1.947	0.2	1.555	0.062	0.133	0.014	0.033	0.002	0.020	<DL
SCH22-B6.d	15.429	0.976	0.1	0.791	0.033	0.070	0.005	0.008	<DL	<DL	<DL
SCH23-B1.d	164.715	27.355	1.2	26.688	2.972	18.723	3.211	8.423	0.902	5.504	0.632
SCH23-B2.d	140.112	47.121	1.8	55.600	7.200	46.426	8.062	21.476	2.220	13.622	1.633
SCH23-B3.d	181.951	68.110	1.9	87.292	11.454	76.311	13.386	35.848	3.767	22.337	2.615
SCH23-B4.d	101.053	23.978	1.2	23.672	2.773	17.167	2.850	7.687	0.826	5.226	0.598
SCH23-B5.d	66.164	17.584	2.1	18.626	2.316	15.679	2.787	7.965	0.919	5.991	0.678
SCH23-C1.d	189.318	53.932	2.6	53.237	7.687	54.071	9.438	28.036	3.571	24.478	2.730
SCH23-C2.d	219.898	77.284	2.3	95.354	12.315	82.705	14.373	38.920	4.073	24.923	2.913
SCH23-C3.d	159.155	41.839	2.6	42.534	5.852	40.171	6.811	19.974	2.478	16.346	1.785
SCH23-C4.d	128.297	34.472	2.0	38.086	4.976	33.402	5.824	16.499	1.739	10.800	1.233
SCH23-C5.d	423.950	99.941	5.8	79.925	10.272	69.083	11.773	35.862	4.823	34.472	3.545
SCH24-1.d	150.815	45.314	3.1	44.619	6.755	48.928	8.604	27.661	3.280	19.043	1.348
SCH24-2.d	80.759	21.295	1.8	21.434	2.982	20.099	3.433	9.869	1.006	4.879	0.291
SCH24-3.d	134.691	33.847	3.6	33.165	4.379	29.760	5.157	14.248	1.350	5.310	0.247
SCH24-4.d	109.254	30.650	1.7	30.413	4.170	28.439	4.976	14.470	1.776	11.217	1.087
SCH24-5.d	117.594	30.344	3.3	30.608	3.974	26.744	4.712	12.802	1.193	4.281	0.175
SCH24-6.d	60.882	12.816	1.2	11.148	1.416	9.410	1.625	4.490	0.485	2.474	0.154
SCH24-7.d	94.937	25.882	2.6	27.661	3.656	25.368	4.323	11.718	1.115	4.851	0.234
SCH24-1A-R.d	161.379	47.816	2.8	46.982	7.006	51.430	9.396	30.719	4.309	33.499	3.934
SCH24-1A-C.d	65.191	15.526	1.8	14.428	1.935	12.899	2.205	5.991	0.616	2.683	0.163
SCH24-2A-R.d	11.537	4.823	0.4	6.255	0.959	6.950	1.223	3.433	0.389	2.544	0.284
SCH24-2A-R1.d	99.385	27.480	2.3	25.576	3.789	28.050	5.060	16.472	2.300	16.360	1.628
SCH25-1.d	32.234	13.302	1.8	16.291	1.911	11.912	2.075	5.769	0.600	3.239	0.329
SCH25-3.d	67.832	27.341	2.3	28.217	2.975	17.292	2.722	5.908	0.449	1.485	0.092
SCH25-4.d	62.133	25.757	2.2	26.132	2.641	14.998	2.335	5.226	0.375	1.305	0.085
SCH25-5B.d	50.735	20.516	1.4	22.560	2.410	15.248	2.521	6.477	0.649	3.350	0.313
SCH25-6B.d	27.036	11.551	1.9	16.861	1.943	12.566	2.267	6.019	0.571	2.891	0.285
SCH26-1.d	79.925	20.391	1.9	20.892	2.786	18.890	3.286	9.257	0.948	4.935	0.364
SCH26-2.d	97.439	24.506	2.4	24.770	3.258	21.823	3.878	11.190	1.150	5.685	0.359
SCH26-3.d	43.229	8.715	0.9	8.618	1.048	6.589	1.136	3.239	0.331	1.889	0.135
SCH26-4.d	19.404	2.572	0.3	2.460	0.265	1.731	0.325	0.966	0.160	0.827	0.090
SCH26-5.d	20.016	2.071	0.3	1.890	0.195	0.992	0.172	0.532	0.073	0.493	0.048
SCH26-6.d	55.044	11.176	1.6	9.744	1.250	8.062	1.426	4.170	0.482	2.572	0.189

Appendix 2.4B (continued)

Point ID	Nd (ppm)	Sm (ppm)	Eu (ppm)	Gd (ppm)	Tb (ppm)	Dy (ppm)	Ho (ppm)	Er (ppm)	Tm (ppm)	Yb (ppm)	Lu (ppm)
SCH26-7.d	43.785	7.993	1.4	7.047	0.881	5.824	1.054	3.114	0.368	1.793	0.120
SCH26-8.d	80.203	15.012	1.33579	13.8861	1.58738	10.7169	1.7653	4.8233	0.5421	2.8217	0.20711
SCH27-C1.d	94.937	17.1109	3.8503	17.1109	2.08083	13.9278	2.58818	8.1176	1.01053	6.1577	0.5421
SCH27-C2.d	48.928	12.4544	1.35108	12.4822	1.46506	9.3825	1.54846	4.1561	0.40727	2.1684	0.18209
SCH27-C3.d	82.566	19.043	2.9329	19.3488	2.47142	17.375	3.14418	9.7856	1.35664	10.9393	1.33996
SCH27-4.d	101.887	24.1443	1.97658	23.769	2.7244	17.8198	3.1136	9.0767	1.08559	6.8527	0.71863
SCH27-5.d	159.711	27.9946	4.2256	26.9382	3.13167	20.4052	3.6696	10.9393	1.38583	8.1871	0.70056
SCH27-6.d	63.384	12.927	1.00497	13.205	1.59989	10.1748	1.74723	4.6426	0.49901	2.6827	0.2363
SD11-C2.d	9.1462	5.6156	3.336	18.8762	4.8233	50.2902	20.8083	76.311	9.8829	58.519	8.1593
SD11-C1b.d	145.394	54.21	10.981	100.497	19.6268	150.954	42.9371	129.687	16.9441	93.408	11.1895
SD11-C1c.d	35.584	15.8321	5.8658	31.97	7.1585	61.438	19.0013	65.052	9.5771	61.438	7.8118
SD11-C1d.d	2.641	1.6958	2.11697	7.0056	1.88345	19.6685	7.6728	25.3536	2.9607	14.2197	1.73194
SD28-sch1.d	82.149	18.5426	3.9337	16.7634	2.2796	12.7324	2.37412	4.0866	0.24742	0.79925	0.051291
SD28-sch1a.d	78.118	21.0724	4.2534	18.9318	2.54926	14.2058	2.88564	6.6581	0.67137	2.5159	0.20016
SD28-sch2.d	69.361	17.1943	6.5747	16.541	2.2796	13.1216	2.62154	6.2411	0.5699	2.0711	0.13066
SD28-sch2a.d	52.264	14.9564	5.56	15.4568	2.13643	12.8158	2.49644	5.3932	0.45731	1.53456	0.12232
SD28-sch2b.d	49.4562	10.9532	5.2125	9.8968	1.32467	7.3809	1.28853	1.97797	0.12371	0.31136	0.015568
SD28-sch3.d	143.726	40.588	6.7554	36.279	4.7399	24.8393	4.8094	11.1617	1.14119	4.5036	0.36279
SD28-sch3a.d	197.519	54.21	8.6736	47.677	6.2689	32.7901	6.6442	16.1657	1.69719	6.811	0.51569
SD28-sch3b.d	59.492	15.9433	5.6434	16.2352	2.24902	12.51	2.57845	5.1847	0.4309	1.52761	0.10981
SD28-sch4.d	50.8879	13.9973	6.255	14.0946	2.01411	11.8428	2.33798	5.0318	0.44897	1.56653	0.09869
SD28-sch4a.d	97.995	26.7575	5.7963	27.4525	3.52504	19.599	3.69879	6.1577	0.36835	0.9035	0.029329
SD28-sch4b.d	123.988	36.557	8.1037	35.7925	4.5036	24.2833	4.9762	11.9401	1.18011	4.5453	0.32526
ITALY-1.d	136.637	50.0817	9.174	62.411	7.8674	55.461	9.8829	28.6201	2.62015	14.4838	1.29965
ITALY-2.d	313.584	115.092	11.9957	131.494	14.8591	93.825	15.1093	39.1007	3.21646	15.0259	1.19957
ITALY-3.d	318.588	111.2	9.6605	128.297	14.0668	88.265	14.1502	36.14	2.85784	12.788	0.95076
ITALY-4.d	254.926	84.373	8.5763	92.018	10.0358	62.55	9.9107	25.02	1.94322	9.0767	0.7228
ITALY-5.d	229.35	77.145	8.2149	85.068	9.3547	57.963	9.2296	23.0184	1.72638	7.8535	0.61299
ITALY-6.d	239.636	82.01	8.2844	91.74	10.2165	64.496	10.147	25.2007	1.88623	8.4095	0.60604
ITALY-7.d	345.832	121.625	8.2983	134.413	14.8174	90.489	13.5386	31.97	2.20454	9.035	0.64079
ITALY-8.d	351.392	120.791	7.7284	136.915	14.9008	91.879	14.2336	33.7909	2.52007	10.4806	0.80759
ITALY-9.d	293.846	89.794	7.8118	94.103	10.1748	64.079	10.0497	24.3667	1.7792	7.6033	0.54349
ITALY-10.d	355.284	118.984	9.2991	128.714	13.9695	85.902	13.1633	32.0673	2.33381	10.0775	0.78257
ITALY-11.d	393.787	128.853	10.0497	136.359	14.8313	91.045	14.1363	34.3469	2.53119	10.8976	0.8479
ITALY-12.d	403.934	130.66	10.0636	140.251	15.4151	96.327	14.6645	36.0149	2.71745	11.8428	0.94937

Appendix 2.4B (continued)

Point ID	Nd (ppm)	Sm (ppm)	Eu (ppm)	Gd (ppm)	Tb (ppm)	Dy (ppm)	Ho (ppm)	Er (ppm)	Tm (ppm)	Yb (ppm)	Lu (ppm)
TSE-1.d	319.7	111.2	6.5469	119.262	23.2686	142.475	27.383	70.195	9.4798	54.905	6.9222
TSE-2.d	333.6	121.069	5.4905	131.077	25.3397	152.622	28.1892	71.724	9.6883	55.044	6.6859
TSE-3.d	393.37	136.081	6.4496	149.425	28.217	170.275	31.831	78.813	10.5501	58.936	7.0056
TSE-4.d	304.549	113.424	10.8698	125.656	25.6177	158.738	29.7738	75.199	10.3138	58.797	7.2558
TSE-5.d	295.792	120.513	7.7006	140.946	30.0935	193.349	37.8497	99.941	14.6228	85.207	10.4111
TSE-6.d	301.63	105.084	5.0735	116.621	22.518	139.139	26.4656	69.778	9.591	54.627	7.0612
TSE-7.d	230.74	86.458	5.2542	99.524	19.9604	126.351	24.4223	62.689	8.2705	45.7588	5.6573
SCH30-1.d	51.986	10.9115	1.8348	9.4659	0.85207	5.977	0.84512	2.7939	0.31136	2.2657	0.21128
SCH30-2.d	70.056	15.9155	2.7661	13.5942	1.23571	8.1037	1.03833	3.0997	0.31275	2.11419	0.19321
SCH30-4.d	116.899	26.271	3.8503	21.8786	2.18647	14.3865	2.00855	5.9214	0.60048	4.0032	0.37808
SCH30-5.d	54.905	15.0954	2.19898	14.5811	1.49842	10.4389	1.5012	4.3785	0.49067	3.5028	0.40171
SCH30-6.d	134.274	23.2964	4.8511	18.0422	1.78893	13.2745	1.99187	7.1863	1.10505	11.9401	1.89596
SCH40-1.d	11.7872	1.9043	0.46843	1.3761	0.12093	0.58658	0.12371	0.27661	0.030302	0.2224	0.028495
SCH40-2.d	1.20374	0.15846	0.63523	0.17514	0.017653	0.04309	0.019043	0.09869	0.019043	0.17931	0.07228
SCH40-3.d	1.3205	0.278	0.83956	0.32109	0.021962	0.19877	0.023074	0.17792	0.026966	0.34055	0.053654
SCH40-4.d	2.9329	0.3336	0.94381	0.33221	0.032526	0.26688	0.044341	0.21962	0.03475	0.37669	0.05838
SCH40-5.d	0.53237	0.09035	0.85207	0.1946	<DL	<DL	<DL	0.10286	0.020572	0.3336	0.038364
SCH40-6.d	2.6271	0.38364	1.0008	0.42673	<DL	0.21267	0.021128	0.28634	0.042812	0.45731	0.039893
SCH40-7.d	1.9877	0.21684	0.92435	0.32387	0.019877	0.18765	0.045175	0.27105	0.07645	0.44202	0.060465
SCH40-8.d	4.2117	0.57546	4.448	0.46843	0.04726	0.30302	0.060187	0.27105	0.025715	0.83539	0.15151
SCH40-9.d	1.58877	0.29468	1.90847	0.26132	<DL	0.2224	0.043368	0.0834	0.034055	0.56851	0.12232
SCH40-10.d	4.5453	0.5282	2.641	0.53098	0.035862	0.45314	0.093964	0.36974	0.081593	0.95354	0.13483
SCH40-11.d	0.60882	0.08062	0.61299	0.1946	0.00417	0.12371	0.025993	0.0973	0.019182	0.24325	0.040449
SCH40-12.d	0.9452	0.4448	0.65052	0.22518	0.04448	0.1668	0.024464	0.14734	0.019321	0.22796	0.03336
SCH44-3.d	3.2109	1.2371	0.28773	1.3205	0.14595	1.01331	0.15429	0.42395	0.028634	0.22796	0.02363
SCH44-4.d	3.2943	0.834	0.17375	0.7367	<DL	0.77284	0.13483	0.3614	0.03753	0.06811	0.032387
SCH44-5.d	1.3761	0.556	0.3614	0.8479	0.10703	0.6394	0.1112	0.34194	0.03614	0.26688	0.017375
SCH44-6.d	1.6263	0.5699	0.14734	0.7506	0.09035	0.64357	0.12232	0.35723	0.028356	0.23074	0.024603
SCH44-7.d	1.251	0.4865	0.17236	0.6394	0.08479	0.57963	0.09869	0.33777	0.03892	0.13622	0.028078
SCH44-8.d	2.7939	1.0147	0.24742	1.0981	0.13761	0.95076	0.16263	0.35028	0.035862	0.18904	0.015707
SCH44-9.d	1.6819	0.38364	0.17375	0.8479	0.09313	0.65052	0.10425	0.28912	0.039476	0.24464	0.015151
YP5B-C3.d	3.0163	0.7506	0.84095	0.7506	0.21684	1.4317	0.33916	0.96744	0.19877	1.9043	0.24742
YP5A-C5a.d	21.267	4.309	2.7383	3.614	0.54905	2.9607	0.53098	1.25656	0.15985	0.94381	0.094103
YP5A-C5b.d	10.842	2.6688	3.058	2.9468	0.59492	4.0588	0.86597	2.363	0.35167	2.1823	0.21406
YP5A-C5b.d	5.1847	1.1676	2.1267	1.3483	0.29468	2.2935	0.47399	1.4595	0.23074	1.4317	0.15568

Appendix 2.4B (continued)

Point ID	Nd (ppm)	Sm (ppm)	Eu (ppm)	Gd (ppm)	Tb (ppm)	Dy (ppm)	Ho (ppm)	Er (ppm)	Tm (ppm)	Yb (ppm)	Lu (ppm)
YP5A-C1a.d	11.676	2.3213	2.085	2.1267	0.34472	2.1684	0.40866	1.16343	0.19182	1.24405	0.14039
YP5A-C1a.d	3.8364	0.8618	2.3769	1.0147	0.20711	1.4317	0.29885	0.96744	0.19182	1.5846	0.21823
YP5A-C1b.d	4.9067	1.05501	2.1823	1.19957	0.25298	1.8209	0.41005	1.23849	0.21823	1.42614	0.16124
YP5A-C3a.d	3.197	0.63801	1.04111	0.60187	0.12371	0.8479	0.16958	0.5004	0.08201	0.55461	0.06116
YP5A-C3a.d	15.2761	3.3221	3.5723	3.4333	0.61855	3.7391	0.7089	1.7097	0.23908	1.4317	0.14317
YP5A-C3b.d	4.7399	1.0981	1.7792	1.2371	0.2641	1.807	0.37808	1.01609	0.15985	0.89099	0.086458
YP5A-C3b.d	13.2189	3.9893	4.031	4.9484	0.97856	6.3801	1.16621	2.8912	0.33916	1.5707	0.14734
YP5A-C1c.d	11.12	2.2518	2.0572	2.0572	0.34333	2.0572	0.41005	1.06891	0.17097	1.04667	0.11537
YP5A-C1d.d	14.039	2.7661	2.8912	2.3074	0.3475	1.9738	0.39893	1.13563	0.2085	1.54985	0.22101
YP5B-C1a.d	4.6982	1.3344	1.3622	1.6819	0.35584	2.5437	0.51013	1.4734	0.27522	2.0711	0.27522
YP5B-C1b.d	1.668	0.4726	0.4448	0.5977	0.12093	0.8757	0.18626	0.55461	0.12649	1.3761	0.25715
YP5B-C3a.d	15.012	3.475	4.4897	4.3646	0.9035	6.811	1.5012	4.4341	0.7367	4.6009	0.53098
YP5B-C2a.d	3.6974	1.1815	1.1815	1.4317	0.29885	2.1406	0.45036	1.2371	0.21823	2.0155	0.30997
ZIV-1.d	26.7992	9.9385	35.5284	12.4683	1.7097	11.8428	1.81812	5.143	0.67276	5.6434	0.62689
ZIV-2.d	265.49	117.316	56.434	150.537	20.4052	125.517	17.097	36.5709	2.57706	9.9107	0.65191
ZIV-3.d	74.643	19.4739	66.581	22.3929	3.63346	29.8155	5.22362	17.2082	2.02106	11.8011	0.92435
ZIV-4.d	239.497	100.358	66.442	132.884	19.4044	131.633	19.5712	45.453	3.41662	14.039	0.92852
ZIV-5.d	244.64	106.335	64.496	148.313	21.5867	145.255	21.3504	49.623	3.82945	15.9572	1.04945
ZIV-6.d	304.827	123.988	55.4749	152.344	20.6693	130.66	18.5287	41.2135	3.14557	13.1772	0.92991
ZIV-7.d	114.397	44.6468	43.5626	55.183	8.1454	55.6139	8.2983	20.6415	1.79449	8.4512	0.59075
ZIV-8.d	230.74	89.099	61.994	120.096	18.4036	130.382	20.6137	51.7636	4.3785	19.2793	1.42058
ZIV-9.d	150.398	54.766	55.5027	66.581	10.0775	70.612	10.5362	26.4239	2.26153	10.2443	0.72697
ZIV-10.d	98.412	34.8612	43.229	43.368	6.4496	45.1472	6.8388	17.6808	1.668	8.0898	0.60604
ZIV-11.d	104.945	47.4268	34.8473	58.102	8.5346	54.627	7.4782	17.0136	1.36081	5.8797	0.3892
ZIV-12.d	286.757	117.455	67.3455	152.9	21.5589	141.502	20.3218	45.9395	3.46944	13.8861	0.91184

Appendix 2.4B (continued)

Point ID	Ta (ppm)	Pb (ppm)	Bi (ppm)	Th (ppm)	U (ppm)	REE	Eu anomaly
Min DL	0.0005	0.002	0.001	0.001	0.001		
Max DL	0.223	0.149	0.129	0.242	0.224		
Cel-L1.d	0.721	3.892	0.054	0.532	0.292	641.570	1.236
Cel-L2.d	0.716	4.045	0.028	0.531	0.264	691.265	1.078
Cel-L3.d	0.653	3.364	0.023	0.548	0.313	610.325	1.443
Cel-L4.d	0.787	3.392	0.015	0.306	0.183	918.978	0.755
Cel-L4.d	0.539	3.711	0.020	0.292	0.236	430.997	1.642
Cel-L5.d	0.716	3.697	0.028	0.559	0.284	618.718	1.218
Cel-L6.d	0.716	3.572	0.031	0.505	0.236	641.370	1.172
Cel-L7.d	0.731	3.364	0.032	0.475	0.250	632.333	1.145
CL16-2-C1a.d	0.250	8.521	0.334	0.042	0.023	93.067	1.324
CL16-2-C2b.d	0.243	8.243	0.121	0.016	0.364	141.182	1.438
CL16-2-C2c.d	0.270	10.898	0.115	0.054	1.170	246.840	1.532
CL16-3-1.d	0.245	9.313	0.099	<DL	0.156	149.792	2.508
CL16-3-2.d	0.252	9.271	0.046	0.041	0.289	125.513	3.347
CL16-3-3.d	0.246	9.285	0.076	<DL	0.067	116.091	3.104
CL16-3-4.d	0.225	8.966	0.061	<DL	0.108	81.205	3.178
CL16-3-5.d	0.239	9.688	0.068	<DL	0.028	88.685	2.283
CC57-1.d	0.460	4.754	0.032	0.225	0.300	1039.897	1.683
CC57-2.d	0.470	5.185	0.034	0.361	0.413	1329.104	1.816
CC57-3.d	0.523	4.240	0.020	0.039	0.008	488.096	0.432
CC57-4.d	0.503	4.935	0.209	0.206	0.213	1049.228	1.877
CC57-5.d	0.484	5.449	0.570	0.229	0.264	1231.931	1.104
CC57-6.d	0.520	5.046	0.022	0.153	0.132	1244.425	0.982
CC57-7.d	0.452	5.365	0.032	0.311	0.197	948.008	1.772
CC57-8.d	0.449	5.699	0.570	0.272	0.250	1483.213	2.724
CC57-9.d	0.487	4.420	0.033	0.723	2.363	954.986	2.208
DG28-C1a.d	0.374	4.156	0.022	0.260	0.088	1162.276	0.329
DG28-C2b.d	0.359	4.713	0.020	0.584	0.225	1469.650	0.315
DG28-C1c.d	0.381	3.823	0.022	0.100	0.039	1374.454	0.248
DG28-C1c.d	0.334	2.850	0.024	0.236	0.072	757.152	0.294
DG28-C3a.d	0.324	4.684	0.020	0.188	0.055	648.113	0.408
DG28-C3b.d	0.353	3.406	0.024	0.156	0.063	886.909	0.349
DG28-C3b.d	0.292	5.199	0.019	9.591	0.765	647.569	0.578

Appendix 2.4B (continued)

Point ID	Ta (ppm)	Pb (ppm)	Bi (ppm)	Th (ppm)	U (ppm)	REE	Eu anomaly
DG28-C3c.d	0.293	2.585	0.020	0.120	0.039	592.949	0.533
FBA711B-SCH2-10.d	1.722	31.803	1.682	25.298	18.487	1887.801	0.140
FBA711B-SCH2-11.d	1.156	38.781	0.867	4.615	3.280	357.037	0.174
FBA711B-SCH2-2.d	2.210	29.607	0.468	4.240	6.464	800.126	0.330
FBA711B-SCH2-3.d	0.826	40.449	1.024	22.657	6.311	445.189	0.233
FBA711B-SCH2-4.d	1.243	24.325	0.385	11.676	7.506	711.676	0.207
FBA711B-SCH2-5.d	1.145	26.744	0.626	2.911	3.892	380.761	0.296
FBA711B-SCH2-6.d	0.339	31.831	2.641	0.024	0.009	17.845	0.202
FBA711B-SCH2-7.d	0.773	34.889	0.824	2.177	5.796	221.848	0.293
FBA711B-SCH2-8.d	0.598	27.244	0.277	0.239	0.356	89.231	0.271
FBA711B-SCH2-9.d	2.196	46.704	1.622	3.429	259.930	632.265	0.374
FBA711B-SCH3-1.d	5.463	58.380	1.209	38.503	100.080	1928.154	0.150
FBA711B-SCH3-2.d	2.811	50.040	0.591	7.256	58.797	925.259	0.301
FBA712B-SCH2-1.d	1.756	37.155	1.079	2.307	171.109	374.359	0.106
FBA712B-SCH2-2.d	4.670	60.882	1.460	21.128	134.830	1136.283	0.133
FBA712B-SCH2-3.d	3.280	36.807	1.279	8.674	114.536	648.548	0.170
FBA712B-SCH2-4.d	2.028	49.693	0.641	5.310	64.079	580.283	0.220
FBA712B-SCH2-6.d	2.127	82.844	2.460	16.124	102.860	548.633	0.241
FBA712B-SCH2-7.d	3.628	46.843	2.294	151.510	132.050	698.211	0.208
FBA712B-SCH2-8.d	3.613	43.507	1.473	14.178	128.853	928.145	0.132
FBA712B-SCH2-9.d	3.322	44.480	1.259	7.159	262.710	1022.401	0.086
FBA712B-SCH3-1.d	3.141	40.310	1.043	11.329	157.070	911.882	0.271
FBA712B-SCH3-3.d	6.616	32.387	0.295	2.961	9.730	826.939	0.132
FBA712B-SCH3-4.d	27.036	40.727	0.505	21.990	37.808	2440.748	0.207
FBA712B-SCH3-5.d	6.283	36.849	0.438	3.123	10.119	937.156	0.258
FBA712B-SCH3-7.d	2.947	33.666	0.334	0.040	0.803	241.152	0.124
FBA712B-SCH3-8.d	17.653	36.779	0.366	6.686	41.283	1405.346	0.321
FBA713A-SCH2-1.d	4.504	27.063	0.232	0.082	0.714	269.591	0.193
FBA713A-SCH2-2.d	43.229	34.514	0.467	9.674	113.980	2540.142	0.186
FBA713A-SCH2-3.d	5.282	33.721	0.211	2.766	5.129	933.902	0.250
FBA713A-SCH2-4.d	5.921	37.071	0.171	2.609	3.975	1125.345	0.439
FBA713A-SCH2-5.d	3.920	36.835	0.136	2.850	6.116	964.071	0.420
FBA713A-SCH3-1.d	2.512	48.650	0.270	3.169	3.211	1219.321	0.530
FBA713A-SCH3-2.d	3.900	52.125	0.321	6.338	4.782	1443.084	0.315
FBA713A-SCH3-3.d	5.074	39.532	0.723	10.119	5.894	2687.885	0.581

Appendix 2.4B (continued)

Point ID	Ta (ppm)	Pb (ppm)	Bi (ppm)	Th (ppm)	U (ppm)	REE	Eu anomaly
FBA713A-SCH3-4.d	19.015	48.233	0.392	8.229	11.815	3234.794	0.433
FBA713A-SCH3-5.d	5.741	48.511	0.473	5.171	4.142	1001.786	0.402
FBA713A-SCH3-6.d	5.755	37.572	0.157	3.503	4.017	952.346	0.462
FBA713A-SCH3-7.d	3.920	43.924	0.361	3.739	3.586	1048.223	0.605
FBA713B-SCH2-1.d	3.196	47.121	0.220	3.267	2.811	753.256	0.273
FBA713B-SCH2-2.d	6.005	44.619	0.189	3.378	3.253	1139.161	0.238
FBA713B-SCH2-3.d	5.852	43.076	0.203	3.465	5.796	956.433	0.235
FBA713B-SCH2-4.d	6.908	52.403	0.626	3.739	4.670	997.312	0.376
FBA713B-SCH2-5.d	6.074	34.389	0.215	4.046	4.170	871.252	0.603
FBEOZ1A-1.d	14.901	40.032	0.639	4.156	3.878	1329.966	0.255
FBEOZ1A-2.d	11.329	33.291	0.556	3.322	6.700	969.048	0.074
FBEOZ1A-3.d	5.685	25.826	0.240	1.633	8.312	1101.920	0.135
FBEOZ1A-4.d	4.073	35.167	1.710	0.357	4.017	152.931	0.260
FBEOZ1A-5.d	12.427	53.932	0.264	2.584	3.624	1100.977	0.119
FBEOZ1A-6.d	14.275	58.380	0.523	2.983	3.663	1258.617	0.253
FBEOZ1A-7.d	30.997	59.770	1.056	2.217	3.799	1141.107	0.196
FBEOZ1B-1.d	9.744	54.488	0.304	1.820	2.822	805.644	0.178
FBEOZ1B-2.d	2.213	66.998	0.411	1.465	2.591	352.004	0.225
FBEOZ1B-3.d	0.619	62.550	1.286	0.099	1.283	127.781	0.181
FBEOZ1B-4.d	10.008	47.121	0.751	3.697	4.587	1286.876	0.233
FBEOZ1B-5.d	0.521	50.040	0.220	0.075	1.321	110.366	0.186
FBK71A-1.d	4.921	46.148	0.260	0.570	1.126	702.909	0.420
FBK71A-2.d	3.684	87.153	4.601	0.357	2.738	441.408	0.436
FBK71A-3.d	2.275	39.198	0.302	1.277	1.230	498.792	0.424
FBK71A-4.d	0.499	58.102	0.056	0.081	1.029	84.077	0.617
FBK71A-5.d	13.010	39.893	0.481	7.145	9.758	2083.026	0.573
FBK71A-6.d	17.973	37.947	0.510	9.939	6.839	2631.423	0.536
FBK7A-SCH3-2.d	6.922	51.152	0.873	0.934	2.572	700.546	0.709
FK11-1-C1a.d	0.261	12.538	0.033	0.036	0.047	240.218	1.659
FK11-1-C1b.d	0.272	19.238	0.086	0.179	0.199	563.666	2.281
FK11-1-C1c.d	0.256	11.732	0.090	0.088	0.139	556.100	1.493
FK11-1-C2a.d	0.238	5.421	0.018	<DL	0.018	162.697	1.362
FK11-1-C2b.d	0.292	9.396	0.026	<DL	0.071	328.614	0.815
FK11-1-C2c.d	0.261	4.809	0.022	<DL	0.014	283.823	0.583
FK11-1-C2d.d	0.242	4.559	0.019	<DL	0.004	126.778	2.335

Appendix 2.4B (continued)

Point ID	Ta (ppm)	Pb (ppm)	Bi (ppm)	Th (ppm)	U (ppm)	REE	Eu anomaly
FK11-1-C2e.d	0.261	6.088	0.016	0.024	0.018	162.480	1.230
FK11-1-C2f.d	0.245	4.337	0.018	0.070	0.074	527.643	1.252
FK11-1-C2g.d	0.246	5.101	0.020	<DL	0.003	113.356	0.673
FK13-1-L1.d	0.281	8.145	0.039	0.139	0.070	429.778	1.708
FK13-1-L1.d	0.523	8.187	0.040	0.125	0.134	644.258	0.835
FK15-L1.d	0.482	26.952	0.204	0.288	0.253	549.090	1.060
FK15-L2.d	0.384	28.259	0.320	0.951	0.404	787.108	1.651
FK15-L2.d	0.555	29.468	0.076	0.678	0.342	842.358	1.082
FK15-L3.d	0.382	28.634	0.286	1.058	0.468	792.287	1.740
FK15-L3.d	0.507	28.773	0.081	0.696	0.373	779.807	1.071
FK15-L4.d	0.382	29.468	0.313	1.004	0.420	796.574	1.727
FK15-L5.d	0.375	28.968	0.185	0.967	0.446	708.732	1.818
FK13-1-L2.d	0.282	16.027	0.101	0.101	0.371	191.324	2.512
FK13-1-L3.d	0.289	16.652	0.035	0.026	0.031	201.204	2.416
FK13-1-L4.d	0.281	16.166	0.046	0.178	0.104	407.121	3.406
FK13-1-L5.d	0.303	16.374	0.063	0.184	0.132	463.155	2.927
FK13-1-L6.d	0.303	16.402	0.044	0.163	0.128	462.099	2.737
FK12-1.d	0.765	10.286	0.067	0.015	0.239	662.418	0.493
FK12-2.d	0.662	11.398	0.653	<DL	0.189	432.193	0.747
FK12-3.d	0.927	13.608	0.070	0.009	0.064	268.131	0.951
FK12-4.d	0.819	7.576	0.167	0.022	0.460	108.110	1.428
FK12-5.d	0.628	12.204	0.150	0.012	0.778	205.004	1.931
FK12-6.d	0.734	23.269	0.110	0.096	0.945	284.451	1.226
FK12-7.d	0.649	16.138	0.292	0.035	0.175	191.143	1.213
FK12-8.d	0.645	20.419	0.306	0.018	0.231	584.982	0.962
FK12-9.d	0.645	18.126	0.217	0.028	0.626	550.579	1.148
Gil-C1.d	0.039	2.043	0.026	0.009	0.011	102.693	2.403
G25-C1a.d	0.041	2.516	<DL	<DL	0.007	101.021	1.067
G25-C1b.d	0.042	2.239	<DL	<DL	0.009	159.950	1.144
G25-C2b.d	0.043	2.072	0.014	<DL	0.020	127.160	1.582
G25-C1c.d	0.038	2.544	0.309	0.014	0.031	98.152	1.507
G25-C3a.d	0.038	1.893	0.027	0.008	0.013	150.822	1.198
G25-C3b.d	0.035	2.009	0.027	0.010	0.015	96.463	2.040
G25-C4.d	0.039	1.775	0.020	<DL	0.010	99.199	1.643
G25-C1a.d	0.221	2.474	0.085	0.011	0.025	102.472	2.080

Appendix 2.4B (continued)

Point ID	Ta (ppm)	Pb (ppm)	Bi (ppm)	Th (ppm)	U (ppm)	REE	Eu anomaly
G25-C1a.d	0.236	2.780	0.071	0.013	0.020	55.353	2.198
G25-C2a.d	0.223	2.341	0.034	0.007	0.034	170.203	0.863
G22-L1.d	0.261	2.599	0.017	0.040	0.005	34.636	1.234
G22-L1.d	0.304	1.548	0.027	0.038	0.023	254.879	0.612
G22-L2.d	0.286	1.796	0.029	0.037	0.040	233.396	0.599
G22-L2.d	0.293	1.622	0.018	0.036	0.040	281.132	0.598
G22-L3.d	0.307	1.619	0.031	0.033	0.049	279.587	0.612
G23-L1.d	0.304	1.642	0.017	0.026	0.023	236.315	0.650
G23-L1.d	0.279	1.529	0.029	0.021	0.027	261.205	0.648
G23-L2.d	0.261	1.813	0.028	0.033	0.064	330.464	0.629
G23-L2.d	0.335	1.669	0.021	0.028	0.092	314.228	0.652
G22-L4.d	0.292	4.309	0.118	0.250	0.017	34.917	1.163
G23-L3.d	0.293	1.682	0.013	<DL	0.028	278.667	0.644
G23-L3.d	0.286	1.654	0.016	<DL	0.004	94.706	0.798
SCH31-1.d	0.767	1.765	0.025	0.029	0.500	0.983	0.382
SCH31-2.d	0.651	1.803	0.139	0.024	<DL	1.024	0.315
SCH31-3.d	0.436	1.681	0.011	0.023	0.002	1.031	0.309
SCH31-4.d	0.689	1.792	0.012	0.022	1.807	0.816	0.433
SCH31-5.d	0.746	1.904	0.017	0.031	<DL	1.800	3.018
SCH31-6.d	0.584	1.843	0.012	<DL	<DL	0.909	0.504
SCH31-7.d	0.491	1.946	0.044	0.017	<DL	3.540	0.317
SCH31-8.d	0.477	1.874	0.007	<DL	0.032	1.168	1.664
SCH31-9.d	0.612	1.915	0.015	<DL	<DL	2.870	0.492
SCH31-10.d	0.605	1.736	0.023	0.010	<DL	2.830	0.568
SCH31-11.d	0.826	1.918	0.012	0.017	0.042	1.731	0.344
SCH11-1.d	0.952	1.017	0.361	0.059	0.065	90.133	0.294
SCH11-2.d	1.430	1.233	0.063	0.093	0.125	109.122	0.469
SCH11-3.d	1.244	1.109	0.278	0.093	0.584	101.452	0.334
SCH11-4.d	4.837	1.850	0.020	0.203	0.140	201.038	0.365
SCH11-5.d	2.531	0.820	0.055	0.174	0.089	211.879	0.353
SCH11-6.d	1.847	0.833	0.019	0.320	<DL	194.067	0.418
SCH11-7.d	3.917	1.739	0.709	0.247	<DL	177.355	0.400
SCH11-8.d	3.545	1.543	0.025	0.730	0.092	255.830	0.433
SCH11-9.d	4.935	1.501	0.041	0.450	0.231	175.461	0.411
SCH11-10.d	4.962	2.780	0.033	0.274	0.063	186.959	0.305

Appendix 2.4B (continued)

Point ID	Ta (ppm)	Pb (ppm)	Bi (ppm)	Th (ppm)	U (ppm)	REE	Eu anomaly
SCH11-11.d	4.740	2.081	<DL	0.154	0.431	174.912	0.317
SCH11-12.d	4.114	0.931	<DL	0.053	0.231	178.120	0.428
INV-1-RIM1.d	0.336	0.641	0.022	0.092	0.096	275.780	1.011
INV-1-RIM2.d	0.571	7.367	0.082	0.157	0.521	186.321	0.591
INV-1-RIM3.d	0.471	20.683	0.075	0.131	0.393	142.881	0.590
INV-1-RIM4.d	0.375	2.905	0.108	0.534	0.491	585.101	0.953
INV-1-RIM5.d	0.489	23.630	0.528	0.411	0.780	311.977	0.349
INV-1-1.d	1.312	3.809	0.589	10.745	11.898	965.773	1.311
INV-1-2.d	1.339	3.068	0.564	11.134	12.302	965.804	1.365
INV-1-3.d	1.223	2.877	0.539	9.174	10.675	911.391	1.396
INV-1-4.d	0.972	3.433	0.297	3.406	4.670	330.643	1.290
INV-1-5.d	1.289	3.823	0.388	8.618	15.818	449.773	1.258
INV-1-6.d	0.905	4.851	0.304	3.978	6.922	363.746	1.219
INV-1-7.d	0.792	11.315	0.260	1.735	1.899	448.736	1.370
M61-1.d	0.610	6.561	2.224	1.696	3.294	217.817	3.094
M61-2.d	0.594	6.213	0.325	0.830	1.043	345.056	5.658
M61-3.d	0.580	7.450	0.167	8.284	16.680	585.368	2.523
M61-4.d	0.596	4.823	0.027	0.445	0.987	223.985	1.965
M61-5.d	0.599	5.101	0.048	0.076	0.107	332.274	2.016
M61A-C1-1.d	0.564	5.282	0.058	2.099	15.568	815.489	1.153
M61A-C2-1.d	0.595	5.365	0.019	0.653	1.446	1202.016	0.587
M62-1.d	0.549	3.336	0.038	0.013	0.032	4.609	0.653
M62-2.d	0.566	0.735	0.115	0.014	0.044	3.549	1.415
M62A-1.d	0.517	3.336	0.181	2.599	1.098	124.324	0.880
M62A-2.d	0.560	0.987	0.139	0.036	0.035	27.057	0.562
KH61A-1.d	0.798	13.288	0.053	1.597	0.373	977.448	1.510
KH61A-2.d	1.106	18.932	0.061	0.092	0.041	641.609	0.515
KH61A-3.d	0.791	11.106	0.145	4.504	1.793	294.260	2.149
KH61A-4.d	0.856	11.759	0.653	1.863	0.448	454.405	3.756
KH61A-5.d	1.257	11.120	0.017	0.231	0.064	945.395	0.799
KH61A-6.d	0.898	9.758	0.023	0.188	0.076	1291.227	0.323
KH61A-7.d	0.926	14.011	0.011	0.434	0.473	914.968	0.627
KH61A-8.d	0.701	16.263	1.211	17.097	7.075	175.988	7.420
KH61A-9.d	1.116	11.092	0.030	0.373	0.068	1340.210	0.476
KH61A-10.d	0.915	8.910	0.022	0.143	0.060	983.064	0.383

Appendix 2.4B (continued)

Point ID	Ta (ppm)	Pb (ppm)	Bi (ppm)	Th (ppm)	U (ppm)	REE	Eu anomaly
KH61A-11.d	0.944	13.358	0.040	0.518	0.182	447.608	2.792
KH61A-12.d	1.207	9.383	0.046	0.862	0.181	949.342	0.752
SCH17-1.d	0.348	127.880	0.032	0.018	0.078	8.819	1.050
SCH17-2.d	0.373	43.090	0.056	0.041	0.403	23.458	0.839
SCH17-3.d	0.396	1.829	0.012	0.015	0.005	43.382	0.210
SCH17-4.d	0.370	1.738	0.008	0.022	0.001	12.480	0.208
SCH17-5.d	0.370	2.267	0.167	0.014	0.044	13.554	0.861
SCH17-6.d	0.382	2.029	0.008	0.051	0.015	37.651	0.262
SCH17-7.d	0.366	2.196	0.008	0.018	0.020	10.548	1.405
SCH17-8.d	0.368	6.783	0.050	0.014	0.163	5.881	0.636
SCH17-9.d	0.350	1.190	0.007	0.011	<DL	1.859	0.524
SCH17-10.d	0.367	1.801	0.007	0.015	0.002	10.308	0.617
SCH17-11.d	0.370	2.075	0.019	0.022	0.016	17.503	0.862
SCH17-12.d	0.375	3.114	0.009	0.026	0.403	14.452	0.708
SCH16-2.d	0.403	2.335	0.002	0.043	<DL	4.779	0.280
SCH16-3.d	0.356	0.974	0.033	0.054	<DL	3.243	0.492
SCH16-6.d	0.420	9.271	0.008	0.734	0.036	18.464	0.342
LT-L1.d	0.687	26.938	0.122	0.118	0.067	2357.176	0.168
LT-L2.d	0.612	26.132	0.081	0.108	0.064	2436.434	0.162
LT-L3.d	0.648	25.590	0.120	0.108	0.057	2395.067	0.163
LT-L4.d	0.538	26.202	0.128	0.177	0.204	2032.667	0.169
LT-L5.d	0.600	27.981	0.070	0.117	0.074	2098.066	0.170
LT-L6.d	1.640	30.566	0.124	0.232	0.082	2796.346	0.128
LT-L7.d	0.785	27.175	0.071	0.141	0.074	2698.921	0.169
LT2-1.d	10.717	16.485	2.224	1.166	0.541	2681.004	0.119
LT2-2.d	7.770	18.668	0.495	1.612	4.726	2895.328	0.095
LT2-3.d	10.439	18.570	0.820	1.820	2.576	3163.306	0.091
LT2-4.d	8.993	16.902	0.250	1.109	0.460	2627.698	0.124
LT2-5.d	9.174	18.626	0.403	0.933	0.571	2302.771	0.152
LT2-6.d	6.088	15.499	0.121	0.714	0.487	1913.224	0.142
MCW3-1-1.d	4.269	19.474	0.016	0.099	0.409	931.969	0.269
MCW3-1-2.d	8.173	21.045	0.014	0.069	0.242	1315.581	0.089
MCW3-1-3.d	4.670	18.126	0.012	0.128	0.456	875.672	0.070
MCW3-1-4.d	10.647	23.630	0.020	0.139	0.424	1736.963	0.064
MCW3-1-5.d	5.824	14.817	0.011	0.076	0.220	430.776	0.096

Appendix 2.4B (continued)

Point ID	Ta (ppm)	Pb (ppm)	Bi (ppm)	Th (ppm)	U (ppm)	REE	Eu anomaly
MCW3-1.d	2.859	15.832	<DL	0.032	0.225	651.524	0.076
MCW3-2.d	3.182	16.110	<DL	0.040	0.247	774.651	0.120
MCW3-3.d	4.320	9.772	0.019	0.027	0.361	501.388	0.087
MCW3-4.d	86.180	13.427	1.020	1.738	50.040	491.604	0.072
MCW3-5.d	3.823	16.958	0.029	0.059	0.393	687.953	0.097
MCW2-D-2.d	11.412	9.466	0.009	0.016	0.110	934.233	0.014
MCW2-D-4.d	10.342	13.288	0.009	0.145	0.299	885.235	0.065
MCW2-D-5.d	61.577	19.696	0.031	0.277	2.016	1265.224	0.086
MCW2-D-6.d	8.145	7.617	0.005	0.047	0.157	660.130	0.016
MCW2-D-7.d	1.012	0.436	0.005	<DL	0.278	290.417	0.062
NP1-C4-L1.d	0.667	3.183	0.119	0.012	0.289	304.267	0.861
NP1-C4-L2.d	0.714	2.534	0.104	0.008	0.181	226.959	0.921
NP1-C4-L3.d	0.873	2.474	0.097	<DL	0.170	276.228	0.832
NP1-C1-L1.d	0.692	2.975	0.107	0.017	0.217	291.051	0.822
NP1-C1-L1.d	1.772	2.877	0.107	0.016	0.318	169.009	0.863
NP1-0.d	0.602	4.003	0.140	0.006	0.231	209.612	1.298
NP1-C2a.d	0.792	1.978	0.085	<DL	0.293	278.847	0.961
NP1-C2b.d	0.676	2.003	0.075	0.021	0.350	322.292	0.860
NP1-C2c.d	0.785	2.035	0.070	0.014	0.284	304.354	0.888
NP1-1-L1.d	1.044	1.738	0.053	<DL	0.265	240.342	1.087
NP1-1-L2.d	1.152	1.988	0.209	0.009	0.331	242.408	1.065
NP1-1-L3.d	0.904	1.947	0.107	<DL	0.218	247.013	0.945
NP1-2-L1.d	1.076	1.793	0.053	<DL	0.284	277.236	1.027
NP1-2-L1.d	1.077	2.016	0.052	<DL	0.203	522.932	0.472
NP1-2-L2.d	1.083	1.849	0.054	<DL	0.228	522.306	0.454
NP1-2-L2.d	0.423	1.890	0.032	0.013	0.090	326.771	0.836
NP1-2-L3.d	1.098	1.932	0.049	<DL	0.254	527.783	0.449
NP1-2-L3.d	0.442	1.988	0.037	<DL	0.143	259.930	0.828
NP1-2-L4.d	0.352	2.630	0.058	0.008	0.085	551.566	1.114
SCH19-1.d	3.517	3.364	0.113	1.251	0.834	1290.615	0.111
SCH19-2.d	6.019	5.435	0.016	0.974	0.370	1759.045	0.091
SCH19-3.d	35.306	5.365	0.017	0.432	0.240	2140.531	0.065
SCH19-4.d	1.778	1.853	0.031	0.133	0.095	670.455	0.116
SCH19-5.d	2.150	3.753	<DL	0.553	0.218	1277.735	0.155
SCH19-7.d	15.902	8.173	<DL	0.776	<DL	2231.937	0.052

Appendix 2.4B (continued)

Point ID	Ta (ppm)	Pb (ppm)	Bi (ppm)	Th (ppm)	U (ppm)	REE	Eu anomaly
SCH19-8.d	5.185	6.881	0.626	0.411	0.177	1351.580	0.162
SCH19-9.d	14.915	6.533	<DL	0.235	0.653	1345.464	0.123
SCH20-1.d	0.865	8.437	<DL	0.058	0.025	438.450	0.242
SCH20-2.d	0.737	47.260	7.228	3.237	1.027	1683.229	0.507
SCH20-3.d	0.546	6.811	0.014	1.726	0.557	1117.769	0.817
SCH20-4.d	0.574	7.131	0.021	1.279	0.381	888.471	0.846
SCH20-5.d	0.674	6.186	0.016	1.322	0.492	1031.172	0.558
SCH20-7.d	0.891	14.734	0.078	0.840	0.209	1070.884	0.382
SCH20-8.d	1.585	8.757	0.178	2.808	0.862	1411.406	0.296
SCH20-9.d	0.714	5.921	0.007	0.121	0.051	532.496	0.519
SCH20-10.d	0.635	6.922	0.047	0.075	0.059	518.474	0.431
SCH20-11.d	0.980	48.650	9.869	0.099	0.086	566.870	0.322
SCH20-12.d	0.820	8.159	0.042	0.342	0.175	766.780	0.485
SCH20-13.d	1.118	4.531	<DL	0.132	0.056	645.059	0.276
SCH21-1.d	0.692	32.665	55.600	0.044	1.251	209.971	0.309
SCH21-2.d	0.783	6.047	<DL	0.334	1.946	255.220	0.590
SCH21-3.d	0.783	6.019	<DL	0.149	0.075	223.387	0.469
SCH21-4.d	2.494	4.921	<DL	1.151	0.848	558.143	0.209
SCH21-5.d	1.473	27.800	0.834	0.117	0.054	291.594	0.222
SCH21-6.d	0.990	7.784	0.082	0.181	<DL	267.022	0.283
SCH21-7.d	0.573	7.089	1.380	0.042	<DL	168.260	0.710
SCH21-8.d	0.610	4.045	0.417	0.051	0.834	206.522	0.349
SCH22-A1.d	0.887	5.115	0.007	0.045	0.027	510.127	0.133
SCH22-A2.d	0.792	2.697	0.016	6.394	0.550	409.465	0.470
SCH22-A4.d	0.535	3.058	0.009	0.446	0.043	399.403	0.547
SCH22-A5.d	0.510	3.670	<DL	0.020	0.008	273.189	0.362
SCH22-A6.d	0.527	1.307	0.250	0.088	0.045	553.536	0.413
SCH22-B1.d	0.954	12.927	0.987	0.044	0.061	112.393	0.228
SCH22-B2.d	0.828	2.572	0.075	0.022	<DL	85.071	0.019
SCH22-B3.d	0.894	10.842	8.757	<DL	<DL	81.536	0.006
SCH22-B4.d	0.523	6.297	1.418	0.015	0.013	95.771	0.244
SCH22-B5.d	0.518	7.506	2.224	0.149	0.250	218.520	0.255
SCH22-B6.d	0.580	13.205	8.618	0.041	0.008	104.283	0.234
SCH23-B1.d	0.762	7.284	0.058	0.081	0.183	612.241	0.130
SCH23-B2.d	2.555	4.420	0.195	0.131	0.250	477.496	0.108

Appendix 2.4B (continued)

Point ID	Ta (ppm)	Pb (ppm)	Bi (ppm)	Th (ppm)	U (ppm)	REE	Eu anomaly
SCH23-B3.d	4.879	33.777	1.015	0.785	0.851	681.826	0.074
SCH23-B4.d	0.771	29.190	1.084	0.056	0.068	318.710	0.148
SCH23-B5.d	0.726	2.891	0.074	0.055	0.022	219.050	0.359
SCH23-C1.d	2.252	12.037	0.014	0.097	0.039	728.600	0.147
SCH23-C2.d	4.295	3.684	0.010	0.124	0.278	800.077	0.083
SCH23-C3.d	1.729	8.132	0.695	0.149	0.111	640.494	0.190
SCH23-C4.d	0.827	21.823	0.973	0.090	0.181	457.250	0.164
SCH23-C5.d	2.444	236.300	4.587	1.029	0.733	1442.792	0.193
SCH24-1.d	1.147	3.433	0.043	0.667	0.737	561.727	0.209
SCH24-2.d	1.391	2.975	0.046	0.232	0.069	292.890	0.253
SCH24-3.d	1.409	3.461	<DL	0.399	0.249	486.624	0.322
SCH24-4.d	2.516	2.238	0.973	0.057	0.051	384.705	0.167
SCH24-5.d	0.844	2.635	4.170	0.254	1.112	410.165	0.328
SCH24-6.d	0.767	2.679	<DL	0.051	0.033	235.174	0.292
SCH24-7.d	1.137	4.823	0.167	0.078	0.045	338.922	0.290
SCH24-1A-R.d	2.184	3.739	0.010	0.078	0.067	619.968	0.177
SCH24-1A-C.d	0.878	2.655	<DL	0.035	0.026	241.708	0.353
SCH24-2A-R.d	0.730	1.227	<DL	<DL	0.013	49.684	0.209
SCH24-2A-R1.d	0.840	6.172	0.375	0.046	0.039	362.939	0.259
SCH25-1.d	0.541	3.489	<DL	<DL	0.005	107.298	0.368
SCH25-3.d	0.716	2.335	0.015	0.016	0.017	186.366	0.249
SCH25-4.d	0.682	2.173	0.010	0.016	0.018	170.307	0.262
SCH25-5B.d	0.542	2.441	0.125	<DL	0.006	152.774	0.202
SCH25-6B.d	0.520	2.961	0.006	<DL	<DL	101.416	0.422
SCH26-1.d	0.941	3.975	0.193	0.032	0.043	274.325	0.282
SCH26-2.d	0.777	6.811	0.025	0.067	0.004	341.271	0.297
SCH26-3.d	0.723	2.969	0.015	0.049	0.074	166.446	0.315
SCH26-4.d	0.556	4.629	0.500	0.086	0.106	134.760	0.416
SCH26-5.d	0.626	10.147	0.556	0.036	0.306	123.311	0.485
SCH26-6.d	0.790	7.228	0.556	0.031	0.054	206.676	0.462
SCH26-7.d	0.682	8.201	<DL	0.048	0.069	208.401	0.563
SCH26-8.d	1.15648	3.3082	<DL	0.07367	0.10981	293.3623	0.278
SCH27-C1.d	0.53237	4.6704	0.11954	0.53098	0.24881	468.1047	0.681
SCH27-C2.d	0.59214	13.5386	3.9059	0.052125	0.047816	183.5551	0.328
SCH27-C3.d	1.82368	10.1748	1.8348	2.8356	7.9091	411.301	0.463

Appendix 2.4B (continued)

Point ID	Ta (ppm)	Pb (ppm)	Bi (ppm)	Th (ppm)	U (ppm)	REE	Eu anomaly
SCH27-4.d	0.834	4.0171	0.027522	0.10425	0.039198	378.636	0.249
SCH27-5.d	0.51708	12.7324	0.973	0.6811	0.36279	782.5895	0.464
SCH27-6.d	1.19818	20.711	2.224	0.11954	0.021962	275.6787	0.233
SD11-C2.d	0.075894	2.3769	0.016819	0.012371	0.005004	272.4066	0.895
SD11-C1b.d	0.58519	3.9337	0.014734	0.24325	0.24464	943.4625	0.449
SD11-C1c.d	0.4448	3.9337	<DL	0.019599	0.09452	359.8571	0.781
SD11-C1d.d	0.06255	2.7661	<DL	0.025993	0.01529	88.63891	1.616
SD28-sch1.d	0.074504	5.1152	<DL	0.036557	0.064774	284.1965	0.669
SD28-sch1a.d	0.13344	8.1315	0.0417	0.57407	1.01748	296.5801	0.638
SD28-sch2.d	0.067693	7.8813	0.04448	0.36418	0.80064	252.7437	1.175
SD28-sch2a.d	0.049901	5.7963	0.019738	0.14456	0.31414	186.6131	1.108
SD28-sch2b.d	0.071585	5.3793	0.02641	0.015429	0.29885	160.2909	1.501
SD28-sch3.d	0.10425	9.2991	0.03614	1.47479	2.15033	491.2149	0.527
SD28-sch3a.d	0.06672	8.479	0.027661	0.81454	1.09254	704.4687	0.510
SD28-sch3b.d	0.055322	5.9214	0.03614	0.22935	0.42395	232.6457	1.062
SD28-sch4.d	0.062272	6.3106	0.017514	0.1807	0.42117	179.7298	1.347
SD28-sch4a.d	0.15012	5.1291	0.013344	0.33499	0.20711	306.5827	0.648
SD28-sch4b.d	0.065191	6.4079	0.021267	0.56712	0.63384	391.2475	0.676
ITALY-1.d	0.68527	0.76172	0.025715	1.60823	0.18904	501.1089	0.501
ITALY-2.d	1.36081	0.77979	0.028495	0.93686	0.107725	1059.676	0.297
ITALY-3.d	2.09334	1.41224	0.032943	0.64218	0.068944	1079.182	0.247
ITALY-4.d	1.91264	0.73114	0.022935	0.5282	0.04865	801.9855	0.296
ITALY-5.d	1.47201	0.67415	0.020016	0.47399	0.040866	720.886	0.309
ITALY-6.d	1.16343	0.70751	0.024325	0.30302	0.034333	763.0308	0.291
ITALY-7.d	1.7097	0.78952	0.016541	0.25159	0.033082	1148.372	0.197
ITALY-8.d	1.90847	0.75616	0.017792	0.27105	0.033777	1178.6	0.183
ITALY-9.d	2.80919	0.86597	0.020016	0.35167	0.071585	1013.075	0.258
ITALY-10.d	1.95712	0.73948	0.021962	0.16402	0.028912	1198.433	0.228
ITALY-11.d	2.12948	0.78813	0.021823	0.21406	0.053654	1332.177	0.230
ITALY-12.d	2.59513	0.84512	0.025159	0.38364	0.046009	1379.225	0.226
TSE-1.d	9.2852	2.9885	0.88821	625.5	18.904	1423.152	0.173
TSE-2.d	10.2721	3.5306	0.834	478.16	14.9842	1428.837	0.132
TSE-3.d	12.9548	4.1978	0.36001	223.79	12.788	1699.789	0.138
TSE-4.d	9.9246	2.2796	0.07228	13.9	8.9516	1448.116	0.277
TSE-5.d	10.6196	2.4464	0.22379	22.518	16.0823	1475.082	0.180

Appendix 2.4B (continued)

Point ID	Ta (ppm)	Pb (ppm)	Bi (ppm)	Th (ppm)	U (ppm)	REE	Eu anomaly
TSE-6.d	8.6736	4.3368	1.7653	383.05	13.082	1418.453	0.139
TSE-7.d	6.2689	2.2657	0.54488	334.99	16.541	1033.952	0.173
SCH40-1.d	0.48789	4.1561	0.01251	0.04309	<DL	46.3319	0.844
SCH40-2.d	0.44897	4.448	0.01807	0.052542	0.13761	12.40589	11.602
SCH40-3.d	0.49206	4.7538	0.2085	0.77284	1.32606	19.41469	8.567
SCH40-4.d	0.48094	4.6704	0.1251	0.58102	0.88404	25.89751	8.571
SCH40-5.d	0.50179	4.7399	0.08201	0.98134	1.41363	14.63865	19.110
SCH40-6.d	0.52959	4.1005	<DL	0.70334	0.96883	32.27955	7.528
SCH40-7.d	0.50735	3.6279	<DL	1.8626	2.6271	29.26687	10.649
SCH40-8.d	0.45592	6.9917	<DL	2.85923	1.6958	45.97814	25.391
SCH40-9.d	0.4309	6.7276	0.556	0.41978	0.40727	10.20774	20.581
SCH40-10.d	0.49067	5.4627	0.139	0.84651	0.8479	43.02898	15.087
SCH40-11.d	0.46843	4.2951	0.016958	0.32526	0.77979	12.07993	14.341
SCH40-12.d	0.45453	3.6418	0.1112	0.08896	0.08062	18.32785	5.604
SCH44-3.d	0.46982	4.865	0.556	0.53515	0.37252	11.82973	0.684
SCH44-4.d	0.49067	7.3114	0.07089	0.74087	0.15429	9.081287	0.663
SCH44-5.d	0.51708	7.923	0.08062	0.19599	0.26549	7.021585	1.606
SCH44-6.d	0.52403	9.3269	0.4726	1.7653	0.15846	7.468609	0.689
SCH44-7.d	0.53793	10.425	2.0016	0.51847	0.2919	8.771178	0.945
SCH44-8.d	0.52681	3.2804	1.668	0.30441	0.26966	9.910839	0.712
SCH44-9.d	0.52264	17.375	3.475	0.26132	0.09452	7.543947	0.903
YP5B-C3.d	0.035167	0.03892	0.01529	0.10842	0.79925	22.29699	3.388
YP5A-C5a.d	0.2502	0.08201	0.012371	1.7097	5.5322	100.5703	2.064
YP5A-C5b.d	0.21684	0.11259	0.010703	0.35445	4.2117	57.36252	3.318
YP5A-C5b.d	0.21684	0.065608	0.010564	0.1807	4.6565	35.94679	5.167
YP5A-C1a.d	0.21962	0.20294	0.010008	0.27244	2.7661	58.91237	2.817
YP5A-C1a.d	0.2363	0.06116	0.014317	0.12927	11.7594	34.81255	7.754
YP5A-C1b.d	0.225736	0.17097	0.014456	0.171387	4.3785	38.60308	5.910
YP5A-C3a.d	0.21684	0.17375	0.015429	0.15985	3.5167	24.78787	5.057
YP5A-C3a.d	0.21128	0.22935	0.013622	0.36696	2.502	79.0354	3.206
YP5A-C3b.d	0.21545	0.08757	0.010842	0.10564	2.06415	31.61444	4.649
YP5A-C3b.d	0.22379	0.07784	0.015568	0.23352	1.5568	68.98987	2.771
YP5A-C1c.d	0.217674	0.48094	0.012788	0.42117	1.7931	61.1322	2.869
YP5A-C1d.d	0.230184	0.12093	0.013344	0.23908	5.8102	68.13502	3.402
YP5B-C1a.d	0.213226	0.23352	0.010564	0.18487	2.1962	39.65531	2.778

Appendix 2.4B (continued)

Point ID	Ta (ppm)	Pb (ppm)	Bi (ppm)	Th (ppm)	U (ppm)	REE	Eu anomaly
YP5B-C1b.d	0.22379	0.16541	0.0139	0.10008	2.0016	31.54466	2.557
YP5B-C3a.d	0.21545	0.22379	0.014317	0.39059	1.3761	89.62998	3.522
YP5B-C2a.d	0.23769	0.5699	0.012649	0.32804	5.004	42.68551	2.774
ZIV-1.d	0.35862	11.6065	0.029885	0.42395	0.57268	188.4187	9.752
ZIV-2.d	0.35584	14.9842	0.01668	0.017653	0.009452	977.5078	1.298
ZIV-3.d	0.35306	26.0764	0.016541	0.056573	0.07506	378.9015	9.718
ZIV-4.d	0.35862	20.8083	0.05838	0.023213	0.019321	925.9707	1.759
ZIV-5.d	0.3614	9.7995	0.021128	0.033638	0.012371	985.0652	1.570
ZIV-6.d	0.33916	11.2729	0.021406	0.010425	0.007645	1105.233	1.233
ZIV-7.d	0.35028	38.3918	0.021545	0.0139	0.015151	464.6297	2.681
ZIV-8.d	0.3614	11.3146	0.019321	0.016819	0.015985	939.5733	1.832
ZIV-9.d	0.33221	42.1031	0.020711	0.013344	0.017514	577.8091	2.807
ZIV-10.d	0.35584	31.9978	0.026966	0.033916	0.018487	406.7779	3.396
ZIV-11.d	0.32526	34.3747	0.024603	0.009174	0.012371	408.1165	2.027
ZIV-12.d	0.33499	10.0358	0.019182	0.024186	0.014317	1085.551	1.536

Appendix 2.5B. R code for RF deposit types model based on scheelite composition.

```
library(ggplot2)
library(cowplot)
library(randomForest)
library(caret)
library(tibble)

#INPUTTING SCHEELITE DATA TO CREATE THE
MODEL============================================================
#the data do not contain missing/censored data
#the data DO NOT HAVE any type of transformation
table=read.csv(file.choose(), header = TRUE, sep = ",", stringsAsFactors = FALSE)
data=table[,c(2:13)]

#INPUTTING THE UNKNOWN
DATA=============================================================================
#make sure that all missing values were imputed
unknown_data <- read.csv(file.choose(),header = TRUE, sep = ",", stringsAsFactors = FALSE)

unknown_data_filter=unknown_data[,c(3:13)] #choose here the columns with elements only!
unknown_data_filter
```

```
#CREATING DATA
PARTITION=============================================================================

#here we divide the scheelite dataset in training and testing data

#seed is set to maintain the same number generation that will be input in the algorithm.

set.seed(1234)

trainIndex = createDataPartition(data$model.1, p = 0.7, list = FALSE)  #choose the "TARGET" for split the data

training = data[trainIndex,]

testing = data[-trainIndex,]

summary(training)

summary(testing)



#CREATING THE RF DEPOSIT TYPE SCHEELITE COMPOSITION
MODEL================================================

control = trainControl(method = "cv", number = 10, p= 0.7)

mtry = 3                #number of variables that will be used in each tree node, sqrt of total variables

metric <- "Accuracy"     #specifies if it is for regression (Rsquared) or for classification (Accuracy)

#tunegrid <- data.frame(mtry = c(1:10))        #with cross validation

tunegrid <- expand.grid(.mtry=mtry)           #number of variable to be used in the each node


rf_default <- train(model.1~ ., data= training, method="rf", metric=metric, tuneGrid=tunegrid,

                    trControl=control)

print(rf_default)
```

```
#PREDICTION OF THE TESTING DATA
pred_RF <- predict(rf_default, testing)
pred_RF
labels <- as.factor(testing$model.1)
mat_RF <- caret::confusionMatrix(data  = pred_RF, reference = labels, dnn = c("Prediction","Reference"))
mat_RF

#GINI DECREASE
varImp <- varImp(rf_default, scale = FALSE) #TRUE if you want to scale the variable importance
view(varImp)
plot(varImp)

#PREDICTIONS OF UNKNOW
SAMPLES================================================================================
#add here the data set to be predicted
pred_unknown_data <- predict(rf_default, newdata = unknown_data_filter, type = "raw")
view(pred_unknown_data)

#CREATING TABLE OF PREDICTED RESULTS
results <- as.data.frame(pred_unknown_data)
results_pred <- cbind(results, unknown_data)
head(results_pred)
#write.table(results_pred,"#add here the path in case you want to save the table in your pc", sep = ",",row.names = FALSE)
```

```
#drawing barplot
ggplot(results_pred, aes(x=factor(pred_unknown_data))) +
  geom_bar(stat="count", width=0.4, aes(fill= unknown_data$Name))+
  theme(panel.background = element_rect(fill = "white",colour = "black",size = 1, linetype = "solid"),
        panel.grid.major = element_line(size = 0, linetype = 'solid',colour = "white"),
        panel.grid.minor = element_line(size = 0, linetype = 'solid',colour = "white"))
```

Appendix 2.6B Scheelite data set to be used in the script for RF deposit type model. The element concentration is given in ppm. The second column is the deposit classification.

Name	model 1	Na	Mg	Mn	As	Sr	Y	Nb	Mo	Pb	REE	EuA
Alta Lode - Bendigo	6Orogenic Au	51	6	0.9	50	4340	244	1.94	0.26	12.6	349.59	9.64
Alta Lode - Bendigo	6Orogenic Au	73	0.45	0.6	2.3	4700	486	2.08	0.32	11.4	955.9	2.79
Alta Lode - Bendigo	6Orogenic Au	89	1	0.7	2.1	4930	439	2.05	0.27	18.6	760.61	2.56
Alta Lode - Bendigo	6Orogenic Au	36	0.42	2.2	0.4	7180	95	1.99	0.53	41.4	177.71	4.06
Alta Lode - Bendigo	6Orogenic Au	152	1	0.9	59	4730	429	2.08	0.34	13.2	723.97	3.13
Alta Lode - Bendigo	6Orogenic Au	126	0.31	0.7	3.6	4600	645	2.33	0.27	11.9	1277.3	2.47
Alta Lode - Bendigo	6Orogenic Au	131	0.47	0.5	20.2	5580	660	2.6	0.25	14.1	1379.9	1.79
Alta Lode - Bendigo	6Orogenic Au	88	0.36	0.6	45.9	5290	499	2.59	0.4	13.5	1018.7	2.14
Alta Lode - Bendigo	6Orogenic Au	40	0.26	0.6	1.6	5160	229	1.95	0.35	12.2	497.55	2.9
Alta Lode - Bendigo	6Orogenic Au	5.32	0.19	0.8	0.42	4530	51	1.71	0.45	14.5	80.96	27.43
Alta Lode - Bendigo	6Orogenic Au	6.56	0.24	0.8	3	5050	136	2.05	0.37	14.5	187.92	21.08
Alta Lode - Bendigo	6Orogenic Au	87	0.24	0.6	1.7	3940	725	1.88	0.43	12	1464.5	2.49
Alta Lode - Bendigo	6Orogenic Au	97	0.24	0.4	2	3800	600	1.99	0.4	12.2	1158.6	2.26
Alta Lode - Bendigo	6Orogenic Au	154	2	0.8	13.3	4080	538	2.33	0.35	12.9	1100.5	2.41
Alta Lode - Bendigo	6Orogenic Au	105	0.42	0.7	24.4	4470	350	2.15	0.33	12	741.71	2.22
Alta Lode - Bendigo	6Orogenic Au	101	0.3	0.5	2.3	4910	510	2.24	0.34	11.5	1089.5	1.9
Alta Lode - Bendigo	6Orogenic Au	148	0.38	0.4	1.5	4260	485	2.44	0.24	10.3	1067.2	1.83
Alta Lode - Bendigo	6Orogenic Au	65	1	0.5	0.35	4220	261	2.35	0.42	10.3	516.29	3.58
Alta Lode - Bendigo	6Orogenic Au	74	4	1.1	8.1	4670	187	1.83	0.42	13.3	379.38	3.97
Alta Lode - Bendigo	6Orogenic Au	51	0.24	0.8	69	4440	336	1.63	0.31	15.8	459.7	13.77
Alta Lode - Bendigo	6Orogenic Au	63	0.22	0.7	1.7	4560	334	2.32	0.3	11.6	580.37	5.4
Alta Lode - Bendigo	6Orogenic Au	70	0.41	0.5	2.2	3730	458	2.29	0.19	9	1004.4	2.07
Alta Lode - Bendigo	6Orogenic Au	44	0.33	0.6	1.2	4230	382	1.94	0.29	9.9	737.36	3.01
Alta Lode - Bendigo	6Orogenic Au	57	0.23	0.7	9.2	4440	308	1.65	0.19	10.5	497.51	6.25
Alta Lode - Bendigo	6Orogenic Au	32	1	1	47.3	4990	149	1.91	0.38	21.2	262.46	6.74
Alta Lode - Bendigo	6Orogenic Au	26	0.29	1.2	1.6	6400	172	2.19	0.34	27.8	245.64	9.64
Alta Lode - Bendigo	6Orogenic Au	33	0.21	0.7	1.4	4670	325	2.02	0.25	17.2	635.52	3.13
Alta Lode - Bendigo	6Orogenic Au	79	0.3	0.5	2	3900	377	2.85	0.2	9.7	976.93	1.77
Alta Lode - Bendigo	6Orogenic Au	31	0.24	1.1	9.3	4860	190	1.58	0.38	20.5	284.36	8.76

Appendix 2.6B (continued)

Name	model 1	Na	Mg	Mn	As	Sr	Y	Nb	Mo	Pb	REE	EuA
Alta Lode - Bendigo	6Orogenic Au	111	0.37	1	2.4	4380	372	2.64	0.44	13.1	777.94	2.33
Alta Lode - Bendigo	6Orogenic Au	109	0.3	1	2.4	4190	279	2.18	0.26	13.6	664.02	2.49
Alta Lode - Bendigo	6Orogenic Au	64	0.23	0.6	1	3230	416	2.02	0.23	7.4	964.31	2.46
Alta Lode - Bendigo	6Orogenic Au	58	2	1.5	117	4700	220	1.7	0.37	17.1	335.94	5.54
Alta Lode - Bendigo	6Orogenic Au	35	0.43	0.9	98	4710	215	1.99	0.3	18.3	356.1	6.85
Alta Lode - Bendigo	6Orogenic Au	56	1	0.9	76	4800	225	1.99	0.23	18.2	375.18	8.58
Alta Lode - Bendigo	6Orogenic Au	49	0.02	0.9	36	5080	197	1.81	0.12	14.1	305.2	9.98
Alta Lode - Bendigo	6Orogenic Au	46	1	0.8	80	4480	155	1.5	0.43	13.5	286.86	4.65
Alta Lode - Bendigo	6Orogenic Au	41	1	0.8	51	4300	176	1.78	0.23	12.2	308.35	6.67
Alta Lode - Bendigo	6Orogenic Au	155	1	0.5	2.3	3770	610	2.41	0.32	9.9	1522.7	1.71
Alta Lode - Bendigo	6Orogenic Au	60	0.02	0.6	0.65	3260	561	2.06	0.25	7.5	805.2	10.77
Alta Lode - Bendigo	6Orogenic Au	64	0.24	0.7	0.64	3910	485	2.1	0.45	8.3	742.98	10.9
Alta Lode - Bendigo	6Orogenic Au	54	0.38	0.5	0.55	4360	375	1.75	0.25	9.3	614.29	9.4
Alta Lode - Bendigo	6Orogenic Au	70	1	0.6	0.51	4190	267	2.21	0.45	9.9	552.93	3.47
Alta Lode - Bendigo	6Orogenic Au	62	0.38	0.6	1.3	4410	286	2.12	0.35	10.2	660.21	2.25
Alta Lode - Bendigo	6Orogenic Au	94	0.25	0.6	1.7	3820	255	2.08	0.21	8.9	611.34	2.1
Alta Lode - Bendigo	6Orogenic Au	124	0.33	0.7	15	3970	279	2.11	0.31	10.4	798.47	2.29
Alta Lode - Bendigo	6Orogenic Au	107	0.32	0.6	39	4510	269	2.07	0.33	10.8	692.74	1.96
Alta Lode - Bendigo	6Orogenic Au	92	0.28	0.6	17	4200	256	2.5	0.23	11.5	624.26	2.68
Alta Lode - Bendigo	6Orogenic Au	113	0.32	0.5	1.8	3820	336	2.43	0.39	10.1	898.33	2.09
Alta Lode - Bendigo	6Orogenic Au	101	0.31	0.6	52	3420	434	2.28	0.41	9.7	977.91	2.23
Alta Lode - Bendigo	6Orogenic Au	59	0.39	1	101	4760	246	1.82	0.27	15	419.94	5.56
Alta Lode - Bendigo	6Orogenic Au	88	1	1.2	134	4130	172	1.65	0.33	17	305.49	4.9
Alta Lode - Bendigo	6Orogenic Au	82	1	0.9	96	4560	297	1.82	0.3	14.4	424.65	8.22
Alta Lode - Bendigo	6Orogenic Au	56	0.21	0.6	0.47	3970	405	1.79	0.23	10.9	567.99	8.9
Alta Lode - Bendigo	6Orogenic Au	40	1	0.6	0.37	3820	237	1.86	0.26	10.3	388.66	11.79
Alta Lode - Bendigo	6Orogenic Au	41	0.24	0.9	0.49	4270	210	1.94	0.32	18.5	289.14	17.51
Alta Lode - Bendigo	6Orogenic Au	44	0.24	1	0.47	4640	206	1.98	0.19	21	268.14	23.19
Alta Lode - Bendigo	6Orogenic Au	39	0.02	1.1	1	5500	102	1.98	0.37	29.3	156.17	36.93
Alta Lode - Bendigo	6Orogenic Au	34	0.18	0.5	0.53	4100	242	1.99	0.25	11.24	371.82	11.14

Appendix 2.6B (continued)

Name	model 1	Na	Mg	Mn	As	Sr	Y	Nb	Mo	Pb	REE	EuA
Alta Lode - Bendigo	6Orogenic Au	65	0.25	0.8	4	5800	151	1.76	0.23	16.6	239.62	14.95
Alta Lode - Bendigo	6Orogenic Au	43	0.35	0.7	33.1	4350	250	1.62	0.15	15	359.82	15.64
Alta Lode - Bendigo	6Orogenic Au	92	27	1.3	260	4250	164	1.94	0.52	19.8	326.25	5.29
Alta Lode - Bendigo	6Orogenic Au	69	0.09	0.4	68	4340	215	1.85	0.21	9.18	524.4	1.94
Alta Lode - Bendigo	6Orogenic Au	74	0.02	0.4	13.5	4820	246	1.84	0.36	8.7	582.75	2.22
Alta Lode - Bendigo	6Orogenic Au	97	0.37	0.6	1.9	4510	294	2.12	0.2	7.75	624.06	2.05
Alta Lode - Bendigo	6Orogenic Au	102	0.51	0.6	0.54	4460	237	2.12	0.24	8.62	534.51	2.3
Alta Lode - Bendigo	6Orogenic Au	94	0.4	0.7	1.1	3380	282	1.89	0.31	8.2	606.82	2.89
Alta Lode - Bendigo	6Orogenic Au	93	0.25	0.6	1.3	3700	320	1.8	0.16	9.7	695.77	2.87
Alta Lode - Bendigo	6Orogenic Au	87	2	0.6	1.1	3570	257	1.79	0.25	8.3	593.72	2.65
Alta Lode - Bendigo	6Orogenic Au	61	1	0.6	0.62	3360	319	1.85	0.25	8.4	644.57	3
Alta Lode - Bendigo	6Orogenic Au	89	0.42	0.6	1.5	3970	351	2.37	0.38	10.7	763.07	2.64
Alta Lode - Bendigo	6Orogenic Au	86	0.23	0.5	1.1	3530	335	2.24	0.19	9.4	684.29	2.69
Alta Lode - Bendigo	6Orogenic Au	79	0.29	0.7	0.64	3970	305	2.09	0.38	8.9	636.41	3.08
Alta Lode - Bendigo	6Orogenic Au	105	1	0.8	7.4	3600	278	1.98	0.79	9.2	611.3	3.07
Alta Lode - Bendigo	6Orogenic Au	86	0.32	0.9	0.43	3730	283	2.1	0.11	9.4	583.45	3.31
Alta Lode - Bendigo	6Orogenic Au	74	0.29	0.6	2.2	3600	268	1.82	0.43	9	588.84	2.69
Alta Lode - Bendigo	6Orogenic Au	138	0.33	0.7	22.7	4620	406	3.57	0.29	12.3	682.08	2.34
Alta Lode - Bendigo	6Orogenic Au	127	0.44	0.4	46	4820	482	4.49	0.2	1.73	694.28	1.98
Alta Lode - Bendigo	6Orogenic Au	136	1	0.6	16.4	4250	347	3.58	0.2	13.2	583.48	2.19
Alta Lode - Bendigo	6Orogenic Au	92	1	0.6	1.9	4190	207	2.16	0.36	11	548.86	2.12
Alta Lode - Bendigo	6Orogenic Au	92	1	0.32	1.6	4090	249	2.39	0.34	11.1	687.98	1.91
Alta Lode - Bendigo	6Orogenic Au	89	0.38	0.5	2.1	3560	225	2.06	0.39	9.5	644.44	1.76
Alta Lode - Bendigo	6Orogenic Au	87	5	0.9	58	4440	287	1.69	0.21	15.2	471.24	8.43
Alta Lode - Bendigo	6Orogenic Au	156	0.5	0.8	70	4370	600	2.61	0.36	12.3	1098.7	3.46
Alta Lode - Bendigo	6Orogenic Au	50	0.02	1.1	207	4940	139	1.86	0.53	17.7	260.53	5.25
Alta Lode - Bendigo	6Orogenic Au	19	0.55	0.8	146	4730	98	1.62	0.76	15.6	150.35	8.53
Alta Lode - Bendigo	6Orogenic Au	75	5	0.9	144	4620	223	1.8	0.52	16.5	478.02	2.41
Alta Lode - Bendigo	6Orogenic Au	156	1	0.5	2.1	5090	480	2.5	0.12	12.9	1359.1	1.51
Alta Lode - Bendigo	6Orogenic Au	86	0.38	0.7	20.4	3480	255	1.88	0.33	9.6	584.82	2.33

Appendix 2.6B (continued)

Name	model 1	Na	Mg	Mn	As	Sr	Y	Nb	Mo	Pb	REE	EuA
Amaruq	6Orogenic Au	39.3	20.3	7.36	1.6	658	54.7	2.05	49	19.24	242.15	3.27
Amaruq	6Orogenic Au	22.9	450	45	1.17	984	40.6	1.93	3.6	34	118.42	3.87
Amaruq	6Orogenic Au	12.84	19.3	14.4	1.02	1205	22.68	1.82	3.43	28.28	54.08	6.99
Amaruq	6Orogenic Au	10.45	5.2	8.63	1.49	1098	25.17	2.27	37.9	35.2	56.05	5.38
Amaruq	6Orogenic Au	15	56	11.4	1.35	1044	32.07	2.85	68.2	47	68.91	3.59
Amaruq	6Orogenic Au	12.4	9	12.8	1.1	1112	22.3	1.94	7.5	34.4	50.73	5.75
Amaruq	6Orogenic Au	10.42	4.1	10.59	1.03	1176	20.46	2.09	44.7	35.3	46.4	6.26
Amaruq	6Orogenic Au	14.07	7	11.21	0.75	1321	243.4	1.8	1.95	34.74	369.78	17.15
Amaruq	6Orogenic Au	22.7	4.48	10.49	0.77	1306	153.9	1.78	2.02	32.73	270.37	29.65
Amaruq	6Orogenic Au	69.1	3.96	8.66	1.26	1310	193.1	2.24	2.19	30.49	479.61	13.16
Amaruq	6Orogenic Au	55.6	13	7.79	1.09	1269	141.6	1.87	1.46	29.2	403.57	26.65
Amaruq	6Orogenic Au	46.9	10.7	11.1	1.11	1263.9	123.1	1.85	1.83	33.53	359.88	30.03
Amaruq	6Orogenic Au	141.8	23.4	15.1	5.07	1327	407	2.24	2.42	28.93	645.81	6.92
Amaruq	6Orogenic Au	128.7	5.1	14.6	5.71	922	304	3.65	2.55	16.8	472.99	1.7
Amaruq	6Orogenic Au	118.9	11.3	13.17	3.13	1192	397	2.26	2.06	27.9	455.95	4.74
Amaruq	6Orogenic Au	133	40	110	8	718	282	11.2	2.71	15.4	419.35	1.02
Amaruq	6Orogenic Au	114	9.5	44	8.2	699	280	16.5	2.9	18.2	433.14	0.92
Amaruq	6Orogenic Au	99.7	4.9	12.2	9.2	713	265	10.8	2.2	21.9	416.74	0.99
Amaruq	6Orogenic Au	89.4	23	68	4.34	887	250	9.9	3.08	19.34	321.42	3.75
Amaruq	6Orogenic Au	123	55	28.2	6.52	981	296	4.88	2.52	23.4	415.64	2.41
Amaruq	6Orogenic Au	115	6.2	21.1	4.7	1012	345	12.1	3.48	19.5	415.17	2.78
Amaruq	6Orogenic Au	138.2	6.6	12.01	5.89	497	325	16.76	5.72	14.66	530.24	0.79
Amaruq	6Orogenic Au	113	11.1	29.7	5.89	876	287	3.78	2.04	19.67	406.33	3.55
Amaruq	6Orogenic Au	82	5.4	14.46	4.75	942	204	4.11	1.45	21.11	948.61	5.73
Amaruq	6Orogenic Au	154.9	16.5	9.52	4.65	1223	440	2.79	2.85	34.37	1295.7	2.43
Amaruq	6Orogenic Au	83.2	13.7	16.3	4.21	996	195	5.9	2.89	25.3	359.42	9.92
Amaruq	6Orogenic Au	263.9	27	14.16	5.28	548	627	15.7	4.83	20.2	1085.5	1.55
Amaruq	6Orogenic Au	200.1	3.36	9.3	4.75	699	586	6.24	3.67	33.22	1102.7	2.87
Amaruq	6Orogenic Au	166.1	3.89	13.34	8.08	538.8	388	17.23	5.46	15.98	627.01	0.8
Barewood	6Orogenic Au	830	165	7.1	7.1	6040	955	76.1	0.58	9.88	1872.2	0.74

Appendix 2.6B (continued)

Name	model 1	Na	Mg	Mn	As	Sr	Y	Nb	Mo	Pb	REE	EuA
Barewood	6Orogenic Au	117.4	5.1	1.3	2.7	5286	979	70.8	0.56	4.7	1876.7	0.77
Barewood	6Orogenic Au	440	101	29.1	17.3	5538	979	76.6	0.64	13.5	1914.9	0.73
Barewood	6Orogenic Au	860	200	41.4	81	4471	780	54.6	0.93	12.9	1595.1	0.77
Barewood	6Orogenic Au	111	17.8	5.7	10.3	3292	509	32.14	0.37	7.93	1031.3	0.75
Barewood	6Orogenic Au	8.7	1.3	2.4	1.3	6540	474	6.39	0.61	8.68	484.31	3.41
Barewood	6Orogenic Au	96	57	27.9	5.2	7080	212	5.92	0.75	13.52	213.35	5.26
Barewood	6Orogenic Au	104	46	420	20.4	5052	909	60.9	0.58	23.4	1479	0.65
Barewood	6Orogenic Au	116	12.6	9	6.4	5680	998	40.4	0.61	7.63	1280.2	0.67
Barewood	6Orogenic Au	101.2	5.8	2	3.3	4352	994	63	0.6	4.38	1668.2	0.86
Barewood	6Orogenic Au	115.8	2	1.3	2.7	4792	1029	70.14	0.57	4.5	1734.4	0.76
Barewood	6Orogenic Au	270	66	2.5	35.2	4676	107	1.8	1.26	56.3	237.92	1.54
Barewood	6Orogenic Au	5.9	4.3	2.1	20.7	3656	53	1.05	1.4	20.05	130.65	3.04
Barewood	6Orogenic Au	4.7	2.4	1.8	5.8	2853	76	1.17	0.36	14.3	197.78	2.37
Barewood	6Orogenic Au	7.6	2.5	1.3	4.4	3525	203	1.58	0.44	5.46	377.86	1.23
Barewood	6Orogenic Au	1.9	1.3	1.9	0.4	4426	59	1.07	0.44	2.88	50.95	4.81
Barewood	6Orogenic Au	6.5	1.8	3.2	2	5100	36	1.14	0.46	5.6	53.78	3.74
Barewood	6Orogenic Au	9.6	1.8	2.6	4.9	4292	48	1.4	0.58	9.07	102.17	3.03
Barewood	6Orogenic Au	2.5	1.5	1.6	0.5	4280	102	1.03	0.44	2.38	179.67	2.52
Barewood	6Orogenic Au	3	1.4	2.2	8.4	4316	69	1.08	0.53	10.31	108.58	3.16
Barewood	6Orogenic Au	86	18.7	4.3	56.8	5107	49	1.25	1.09	50.4	91.72	2.64
Barewood	6Orogenic Au	730	116	1.7	14.5	4152	814	41.4	0.74	14.8	2584.7	0.67
Barewood	6Orogenic Au	49.5	1.2	1.2	1.8	4276	848	28.77	0.78	3.94	1054.2	2.77
Barewood	6Orogenic Au	133.3	1.4	1	8	5260	955	87	0.58	8.56	2131.1	0.65
Barewood	6Orogenic Au	97.8	1.3	1.3	8.6	4438	721	57.69	0.78	10.9	1640.1	0.79
Barewood	6Orogenic Au	10.2	28	1.3	0.9	3515	66	1.21	0.25	1.95	131.22	8.91
Barewood	6Orogenic Au	3	1.7	0.5	1.1	2352	109	0.95	0.19	0.98	125.36	17.12
Barewood	6Orogenic Au	8.1	1.7	0.7	0.9	3334	109	1.35	0.17	1.26	302.63	3.28
Barewood	6Orogenic Au	8.9	18.4	1.9	3.8	3055	120	1.32	0.26	2.46	211.89	6.07
Barewood	6Orogenic Au	0.31	1.6	0.8	0.9	3541	66	0.94	0.16	1.16	126.56	5.73
Barewood	6Orogenic Au	1.7	1.7	0.5	0.7	2304	105	0.97	0.21	0.83	280.73	11.45

Appendix 2.6B (continued)

Name	model 1	Na	Mg	Mn	As	Sr	Y	Nb	Mo	Pb	REE	EuA
Barewood	6Orogenic Au	6.3	1.6	2.8	18.4	4855	50	1.26	0.82	25.4	95.9	1.95
Barewood	6Orogenic Au	16.1	13.3	1.1	2.1	3045	83	1.49	0.66	1.68	147.47	9.41
Barewood	6Orogenic Au	0.39	1.7	0.6	0.9	2768	140	1.25	0.16	0.94	216.68	6.87
Barewood	6Orogenic Au	4.1	1.7	0.6	0.8	2777	107	1.21	0.18	1.06	165.52	7.17
Barewood	6Orogenic Au	4.7	4.9	2.7	2	2538	135	1.47	0.54	1.3	270.27	4.65
Barewood	6Orogenic Au	52	3.3	0.9	1.5	2538	95	1.17	1.94	1.72	207.04	7.68
Barewood	6Orogenic Au	0.33	1.7	0.6	0.8	2583	102	1.1	0.4	0.96	198.16	6.11
Barewood	6Orogenic Au	2.4	1.7	1	0.6	3284	29	1.11	0.18	1.48	58.41	16.88
Barewood	6Orogenic Au	1.3	1.8	0.6	1.1	2519	94	1.12	0.15	1.14	190.41	7.88
Barewood	6Orogenic Au	2.2	1.7	0.6	0.7	2893	69	1.18	0.15	1.06	136.8	8.69
Batemans	3Quartz vein/Greisen	273	15	37.7	0.9	70	758	290.6	8.8	15.4	651.7	0.26
Batemans	3Quartz vein/Greisen	239	19	48.9	0.5	73	739	303.9	7.4	8.2	392.5	0.85
Batemans	3Quartz vein/Greisen	211	12	53	0.5	74	657	281.3	8.6	11.5	358.9	0.89
Batemans	3Quartz vein/Greisen	304	12	40.2	0.9	69	881	352.7	11.3	13.2	579.7	0.45
Batemans	3Quartz vein/Greisen	229	10	47.8	1.2	82	934	313.9	11.6	9.5	593.6	0.49
Batemans	3Quartz vein/Greisen	230	11	45.4	0.7	67	827	288.4	10.6	11.6	489.3	0.75
Batemans	3Quartz vein/Greisen	279	15	40.9	0.8	64	796	273.4	11.3	11.6	526.5	0.53
Batemans	3Quartz vein/Greisen	249	19	47.5	0.9	65	652	288.5	10.4	15.5	443.4	0.39
Batemans	3Quartz vein/Greisen	245	16	40.8	2.3	128	568	206.7	7.7	17.8	381.8	0.51
Batemans	3Quartz vein/Greisen	255	17	48.4	2.9	73	593	290.6	10.7	12.4	438.6	0.35
Batemans	3Quartz vein/Greisen	265	15	40.4	4.5	92	627	337.8	11.4	11.5	464.3	0.32
Batemans	3Quartz vein/Greisen	220	21	41.5	2.1	71	322	128.8	8.3	10.7	267.7	0.53
Batemans	3Quartz vein/Greisen	171	15	47.8	1.6	67	333	144.4	8.2	10.4	280.7	0.56
Batemans	3Quartz vein/Greisen	161	33	36.2	0.8	62	274	163.8	7.6	8.3	268.8	0.42
Batemans	3Quartz vein/Greisen	159	15	49.2	0.7	63	432	173.5	10	15.4	268.6	0.56
Batemans	3Quartz vein/Greisen	210	18	52.2	1.2	78	567	271.4	10	16.6	411.3	0.39
Batemans	3Quartz vein/Greisen	144	19	39.8	2.3	114	399	255.9	9.7	14.7	308.3	0.38
Batemans	3Quartz vein/Greisen	290	19	51	1	67	803	341.9	10	11.4	516	0.41
Batemans	3Quartz vein/Greisen	278	19	42.9	1	67	868	398.9	9.5	11	539	0.44
Batemans	3Quartz vein/Greisen	193	20	46.5	0.7	69	512	225.1	11.5	12.8	326.3	0.49

Appendix 2.6B (continued)

Name	model 1	Na	Mg	Mn	As	Sr	Y	Nb	Mo	Pb	REE	EuA
Batemans	3Quartz vein/Greisen	232	3.68	36.8	0.9	114	538	231.2	8.5	9.9	329.8	1.15
Batemans	3Quartz vein/Greisen	312	17	55.2	0.5	68	825	189.9	10.7	8.6	449.8	1.1
Batemans	3Quartz vein/Greisen	296	14	47.7	0.9	69	778	358.4	10.1	9.4	519.8	0.38
Batemans	3Quartz vein/Greisen	328	11	47.1	0.9	65	818	284	11	28.3	532.8	0.5
Batemans	3Quartz vein/Greisen	248	13	46.5	1	75	687	321.7	9.7	13	429.6	0.49
Batemans	3Quartz vein/Greisen	318	21	38.3	3.4	103	817	483	9.9	0.02	547.2	0.44
Batemans	3Quartz vein/Greisen	274	20	49.2	0.9	65	840	395.2	9.3	7.3	523.1	0.5
Batemans	3Quartz vein/Greisen	228	19	42.8	1.1	71	705	378.9	10	8.7	465.2	0.45
Batemans	3Quartz vein/Greisen	281	12	38.6	3.2	149	426	190.2	6.8	13.5	341.7	0.43
Batemans	3Quartz vein/Greisen	294	10	44.2	1.9	101	610	314.2	9	14.4	478.8	0.35
Batemans	3Quartz vein/Greisen	175	8	41.4	5.8	166	587	400.7	11.7	13.3	480.6	0.34
Batemans	3Quartz vein/Greisen	223	13	35.3	3.1	134	654	405	11.2	10.3	485.5	0.32
Batemans	3Quartz vein/Greisen	269	11	42.2	2.6	110	610	340	10.1	11.3	456.8	0.38
Batemans	3Quartz vein/Greisen	295	15	40.6	3	93	630	256	10.6	11.2	455.9	0.45
Batemans	3Quartz vein/Greisen	450	13	49.4	1.8	67	1474	552	8.3	8.6	1219.6	0.2
Batemans	3Quartz vein/Greisen	448	14	61.2	2	68	1078	363	7.2	8.1	1357.3	0.33
Batemans	3Quartz vein/Greisen	366	13	59.6	2.9	58	976	732	7.9	9	1568.2	0.11
Batemans	3Quartz vein/Greisen	328	13	37.5	4.1	66	633	411.1	7.8	1.7	971.8	0.12
Batemans	3Quartz vein/Greisen	418	15	41.6	2.7	68	1039	573.2	8.8	0.02	823	0.22
Batemans	3Quartz vein/Greisen	281	18	40.4	1.3	61	677	298.2	10.8	0.02	345	1.26
Batemans	3Quartz vein/Greisen	243	4.09	29	4	75	831	413.5	10.1	8.1	575	0.57
Batemans	3Quartz vein/Greisen	227	3.42	33.3	1.8	61	921	369.9	10.4	0.01	675.9	0.86
Batemans	3Quartz vein/Greisen	152	27	27.5	1.8	72	369	260.6	8.7	0.02	387	0.38
Batemans	3Quartz vein/Greisen	252	3.61	33.3	2.1	71	841	328	11.6	0.02	562.9	0.81
Batemans	3Quartz vein/Greisen	268	17	34	1.8	67	852	369.2	9.7	0.02	596.2	0.99
Batemans	3Quartz vein/Greisen	243	5.02	41.9	1.3	68	811	247.2	10.3	0.01	501	0.6
Batemans	3Quartz vein/Greisen	322	4.58	38.7	1.3	67	967	340.9	10	0.02	655.8	0.43
Batemans	3Quartz vein/Greisen	314	4.04	40.7	1.8	65	1043	342.1	9.9	0.02	712.4	0.41
Batemans	3Quartz vein/Greisen	256	17	52	1.4	61	739	370.9	10.4	4.5	475.4	0.49
Batemans	3Quartz vein/Greisen	320	13	47.3	1.6	74	1355	551.2	7.5	7.7	1014.4	0.28

Appendix 2.6B (continued)

Name	model 1	Na	Mg	Mn	As	Sr	Y	Nb	Mo	Pb	REE	EuA
Batemans	3Quartz vein/Greisen	230	3.64	39.6	1.2	63	727	263	10.1	0.01	502.6	0.57
Batemans	3Quartz vein/Greisen	385	4.7	39	1.8	68	1161	269.2	8.9	0.02	783.3	0.66
Batemans	3Quartz vein/Greisen	251	3.01	47.3	1.7	66	998	389	10.4	0.02	747.2	0.53
Batemans	3Quartz vein/Greisen	245	2.67	43.2	1.4	65	946	366.6	9.7	0.01	656.9	0.45
Batemans	3Quartz vein/Greisen	342	3.65	32.8	1.7	90	1261	409.2	7.5	18.1	839.7	0.53
Batemans	3Quartz vein/Greisen	176	3.95	39.9	1.2	84	724	325	10.5	1.2	495.4	0.46
Batemans	3Quartz vein/Greisen	122	3.27	56.4	1	61	687	353.2	10.8	0.02	444.5	0.55
Batemans	3Quartz vein/Greisen	159	3.39	57.1	0.9	61	603	278.3	12	0.02	369.5	0.52
Batemans	3Quartz vein/Greisen	204	4.87	42.7	1.4	64	904	355.3	10.4	10.6	601.7	0.39
Batemans	3Quartz vein/Greisen	223	4.31	44.7	1	59	805	290.5	11.3	0.02	494.7	0.52
Batemans	3Quartz vein/Greisen	133	3.93	49.3	0.8	73	571	212.8	9.1	0.02	359.1	0.55
Batemans	3Quartz vein/Greisen	151	19	42.5	2.3	75	357	131.5	9.2	13.2	328.4	0.52
Batemans	3Quartz vein/Greisen	250	19	40.9	1.1	54	380	169.9	8.3	12.1	331	0.47
Batemans	3Quartz vein/Greisen	203	26	40.8	1.4	59	304	126	7.8	11.7	280.9	0.47
Batemans	3Quartz vein/Greisen	364	13	30.9	1.2	61	898	396.9	12.3	9.3	623.2	0.32
Batemans	3Quartz vein/Greisen	266	12	31.5	1.4	66	941	664	10.4	10.4	642	0.32
Batemans	3Quartz vein/Greisen	354	4.1	26.4	2.1	130	884	420.3	11.2	0.02	599.3	0.24
Batemans	3Quartz vein/Greisen	431	4.62	34.4	1.6	61	901	423.6	10.6	0.02	595.7	0.3
Batemans	3Quartz vein/Greisen	422	4.19	31.3	1.5	93	1091	532.6	12.2	12.9	792.2	0.28
Batemans	3Quartz vein/Greisen	303	18	35	0.3	70	493	96.6	7.3	10.7	275.5	2
Batemans	3Quartz vein/Greisen	205	3.59	43.8	0.6	68	838	286.1	10.3	10.9	457	1.01
Batemans	3Quartz vein/Greisen	343	13	27.4	0.9	71	1075	337.1	10.7	12	617.6	0.7
Batemans	3Quartz vein/Greisen	195	16	34.5	0.7	75	602	322.1	10.1	10.8	404	0.81
Batemans	3Quartz vein/Greisen	214	23	34.5	0.28	75	626	324.7	10.7	12.3	437.2	0.79
Batemans	3Quartz vein/Greisen	134	2.93	32.9	0.8	74	609	328.3	10.3	8.8	404.3	0.8
Batemans	3Quartz vein/Greisen	288	15	32.7	0.9	65	998	317.7	10.1	11.1	557.6	0.78
Batemans	3Quartz vein/Greisen	275	16	34	0.9	73	744	389.8	9.1	11	485.4	0.46
Batemans	3Quartz vein/Greisen	252	16	24.9	1.2	81	835	378.7	10.4	13.4	555.4	0.37
Batemans	3Quartz vein/Greisen	282	13	26.3	1.2	80	821	366.5	11	15.2	564.3	0.38
Batemans	3Quartz vein/Greisen	298	17	39.1	0.6	65	653	174.5	9.3	10.4	390.2	0.78

Appendix 2.6B (continued)

Name	model 1	Na	Mg	Mn	As	Sr	Y	Nb	Mo	Pb	REE	EuA
Batemans	3Quartz vein/Greisen	269	10	36.8	0.7	63	918	261.1	10.8	9.7	530.1	0.72
Batemans	3Quartz vein/Greisen	152	2.52	49	0.27	86	890	374.1	10	9.6	525.5	0.73
Batemans	3Quartz vein/Greisen	265	15	37.5	0.9	69	900	295.3	11.2	9.6	547.8	0.95
Batemans	3Quartz vein/Greisen	245	14	37.1	0.27	69	789	293	11.1	10.6	417.7	1.12
Batemans	3Quartz vein/Greisen	257	15	37.7	1.3	65	772	323.3	11.2	9.7	449.3	0.64
Batemans	3Quartz vein/Greisen	254	3.85	35.7	1.8	68	978	732.6	11.7	0.02	727.1	0.39
Batemans	3Quartz vein/Greisen	224	3.08	30.3	1.7	73	864	332	11.1	0.02	723.6	0.35
Batemans	3Quartz vein/Greisen	338	3.77	29.4	2.2	65	979	349.6	12.3	0.02	896.3	0.6
Batemans	3Quartz vein/Greisen	336	3.03	28.5	2	68	1351	727.5	9.7	0.02	1094	0.24
Batemans	3Quartz vein/Greisen	330	3.46	37.3	2.1	65	1223	496.9	10.1	0.02	904.7	0.55
Batemans	3Quartz vein/Greisen	240	14	27.5	3	84	953	458.4	7.9	0.02	782.4	0.33
Batemans	3Quartz vein/Greisen	254	13	24.5	2.7	78	779	362.1	10.7	0.02	580.3	0.33
Batemans	3Quartz vein/Greisen	99	3.18	27.8	2.8	89	433	178.7	7.4	1.2	409.9	0.31
Batemans	3Quartz vein/Greisen	259	2.8	25.4	2.7	72	1127	700	9.6	1.8	960.5	0.22
Batemans	3Quartz vein/Greisen	239	4.91	30.6	3.9	67	528	455.2	7.3	2.8	1114.4	0.1
Batemans	3Quartz vein/Greisen	731	21	26.4	3.3	101	737	350.9	10.1	0.02	582.8	0.26
Batemans	3Quartz vein/Greisen	208	192	21.3	1	195	248	13.9	8.2	18.4	326.7	0.77
Batemans	3Quartz vein/Greisen	257	75	14.7	0.33	205	150	7.7	9.4	11.7	167.8	1.26
Batemans	3Quartz vein/Greisen	218	74	19.5	0.8	229	465	14.9	4.9	11.1	511	2.75
Batemans	3Quartz vein/Greisen	184	3.19	12.1	0.2	174	286	51.1	4.8	23.8	203.7	3.9
Batemans	3Quartz vein/Greisen	187	16	18.4	0.5	191	247	9.1	6	24.8	165.9	3.4
Batemans	3Quartz vein/Greisen	176	5.78	29	1.3	212	486	11.6	4.1	12.6	660.2	1.39
Batemans	3Quartz vein/Greisen	293	51	13	0.32	222	339	13.8	4.6	15.7	280.4	1.28
Batemans	3Quartz vein/Greisen	281	49	60	1.6	260	250	66.7	7.2	14.9	1174	1.3
Batemans	3Quartz vein/Greisen	275	338	50.7	1	430	102	38	6.1	21.5	627.2	1.56
Batemans	3Quartz vein/Greisen	376	45	24.8	2.3	388	206	62.6	6	26.9	1037.4	0.84
Batemans	3Quartz vein/Greisen	256	69	98.6	2.7	310	266	70.1	6.1	18.3	1685	0.79
Batemans	3Quartz vein/Greisen	293	42	42.9	1.3	173	513	74.2	7.2	7.7	683.6	0.46
Batemans	3Quartz vein/Greisen	229	38	53	1.2	175	474	72.1	7	9.4	661.4	0.37
Batemans	3Quartz vein/Greisen	186	56	62.4	0.18	242	60	13.1	6.4	11.1	262.5	5.03

Appendix 2.6B (continued)

Name	model 1	Na	Mg	Mn	As	Sr	Y	Nb	Mo	Pb	REE	EuA
Batemans	3Quartz vein/Greisen	154	86	74.5	0.32	274	60	24.1	7.1	17.9	324.2	7.32
Batemans	3Quartz vein/Greisen	176	91	70.7	0.35	276	126	15	7.8	15.9	430.5	8.57
Batemans	3Quartz vein/Greisen	282	42	27.9	1	250	216	26.7	5.3	16.8	692.7	1.47
Batemans	3Quartz vein/Greisen	568	38	13.3	2.7	565	220	33.3	5.5	49.4	421.3	1.02
Batemans	3Quartz vein/Greisen	186	48	64.3	1.1	250	147	33.2	5	14.7	586.2	0.99
Batemans	3Quartz vein/Greisen	234	30	19.6	0.7	345	166	13.7	5.3	27.7	327	2.27
Batemans	3Quartz vein/Greisen	530	61	16.3	2.1	832	146	19.5	4.8	45.1	308.4	1.66
Batemans	3Quartz vein/Greisen	270	37	23	0.9	213	380	25.9	5.8	14.1	519.4	1.21
Batemans	3Quartz vein/Greisen	477	31	10.4	1.7	364	396	44.8	7	50.2	509.1	0.64
Batemans	3Quartz vein/Greisen	286	59	30.7	1.2	264	163	20.7	6.3	27.3	745.1	1.35
Batemans	3Quartz vein/Greisen	112	36	39	0.5	260	129	14.1	5	13	291.6	2.75
Batemans	3Quartz vein/Greisen	181	41	32.9	0.8	255	129	24.7	5.4	17.5	431.2	1.57
Batemans	3Quartz vein/Greisen	284	30	20	0.8	269	220	27.5	5.4	25.3	364.6	1.23
Batemans	3Quartz vein/Greisen	273	72	20.5	1	302	169	13.4	6.5	29.8	305.8	1.47
Batemans	3Quartz vein/Greisen	265	59	34.3	1.1	274	189	50.3	5	13.2	595.6	0.93
Batemans	3Quartz vein/Greisen	274	23	19.8	1.5	277	204	20.4	4.7	13.9	682.7	0.89
Batemans	3Quartz vein/Greisen	153	19	24.6	0.8	329	129	14.8	5	27.5	408.7	1.37
Batemans	3Quartz vein/Greisen	590	73	26.2	1.1	397	66	50.3	7.5	43.7	387.6	0.72
Batemans	3Quartz vein/Greisen	432	362	322	14.6	2096	273	45.6	6.4	80.3	614.6	0.79
Batemans	3Quartz vein/Greisen	437	54	14.2	3.8	895	172	59.6	7.3	49.4	742.5	0.65
Batemans	3Quartz vein/Greisen	820	170	24	1	364	69	34.1	8	37.2	409.7	2.54
Batemans	3Quartz vein/Greisen	380	168	16.2	3.6	965	166	65.8	7.8	52.9	588.5	0.78
Beaufor	6Orogenic Au	110.8	5.72	1.59	9.68	558	448	6	63.5	6.52	628.75	0.74
Beaufor	6Orogenic Au	132	4.63	2.81	11.9	563	483	6.92	61.1	5.69	689.83	0.7
Beaufor	6Orogenic Au	103	5.8	3.6	9	493	327	4.62	63.1	5.31	500.06	0.72
Beaufor	6Orogenic Au	152	3.39	2.89	7.4	541	419	4.11	65.6	11.6	720.97	0.76
Beaufor	6Orogenic Au	196	3.36	3.31	7.7	589	471	4.86	67	7.6	765.18	0.75
Beaufor	6Orogenic Au	82.2	4.08	2.97	11.3	574	238	3.7	209	9.6	412.35	0.63
Beaufor	6Orogenic Au	97	4.28	3.01	6.9	554	397	4.38	61.1	7.87	652.91	0.74
Beaufor	6Orogenic Au	82.2	8.2	3.7	7.66	579	393	4.5	61.7	6.74	645.74	0.76

Appendix 2.6B (continued)

Name	model 1	Na	Mg	Mn	As	Sr	Y	Nb	Mo	Pb	REE	EuA
Beaufor	6Orogenic Au	158	3.33	3.78	6.4	560	418	4.84	68.3	8.55	766.2	0.72
Beaufor	6Orogenic Au	120	4.32	3.42	7.4	561	394	4.36	79	8.28	665.82	0.73
Beaufor	6Orogenic Au	85.8	3.82	4.37	9.1	538	612	6.8	67.1	15.5	845.34	0.61
Beaufor	6Orogenic Au	82	4.09	4.11	9.95	542	540	5.43	65.8	14.82	774.46	0.63
Beaufor	6Orogenic Au	66.8	3.86	4.26	11.1	544	348	4.42	61.2	15	594.7	0.71
Beaufor	6Orogenic Au	215.9	4.45	2.88	3.17	667	853	7.84	16.9	16	2025.9	0.53
Beaufor	6Orogenic Au	324	4.28	3.36	6.8	660	780	7.27	25	7.31	3559.3	0.55
Beaufor	6Orogenic Au	272	4.55	2.99	4.3	672	842	7.81	19.8	34	2492.9	0.54
Beaufor	6Orogenic Au	160.8	4.95	4.15	2	651	267.5	3.95	18.99	23	688.51	0.66
Beaufor	6Orogenic Au	362	5.18	3.78	3.43	700	661	8.64	17.97	13.1	1812	0.51
Beaufor	6Orogenic Au	277	5.7	3.26	3.19	653	800	9.72	18.8	25	2070.1	0.53
Beaufor	6Orogenic Au	314	4.44	3.86	2.74	635	576	7.14	17.2	12.11	1531.9	0.55
Beaufor	6Orogenic Au	310	4.95	3.46	3.06	658	657	7.97	17.87	16.5	1735.8	0.53
Beaufor	6Orogenic Au	247.9	6	3.07	5.9	654	492	7.05	19	18.6	1344	0.52
Beaufor	6Orogenic Au	247	5.81	2.9	4.33	656	589	7.47	19.5	31	1501.4	0.54
Bomfim	5Reduced skarn	32.8	4.48	15.46	0.69	192.93	61.3	23.07	832.6	3.45	183.27	0.73
Bomfim	5Reduced skarn	25.16	3.81	14.18	0.82	185.43	50.46	22.74	807.6	3.7	153.21	0.66
Bomfim	5Reduced skarn	28.75	3.67	13.84	0.74	186.54	53.24	23.24	817.3	3.35	167.33	0.77
Bomfim	5Reduced skarn	29.05	4.34	12.93	0.81	183.76	46.29	23	828.4	4.2	145.96	0.63
Bomfim	5Reduced skarn	26.66	3.64	12.7	0.82	176.11	47.68	20.92	736.7	3.14	166.36	0.67
Bomfim	5Reduced skarn	28.37	3.54	14.6	0.78	184.87	50.74	22.17	764.5	2.9	175.93	0.7
Bomfim	5Reduced skarn	14.39	3.34	11.31	0.78	178.62	33.55	19.52	743.7	3.38	109.83	0.56
Bomfim	5Reduced skarn	13.37	3.61	9.27	0.86	181.95	36.89	19.99	774.2	3.25	115.64	0.54
Bonne Jean - Glenorchy	6Orogenic Au	480	52	4.5	20	6100	111	1.87	0.79	2.2	465.78	1.67
Bonne Jean - Glenorchy	6Orogenic Au	460	100	8	13	5200	122	1.28	0.42	2.9	488.47	1.26
Bonne Jean - Glenorchy	6Orogenic Au	360	71	2	6.3	4580	108	1.49	0.29	1.37	491.32	1.17
Bonne Jean - Glenorchy	6Orogenic Au	180	49	2.9	13	5100	168	1.15	0.39	1.97	893.14	1.26
Bonne Jean - Glenorchy	6Orogenic Au	250	210	3	9.6	6300	101	1.41	0.2	1.73	716.01	1.17
Bonne Jean - Glenorchy	6Orogenic Au	580	100	3.1	16	4400	92	0.89	0.35	1.89	354.52	1.43
Bonne Jean - Glenorchy	6Orogenic Au	160	64	2	9.5	3600	51	1.17	0.48	1.17	452.97	0.7

Appendix 2.6B (continued)

Name	model 1	Na	Mg	Mn	As	Sr	Y	Nb	Mo	Pb	REE	EuA
Bonne Jean - Glenorchy	6Orogenic Au	90	15	2	2.8	5800	38	1.65	0.22	3.1	104.25	2.52
Bonne Jean - Glenorchy	6Orogenic Au	71	20	2.4	2.4	7300	23	1.64	0.19	3.12	71.28	3.98
Bonne Jean - Glenorchy	6Orogenic Au	120	24	2.1	2.7	6400	47	1.76	0.3	3.3	136.46	2.33
Bonne Jean - Glenorchy	6Orogenic Au	220	22	2.9	7.3	5400	97	2.58	0.32	2.05	236.63	4
Bonne Jean - Glenorchy	6Orogenic Au	25	2	3.6	2	4300	59	3.2	0.23	1.67	163.27	2.64
Bonne Jean - Glenorchy	6Orogenic Au	180	29	2.5	1.9	6400	26	2.7	0.51	2.3	67.2	6.94
Bonne Jean - Glenorchy	6Orogenic Au	67	13	2.2	2.8	5200	35	2.91	0.1	2.24	102.23	2.06
Bonne Jean - Glenorchy	6Orogenic Au	900	150	3.5	23	4230	82	3.41	0.58	1.66	374.97	0.93
Bonne Jean - Glenorchy	6Orogenic Au	30	2	1.1	0.43	5820	35	1.67	0.15	1.69	103.72	2.9
Bonne Jean - Glenorchy	6Orogenic Au	58	7	1.7	1.4	4550	25	1.26	0.08	2.6	63.54	2.39
Bonne Jean - Glenorchy	6Orogenic Au	53	9	2.4	3.1	5500	20	1.14	0.12	1.62	58.43	3.41
Bonne Jean - Glenorchy	6Orogenic Au	20	4	1.5	1.3	4500	16	0.9	0.02	1.34	40.5	6.61
Bonne Jean - Glenorchy	6Orogenic Au	37	5	1.6	0.67	6700	23	1.57	0.18	1.68	93.79	2.47
Bonne Jean - Glenorchy	6Orogenic Au	79	12	1.5	0.5	5400	96	3.9	0.9	1.43	271.89	1.15
Bonne Jean - Glenorchy	6Orogenic Au	170	19	0.8	5.6	5200	142	1.71	0.23	1.59	716.33	0.9
Bonne Jean - Glenorchy	6Orogenic Au	420	80	1.5	11	4200	133	1.41	0.29	1.52	540.18	1.18
Bonne Jean - Glenorchy	6Orogenic Au	400	67	1.4	12	5600	202	1.36	0.18	2.3	1074.2	1.13
Bonne Jean - Glenorchy	6Orogenic Au	380	60	2.5	9.8	5900	50	1.42	0.4	2.4	168.36	1.72
Bonne Jean - Glenorchy	6Orogenic Au	520	100	2.9	6.8	7400	37	1.49	0.46	3	102.58	2.15
Bonne Jean - Glenorchy	6Orogenic Au	520	100	3.8	11	5500	38	1.43	0.34	5.9	131.26	2.22
Bonne Jean - Glenorchy	6Orogenic Au	720	180	55	25	4300	173	0.79	0.78	1.79	666.65	1.84
Bonne Jean - Glenorchy	6Orogenic Au	140	18	2.2	7.7	6300	68	1.62	0.36	2.08	320.53	1.91
Bonne Jean - Glenorchy	6Orogenic Au	89	18	1.2	1.5	5300	40	1.48	0.27	1.52	151.61	2.07
Bonne Jean - Glenorchy	6Orogenic Au	900	130	3.1	14	5800	62	1.19	0.32	2.09	166.3	2.2
Bonne Jean - Glenorchy	6Orogenic Au	900	90	2.6	12	5370	29	1.38	0.25	2.06	74.82	4.78
Bonne Jean - Glenorchy	6Orogenic Au	700	90	3.5	22	5600	33	1.24	0.33	2.71	85.32	2.51
Bonne Jean - Glenorchy	6Orogenic Au	190	33	3.3	8.8	7800	31	1.31	0.79	3.02	90.32	2.67
Brejui	4Oxidized skarn	10.98	25.19	15.6	1.84	678.88	3.41	5.54	6483	9.47	36.06	0.78
Brejui	4Oxidized skarn	3.64	23.85	18.18	1.45	601.31	2.24	5.9	6213	12.82	29.47	0.77
Brejui	4Oxidized skarn	3.77	23.76	17.82	1.29	569.76	2.02	5.78	6186	11.76	26.08	0.77

Appendix 2.6B (continued)

Name	model 1	Na	Mg	Mn	As	Sr	Y	Nb	Mo	Pb	REE	EuA
Brejui	4Oxidized skarn	13.34	23.99	16.76	1.67	563.23	3.11	4.66	5796	6.92	18	0.77
Brejui	4Oxidized skarn	1.39	14.73	4.87	2.07	289.82	1.14	7.33	5185	6.42	1.66	0.29
Brejui	4Oxidized skarn	1.47	14.89	4.82	1.97	288.01	1.07	7.31	4964	6.82	1.63	0.36
Brejui	4Oxidized skarn	0.97	13.8	4.52	2.4	300.24	0.66	7.24	5486	6.31	1.82	0.34
Brejui	4Oxidized skarn	1.4	14.07	4.49	2.2	303.3	0.74	6.99	5496	6.42	1.58	0.48
Brejui	4Oxidized skarn	4.71	14.86	5.04	2.24	251.03	1.25	5.4	4452	6.31	1.16	0.39
Brejui	4Oxidized skarn	2.78	15.19	4.76	1.84	305.94	0.63	7.03	5842	6.45	1.27	0.35
Brejui	4Oxidized skarn	8.62	13.91	4.95	1.98	262.99	1.14	5.49	4852	6.23	1.07	0.36
Brejui	4Oxidized skarn	0.44	13.73	4.89	2.02	289.68	0.56	5.85	5465	6.42	1.66	0.49
Brejui	4Oxidized skarn	0.76	13.66	4.82	1.86	289.4	0.59	6.02	5379	6.38	1.52	0.34
Brejui	4Oxidized skarn	3.68	22.84	18.13	1.4	593.25	2.34	5.73	6302	11.55	28.06	0.75
Brejui	4Oxidized skarn	4.34	23.48	14.34	1.75	578.1	3.01	4.93	5791	6.2	30.2	0.74
Brejui	4Oxidized skarn	2.65	22.46	13.25	1.32	548.08	3.2	4.5	5731	5.63	21.24	0.72
Brejui	4Oxidized skarn	9.04	17.58	19.29	0.63	505.27	4.18	4.16	5980	9.51	9.36	0.68
Brejui	4Oxidized skarn	0.4	15.42	5.23	1.6	303.58	0.66	7.25	5406	6.59	1.85	0.39
Buzwagi	6Orogenic Au	52.9	80	32.73	4.01	1948	94.4	2.1	142.5	34.4	262.13	0.92
Canaan Downs	3Quartz vein/Greisen	187	19	6.9	23.2	730	361	30.5	40.6	0.01	1204.1	1.17
Canaan Downs	3Quartz vein/Greisen	213	38	7.9	30.5	706	304	22.2	94.6	32.4	1009.9	1.17
Canaan Downs	3Quartz vein/Greisen	174	46	6.9	26.8	532	407	22.3	46.7	0.01	1705.5	1.2
Canaan Downs	3Quartz vein/Greisen	29.78	4.52	6.3	32.2	892	446	23.4	74.1	0.01	1422.5	1.1
Canaan Downs	3Quartz vein/Greisen	26.79	6.4	10.7	22.4	758	406	25.5	55.6	0.01	1020.6	1.34
Canaan Downs	3Quartz vein/Greisen	189	33	5.9	27.1	510	423	20.6	45.3	0.02	2043.2	1.12
Canaan Downs	3Quartz vein/Greisen	38.89	37	8.2	22.1	537	221	36.2	96.4	0.02	1681.7	1.08
Canaan Downs	3Quartz vein/Greisen	193	40	6.7	23.8	708	430	22.9	64	8.2	1224.4	1.27
Canaan Downs	3Quartz vein/Greisen	134	38	7.3	17.8	654	394	23.3	46.8	67.7	1283.8	1.47
Canaan Downs	3Quartz vein/Greisen	94	4.91	7.8	40.2	1125	652	23	84.6	0.02	2319.6	1.17
Canaan Downs	3Quartz vein/Greisen	272	50	7.8	23.1	569	650	12.6	73.1	0.01	1672.2	1.62
Canaan Downs	3Quartz vein/Greisen	151	63	8.3	24.4	550	774	8.7	74.3	92	3447.3	1.51
Canaan Downs	3Quartz vein/Greisen	343	35	6.7	87.2	1340	806	64.8	66.5	7.6	2785.2	1.12
Canaan Downs	3Quartz vein/Greisen	248	67	9	21.3	402	679	15.5	59.8	0.02	1717.5	1.55

Appendix 2.6B (continued)

Name	model 1	Na	Mg	Mn	As	Sr	Y	Nb	Mo	Pb	REE	EuA
Canaan Downs	3Quartz vein/Greisen	245	27	6.2	31.8	913	422	21.1	83.9	17.1	1529.4	1.33
Canaan Downs	3Quartz vein/Greisen	234	41	8.6	33.6	759	471	24.2	68.8	0.02	1420.4	1.3
Canaan Downs	3Quartz vein/Greisen	51.29	28	9	22.9	698	446	29.5	53.6	14.8	2004.2	1.35
Canaan Downs	3Quartz vein/Greisen	245	27	6.2	31.8	913	422	21.1	83.9	17.1	1529.4	1.33
Canaan Downs	3Quartz vein/Greisen	234	41	8.6	33.6	759	471	24.2	68.8	0.02	1420.4	1.3
Canaan Downs	3Quartz vein/Greisen	304	37	5.9	23	729	629	26.9	62.7	17.9	1558.7	1.45
Canaan Downs	3Quartz vein/Greisen	39.32	30	7.5	27	702	802	31	83.7	0.02	2104.6	1.41
Canaan Downs	3Quartz vein/Greisen	45.16	49	10.4	27.8	783	917	21.7	69.6	0.02	2457.2	1.49
Canaan Downs	3Quartz vein/Greisen	172	41	9.6	23.2	491	328	22.7	44.5	0.03	2165.6	1.25
Canaan Downs	3Quartz vein/Greisen	213	5.36	7	37	1039	393	22.8	71.2	0.02	1073.9	1.13
Canaan Downs	3Quartz vein/Greisen	44.23	19	7	39.7	1074	525	25.2	72.2	0.001	1883.1	1.15
Canaan Downs	3Quartz vein/Greisen	60.88	67	10.4	13.4	437	390	9.5	72.5	0.02	1471.7	1.93
Canaan Downs	3Quartz vein/Greisen	203	74	10.3	19.4	427	729	12.8	76.4	0.03	2092.9	1.81
Canaan Downs	3Quartz vein/Greisen	47.47	29	8.4	22.3	555	488	9.9	58.4	0.02	1405.5	1.44
Canaan Downs	3Quartz vein/Greisen	67.28	81	8.4	16.9	460	667	10.6	86.1	0.02	1805.6	1.82
Canaan Downs	3Quartz vein/Greisen	40.24	24	9.5	27.7	746	923	29.8	74.9	0.02	2361.9	1.36
Canaan Downs	3Quartz vein/Greisen	60.47	28	8.9	30.5	658	644	30.4	70.2	2.4	1443.6	1.36
Canaan Downs	3Quartz vein/Greisen	54.11	31	10.5	31.8	729	500	27.1	70.3	30.9	1180.9	1.22
Canaan Downs	3Quartz vein/Greisen	48.6	37	9.3	26.3	648	720	24.5	86.7	3.7	1968.8	1.43
Canaan Downs	3Quartz vein/Greisen	51.86	72	12.5	18.4	483	561	9.4	48.5	0.02	2259.3	1.49
Canaan Downs	3Quartz vein/Greisen	47.55	41	7.9	20.1	606	455	9	58.7	0.02	1715	1.53
Canaan Downs	3Quartz vein/Greisen	110	50	9.1	21.1	493	542	12.3	75.3	0.02	1444.9	1.66
Canaan Downs	3Quartz vein/Greisen	201	43	6.1	20.8	638	359	10.7	63.2	0.02	652.5	1.7
Canaan Downs	3Quartz vein/Greisen	164	59	8.3	26.6	654	669	11.7	100.9	0.02	2307.3	1.39
Canaan Downs	3Quartz vein/Greisen	402	26	5.9	41.1	991	679	25.3	73.8	0.02	2192.9	1.15
Canaan Downs	3Quartz vein/Greisen	284	36	4.7	25.7	812	388	18.1	75.5	0.02	1395.5	1.4
Canaan Downs	3Quartz vein/Greisen	156	24	8	42.9	1083	657	24.7	74	2.8	2448.8	1.11
Canaan Downs	3Quartz vein/Greisen	317	26	6	38.8	1075	565	22.7	75.3	76	2895.3	1.11
Canaan Downs	3Quartz vein/Greisen	36.46	47	8.9	23.8	516	765	11.8	69.2	0.02	2094.3	1.68
Canaan Downs	3Quartz vein/Greisen	300	25	5.7	26.4	1216	337	29.8	100	14.6	964.3	1.24

Appendix 2.6B (continued)

Name	model 1	Na	Mg	Mn	As	Sr	Y	Nb	Mo	Pb	REE	EuA
Canaan Downs	3Quartz vein/Greisen	261	54	9.2	17.8	526	148	21.3	91.6	20	968.7	1.21
Canaan Downs	3Quartz vein/Greisen	144	48	11.8	21.4	443	147	33.4	55.2	0.02	1586.3	1.07
Canaan Downs	3Quartz vein/Greisen	145	36	7.7	20.4	747	332	15.3	93.3	11.3	1416.7	1.33
Canaan Downs	3Quartz vein/Greisen	193	71	8	18.7	669	211	11.5	147.8	37.1	1317.3	1.59
Canaan Downs	3Quartz vein/Greisen	37.29	29	9.1	26.6	793	298	18.9	81.3	61.4	1515.6	1.05
Canaan Downs	3Quartz vein/Greisen	155	39	6.3	24.8	822	248	14.9	72.5	0.02	876.2	1.36
Canaan Downs	3Quartz vein/Greisen	237	40	7.1	22.6	593	385	16.7	67.8	11.5	1475.3	1.36
Canaan Downs	3Quartz vein/Greisen	159	31	7.4	26.1	761	415	19.7	68.6	0.02	1923.3	1.16
Canaan Downs	3Quartz vein/Greisen	189	84	9.5	27.7	566	485	31.9	133.5	26.6	2770.6	1.14
Canaan Downs	3Quartz vein/Greisen	326	50	6.1	24	595	398	18.2	69.1	0.01	1617.8	1.3
Canaan Downs	3Quartz vein/Greisen	212	39	7.1	29.2	723	496	20.1	68.8	6.1	2131.6	1.17
Canaan Downs	3Quartz vein/Greisen	389	35	6.3	44.8	1004	751	23.5	75.5	5.9	2675.9	1.2
Canaan Downs	3Quartz vein/Greisen	233	31	6.3	34.5	772	539	23.5	58.8	0.01	1990.9	1.24
Canaan Downs	3Quartz vein/Greisen	289	33	6.2	34.1	1166	602	21.5	77.6	3	2213.1	1.17
Canaan Downs	3Quartz vein/Greisen	324	45	7.2	22.2	629	408	29.2	46	12.5	1838.5	1.18
Canaan Downs	3Quartz vein/Greisen	54.43	68	12.9	63.4	578	462	48.4	137.1	17.4	2342.9	1.12
Canaan Downs	3Quartz vein/Greisen	98	33	9.4	25.1	612	526	39.4	59.6	0.02	1760.5	1.33
Canaan Downs	3Quartz vein/Greisen	39.15	35	9	19.4	623	441	24	46.5	0.02	1376.5	1.56
Canaan Downs	3Quartz vein/Greisen	72	38	9.8	19.4	610	501	23	39.1	0.02	1618.8	1.62
Canaan Downs	3Quartz vein/Greisen	91	31	11.8	19.8	562	487	19.8	51.9	29.7	1525	1.7
Canaan Downs	3Quartz vein/Greisen	158	36	8.9	17.5	594	443	22.3	46.1	8.7	1433.2	1.6
Canaan Downs	3Quartz vein/Greisen	189	31	7.6	39.1	687	577	28.4	65.2	0.02	2165.2	1.17
Canaan Downs	3Quartz vein/Greisen	153	37	8.8	24.8	761	429	24	51.1	6.4	1988.2	1.4
Canaan Downs	3Quartz vein/Greisen	194	22	8.6	36	1052	745	15.1	70.6	2.1	2390.4	1.58
Canaan Downs	3Quartz vein/Greisen	95	22	8.1	33.7	1167	467	22.1	69.6	2.3	1949.7	1.13
Canaan Downs	3Quartz vein/Greisen	221	40	7.7	32.6	911	402	22.4	68	88	1378.4	1.18
Canaan Downs	3Quartz vein/Greisen	177	24	7.3	28.2	809	390	21	51.3	0.02	1283.8	1.21
Canaan Downs	3Quartz vein/Greisen	163	28	8.8	35.1	1113	453	20.6	75.9	21.3	1618.4	1.18
Canaan Downs	3Quartz vein/Greisen	77	48	11.5	19.6	864	346	26.7	118.2	5.7	1551.3	1.4
Canaan Downs	3Quartz vein/Greisen	80	24	11.8	24.8	929	366	26.6	47.4	0.01	1936.3	1.15

Appendix 2.6B (continued)

Name	model 1	Na	Mg	Mn	As	Sr	Y	Nb	Mo	Pb	REE	EuA
Canaan Downs	3Quartz vein/Greisen	125.57	4.93	0.78	23.3	4670	164	23	72.3	0.06	809.2	1.14
Canaan Downs	3Quartz vein/Greisen	124	28	10.1	25	797	394	24.1	55.4	0.02	1108	1.43
Canaan Downs	3Quartz vein/Greisen	34.4	42	26.8	67.3	0.09	338	13.8	62.5	36.5	1428.5	1.34
Canaan Downs	3Quartz vein/Greisen	30.55	53	36.8	20.6	0.09	131	15.9	37	44.6	1025	1.13
Canaan Downs	3Quartz vein/Greisen	25.17	66	59.9	15.4	0.09	71	18.8	63	10.9	1019.9	1.12
Canaan Downs	3Quartz vein/Greisen	20.3	26	42	33.7	0.09	390	22.9	49.3	0.08	1722.6	1.14
Canaan Downs	3Quartz vein/Greisen	11.16	28	49.4	34.6	0.09	476	17.3	62.9	0.001	2305.2	1.11
Canaan Downs	3Quartz vein/Greisen	42.28	47	95.2	27.1	0.1	123	18.2	60	60.2	863.3	1.12
Canaan Downs	3Quartz vein/Greisen	40.47	34	85	35.3	0.01	369	17.1	81.9	0.02	1772	1.12
Canaan Downs	3Quartz vein/Greisen	40.91	79	139	21	0.02	40	25	84.7	60.9	663.3	1.01
Canaan Downs	3Quartz vein/Greisen	183.01	59	284	22.2	0.03	54	23.3	80.2	52	785.6	1.04
Canaan Downs	3Quartz vein/Greisen	233.15	8.67	284.9	33.2	0.04	392	17.6	80.2	0.01	2020.3	1.27
Canaan Downs	3Quartz vein/Greisen	134	48	10.5	20.6	502	254	26.3	39.8	0.001	1788.8	1.13
Canaan Downs	3Quartz vein/Greisen	150	61	10.5	20.4	406	382	21.5	41.8	0.03	2193.8	1.15
Canaan Downs	3Quartz vein/Greisen	196	30	7.8	25.1	792	322	17.7	66.8	0.02	1347.8	1.24
Canaan Downs	3Quartz vein/Greisen	109	29	8.7	21.9	736	361	18.5	76.8	0.02	1593.9	1.28
Canaan Downs	3Quartz vein/Greisen	187	37	7.1	20.3	822	162	23.7	87.7	0.02	775.3	1.06
Canaan Downs	3Quartz vein/Greisen	271	49	8.1	25.4	846	241	27.6	81.4	0.02	1220.6	1.06
Canaan Downs	3Quartz vein/Greisen	188	52	8.1	17.3	983	205	18.9	72.6	53.3	1099	1.13
Canaan Downs	3Quartz vein/Greisen	151	31	7.7	25.8	782	421	19.3	67.4	28	1891.7	1.11
Canaan Downs	3Quartz vein/Greisen	219	33	7.7	27.2	773	446	21.3	72.2	0.02	1813.1	1.23
Canaan Downs	3Quartz vein/Greisen	262	62	9.4	16.3	1104	103	12.8	79.4	64	614.9	1.25
Canaan Downs	3Quartz vein/Greisen	207	53	11.1	20.5	1020	245	15.8	67.7	27.6	1164.5	1.23
Canaan Downs	3Quartz vein/Greisen	192	33	6.9	26	811	501	19.7	67.6	0.02	2224.6	1.15
Canaan Downs	3Quartz vein/Greisen	131	38	9.3	15.6	612	168	26.3	119.9	28.3	1566.2	0.99
Canaan Downs	3Quartz vein/Greisen	164	40	9.5	21.9	590	305	22.2	46.4	0.02	1811.6	1.11
Canaan Downs	3Quartz vein/Greisen	152	39	8.9	19.1	588	301	31.1	38.5	0.02	1706.9	1.12
Canaan Downs	3Quartz vein/Greisen	130	72	8.1	23.5	730	394	19.2	67.6	0.02	1905.1	1.11
Canaan Downs	3Quartz vein/Greisen	205	21	6.3	30.5	1067	417	20.7	73.1	3.3	1520.7	1.14
Canaan Downs	3Quartz vein/Greisen	200	33	8.6	25.9	607	335	18.5	80.6	14.7	1154.6	1.34

Appendix 2.6B (continued)

Name	model 1	Na	Mg	Mn	As	Sr	Y	Nb	Mo	Pb	REE	EuA
Canaan Downs	3Quartz vein/Greisen	141	41	9.7	13.4	663	62	15.3	150.2	22.8	782.4	1.34
Canaan Downs	3Quartz vein/Greisen	190	23	7.7	28.7	760	386	19.3	54.6	0.02	1341.6	1.2
Canaan Downs	3Quartz vein/Greisen	156	34	8.3	25.4	701	341	17.1	70.7	2.7	1427.3	1.23
Canaan Downs	3Quartz vein/Greisen	153	33	8.5	25	676	277	17.1	77.8	15.3	1426	1.16
Canaan Downs	3Quartz vein/Greisen	166	35	7.6	25.5	754	260	22.9	67.6	6.8	1259	1.13
Canaan Downs	3Quartz vein/Greisen	161	29	7.4	24.9	835	361	18	62.9	0.02	1786.2	1.12
Canaan Downs	3Quartz vein/Greisen	148	47	9.6	17.8	447	303	19.2	31	0.02	1718.1	1.12
Canaan Downs	3Quartz vein/Greisen	149	29	7.6	23.4	734	398	30.3	53.1	0.02	1825.5	1.18
Canaan Downs	3Quartz vein/Greisen	152	26	6.5	21	922	335	19.3	73.9	0.02	1465.2	1.18
Canaan Downs	3Quartz vein/Greisen	135	47	7.3	23.3	631	236	19.4	58	42.2	1073.1	1.14
Canaan Downs	3Quartz vein/Greisen	158	26	7.3	20.5	950	207	15.8	69.2	11.6	789.4	1.31
Canaan Downs	3Quartz vein/Greisen	147	31	7.5	24.9	715	370	21.3	64.8	0.02	1632.9	1.22
Canaan Downs	3Quartz vein/Greisen	135	25	8	28.5	1026	540	18.9	79	0.02	1477.6	1.18
Canaan Downs	3Quartz vein/Greisen	151	25	6.3	21.4	913	253	15.9	56.2	0.02	1164.1	1.33
Canaan Downs	3Quartz vein/Greisen	207	27	7.9	34.4	940	631	19.2	76	0.02	2219.6	1.38
Canaan Downs	3Quartz vein/Greisen	195	41	7.9	22.5	676	466	20.8	78.9	48	1991.6	1.22
Canaan Downs	3Quartz vein/Greisen	244	39	5.6	22.1	885	271	16.9	68.9	4.8	880.7	1.22
Canaan Downs	3Quartz vein/Greisen	127	60	9	28	657	515	33.5	144.6	0.02	2731	1.11
Canaan Downs	3Quartz vein/Greisen	161	36	7.6	23.3	638	344	17.2	79.3	6.2	1463.8	1.17
Canaan Downs	3Quartz vein/Greisen	103	28	8.5	18.9	654	156	26.8	118.2	0.02	1357.7	1.1
Canaan Downs	3Quartz vein/Greisen	84	37	8.8	15.1	615	86	16.1	158.9	0.02	1477.4	1.28
Canaan Downs	3Quartz vein/Greisen	173	28	7.7	23.9	762	329	29.5	64.7	0.03	1406.3	1.18
Canaan Downs	3Quartz vein/Greisen	150	36	7.7	24.7	618	302	26.3	45.9	0.02	1680.5	1.06
Canaan Downs	3Quartz vein/Greisen	168	24	7.8	23.9	720	333	22.6	115	11.1	1598.1	1.15
Canaan Downs	3Quartz vein/Greisen	143	42	9.4	19.4	459	164	30.5	64.9	15.9	1694.4	1.16
Canaan Downs	3Quartz vein/Greisen	76	36	8.4	12.8	664	70	13.7	153.6	49	900.4	1.31
Canaan Downs	3Quartz vein/Greisen	141	36	7.8	24.6	705	407	20	49.6	0.02	1730.2	1.21
Canaan Downs	3Quartz vein/Greisen	88	34	8.2	23	723	169	18.7	324.5	39.3	921.3	0.97
Canaan Downs	3Quartz vein/Greisen	176	45	8	22.4	982	163	19.6	95.4	62	883.6	0.98
Canaan Downs	3Quartz vein/Greisen	209	40	8.8	14.1	738	116	15.9	134.1	41	900.5	1.22

Appendix 2.6B (continued)

Name	model 1	Na	Mg	Mn	As	Sr	Y	Nb	Mo	Pb	REE	EuA
Canaan Downs	3Quartz vein/Greisen	80	30	7.4	15.2	850	43	20.2	231.5	0.02	627.8	1.02
Canaan Downs	3Quartz vein/Greisen	154	34	6.8	21.7	642	164	17.7	304.3	27.8	801.4	0.98
Canaan Downs	3Quartz vein/Greisen	97	30	7.1	20.4	614	272	24.1	44.4	19.2	1286	1.09
Canaan Downs	3Quartz vein/Greisen	240	43	7.9	21.5	999	275	24.3	76.2	0.02	1150.1	1.06
Canaan Downs	3Quartz vein/Greisen	228	41	8.2	20.6	834	189	19.5	98.9	41	948.3	1.03
Canaan Downs	3Quartz vein/Greisen	249	39	8	19.7	761	228	18.4	78.3	1.1	1008.9	1.2
Canaan Downs	3Quartz vein/Greisen	162	33	7.7	25.6	1029	276	19	95.5	49.4	992.9	1.04
Canaan Downs	3Quartz vein/Greisen	209	114	11.1	17.6	518	317	12.8	97.4	18.8	1301.5	2.02
Canaan Downs	3Quartz vein/Greisen	233	41	15.7	22.3	893	272	20.3	61.2	30.3	1231	1.27
Canaan Downs	3Quartz vein/Greisen	220	43	7.8	18.7	691	255	15.4	59.1	6.8	1014.9	1.22
Canaan Downs	3Quartz vein/Greisen	234	34	8.8	20.5	734	370	22.9	56.9	58.4	1212	1.45
Canaan Downs	3Quartz vein/Greisen	190	34	9	22.2	684	330	26.7	69.4	53.9	1092.1	1.44
Canaan Downs	3Quartz vein/Greisen	198	39	7.7	22.1	658	299	17.5	79.4	43	1133.9	1.21
Canaan Downs	3Quartz vein/Greisen	212	23	6.6	29.2	1041	338	18.9	84	12.5	1175.6	1.13
Canaan Downs	3Quartz vein/Greisen	282	33	6.4	24.6	788	329	18.9	98.5	22	1178.9	1.15
Canaan Downs	3Quartz vein/Greisen	232	27	7.1	29.2	908	370	21.8	79.6	3	1176.1	1.22
Canaan Downs	3Quartz vein/Greisen	178	48	8.2	22.1	1088	133	9.1	107.3	53.2	665.9	1.04
Canaan Downs	3Quartz vein/Greisen	86	36	9.9	14	746	248	12.6	244.3	37.8	1432.4	0.82
Canaan Downs	3Quartz vein/Greisen	102	39	7.4	24	699	370	18	64.9	0.02	1822.4	1.09
Canaan Downs	3Quartz vein/Greisen	125	28	6.9	24.5	833	343	18.4	75.6	0.02	1494.8	1.13
Canaan Downs	3Quartz vein/Greisen	101	59	10.5	44.6	1133	231	17.1	110.1	6.8	1306.7	1.05
Canaan Downs	3Quartz vein/Greisen	195	43	9.4	20.9	532	287	25.7	143	17.9	1773.5	1.08
Canaan Downs	3Quartz vein/Greisen	198	73	14.3	48.1	743	186	21.4	96.4	12	1231.6	1.04
Canaan Downs	3Quartz vein/Greisen	94	34	9.6	22.1	646	253	28.9	119.2	25.6	1735.2	0.98
Canaan Downs	3Quartz vein/Greisen	154	68	13.3	33.1	579	167	24.6	89	3.4	1415.5	1.14
Canaan Downs	3Quartz vein/Greisen	94	54	13.8	16.9	413	162	23.9	81.6	12.2	1747.8	1.25
Canaan Downs	3Quartz vein/Greisen	190	62	11.3	14.9	323	145	18.1	102.9	0.02	1750.7	1.28
Canaan Downs	3Quartz vein/Greisen	196	30	8.5	79	1149	473	23.3	79.8	21.7	1886.8	1.16

Appendix 2.6B (continued)

Name	model 1	Na	Mg	Mn	As	Sr	Y	Nb	Mo	Pb	REE	EuA
Canaan Downs	3Quartz vein/Greisen	102	45	12.8	17.8	484	117	28.8	105.4	0.02	1301.4	1.06
Canaan Downs	3Quartz vein/Greisen	157	176	9	20.5	679	132	19.6	113.2	26.5	853.1	1.11
Canaan Downs	3Quartz vein/Greisen	144	57	9.1	18.4	418	319	17.5	45.1	0.02	1893.6	1.2
Canaan Downs	3Quartz vein/Greisen	112	50	13.3	24.4	786	290	12.1	93.4	25.7	1547	0.99
Canaan Downs	3Quartz vein/Greisen	20.58	42	9.3	18.9	535	179	31.5	73.3	9	1589.7	1.1
Canaan Downs	3Quartz vein/Greisen	79	41	11.4	17.9	638	218	25.9	126.4	57.9	1595.9	1.01
Canaan Downs	3Quartz vein/Greisen	134	61	17.5	16.3	465	168	21.5	87.2	74.5	1571.1	1.25
Canaan Downs	3Quartz vein/Greisen	19.76	38	9.7	18.7	589	220	32.6	92.6	0.02	1759.8	1.07
Canaan Downs	3Quartz vein/Greisen	88	49	10.3	20.3	516	264	22.2	98.9	0.02	1958.3	1.05
Canaan Downs	3Quartz vein/Greisen	54.42	53	10.8	32.2	470	112	34.1	76.6	11.5	1139.3	1.12
Canaan Downs	3Quartz vein/Greisen	183	50	10.3	20.7	645	149	20.6	98.5	5.1	1070.8	0.95
Canaan Downs	3Quartz vein/Greisen	36.72	31	10.4	21.9	677	220	28.8	112.3	8	1530.4	0.96
Canaan Downs	3Quartz vein/Greisen	23.25	62	15.3	16.7	285	149	19.5	109.9	0.02	1874.6	1.25
Canaan Downs	3Quartz vein/Greisen	192	105	26.2	2.1	88	44	30.7	671.4	0.9	866.5	0.36
Canaan Downs	3Quartz vein/Greisen	251	121	26.1	2.8	95	42	65.1	705.2	1.1	838.7	0.37
Canaan Downs	3Quartz vein/Greisen	238	100	23.9	1.6	84	41	20.3	645.5	0.9	797	0.34
Canaan Downs	3Quartz vein/Greisen	240	15	3.4	3	478	22	4.4	32.2	11.4	487.8	1.16
Canaan Downs	3Quartz vein/Greisen	216	11	2.9	4.5	380	29	6	29.5	9.7	679.1	1.66
Canaan Downs	3Quartz vein/Greisen	197	4.87	3.7	3.8	366	27	5.5	26.8	9.5	640	1.39
Canaan Downs	3Quartz vein/Greisen	214	12	3.4	4.1	407	26	5	27.4	10	615.8	1.26
Canaan Downs	3Quartz vein/Greisen	240	4.02	3.7	2.7	464	26	4.2	14.1	14.7	465.4	1.05
Canaan Downs	3Quartz vein/Greisen	240	10	4	4	485	32	5.8	24.3	11.9	605.7	1.15
Canaan Downs	3Quartz vein/Greisen	143	4.02	5.2	3.5	316	30	5.6	40.3	8.4	589.4	1.43
Canaan Downs	3Quartz vein/Greisen	244	8	3.3	4.9	353	38	6.9	32.7	10.5	707.2	1.66
Canaan Downs	3Quartz vein/Greisen	224	11	3.3	2.8	432	19	3.4	27.7	11.4	427.3	1.06
Canaan Downs	3Quartz vein/Greisen	340	32	11.2	26.4	618	238	60.1	100.4	14.9	1497.3	0.9
Canaan Downs	3Quartz vein/Greisen	250	32	10.9	18.5	622	361	43.4	126.5	13.5	1983.6	1.15
Canaan Downs	3Quartz vein/Greisen	264	36	11.3	19.3	649	474	51.3	154.7	16.8	2113.9	1.18
Canaan Downs	3Quartz vein/Greisen	291	29	11.1	20.4	675	411	51.3	123.7	16.9	1757.2	1.11
Canaan Downs	3Quartz vein/Greisen	176	25	13.5	20.6	758	366	47	130.7	18.2	1773	1.16

Appendix 2.6B (continued)

Name	model 1	Na	Mg	Mn	As	Sr	Y	Nb	Mo	Pb	REE	EuA
Canaan Downs	3Quartz vein/Greisen	320	37	11.8	19.1	605	313	40.2	137	14.7	1662.1	1.04
Canaan Downs	3Quartz vein/Greisen	222	16	4	4.1	350	35	6.6	33.2	11.4	683.1	1.83
Canaan Downs	3Quartz vein/Greisen	300	43	10.9	20.3	513	301	44	90.5	10.7	1877.7	1.08
Canaan Downs	3Quartz vein/Greisen	269	45	10.1	3.5	690	16	16	117.7	31.7	395.1	0.79
Canaan Downs	3Quartz vein/Greisen	168	30	14.2	5.2	825	79	39.7	193.4	19.6	567.8	0.87
Canaan Downs	3Quartz vein/Greisen	260	30	12.4	4.6	801	74	33.6	194.3	28.4	567.4	0.87
Canaan Downs	3Quartz vein/Greisen	228	34	12.4	4.2	810	52	12.4	219.1	21.5	438.8	0.88
Canaan Downs	3Quartz vein/Greisen	297	35	14	11.8	620	115	36.1	205.2	21.8	791.5	1.21
Canaan Downs	3Quartz vein/Greisen	242	26	13	6.1	698	83	27.6	198.6	27.7	614	1.14
Canaan Downs	3Quartz vein/Greisen	242	24	10.4	22.7	1137	256	28.9	135.9	21.9	1413.9	0.99
Canaan Downs	3Quartz vein/Greisen	293	35	10.7	17.6	488	419	42.8	183.1	14.9	1813.1	0.95
Canaan Downs	3Quartz vein/Greisen	300	34	12.2	23.1	604	469	37.3	133.3	17.8	1871.9	1.02
Canaan Downs	3Quartz vein/Greisen	278	30	12	21.9	749	423	57.7	125.3	18.2	1826.9	1.09
Canaan Downs	3Quartz vein/Greisen	330	38	11.2	22.3	622	438	52.9	131.2	15.2	2036.6	1.14
Canadian Malartic	6Orogenic Au	92	32.6	7.14	36	1846	48.8	1.06	1395	56.4	181.53	0.86
Canadian Malartic	6Orogenic Au	118	20.9	8.27	12.4	1980	144	3.96	914	40.5	412.99	0.66
Canadian Malartic	6Orogenic Au	128	34	9.69	22.6	2083	159.7	2.62	871	41.2	404.32	0.72
Canadian Malartic	6Orogenic Au	85	24.9	8.3	9.4	1656	34.2	1.49	1482	36.4	195.04	1.06
Canadian Malartic	6Orogenic Au	132	36.8	9.51	28	1734	34.3	1.34	1408	38.3	196.04	0.96
Celine	1RIRGS	113.98	3.73	13.79	3.22	43.97	154.3	61.3	1970	3.89	641.57	1.24
Celine	1RIRGS	117.73	3.49	14.28	3.24	44.33	166.1	61.72	2056	4.04	691.27	1.08
Celine	1RIRGS	104.67	3.68	15.55	3.34	44.66	139.8	58.94	1939	3.36	610.33	1.44
Celine	1RIRGS	169.3	3.56	13.21	4.14	46.01	200.6	61.58	1932	3.39	918.98	0.76
Celine	1RIRGS	69.78	3.25	13.44	3.07	46.06	85.49	48.5	2116	3.71	431	1.64
Celine	1RIRGS	108.7	3.82	13.75	3.1	43.85	145	60.47	1927	3.7	618.72	1.22
Celine	1RIRGS	99.25	3.82	16.33	2.86	46.08	141.5	59.08	2078	3.57	641.37	1.17
Celine	1RIRGS	107.17	3.67	13.43	2.96	47.4	155	63.66	1967	3.36	632.33	1.14
Celine	1RIRGS	38.92	10.7	10.49	17.42	26.09	148.7	31.83	2783	1.69	211.64	0.42
Celine	1RIRGS	35.86	115.37	27.24	17.9	31.3	100.6	37.67	2697	2	129.9	0.46
Celine	1RIRGS	25.42	2.64	9.34	4.7	25.26	89.66	16.62	2325	1.22	94.96	0.62

Celine	1RIRGS	88.96	61.16	9.92	4.78	28.37	92.3	8.85	2442	2.53	101.93	0.52
Celine	1RIRGS	33.36	14.04	12.65	10.9	37.39	52.82	16	2434	1.92	100.98	0.52
Cetoraz u Pacova	3Quartz vein/Greisen	304.41	3.78	328.87	16.76	533.76	583.8	247.1	0.39	38.09	2193.4	1.7
Cetoraz u Pacova	3Quartz vein/Greisen	278.97	3.36	287.87	19.74	539.32	551.8	289.4	0.43	29.3	2112.9	1.77

,

Appendix 2.6B (continued)

Name	model 1	Na	Mg	Mn	As	Sr	Y	Nb	Mo	Pb	REE	EuA
Cetoraz u Pacova	3Quartz vein/Greisen	189.74	3.73	481.5	23.07	1494.25	294.8	117.9	153.5	123	1469	1.13
Cetoraz u Pacova	3Quartz vein/Greisen	235.88	13.9	211.14	15.15	532.37	464.3	244	0.41	21.32	1805.7	1.16
Cetoraz u Pacova	3Quartz vein/Greisen	237.13	3.36	283.42	14.04	606.04	512.9	287	0.44	21.8	1890.5	1.17
Cetoraz u Pacova	3Quartz vein/Greisen	262.85	3.71	347.36	18.21	567.12	508.7	291.6	0.49	27.83	2091.6	1.37
Cetoraz u Pacova	3Quartz vein/Greisen	15.68	11.4	442.02	0.37	865.97	56.3	361.4	5.14	63.25	99	8.23
Cetoraz u Pacova	3Quartz vein/Greisen	50.04	3.73	165.55	1.18	296.77	102.7	19.07	81.87	31	199.72	2.03
Cetoraz u Pacova	3Quartz vein/Greisen	22.6	3.46	196.41	0.7	822.88	63.94	33.82	25.97	43.65	126.54	5.95
Cetoraz u Pacova	3Quartz vein/Greisen	48.51	3.17	156.38	0.61	305.52	109.4	9.56	82.01	28.33	202.71	2.03
Cetoraz u Pacova	3Quartz vein/Greisen	38.92	15.29	177.64	0.38	597.7	70.2	47.68	34.33	31.55	138	4.34
Cínovec 3. p.	3Quartz vein/Greisen	16.68	5.35	0.24	4434.1	360.01	5.41	8.44	4601	0.45	44.2	0.4
Cínovec 3. p.	3Quartz vein/Greisen	6.41	4.71	1.28	1481.7	467.04	7.31	2.47	1579	0.26	40.77	0.01
Cínovec 3. p.	3Quartz vein/Greisen	2.78	4.82	1.25	1768.1	440.63	2.81	3.22	1706	2.06	14.9	8.67
Cínovec 3. p.	3Quartz vein/Greisen	0.4	5.71	0.78	4726	385.03	3.24	15.01	4921	0.63	24.26	0.03
Cínovec 3. p.	3Quartz vein/Greisen	13.9	5.89	1.03	4851.1	453.14	10.93	18.53	4545	1.46	84.61	0.02
Cínovec 3. p.	3Quartz vein/Greisen	18.07	5.63	5.84	5949.2	332.21	4.64	19.5	8145	29.61	57.53	0.06
Cínovec 3. p.	3Quartz vein/Greisen	5.53	5.62	0.23	6769.3	310.94	14.8	41.84	11134	3.61	168.25	0.02
Cínovec 3. p.	3Quartz vein/Greisen	6.94	8.2	0.97	6366.2	404.49	4.11	30.44	13886	3.74	23.18	0.25
Cínovec 3. p.	3Quartz vein/Greisen	3.21	5.62	0.21	5838	336.38	8.26	16.33	7478	1.24	120.56	0.02
Cínovec 3. p.	3Quartz vein/Greisen	7.9	5.85	6.81	6018.7	351.67	7.56	26.55	12997	4.85	56.77	0.02
Cínovec 3. p.	3Quartz vein/Greisen	7.96	5.32	0.21	5615.6	207.81	3.43	11.01	7937	1.49	55.66	0.03
Cínovec Vojenská jáma 3.	3Quartz vein/Greisen	14.79	29.05	110.51	10800	255.2	2.54	24.49	4096	1343	19.86	0.32
Cínovec Vojenská jáma 3.	3Quartz vein/Greisen	4.23	34.75	82.15	10050	259.37	3.49	15.97	3781	1220	11.01	0.19
Cínovec Vojenská jáma 3.	3Quartz vein/Greisen	20.32	22.05	106.2	11190	327.21	4.96	40.62	3601	3709	37.72	0.32
Cínovec Vojenská jáma 3.	3Quartz vein/Greisen	13.77	20.38	34.89	10800	254.23	87.57	42.81	6172	14373	220.75	0.2
Cínovec Vojenská jáma 3.	3Quartz vein/Greisen	13.76	26.55	96.33	10328	287.87	2.27	25.44	4142	1587	17.03	0.29
Cínovec Vojenská jáma 3.	3Quartz vein/Greisen	12.19	26.91	93.69	11551	260.76	11.72	22.43	5977	2077	38.05	0.23
Cínovec Vojenská jáma 3.	3Quartz vein/Greisen	9.2	23.95	45.18	11787	231.3	98.13	40.45	5685	14859	330.46	0.1
Celine	1RIRGS	44.48	10.01	8.12	15.57	31.97	129.6	20.54	2275	1.71	156.82	0.41
Celine	1RIRGS	32.25	2.07	9.56	5	27.37	106.9	14.07	2588	2.4	124.84	0.53
Celine	1RIRGS	51.43	14.46	8.48	10.88	26.28	114.8	18.61	4198	1.54	129.91	0.46

Appendix 2.6B (continued)

Name	model 1	Na	Mg	Mn	As	Sr	Y	Nb	Mo	Pb	REE	EuA
Cínovec Vojenská jáma 3.	3Quartz vein/Greisen	19.63	15.96	81.32	14442	281.06	25.58	53.04	5657	10661	116.42	0.16
Cínovec Vojenská jáma 3.	3Quartz vein/Greisen	18.82	13.8	96.05	12037	339.44	5.64	44.05	3406	5949	42.25	0.33
Cínovec Vojenská jáma 3.	3Quartz vein/Greisen	19.28	23.21	106.47	11871	337.35	5.53	42.4	3874	3700	38.63	0.34
Colbert Lode	1RIRGS	18.61	5.49	12.45	1.05	137.75	56.3	16.35	2000	8.52	93.07	1.32
Colbert Lode	1RIRGS	35.58	5.32	12.5	1.61	140.67	111.5	23.35	2028	8.24	141.18	1.44
Colbert Lode	1RIRGS	15.22	5.48	14.44	4.17	146.51	203.9	102.4	1847	10.9	246.84	1.53
Colbert Lode	1RIRGS	36.64	4.98	12.93	1.25	138.03	107.7	15.25	1900	9.31	149.79	2.51
Colbert Lode	1RIRGS	22.02	4.45	12.15	1.58	142.75	72.14	26.49	1870	9.27	125.51	3.35
Colbert Lode	1RIRGS	22.91	4.48	12.27	0.83	135.53	62.13	9.29	1920	9.29	116.09	3.1
Colbert Lode	1RIRGS	12.76	4.67	12.8	0.96	133.3	59.35	11.54	1838	8.97	81.21	3.18
Colbert Lode	1RIRGS	9.59	5.41	14.03	0.99	134.69	55.04	13.8	1820	9.69	88.68	2.28
Crown Footwall	6Orogenic Au	354	6.6	10.19	11.4	286.3	1510	359	0.79	11.58	3901.7	0.52
Crown Footwall	6Orogenic Au	328	3.77	14.33	8	320	1680	305	0.95	13.7	3626	0.6
Crown Footwall	6Orogenic Au	379	4.47	16.67	6.8	302.3	858	251	0.76	17.14	1890.6	0.75
Crown Footwall	6Orogenic Au	61.1	4.01	21.7	0.09	252.9	91.7	6.57	0.75	20	167.48	12.28
Crown Footwall	6Orogenic Au	66.7	4.73	22.6	0.56	235	90.7	2.88	0.56	20.14	175.45	11.49
Crown Footwall	6Orogenic Au	105	5.8	21.05	3.13	249.7	167	16.6	0.68	24.41	308.16	4.88
Crown Footwall	6Orogenic Au	79.2	4.94	21.85	1.61	246.6	123	8.5	0.68	22.25	223.24	7.61
Crown Footwall	6Orogenic Au	109.9	6.1	5.44	1.12	120.8	120.5	0.5	2.86	13.93	293.06	7.59
Crown Footwall	6Orogenic Au	55	4.11	6.83	6.74	325	52.4	0.25	0.15	16.02	105.15	15.15
Crown Footwall	6Orogenic Au	39.3	4.3	6.02	8.73	316	87.3	0.51	0.7	14.53	140.36	6.69
Cuiaba	6Orogenic Au	16.3	7	5.03	0.85	833	54.9	0.26	0.09	24.82	108.16	24.96
Cuiaba	6Orogenic Au	19.2	13	7.2	1.09	832	42.7	0.25	0.09	27.85	76.89	23.88
Cuiaba	6Orogenic Au	26.1	4.43	15.4	0.08	764	44.1	0.26	0.04	31.5	105	13.13
Cuiaba	6Orogenic Au	86	17.3	18.9	2.33	728	138	0.27	0.07	38.9	256.11	6.96
Dolphin Mine	4Oxidized skarn	17.67	4.49	16.71	7.88	119.12	0.47	44.9	18070	7.94	224.76	1.19
Dolphin Mine	4Oxidized skarn	21.42	3.91	14.48	15.33	125.24	0.72	29.47	25479	8.08	236.03	1.54
Celine	1RIRGS	27.23	168.19	21.13	11.79	27.95	95.08	21.11	3628	1.87	116.09	0.53
Celine	1RIRGS	54.21	0.43	7.85	12.86	26.13	240.3	66.44	2331	2.02	199.73	0.48

Appendix 2.6B (continued)

Name	model 1	Na	Mg	Mn	As	Sr	Y	Nb	Mo	Pb	REE	EuA
Dolphin Mine	4Oxidized skarn	15.3	6.67	14.4	5.84	151.23	1.45	28.63	20336	7.48	166.38	1.8
Dolphin Mine	4Oxidized skarn	16.96	4.31	14.5	6.95	122.18	0.62	48.79	20961	7.76	220.8	1.44
Dolphin Mine	4Oxidized skarn	22.5	4.25	14.82	6.81	114.81	1.64	43.66	22310	7.8	244.29	1.05
Dolphin Mine	4Oxidized skarn	15.21	4.63	12.25	10.2	138.72	0.81	68.11	21837	6.49	245.46	0.91
Dolphin Mine	4Oxidized skarn	18.81	4.64	13.27	11.47	134.14	1.65	46.43	25423	8.17	247.11	0.96
Dolphin Mine	4Oxidized skarn	15.03	8.48	17.29	8.35	140.81	0.7	35.63	26535	9.05	182.55	1.09
Dolphin Mine	4Oxidized skarn	17.71	2.54	18.49	9.69	158.88	16.36	31.83	18543	8.1	251.83	1.07
Dolphin Mine	4Oxidized skarn	6.34	7.23	18.77	11.98	91.18	0.95	27.88	17556	9.72	200.62	0.54
Dolphin Mine	4Oxidized skarn	12.52	5.7	15.85	9.16	83.4	1.36	33.9	18459	10.43	225.55	0.47
Dolphin Mine	4Oxidized skarn	19.08	23.63	15.97	9.27	90.35	0.95	35.03	15443	9.19	223.71	0.57
Dolphin Mine	4Oxidized skarn	23.21	2.59	17.47	10.81	98.97	1.28	49.76	12732	9.04	266.82	0.39
Dolphin Mine	4Oxidized skarn	43.09	2.93	19.04	9.19	96.19	1.43	50.32	12691	6.76	278.91	0.41
Dolphin Mine	4Oxidized skarn	21.25	3.16	19.46	9.81	91.05	1.64	56.99	11662	9.02	278.67	0.41
Dolphin Mine	4Oxidized skarn	14.87	2.88	14.87	8.15	102.72	2.55	34.35	16277	21.96	201.61	0.71
Dome	6Orogenic Au	189	5.17	1.36	8.77	923	585	6.56	3.98	28.8	1417.1	1.71
Dome	6Orogenic Au	213	6.3	3.6	9.52	928	710	6.44	3.67	31.06	1449.7	1.64
Dome	6Orogenic Au	212.6	14	2.41	8.92	1025	480	5.99	3.02	24.6	1124.1	1.22
Dome	6Orogenic Au	180.7	1.47	1.17	12.08	1029.99	690.8	5.3	3.2	25.44	1977.8	1.34
Dome	6Orogenic Au	200.16	1.53	1.33	9.13	1167.6	569.9	5.42	2.43	20.22	1138.2	1.39
Dome	6Orogenic Au	162.91	1.78	1.97	9.7	1061.96	729.8	6.03	3.41	25.94	1292.1	1.55
Dome	6Orogenic Au	218.37	5.14	2.61	7.06	1074.47	621.3	4.78	1.45	23.2	1371.1	1.49
Dome	6Orogenic Au	166.8	1.92	1.99	8.9	1095.32	474.3	4.27	2.34	18.13	997.23	1.01
Dome	6Orogenic Au	77.42	2.35	2.25	8.09	1027.21	418.8	5.18	2.84	26.62	891.89	0.9
Dome	6Orogenic Au	108.42	2.06	2.5	9.1	1035.55	473.7	5.46	3.1	25.49	899.21	0.97
Dublin Gulch	1RIRGS	149.56	11.82	10.54	3.31	261.32	54.86	115.2	872.9	4.16	1162.3	0.33
Dublin Gulch	1RIRGS	195.71	13.21	11.19	3.56	223.23	65.01	120.1	1183	4.71	1469.7	0.31
Dublin Gulch	1RIRGS	181.4	14.46	9.22	4.03	279.53	60.47	119.8	1279	3.82	1374.5	0.25
Celine	1RIRGS	10.31	5.84	8.58	19.75	36.56	70.89	14.07	2524	2.44	97.06	0.43
Celine	1RIRGS	11.68	51.43	14.18	14.09	34.19	61.16	20.47	2854	2.13	101.85	0.54
Celine	1RIRGS	23.63	1.28	9.17	11.16	19.64	119.3	24.88	6199	0.52	167.53	0.41

Appendix 2.6B (continued)

Name	model 1	Na	Mg	Mn	As	Sr	Y	Nb	Mo	Pb	REE	EuA
Dublin Gulch	1RIRGS	97.3	13.34	7.8	4.78	387.12	41.95	88.82	910.5	2.85	757.15	0.29
Dublin Gulch	1RIRGS	82.29	35.03	12.34	2.39	352.5	31.83	82.01	989.7	4.68	648.11	0.41
Dublin Gulch	1RIRGS	116.62	13.07	10.23	3.04	336.8	46.43	92.3	1362	3.41	886.91	0.35
Dublin Gulch	1RIRGS	72.56	22.66	16.82	3.46	261.6	21.29	79.51	1011	5.2	647.57	0.58
Dublin Gulch	1RIRGS	82.98	15.01	7.85	2.45	365.57	31.55	44.2	3016	2.59	592.95	0.53
E Zone	5Reduced skarn	10.19	9.17	127.88	0.37	58.77	62.13	62.69	49.9	5.73	259.12	6.64
E Zone	5Reduced skarn	6.67	4.53	31.94	0.28	44.34	38.64	26.83	98.69	3.24	57.27	1.5
E Zone	5Reduced skarn	44.62	10.7	31.84	0.92	33.46	49.26	114.7	551.3	2.51	450.87	0.35
E Zone	5Reduced skarn	12.37	10.43	25.87	0.61	47.82	21.66	37.39	115.8	3.03	113.68	1.55
E Zone	5Reduced skarn	37.53	6.95	26.62	0.82	36.68	64.91	116.5	565.7	2.47	358.67	0.32
E Zone	5Reduced skarn	34.75	6.38	28.22	0.57	40.85	40.31	84.37	520	3.04	330.37	0.51
E Zone	5Reduced skarn	51.99	4.71	35.51	0.81	40.41	72.14	97.86	538.4	2.63	443.86	0.35
E Zone	5Reduced skarn	29.75	5.85	16.3	2.25	12.98	133.2	218.2	1932	1.38	396.53	0.13
E Zone	5Reduced skarn	44.9	50.04	34.89	1.11	40.03	80.48	122.9	526.8	2.72	395.49	0.3
E Zone	5Reduced skarn	64.91	5.43	34.42	0.9	47.4	175.1	166.5	537.9	2.55	472.74	0.22
E Zone	5Reduced skarn	37.11	3.92	29.59	0.72	35.06	94.52	152.9	703.3	2.11	417.11	0.31
E Zone	5Reduced skarn	9.73	7.02	24.24	0.84	64.5	18.49	50.18	5630	12.23	101.67	0.57
E Zone	5Reduced skarn	9.87	5.55	35.31	0.51	84.23	11.95	53.24	4962	5.31	100.08	0.81
E Zone	5Reduced skarn	10.72	3.81	18	0.71	50.04	31.14	49.62	7840	1.89	111.59	0.6
E Zone	5Reduced skarn	7.55	4	20.64	0.57	76.17	22.71	54.49	6408	2.54	105.41	0.62
E Zone	5Reduced skarn	7.05	6.12	47.26	0.78	63.52	23.78	54.49	6394	2.62	109.83	0.51
E Zone	5Reduced skarn	25.02	4.89	34.19	0.65	86.6	5.05	38.64	7798	1.72	87.64	0.74
E Zone	5Reduced skarn	4.57	4.25	23.82	0.54	99.8	5.38	48.09	6047	2	101.1	0.55
E Zone	5Reduced skarn	5.52	4.57	23.35	0.43	66.86	9.73	48.93	3461	1.95	105.29	0.56
E Zone	5Reduced skarn	6.67	5.56	21	0.72	67.97	6.32	28.77	3684	2.65	77.91	0.68
E Zone	5Reduced skarn	9.17	7.37	20.57	0.96	64.08	9.29	34.35	6630	3.35	91.43	0.53
E Zone	5Reduced skarn	5.32	5.92	33.69	0.3	39.32	1.99	14.57	149.2	3.6	96.53	14.35
Celine	1RIRGS	88.96	61.16	9.92	4.78	28.37	92.3	8.85	2442	2.53	101.93	0.52
Celine	1RIRGS	33.36	14.04	12.65	10.9	37.39	52.82	16	2434	1.92	100.98	0.52
Cetoraz u Pacova	3Quartz vein/Greisen	304.41	3.78	328.87	16.76	533.76	583.8	247.1	0.39	38.09	2193.4	1.7

Appendix 2.6B (continued)

Name	model 1	Na	Mg	Mn	As	Sr	Y	Nb	Mo	Pb	REE	EuA
E Zone	5Reduced skarn	2.53	4.87	36.5	0.31	31.5	0.85	76.17	134	3.56	49.33	10.12
E Zone	5Reduced skarn	28.5	8.47	38.5	0.48	70.01	71.86	92.02	44.06	7.27	287.02	33.87
E Zone	5Reduced skarn	13.21	11.82	41.98	0.27	57.96	44.48	76.31	63.11	6.57	257.52	43.54
E Zone	5Reduced skarn	4.28	33.22	36.56	0.19	41.42	3.81	25.44	61.3	3.31	64.55	9.86
E Zone	5Reduced skarn	20.85	17.51	35.31	0.48	62.41	3.28	16.54	303	2.71	49.77	2.71
E Zone	5Reduced skarn	4.67	36.14	51.57	0.24	39.48	1.42	15.19	104.7	3.49	109.23	9.81
E Zone	5Reduced skarn	2.72	4.32	12.93	0.54	62.83	1.93	11.31	436.5	1.62	37.14	2.2
E Zone	5Reduced skarn	7.34	11.82	34.17	0.33	38.5	3.81	23.77	71.31	4.7	98.08	27.25
E Zone	5Reduced skarn	6.44	5.7	37.11	0.6	45.51	2.91	10.43	509.9	1.9	97.71	2.92
E Zone	5Reduced skarn	19.04	27.11	43.23	0.37	47.68	164	122.3	53.65	4.39	154.32	2.22
E Zone	5Reduced skarn	14.6	27.52	246.03	0.54	53.79	5.81	7.78	515.6	2.22	29.82	5.4
E Zone	5Reduced skarn	10.98	4.71	22.52	0.37	48.37	1.32	12	211.3	2.32	114.73	3.95
E Zone	5Reduced skarn	13.34	4.71	13.96	0.46	64.5	2.45	12.23	382.3	1.82	80.94	4.04
E Zone	5Reduced skarn	18.77	7.78	21.27	0.44	63.52	7.1	26.83	289.1	2.67	98.57	1.28
Edward's Find	6Orogenic Au	51	6.5	4.5	8.37	734	25.64	0.34	0.05	8.69	49.68	4.29
Edward's Find	6Orogenic Au	6.4	2.62	5.4	9	790	27	0.33	0.001	8.67	50.99	4.2
Edward's Find	6Orogenic Au	8.4	2.33	6.13	8	712	29.9	0.31	0.001	10.4	58.96	3.72
Edward's Find	6Orogenic Au	7.4	2.34	5.25	6.4	901	25.4	0.24	0.04	7.57	46.6	4.24
Edward's Find	6Orogenic Au	11.2	2.06	4.6	12.55	823	40	0.34	0.001	6.89	64.18	3.86
Edward's Find	6Orogenic Au	11.8	2.25	5.69	13.45	680	50.8	0.26	0.001	2.39	89.12	3.61
Essakane	6Orogenic Au	73.2	5.99	3.63	1.4	2486	113	0.42	0.71	47.6	210.66	5.3
Essakane	6Orogenic Au	79	15.2	7.3	18	2406	142	0.49	0.64	57.1	344.45	3.39
Essakane	6Orogenic Au	25.4	14.8	1.79	0.64	2298	54.7	0.3	0.38	48.5	156.6	10.17
Essakane	6Orogenic Au	46	33	1.66	1.29	2154	145	0.3	0.37	43.1	429.25	6.51
Essakane	6Orogenic Au	36	17.8	5.82	1.4	2331	46.7	0.31	0.54	48.9	139.26	35.25
Essakane	6Orogenic Au	34.3	14.6	2.88	1.04	3152	66	0.26	0.14	49.1	145.45	8.2
Essakane	6Orogenic Au	26.9	4.39	3.14	0.79	2680	65.9	0.22	0.19	37	128.95	13.05

Appendix 2.6B (continued)

Name	model 1	Na	Mg	Mn	As	Sr	Y	Nb	Mo	Pb	REE	EuA
Essakane	6Orogenic Au	23.9	5.2	2.08	0.9	2990	54.2	0.19	0.12	41.2	114.18	11.87
Essakane	6Orogenic Au	88.7	8.1	2.24	1.8	2470	250	0.25	0.08	32	429.51	6.46
Essakane	6Orogenic Au	85	4.13	2.92	0.93	2860	242	0.29	0.22	35.1	383.55	13.67
Essakane	6Orogenic Au	41.9	5.14	2.94	0.98	2705	109	0.22	0.15	36.9	195.56	10.26
Essakane	6Orogenic Au	47.4	4.8	1.35	1.66	2340	116	0.2	0.13	33.6	187.69	8.38
Essakane	6Orogenic Au	84	4.5	0.21	1.73	2650	207	0.31	0.31	36.1	322.18	8.07
Essakane	6Orogenic Au	63	7.2	0.99	1.5	2890	138	0.27	0.19	40.6	251.53	7.04
Essakane	6Orogenic Au	65	5.37	1.14	1.67	2440	164	0.27	0.15	33.2	275.57	6.16
Essakane	6Orogenic Au	123	4.79	0.22	2.24	2330	305	0.44	0.17	29.1	506.25	4.12
Essakane	6Orogenic Au	16.1	9.1	2.87	0.44	2682	53.3	0.64	0.08	38	141.58	16.33
Essakane	6Orogenic Au	10.9	5	2.52	0.07	2830	87	0.36	0.08	47.5	219.97	11.37
Essakane	6Orogenic Au	31.2	6.85	2.42	0.07	2752	31	0.4	0.07	44.8	87.9	17.1
Essakane	6Orogenic Au	20.8	5.86	2.38	0.07	2824	47.7	0.38	0.09	46.5	125.99	14.54
Essakane	6Orogenic Au	15.4	6.5	3	1.19	3580	37	0.49	0.001	71.6	145.86	27.98
Felbertal	3Quartz vein/Greisen	68.53	45.73	36.06	20.2	66.3	849.3	1283	5504	40.03	1330	0.14
Felbertal	3Quartz vein/Greisen	23.21	7.23	18.4	30.58	259.24	717.2	1126	6630	33.29	969.05	0.17
Felbertal	3Quartz vein/Greisen	57.82	107.45	51.39	19.27	58.24	682.5	899.3	5240	48.51	1001.8	0.33
Felbertal	3Quartz vein/Greisen	55.88	108.84	53.79	18.95	74.37	674.2	897.9	5685	37.57	952.35	0.23
Felbertal	3Quartz vein/Greisen	50.04	92.3	55.88	18.82	46.29	550.4	874.3	6380	43.92	1048.2	0.21
Felbertal	3Quartz vein/Greisen	62.69	77.42	48.65	12.52	49.21	422.6	560.2	6978	47.12	753.26	0.3
Felbertal	3Quartz vein/Greisen	53.93	109.25	56.3	21.55	47.96	697.8	1034	6589	44.62	1139.2	0.2
Felbertal	3Quartz vein/Greisen	74.64	62.83	27.93	19.56	139.83	679.7	879.9	5004	43.08	956.43	0.29
Felbertal	3Quartz vein/Greisen	81.04	62.55	29.61	19.27	92.16	728.4	896.6	5671	52.4	997.31	0.27
Felbertal	3Quartz vein/Greisen	50.04	96.47	49.82	18.04	68.53	702	900.7	5699	34.39	871.25	0.37
Felbertal	3Quartz vein/Greisen	45.04	35.72	24.09	20.11	258.4	593.5	977.2	5213	25.83	1101.9	0.15
Felbertal	3Quartz vein/Greisen	9.19	7.92	12.32	9.45	385.03	258.5	246	234.9	35.17	152.93	0.3
Felbertal	3Quartz vein/Greisen	54.63	7.83	15.39	32.8	165.97	2182	3211	5782	34.51	2540.1	0.11

Appendix 2.6B (continued)

Name	model 1	Na	Mg	Mn	As	Sr	Y	Nb	Mo	Pb	REE	EuA
Felbertal	3Quartz vein/Greisen	33.22	6.41	14.79	19.77	177.36	696.4	993.9	4823	33.72	933.9	0.13
Felbertal	3Quartz vein/Greisen	43.09	22.52	38.09	20.24	78.26	707.5	1081	6338	37.07	1125.4	0.17
Felbertal	3Quartz vein/Greisen	44.52	16.14	18.47	24.01	111.76	850.7	1093	5741	36.84	964.07	0.22
Felbertal	3Quartz vein/Greisen	68.25	40.03	79.23	21.81	56.99	992.5	1272	5157	48.65	1219.3	0.24
Felbertal	3Quartz vein/Greisen	82.71	57.55	32.67	22.91	44.76	1176	1532	5379	52.13	1443.1	0.21
Felbertal	3Quartz vein/Greisen	225.18	117.87	46.15	32.39	36.42	1500	2423	5449	39.53	2687.9	0.13
Felbertal	3Quartz vein/Greisen	103.97	59.77	23.2	39.48	55.6	1849	2961	4434	48.23	3234.8	0.09
Felbertal	3Quartz vein/Greisen	54.21	3.48	11.88	20.11	187.09	760.3	657.5	182.1	35.03	413.9	0.27
Felbertal	3Quartz vein/Greisen	67.97	38.79	26.76	38.92	92.71	1824	2738	6172	40.73	2440.8	0.13
Felbertal	3Quartz vein/Greisen	48.65	48.65	18.18	22.2	161.8	854.9	1076	5630	36.85	937.16	0.21
Felbertal	3Quartz vein/Greisen	15.16	8.9	14.58	23.98	254.51	459.3	436.7	161.2	32.01	236.27	0.26
Felbertal	3Quartz vein/Greisen	37.25	10.2	15.57	34.47	195.02	1396	1946	5143	36.78	1405.4	0.12
Felbertal	3Quartz vein/Greisen	27.77	2.88	10.31	17.96	149.15	492.1	447.4	351.7	27.06	269.59	0.32
Felbertal	3Quartz vein/Greisen	93.55	40.67	26.34	25.58	100.78	1208	1879	5755	39.89	2083	0.19
Felbertal	3Quartz vein/Greisen	129.41	63.8	31.53	31.97	60.74	1491	2359	5838	37.95	2631.4	0.19
Felbertal	3Quartz vein/Greisen	80.2	42.77	25.52	19.29	72.84	1229	1835	5477	34.47	1746.3	0.25
Felbertal	3Quartz vein/Greisen	79.23	52.96	27.01	16.43	145.67	428.1	585.2	15721	51.15	700.55	0.44
Felbertal	3Quartz vein/Greisen	48.51	60.33	23.42	15.47	110.09	397.5	550.4	15207	50.32	666.44	0.42
Felbertal	3Quartz vein/Greisen	34.06	13.11	22.24	9.94	293.29	180.7	66.03	126.4	62.55	127.78	0.53
Felbertal	3Quartz vein/Greisen	82.01	47.26	33.62	20.81	131.36	879.9	1297	6047	47.12	1286.9	0.31
Felbertal	3Quartz vein/Greisen	35.17	19.35	14.91	4.16	296.07	112.3	49.48	163.1	50.04	110.37	0.58
Felbertal	3Quartz vein/Greisen	57.96	37.67	23.81	17.04	160.13	305.2	405.9	10634	46.15	702.91	0.43
Felbertal	3Quartz vein/Greisen	43.09	35.06	17.44	10.68	201.13	244.6	322.5	10550	87.15	441.41	0.4
Felbertal	3Quartz vein/Greisen	63.94	49.62	30.55	9.95	96.19	228	383.9	7145	39.2	498.79	0.46
Felbertal	3Quartz vein/Greisen	29.19	27.7	15.42	3.28	223.93	82.15	40.73	187.2	58.1	84.08	0.6
Felbertal	3Quartz vein/Greisen	55.6	34.57	22.38	26.34	127.05	575.5	973	7228	53.93	1101	0.27
Felbertal	3Quartz vein/Greisen	69.08	43.69	21.06	29.33	134.27	638	1069	6936	58.38	1258.6	0.24

Appendix 2.6B (continued)

Name	model 1	Na	Mg	Mn	As	Sr	Y	Nb	Mo	Pb	REE	EuA
Felbertal	3Quartz vein/Greisen	59.21	47.26	33.08	29.75	159.02	654.7	1515	8062	59.77	1141.1	0.23
Felbertal	3Quartz vein/Greisen	36.84	47.26	19.18	18.77	144.56	414.5	682.5	10036	54.49	805.64	0.38
Felbertal	3Quartz vein/Greisen	20.24	29.61	20.74	12.95	188.76	203.2	302.7	6728	67	352	0.6
Felbertal	3Quartz vein/Greisen	11.72	22.24	58.42	30.86	14.58	406.2	875.7	8340	46.7	632.27	0.25
Felbertal	3Quartz vein/Greisen	90.49	14.66	30.68	40.45	22.03	1119	1712	8173	58.38	1928.2	0.07
Felbertal	3Quartz vein/Greisen	49.07	13.1	38.7	46.29	27.52	647.7	999.4	8020	50.04	925.26	0.13
Felbertal	3Quartz vein/Greisen	9.45	10.12	54.43	19.78	12.25	253.5	588	7715	37.15	374.36	0.26
Felbertal	3Quartz vein/Greisen	75.89	18.07	30.19	64.36	26.9	742.3	1277	8145	60.88	1136.3	0.12
Felbertal	3Quartz vein/Greisen	12.86	14.28	62.23	11.58	12.3	405.1	882.7	7728	36.81	648.55	0.25
Felbertal	3Quartz vein/Greisen	36.14	17.52	34.25	25.3	31.29	390.6	668.6	8006	49.69	580.28	0.2
Felbertal	3Quartz vein/Greisen	20.99	19.6	27.86	47.4	38.64	578.2	781.2	5491	82.84	548.63	0.18
Felbertal	3Quartz vein/Greisen	20.16	18.64	38.18	39.48	47.26	533.8	906.3	7284	46.84	698.21	0.23
Felbertal	3Quartz vein/Greisen	59.77	12.33	60.88	14.07	10.83	578.2	946.6	8771	43.51	928.14	0.18
Felbertal	3Quartz vein/Greisen	105.64	15.46	49.07	20.02	16.3	608.8	1165	8854	44.48	1022.4	0.23
Felbertal	3Quartz vein/Greisen	33.92	14.49	42.94	27.38	16.3	533.8	1079	7589	40.31	911.88	0.19
Felbertal	3Quartz vein/Greisen	33.36	12.47	46.57	26.13	235.05	453.1	561.6	5810	31.8	1887.8	0.42
Felbertal	3Quartz vein/Greisen	23.02	10.29	13.96	12.87	333.6	225.5	301.5	6144	38.78	357.04	0.44
Felbertal	3Quartz vein/Greisen	46.01	13.43	15.29	31.14	178.75	526.8	728.4	6074	29.61	800.13	0.42
Felbertal	3Quartz vein/Greisen	16.49	10.45	15.05	12.09	286.34	165.4	205	5518	40.45	445.19	0.62
Felbertal	3Quartz vein/Greisen	59.77	15.43	15.12	28.36	199.47	332.2	412.8	6047	24.33	711.68	0.57
Felbertal	3Quartz vein/Greisen	34.75	6.46	13.21	20.16	186.96	237.6	309.7	5935	26.74	380.76	0.54
Felbertal	3Quartz vein/Greisen	17.36	6.19	14.57	11.19	163.6	127.1	172.4	6158	34.89	221.85	0.71
Fort Knox	1RIRGS	11.29	4.03	11.29	1.06	223.23	80.06	18.36	1183	12.54	240.22	1.66
Fort Knox	1RIRGS	17.93	4.48	17.51	1.67	348.06	157.1	20.56	1186	19.24	563.67	2.28
Fort Knox	1RIRGS	32.25	4.21	12.7	2.15	313.31	209.2	27.16	1173	11.73	556.1	1.49
Fort Knox	1RIRGS	26.7	3.6	9.38	1.75	325.68	98.41	20.11	836.8	5.42	162.7	1.36
Fort Knox	1RIRGS	18.49	3.35	10.55	3.03	386.98	182.2	54.35	781.2	9.4	328.61	0.81

Appendix 2.6B (continued)

Name	model 1	Na	Mg	Mn	As	Sr	Y	Nb	Mo	Pb	REE	EuA
Fort Knox	1RIRGS	24.88	4.73	10.54	1.83	340.41	150.5	10.83	948	4.81	283.82	0.58
Fort Knox	1RIRGS	9.12	3.35	9.99	0.78	469.13	37.29	7.21	921.6	4.56	126.78	2.34
Fort Knox	1RIRGS	30.3	3.6	10.09	1.5	441.74	72.28	12.02	1126	6.09	162.48	1.23
Fort Knox	1RIRGS	29.05	3.68	9.45	1.79	553.22	145.4	8.01	797.9	4.34	527.64	1.25
Fort Knox	1RIRGS	19.53	3.6	9.4	1.33	319.56	57.55	9.99	917.4	5.1	113.36	0.67
Fort Knox	1RIRGS	53.65	5.05	16.26	1.49	365.57	46.11	14.51	810.4	8.15	429.78	1.71
Fort Knox	1RIRGS	65.19	4.64	17.25	2.22	425.06	168.6	46.87	818.7	8.19	644.26	0.83
Fort Knox	1RIRGS	27.59	10.4	36.28	2.42	305.66	72.14	19.33	2997	26.95	549.09	1.06
Fort Knox	1RIRGS	25.6	13.8	38.34	3.6	308.58	83.4	20.25	4814	28.26	787.11	1.65
Fort Knox	1RIRGS	33.22	6.38	36.97	3.29	319.42	107.7	25.26	3586	29.47	842.36	1.08
Fort Knox	1RIRGS	26.84	12.86	39.1	3.45	307.33	81.87	20.75	4983	28.63	792.29	1.74
Fort Knox	1RIRGS	33.5	6.81	37.85	3.21	312.47	104.3	25.31	3518	28.77	779.81	1.07
Fort Knox	1RIRGS	29.25	12.62	38.49	3.28	309.41	83.82	21.25	5015	29.47	796.57	1.73
Fort Knox	1RIRGS	27.24	10.83	38.1	3.5	305.24	76.73	20.57	4948	28.97	708.73	1.82
Fort Knox	1RIRGS	11.83	6.55	16.86	0.78	347.5	22.23	9.79	520.8	16.03	191.32	2.51
Fort Knox	1RIRGS	10.7	4.81	15.9	0.81	351.67	23.07	9.49	511.8	16.65	201.2	2.42
Fort Knox	1RIRGS	11.79	4.5	16.94	1.18	367.79	48.25	11.37	528.3	16.17	407.12	3.41
Fort Knox	1RIRGS	14.46	4.74	16.71	1.18	366.13	52.56	11.4	548.2	16.37	463.15	2.93
Fort Knox	1RIRGS	13.01	4.81	15.93	1.17	360.43	50.37	11.18	559.1	16.4	462.1	2.74
Fort Knox	1RIRGS	24.74	14.87	23.63	4.46	157.07	387.8	41.28	772.8	10.29	662.42	0.49
Fort Knox	1RIRGS	47.96	15.99	15.67	4.14	140.67	348.9	23.92	1118	11.4	432.19	0.75
Fort Knox	1RIRGS	37.95	14.18	16.72	2.47	189.04	169.6	28.12	1086	13.61	268.13	0.95
Fort Knox	1RIRGS	14.83	9.88	17.04	1.74	143.45	65.61	22.95	1765	7.58	108.11	1.43
Fort Knox	1RIRGS	30.58	11.5	15.33	2.74	131.36	174.5	16.36	1711	12.2	205	1.93
Fort Knox	1RIRGS	20.03	14.26	14.53	16.47	127.46	223.9	174.6	1434	23.27	284.45	1.23
Fort Knox	1RIRGS	27.19	18.77	16.05	7.14	121.9	110.6	23.13	3057	16.14	191.14	1.21
Fort Knox	1RIRGS	10.27	18.07	15.21	5.21	137.19	395.5	18.79	1753	20.42	584.98	0.96

Appendix 2.6B (continued)

Name	model 1	Na	Mg	Mn	As	Sr	Y	Nb	Mo	Pb	REE	EuA
Fort Knox	1RIRGS	12.83	24.56	17.04	6.03	141.22	420.8	17.12	2503	18.13	550.58	1.15
Gil	1RIRGS	1.4	2.75	2.52	0.78	155.12	102.2	4.24	495.4	2.04	102.69	2.4
Gil	1RIRGS	2.11	2.63	1.77	1.11	203.5	54.07	4.64	963.3	2.52	101.02	1.07
Gil	1RIRGS	2.02	2.45	2.2	1.01	163.46	96.05	5.84	725.6	2.24	159.95	1.14
Gil	1RIRGS	1.19	2.64	2.25	0.71	152.48	108.7	4.85	617.2	2.07	127.16	1.58
Gil	1RIRGS	5.02	2.72	4.03	2.95	156.38	69.92	6.6	686.7	2.54	98.15	1.51
Gil	1RIRGS	1.9	2.46	2.02	1.18	163.88	92.16	5.92	707.5	1.89	150.82	1.2
Gil	1RIRGS	1.25	2.4	2.39	0.93	157.9	33.47	4.88	743.7	2.01	96.46	2.04
Gil	1RIRGS	1.3	2.56	2.31	0.93	152.9	72.84	4.6	526.8	1.78	99.2	1.64
Gil	1RIRGS	5.03	11.4	3.18	1.28	159.16	87.71	5.5	594.9	2.47	102.47	2.08
Gil	1RIRGS	6.53	4.88	2.04	1.96	160.41	39.48	20.09	468.4	2.78	55.35	2.2
Gil	1RIRGS	4.99	4.53	1.93	1.19	211.28	125.8	7.13	1216	2.34	170.2	0.86
Gil	1RIRGS	4.31	4.34	2.29	0.74	118.01	44.48	7.08	308.6	2.6	34.64	1.23
Gil	1RIRGS	10.31	3.84	2.32	2.27	142.48	275.4	19.25	892.4	1.55	254.88	0.61
Gil	1RIRGS	11.68	3.85	2.56	2.81	144.7	252.6	23.49	921.6	1.8	233.4	0.6
Gil	1RIRGS	12.44	4.55	2.21	2.77	147.06	305.8	23.67	1012	1.62	281.13	0.6
Gil	1RIRGS	11.95	3.93	2.15	2.45	156.38	297.5	17.25	1248	1.62	279.59	0.61
Gil	1RIRGS	8.4	4.09	2.78	1.81	142.06	224.5	16.07	789.5	1.64	236.32	0.65
Gil	1RIRGS	10.2	4.1	2.74	2.25	145.12	239.4	19.42	1091	1.53	261.2	0.65
Gil	1RIRGS	9.37	3.89	3.18	3.6	151.37	346.7	25.92	981.3	1.81	330.46	0.63
Gil	1RIRGS	9.35	3.85	3.09	3.43	151.51	347.9	26.67	902.1	1.67	314.23	0.65
Gil	1RIRGS	11.54	27.8	1.83	1.95	121.35	42.7	8.41	344.3	4.31	34.92	1.16
Gil	1RIRGS	11.29	4.13	2.38	1.9	147.9	248.4	18.7	1109	1.68	278.67	0.64
Gil	1RIRGS	8.23	5.03	2.31	1.26	135.11	39.34	8.67	2583	1.65	94.71	0.8
H. Slavkov Huber	3Quartz vein/Greisen	1.01	16.4	4.41	0.05	205.72	2.21	10.08	9.73	0.22	7.89	0.87
H. Slavkov Huber	3Quartz vein/Greisen	2.95	10.65	6.03	19.18	249.64	0.22	8.56	0.02	0.35	1.73	13.85
H. Slavkov Huber	3Quartz vein/Greisen	9.73	16.68	3.81	0.06	311.22	0.07	8.17	0.54	0.28	1.21	8.51
H. Slavkov Huber	3Quartz vein/Greisen	37.53	8.37	2.74	0.03	172.5	0.31	6.32	0.67	0.15	0.7	1.4

Appendix 2.6B (continued)

Name	model 1	Na	Mg	Mn	As	Sr	Y	Nb	Mo	Pb	REE	EuA
H. Slavkov Huber	3Quartz vein/Greisen	7.09	8.49	2.89	0.04	157.77	0.05	6.26	0.01	0.01	0.82	0.84
H. Slavkov Huber	3Quartz vein/Greisen	1.35	8.92	2.78	0.05	215.17	0.04	6.88	0.07	0.21	0.84	6.13
H. Slavkov Huber	3Quartz vein/Greisen	0.36	8.38	3.14	0.01	277.31	0.06	7.48	0.21	0.02	1	67.79
H. Slavkov Huber	3Quartz vein/Greisen	0.38	16.68	4.13	0.03	285.23	0.06	9.74	0.9	0.36	1.26	32.87
Hazlov u Chebu výchoz	5Reduced skarn	2.64	5.95	0.26	0.58	1662.44	0.41	29.45	193.2	1.77	0.98	0.38
Hazlov u Chebu výchoz	5Reduced skarn	30.58	9.31	0.44	0.47	1720.82	0.49	23.52	204.2	1.8	1.02	0.31
Hazlov u Chebu výchoz	5Reduced skarn	10.29	4.91	0.29	0.3	1569.31	0.49	11.11	197.7	1.68	1.03	0.31
Hazlov u Chebu výchoz	5Reduced skarn	0.78	5.32	0.53	0.47	1634.64	0.39	23.95	196.7	1.79	0.82	0.43
Hazlov u Chebu výchoz	5Reduced skarn	2.22	5.77	4.73	0.97	1599.89	0.9	28.19	196	1.9	1.8	3.02
Hazlov u Chebu výchoz	5Reduced skarn	27.52	6.26	5.14	0.94	1604.06	0.69	25.02	219.6	1.84	0.91	0.5
Hazlov u Chebu výchoz	5Reduced skarn	84.79	4.46	0.3	2.49	1506.76	2.38	17.14	203.4	1.95	4.04	0.32
Hazlov u Chebu výchoz	5Reduced skarn	0.78	4.82	0.79	0.38	1535.95	0.53	16.04	212.1	1.87	1.17	1.66
Hazlov u Chebu výchoz	5Reduced skarn	2.02	10.84	0.81	0.68	1587.38	1.37	28.77	211.3	1.92	2.87	0.49
Hazlov u Chebu výchoz	5Reduced skarn	11.4	244.64	2.71	2.21	1570.7	1.64	20.59	211.7	1.74	2.83	0.57
Hazlov u Chebu výchoz	5Reduced skarn	1.75	6.67	0.35	0.82	1594.33	0.78	47.26	204.2	1.92	1.73	0.34
Hollinger	6Orogenic Au	13.4	530	922	0.08	148.4	2.57	0.01	0.05	1.43	5.88	2.6
Hollinger	6Orogenic Au	4.7	368.2	935	0.07	98.3	5.38	0.01	0.04	1.22	16.59	2.06
Hollinger	6Orogenic Au	10.5	197	1022	0.07	115.1	11.1	0.01	0.01	0.89	8.41	3.07
Horní Babákov u Hlinska	3Quartz vein/Greisen	493.45	288.56	72.42	7.52	263.82	512.9	23.76	9.77	4.73	3137.7	0.17
Horní Babákov u Hlinska	3Quartz vein/Greisen	442.16	284.81	73.25	7.26	244.5	478.6	25.55	9.66	4.42	2906	0.16
Horní Babákov u Hlinska	3Quartz vein/Greisen	500.4	297.32	73.81	7.03	253.95	511.5	27.73	10.38	5.98	2942.7	0.17
Horní Babákov u Hlinska	3Quartz vein/Greisen	421.17	281.34	74.78	6.85	233.38	453.1	25.66	11.82	4.32	2934.2	0.16
Horní Babákov u Hlinska	3Quartz vein/Greisen	485.11	297.74	75.76	6.89	256.46	476.9	25.06	9.54	4.64	2978	0.17
Horní Babákov u Hlinska	3Quartz vein/Greisen	343.33	247	69.5	8.23	271.75	375	63.25	11.59	7.05	2700.7	0.17
Horní Babákov u Hlinska	3Quartz vein/Greisen	331.38	243.53	70.46	8.34	259.65	407.4	73.25	11.91	6.6	2715.1	0.17
Horní Babákov u Hlinska	3Quartz vein/Greisen	338.74	250.34	74.23	8.19	287.45	413.9	68.39	11.91	6.92	2896.9	0.17
Horní Babákov u Hlinska	3Quartz vein/Greisen	333.88	242.97	72.56	8.3	271.61	391.3	69.5	11.04	6.52	2801.7	0.17
Horní Babákov u Hlinska	3Quartz vein/Greisen	393.37	318.31	79.09	43.09	295.1	373.1	36.07	13.21	4.64	2981.9	0.2
Horní Babákov u Hlinska	3Quartz vein/Greisen	549.05	304.41	93.83	7.62	333.32	829.8	48.37	9.2	5.39	3146.4	0.18
Horní Babákov u Hlinska	3Quartz vein/Greisen	792.3	285.65	86.04	8.31	264.38	950.8	42.96	10.56	4.77	3219.9	0.16

Appendix 2.6B (continued)

Name	model 1	Na	Mg	Mn	As	Sr	Y	Nb	Mo	Pb	REE	EuA
Hostákov u T?ebí?e	5Reduced skarn	12.51	26.41	9.24	1.97	48.23	6.35	38.91	2125	1.02	90.13	0.29
Hostákov u T?ebí?e	5Reduced skarn	19.46	11.26	11.29	1.61	50.46	7.58	55.32	2469	1.23	109.12	0.47
Hostákov u T?ebí?e	5Reduced skarn	2.92	3.77	10.19	1.64	47.26	7.17	48.51	2198	1.11	101.45	0.33
Hostákov u T?ebí?e	5Reduced skarn	2.95	7.05	6.8	1.42	41.01	9.24	117.9	592.1	1.85	201.04	0.37
Hostákov u T?ebí?e	5Reduced skarn	4.27	0.03	9.76	2.4	37.81	7.7	99.8	571.3	0.82	211.88	0.35
Hostákov u T?ebí?e	5Reduced skarn	18.07	0.02	10.51	1.89	37.24	9.55	92.71	568.5	0.83	194.07	0.42
Hostákov u T?ebí?e	5Reduced skarn	2.57	7.06	8.88	1.4	39.34	9.09	107.2	594.9	1.74	177.35	0.4
Hostákov u T?ebí?e	5Reduced skarn	3	8.26	10.84	1.56	35.86	8.72	151.4	590.8	1.54	255.83	0.43
Hostákov u T?ebí?e	5Reduced skarn	2.04	7.94	10.58	1.07	36.28	10.16	108.8	601.9	1.5	175.46	0.41
Hostákov u T?ebí?e	5Reduced skarn	0.52	19.46	6.17	1.06	41.28	11.23	124.1	657.5	2.78	186.96	0.3
Hostákov u T?ebí?e	5Reduced skarn	0.51	11.12	6.52	1.33	41.44	10.98	113	702	2.08	174.91	0.32
Hostákov u T?ebí?e	5Reduced skarn	0.79	7.1	6.78	1.17	37.95	12.45	108.6	593.5	0.93	178.12	0.43
Hutti	6Orogenic Au	145.2	4.08	22.3	7.3	344	473	10.22	0.38	8.43	658.67	2.93
Hutti	6Orogenic Au	108	4.34	16.8	12.6	252	364	11.6	1.85	6.16	375.01	2.61
Hutti	6Orogenic Au	44.2	3.36	9.01	17.7	171	241	13.1	2.53	4.14	188.24	1.75
Hutti	6Orogenic Au	180	4.05	5.7	11.1	127	186	20.8	3.78	2.88	147.26	1.92
Hutti	6Orogenic Au	47.6	8.6	9.61	19.6	150	229	24.7	3	4.02	194.41	1.16
Hutti	6Orogenic Au	36.4	3.32	14.8	13.3	247	154	1.82	0.38	5.48	159.27	2.05
Hutti	6Orogenic Au	41	9.6	9	21	202	185	2.48	0.28	4.52	142.55	1.56
Hutti	6Orogenic Au	38.9	6.7	10.18	22.3	176.6	250	30	1.45	4.42	196.34	1.17
Hutti	6Orogenic Au	42.2	7.2	10.48	19.3	183.7	210.2	15.8	1.52	4.46	176.04	1.37
Hutti	6Orogenic Au	56	19	7.1	14.7	131	188	18.7	2.43	8.8	150.58	0.95
Hutti	6Orogenic Au	53.4	14	9.1	16.3	147	194.2	15.3	1.94	7.2	167.16	1

Appendix 2.6B (continued)

Name	model 1	Na	Mg	Mn	As	Sr	Y	Nb	Mo	Pb	REE	EuA
Hutti	6Orogenic Au	50.7	6.4	10.7	18.6	178	208	9.32	1.43	5.2	191.46	1.06
Hutti	6Orogenic Au	37.7	4.3	7.8	24.1	167	249	14.1	1.06	4	197.06	1.05
Hutti	6Orogenic Au	31	3.31	9.3	14	136	187	12.2	0.78	2.9	166.83	1.14
Hutti	6Orogenic Au	41.8	3.7	10.7	16.7	208	192.6	2.11	0.46	4.94	181.1	2.05
Hutti	6Orogenic Au	33.4	6.9	12.3	5.03	403	89.4	1	0.44	10.1	98.08	3.35
Hutti	6Orogenic Au	40.5	8.3	7.7	12.3	239	192	48	4.5	5.5	182.81	1.32
Hutti	6Orogenic Au	57	8.2	6.27	17.6	236	208	32	1.47	8.5	195.62	1.27
Hutti	6Orogenic Au	44.5	7.32	9.7	10.4	315	148	13.1	1.18	8.16	151.51	1.8
Hutti	6Orogenic Au	70.8	10.9	8.3	1.55	426	156	1.29	0.52	8.54	154.43	5.94
Hutti	6Orogenic Au	19.7	9.5	16.9	17.2	481	31.8	0.24	0.31	18.9	56.8	3.67
Hutti	6Orogenic Au	25.5	10	15.9	24.4	477	54	0.27	0.35	17.86	93.6	3.05
Hutti	6Orogenic Au	56	19.6	12.6	63	417	166.3	0.37	0.2	13.5	267.22	2.52
Hutti	6Orogenic Au	10.6	6.5	19.8	7.92	510	15.3	0.24	0.53	20.3	27.52	8.7
Hutti	6Orogenic Au	24.1	14.5	12.18	18.8	556	35.6	0.28	0.44	21.3	48.72	5.35
Hutti	6Orogenic Au	31	15.5	19.3	19.1	556	39.3	0.29	0.69	25.1	65.2	3.82
Invincible Mine	5Reduced skarn	59.91	27.11	1.14	0.46	504.29	24.33	4.61	3.22	0.64	275.78	1.01
Invincible Mine	5Reduced skarn	18.77	2.71	21.34	0.56	77.7	8.26	106.8	1914	7.37	186.32	0.59
Invincible Mine	5Reduced skarn	30.02	3.14	21.71	0.48	89.93	8.95	69.36	1840	20.68	142.88	0.59
Invincible Mine	5Reduced skarn	42.81	3.95	3.99	0.87	593.53	38.78	18.49	316.9	2.91	585.1	0.95
Invincible Mine	5Reduced skarn	30.58	9.59	29.5	0.82	76.87	86.04	195	2613	23.63	311.98	0.35
Invincible Mine	5Reduced skarn	4.66	2.31	52.5	1.82	33.92	32.61	495.3	6154	3.81	965.77	1.31
Invincible Mine	5Reduced skarn	3.92	2.39	51.56	1.82	34.01	31.8	502.5	6297	3.07	965.8	1.36
Invincible Mine	5Reduced skarn	6.44	2.45	50.89	1.78	34.62	28.97	466.6	6047	2.88	911.39	1.4
Invincible Mine	5Reduced skarn	6.12	2.27	44.2	0.62	41.44	10.97	355.2	5472	3.43	330.64	1.29
Invincible Mine	5Reduced skarn	4.24	2.45	38.98	1.04	59.35	25.51	601.9	5370	3.82	449.77	1.26
Invincible Mine	5Reduced skarn	14.6	3.07	35.46	0.95	79.65	17.5	360.6	4701	4.85	363.75	1.22
Invincible Mine	5Reduced skarn	27.8	3	49.48	1.24	56.3	17.67	174.7	4798	11.31	448.74	1.37

Appendix 2.6B (continued)

Name	model 1	Na	Mg	Mn	As	Sr	Y	Nb	Mo	Pb	REE	EuA
Jiama	4Oxidized skarn	56.85	4.17	4.89	20.39	85.07	25.15	21.63	1E+05	8.02	487.97	3.43
Jiama	4Oxidized skarn	39.62	3.78	6.14	8.6	86.46	12.18	10.98	1E+05	5.92	317	1.66
Jiama	4Oxidized skarn	27.65	3.74	4.78	13	76.03	6.99	8.94	2E+05	5.89	250.89	2.01
Jiama	4Oxidized skarn	44.48	4.52	4.31	20.11	69.78	14.32	11.45	2E+05	4.34	302.39	1.73
Jiama	4Oxidized skarn	68.94	3.77	4.46	8.9	98.41	12.11	13.19	1E+05	6.56	508.11	2.93
Jiama	4Oxidized skarn	51.43	4.11	4.38	16.9	64.91	21.49	8.73	2E+05	5.66	351.61	1.46
Jiama	4Oxidized skarn	49.48	116.76	15.29	14.22	91.74	12.29	12.05	1E+05	5.55	378.04	1.67
Jiama	4Oxidized skarn	27.94	6.12	11.12	13.58	79.37	10.51	13.07	1E+05	5.1	260.08	1.77
Jiama	4Oxidized skarn	46.09	3.67	4.1	21.13	78.4	24.09	17.04	1E+05	5.56	397.63	2.17
Jiama	4Oxidized skarn	30.05	52.4	100.08	3.52	36.88	18.89	2.65	1861	34.75	199.97	1.15
Jiama	4Oxidized skarn	42.67	134.83	125.52	20.85	32.12	24.73	2.54	2184	40.31	224.53	1.18
Jiama	4Oxidized skarn	72.28	19.18	78.4	3.02	36.56	39.34	1.73	2259	52.82	369.72	1.07
Jiama	4Oxidized skarn	85.76	28.5	92.71	4.74	32.33	42.95	1.43	1963	34.33	513.78	1.23
Jiama	4Oxidized skarn	9.22	6.28	43.92	6.03	57.96	1.97	4.31	55044	10.51	73.07	0.89
Jiama	4Oxidized skarn	10.79	48.65	80.06	2.93	57.13	5.03	9.98	8201	10.43	78.08	1.27
Jiama	4Oxidized skarn	9.47	14	80.9	1.1	63.52	5.1	9.55	2207	13.97	69.98	1.14
Jiama	4Oxidized skarn	8.84	8.81	48.09	4.17	60.05	4.14	4.6	1821	12.93	62.39	1.17
Jiama	4Oxidized skarn	27.8	12.79	78.67	5.46	59.21	2.63	4.91	39337	11.72	68.46	0.79
Kanbauk	4Oxidized skarn	30.16	45.45	185.15	0.97	80.62	5.7	4.41	42.12	6.56	217.82	3.09
Kanbauk	4Oxidized skarn	54.63	69.92	68.67	0.95	61.58	8.84	3.13	248.8	6.21	345.06	5.66
Kanbauk	4Oxidized skarn	82.98	129.27	47.96	2.5	107.59	18.1	1.83	77.7	7.45	585.37	2.52
Kanbauk	4Oxidized skarn	41.7	45.18	224.9	0.93	53.79	9.04	3.02	344.9	4.82	223.98	1.97
Kanbauk	4Oxidized skarn	39.92	60.47	98	1.32	46.95	9.27	2.35	208.5	5.1	332.27	2.02
Kanbauk	4Oxidized skarn	83.12	89.38	105.78	2.34	67.83	7.91	4.2	118.2	5.28	815.49	1.15
Kanbauk	4Oxidized skarn	167.5	103.56	67.55	3.79	65.61	15.92	4.45	21.82	5.37	1210.9	0.59
Kanbauk	4Oxidized skarn	15.29	17.58	14.73	1.82	15.53	0.19	3.12	12357	3.34	4.62	0.65
Kanbauk	4Oxidized skarn	3.11	21.6	11.66	2.65	13.96	0.03	4.57	10634	0.74	3.59	1.41

Appendix 2.6B (continued)

Name	model 1	Na	Mg	Mn	As	Sr	Y	Nb	Mo	Pb	REE	EuA
Kanbauk	4Oxidized skarn	50.04	21.27	34.89	2.36	39.89	0.64	1.51	9661	3.34	124.32	0.88
Kanbauk	4Oxidized skarn	7.78	29.19	13.04	1.99	23.59	0.14	1.94	12399	0.99	27.07	0.56
Kara	4Oxidized skarn	6.87	6.46	8.07	20	162.77	1.37	5.59	30045	4.34	109.95	0.74
Kara	4Oxidized skarn	4.3	9.73	8.62	16.64	174.58	1.62	8.84	35723	3.41	95.72	0.96
Kara	4Oxidized skarn	9.45	3.2	7.52	23.35	150.95	1.12	2.34	24367	5.28	124.19	0.26
Kara	4Oxidized skarn	16.68	9.17	7.34	16.75	217.12	1.46	13.46	47260	3.68	78.5	0.52
Kara	4Oxidized skarn	7.92	12.51	9.12	18.82	177.78	1.6	7.49	33443	4.59	101.84	0.68
Kara	4Oxidized skarn	12.3	10.84	8.23	17.79	197.45	1.53	10.47	40352	4.14	90.17	0.6
Kara	4Oxidized skarn	27.52	4.11	16.44	8.2	118.98	0.26	49.83	17431	9.02	257.41	1.18
Kara	4Oxidized skarn	31.28	5.43	13.36	12.64	118.85	0.46	62.55	25340	25.02	291.9	0.83
Kara	4Oxidized skarn	30.16	4.73	11.84	8.84	105.36	0.41	36.84	20086	15.6	208.58	1.03
Kara	4Oxidized skarn	33.5	4.48	15.79	6.74	97.3	0.4	40.59	20225	10.09	265.08	1.23
Kara	4Oxidized skarn	29.89	4.2	15.3	8.87	105.92	0.29	46.23	21906	9.02	251.78	1.01
Kara	4Oxidized skarn	31.83	4.41	17.04	6.52	94.52	0.48	37.85	19085	11.08	250.05	1.21
Kara	4Oxidized skarn	33.78	5.1	18.26	7.66	101.61	0.37	42.67	23060	11.04	261.61	1.04
Kara	4Oxidized skarn	30.86	4.13	16.57	7.74	98.69	0.44	40.84	22476	10.08	265.62	1.07
Kara	4Oxidized skarn	31.14	4.3	16.57	9.31	97.72	0.63	41.56	20072	10.33	255.56	1.1
Kara	4Oxidized skarn	29.19	79.23	33.36	2.57	11.63	30.72	58.52	1815	0.65	335.33	0.64
Kara	4Oxidized skarn	33.64	88.27	25.85	7.09	23.32	36.7	75.34	1582	0.9	460.86	0.46
Kara	4Oxidized skarn	16.01	28.22	16.68	7.37	4.02	102.3	76.59	1293	1.67	623.02	0.76
Kara	4Oxidized skarn	6.49	33.69	7.67	2.1	17.6	21.39	52.26	3272	0.35	178.69	0.28
Kara	4Oxidized skarn	34.61	126.49	17.79	3.54	5.39	46.84	47.97	1494	1.33	522.35	0.38
Kara	4Oxidized skarn	130.66	31.72	18.77	12.5	3.6	196.4	33.5	1300	1.15	2740	0.24
Kara	4Oxidized skarn	71.86	48.37	13.54	5.28	6.48	46.29	63.66	870.1	1.09	1024.6	0.23
Kirwans Hill	3Quartz vein/Greisen	97.3	32.11	69.78	2.21	301.77	485.1	46.43	4.92	13.29	977.45	1.51
Kirwans Hill	3Quartz vein/Greisen	133.44	32.53	21.96	19.46	510.13	285.8	71.86	4.45	18.93	641.61	0.52
Kirwans Hill	3Quartz vein/Greisen	72.28	30.16	35.72	1.15	265.91	154.3	20.89	5.64	11.11	294.26	2.15

Appendix 2.6B (continued)

Name	model 1	Na	Mg	Mn	As	Sr	Y	Nb	Mo	Pb	REE	EuA
Kirwans Hill	3Quartz vein/Greisen	31	32.71	59.35	1.22	226.85	339.2	31.12	7.02	11.76	454.4	3.76
Kirwans Hill	3Quartz vein/Greisen	103.42	36.04	41.6	4.73	181.53	827.1	96.88	6.66	11.12	945.39	0.8
Kirwans Hill	3Quartz vein/Greisen	96.19	64.36	58.1	2.59	174.17	841	76.87	5.39	9.76	1291.2	0.32
Kirwans Hill	3Quartz vein/Greisen	115.51	23.77	58.1	2.27	213.37	482.3	70.06	4.38	14.01	914.97	0.63
Kirwans Hill	3Quartz vein/Greisen	51.43	24.6	59.55	29.19	293.71	84.93	7.84	8.17	16.26	175.99	7.42
Kirwans Hill	3Quartz vein/Greisen	87.01	61.99	65.05	2.75	180.98	785.4	89.66	7.51	11.09	1340.2	0.48
Kirwans Hill	3Quartz vein/Greisen	80.62	67.55	55.28	2.57	175.14	622.7	53.65	4.87	8.91	983.06	0.38
Kirwans Hill	3Quartz vein/Greisen	58.94	27.55	36.46	0.71	237.27	446.2	46.01	5.39	13.36	447.61	2.79
Kirwans Hill	3Quartz vein/Greisen	94.66	48.51	47.82	1.78	223.79	661.6	123.9	5.7	9.38	949.34	0.75
Kochkar	6Orogenic Au	65	13.5	13.1	54	830	33.7	4.91	75.1	23.1	421.77	2.63
Kochkar	6Orogenic Au	69	19	16.2	101	1115	52.1	6.13	65	31.1	489.15	2.12
Kochkar	6Orogenic Au	52.8	5.94	10.98	21.1	667	23.3	4.31	80.7	18.4	384.96	2.93
Kochkar	6Orogenic Au	40.5	6.78	7.16	21.3	820	14.2	9.8	97.7	18.2	293	10.69
Kochkar	6Orogenic Au	56.3	8	7.19	35.8	811	17.6	4.94	99.8	19.8	493.06	8.58
Kochkar	6Orogenic Au	43.5	4.89	6.32	138	771	23.2	6.38	84.4	18.5	289.22	2.41
Kochkar	6Orogenic Au	65.3	10.2	11.1	34	900	29	6.7	82.2	22.5	381.04	4.67
Kochkar	6Orogenic Au	49.2	12.3	9.85	27.3	883	22.4	4.74	114	22.3	295.3	7.12
Kochkar	6Orogenic Au	620	127	3.6	4.87	1042	5.86	1.97	567	36.3	26.57	10.27
Kochkar	6Orogenic Au	380	68	3.43	4.41	1057	5.67	1.99	516	35	20.77	10.85
Kochkar	6Orogenic Au	980	176	3.86	6.8	970	7.99	2.15	619	39.1	42.34	8.82
Kochkar	6Orogenic Au	17.9	5.41	2.03	1.81	897	9.6	0.45	334	28.9	82.79	4.3
Kochkar	6Orogenic Au	11.1	5	2.01	5.51	960	7.39	0.88	428	28.21	52.04	4.52
Kochkar	6Orogenic Au	7	4.9	2.34	7.1	1024	9.81	1.31	549	30.2	54.79	5.24
Kochkar	6Orogenic Au	7.5	5.9	2.4	6.9	985	5.51	0.93	404	27	41	4.56
Kochkar	6Orogenic Au	19.5	16.2	3.05	16	921	8.6	5.35	467	34.12	51.97	3.24
Kochkar	6Orogenic Au	11.7	8.4	1.74	7.64	891	5.4	4.76	383	33.9	31.21	2.67
Kochkar	6Orogenic Au	17.3	9.9	2.51	16.5	960	9.72	5.59	517	34	55.5	4.13

Appendix 2.6B (continued)

Name	model 1	Na	Mg	Mn	As	Sr	Y	Nb	Mo	Pb	REE	EuA
Kochkar	6Orogenic Au	16.4	11.6	2.6	16.6	943	10.14	5.39	509	33.9	60.13	3.58
Kotel (Krkonoše)	5Reduced skarn	2.22	8.48	0.72	3.89	239.78	6.26	1.72	412.8	127.9	8.82	1.05
Kotel (Krkonoše)	5Reduced skarn	1.9	2.99	0.99	7.37	176.53	25.55	1.92	257.2	43.09	23.46	0.84
Kotel (Krkonoše)	5Reduced skarn	13.48	5.42	0.88	0.95	340.97	32.22	2	190.6	1.83	43.38	0.21
Kotel (Krkonoše)	5Reduced skarn	1.81	2.74	0.68	1.54	283.56	9.99	2.14	187.7	1.74	12.48	0.21
Kotel (Krkonoše)	5Reduced skarn	9.73	3.88	1.06	1.49	250.2	12.32	1.83	365.9	2.27	13.55	0.86
Kotel (Krkonoše)	5Reduced skarn	0.44	3.09	0.82	1.49	404.49	30.87	2.08	204.2	2.03	37.65	0.26
Kotel (Krkonoše)	5Reduced skarn	10.98	3.27	0.4	0.86	248.39	10.3	1.72	369.7	2.2	10.55	1.4
Kotel (Krkonoše)	5Reduced skarn	0.71	11.12	1.03	3.57	124.96	2.15	1.48	233.8	6.78	5.88	0.64
Kotel (Krkonoše)	5Reduced skarn	12.51	3.56	1.95	0.41	108	1.19	1.43	72.14	1.19	1.86	0.52
Kotel (Krkonoše)	5Reduced skarn	1.22	3.98	1	0.54	269.66	10.23	1.57	312.6	1.8	10.31	0.62
Kotel (Krkonoše)	5Reduced skarn	1.63	11.4	0.92	0.78	191.54	21.81	1.84	218.2	2.08	17.5	0.86
Kotel (Krkonoše)	5Reduced skarn	9.31	5.56	1.47	3.34	208.64	12.44	1.69	310.1	3.11	14.45	0.71
Ková?ská	4Oxidized skarn	10.84	7.2	2.78	0.31	105.5	4.16	1.67	1015	2.34	4.78	0.28
Ková?ská	4Oxidized skarn	1.52	16.68	2.13	0.65	111.9	4.52	1.5	977.2	0.97	3.24	0.49
Ková?ská	4Oxidized skarn	1.74	11.47	107.03	0.53	103.42	2.71	1.56	1052	9.27	18.46	0.34
Kumbel	4Oxidized skarn	12.23	3.88	1.38	100.91	104.11	0.17	1.51	11481	1.71	512.54	0.85
Kumbel	4Oxidized skarn	10.09	4.04	1.29	99.25	103.14	0.27	1.47	12232	1.53	506.18	0.85
Kumbel	4Oxidized skarn	8.58	3.71	1.39	87.99	71.72	0.05	1.63	10606	1.19	244.95	1.28
Kumbel	4Oxidized skarn	10.17	3.45	1.29	84.79	71.17	0.05	1.7	10522	1.23	241.74	1.2
Kumbel	4Oxidized skarn	11.45	3.5	1.31	85.76	71.38	0.06	1.64	10522	1.25	239.44	1.17
Kumbel	4Oxidized skarn	14.04	3.49	1.52	82.57	70.75	0.12	1.6	11064	1.5	232.57	1.37
Kumbel	4Oxidized skarn	10.15	3.53	1.49	82.98	70.61	0.04	1.72	10634	1.16	236.52	1.2
Kumbel	4Oxidized skarn	15.57	3.71	1.35	92.3	103.56	0.15	1.48	10898	1.33	501.41	0.94
Kumbel	4Oxidized skarn	12.51	3.67	1.22	102.86	103.56	0.12	1.52	11301	1.79	508.53	0.72
Kumtor	6Orogenic Au	8.4	3.77	1.36	6.7	7300	13.2	0.38	196	86	78.39	0.84
Kumtor	6Orogenic Au	33	5.4	2.14	10.3	2820	6.1	0.39	240	25	180.45	0.68

Appendix 2.6B (continued)

Name	model 1	Na	Mg	Mn	As	Sr	Y	Nb	Mo	Pb	REE	EuA
Kumtor	6Orogenic Au	12.3	3.46	2.61	5.9	6340	2.14	0.39	195.6	94.7	14.2	0.76
Kumtor	6Orogenic Au	24.6	4.31	2.66	9.4	5570	5.2	0.41	211	76.4	71.66	0.94
Lamaque	6Orogenic Au	253	19	2.19	43	812	575	2.26	46.6	179	2067.6	0.75
Lamaque	6Orogenic Au	204	13.5	2.04	21.5	772	328	2.02	42.5	155	1259.1	0.83
Lamaque	6Orogenic Au	229	23.9	2.38	35.1	788	504	2.19	42.1	168	1728.4	0.71
Lened	5Reduced skarn	5.42	4.14	51.43	1.15	91.88	1.42	15.29	4879	1.56	62.04	1.51
Lened	5Reduced skarn	25.99	2.59	11.69	1.22	57.32	20.41	51.85	3315	1.47	272.49	0.58
Lened	5Reduced skarn	16.4	2.84	7.85	1.29	48.37	53.93	103	3652	1.65	217.48	0.41
Lened	5Reduced skarn	9.17	3.2	60.19	1.03	55.32	13.33	44.76	4031	1.5	160.91	0.39
Lened	5Reduced skarn	18.35	2.85	15.85	1.24	62.83	11.26	23.34	4476	1.31	312.07	0.38
Lened	5Reduced skarn	1.03	2.96	9.8	0.31	27.66	1.57	15.99	746.4	0.93	36.5	0.64
Lened	5Reduced skarn	9.34	2.43	9.27	1.31	64.64	6.1	22.21	4579	1	111.01	0.52
Lened	5Reduced skarn	15.43	2.35	11.72	1.52	66.86	9.13	57.82	4177	1.3	193.54	0.44
Lened	5Reduced skarn	11.86	2.71	13.48	1.36	67.55	7.95	31.14	4139	1.24	142.41	0.61
Lened	5Reduced skarn	8.48	2.88	9.33	1.17	95.35	2.98	18.83	4084	1.35	66.99	0.6
Lened	5Reduced skarn	17.38	14.6	17.38	2.46	39.09	42.67	35.03	332.4	1.07	331.78	1.04
Lened	5Reduced skarn	6.02	3.77	16.28	1.17	37.74	86.74	46.57	337.4	1.04	505.03	0.83
Lened	5Reduced skarn	6.19	3.74	15.54	0.82	37.95	39.48	28.55	374.3	1.05	390.53	0.98
Lened	5Reduced skarn	10.29	6.81	14.54	1.63	40.35	38.09	36	418.4	1.06	486.94	1.16
Lened	5Reduced skarn	4.75	5.23	15.78	1.53	37.04	83.54	38.23	390.2	0.98	812.26	0.72
Lened	5Reduced skarn	4.87	4.13	14.89	1.99	39.2	42.95	79.09	461.5	1.01	698.98	0.69
Lened	5Reduced skarn	9.98	5.2	20.63	0.67	45.26	208.5	88.96	163.6	1.55	355.05	0.72
Lened	5Reduced skarn	2.52	4.14	18.07	1.38	40.1	187.1	32.73	337.4	1.26	546.7	0.73
Lened	5Reduced skarn	3.81	4.81	19.61	0.49	39.28	59.91	52.26	266.6	1.29	133.95	1.44
Lened	5Reduced skarn	17.03	36.14	30.44	0.75	46.57	4.93	31	2533	1.56	160.05	0.41
Lened	5Reduced skarn	15.01	13.34	27.11	0.75	61.58	15.47	49.21	2947	2.35	141.05	0.4
Lened	5Reduced skarn	17.79	119.54	37.53	0.88	58.1	13.34	43.37	2585	2.38	133.8	0.41

Appendix 2.6B (continued)

Name	model 1	Na	Mg	Mn	As	Sr	Y	Nb	Mo	Pb	REE	EuA
Lened	5Reduced skarn	10.91	17.24	27.09	0.61	72.09	8.67	33.64	1986	1.86	140.79	0.48
Lened	5Reduced skarn	11.61	19.46	43.92	0.39	75.2	26.85	86.46	1305	1.68	184.54	0.68
Lened	5Reduced skarn	9.31	19.46	41.01	0.53	65.33	35	119	1287	1.84	203.61	0.47
Lened	5Reduced skarn	20.43	7.37	21.96	0.38	60.19	36.14	76.17	1133	1.41	179.18	0.53
Lened	5Reduced skarn	11.12	15.01	61.16	0.7	86.74	18.49	81.59	1854	1.63	150.15	0.46
Lened	5Reduced skarn	11.4	7.87	25.59	0.43	78.26	26.37	92.44	1881	1.3	167.33	0.48
Lened	5Reduced skarn	18	10.56	21.82	0.63	72.98	24.05	78.95	1985	1.05	191.02	0.34
Lened	5Reduced skarn	23.56	6.67	18.7	0.57	88.4	37.39	69.36	2010	1.34	195.1	0.42
Lened	5Reduced skarn	17.03	3.38	17.96	0.44	88.54	25.65	80.9	1508	1.32	199.85	0.52
Lened	5Reduced skarn	6.44	2.88	164.02	0.46	176.53	2.63	32.53	746.4	2.09	119.2	1.13
Lened	5Reduced skarn	6.8	3.77	16.03	0.68	34.29	14.86	22.55	1939	1.71	179.42	1.3
Lened	5Reduced skarn	7.7	3.28	14.29	0.58	36.24	7.27	16	1992	1.53	94.09	0.98
Lened	5Reduced skarn	11.22	3.35	16.6	1.18	62.97	13.47	16.62	2570	1.61	102.01	0.7
Lened	5Reduced skarn	4.17	2.95	28.63	0.54	47.68	2.03	95.77	1689	2.34	137.04	1.71
Lened	5Reduced skarn	8.92	4.42	27.08	0.88	68.53	12.15	12.41	1362	1.71	84.09	0.58
Lened	5Reduced skarn	7.77	3.82	37.53	0.47	114.81	1.71	20.74	1097	1.75	70.89	0.99
Lened	5Reduced skarn	5.73	2.91	23.94	0.65	158.04	4.24	84.51	824.3	2.38	217.58	0.86
Lened	5Reduced skarn	3.95	3.79	184.87	0.42	97.86	2.24	34.75	1407	1.86	93.41	0.96
Lened	5Reduced skarn	12.79	7.23	13.48	0.83	37.53	7.31	14.48	2253	1.81	105.52	0.65
Lened	5Reduced skarn	21.41	5.07	14.3	0.67	33.53	12.73	7.42	2405	1.93	159.39	1.61
Lened	5Reduced skarn	11.13	4.34	21.27	0.85	31.55	10.34	7.96	2399	2.82	109.33	1.79
Lened	5Reduced skarn	20.02	6.67	15.25	0.7	27.66	11.76	7.95	2243	1.78	153.68	1.37
Lened	5Reduced skarn	19.6	4.41	16.37	0.64	40.73	12.97	12.65	2138	1.67	136.93	1.2
Lermo	5Reduced skarn	7.14	4.49	11.31	1.36	17.01	85.9	10.7	14.57	2.11	161.74	2.98
Lermo	5Reduced skarn	9.04	4.16	15.5	0.75	21.42	90.63	12.47	14.22	2.42	354.16	18.68
Lermo	5Reduced skarn	13.77	3.77	12.01	0.98	21.74	125.1	36	12.91	2.02	122.85	0.49
Lermo	5Reduced skarn	12.02	3.73	17.32	1.04	22.1	175.6	142.8	12.65	2.92	299.42	6.75

Appendix 2.6B (continued)

Name	model 1	Na	Mg	Mn	As	Sr	Y	Nb	Mo	Pb	REE	EuA
Lermo	5Reduced skarn	25.3	13.07	26.27	1.11	22.53	269.7	38.78	31.11	2.97	346.11	0.38
Lermo	5Reduced skarn	16.82	34.75	13.01	1.18	32.94	196.8	18.49	31	3.14	296.6	0.65
Lermo	5Reduced skarn	12.79	8.06	15.05	0.88	20.54	196.3	14.89	34.71	1.89	298.6	0.85
Lermo	5Reduced skarn	26.69	17.93	26.69	1.14	22.73	232.8	19.4	27.08	2.56	437.2	0.44
Lermo	5Reduced skarn	36.84	51.43	13.51	1.74	24.63	314.1	38.36	29.75	3.17	439.28	0.27
Lermo	5Reduced skarn	12.93	58.38	13.34	1.74	14.55	373.9	135.3	117.3	1.14	397.25	0.11
Lermo	5Reduced skarn	21.99	3.29	14.61	0.44	16.65	348.9	78.81	20.99	1.85	231.89	0.92
Lermo	5Reduced skarn	8.74	3.81	15.48	0.33	17.5	124.8	30.16	16.36	2.63	135.19	1.72
Lermo	5Reduced skarn	13.34	3.95	9.34	1.44	13.01	379.8	174.7	104.7	1.26	282.06	0.09
Lermo	5Reduced skarn	13.76	3.41	26.83	0.34	25.49	129.6	22.24	19.32	2.79	228.96	4.01
Lermo	5Reduced skarn	5.74	3.47	16.97	0.18	19.21	130	11.82	15.14	2.2	251.89	23.12
Lermo	5Reduced skarn	23.63	7.09	12.13	1.14	12.07	418.4	98.69	84.79	1	276.95	0.1
Lermo	5Reduced skarn	21.68	5.09	51.29	0.6	21.7	56.99	51.57	357.2	2.81	140.7	0.46
Lermo	5Reduced skarn	18.77	55.6	38.5	0.57	24.05	23.63	243.3	1849	4.73	254.2	0.64
Lermo	5Reduced skarn	9.34	4.61	15.82	0.33	20.92	184.3	11.25	14.39	2.28	294.07	5.55
Lermo	5Reduced skarn	10.7	21.41	9.31	0.38	20.16	123.7	23.63	23.77	1.54	92.12	0.95
Lermo	5Reduced skarn	11.4	4.78	13.62	0.37	22.2	138.9	10.13	16.79	1.96	236.1	4.68
Lermo	5Reduced skarn	39.34	38.92	29.33	0.77	28.12	193.2	57.82	25.3	2.93	331.68	0.53
Lermo	5Reduced skarn	12	4.52	10.48	1.89	11.8	563	66.16	148.6	1.03	376.86	0.04
Lermo	5Reduced skarn	15.15	65.33	38.64	0.32	30.98	73.53	11.95	14.83	3.45	161.89	7.77
Lermo	5Reduced skarn	54.91	5.56	46.88	1.24	34.79	276.6	32.94	9.83	3.96	690.46	0.71
Lermo	5Reduced skarn	19.32	3.7	13.43	2.43	11.44	325.3	41.14	224.6	0.69	384.98	0.07
Logtung	2Porphyry	294.68	204.89	154.85	14.41	98.13	799.3	224.8	287	26.94	2357.2	0.17
Logtung	2Porphyry	295.93	234.49	165.41	13.64	97.16	881.3	213.5	290.8	26.13	2436.4	0.16
Logtung	2Porphyry	293.71	234.77	166.94	13.72	93.27	879.9	221.4	277.6	25.59	2395.1	0.16
Logtung	2Porphyry	270.77	202.38	150.82	11.62	108.7	692.2	165.4	288.7	26.2	2032.7	0.17
Logtung	2Porphyry	293.01	207.25	166.11	12.66	108.28	699.2	170.3	285.7	27.98	2098.1	0.17

Appendix 2.6B (continued)

Name	model 1	Na	Mg	Mn	As	Sr	Y	Nb	Mo	Pb	REE	EuA
Logtung	2Porphyry	300.94	211.28	203.91	12.15	130.1	767.3	415.6	307.3	30.57	2796.4	0.13
Logtung	2Porphyry	361.12	206.97	158.18	17.63	99.39	877.1	263.7	292.6	27.17	2698.9	0.17
Logtung	2Porphyry	232.96	210.72	144.28	17.51	91.18	956.3	939.6	1441	16.49	2681	0.12
Logtung	2Porphyry	218.37	218.65	153.87	20.63	144.84	1223	980	1277	18.67	2895.3	0.1
Logtung	2Porphyry	201.13	258.96	166.52	21.68	117.59	1223	1204	1365	18.57	3163.3	0.09
Logtung	2Porphyry	230.6	217.81	147.2	16.99	91.74	917.4	911.8	1473	16.9	2627.7	0.12
Logtung	2Porphyry	236.3	207.11	145.95	15.28	102.58	746.4	841	1236	18.63	2302.8	0.15
Logtung	2Porphyry	204.75	191.96	123.29	16.82	99.11	668.6	629.7	1045	15.5	1913.2	0.14
Machwi	3Quartz vein/Greisen	33.47	5.63	124.27	1.17	20.64	878.5	302.1	8.48	19.47	931.97	0.27
Machwi	3Quartz vein/Greisen	56.57	3.74	125.8	2.03	20.2	971.6	499	1.77	21.04	1315.6	0.09
Machwi	3Quartz vein/Greisen	33	3.53	125.24	1.2	19.43	1023	329.4	1.74	18.13	875.67	0.07
Machwi	3Quartz vein/Greisen	83.26	9.31	113.56	2.75	21.73	946.6	688.1	2.92	23.63	1737	0.06
Machwi	3Quartz vein/Greisen	25.3	2.93	77.01	0.73	25.63	414.6	307.2	1.06	14.82	430.78	0.1
Machwi	3Quartz vein/Greisen	27.41	3.2	98	0.47	23	640.8	201.8	1.38	15.83	651.52	0.08
Machwi	3Quartz vein/Greisen	28.66	3.21	99.39	0.7	23.48	752	233.9	1.22	16.11	774.65	0.12
Machwi	3Quartz vein/Greisen	28.44	2.92	73.81	1.07	24.06	544.9	387.8	1.95	9.77	501.39	0.09
Machwi	3Quartz vein/Greisen	20.41	3.67	73.67	18.49	54.77	411.4	881.3	3.91	13.43	491.6	0.07
Machwi	3Quartz vein/Greisen	51.43	15.29	93.13	0.71	29.36	761.7	314	10.43	16.96	687.95	0.1
Machwi	3Quartz vein/Greisen	45.59	17.42	58.24	1	26.15	946.6	179.9	0.42	9.47	934.23	0.01
Machwi	3Quartz vein/Greisen	30	8.48	96.74	1.22	30.29	867.4	197.9	4.17	13.29	885.24	0.06
Machwi	3Quartz vein/Greisen	66.72	4.93	98	2.82	76.73	795.1	867.4	2.36	19.7	1265.2	0.09
Machwi	3Quartz vein/Greisen	44.76	19.46	45.05	0.77	27.41	920.2	256.7	0.09	7.62	660.13	0.02
Machwi	3Quartz vein/Greisen	7.62	21.49	34.19	0.42	162.21	243	33.64	1.54	0.44	290.42	0.06
Macraes	6Orogenic Au	28.5	277	4.39	63	5050	182	0.57	0.17	3.92	396.45	1.67
Macraes	6Orogenic Au	68.1	16.2	7.6	2.2	6470	145	0.28	0.001	8.6	215.1	2.07
Macraes	6Orogenic Au	49.8	15.4	5.88	0.98	6910	73	0.3	0.001	8.97	104.38	2.08
Macraes	6Orogenic Au	73	37	5.8	4.1	6340	208	0.39	0.001	6.1	248.02	2.46

Appendix 2.6B (continued)

Name	model 1	Na	Mg	Mn	As	Sr	Y	Nb	Mo	Pb	REE	EuA
Macraes	6Orogenic Au	37	13.9	1.82	2.22	3500	176	0.65	0.001	2	344.08	1.5
Macraes	6Orogenic Au	35.1	12.1	4.31	0.8	6780	74.2	0.36	0.001	6.12	103.39	2.2
Macraes	6Orogenic Au	53.1	15.9	6.19	1.56	6620	112.8	0.33	0.001	8.02	166.11	2.06
Macraes	6Orogenic Au	52.7	18.8	4.6	1.12	6090	100.4	0.3	0.06	4.27	132.79	2.56
Macraes	6Orogenic Au	62.5	17.5	6.01	1.12	7050	166	0.36	0.07	6	181.93	1.84
Macraes	6Orogenic Au	79	19.7	5.8	1.87	6400	250	0.37	0.23	6.7	316.97	2.83
Macraes	6Orogenic Au	40.4	11.4	1.22	1.48	2250	536	0.53	0.17	0.71	643.1	5.12
Macraes	6Orogenic Au	68	21.8	4.31	0.09	5130	115	0.36	0.07	2.96	137.44	2.49
Macraes	6Orogenic Au	62.4	18	5.27	1.37	5830	214	0.4	0.12	4.99	255.81	3.46
Macraes	6Orogenic Au	74	57	2.7	8.2	5160	248	0.42	0.19	2.69	441.52	1.47
Macraes	6Orogenic Au	55	19	5.51	1.6	6020	71.7	0.27	0.07	7.4	94.57	1.95
Macraes	6Orogenic Au	66	32	5	10	4780	124	0.51	0.05	3.46	193.42	1.41
Macraes	6Orogenic Au	56	14.8	3.2	2.22	5000	421	0.54	0.15	2.94	636.01	1.14
Macraes	6Orogenic Au	48.7	17.3	5.98	2.67	5410	106.2	0.31	0.06	6.05	129.83	1.77
Macraes	6Orogenic Au	55.6	21	4.89	2.78	5540	137	0.36	0.09	5.8	197.76	1.51
Mactung	5Reduced skarn	10.13	3.24	8.16	0.88	37.81	6.81	19.6	2473	2.27	155.95	0.66
Mactung	5Reduced skarn	7.67	3.39	8.21	0.74	37.74	6.02	26.27	2491	2.37	185.87	0.67
Mactung	5Reduced skarn	8.9	3.45	9.62	0.44	39.17	31.47	13.08	1532	2.79	94.55	0.47
Mactung	5Reduced skarn	10.37	5.28	134.83	0.65	36.84	53.38	212.7	1761	3.53	342.11	0.59
Mactung	5Reduced skarn	10.44	3.68	7.31	0.82	40.57	15.03	68.67	2178	2.97	185.1	1.15
Mactung	5Reduced skarn	10.16	4.32	10.49	0.71	34.99	48.93	159.2	1794	3.7	313.74	0.72
Mactung	5Reduced skarn	7.41	4.71	9.84	0.39	49.07	9.67	101.9	1847	3.1	200.17	1.33
Mactung	5Reduced skarn	7.2	3.81	9.79	0.6	39.31	10.26	114.4	2369	3.05	236.19	0.93
Mactung	5Reduced skarn	5.45	6.94	15.86	0.18	136.08	1.78	4	336.4	2.15	25.16	1.17
Mactung	5Reduced skarn	8.19	8.45	19.14	0.13	91.6	4.66	5.49	348.9	1.87	51.49	0.53
Mactung	5Reduced skarn	7.83	8.33	20.57	0.29	52.82	4.74	5.96	199.6	2.48	59.6	0.7
Mactung	5Reduced skarn	7.65	13.65	148.45	0.14	47.26	20.11	186.3	29.09	13.23	109.7	3.36

Appendix 2.6B (continued)

Name	model 1	Na	Mg	Mn	As	Sr	Y	Nb	Mo	Pb	REE	EuA
Mactung	5Reduced skarn	3.17	14.37	123.57	0.08	54.07	25.58	173.8	72.14	12.09	82.25	1.34
Mactung	5Reduced skarn	32.53	41.7	22.38	0.44	13.89	45.45	75.06	421.2	3	289.6	0.29
Mactung	5Reduced skarn	37.25	4.06	13.14	0.72	12.45	74.23	157.9	493.5	3.34	441.99	0.32
Mactung	5Reduced skarn	24.67	5.06	16.21	0.5	12.11	45.45	121.9	582.8	2.76	310.18	0.35
Mactung	5Reduced skarn	39.62	4.42	13.23	0.71	14.64	72.84	142.9	526.4	3.75	400.26	0.31
Mactung	5Reduced skarn	25.85	4.09	14.79	0.49	14.6	48.23	123.3	551.8	3.46	311.66	0.3
Mactung	5Reduced skarn	21.43	3.85	15.43	0.48	19.52	38.78	98.83	639.4	2.79	263.11	0.26
Mactung	5Reduced skarn	14.46	5.03	15.67	0.53	15.26	81.32	311.4	478.2	3.84	497.84	0.19
Mactung	5Reduced skarn	22.8	3.93	19.46	0.78	12.43	80.06	167.9	518.6	3.41	482.2	0.32
Mactung	5Reduced skarn	11.54	5.07	17.28	0.24	31.41	37.95	104	295.2	8.19	181.62	3.22
Mactung	5Reduced skarn	22.66	31.28	24.88	0.43	61.02	30.72	88.4	295.1	6.78	161.97	2.03
Mactung	5Reduced skarn	11.58	5.32	18.63	0.2	28.15	28.91	46.98	273.7	8.17	120.39	7.32
Mactung	5Reduced skarn	16.68	3.75	21.17	0.25	38.5	52.68	160	351.7	7.78	304.65	0.9
Mactung	5Reduced skarn	11.82	3.54	24.98	0.21	32.01	33.36	140.4	260.2	9.12	162.01	1.99
Mactung	5Reduced skarn	5.05	3.82	28.51	0.14	30.4	19.17	137.6	286.6	9.94	77.63	7.36
Mactung	5Reduced skarn	31.28	44.48	33.64	0.81	37.67	43.23	91.74	296.1	15.01	190.37	6.04
Mactung	5Reduced skarn	20.02	26.27	41.98	0.7	37.54	24.33	127.9	272.2	17.63	115.41	12.15
Mactung	5Reduced skarn	24.16	6.81	15.22	0.37	33.64	47.36	111.6	369.5	7.96	280.9	1.2
Mactung	5Reduced skarn	19.74	5.17	12.64	0.42	35.58	54.21	121.8	313.7	7.95	264.31	2.14
Mactung	5Reduced skarn	14.32	8.62	37.53	0.31	25.1	35.83	51.29	355	6.7	120.84	1.36
Mactung	5Reduced skarn	7.73	4.16	28.16	0.25	31.29	24.83	112.5	283.4	10.79	181.44	20.18
Mactung	5Reduced skarn	64.36	7.65	15.26	0.85	47.26	105.1	121.8	285.5	4.07	473.02	0.42
Mactung	5Reduced skarn	28.22	13.07	10.08	0.48	80.48	53.38	107	293.3	3.13	313.2	0.64
Mactung	5Reduced skarn	46.43	5.63	10.19	0.61	89.66	74.64	88.54	404.5	3.14	340.52	0.44
Mactung	5Reduced skarn	25.99	9.87	11.55	0.37	90.77	31.46	43.37	468.4	2.85	192.34	0.66
Mactung	5Reduced skarn	3.82	6.81	16.3	0.24	31.55	30.44	196	262.7	6.28	186.32	1.01
Mactung	5Reduced skarn	4.45	4.78	18.06	0.15	22.52	9.84	80.06	258.5	5	62.72	2.26

Appendix 2.6B (continued)

Name	model 1	Na	Mg	Mn	As	Sr	Y	Nb	Mo	Pb	REE	EuA
Mactung	5Reduced skarn	11.15	11.82	25.28	0.09	31	22.1	57.96	390.6	4.59	112.46	1.34
Mactung	5Reduced skarn	29.19	5.74	12.15	0.56	74.92	34.64	48.93	138.4	3.6	232.78	2.28
Mactung	5Reduced skarn	8.53	7.02	12.3	0.38	124.27	28.59	35.86	515.7	2.59	132.79	0.73
Mactung	5Reduced skarn	38.78	11.82	11.51	0.54	104.11	44.9	53.93	444.8	2.95	275.01	0.7
Mactung	5Reduced skarn	11.4	8.28	13.75	0.36	56.3	23.85	85.35	400.3	5.03	147.44	1.66
Mactung	5Reduced skarn	5.42	4.93	13.11	0.28	24.7	21.82	78.81	314.7	5.23	96.53	1.23
Mactung	5Reduced skarn	3.71	19.04	46.25	0.29	62.41	7.62	25.23	32.08	6.85	54.02	3.16
Mactung	5Reduced skarn	3.64	11.84	86.88	0.14	63.25	0.69	443.4	27.87	10.74	11.54	29.52
Mactung	5Reduced skarn	2.34	14.23	79.93	0.21	50.62	2.29	54.07	45.59	6.8	35.66	49.33
Mactung	5Reduced skarn	4.59	15.89	54.14	0.24	56.16	1.67	49.76	38.23	7.19	33.29	56.32
Mactung	5Reduced skarn	1.71	14.41	57.13	0.21	53.93	1.72	19.54	47.26	6.66	26.3	46.03
Mararoa Norseman	6Orogenic Au	92	2.93	22.22	2.95	314.8	196.2	30.2	0.65	23.09	289.86	3.51
Mararoa Norseman	6Orogenic Au	24.8	3.41	23.7	1.96	256	40.2	5.2	0.82	25.98	91.83	16.91
Mararoa Norseman	6Orogenic Au	58.9	5	21.46	15.8	221	149	37.7	0.84	33	239.69	2.41
Mararoa Norseman	6Orogenic Au	77.3	3.05	21.31	18.7	229.4	199	24.5	0.78	30.6	257.79	3.91
Mararoa Norseman	6Orogenic Au	39.8	2.97	23.24	4.2	277	88.1	20.3	0.61	25.54	136.67	9.34
Mararoa Norseman	6Orogenic Au	59	3.74	20.59	3.2	285	69.4	11.3	0.71	24.81	134.24	8.5
Marn	5Reduced skarn	7.33	3.68	2.97	3.27	195.71	100.9	21.96	454.5	1.3	252.2	0.6
Marn	5Reduced skarn	18.07	3.66	4.53	2.91	203.5	106.5	22.27	493.7	1.82	218.49	0.74
Marn	5Reduced skarn	7.35	3.91	3.36	2.61	198.21	103.7	22.18	489.3	1.38	213.57	0.75
Marn	5Reduced skarn	8.65	3.56	2.96	3.07	201.27	108.6	19.27	484.7	1.31	264.22	0.69
Marn	5Reduced skarn	7.73	4.04	3.63	2.82	202.8	103.6	21.03	475.5	2.47	221.55	0.74
Marn	5Reduced skarn	21.68	4.55	15.15	14.98	160.96	106.3	59.21	522.1	3.75	208.51	0.73
Marn	5Reduced skarn	7.91	3.86	2.43	4.75	172.5	130.5	19.28	604.7	1.33	347.6	0.73
Marn	5Reduced skarn	8.67	3.91	1.4	5.32	171.25	151.9	14.19	564.3	1.31	417.23	0.63
Marn	5Reduced skarn	11.77	3.93	3	3.28	180.14	87.01	15.72	618.6	1.54	288.14	0.6
Marn	5Reduced skarn	12.41	3.91	2.72	4.49	165.69	153.9	13.61	523.6	1.3	331.16	0.73

Appendix 2.6B (continued)

Name	model 1	Na	Mg	Mn	As	Sr	Y	Nb	Mo	Pb	REE	EuA
Marvel Loch	6Orogenic Au	16.8	4.89	11.56	7.92	684	12.57	0.29	0.03	19.6	46.4	20.62
Marvel Loch	6Orogenic Au	13.6	4.81	11.44	9.55	693	13.77	0.3	0.02	18.87	51.19	15.78
Marvel Loch	6Orogenic Au	99	7.9	10.96	12.38	668.2	16.83	0.36	0.02	19.49	64.12	8.75
Marvel Loch	6Orogenic Au	66.2	5.29	9.1	11.47	621	14.02	0.39	0.26	18.63	54.63	11.31
Marvel Loch	6Orogenic Au	47.6	9.4	9.34	8.22	1084	11.11	0.52	3.1	23.94	48.21	2.31
Marvel Loch	6Orogenic Au	232	8.3	9.61	9.8	1061	11.65	0.65	20.1	25.5	53.93	1.88
Marvel Loch	6Orogenic Au	125	5.29	9	10.3	1053	13.06	1.19	92	23.4	55.96	1.34
Marvel Loch	6Orogenic Au	37	4.65	8.1	9.2	1071	13.5	1.21	10.3	21.5	52.73	2.05
Marvel Loch	6Orogenic Au	84	6.5	9.08	8.82	1091	11.92	0.73	20.3	24.36	51.5	2.09
Marvel Loch	6Orogenic Au	54.6	5.06	9.68	10.47	689	12.48	0.33	0.03	19.8	53.34	16.29
Marvel Loch	6Orogenic Au	72	5.92	9.79	10.02	656	12.52	0.36	0.03	19.2	53.69	12.93
Mount Charlotte	6Orogenic Au	34.1	4.41	2.54	0.08	1160	52.4	0.26	0.79	26.1	96.84	26.28
Mount Charlotte	6Orogenic Au	42.8	5.92	2.09	0.08	1275	58.1	0.27	0.54	27.32	109.69	21.1
Mount Charlotte	6Orogenic Au	164	4.33	3.14	2.4	1067	393	0.67	0.31	23.4	1157	1.95
Mount Charlotte	6Orogenic Au	92	4	2.76	2.12	1010	504	0.64	0.54	23	1048.2	2.91
Mount Charlotte	6Orogenic Au	129.8	4.79	2.81	2.08	1031	391	0.61	0.37	22.5	983.34	2.41
Mount Charlotte	6Orogenic Au	9.4	3.56	1.63	0.08	1391	85	0.27	0.57	26.72	167.84	12.2
Mount Charlotte	6Orogenic Au	150	6.1	2.49	3.56	883	470	0.49	0.3	20.07	909.79	3.23
Mount Charlotte	6Orogenic Au	217	6.2	2.38	4.5	1281	420	0.6	0.45	25	1423.9	1.48
Mount Charlotte	6Orogenic Au	203	6.4	2.1	3.9	1043	305	0.72	0.41	20.8	1311.6	1.36
Mount Charlotte	6Orogenic Au	73.4	4.3	1.69	1.63	669	93.2	0.56	0.8	12.8	389.27	1.66
Mount Charlotte	6Orogenic Au	173	7.2	2.24	2.99	914	256	0.64	0.51	20.4	936.08	1.44
Mount Charlotte	6Orogenic Au	82.1	4.18	2.39	0.68	591	202	0.41	0.36	18.25	410.9	12.65
Mount Charlotte	6Orogenic Au	75.6	3.92	2.42	0.81	576	181	0.38	0.33	18.02	358.79	13.45
Mount Charlotte	6Orogenic Au	26.2	3.63	2.05	0.08	542	69.5	0.36	0.32	18.73	140.91	35.29
Mount Charlotte	6Orogenic Au	55.5	3.87	2.26	0.72	555	135	0.36	0.34	18.71	267.78	16.67
Mount Pleasant	6Orogenic Au	265.9	10.7	2.05	4.57	1674	710	11.03	0.29	15.63	2059.6	1.04

Appendix 2.6B (continued)

Name	model 1	Na	Mg	Mn	As	Sr	Y	Nb	Mo	Pb	REE	EuA
Mount Pleasant	6Orogenic Au	280	8.3	3.04	4.74	1246	559	6.12	0.94	18.23	2100.1	0.92
Mount Pleasant	6Orogenic Au	242	12.2	4.34	4.3	1958	509	16.82	0.18	17.48	1852.6	0.94
Mount Pleasant	6Orogenic Au	135.3	4.67	1.61	2.26	1207	374.9	2.29	0.64	20.82	947.82	1.7
Mount Pleasant	6Orogenic Au	173	9.6	3.4	1.75	1208	748	1.66	0.48	19.76	982.87	5.57
Mount Pleasant	6Orogenic Au	361	5.99	2.96	3.07	1440	1090	16.8	0.46	27.3	1459.1	2.23
Mount Pleasant	6Orogenic Au	226	7.1	3.08	2.8	1241	812	7	0.51	21	1325.1	3.28
Mount Pleasant	6Orogenic Au	107	4.14	2.77	1.6	1299	707	1.78	0.58	23.3	1098.4	3.52
Nevoria	5Reduced skarn	4.2	2.5	6.04	3.52	83.5	4.95	31.6	11060	4.34	70.77	1.28
Nevoria	5Reduced skarn	6.1	2.35	6.2	3.05	134.1	8.84	21.83	10690	5.9	48.2	1.5
Nevoria	5Reduced skarn	6.3	2.35	6.26	3.37	106.4	6.06	25.49	10910	5.46	56.65	1.43
Nevoria	5Reduced skarn	44	5.83	6.6	2.33	212.4	12.5	12.05	14590	5.93	15.42	1.1
Nevoria	5Reduced skarn	19.1	6.1	10.9	3.58	243	16.9	12.5	14620	8.12	22.19	1.06
Nevoria	5Reduced skarn	15.6	4.71	6.15	0.85	172.7	4.71	6.74	14670	4.75	5.78	1.54
North Royal Norseman	6Orogenic Au	12	6.76	1.9	0.07	471	41	0.28	0.28	17.17	53.48	17.89
North Royal Norseman	6Orogenic Au	17	5.98	5.17	0.08	448	21.6	0.26	0.36	17.11	28.32	12.52
North Royal Norseman	6Orogenic Au	15.4	4.48	3.57	0.07	684	11.6	0.29	0.26	7.9	26.95	10.68
North Royal Norseman	6Orogenic Au	39	4.47	5.35	0.77	579	26.2	0.54	0.34	31.1	35.87	5.15
North Royal Norseman	6Orogenic Au	37	3.76	4.9	0.59	577	25.4	0.65	0.35	29.8	23.77	13.14
North Royal Norseman	6Orogenic Au	15.7	5.45	6.63	0.69	430	26.6	0.27	0.38	15.5	27.97	8.46
North Royal Norseman	6Orogenic Au	34.2	6.2	4.56	0.08	418	26.1	0.26	0.27	14.04	38.59	6.07
North Royal Norseman	6Orogenic Au	27.6	4.93	6.23	0.33	466	30.4	0.34	0.24	18.8	35.89	15.31
Nui Phao	5Reduced skarn	6.3	27.12	15.89	0.38	59.33	254.2	24.48	338.3	3.18	304.27	0.86
Nui Phao	5Reduced skarn	11.4	27.42	15.46	0.36	63.8	206	26.95	339	2.53	226.96	0.92
Nui Phao	5Reduced skarn	9.24	27.37	15.16	0.5	66.72	239.8	29.38	302.7	2.47	276.23	0.83
Nui Phao	5Reduced skarn	6.69	25.52	15.47	0.35	62.55	239.4	25.77	331.5	2.97	291.05	0.82
Nui Phao	5Reduced skarn	12.37	30.57	17.63	0.82	71.45	146.9	85.9	368.2	2.88	169.01	0.86
Nui Phao	5Reduced skarn	9.45	29.63	16.76	0.36	56.17	155.4	25.62	320.3	4	209.61	1.3

Appendix 2.6B (continued)

Name	model 1	Na	Mg	Mn	As	Sr	Y	Nb	Mo	Pb	REE	EuA
Nui Phao	5Reduced skarn	9.35	27.02	15.86	0.45	57.55	179.2	25.52	307.9	1.98	278.85	0.96
Nui Phao	5Reduced skarn	2.18	27.2	16.04	0.41	57.96	264.7	24.6	317.3	2	322.29	0.86
Nui Phao	5Reduced skarn	2.5	25.88	16.25	0.37	59.63	256.3	25.12	308.3	2.03	304.35	0.89
Nui Phao	3Quartz vein/Greisen	8.76	34.15	10.06	0.41	78.03	280	49.76	144	1.74	240.34	1.09
Nui Phao	3Quartz vein/Greisen	9.04	35.36	9.77	0.31	80.9	289.1	55.46	145.5	1.99	242.41	1.06
Nui Phao	3Quartz vein/Greisen	16.12	34.29	10.87	0.31	74.53	284.1	44.34	134.1	1.95	247.01	0.94
Nui Phao	3Quartz vein/Greisen	3.84	35.49	10.16	0.42	78.4	314.1	51.43	145.1	1.79	277.24	1.03
Nui Phao	3Quartz vein/Greisen	10.7	39.2	12.84	0.64	74.23	421.2	60.74	152.9	2.02	522.93	0.47
Nui Phao	3Quartz vein/Greisen	9.24	40.17	13.01	0.59	76.73	424	63.52	152.8	1.85	522.31	0.45
Nui Phao	3Quartz vein/Greisen	6.14	27.8	13.29	0.63	64.64	243	30.54	268.6	1.89	326.77	0.84
Nui Phao	3Quartz vein/Greisen	8.92	41.14	13.04	0.61	77.15	428.1	65.61	153.2	1.93	527.78	0.45
Nui Phao	3Quartz vein/Greisen	9.45	32.94	11.47	0.32	75.62	211.3	30.97	215.2	1.99	259.93	0.83
Nui Phao	3Quartz vein/Greisen	17.65	18	20.81	0.74	53.08	253	12.91	136.4	2.63	551.57	1.11
Ob?í d?l	4Oxidized skarn	113.98	3.06	3.21	16.37	47.68	485.1	544.9	5352	3.36	1290.6	0.11
Ob?í d?l	4Oxidized skarn	206.28	10.29	27.8	8.76	43.92	703.3	645	5046	5.43	1759.1	0.09
Ob?í d?l	4Oxidized skarn	290.65	2.79	8.58	14.79	40.57	1341	1005	5087	5.37	2140.5	0.07
Ob?í d?l	4Oxidized skarn	61.44	10.29	6.74	23.82	43.37	299.8	287	5213	1.85	670.46	0.12
Ob?í d?l	4Oxidized skarn	138.72	2.97	12.05	8.58	46.15	298.7	376.7	7089	3.75	1277.7	0.16
Ob?í d?l	4Oxidized skarn	305.8	2.18	22.8	10.54	42.4	1476	1168	4726	8.17	2231.9	0.05
Ob?í d?l	4Oxidized skarn	168.19	1.52	17.22	8.7	36.7	479.6	437.9	3975	6.88	1351.6	0.16
Ob?í d?l	4Oxidized skarn	174.72	2.84	13.48	10.7	35.45	715.9	588	3118	6.53	1345.5	0.12
Ob?í d?l	4Oxidized skarn	58.24	2.95	12.01	5.42	38.11	116.5	89.66	4990	8.44	438.45	0.24
Ob?í d?l	4Oxidized skarn	251.59	2.38	18.07	7.02	39.85	369.9	298.4	7728	47.26	1683.2	0.51
Ob?í d?l	4Oxidized skarn	124.13	5.56	10.36	4.04	38.77	150.8	153.2	7673	6.81	1117.8	0.82
Ob?í d?l	4Oxidized skarn	102.72	2.79	10.66	3.6	37.61	138.3	127.1	7437	7.13	888.47	0.85
Ob?í d?l	4Oxidized skarn	147.34	3.16	8.78	5.64	38.66	210.3	183.8	7367	6.19	1031.2	0.56
Ob?í d?l	4Oxidized skarn	131.36	0.03	16.54	12.62	42.94	245.3	236.3	7131	14.73	1070.9	0.38

Appendix 2.6B (continued)

Name	model 1	Na	Mg	Mn	As	Sr	Y	Nb	Mo	Pb	REE	EuA
Ob?í d?l	4Oxidized skarn	128.3	3.24	10.72	9.54	43.51	373.9	471.2	7270	8.76	1411.4	0.3
Ob?í d?l	4Oxidized skarn	76.59	3.02	11.36	4	47.4	80.34	78.54	8562	5.92	532.5	0.52
Ob?í d?l	4Oxidized skarn	55.04	2.89	8.6	7.26	40.52	94.8	110.8	8493	6.92	518.47	0.43
Ob?í d?l	4Oxidized skarn	65.33	8.2	12.37	17.35	45.04	92.16	146.5	7520	48.65	566.87	0.32
Ob?í d?l	4Oxidized skarn	91.6	7.09	11.12	5.71	42.4	154.9	171	7089	8.16	766.78	0.49
Ob?í d?l	4Oxidized skarn	73.39	11.12	9.23	5.03	53.38	154.7	131.8	6186	4.53	645.06	0.28
Ob?í d?l	4Oxidized skarn	59.77	4.67	18.97	54.91	31.26	52.4	74.23	7742	32.67	209.97	0.31
Ob?í d?l	4Oxidized skarn	47.26	3.22	14.73	30.58	29.41	25.19	56.85	18390	6.05	255.22	0.59
Ob?í d?l	4Oxidized skarn	51.43	2.49	25.02	22.1	32.53	48.65	56.3	6742	6.02	223.39	0.47
Ob?í d?l	4Oxidized skarn	39.62	72.98	87.99	18.43	41.14	181.3	341.9	10981	4.92	558.14	0.21
Ob?í d?l	4Oxidized skarn	184.87	4.11	45.87	27.66	37.53	95.49	97.86	10453	27.8	291.59	0.22
Ob?í d?l	4Oxidized skarn	33.22	3.42	7.23	20.52	36.49	78.95	96.74	9508	7.78	267.02	0.28
Ob?í d?l	4Oxidized skarn	50.04	2.82	16.4	14.34	32.54	3.54	47.54	23338	7.09	168.26	0.71
Ob?í d?l	4Oxidized skarn	34.06	3.04	6.55	15.79	44.62	47.4	49.21	22685	4.04	206.52	0.35
Ob?í d?l	4Oxidized skarn	64.64	7.51	14.18	3.6	39.48	158.3	123	515.7	5.12	510.13	0.13
Ob?í d?l	4Oxidized skarn	49.76	3.13	5.52	4.93	32.69	149.3	103.4	991.1	2.7	409.46	0.47
Ob?í d?l	4Oxidized skarn	72.28	3.09	5.71	3.38	30.51	140.4	25.99	692.2	3.06	399.4	0.55
Ob?í d?l	4Oxidized skarn	42.26	5.56	7.35	2.56	31.14	75.48	26.69	1097	3.67	273.19	0.36
Ob?í d?l	4Oxidized skarn	102.86	2.57	4.88	2.17	35.14	167.9	30.43	692.2	1.31	553.54	0.41
Ob?í d?l	4Oxidized skarn	24.74	3.45	3.02	19.54	49.62	0.5	32.96	18237	12.93	112.41	0.23
Ob?í d?l	4Oxidized skarn	22.24	2.68	3.04	26.37	47.12	0.38	17.88	23366	2.57	85.08	0.02
Ob?í d?l	4Oxidized skarn	4.1	1.9	2.49	18.29	66.03	0.29	24.92	27230	10.84	81.54	0.01
Ob?í d?l	4Oxidized skarn	5.98	1.83	3.56	64.36	47	0.31	2.73	24047	6.3	95.77	0.24
Ob?í d?l	4Oxidized skarn	17.93	4.17	4.06	69.36	71.17	0.35	3.99	29009	7.51	218.52	0.26
Ob?í d?l	4Oxidized skarn	17.79	3.43	3.93	50.74	65.47	0.12	4.57	28467	13.21	104.29	0.23
Ob?í d?l	4Oxidized skarn	117.59	7.7	38.09	10.04	67.14	64.08	57.27	1843	7.28	612.24	0.13
Ob?í d?l	4Oxidized skarn	62.55	4.21	17.24	13.21	52.26	181.7	163.9	727	4.42	477.5	0.11

Appendix 2.6B (continued)

Name	model 1	Na	Mg	Mn	As	Sr	Y	Nb	Mo	Pb	REE	EuA
Ob?í d?l	4Oxidized skarn	79.23	4.2	15.15	10.55	51.85	321	362.8	867.4	33.78	681.83	0.07
Ob?í d?l	4Oxidized skarn	55.18	3.66	8.66	6.56	48.79	63.25	29.34	854.9	29.19	318.71	0.15
Ob?í d?l	4Oxidized skarn	29.05	3.18	11.54	10.58	51.71	62.55	29.47	539.3	2.89	219.05	0.36
Ob?í d?l	4Oxidized skarn	111.2	3.42	10.52	8.23	44.48	269.1	235.6	5213	12.04	728.6	0.15
Ob?í d?l	4Oxidized skarn	95.91	3.16	8.52	8.55	44.2	343.9	293.6	522.6	3.68	800.08	0.08
Ob?í d?l	4Oxidized skarn	70.33	3.06	10.59	12.04	50.04	166.1	183.6	8062	8.13	640.49	0.19
Ob?í d?l	4Oxidized skarn	61.02	4.11	9.83	7.99	40.84	134.7	66.3	575.5	21.82	457.25	0.16
Ob?í d?l	4Oxidized skarn	181.4	3.71	12.9	10.24	38.92	326.7	344.7	4879	236.3	1442.8	0.19
Ob?í d?l	4Oxidized skarn	109.81	3.02	9.59	13.65	40.45	237.7	182	6950	3.43	561.73	0.21
Ob?í d?l	4Oxidized skarn	56.99	15.29	30.58	18.96	40.73	87.29	121.4	7506	2.97	292.89	0.25
Ob?í d?l	4Oxidized skarn	87.57	2.84	6.23	13.62	42.26	130.1	195.7	7784	3.46	486.62	0.32
Ob?í d?l	4Oxidized skarn	32.39	3.09	4.42	30.02	53.1	120.5	173.1	6908	2.24	384.7	0.17
Ob?í d?l	4Oxidized skarn	51.15	0.93	4.24	20.02	37.14	114.8	128.6	7131	2.64	410.17	0.33
Ob?í d?l	4Oxidized skarn	28.5	0.02	6.44	20.67	39.62	41.84	77.15	14164	2.68	235.17	0.29
Ob?í d?l	4Oxidized skarn	209.89	7.65	10.56	9.94	41.48	107.3	93.13	7659	4.82	338.92	0.29
Ob?í d?l	4Oxidized skarn	79.23	3.25	6.21	6.73	33.64	271.6	283.3	3595	3.74	619.97	0.18
Ob?í d?l	4Oxidized skarn	28.36	2.99	4.7	10.48	32.4	56.57	94.66	9341	2.65	241.71	0.35
Ob?í d?l	4Oxidized skarn	0.55	3.48	0.27	0.11	28.27	29.05	21.13	1763	1.23	49.68	0.21
Ob?í d?l	4Oxidized skarn	264.1	4.18	25.85	0.13	32.19	129.3	122.6	4087	6.17	362.94	0.26
Ob?í d?l	4Oxidized skarn	26.41	3.04	7.3	3.14	28.51	41.01	10.9	942.4	3.49	107.3	0.37
Ob?í d?l	4Oxidized skarn	33.08	2.93	6.48	4.74	22.87	53.1	31.28	2738	2.34	186.37	0.25
Ob?í d?l	4Oxidized skarn	27.66	2.78	12.37	4.43	23.19	47.82	22.38	2622	2.17	170.31	0.26
Ob?í d?l	4Oxidized skarn	65.33	2.95	19.46	2.07	22.78	53.38	15.73	825.7	2.44	152.77	0.2
Ob?í d?l	4Oxidized skarn	16.72	3.11	5.34	2.99	34.61	43.23	10.69	1230	2.96	101.42	0.42
Ob?í d?l	4Oxidized skarn	23.91	37.81	20.85	17.46	56.02	71.45	97.72	9577	3.98	274.32	0.28
Ob?í d?l	4Oxidized skarn	116.76	3.14	11.4	12.09	36.56	94.66	98.97	7617	6.81	341.27	0.3
Ob?í d?l	4Oxidized skarn	13.33	3.56	7.87	15.37	64.22	26.76	50.32	18904	2.97	166.45	0.32

Appendix 2.6B (continued)

Name	model 1	Na	Mg	Mn	As	Sr	Y	Nb	Mo	Pb	REE	EuA
Ob?í d?l	4Oxidized skarn	33.36	7.92	12.75	12.34	50.04	9.62	40.17	53932	4.63	134.76	0.42
Ob?í d?l	4Oxidized skarn	47.26	3.98	10.24	14.78	53.93	5.17	25.12	31581	10.15	123.31	0.48
Ob?í d?l	4Oxidized skarn	16.4	10.29	14.04	13.12	50.32	38.5	80.34	16847	7.23	206.68	0.46
Ob?í d?l	4Oxidized skarn	20.71	12.09	27.8	16.82	45.87	29.87	56.99	52403	8.2	208.4	0.56
Ob?í d?l	4Oxidized skarn	19.18	12.23	15.99	18.07	58.52	41.01	99.66	21031	3.31	293.36	0.28
Ob?í d?l	4Oxidized skarn	44.9	3.03	9.95	6.12	42.49	67	98.97	8132	4.67	468.1	0.68
Ob?í d?l	4Oxidized skarn	22.52	3.2	8.4	14.09	44.06	36.6	45.87	15429	13.54	183.56	0.33
Ob?í d?l	4Oxidized skarn	69.5	3.35	10.41	19.11	38.64	73.53	67.69	11231	10.17	411.3	0.46
Ob?í d?l	4Oxidized skarn	31.69	7.45	8.21	19.5	51.57	77.01	131.9	6867	4.02	378.64	0.25
Ob?í d?l	4Oxidized skarn	109.25	3.28	4.61	6.26	45.87	91.18	67.55	7214	12.73	782.59	0.46
Ob?í d?l	4Oxidized skarn	45.04	3.22	5.88	16.79	54.63	40.73	71.31	10050	20.71	275.68	0.23
Open Pit	5Reduced skarn	378.08	4.87	29.9	2.92	61.72	807.6	183.3	97.3	5.03	1491.3	0.14
Open Pit	5Reduced skarn	724.19	21.55	137.61	8.8	69.78	1441	949.4	94.94	5.63	3013	0.05
Open Pit	5Reduced skarn	661.64	3.09	37.25	7.53	63.66	982.7	440.2	112.6	5.21	3581.8	0.07
Open Pit	5Reduced skarn	641.21	4.32	37.03	6.28	61.86	1094	488.5	86.88	5.03	3127.2	0.09
Open Pit	5Reduced skarn	639.4	3.36	26.54	5.42	65.33	1607	661.6	71.31	5.31	2850.9	0.1
Open Pit	5Reduced skarn	701.95	4.02	41.01	4.91	69.36	1883	455.9	52.68	5.87	3111	0.22
Open Pit	5Reduced skarn	707.51	6.12	73.53	6.28	70.33	1979	314.1	30.71	9.44	4433.1	0.22
Open Pit	5Reduced skarn	542.1	3.42	44.2	5.17	69.5	1807	313.3	54.91	6.37	3639	0.17
Open Pit	5Reduced skarn	76.03	15.8	41.48	1.28	61.86	308	222.4	23.8	8.47	661.44	0.36
Open Pit	5Reduced skarn	194.6	5.09	44.76	1.61	63.11	503.2	295.2	61.58	5.69	905.74	0.09
Open Pit	5Reduced skarn	173.19	4.87	35.58	1.32	60.88	626.9	449	87.85	5.88	780.26	0.18
Open Pit	5Reduced skarn	166.8	70.89	40.59	0.63	46.57	111.1	83.54	61.86	4.82	175.56	1.61
Open Pit	5Reduced skarn	75.06	38.92	43.09	0.93	50.46	164.4	162.1	79.65	6.52	293.83	1.59
Open Pit	5Reduced skarn	110.09	5.27	39.09	1.22	62.97	304	186.7	90.63	5.92	460.15	0.23
Open Pit	5Reduced skarn	103.28	4.74	39.21	1.42	59.77	797.9	771.5	126.4	3.91	764.63	0.14
Open Pit	5Reduced skarn	50.32	59.77	37.67	0.81	55.73	233	176.1	201.3	3.02	316.51	0.35

Appendix 2.6B (continued)

Name	model 1	Na	Mg	Mn	As	Sr	Y	Nb	Mo	Pb	REE	EuA
Open Pit	5Reduced skarn	19.03	3.02	52.13	0.42	56.16	85.49	38.21	48.79	6.2	773.29	10.01
Open Pit	5Reduced skarn	49.48	7.83	13.01	0.5	27.93	137.8	21.68	138	3.35	185.38	1.21
Open Pit	5Reduced skarn	15.85	6.06	17.36	0.7	53.93	60.74	42.4	174.2	2.45	154.38	0.91
Open Pit	5Reduced skarn	74.78	8.05	43.23	0.77	64.84	114.8	58.52	47.51	5.47	624.22	3.29
Open Pit	5Reduced skarn	44.2	75.06	26.97	2.13	40.12	397.5	104	106.6	3.08	1927.8	0.74
Open Pit	5Reduced skarn	157.07	18.21	41.42	2.06	59.05	934.1	731.1	151.5	13.62	1195.6	0.17
Open Pit	5Reduced skarn	72.14	4.78	32.1	1.17	69.36	461.5	202.9	95.22	4.41	810.23	0.73
Open Pit	5Reduced skarn	119.12	12.79	29.2	1.46	69.88	358.6	112.2	112.5	4.46	699.5	0.79
Open Pit	5Reduced skarn	98	33.36	25.48	1	70.2	455.9	219.6	85.35	4.21	642.21	0.26
Open Pit	5Reduced skarn	146.65	3.37	43.53	1.41	68.26	599.1	240.5	57.82	5.06	1027.9	0.38
Open Pit	5Reduced skarn	50.6	4.35	29.51	1.16	70.89	625.5	174.2	70.75	4.21	725.82	0.37
Ovesná Lhota	3Quartz vein/Greisen	195.57	4.06	40.38	1.96	227.82	1081	67.69	1.61	10.56	1891.6	1.04
Ovesná Lhota	3Quartz vein/Greisen	198.77	4.55	31.53	1.07	261.6	615.8	50.18	1.77	11.69	1068.2	2.84
Ovesná Lhota	3Quartz vein/Greisen	96.19	4.31	39.06	0.64	215.59	298.7	25.41	1.72	10.59	499.23	5.89
Ovesná Lhota	3Quartz vein/Greisen	125.93	5.3	36.01	0.97	231.3	352.2	23.03	6.12	13.96	674.75	6.31
Ovesná Lhota	3Quartz vein/Greisen	120.37	4.32	46.43	0.6	252.98	353.2	22.11	1.71	10.76	688.4	4.04
Ovesná Lhota	3Quartz vein/Greisen	129.27	4.85	34.76	1.25	272.3	633.3	108.8	1.75	14.14	1029.9	2.52
Ovesná Lhota	3Quartz vein/Greisen	59.77	4.42	42.46	0.53	209.33	357	20.67	1.56	11.63	867.78	16.67
Ovesná Lhota	3Quartz vein/Greisen	237	4.84	33.3	1.49	258.96	797.9	67.42	1.52	11.76	1177	1.19
Ovesná Lhota	3Quartz vein/Greisen	97.3	4.7	37.88	0.58	239.64	294.7	30.09	1.77	8.67	491.62	2.98
Paddington	6Orogenic Au	244	59	5.1	5.1	584	442	0.46	0.4	18.3	919.37	3.04
Paddington	6Orogenic Au	176	56	4.55	5	548	358	0.41	0.44	19.79	799.64	3.88
Paddington	6Orogenic Au	116	41.7	3.6	4	594	307	0.56	0.39	21.42	717.41	2.85
Paddington	6Orogenic Au	66.1	8.13	1.75	1.45	661	238	0.35	0.17	19.75	463.93	6.45
Paddington	6Orogenic Au	176	23.8	3.14	3.16	530	429	0.51	0.22	16.02	910.38	2.57
Paddington	6Orogenic Au	119.8	14.2	1.3	2.35	493	308	0.58	0.14	15.35	781.66	2.66
Paddington	6Orogenic Au	42.8	10.9	1.26	1.15	412.9	207	0.34	0.32	18.82	480.02	10.38

Appendix 2.6B (continued)

Name	model 1	Na	Mg	Mn	As	Sr	Y	Nb	Mo	Pb	REE	EuA
Paddington	6Orogenic Au	132	10.6	1.07	2.21	605	322	0.52	0.23	13.73	706.16	3.88
Paddington	6Orogenic Au	94	14.6	1.29	1.92	472	275	0.45	0.26	16.49	643.96	4.43
Paddington	6Orogenic Au	66	14.6	2.25	1.22	420	192	0.28	0.22	19.5	416.09	6.95
Paddington	6Orogenic Au	54.2	12.3	1.26	1.12	415	272	0.31	0.38	20.3	590.53	9.37
Paddington	6Orogenic Au	120	16.8	0.24	2.42	584	451	0.53	0.28	16.7	837.7	3.02
Paddington	6Orogenic Au	71.5	14.7	1.56	1.53	449	291	0.33	0.29	19.09	593.75	6.13
Paddington	6Orogenic Au	56	5.5	1.66	0.94	1696	63.7	0.37	0.16	7.49	180.18	5.81
Paddington	6Orogenic Au	31	4.44	1.17	0.06	1575	24.4	0.3	0.04	7.05	105.74	9.48
Paddington	6Orogenic Au	19	3.74	1.74	0.07	1622	11.2	0.28	0.12	6.17	43.79	11.59
Paddington	6Orogenic Au	43.6	4.96	1.76	0.77	1633	39.4	0.33	0.12	7.05	125.69	6.84
Paddington	6Orogenic Au	35	4.13	3.02	0.08	468	18.9	0.28	0.34	21.4	30.75	5.49
Paddington	6Orogenic Au	28.6	3.68	2.76	0.08	469.7	32.9	0.3	0.45	22.09	56.12	6.92
Paddington	6Orogenic Au	46.8	3.39	2.99	0.08	522	115	0.31	0.46	24.52	189.66	9.06
Paddington	6Orogenic Au	17.8	3.57	2.54	0.07	465	12.87	0.32	0.57	23.3	22.81	6.57
Paddington	6Orogenic Au	246	7.1	2.48	0.08	505	15.3	0.31	0.61	25.7	26.68	10.54
Paddington	6Orogenic Au	20.2	3.69	3.4	0.07	504	17.6	0.28	0.54	22.95	31.2	8.89
Paddington	6Orogenic Au	33.5	3.31	2.63	0.71	484	15.73	0.23	0.51	23.9	23.58	13.73
Paddington	6Orogenic Au	75	4.42	2.89	0.07	493.7	15.72	0.27	0.5	23.83	25.87	12.34
Paddington	6Orogenic Au	65	5.03	2.83	2	1431	20.5	0.31	0.07	14.91	92.35	20
Paddington	6Orogenic Au	104	4.7	2.93	0.92	1150	58	0.3	0.06	19.3	120.2	7.02
Paddington	6Orogenic Au	93	4.92	3.44	2.2	890	136	0.34	0.09	26.4	333.56	2.12
Paddington	6Orogenic Au	71.9	5.14	2.94	1.49	1315	48	0.31	0.08	18.8	142.79	7.69
Paddington	6Orogenic Au	60	4.39	3.28	0.44	467.7	15.63	0.29	0.5	23.77	26.69	9.11
Pine Creek	5Reduced skarn	28.22	18.32	30.48	3.1	513.61	11.45	93.55	3864	13.14	183.3	1.71
Pine Creek	5Reduced skarn	5.6	20.43	26.47	11.12	486.92	7.03	65.68	3072	12.72	142.16	0.87
Pine Creek	5Reduced skarn	5.95	18.2	29.54	3.13	558.09	6.27	75.89	3442	9.2	169.48	1.09
Pine Creek	5Reduced skarn	6.35	37.53	34.47	18.07	519.3	6.39	73.81	3326	10.37	162.1	1.11

Appendix 2.6B (continued)

Name	model 1	Na	Mg	Mn	As	Sr	Y	Nb	Mo	Pb	REE	EuA
Pine Creek	5Reduced skarn	46.7	19.59	28.54	9.17	475.38	12.97	102.6	3204	9.66	184.53	1.4
Pine Creek	5Reduced skarn	6.24	17.26	27.83	4.31	547.66	6.82	87.71	4308	14.73	183.51	0.72
Pine Creek	5Reduced skarn	6.81	43.09	41.01	26.41	478.72	8.77	74.64	3283	15.29	154.29	0.81
Pine Creek	5Reduced skarn	5.96	53.38	52.68	2.78	440.35	8.44	73.39	3645	11.09	148.31	0.84
Pine Creek	5Reduced skarn	4.63	18.77	24.95	2.1	462.87	9.02	70.47	2788	10.73	142.39	0.91
Ray Gulch	5Reduced skarn	60.88	3.79	10.86	3.96	140.81	47.96	103.4	713.1	4.6	536.19	0.47
Ray Gulch	5Reduced skarn	73.25	3.98	16.3	1.88	106.34	42.21	112.2	679.7	10.45	628.82	0.5
Ray Gulch	5Reduced skarn	54.63	3.63	10.31	3.2	164.02	88.27	174.9	835.4	4.6	566.08	0.39
Ray Gulch	5Reduced skarn	52.96	3.64	13.32	3.16	122.32	77.15	128.6	852.1	5.94	493.89	0.32
Ray Gulch	5Reduced skarn	33.94	3.68	10.05	3.92	165.41	75.06	136.4	1061	4.06	372.59	0.26
Ray Gulch	5Reduced skarn	46.15	15.15	14.68	4.02	141.09	78.81	138.3	975.8	6	461.03	0.28
Ray Gulch	5Reduced skarn	39.62	47.96	23.49	3.67	148.59	68.11	150	961.9	5.3	435.33	0.33
Ray Gulch	5Reduced skarn	36.77	6.88	15.64	2.35	115.79	66.58	125.1	1280	5.39	388.68	0.3
Ray Gulch	5Reduced skarn	54.49	3.71	12.55	2.65	123.85	86.32	144.8	970.2	6.24	504.96	0.34
Salau	5Reduced skarn	38.92	4.71	52.82	2.59	34.49	307.8	97.16	19.85	4.45	1454	0.63
Salau	5Reduced skarn	44.48	4.14	45.45	0.85	40.59	87.71	45.45	29.47	4.31	731.37	4.98
Salau	5Reduced skarn	10.7	5	12.57	3.75	39.92	36.04	17.29	66.3	1.85	55.12	0.54
Salau	5Reduced skarn	10.41	3.74	11.16	0.89	34.11	67.83	35.45	81.45	1.22	49.59	0.83
Salau	5Reduced skarn	11.82	4.88	18.49	1.53	28.55	140.4	41.28	83.4	1.7	402.55	0.46
Salau	5Reduced skarn	40.31	4.48	14.04	2.5	35.01	182	113.3	85.76	1.21	145.06	0.76
Salau	5Reduced skarn	9.74	4.04	20.63	1.1	44.92	120.5	112.7	74.64	2.03	86.73	0.89
Salau	5Reduced skarn	13.97	3.59	16.47	0.25	35.89	80.34	41.13	82.15	1.72	57.71	0.79
Salau	5Reduced skarn	7.87	3.95	9.04	1.15	23.7	15.04	14.85	200.2	0.71	96.94	0.95
Salau	5Reduced skarn	9.12	4.36	6.41	1.43	23.63	18.72	9.47	199.1	0.71	103.14	0.71
Salau	5Reduced skarn	55.6	44.48	13.9	1.71	23.92	13.32	17.79	200.2	0.95	90.42	0.82
Salau	5Reduced skarn	20.85	3.98	5.78	1.46	29.16	7.01	16.4	180.4	0.67	96.15	0.97
Salau	5Reduced skarn	80.62	4.31	9.81	1.47	37.38	4.5	8.76	202.5	1.08	63.39	0.79

Appendix 2.6B (continued)

Name	model 1	Na	Mg	Mn	As	Sr	Y	Nb	Mo	Pb	REE	EuA
Scheelite Dome	1RIRGS	10.34	2.25	7.58	5.64	96.88	104.1	299.1	1560	5.1	440.3	0.51
Scheelite Dome	1RIRGS	11.82	2.29	6.27	3.71	101.89	116.1	131.2	1546	5.55	476.07	0.5
Scheelite Dome	1RIRGS	16.4	2.31	7.08	3.84	104.39	88.13	282.6	1475	5.32	496.93	0.72
Scheelite Dome	1RIRGS	7.09	7.81	7.2	2.45	98.41	69.36	329.2	1409	5.62	411.25	0.78
Scheelite Dome	1RIRGS	36.84	2.64	9.04	3.17	103	74.92	140.1	1461	4.82	347.82	0.77
Scheelite Dome	1RIRGS	27.66	2.34	7.98	3.25	100.91	72.28	131.9	1380	5.18	354.51	0.9
Scheelite Dome	1RIRGS	7.92	2.17	4.71	2.21	96.88	71.72	115.2	1434	5.12	398.44	0.89
Scheelite Dome	1RIRGS	5.18	2.54	11.68	6.03	64.91	492.1	19.68	107.3	2.38	272.41	0.89
Scheelite Dome	1RIRGS	51.57	3.1	11.43	4.91	56.3	1120	99.25	60.33	3.93	943.46	0.45
Scheelite Dome	1RIRGS	50.8	3.2	10.45	4.52	69.5	518.5	84.65	56.71	3.93	359.86	0.78
Scheelite Dome	1RIRGS	40.53	3.17	15.25	6.38	48.86	189.9	21.98	86.88	2.77	88.64	1.62
Scheelite Dome	1RIRGS	35.45	2.14	4.7	11.23	109.81	60.6	24.85	1601	5.12	284.2	0.67
Scheelite Dome	1RIRGS	38.92	2.4	7.85	3.48	135.53	77.7	153.7	1536	8.13	296.58	0.64
Scheelite Dome	1RIRGS	36.28	2.6	7.63	3.21	139.14	72	46.15	1603	7.88	252.74	1.18
Scheelite Dome	1RIRGS	107.03	2.54	6.85	2.63	123.99	59.91	43.81	1696	5.8	186.61	1.11
Scheelite Dome	1RIRGS	15.94	2.46	5.82	5.53	135.53	29.5	40.39	2027	5.38	160.29	1.5
Scheelite Dome	1RIRGS	40.59	2.29	9.58	4.42	159.99	120.4	212.3	1642	9.3	491.21	0.53
Scheelite Dome	1RIRGS	14.26	2.72	9.19	2.77	145.53	173.3	72.28	1653	8.48	704.47	0.51
Scheelite Dome	1RIRGS	30.3	2.39	7.6	3.73	108.56	59.63	31.44	1590	5.92	232.65	1.06
Scheelite Dome	1RIRGS	18.35	2.5	6.21	2.4	122.74	61.02	42.67	1715	6.31	179.73	1.35
Scheelite Dome	1RIRGS	40.59	2.49	7.13	6.35	116.9	83.54	51.79	892.4	5.13	306.58	0.65
Scheelite Dome	1RIRGS	61.02	2.21	6.81	3.32	137.19	113.8	58.94	1582	6.41	391.25	0.68
Shizhuyuan	4Oxidized skarn	33.36	38.73	20.85	5.21	56.16	0.64	52.96	25896	4.67	133.39	0.08
Shizhuyuan	4Oxidized skarn	35.58	25.02	12.51	6.12	42.81	1.3	28.91	19113	5.94	103.28	0.12
Shizhuyuan	4Oxidized skarn	76.45	35.03	12.7	12.89	43.37	2.75	53.1	32248	1.96	190.31	0.08
Shizhuyuan	4Oxidized skarn	8.34	28.65	16.96	14.82	77.42	1.04	42.53	26354	10.29	142.45	0.11
Shizhuyuan	4Oxidized skarn	14.46	32.35	18.99	6.23	51.15	0.44	32.18	37544	10.01	102.89	0.25

Appendix 2.6B (continued)

Name	model 1	Na	Mg	Mn	As	Sr	Y	Nb	Mo	Pb	REE	EuA
Shizhuyuan	4Oxidized skarn	11.82	65.19	20.99	23.77	58.94	1.21	33.42	44689	25.3	165.26	0.18
Shizhuyuan	4Oxidized skarn	5.28	8.2	1.2	0.72	32.22	0.64	1.63	1348	0.56	1.2	0.47
Shizhuyuan	4Oxidized skarn	8.62	7.31	0.44	0.48	35.71	1	1.51	1347	0.76	1.99	0.41
Shizhuyuan	4Oxidized skarn	15.29	5.6	1.65	8.62	31.15	0.04	9.81	1683	1.25	0.55	0.21
Shizhuyuan	4Oxidized skarn	2.22	5.46	2.64	0.89	20.22	0.06	1.69	1300	0.47	0.08	0.64
Shizhuyuan	4Oxidized skarn	29.19	4.45	4.68	9.37	50.46	0.05	3.77	42951	2.36	211.47	0.36
Shizhuyuan	4Oxidized skarn	72.28	10.29	5.39	9.24	55.74	0.12	6.09	39045	1.97	176.38	0.35
Shizhuyuan	4Oxidized skarn	108.98	13.34	4.48	11.09	110.23	70.61	29.5	28134	2.57	784.96	0.45
Sigma	6Orogenic Au	240.1	2.98	9.39	9.33	267	605	2.45	5.54	16.3	1023.5	4.29
Sigma	6Orogenic Au	101.7	4.76	3.25	6.64	266.1	521	2.24	5.07	31.8	649.02	5.1
Sigma	6Orogenic Au	172	7	6.25	8.45	265.6	630	2.4	5.22	24	1074.9	4.38
Sigma	6Orogenic Au	127.2	3.96	3.69	6.41	295.2	606	2.57	5.1	27.9	991.8	4.92
Sigma	6Orogenic Au	275	2.88	5.57	8.84	288	664	3.41	5.66	26.4	1235.4	3.21
Sigma	6Orogenic Au	157	3.93	3.98	7.05	293.4	636	2.68	5.29	26.68	1034.6	4.56
Sigma	6Orogenic Au	274	63	8.08	13.6	254.1	600	3.12	5.02	18.6	1123.4	2.95
Sigma	6Orogenic Au	115.8	6.96	4	11.42	255.4	624	3.86	4.83	71.2	1175.1	2.62
Sigma	6Orogenic Au	245.1	9.52	3.23	13.05	213	648	4.27	4.71	61.7	1352.7	2.54
Sigma	6Orogenic Au	184	8.24	3.72	11.86	233.6	608	3.87	4.81	65.1	1208.7	2.61
Sigma	6Orogenic Au	289.3	10.64	10.04	9.81	199.9	589.8	4.02	4.48	63	1153.1	2.44
Sigma	6Orogenic Au	105.6	15.6	2.92	10.71	211.1	660	4.63	4.88	77.6	1567.7	1.95
Sigma	6Orogenic Au	300	49.6	7.89	8.32	253.2	551	2.65	5.45	128.5	1019	3.46
Sigma	6Orogenic Au	151	21.5	5.25	11.3	247.9	646	4.02	5.21	103.8	1256	2.56
Sigma	6Orogenic Au	130.3	7.17	3.37	8.01	268.2	533	2.86	5.1	71.6	901.1	4.25
Tarmoola	6Orogenic Au	199	74	5.2	16.7	2286	149.2	1.03	4.7	99	481.01	6.87
Tarmoola	6Orogenic Au	228	64	1.6	14.3	2380	235	1.2	10	26.7	857.06	3.95
Tarmoola	6Orogenic Au	234	69	3.7	14.3	2120	214	1.38	8	34	673.43	3.4
Tarmoola	6Orogenic Au	121	47	7.6	6.6	2396	84.4	0.44	3.8	46.1	301.86	12.48

Appendix 2.6B (continued)

Name	model 1	Na	Mg	Mn	As	Sr	Y	Nb	Mo	Pb	REE	EuA
Tarmoola	6Orogenic Au	133	39	4.72	9.7	2410	110.5	0.66	2.46	57.4	366.21	7.1
Tarmoola	6Orogenic Au	213	49	4.03	7.8	2178	190	1	2.2	57	685.58	4.72
Tarmoola	6Orogenic Au	146	43.9	5.66	7.79	2349	116.3	0.63	2.95	49.7	412.62	7.6
Tarmoola	6Orogenic Au	109	19.5	3.36	5.7	2386	131	1.39	1.49	65	397.22	4.22
Tarmoola	6Orogenic Au	151	55	5.13	12.1	2250	114.5	1.02	2.15	66	386.69	6.28
Tarmoola	6Orogenic Au	113	24.5	5.85	6.3	2649	99	0.58	2.38	85	327.69	9.01
Tarmoola	6Orogenic Au	108	21.5	4.7	7.1	2485	122	0.88	2.35	84.9	395.98	5.4
Tarmoola	6Orogenic Au	156	23.8	4.01	10.6	2310	210	1.81	2.56	109	670.83	3.34
Trasevella	4Oxidized skarn	1.1	1.57	1.39	134.97	59.21	292	221	3621	0.76	501.11	0.5
Trasevella	4Oxidized skarn	4.82	2.24	1.49	274.94	59.77	462	292.3	3515	0.78	1059.7	0.3
Trasevella	4Oxidized skarn	7.92	1.72	1.43	281.48	82.29	442.3	258	4173	1.41	1079.2	0.25
Trasevella	4Oxidized skarn	3.75	2.36	1.45	186.54	62.41	250.9	185	4198	0.73	801.99	0.3
Trasevella	4Oxidized skarn	3.71	2.38	1.43	178.34	60.88	224.2	146.2	4265	0.67	720.89	0.31
Trasevella	4Oxidized skarn	3.78	1.81	1.45	204.89	60.6	292.3	140.4	4274	0.71	763.03	0.29
Trasevella	4Oxidized skarn	6.28	1.65	1.58	307.33	62.83	424.4	166	5121	0.79	1148.4	0.2
Trasevella	4Oxidized skarn	6.53	1.77	1.64	324.84	64.22	455.1	170.6	5281	0.76	1178.6	0.18
Trasevella	4Oxidized skarn	3.2	1.67	1.97	309.97	62.69	280.2	257.7	4937	0.87	1013.1	0.26
Trasevella	4Oxidized skarn	8.17	1.74	1.58	289.95	62.55	401.2	162.5	4676	0.74	1198.4	0.23
Trasevella	4Oxidized skarn	7.58	1.82	1.95	340.69	64.22	434.5	182.7	4814	0.79	1332.2	0.23
Trasevella	4Oxidized skarn	9.06	1.88	1.65	362.79	65.75	465.7	198.8	4657	0.85	1379.2	0.23
TSE	2Porphyry	89.66	102.72	18.29	3.91	82.84	357.2	617.2	403.1	2.99	1423.2	0.17
TSE	2Porphyry	112.59	103	18.9	23.63	87.29	394.8	640.8	338.1	3.53	1428.8	0.13
TSE	2Porphyry	145.39	128.58	19.53	4.07	73.95	446.2	679.7	357	4.2	1699.8	0.14
TSE	2Porphyry	98.27	181.26	15.68	40.31	59.49	359	558.8	435.1	2.28	1448.1	0.28
TSE	2Porphyry	137.05	139.97	12.57	3.42	57.69	511.5	592.1	524	2.45	1475.1	0.18
TSE	2Porphyry	64.5	79.79	20.89	3.74	114.4	415.6	617.2	376.7	4.34	1418.5	0.14
TSE	2Porphyry	85.62	88.96	16.43	3.81	88.68	341.4	454.1	338.1	2.27	1034	0.17

Appendix 2.6B (continued)

Name	model 1	Na	Mg	Mn	As	Sr	Y	Nb	Mo	Pb	REE	EuA
Vacíkov Petrá?kova hora	1RIRGS	113.42	3.21	7.8	9.33	145.67	59.35	39.53	1177	5.7	1196.6	0.07
Vacíkov Petrá?kova hora	1RIRGS	153.18	262.71	9.88	11.36	133.16	53.38	47.96	1697	5.64	1368.1	0.27
Vacíkov Petrá?kova hora	1RIRGS	53.65	84.79	8.35	19.82	176.95	38.85	24.84	1213	7.96	624.28	0.4
Vacíkov Petrá?kova hora	1RIRGS	137.61	2.36	8.15	8.05	150.82	33.86	37.95	1743	6.56	939.33	0.35
Vacíkov Petrá?kova hora	1RIRGS	129.13	0.4	7.34	10.84	143.31	42.4	40.45	1815	5.87	1163.3	0.31
Vacíkov Petrá?kova hora	1RIRGS	80.2	32.53	7.35	16.29	170.69	36.28	40.38	1820	7.24	783.94	0.36
Vacíkov Petrá?kova hora	1RIRGS	100.08	5.28	7.74	13.16	166.38	36.28	20.84	1036	6.55	1248.7	0.43
Vacíkov Petrá?kova hora	1RIRGS	71.03	0.02	6.39	20.74	172.92	37.85	32.25	2084	8.41	666.21	0.28
Vacíkov Petrá?kova hora	1RIRGS	134.41	2.84	7.83	12.93	155.82	87.85	56.99	2761	6.69	1192.3	0.17
Vacíkov Petrá?kova hora	1RIRGS	62.55	123.71	7.3	39.06	180.84	32.41	29.45	2698	8.13	612.72	0.28
Vacíkov Petrá?kova hora	1RIRGS	116.9	16.68	6.67	9.22	149.01	30.91	31.55	1947	7.2	934.54	0.45
Vostok-2	5Reduced skarn	22.1	5.52	40.34	0.93	22	76.45	66.03	126.6	3.29	223.32	0.9
Vostok-2	5Reduced skarn	9.24	7.65	34.78	1.04	17.29	37.95	28.36	101.8	3.17	133.56	4.06
Vostok-2	5Reduced skarn	10.7	3.95	16.35	1.28	12.22	131.6	76.03	209.8	2.07	171.3	0.77
Vostok-2	5Reduced skarn	9.59	4.31	50.6	1.7	24.13	31.14	68.39	103.3	4.34	70.15	3.75
Vostok-2	5Reduced skarn	28.63	4.71	30.72	1.39	21.39	107.5	86.6	176.5	2.63	271.83	0.2
Vostok-2	5Reduced skarn	30.86	4.04	19.79	1.69	63.25	472.6	56.16	88.4	2.46	624.85	0.99
Vostok-2	5Reduced skarn	19.22	4.41	27.79	1.13	52.96	162.9	34.9	70.33	2.4	827.72	2.55
Vostok-2	5Reduced skarn	38.92	3.94	23.92	1.92	30.55	567.1	58.38	77.7	2.64	744.89	0.69
Vostok-2	5Reduced skarn	37.95	4.66	26.35	1.15	44.87	119.4	30.91	63.52	2.5	577.16	2.58
Vostok-2	5Reduced skarn	4.18	3.54	10.2	1.35	17.92	135.1	21.66	168.1	2.04	155.02	0.69
Vostok-2	5Reduced skarn	5.74	7.09	11.8	2.18	17.88	90.91	29.75	171.8	1.21	179.49	0.78
Vostok-2	5Reduced skarn	4.59	3.45	12.91	0.73	18.95	95.91	14.9	136.1	1.76	83.55	0.87
Vostok-2	5Reduced skarn	48.93	3.68	35.72	1.85	50.32	382.3	48.79	6.52	6.42	792.17	0.57
Vostok-2	5Reduced skarn	4.84	4.3	12.55	0.67	19.92	35.31	15.75	102.9	1.97	31.32	1.83
Vostok-2	5Reduced skarn	21.82	291.9	63.94	1.03	25.52	129.6	35.17	77.56	2.22	124.84	0.64
Vostok-2	5Reduced skarn	11.68	111.2	28.63	0.53	21.35	49.21	14.05	107.7	1.89	48.25	1.38

Appendix 2.6B (continued)

Name	model 1	Na	Mg	Mn	As	Sr	Y	Nb	Mo	Pb	REE	EuA
Vostok-2	5Reduced skarn	24.6	3.29	24.46	1.06	27.94	437.9	68.67	14.73	3.13	413.94	0.37
Vostok-2	5Reduced skarn	12.23	4.64	14.83	0.95	22.91	162.6	21.82	132.8	2.1	166.05	0.63
Vostok-2	5Reduced skarn	10.54	102.86	19.74	0.93	21.13	152.9	19.32	138.3	1.88	100.58	0.84
Vostok-2	5Reduced skarn	7.35	8.76	16.54	1.15	23.16	76.17	19	115.2	2.29	58.63	1.08
Vrbík u Horaž?ovic	5Reduced skarn	12.51	0.05	4.3	2.06	53.52	2.59	23.89	1187	4.16	46.33	0.84
Vrbík u Horaž?ovic	5Reduced skarn	15.29	3.07	6.44	1.39	47.26	1.04	20.99	725.6	4.45	12.41	11.6
Vrbík u Horaž?ovic	5Reduced skarn	2.45	2.81	5.05	2.22	47.68	1.73	60.88	857.6	4.75	19.41	8.57
Vrbík u Horaž?ovic	5Reduced skarn	1.46	11.12	5.02	1.97	50.32	2.11	51.01	902.1	4.67	25.9	8.57
Vrbík u Horaž?ovic	5Reduced skarn	73.67	6.39	5.42	3.75	49.62	0.88	67.42	906.3	4.74	14.7	19.11
Vrbík u Horaž?ovic	5Reduced skarn	40.31	2.71	4.28	2.68	47.96	2.72	58.94	936.9	4.1	32.28	7.53
Vrbík u Horaž?ovic	5Reduced skarn	3.49	2.71	4.43	3.09	51.85	2.4	79.23	1047	3.63	29.27	10.65
Vrbík u Horaž?ovic	5Reduced skarn	19.46	13.07	11.33	0.62	82.71	2.34	24.21	526.8	6.99	45.98	25.39
Vrbík u Horaž?ovic	5Reduced skarn	15.01	1.36	9.35	0.27	73.11	1.26	7.39	717.2	6.73	10.21	20.58
Vrbík u Horaž?ovic	5Reduced skarn	4.73	22.24	8.16	1.03	55.46	4.1	25.99	714.5	5.46	43.03	15.09
Vrbík u Horaž?ovic	5Reduced skarn	1.33	2.38	5.55	0.96	41.56	1.1	36.28	839.6	4.3	12.08	14.34
Vrbík u Horaž?ovic	5Reduced skarn	5.14	36.14	7.65	0.71	46.15	1.43	12.3	939.6	3.64	18.33	5.6
Vykmanov u Ková?ské	4Oxidized skarn	21.13	94.52	5.07	0.86	124.82	3.61	1.38	1496	4.87	11.83	0.68
Vykmanov u Ková?ské	4Oxidized skarn	5	21.41	5.32	0.07	74.64	3.14	1.6	2446	7.31	9.08	0.66
Vykmanov u Ková?ské	4Oxidized skarn	69.5	59.77	4.6	0.7	107.31	2.68	1.86	1251	7.92	7.02	1.61
Vykmanov u Ková?ské	4Oxidized skarn	22.38	92.44	33.64	0.67	99.25	3.13	1.37	1553	9.33	7.47	0.69
Vykmanov u Ková?ské	4Oxidized skarn	26.55	24.33	4.03	0.56	137.33	2.99	1.44	2085	10.43	8.77	0.94
Vykmanov u Ková?ské	4Oxidized skarn	10.56	127.88	10.01	1.18	159.16	2.91	2.22	949.4	3.28	9.91	0.71
Vykmanov u Ková?ské	4Oxidized skarn	6.95	108.7	34.61	0.43	101.19	2.92	1.54	1237	17.38	7.54	0.9
Xiaoyao	4Oxidized skarn	27.38	7.78	3.28	11.54	47.58	0.12	1.54	62550	3.48	192.25	0.15
Xiaoyao	4Oxidized skarn	35.86	4.18	3.52	18.21	55.46	0.14	2.73	57894	3.98	174.58	0.28
Xiaoyao	4Oxidized skarn	39.34	3.31	3.63	10.9	55.99	0.3	12.57	55002	3.67	209.47	0.39
Xiaoyao	4Oxidized skarn	148.73	3.28	3.95	16.82	103.42	46.98	20.32	32262	2.84	543.28	1.35

Appendix 2.6B (continued)

Name	model 1	Na	Mg	Mn	As	Sr	Y	Nb	Mo	Pb	REE	EuA
Xiaoyao	4Oxidized skarn	98.69	3.7	6.67	35.72	130.24	60.88	29.34	17903	3.32	668.71	0.6
Xiaoyao	4Oxidized skarn	16.62	3.5	5.57	51.01	110.51	7.69	31.93	40588	2.85	297.09	0.75
Xiaoyao	4Oxidized skarn	24.6	3.52	3.98	9.04	61.86	0.2	12.89	40199	2.69	192.95	0.42
Xiaoyao	4Oxidized skarn	90.07	4.32	4.16	8.6	122.18	52.82	14.53	22476	4.49	592.26	0.94
Xiaoyao	4Oxidized skarn	66.58	3.21	3.29	34.06	125.1	37.67	15.39	18279	3.34	577.33	0.87
Young Davidson	6Orogenic Au	165	12.3	2.35	5.71	1828	295	0.45	47	152	561.86	1.24
Young Davidson	6Orogenic Au	310	11	4.3	7.41	2900	433	0.72	50	140	742.42	1.8
Young Davidson	6Orogenic Au	225	11.4	3	6.66	2080	328	0.49	65	158	675.61	1.42
Young Davidson	6Orogenic Au	168.5	7.3	1.42	10.4	3520	446	0.84	115	93.2	3672.8	1.48
Young Davidson	6Orogenic Au	218	6	1.07	7.46	3610	383	0.67	14.8	91	843.62	2.06
Young Davidson	6Orogenic Au	124	5.3	1.61	6.75	3330	402	0.78	11.3	77.9	833.26	1.97
Young Davidson	6Orogenic Au	166	8.9	1.47	8.65	3508	412	0.79	54	90.2	1916	1.72
Young Davidson	6Orogenic Au	210	13.7	1.99	7.61	3480	418	0.82	11.3	132.2	946.49	1.94
Zhuxi	5Reduced skarn	3.67	7.33	5.55	3.61	56.16	0.18	5.05	1151	1.58	0.92	1.88
Zhuxi	5Reduced skarn	12.51	19.46	5.07	0.11	55.88	0.23	7.13	1104	1.67	0.94	7.87
Zhuxi	5Reduced skarn	0.93	16.82	5.32	0.2	30.12	0.11	22.66	950.8	1.22	0.62	0.87
Zhuxi	5Reduced skarn	0.38	8.2	4.39	0.27	78.95	0.04	5.73	1015	2.5	0.25	0.53
Zhuxi	5Reduced skarn	18.49	13.18	6.03	1.95	57.82	1	47.82	1237	1.45	3.34	1.34
Zhuxi	5Reduced skarn	10.98	9.45	5.3	0.93	54.21	0.91	36.14	1125	1.51	1.88	1.35
Zhuxi	5Reduced skarn	17.79	11.86	6.49	1.93	58.66	1.16	52.13	1190	1.53	2.67	0.89
Zhuxi	5Reduced skarn	4.49	11.54	5.28	1.95	73.81	0.13	4.92	1005	2.5	0.54	1.31
Zhuxi	5Reduced skarn	20.85	9.73	5.74	1.35	55.16	0.37	8.88	1145	1.53	1.45	1.62
Zhuxi	5Reduced skarn	13.76	33.36	5.5	0.76	71.72	0.07	10.04	1130	1.47	0.21	1.62
Zhuxi	5Reduced skarn	1	12.23	7.65	0.24	43.76	0.24	11.88	393.4	2.45	4.09	19.61
Zhuxi	5Reduced skarn	7.37	13.51	9.99	0.4	31.01	0.37	8.45	621.3	2.05	7.96	9.19
Zhuxi	5Reduced skarn	1.67	16.93	20.29	1.26	46.44	0.42	26.55	613	2.39	6.52	10.48
Zhuxi	5Reduced skarn	3.13	23.63	16.26	0.39	30.77	0.57	9.31	495.5	2.46	11.18	15.54

Appendix 2.6B (continued)

Name	model 1	Na	Mg	Mn	As	Sr	Y	Nb	Mo	Pb	REE	EuA
Zhuxi	5Reduced skarn	1.32	10.15	5.23	0.46	41.07	0.18	3.98	847.9	1.77	1.34	18.68
Zhuxi	5Reduced skarn	11.12	19.35	14.87	0.29	42.35	0.55	10.65	448.4	1.97	11.56	15.48
Zhuxi	5Reduced skarn	6.39	31.23	67	0.49	42.52	0.36	12.3	615.8	2.72	7.2	9.51
Zinnwald	3Quartz vein/Greisen	37.95	3.06	1.43	0.31	1138.41	74.64	0.43	0.13	11.61	188.42	9.75
Zinnwald	3Quartz vein/Greisen	168.19	2.7	1.89	2.85	1252.39	354.5	1.63	0.1	14.98	977.51	1.3
Zinnwald	3Quartz vein/Greisen	90.63	2.59	3.36	0.64	1212.08	257.4	0.55	0.08	26.08	378.9	9.72
Zinnwald	3Quartz vein/Greisen	218.23	2.99	2.67	1.99	1245.44	448	1.93	0.1	20.81	925.97	1.76
Zinnwald	3Quartz vein/Greisen	166.8	2.64	1.36	1.86	1160.65	487.9	1.99	0.09	9.8	985.07	1.57
Zinnwald	3Quartz vein/Greisen	54.78	1.78	1.82	2.06	1380.27	383.1	2.96	0.12	11.27	1105.2	1.23
Zinnwald	3Quartz vein/Greisen	100.08	2.93	5.03	1.28	1232.93	204.3	0.98	0.07	38.39	464.63	2.68
Zinnwald	3Quartz vein/Greisen	140.39	1.79	1.65	1.92	1189.84	490.7	2.61	0.11	11.31	939.57	1.83
Zinnwald	3Quartz vein/Greisen	90.35	2.91	4.93	1.54	1301.04	299.4	1.11	0.09	42.1	577.81	2.81
Zinnwald	3Quartz vein/Greisen	99.8	2.52	4.71	1.07	1269.07	183.1	0.78	0.08	32	406.78	3.4
Zinnwald	3Quartz vein/Greisen	59.08	2.53	3.31	1.35	1167.6	143.2	1.24	0.13	34.37	408.12	2.03
Zinnwald	3Quartz vein/Greisen	78.95	2.13	1.53	1.86	1298.26	460.2	2.32	0.1	10.04	1085.6	1.54
Yangjiashan	3Quartz vein/Greisen	186	2.1	124	2.17	84.8	149	12.9	45.4	41.3	1172	1.1
Yangjiashan	3Quartz vein/Greisen	160	2.23	126	1.79	86.2	126	13	45.7	41.4	943	1
Yangjiashan	3Quartz vein/Greisen	180	2.7	115	1.88	116	183	11.8	41	46	1047	2.2
Yangjiashan	3Quartz vein/Greisen	163	2.36	124	1.73	102	219	19.5	44.5	44.6	938	1.6
Yangjiashan	3Quartz vein/Greisen	157	2.04	132	1.79	85.7	148	13.5	42.7	44.1	973	1.1
Yangjiashan	3Quartz vein/Greisen	66.3	7.82	39.3	2.79	61.9	958	296	11.8	36.2	858	0.9
Yangjiashan	3Quartz vein/Greisen	65.7	5.7	47.8	1.78	62.7	1064	152	15.3	35.4	1082	1.2
Yangjiashan	3Quartz vein/Greisen	72.8	5.01	47.9	1.74	60.2	1022	139	14.7	34.2	1061	0.9
Yangjiashan	3Quartz vein/Greisen	77.7	6.13	45.6	1.93	61.2	1091	148	14.7	34.8	1056	0.9
Yangjiashan	3Quartz vein/Greisen	107	4.53	47.5	1.71	62.7	1044	107	13.8	34.8	918	1.4
Yangjiashan	3Quartz vein/Greisen	112	6.88	42.1	2.88	65.6	984	174	13.9	32.9	927	0.8
Yangjiashan	3Quartz vein/Greisen	68.3	5.9	43.1	1.5	72.6	667	124	15.3	32.8	522	1.6

Appendix 2.6B (continued)

Name	model 1	Na	Mg	Mn	As	Sr	Y	Nb	Mo	Pb	REE	EuA
Yangjiashan	3Quartz vein/Greisen	56.1	5.59	48.7	1.59	59.5	1015	128	13.2	33.6	782	1.4
Yangjiashan	3Quartz vein/Greisen	45.2	13.3	40.5	2.15	61.3	1100	256	7.62	30.2	1047	0.8
Yangjiashan	3Quartz vein/Greisen	80.3	8.34	33.6	2.18	139	874	204	10.5	24.4	762	0.8
Yangjiashan	3Quartz vein/Greisen	76.9	8.2	47.4	2.38	57.6	1196	261	11.5	34.1	989	0.9
Yangjiashan	3Quartz vein/Greisen	73.4	5.46	43.1	1.5	59.8	926	126	14	31.2	696	1.4
Yangjiashan	3Quartz vein/Greisen	64.2	18.1	38.1	1.3	48.9	1072	212	6.99	33.9	689	0.5
Yangjiashan	3Quartz vein/Greisen	79	24.6	36.7	2.7	51.4	1201	604	8.18	31.9	725	0.2
Yangjiashan	3Quartz vein/Greisen	79.7	26.2	40.9	2.72	52.1	1160	493	10.1	33.7	656	0.3
Yangjiashan	3Quartz vein/Greisen	110	23.2	38.8	3.71	53.6	1380	732	12.1	37.4	818	0.2
Yangjiashan	3Quartz vein/Greisen	76.8	26.3	29.3	1.91	153	954	286	7.37	20.8	524	0.6
Yangjiashan	3Quartz vein/Greisen	60.2	21.9	32.5	3.42	59.5	1056	224	8.55	28.1	675	0.6
Yangjiashan	3Quartz vein/Greisen	76.4	24.5	39.1	3.18	62.1	1041	422	9.37	31.3	619	0.3
Yangjiashan	3Quartz vein/Greisen	62.8	26.6	38.4	1.73	51.4	1188	385	7.51	29.9	650	0.5
Yangjiashan	3Quartz vein/Greisen	72	25.4	39.2	2.38	56.2	1221	516	9.57	33.9	694	0.3
Yangjiashan	3Quartz vein/Greisen	55.6	18.2	30.6	1.57	53.8	1054	212	7.9	26.1	668	0.6
Yangjiashan	3Quartz vein/Greisen	51.4	23.3	26.1	3.61	73.9	1028	440	21.8	34.3	699	0.4
Yangjiashan	3Quartz vein/Greisen	47.8	51.9	30.4	2.02	59	1022	356	14.7	34.5	682	0.5
Yangjiashan	3Quartz vein/Greisen	38.9	27	24.7	1.97	59.6	794	200	13.8	29.5	565	0.8
Yangjiashan	3Quartz vein/Greisen	34.9	25.3	25.6	1.46	70	821	198	12.7	28.3	568	0.9
Yangjiashan	3Quartz vein/Greisen	95.1	9.27	56	1.69	63.8	457	150	19.5	40.9	919	0.9
Yangjiashan	3Quartz vein/Greisen	143	12.2	42.5	6.72	89.6	401	146	13	31	752	1.1
Yangjiashan	3Quartz vein/Greisen	66.7	15.9	38.8	1.79	81	263	92.9	11.7	28.3	612	1.3
Yangjiashan	3Quartz vein/Greisen	55.1	8.55	52.1	1.94	64.9	374	110	20.9	40.8	909	1.7
Yangjiashan	3Quartz vein/Greisen	133	13.3	40.2	5.94	106	368	125	13.5	28.3	659	1.2
Yangjiashan	3Quartz vein/Greisen	86.3	3.33	66.8	2.21	57.1	690	272	17.8	43	966	0.6
Yangjiashan	3Quartz vein/Greisen	109	4.78	63.8	2.49	57.1	802	271	16.7	46.3	980	0.6
Yangjiashan	3Quartz vein/Greisen	99.4	4.37	66.6	2.41	56.8	747	259	18.6	45.9	1027	0.7

Appendix 2.6B (continued)

Name	model 1	Na	Mg	Mn	As	Sr	Y	Nb	Mo	Pb	REE	EuA
Yangjiashan	3Quartz vein/Greisen	105	4.46	49.7	2.09	62.6	1028	76.8	13.3	39.5	1271	1.2
Yangjiashan	3Quartz vein/Greisen	104	5.69	42.3	2.19	63.8	931	92.5	12.2	34.5	1107	1.3
Yangjiashan	3Quartz vein/Greisen	94.4	6.12	43.9	1.62	68.5	694	125	11.5	36.6	747	1.5
Yangjiashan	3Quartz vein/Greisen	111	2.92	52.1	1.99	61.2	1028	130	13	35.2	1202	0.8
Yangjiashan	3Quartz vein/Greisen	95.8	5.07	53.2	2.06	64	1122	151	12.2	38.2	1490	0.8
Yangjiashan	3Quartz vein/Greisen	121	9.37	46.8	2.47	53.8	1349	110	15.3	38.7	1632	0.9
Yangjiashan	3Quartz vein/Greisen	86.3	5.03	52.3	2.97	74.8	1040	114	13.6	39.9	1436	0.9
Yangjiashan	3Quartz vein/Greisen	123	7.74	47.1	5.33	81.2	1027	113	14.5	42.2	1667	1
Yangjiashan	3Quartz vein/Greisen	84.9	9.8	54.1	1.32	81.7	580	206	24.2	49	609	0.9
Yangjiashan	3Quartz vein/Greisen	129	8.82	59.9	3.41	72.4	976	340	21.3	53	1335	0.2
Yangjiashan	3Quartz vein/Greisen	173	8.43	54.3	3.13	70.2	893	264	14.6	50.2	1172	0.3
Yangjiashan	3Quartz vein/Greisen	174	9.04	51.4	2.47	73.6	976	285	11.2	42.9	1182	0.2
Yangjiashan	3Quartz vein/Greisen	64.9	5.44	51.5	2	60.6	987	84.9	7.06	33	1383	1
Yangjiashan	3Quartz vein/Greisen	91	10.6	49.2	2.37	75.3	934	116	7.39	34.7	1356	1
Yangjiashan	3Quartz vein/Greisen	64.9	8.77	48.5	2.47	71.2	957	84	6.93	34.1	1476	0.9
Yangjiashan	3Quartz vein/Greisen	85.6	4.6	45.8	2.65	70.1	1060	62.5	8.35	32	1377	0.9
Yangjiashan	3Quartz vein/Greisen	77.8	5.96	47.4	2.44	68.2	1016	73.9	8.88	35.5	1428	0.9
Yangjiashan	3Quartz vein/Greisen	79.2	12.8	53.6	2.02	59.8	1033	233	8.48	35.9	998	0.4
Yangjiashan	3Quartz vein/Greisen	183	5.92	22.9	2.14	176	883	292	7.8	23.8	919	0.3
Yangjiashan	3Quartz vein/Greisen	120	5.6	60.7	2.47	63	1008	318	20	50.9	1325	0.2
Yangjiashan	3Quartz vein/Greisen	105	4.76	64.5	2.33	61.5	919	251	26.1	46.3	1146	0.2
Yangjiashan	3Quartz vein/Greisen	125	4.08	58.2	1.7	74.6	924	187	27.7	40.9	1113	0.5
Yangjiashan	3Quartz vein/Greisen	150	6.46	56.2	2.23	70.9	861	220	24.8	44.9	1058	0.3
Yangjiashan	3Quartz vein/Greisen	120	8.12	63.1	1.79	69.3	695	104	29.4	41.5	1079	0.4
Yangjiashan	3Quartz vein/Greisen	27.2	39.4	38.1	1.25	58.4	1046	135	9.69	25.1	608	0.9
Yangjiashan	3Quartz vein/Greisen	28.4	73.6	37.2	1.66	67.9	631	137	9.63	26.4	445	0.8
Yangjiashan	3Quartz vein/Greisen	45.6	35.1	35.8	1.45	53.7	1095	269	11.3	28	801	0.4

Appendix 2.6B (continued)

Name	model 1	Na	Mg	Mn	As	Sr	Y	Nb	Mo	Pb	REE	EuA
Yangjiashan	3Quartz vein/Greisen	55.1	36	33.8	1.42	53.6	1048	257	11.1	28.3	781	0.3
Yangjiashan	3Quartz vein/Greisen	65.6	32.1	35.2	6.46	54.6	1190	126	12.5	31.5	727	0.9
Yangjiashan	3Quartz vein/Greisen	64.6	32.1	33.9	1.3	60	698	91	9.87	24.3	474	1.2
Yangjiashan	3Quartz vein/Greisen	28.6	59.7	37.3	0.9	49.3	800	54.4	8.43	25.5	511	1.4
Yangjiashan	3Quartz vein/Greisen	52.2	32	33.1	3.72	57	804	80.5	8.18	22	417	1.8
Yangjiashan	3Quartz vein/Greisen	30.1	48.4	34.6	1.15	50	956	85.2	8.9	24.6	547	1.3
Yangjiashan	3Quartz vein/Greisen	117	51.6	34.2	2.51	67.8	917	77.6	8.09	22.1	431	3.4
Yangjiashan	3Quartz vein/Greisen	58	46.5	31.8	0.7	75.1	665	68.9	8.11	22	356	2.3
Yangjiashan	3Quartz vein/Greisen	49.4	37.9	35	0.77	51.6	771	60.4	7.5	24.3	390	2.1
Yangjiashan	3Quartz vein/Greisen	29.8	28.2	34.2	0.7	53.7	739	50.9	6.32	23.4	354	2.4
Yangjiashan	3Quartz vein/Greisen	138	25.6	26.1	2.59	70.1	945	179	9.34	22.6	484	1.7
Yangjiashan	3Quartz vein/Greisen	155	10.2	41.2	5.26	88.2	778	300	11.6	24.9	833	0.4
Yangjiashan	3Quartz vein/Greisen	92	23.7	11.7	1.15	76.1	316	34.8	5.24	15.2	481	0.8
Yangjiashan	3Quartz vein/Greisen	14.1	37	34.4	0.69	44.8	458	35.4	6.7	21.4	443	1.8
Yangjiashan	3Quartz vein/Greisen	39.1	53.7	40.5	1.57	53.5	1285	124	9.76	31.3	541	2.2
Yangjiashan	3Quartz vein/Greisen	17.3	50.5	37.8	0.63	48.8	967	74.3	8.46	27.8	510	1.5
Yangjiashan	3Quartz vein/Greisen	50.3	70.8	44.2	5.26	57.8	1370	409	10.4	37.7	574	2.2
Yangjiashan	3Quartz vein/Greisen	54.7	64.6	43.8	5.14	65.3	1104	373	11.2	44.3	488	2
Yangjiashan	3Quartz vein/Greisen	19.7	49.7	39	2.47	49.6	1002	77.5	8.85	27	538	1.4
Yangjiashan	3Quartz vein/Greisen	48.4	38	32	1.56	59.3	1189	121	11.8	27.1	687	1
Yangjiashan	3Quartz vein/Greisen	53.4	40.7	33.1	4.11	53	1337	131	13.5	22.4	756	0.7
Yangjiashan	3Quartz vein/Greisen	24.4	30.1	29.4	0.89	57.8	1101	89.6	9.17	23	524	1.7
Yangjiashan	3Quartz vein/Greisen	64.4	34.9	20.9	1.63	66.8	896	119	10.2	21	495	1.1
Yangjiashan	3Quartz vein/Greisen	42.3	47	36.8	1.38	48.8	1351	85.4	12.5	26.1	730	0.9
Yangjiashan	3Quartz vein/Greisen	41.3	52.4	41.3	2.06	50.8	1347	89.8	12.5	28.2	675	1.1
Yangjiashan	3Quartz vein/Greisen	48.4	41.4	39.7	1.36	56.1	1420	127	13.7	26.5	807	0.7
Yangjiashan	3Quartz vein/Greisen	45.2	48.5	37.7	1.67	52.4	1037	113	11.8	26	636	0.6

Appendix 2.6B (continued)

Name	model 1	Na	Mg	Mn	As	Sr	Y	Nb	Mo	Pb	REE	EuA
Yangjiashan	3Quartz vein/Greisen	78.8	39.6	31	1.94	59.2	897	155	10.3	24.7	637	0.7
Yangjiashan	3Quartz vein/Greisen	41.1	34.5	22.4	1.76	81.8	602	83	9.04	20.5	565	0.9
Yangjiashan	3Quartz vein/Greisen	51.9	35	18.1	3.33	96.4	525	63.1	8.99	19	489	1.1
Yangjiashan	3Quartz vein/Greisen	103	4.05	65.4	2.08	51.2	964	322	9.73	39.1	1032	1.1
Yangjiashan	3Quartz vein/Greisen	120	4.5	66.1	1.53	53.8	869	296	9.67	40.9	999	1.1
Yangjiashan	3Quartz vein/Greisen	146	4.94	63.5	2.06	77.1	892	315	9.52	39.4	1003	1.1
Yangjiashan	3Quartz vein/Greisen	82.1	5.9	70.4	1.69	68.2	900	256	8.84	37.3	1002	1.1
Yangjiashan	3Quartz vein/Greisen	80.9	4.69	74.8	1.94	55.8	921	256	9.53	39.2	1003	1.1
Yangjiashan	3Quartz vein/Greisen	80.2	5.65	79.8	1.96	47.8	1079	353	9.93	37.1	1079	0.9
Yangjiashan	3Quartz vein/Greisen	89.6	5.63	79.9	1.97	64.9	1051	371	9.2	38.2	1071	0.8
Yangjiashan	3Quartz vein/Greisen	77.2	5.09	73.3	2.08	50.3	1052	315	9.04	37.4	1117	0.8
Yangjiashan	3Quartz vein/Greisen	104	5.57	71.7	1.82	49.2	948	345	9.54	36.4	987	1.3
Yangjiashan	3Quartz vein/Greisen	98.9	5.82	73.2	1.91	54.9	953	384	9.33	36.2	1053	1
Yangjiashan	3Quartz vein/Greisen	133	4.05	60.3	2.33	78.6	927	353	7.84	34.6	903	0.7
Yangjiashan	3Quartz vein/Greisen	186	5.58	65.1	2.17	80.2	898	328	9.11	38.5	1013	1.1
Yangjiashan	3Quartz vein/Greisen	120	5.33	74.8	3.01	53.7	1251	561	10.7	43.1	1360	0.5
Yangjiashan	3Quartz vein/Greisen	152	4.74	67	2.66	91.7	1182	502	11	42.9	1303	0.5
Yangjiashan	3Quartz vein/Greisen	149	5.21	63.7	2.21	51	1146	415	11.1	38.5	1258	0.6
Yangjiashan	3Quartz vein/Greisen	109	4.73	81.6	2.44	69.1	1188	430	11.3	39.8	1225	0.6
Yangjiashan	3Quartz vein/Greisen	150	5.38	75.2	2.61	57.8	1225	561	11.4	39.2	1352	0.5
Yangjiashan	3Quartz vein/Greisen	78	5.54	68.6	2.08	55.4	899	449	8.84	40.4	1184	0.8
Yangjiashan	3Quartz vein/Greisen	74.6	5.69	73.5	1.63	48.2	803	272	7.77	38.6	996	1
Yangjiashan	3Quartz vein/Greisen	78.5	5.07	70.9	1.65	47	789	274	7.65	37.1	905	1
Yangjiashan	3Quartz vein/Greisen	98.3	5.3	64.3	2.05	47.9	859	314	8.53	37	1014	1
Yangjiashan	3Quartz vein/Greisen	90.6	4.56	66.9	2.13	49.8	895	397	8.69	38.1	1085	0.8
Yangjiashan	3Quartz vein/Greisen	86.7	5.22	64	1.76	56.5	855	407	16	39.7	1057	0.8
Yangjiashan	3Quartz vein/Greisen	78	4.83	64.8	1.51	66	870	426	8.66	41.5	1070	0.8

Appendix 2.6B (continued)

Name	model 1	Na	Mg	Mn	As	Sr	Y	Nb	Mo	Pb	REE	EuA
Yangjiashan	3Quartz vein/Greisen	76.2	6.99	71.3	2.63	52.3	864	381	8.28	35.2	1024	0.7
Yangjiashan	3Quartz vein/Greisen	77.3	5.67	72.4	1.8	48.2	830	339	8.45	37.6	959	0.8
Yangjiashan	3Quartz vein/Greisen	77.1	8.84	61.5	2.2	101	463	110	21.6	34.1	1292	1.7
Yangjiashan	3Quartz vein/Greisen	61.8	10	59.1	1.85	82.5	111	47.9	19.1	36.1	797	2.7
Yangjiashan	3Quartz vein/Greisen	50.2	6.29	71.4	1.93	83.4	180	73.3	26.5	40.7	1674	2.2
Yangjiashan	3Quartz vein/Greisen	29.1	5.47	72.4	1.01	84.1	81.9	45.7	33	49.1	886	8
Yangjiashan	3Quartz vein/Greisen	133	6.15	53.9	2.97	113	161	58.1	12.6	34.1	1029	3.1
Yangjiashan	3Quartz vein/Greisen	24.5	3.32	84.9	0.99	70.6	166	48	32.7	49.9	1125	10.2
Yangjiashan	3Quartz vein/Greisen	37.6	3.48	81.1	1.58	67.9	280	68.7	31.6	44.8	1656	5.8
Yangjiashan	3Quartz vein/Greisen	37.2	3	83.7	1.17	63.7	209	67.7	33.7	44.6	1286	8.6
Yangjiashan	3Quartz vein/Greisen	45.1	3.05	79.2	1.66	66.8	462	102	30.5	43	1605	4.7
Yangjiashan	3Quartz vein/Greisen	41	2.45	81	2.05	69.2	227	83.6	30.5	42.3	1762	2.6
Yangjiashan	3Quartz vein/Greisen	94.3	1.92	64	1.33	68.9	401	98.8	30.6	45.2	1185	4.8
Yangjiashan	3Quartz vein/Greisen	21.9	2.8	77.8	1.26	70.1	140	46.6	36	53.1	929	14.7
Yangjiashan	3Quartz vein/Greisen	43	2.09	81.4	1.63	68.1	275	84.1	32.3	44.3	1691	3.2
Yangjiashan	3Quartz vein/Greisen	35.4	2.2	75.3	1.73	76.9	167	55.8	30.5	47	1476	3
Yangjiashan	3Quartz vein/Greisen	25.9	2.69	74.2	0.88	79.4	93.4	38.3	32.4	53.2	867	7
Yangjiashan	3Quartz vein/Greisen	62	3.66	72.5	1.81	105	253	52.7	20.3	41.8	676	5.8
Yangjiashan	3Quartz vein/Greisen	9.5	5.29	92.2	0.74	100	114	26.1	20.4	46.7	756	10.6
Yangjiashan	3Quartz vein/Greisen	49.9	2.96	68.6	1.87	90.5	482	61.5	18.7	40.2	1028	2.6
Yangjiashan	3Quartz vein/Greisen	33.7	3.27	68.9	0.92	93.3	274	54	20.6	42.2	866	4.7
Yangjiashan	3Quartz vein/Greisen	63.9	3.06	90.5	1.26	95	555	77.1	26.3	37.1	982	2.4
Yangjiashan	3Quartz vein/Greisen	48.1	2.57	75.2	0.81	93.9	337	33.4	31.7	36.5	719	4.2
Yangjiashan	3Quartz vein/Greisen	57.7	2.36	71.7	2.11	101	460	61.8	29	41.3	1432	2.4
Yangjiashan	3Quartz vein/Greisen	56.3	2.43	69.8	2.02	93.4	404	64.1	26.9	43.3	1704	2.3
Yangjiashan	3Quartz vein/Greisen	57	4.02	77.6	3.94	101	389	62.7	33.4	42.5	1434	2
Yangjiashan	3Quartz vein/Greisen	85.2	4.82	62.9	1.42	135	251	40.4	18.2	35.4	773	4.1

Appendix 2.6B (continued)

Name	model 1	Na	Mg	Mn	As	Sr	Y	Nb	Mo	Pb	REE	EuA
Yangjiashan	3Quartz vein/Greisen	58.9	3.24	71.9	0.6	113	133	21.9	17.5	35.5	694	6.5
Yangjiashan	3Quartz vein/Greisen	68.2	3.21	73.3	1.49	110	624	87.8	16.9	37.9	1077	3.2
Yangjiashan	3Quartz vein/Greisen	56	4.68	84.9	1.22	111	93.6	11.4	20.2	37	464	8.9
Yangjiashan	3Quartz vein/Greisen	26.5	4.74	68.9	0.74	102	159	8.85	20.8	36.8	758	8.6
Yangjiashan	3Quartz vein/Greisen	38.4	3.55	72.9	0.98	90.2	195	31.2	18.2	34.8	1095	3.2
Yangjiashan	3Quartz vein/Greisen	57.6	6.13	87.6	3.77	145	371	56.6	16.9	36.8	1063	4.4
Yangjiashan	3Quartz vein/Greisen	75.3	4.51	78.1	2	118	584	83	17.1	35.8	1040	3.7
Yangjiashan	3Quartz vein/Greisen	85	4.04	78.8	2.1	107	493	90	15.6	34.2	1163	3
Yangjiashan	3Quartz vein/Greisen	84.1	3.45	64.8	2.46	112	653	110	24.7	34.7	1107	2.2
Yangjiashan	3Quartz vein/Greisen	32.9	3.11	81.3	1.26	88.2	449	57.4	17.9	36.6	1302	3.5
Yangjiashan	3Quartz vein/Greisen	52.3	2.85	77.6	1.44	87.6	675	80.1	16.3	34.7	1494	2.6
Yangjiashan	3Quartz vein/Greisen	67.7	3.89	58	1.29	156	512	79.5	11.4	28.8	1021	2.4
Yangjiashan	3Quartz vein/Greisen	41.9	2.19	69.1	1.1	96.5	557	50.4	21.1	46.1	487	10.1
Yangjiashan	3Quartz vein/Greisen	28.3	3.22	70.7	1.56	114	380	58.7	21.4	50.3	434	14.1
Yangjiashan	3Quartz vein/Greisen	44.7	4.98	52.8	1.81	193	209	23.6	19.9	38.1	219	13.4
Yangjiashan	3Quartz vein/Greisen	44	2.13	70.3	1.52	139	732	74.1	21.1	51.9	716	2.6
Yangjiashan	3Quartz vein/Greisen	74.4	17.5	27	7.2	45.1	546	213	7.66	27.9	526	0.3
Yangjiashan	3Quartz vein/Greisen	64	26.7	26.1	2.94	62.1	637	271	8.81	30	650	0.4
Yangjiashan	3Quartz vein/Greisen	38.7	22.9	29.4	2.51	55.2	364	113	4.33	13.6	368	0.6
Yangjiashan	3Quartz vein/Greisen	27.6	27.8	23.4	4.66	65.9	498	192	8.02	19.9	387	0.8
Yangjiashan	3Quartz vein/Greisen	47	19.1	22.7	3.03	56.6	503	169	5.36	16.7	464	0.5
Yangjiashan	3Quartz vein/Greisen	100	19.9	39.8	3.12	107	607	250	5.51	19.8	495	0.5
Yangjiashan	3Quartz vein/Greisen	76	23	28	2.35	53.2	900	244	6.78	26.4	695	0.6
Yangjiashan	3Quartz vein/Greisen	95	24.7	31.6	3.06	65.8	735	230	5.67	25.8	490	0.8
Yangjiashan	3Quartz vein/Greisen	300	25.9	29.1	2	82.7	693	164	5.88	22.2	410	2.9
Yangjiashan	3Quartz vein/Greisen	64	21.1	24.1	2.3	76.7	700	229	5.55	20.5	583	0.6
Yangjiashan	3Quartz vein/Greisen	78.5	20.5	28.6	3.04	61.4	756	234	6.3	25.5	615	0.6

Appendix 2.6B (continued)

Name	model 1	Na	Mg	Mn	As	Sr	Y	Nb	Mo	Pb	REE	EuA
Yangjiashan	3Quartz vein/Greisen	77	24.4	32	3.54	42.2	994	543	9.15	32.7	904	0.2
Yangjiashan	3Quartz vein/Greisen	24.3	27.4	26.2	3.23	72	698	165	6.97	21.5	382	3.3
Yangjiashan	3Quartz vein/Greisen	44.5	21.9	25.8	2.73	66.1	824	213	6.22	23.1	490	1.9
Yangjiashan	3Quartz vein/Greisen	37.9	21.4	28.1	2.17	63.7	779	206	6.73	24	462	1.8
Yangjiashan	3Quartz vein/Greisen	43.6	22.4	26.3	1.75	68.3	756	181	6.65	24.1	450	2.3
Yangjiashan	3Quartz vein/Greisen	50.9	19.5	28.6	2.04	53.9	788	236	7.18	27.8	624	0.6
Yangjiashan	3Quartz vein/Greisen	97.8	19.6	23.9	3.75	43.8	652	202	6.78	23.8	587	0.2
Yangjiashan	3Quartz vein/Greisen	48.6	22.8	27.4	2.12	51.1	622	280	7.04	25.6	551	0.4
Yangjiashan	3Quartz vein/Greisen	62.7	21.1	28.9	3.54	47.7	653	249	7.46	28.9	568	0.3
Yangjiashan	3Quartz vein/Greisen	45.8	22	23.2	3.59	58	591	251	7.03	20.7	510	0.5
Yangjiashan	3Quartz vein/Greisen	80	19.2	24.1	5.38	57.2	616	267	6.3	23.9	538	0.4
Yangjiashan	3Quartz vein/Greisen	26.3	26.8	23.3	2.47	56.7	263	82	5.72	16.7	265	0.6
Yangjiashan	3Quartz vein/Greisen	22.4	23.2	25.7	28	66.6	141	32.6	4.09	11.5	184	0.9
Yangjiashan	3Quartz vein/Greisen	31.1	20.8	25.7	1.83	50.5	213	46.5	4.88	15	205	0.7
Yangjiashan	3Quartz vein/Greisen	131	4.19	73.5	3.07	67.9	1238	412	22.9	52.6	1631	0.6
Yangjiashan	3Quartz vein/Greisen	130	3.65	67.4	3.07	70.8	1002	302	27	55.4	1564	0.9
Yangjiashan	3Quartz vein/Greisen	113	4.76	90.9	2.55	75.2	975	292	32.1	48.2	1746	1
Yangjiashan	3Quartz vein/Greisen	95.8	3.73	82.6	2.39	80.2	803	211	35.7	46.7	1586	1
Yangjiashan	3Quartz vein/Greisen	70.4	3.24	81.2	2.42	80.1	504	112	34.8	42.8	1801	1.5
Yangjiashan	3Quartz vein/Greisen	9.6	5.42	59.2	0.52	60.6	124	31.6	9.29	35.9	477	10.1
Yangjiashan	3Quartz vein/Greisen	30	8.63	52.8	0.61	46.4	69.4	32.5	18.6	39	174	10.3
Yangjiashan	3Quartz vein/Greisen	44.9	8.54	43.1	0.58	41.9	87.9	14.3	18.4	28.2	167	4.2
Yangjiashan	3Quartz vein/Greisen	78.1	5.58	49	2.86	63.5	913	273	12.2	43.3	947	1
Yangjiashan	3Quartz vein/Greisen	64.7	6.83	49.1	2.45	69.6	845	145	12.5	38.6	1009	0.9
Yangjiashan	3Quartz vein/Greisen	109	4.69	46.6	2.76	64.4	1023	195	11.8	35.9	1458	0.6
Yangjiashan	3Quartz vein/Greisen	114	5.07	46.7	2.98	118	962	310	26.2	35.1	829	1
Yangjiashan	3Quartz vein/Greisen	65.6	7.79	53.2	2.57	67.9	869	140	11.6	37.7	1124	0.9

Appendix 2.6B (continued)

Name	model 1	Na	Mg	Mn	As	Sr	Y	Nb	Mo	Pb	REE	EuA
Yangjiashan	3Quartz vein/Greisen	59.6	7.12	51.4	3.11	72.3	864	141	11.7	43.3	1179	0.8
Yangjiashan	3Quartz vein/Greisen	63.3	6.92	70.7	1.95	66.5	238	16.7	30.6	38.7	1546	1.1
Yangjiashan	3Quartz vein/Greisen	56.7	7.92	69.3	1.53	67.3	272	16.6	30.8	38.1	1339	1.8
Yangjiashan	3Quartz vein/Greisen	35.2	8.59	60.9	1.03	62.2	217	10.7	30	36.5	645	5.7
Yangjiashan	3Quartz vein/Greisen	250	28.5	24.1	0.55	97.3	217	38.3	3.93	12.6	336	0.7
Yangjiashan	3Quartz vein/Greisen	88.9	19.3	38.2	2.47	66.3	1077	312	11.1	32.4	951	0.4
Yangjiashan	3Quartz vein/Greisen	136	19.6	32.6	2.93	112	754	280	10	28.4	653	0.6
Yangjiashan	3Quartz vein/Greisen	160	8.83	44.8	3.45	102	919	209	11.5	40.9	928	0.3
Yangjiashan	3Quartz vein/Greisen	159	3.2	69.9	2.29	77.2	753	197	28.4	41.4	1337	1.5
Yangjiashan	3Quartz vein/Greisen	80.5	5.31	67.8	1.43	81.7	122	35.7	30.9	45.2	785	4.3
Yangjiashan	3Quartz vein/Greisen	75	3.9	76.1	1.88	79.6	196	82.7	32.7	42.1	1609	2.3
Yangjiashan	3Quartz vein/Greisen	81.1	4.57	66.2	2.57	76.4	210	82.7	22.5	38	1475	2.6
Yangjiashan	3Quartz vein/Greisen	87.4	5.07	57.3	1.77	116	99.2	34.9	27.7	40.7	823	6.4
Yangjiashan	3Quartz vein/Greisen	73.4	16.1	31.5	2.89	142	224	64.9	6.62	19.9	433	1.7
Yangjiashan	3Quartz vein/Greisen	58.7	21.2	22.9	1.94	179	129	31.2	4.93	13.6	279	1.2
Yangjiashan	3Quartz vein/Greisen	133	14.1	22.2	1.1	352	274	67.1	7.02	16.5	317	2.2
Yangjiashan	3Quartz vein/Greisen	89	23.9	36.3	2.95	86.4	174	49.7	7.32	23	503	1.2
Yangjiashan	3Quartz vein/Greisen	100	19.7	22.8	1.38	145	200	38.9	8.47	16.3	276	1.8
Yangjiashan	3Quartz vein/Greisen	48.1	5.98	41.5	2.03	67.3	355	81.3	9.55	25.2	592	2.5
Yangjiashan	3Quartz vein/Greisen	102	11.4	42.8	2.4	149	200	76.4	29.4	25.6	558	1.2
Yangjiashan	3Quartz vein/Greisen	152	10.8	28.5	1.37	123	386	116	16.8	31.1	696	2.1
Yangjiashan	3Quartz vein/Greisen	171	5.44	36	1.54	79.7	369	108	25.3	40.2	773	1.9
Yangjiashan	3Quartz vein/Greisen	13.2	22.8	27	0.54	155	113	52	3.13	12.5	217	1.1
Yangjiashan	3Quartz vein/Greisen	79.6	5.38	44.8	2.52	77.2	421	46.2	29	29.7	1178	0.7
Yangjiashan	3Quartz vein/Greisen	75	7.1	54.8	1.57	85.7	278	21.4	30.4	30.2	1243	0.8
Yangjiashan	3Quartz vein/Greisen	24.4	18.7	7.67	1.51	72.6	211	131	4.24	4.68	196	0.3
Yangjiashan	3Quartz vein/Greisen	29.8	17.6	6.86	1.14	107	161	79.7	3.78	4.45	183	0.3

Appendix 2.6B (continued)

Name	model 1	Na	Mg	Mn	As	Sr	Y	Nb	Mo	Pb	REE	EuA
Yangjiashan	3Quartz vein/Greisen	42.3	13.2	24.3	1.86	65.9	164	42.9	17.6	18.2	485	0.7
Yangjiashan	3Quartz vein/Greisen	19.2	15.5	10.3	0.82	45.5	123	49.9	3.9	5.03	179	0.3
Yangjiashan	3Quartz vein/Greisen	13.9	14	11.3	1.08	43.3	128	69.9	10.8	5.12	167	0.4
Yangjiashan	3Quartz vein/Greisen	42.3	10.1	28.3	1.07	100	226	56.6	22.9	20.8	318	0.9
Yangjiashan	3Quartz vein/Greisen	19.3	20.9	10.1	1.34	56	179	84.3	3.79	4.61	195	0.2
Yangjiashan	3Quartz vein/Greisen	22.4	19.4	8.44	1.4	85.5	177	86.9	6.89	5.15	201	0.2
Yangjiashan	3Quartz vein/Greisen	78	15.8	14.6	1.64	65.7	382	140	4.53	13.1	540	0.4
Yangjiashan	3Quartz vein/Greisen	140	13.7	26.7	3.06	81.3	690	107	7.75	23.1	1094	0.5
Yangjiashan	3Quartz vein/Greisen	79.6	12.2	21.9	1.87	51.1	588	153	5.44	18.6	720	0.5
Yangjiashan	3Quartz vein/Greisen	131	3.63	68.3	2.6	56.9	779	204	13.3	49.7	986	0.5
Yangjiashan	3Quartz vein/Greisen	174	6.02	65.5	3.07	55.9	730	206	12.8	44.3	921	0.5
Yangjiashan	3Quartz vein/Greisen	110	5.71	65.4	2.88	51.6	744	194	13	44.6	829	0.6
Yangjiashan	3Quartz vein/Greisen	121	5.07	65.8	2.08	55.7	722	187	13.4	46.1	771	0.7
Yangjiashan	3Quartz vein/Greisen	114	7	48.5	2.03	259	772	300	9.1	35.7	884	0.6
Yangjiashan	3Quartz vein/Greisen	143	5.32	63.1	2.27	68.6	770	220	13.4	47	898	0.6
Yangjiashan	3Quartz vein/Greisen	18.7	13.2	4.69	0.48	696	97.3	35.6	5.32	1.5	88.2	0.6
Yangjiashan	3Quartz vein/Greisen	64.1	10.1	14.6	1.47	495	237	108	26.4	11.3	415	0.8
Yangjiashan	3Quartz vein/Greisen	23.2	7.27	2.13	0.54	532	80.6	40.8	1.28	0.69	90.5	0.5
Yangjiashan	3Quartz vein/Greisen	56	16.1	4.58	0.62	711	44.3	3.71	3.75	0.48	51.2	2.1
Yangjiashan	3Quartz vein/Greisen	52	20.7	34.2	0.45	796	48.8	5.03	4.19	1.04	72.6	1.2
Yangjiashan	3Quartz vein/Greisen	33.8	24.1	22.7	1.32	184	91.7	18.8	4.18	7.98	214	0.9
Yangjiashan	3Quartz vein/Greisen	48.5	25.4	32.1	3.16	131	127	39.8	12.3	17.8	650	1.4
Yangjiashan	3Quartz vein/Greisen	70.5	18.9	21.7	1.28	182	100	28	9.72	16.2	580	1.6
Yangjiashan	3Quartz vein/Greisen	63.2	22.9	15.1	1.23	254	98.1	25.6	5.77	9.4	359	1
Yangjiashan	3Quartz vein/Greisen	10.3	19.7	11.4	0.63	78.4	77.6	10.5	2.76	3.58	149	0.5

Electronic Supplementary Materials associated with the chapter 3

Appendix 3.1A. Work flow diagram showing the sequence of data analysis procedures: compilation, preprocessing, RF model and predictions/results.

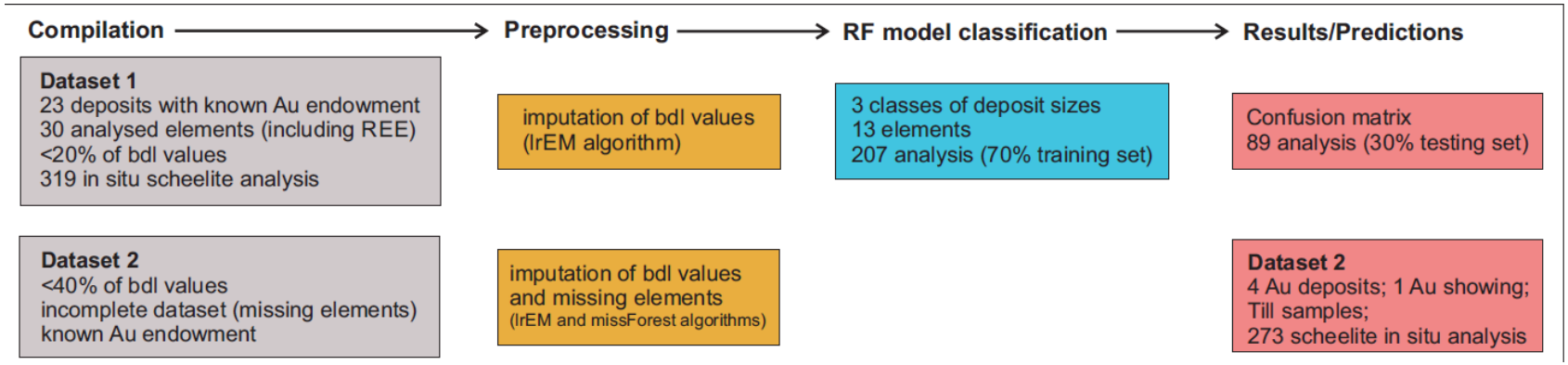

Appendix 3.1B. Scheelite composition used in the RF model (Dataset 1). Censored data already imputed.

Name	RF classification	Mg (ppm)	V (ppm)	Mn (ppm)	As (ppm)	Sr (ppm)	Y (ppm)	Nb (ppm)	Mo (ppm)	Ba (ppm)
Dome	>300t	5.17	0.01	1.36	8.77	923	585	6.56	3.98	0.96
Dome	>300t	6.3	0.065	3.6	9.52	928	710	6.44	3.67	1.36
Dome	>300t	14	0.071	2.41	8.92	1025	480	5.99	3.02	1.91
Dome	>300t	1.473	0.032	1.168	12.079	1029.99	690.83	5.296	3.197	0.136
Dome	>300t	1.779	0.02	1.974	9.702	1061.96	729.75	6.033	3.406	0.348
Dome	>300t	5.143	0.014	2.613	7.061	1074.47	621.33	4.782	1.446	0.917
Dome	>300t	1.918	0.014	1.988	8.896	1095.32	474.268	4.267	2.335	2.377
Dome	>300t	2.057	0.04	2.502	9.105	1035.55	473.712	5.463	3.1	1.223
Hollinger	>300t	530	0.157	922	0.077	148.4	2.57	0.001	0.047	0.24
Hollinger	>300t	368.2	0.093	935	0.072	98.3	5.38	0.001	0.037	0.46
Hollinger	>300t	197	0.008	1022	0.071	115.1	11.1	0.001	0.002	0.2

Appendix 3.1B. (continued)

Name	RF classification	Mg	V	Mn	As	Sr	Y	Nb	Mo	Ba
Young Davidson	100-300t	11	1.97	4.3	7.41	2900	433	0.72	50	1.6
Young Davidson	100-300t	11.4	2.26	3	6.66	2080	328	0.492	65	1.97
Young Davidson	100-300t	5.3	1.11	1.61	6.75	3330	402	0.78	11.3	0.21
Canadian Malartic	>300t	20.9	1.36	8.27	12.4	1980	144	3.96	914	1.41
Canadian Malartic	>300t	24.9	0.27	8.3	9.4	1656	34.2	1.49	1482	2.07
Canadian Malartic	>300t	36.8	0.348	9.51	28	1734	34.3	1.337	1408	2.9
Beaufor	<100t	4.63	0.74	2.81	11.9	563	483	6.92	61.1	0.26
Beaufor	<100t	5.8	0.7	3.6	9	493	327	4.62	63.1	0.41
Beaufor	<100t	3.39	0.64	2.89	7.4	541	419	4.11	65.6	0.21
Beaufor	<100t	3.36	0.7	3.31	7.7	589	471	4.86	67	0.47
Beaufor	<100t	4.08	0.55	2.97	11.3	574	238	3.7	209	0.35
Beaufor	<100t	8.2	0.62	3.7	7.66	579	393	4.5	61.7	0.48
Beaufor	<100t	3.33	0.7	3.78	6.4	560	418	4.84	68.3	0.138
Beaufor	<100t	4.32	0.621	3.42	7.4	561	394	4.36	79	0.289
Beaufor	<100t	4.45	0.219	2.88	3.17	667	853	7.84	16.9	0.109
Beaufor	<100t	4.28	0.217	3.36	6.8	660	780	7.27	25	0.27
Beaufor	<100t	4.55	0.201	2.99	4.3	672	842	7.81	19.8	0.145
Beaufor	<100t	4.95	0.096	4.15	2	651	267.5	3.95	18.99	0.265
Beaufor	<100t	4.44	0.254	3.86	2.74	635	576	7.14	17.2	0.28
Beaufor	<100t	4.95	0.223	3.46	3.06	658	657	7.97	17.87	0.166
Beaufor	<100t	6	0.248	3.07	5.9	654	492	7.05	19	0.4
Beaufor	<100t	5.81	0.281	2.9	4.33	656	589	7.47	19.5	0.4
Sigma-Lamaque	>300t	2.98	0.129	9.39	9.33	267	605	2.45	5.54	0.103
Sigma-Lamaque	>300t	4.76	0.119	3.25	6.64	266.1	521	2.24	5.07	0.177
Sigma-Lamaque	>300t	7	0.144	6.25	8.45	265.6	630	2.404	5.22	0.108
Sigma-Lamaque	>300t	3.96	0.105	3.69	6.41	295.2	606	2.57	5.1	0.034
Sigma-Lamaque	>300t	2.88	0.13	5.57	8.84	288	664	3.41	5.66	0.147
Sigma-Lamaque	>300t	3.93	0.119	3.98	7.05	293.4	636	2.68	5.29	0.084
Sigma-Lamaque	>300t	9.52	0.16	3.23	13.05	213	648	4.27	4.71	0.135
Sigma-Lamaque	>300t	8.24	0.131	3.72	11.86	233.6	608	3.87	4.81	0.141
Sigma-Lamaque	>300t	10.64	0.164	10.04	9.81	199.9	589.8	4.02	4.48	0.174
Sigma-Lamaque	>300t	15.6	0.176	2.92	10.71	211.1	660	4.63	4.88	0.152

Appendix 3.1B. (continued)

Name	RF classification	Mg	V	Mn	As	Sr	Y	Nb	Mo	Ba
Sigma-Lamaque	>300t	49.6	0.101	7.89	8.32	253.2	551	2.65	5.45	0.28
Sigma-Lamaque	>300t	7.17	0.129	3.37	8.01	268.2	533	2.855	5.1	0.124
Sigma-Lamaque	>300t	13.5	1.34	2.04	21.5	772	328	2.02	42.5	0.198
Sigma-Lamaque	>300t	23.9	1.487	2.38	35.1	788	504	2.188	42.1	0.34
Cuiaba	100-300t	7	0.065	5.03	0.85	833	54.9	0.262	0.088	0.265
Cuiaba	100-300t	13	0.075	7.2	1.09	832	42.7	0.246	0.094	0.348
Cuiaba	100-300t	4.43	0.005	15.4	0.08	764	44.1	0.264	0.039	0.42
Cuiaba	100-300t	17.3	0.095	18.9	2.33	728	138	0.274	0.072	0.57
Essakane	100-300t	15.2	0.057	7.3	18	2406	142	0.487	0.636	0.559
Essakane	100-300t	33	0.35	1.66	1.29	2154	145	0.302	0.374	0.165
Essakane	100-300t	17.8	0.105	5.82	1.4	2331	46.7	0.309	0.538	0.44
Essakane	100-300t	14.6	0.073	2.88	1.04	3152	66	0.262	0.141	0.55
Essakane	100-300t	4.39	0.007	3.14	0.79	2680	65.9	0.216	0.185	0.37
Essakane	100-300t	5.2	0.005	2.08	0.9	2990	54.2	0.19	0.117	0.95
Essakane	100-300t	8.1	0.006	2.24	1.8	2470	250	0.252	0.076	0.53
Essakane	100-300t	4.13	0.005	2.92	0.93	2860	242	0.29	0.22	0.61
Essakane	100-300t	5.14	0.006	2.94	0.98	2705	109	0.222	0.147	0.45
Essakane	100-300t	4.5	0.006	0.212	1.73	2650	207	0.31	0.31	0.35
Essakane	100-300t	7.2	0.006	0.99	1.5	2890	138	0.265	0.186	0.39
Essakane	100-300t	4.79	0.006	0.219	2.24	2330	305	0.44	0.166	0.27
Essakane	100-300t	9.1	0.006	2.87	0.44	2682	53.3	0.64	0.078	0.204
Essakane	100-300t	5	0.005	2.52	0.069	2830	87	0.363	0.077	0.075
Essakane	100-300t	6.85	0.006	2.42	0.068	2752	31	0.403	0.066	0.15
Hutti	100-300t	4.34	0.093	16.8	12.6	252	364	11.6	1.85	0.7
Hutti	100-300t	3.36	0.174	9.01	17.7	171	241	13.1	2.53	0.9
Hutti	100-300t	4.05	0.01	5.7	11.1	127	186	20.8	3.78	0.66
Hutti	100-300t	8.6	0.117	9.61	19.6	150	229	24.7	3	1.14
Hutti	100-300t	9.6	0.12	9	21	202	185	2.48	0.28	1.53
Hutti	100-300t	6.7	0.09	10.18	22.3	176.6	250	30	1.45	1.15
Hutti	100-300t	7.2	0.099	10.48	19.3	183.7	210.2	15.8	1.52	1.05
Hutti	100-300t	19	0.148	7.1	14.7	131	188	18.7	2.43	1.93
Hutti	100-300t	4.3	0.108	7.8	24.1	167	249	14.1	1.06	1.54

Appendix 3.1B. (continued)

Name	RF classification	Mg	V	Mn	As	Sr	Y	Nb	Mo	Ba
Hutti	100-300t	3.31	0.011	9.3	14	136	187	12.2	0.78	0.98
Hutti	100-300t	3.7	0.009	10.7	16.7	208	192.6	2.11	0.46	0.83
Hutti	100-300t	6.9	0.102	12.3	5.03	403	89.4	1	0.44	0.52
Hutti	100-300t	6.5	0.011	19.8	7.92	510	15.3	0.242	0.53	1.02
Hutti	100-300t	14.5	0.091	12.18	18.8	556	35.6	0.28	0.44	1.01
Kochkar	>300t	13.5	0.146	13.1	54	830	33.7	4.91	75.1	4.4
Kochkar	>300t	19	0.14	16.2	101	1115	52.1	6.13	65	3.4
Kochkar	>300t	5.94	0.127	10.98	21.1	667	23.3	4.31	80.7	0.7
Kochkar	>300t	6.78	0.29	7.16	21.3	820	14.2	9.8	97.7	1.7
Kochkar	>300t	4.89	0.2	6.32	138	771	23.2	6.38	84.4	1.26
Kochkar	>300t	10.2	0.311	11.1	34	900	29	6.7	82.2	56
Kochkar	>300t	127	0.118	3.6	4.87	1042	5.86	1.97	567	1.88
Kochkar	>300t	68	0.008	3.43	4.41	1057	5.67	1.99	516	1.24
Kochkar	>300t	4.9	0.085	2.34	7.1	1024	9.81	1.31	549	0.13
Kochkar	>300t	16.2	0.227	3.05	16	921	8.6	5.35	467	48
Kochkar	>300t	8.4	0.01	1.74	7.64	891	5.4	4.76	383	13
Kumtor	>300t	3.77	0.94	1.36	6.7	7300	13.2	0.38	196	0.35
Kumtor	>300t	5.4	0.64	2.14	10.3	2820	6.1	0.39	240	1.32
Kumtor	>300t	3.46	2.96	2.61	5.9	6340	2.14	0.385	195.6	1.21
Kumtor	>300t	4.31	1.66	2.66	9.4	5570	5.2	0.413	211	1.12
Marvel Loch	<100t	4.81	0.597	11.44	9.55	693	13.77	0.295	0.021	0.217
Marvel Loch	<100t	5.29	0.427	9.1	11.47	621	14.02	0.388	0.26	0.36
Marvel Loch	<100t	9.4	0.171	9.34	8.22	1084	11.11	0.519	3.1	0.56
Marvel Loch	<100t	8.3	0.309	9.61	9.8	1061	11.65	0.649	20.1	0.53
Marvel Loch	<100t	5.29	0.238	9	10.3	1053	13.06	1.19	92	0.41
Marvel Loch	<100t	4.65	0.22	8.1	9.2	1071	13.5	1.21	10.3	0.44
Edward's Find	<100t	6.5	0.963	4.5	8.37	734	25.64	0.337	0.049	1.8
Edward's Find	<100t	2.62	1.21	5.4	9	790	27	0.329	0.005	0.46
Edward's Find	<100t	2.33	1.03	6.13	8	712	29.9	0.305	0.004	0.64
Edward's Find	<100t	2.06	1.79	4.6	12.55	823	40	0.34	0.004	0.39
Edward's Find	<100t	2.25	4.54	5.69	13.45	680	50.8	0.262	0.004	0.24
Tarmoola	<100t	74	0.3	5.2	16.7	2286	149.2	1.034	4.7	1.74

Appendix 3.1B. (continued)

Name	RF classification	Mg	V	Mn	As	Sr	Y	Nb	Mo	Ba
Tarmoola	<100t	69	0.46	3.7	14.3	2120	214	1.38	8	1.11
Tarmoola	<100t	47	0.144	7.6	6.6	2396	84.4	0.443	3.8	1.22
Tarmoola	<100t	39	0.108	4.72	9.7	2410	110.5	0.66	2.46	1.87
Tarmoola	<100t	49	0.213	4.03	7.8	2178	190	1	2.2	0.99
Tarmoola	<100t	43.9	0.146	5.66	7.79	2349	116.3	0.632	2.95	1.29
Tarmoola	<100t	19.5	0.062	3.36	5.7	2386	131	1.39	1.49	1.43
Tarmoola	<100t	55	0.23	5.13	12.1	2250	114.5	1.02	2.15	1.54
Tarmoola	<100t	23.8	0.09	4.01	10.6	2310	210	1.81	2.56	2.91
Paddington	100-300t	59	0.129	5.1	5.1	584	442	0.459	0.4	1.87
Paddington	100-300t	56	0.136	4.55	5	548	358	0.41	0.437	1.97
Paddington	100-300t	8.13	0.007	1.75	1.45	661	238	0.349	0.166	0.65
Paddington	100-300t	14.2	0.009	1.3	2.35	493	308	0.583	0.135	0.22
Paddington	100-300t	10.9	0.008	1.26	1.15	412.9	207	0.336	0.32	0.269
Paddington	100-300t	10.6	0.008	1.07	2.21	605	322	0.518	0.23	0.52
Paddington	100-300t	14.6	0.009	1.29	1.92	472	275	0.445	0.26	0.322
Paddington	100-300t	12.3	0.054	1.26	1.12	415	272	0.305	0.38	0.219
Paddington	100-300t	16.8	0.009	0.238	2.42	584	451	0.529	0.28	0.14
Paddington	100-300t	14.7	0.049	1.56	1.53	449	291	0.33	0.293	0.187
Paddington	100-300t	5.5	0.049	1.66	0.94	1696	63.7	0.366	0.16	0.83
Paddington	100-300t	4.44	0.003	1.17	0.065	1575	24.4	0.296	0.041	0.23
Paddington	100-300t	4.13	0.007	3.02	0.077	468	18.9	0.28	0.344	0.41
Paddington	100-300t	3.68	0.007	2.76	0.079	469.7	32.9	0.303	0.446	0.5
Paddington	100-300t	3.39	0.007	2.99	0.085	522	115	0.307	0.46	1.26
Paddington	100-300t	3.69	0.007	3.4	0.073	504	17.6	0.283	0.54	0.38
Paddington	100-300t	3.31	0.009	2.63	0.71	484	15.73	0.234	0.51	0.42
Paddington	100-300t	5.03	0.008	2.83	2	1431	20.5	0.313	0.069	1.96
Paddington	100-300t	4.7	0.007	2.93	0.92	1150	58	0.3	0.058	0.69
Paddington	100-300t	4.92	0.008	3.44	2.2	890	136	0.338	0.092	1.92
Paddington	100-300t	5.14	0.007	2.94	1.49	1315	48	0.306	0.083	1.67
Paddington	100-300t	4.39	0.008	3.28	0.44	467.7	15.63	0.291	0.503	0.259
Mount Pleasant	100-300t	12.2	0.005	4.34	4.3	1958	509	16.82	0.177	0.77
Mount Pleasant	100-300t	9.6	0.045	3.4	1.75	1208	748	1.66	0.476	0.44

Appendix 3.1B. (continued)

Name	RF classification	Mg	V	Mn	As	Sr	Y	Nb	Mo	Ba
Mount Pleasant	100-300t	5.99	0.005	2.96	3.07	1440	1090	16.8	0.46	0.75
Mount Pleasant	100-300t	7.1	0.036	3.08	2.8	1241	812	7	0.513	0.62
Mount Pleasant	100-300t	4.14	0.005	2.77	1.6	1299	707	1.78	0.581	0.331
North Royal Norseman	<100t	6.76	0.005	1.9	0.075	471	41	0.284	0.276	0.332
North Royal Norseman	<100t	5.98	0.005	5.17	0.076	448	21.6	0.264	0.364	0.65
North Royal Norseman	<100t	4.48	0.005	3.57	0.075	684	11.6	0.287	0.255	0.44
North Royal Norseman	<100t	4.47	0.006	5.35	0.77	579	26.2	0.537	0.34	0.52
North Royal Norseman	<100t	5.45	0.006	6.63	0.69	430	26.6	0.274	0.376	0.55
North Royal Norseman	<100t	6.2	0.007	4.56	0.079	418	26.1	0.256	0.27	0.68
Crown Footwall Norseman	<100t	6.6	0.086	10.19	11.4	286.3	1510	359	0.79	0.139
Crown Footwall Norseman	<100t	3.77	0.01	14.33	8	320	1680	305	0.95	0.218
Crown Footwall Norseman	<100t	4.73	0.005	22.6	0.56	235	90.7	2.88	0.56	0.32
Crown Footwall Norseman	<100t	5.8	0.008	21.05	3.13	249.7	167	16.6	0.68	0.33
Crown Footwall Norseman	<100t	4.94	0.006	21.85	1.61	246.6	123	8.5	0.679	0.276
Crown Footwall Norseman	<100t	4.11	0.095	6.83	6.74	325	52.4	0.245	0.15	1.42
Crown Footwall Norseman	<100t	4.3	0.161	6.02	8.73	316	87.3	0.51	0.7	2.1
Mararoa Norseman	<100t	2.93	0.01	22.22	2.95	314.8	196.2	30.2	0.65	0.394
Mararoa Norseman	<100t	3.41	0.044	23.7	1.96	256	40.2	5.2	0.82	0.289
Mararoa Norseman	<100t	5	0.221	21.46	15.8	221	149	37.7	0.84	0.65
Mararoa Norseman	<100t	3.05	0.277	21.31	18.7	229.4	199	24.5	0.78	0.6
Mararoa Norseman	<100t	2.97	0.065	23.24	4.2	277	88.1	20.3	0.611	0.26
Mount Charlotte	100-300t	4.41	0.006	2.54	0.079	1160	52.4	0.264	0.79	0.35
Mount Charlotte	100-300t	5.92	0.007	2.09	0.083	1275	58.1	0.274	0.54	0.51
Mount Charlotte	100-300t	4.33	0.085	3.14	2.4	1067	393	0.674	0.307	0.58
Mount Charlotte	100-300t	4	0.112	2.76	2.12	1010	504	0.635	0.54	0.39
Mount Charlotte	100-300t	4.79	0.087	2.81	2.08	1031	391	0.614	0.365	0.74

Appendix 3.1B. (continued)

Name	RF classification	Mg	V	Mn	As	Sr	Y	Nb	Mo	Ba
Mount Charlotte	100-300t	6.1	0.126	2.49	3.56	883	470	0.488	0.297	0.58
Mount Charlotte	100-300t	6.4	0.109	2.1	3.9	1043	305	0.72	0.41	1.56
Mount Charlotte	100-300t	4.3	0.008	1.69	1.63	669	93.2	0.56	0.8	0.71
Mount Charlotte	100-300t	7.2	0.112	2.24	2.99	914	256	0.639	0.511	1.16
Mount Charlotte	100-300t	4.18	0.007	2.39	0.68	591	202	0.411	0.36	0.91
Mount Charlotte	100-300t	3.92	0.007	2.42	0.81	576	181	0.377	0.33	0.74
Mount Charlotte	100-300t	3.87	0.007	2.26	0.72	555	135	0.356	0.341	0.59
Macraes	>300t	277	2.01	4.39	63	5050	182	0.565	0.17	17.1
Macraes	>300t	16.2	0.006	7.6	2.2	6470	145	0.282	0.002	4.54
Macraes	>300t	15.4	0.005	5.88	0.98	6910	73	0.299	0.002	4.4
Macraes	>300t	37	0.2	5.8	4.1	6340	208	0.39	0.002	4.9
Macraes	>300t	13.9	0.005	1.82	2.22	3500	176	0.65	0.003	3.1
Macraes	>300t	12.1	0.053	4.31	0.8	6780	74.2	0.357	0.002	1.8
Macraes	>300t	15.9	0.044	6.19	1.56	6620	112.8	0.334	0.002	3.67
Macraes	>300t	17.5	0.005	6.01	1.12	7050	166	0.359	0.073	2.51
Macraes	>300t	19.7	0.007	5.8	1.87	6400	250	0.37	0.23	4.1
Macraes	>300t	18	0.006	5.27	1.37	5830	214	0.397	0.118	3
Macraes	>300t	19	0.006	5.51	1.6	6020	71.7	0.271	0.073	5.4
Macraes	>300t	32	0.009	5	10	4780	124	0.51	0.05	7.4
Amaruq	100-300t	8.5	0.014169	23.36	2.14	927	29.72	4.33	0.030625	1.01
Amaruq	100-300t	3.82	0.47	9.71	0.454331	4785	10.13	2.08	0.018671	0.51
Amaruq	100-300t	4.24	0.54	9.64	0.303309	3616.5	20.81	2.23	0.027064	2.21
Amaruq	100-300t	20.39	0.02145	39.41	2.38	736.63	29.31	2.32	0.022854	1.1
Amaruq	100-300t	200	0.11	8.9	4.84	1938	153.9	81.3	2430	1.49
Amaruq	100-300t	74	0.12	6.16	4.61	2590	97.6	59.9	1436.5	1.58
Amaruq	100-300t	61.5	0.11	15.09	4.02	2890.5	53.6	41	777.5	2.95
Amaruq	100-300t	72	0.16	12.69	3.3	3180	48.8	128	703	5.15
Amaruq	100-300t	1577.5	0.53	21.64	2.11	2990	73.45	41.15	658.5	5.72
Amaruq	100-300t	87.71	0.11	13.61	0.87	1036.14	34.5	2.25	31.4	1.3
Amaruq	100-300t	67	0.27	103	4.56	2950	89.7	61.1	26.8	4.9
Amaruq	100-300t	52	0.17	59.2	11.9	3760	146	44	15	2.31
Amaruq	100-300t	81	0.25	66	8.77	3340	128.3	28.5	12.8	3.12

Appendix 3.1B. (continued)

Name	RF classification	Mg	V	Mn	As	Sr	Y	Nb	Mo	Ba
Amaruq	100-300t	6.6	0.026568	14.23	0.81	708.33	61.93	2.17	10.06	4.62
Amaruq	100-300t	5.51	0.37	10.91	4.87	517.9	393	17.9	5.73	1.78
Amaruq	100-300t	100	0.14	81.4	8.24	3160	150.5	33.7	5.28	3.28
Amaruq	100-300t	29	0.93	12.18	3.68	549	690	16.5	4.94	0.62
Amaruq	100-300t	3.5	0.67	7.99	3.32	700	645	6.57	3.75	0.27
Amaruq	100-300t	10.8	0.17	15.62	2.47	1324.9	629.3	5.64	3.31	0.41
Amaruq	100-300t	32.3	0.41	21.25	3.9	996	353.5	8.97	3.07	1.47
Amaruq	100-300t	3.86	0.09	11.44	1.94	1380.75	409.25	4.45	3.02	0.33
Amaruq	100-300t	14.4	0.19	14.02	2.94	997	215	6.3	2.96	1.57
Amaruq	100-300t	17.4	0.46	8.2	3.24	1223	485	2.94	2.92	0.62
Amaruq	100-300t	18.88	0.48	42.57	4.58	841.4	325.2	10.68	2.66	2.08
Amaruq	100-300t	5.94	0.14	11.04	3.03	1407.2	526.2	3.33	2.59	0.29
Amaruq	100-300t	3.23	0.08	11.91	1.38	1400	435	2.58	2.58	0.14
Amaruq	100-300t	3.31	0.14	11.11	2.06	1385.43	561	2.92	2.51	0.010567
Amaruq	100-300t	4.09	0.25	13.42	4.89	1317	916	5.64	2.49	0.19
Amaruq	100-300t	107.33	0.53	16.33	2.64	1404.33	858	3.54	2.45	1.02
Amaruq	100-300t	121	0.64	143	4.51	986	879	7.7	2.42	0.54
Amaruq	100-300t	0.040066	0.012719	11.19	0.33	609.85	39.6	1.98	2.1	2.27
Amaruq	100-300t	6.17	0.04	9.37	0.53	1310.5	219.85	1.89	2.04	0.13
Amaruq	100-300t	9.92	0.045432	7.93	0.8	1278.67	168.73	2.09	1.88	0.5
Amaruq	100-300t	8.65	0.21	19.02	3.71	909.5	271	4.15	1.79	1.97
Amaruq	100-300t	3.29	1.01	7.63	1.37	1274.5	18.45	2.34	1.65	2.32
Amaruq	100-300t	145.85	0.44	1343.9	6.65	5370	89.55	167.15	1.27	1.75
Amaruq	100-300t	283.75	1.32	46.28	3.44	573.75	35.35	2.44	1.24	2.98
Amaruq	100-300t	3.39	0.4	8.34	2.62	1606	75.75	3.42	1.03	3.78
Amaruq	100-300t	4.92	0.01542	15.34	2.73	2402	35.96	2.69	0.33	0.44
Amaruq	100-300t	8.5	0.15	11.3	1.28	3870	24.4	2.23	0.03	4.49

Appendix 3.1B (continued)

Name	Pb (ppm)	U (ppm)	REE (ppm)	EuA (ppm)
Dome	28.8	0.02	1417.08	1.707
Dome	31.06	0.011	1449.7	1.639
Dome	24.6	0.007	1124.13	1.224
Dome	25.437	0.009	1977.748	1.343
Dome	25.937	0.01	1292.09	1.555
Dome	23.199	0.008	1371.053	1.488
Dome	18.126	0.005	997.2277	1.009
Dome	25.493	0.01	899.2132	0.975
Hollinger	1.43	0.001	5.8801	2.600
Hollinger	1.22	0.001	16.589	2.065
Hollinger	0.89	0.001	8.4116	3.074
Young Davidson	140	0.022	742.42	1.802
Young Davidson	158	0.05	675.61	1.417
Young Davidson	77.9	1.3	833.263	1.965
Canadian Malartic	40.5	0.004	412.99	0.655
Canadian Malartic	36.4	0.137	195.037	1.056
Canadian Malartic	38.3	0.016	196.0399	0.962
Beaufor	5.69	0.014	689.831	0.697
Beaufor	5.31	0.015	500.063	0.719
Beaufor	11.6	0.002	720.97	0.765
Beaufor	7.6	0.006	765.177	0.753
Beaufor	9.6	0.007	412.349	0.633
Beaufor	6.74	0.004	645.74	0.762
Beaufor	8.55	0.003	766.2	0.718
Beaufor	8.28	0.005	665.819	0.730
Beaufor	16	0.011	2025.85	0.534
Beaufor	7.31	0.024	3559.29	0.545
Beaufor	34	0.014	2492.91	0.542
Beaufor	23	0.006	688.513	0.656
Beaufor	12.11	0.007	1531.88	0.551
Beaufor	16.5	0.01	1735.79	0.531
Beaufor	18.6	0.008	1344	0.518
Beaufor	31	0.015	1501.41	0.544
Sigma-Lamaque	16.3	0.005	1023.523	4.288
Sigma-Lamaque	31.8	0.005	649.02	5.096
Sigma-Lamaque	24	0.006	1074.92	4.378
Sigma-Lamaque	27.9	0.007	991.8	4.922
Sigma-Lamaque	26.4	0.002	1235.44	3.214
Sigma-Lamaque	26.68	0.006	1034.6	4.563
Sigma-Lamaque	61.7	0.005	1352.72	2.543
Sigma-Lamaque	65.1	0.005	1208.72	2.611
Sigma-Lamaque	63	0.004	1153.084	2.439
Sigma-Lamaque	77.6	0.005	1567.65	1.954
Sigma-Lamaque	128.5	0.008	1019.04	3.463
Sigma-Lamaque	71.6	0.008	901.1	4.245
Sigma-Lamaque	155	0.026	1259.06	0.828

Appendix 3.1B (continued)

Name	Pb (ppm)	U (ppm)	REE (ppm)	EuA (ppm)
Sigma-Lamaque	168	0.13	1728.38	0.714
Cuiaba	24.82	4.55	108.161	24.958
Cuiaba	27.85	4.31	76.885	23.883
Cuiaba	31.5	3.32	104.996	13.130
Cuiaba	38.9	2.32	256.11	6.963
Essakane	57.1	4.84	344.45	3.392
Essakane	43.1	0.84	429.25	6.509
Essakane	48.9	4.36	139.258	35.251
Essakane	49.1	12.38	145.447	8.203
Essakane	37	4.5	128.953	13.052
Essakane	41.2	10.7	114.18	11.872
Essakane	32	5.9	429.51	6.461
Essakane	35.1	6.9	383.55	13.669
Essakane	36.9	6.2	195.56	10.256
Essakane	36.1	8.7	322.18	8.072
Essakane	40.6	9	251.53	7.035
Essakane	29.1	1.8	506.25	4.118
Essakane	38	6.03	141.576	16.328
Essakane	47.5	6.72	219.97	11.368
Essakane	44.8	7.32	87.898	17.105
Hutti	6.16	0.95	375.01	2.612
Hutti	4.14	0.109	188.24	1.749
Hutti	2.88	0.6	147.26	1.921
Hutti	4.02	1.8	194.41	1.164
Hutti	4.52	4.3	142.55	1.564
Hutti	4.42	1.03	196.34	1.173
Hutti	4.46	3.4	176.036	1.365
Hutti	8.8	0.39	150.581	0.946
Hutti	4	0.102	197.06	1.054
Hutti	2.9	0.97	166.83	1.136
Hutti	4.94	5.3	181.104	2.053
Hutti	10.1	8	98.076	3.348
Hutti	20.3	0.5	27.52	8.704
Hutti	21.3	0.73	48.716	5.354
Kochkar	23.1	0.135	421.773	2.628
Kochkar	31.1	0.112	489.152	2.122
Kochkar	18.4	0.152	384.964	2.928
Kochkar	18.2	0.232	292.998	10.693
Kochkar	18.5	0.045	289.224	2.415
Kochkar	22.5	0.328	381.043	4.670
Kochkar	36.3	7.3	26.5683	10.266
Kochkar	35	3.62	20.7652	10.846
Kochkar	30.2	5.64	54.789	5.245
Kochkar	34.12	1.77	51.9679	3.239
Kochkar	33.9	0.632	31.2099	2.671
Kumtor	86	7.2	78.3886	0.837

Appendix 3.1B (continued)

Name	Pb (ppm)	U (ppm)	REE (ppm)	EuA (ppm)
Kumtor	25	3.09	180.4493	0.683
Kumtor	94.7	2.4	14.204	0.759
Kumtor	76.4	3.68	71.6565	0.944
Marvel Loch	18.87	0.22	51.1903	15.779
Marvel Loch	18.63	0.015	54.6348	11.307
Marvel Loch	23.94	0.002	48.205	2.311
Marvel Loch	25.5	0.001	53.931	1.885
Marvel Loch	23.4	0.003	55.955	1.338
Marvel Loch	21.5	0.006	52.731	2.046
Edward's Find	8.69	0.011	49.6829	4.291
Edward's Find	8.67	0.008	50.986	4.200
Edward's Find	10.4	0.007	58.964	3.721
Edward's Find	6.89	0.003	64.184	3.863
Edward's Find	2.39	0.006	89.119	3.606
Tarmoola	99	1.99	481.012	6.872
Tarmoola	34	0.124	673.434	3.396
Tarmoola	46.1	1.92	301.862	12.476
Tarmoola	57.4	0.108	366.206	7.100
Tarmoola	57	0.078	685.584	4.719
Tarmoola	49.7	0.78	412.62	7.602
Tarmoola	65	3.3	397.224	4.216
Tarmoola	66	0.15	386.685	6.282
Tarmoola	109	1.03	670.825	3.342
Paddington	18.3	0.008	919.37	3.039
Paddington	19.79	0.011	799.64	3.878
Paddington	19.75	0.107	463.93	6.452
Paddington	15.35	0.008	781.66	2.664
Paddington	18.82	0.017	480.02	10.378
Paddington	13.73	0.017	706.16	3.877
Paddington	16.49	0.014	643.963	4.426
Paddington	20.3	0.019	590.53	9.375
Paddington	16.7	0.009	837.7	3.019
Paddington	19.09	0.017	593.75	6.126
Paddington	7.49	0.292	180.18	5.812
Paddington	7.05	1.62	105.735	9.477
Paddington	21.4	0.005	30.746	5.493
Paddington	22.09	0.02	56.12	6.922
Paddington	24.52	0.108	189.66	9.058
Paddington	22.95	0.009	31.199	8.886
Paddington	23.9	0.005	23.575	13.734
Paddington	14.91	0.15	92.35	20.003
Paddington	19.3	0.03	120.2	7.024
Paddington	26.4	0.055	333.56	2.122
Paddington	18.8	0.278	142.791	7.690
Paddington	23.77	0.01	26.6927	9.111
Mount Pleasant	17.48	0.008	1852.64	0.945

Appendix 3.1B (continued)

Name	Pb (ppm)	U (ppm)	REE (ppm)	EuA (ppm)
Mount Pleasant	19.76	0.066	982.87	5.572
Mount Pleasant	27.3	0.044	1459.11	2.233
Mount Pleasant	21	0.059	1325.09	3.282
Mount Pleasant	23.3	0.285	1098.42	3.522
North Royal Norseman	17.17	0.434	53.476	17.888
North Royal Norseman	17.11	0.462	28.321	12.524
North Royal Norseman	7.9	0.59	26.946	10.682
North Royal Norseman	31.1	0.179	35.874	5.150
North Royal Norseman	15.5	0.203	27.969	8.464
North Royal Norseman	14.04	0.182	38.591	6.074
Crown Footwall Norseman	11.58	0.065	3901.7	0.520
Crown Footwall Norseman	13.7	0.117	3626	0.596
Crown Footwall Norseman	20.14	0.28	175.446	11.494
Crown Footwall Norseman	24.41	1.28	308.159	4.877
Crown Footwall Norseman	22.25	2.05	223.241	7.611
Crown Footwall Norseman	16.02	0.011	105.154	15.153
Crown Footwall Norseman	14.53	0.014	140.36	6.686
Mararoa Norseman	23.09	0.034	289.856	3.515
Mararoa Norseman	25.98	8.9	91.83	16.911
Mararoa Norseman	33	2.4	239.69	2.413
Mararoa Norseman	30.6	2.75	257.785	3.908
Mararoa Norseman	25.54	4.6	136.674	9.342
Mount Charlotte	26.1	0.327	96.837	26.275
Mount Charlotte	27.32	0.389	109.693	21.100
Mount Charlotte	23.4	0.004	1157.03	1.949
Mount Charlotte	23	0.002	1048.22	2.915
Mount Charlotte	22.5	0.004	983.34	2.406
Mount Charlotte	20.07	0.003	909.79	3.232
Mount Charlotte	20.8	0.002	1311.56	1.360
Mount Charlotte	12.8	0.001	389.271	1.661
Mount Charlotte	20.4	0.002	936.08	1.441
Mount Charlotte	18.25	0.004	410.9	12.646
Mount Charlotte	18.02	0.002	358.79	13.449
Mount Charlotte	18.71	0.004	267.78	16.672
Macraes	3.92	0.67	396.451	1.666
Macraes	8.6	1	215.1	2.074
Macraes	8.97	1.51	104.376	2.079
Macraes	6.1	0.77	248.02	2.458
Macraes	2	1.23	344.08	1.497
Macraes	6.12	1.87	103.39	2.199

Appendix 3.1B (continued)

Name	Pb (ppm)	U (ppm)	REE (ppm)	EuA (ppm)
Macraes	8.02	1.35	166.107	2.055
Macraes	6	0.766	181.93	1.845
Macraes	6.7	0.66	316.97	2.835
Macraes	4.99	0.75	255.81	3.464
Macraes	7.4	1.73	94.565	1.945
Macraes	3.46	1.92	193.42	1.405
Amaruq	29.67	0.89	80.04	10.266
Amaruq	8.55	0.001244	31.07	3.659
Amaruq	16.53	0.000563	47	2.011
Amaruq	11.82	0.000616	117.73	0.947
Amaruq	15.5	0.000714	330.41	0.443
Amaruq	21.8	0.001159	300.51	0.617
Amaruq	6.99	0.02	260.73	0.702
Amaruq	11.75	0.08	336.16	0.596
Amaruq	9.72	0.02	301.66	0.715
Amaruq	32.47	0.001396	92.44	3.706
Amaruq	42.7	0.09	211.29	3.478
Amaruq	37.6	0.21	511.31	2.165
Amaruq	34.3	0.06	393.26	2.541
Amaruq	18.74	0.04	147.64	15.913
Amaruq	14.73	0.01	602.9	0.747
Amaruq	31.65	0.09	336.41	2.005
Amaruq	19.3	0.01	1116.02	1.458
Amaruq	31.72	0.03	1113	2.691
Amaruq	34.48	4.8	1440.23	6.360
Amaruq	20.65	4.8	430.75	2.418
Amaruq	32.8	13.53	478.1	15.526
Amaruq	24.2	3.89	363.89	9.291
Amaruq	32.95	0.99	1297.11	2.279
Amaruq	19.83	2.2	424.34	1.891
Amaruq	36.75	11.86	712.71	13.002
Amaruq	37.55	8.72	691.71	21.989
Amaruq	34.99	4.84	887.48	14.482
Amaruq	31.65	1.75	1776.87	3.516
Amaruq	30.7	2.6	1018.44	6.045
Amaruq	21.9	0.2	1127.84	1.499
Amaruq	14.03	0.11	105.84	27.198
Amaruq	32.76	3.86	325.9	20.475
Amaruq	30.1	2.18	415.28	19.647
Amaruq	19.58	1.77	679.8	4.543
Amaruq	17.2	0.00081	50.17	2.840
Amaruq	58.85	0.82	354.8	3.272
Amaruq	9.99	4.28E-05	119.48	0.501
Amaruq	22.5	2.68	114.61	3.471
Amaruq	35.2	0.07	54.51	2.176

Appendix 3.2B. Literature scheelite data (Dataset 2) used to assess the effectiveness of the RF model.

Deposit	Mg (ppm)	V (ppm)	Mn (ppm)	As (ppm)	Sr (ppm)	Y (ppm)	Nb (ppm)	Mo (ppm)	Ba (ppm)	Pb (ppm)	U (ppm)	REE	Eu anomaly
Whale Tail down deposit	10	0.02	9	0.22	1067	5.8	1.97		1.23	12.2	0.06	12.77	4.05
Whale Tail down deposit	8.6	0.03	55.8	3.11	2071	37.3	2.06	0.13	1.61	38	0.22	94.17	12.08
Whale Tail down deposit	4.86	0.09	17.45	1.01	894	29.8	2.65	32.75	1.08	6.39	<DL	51.19	2.20
Whale Tail down deposit	82	0.37	16.7	4.33	1560	47.0	8.75	81	8.7	21.7	0.06	107.85	4.58
Whale Tail down deposit	2.87	0.08	7.62	1.88	938	13.8	1.95	0.38	1.74	13.55	0.04	28.09	8.36
Whale Tail down deposit	3.01	0.07	16.3	2.04	1239	55.6	4.58	191.1	0.54	8.49	0.0013	481.48	0.71
Whale Tail down deposit	5.7	0.02	10.17	0.18	215	6.8	2.25	9.33	0.41	4.89	<DL	5.96	6.05
Whale Tail down deposit	4.09	0.02	20.49	0.24	1004	7.4	1.96	0.84	0.56	5.05	0.01	18.58	3.67
Whale Tail down deposit	3.47	0.03	33.4	1.45	1065	25.5	1.94	8.1	1.18	9.56	<DL	18.29	2.21
Whale Tail down deposit	2.92	0.01	10.68	0.03	248	5.0	1.87	21.6	0.81	6.72	<DL	5.81	64.76
Whale Tail down deposit	28	0.47	8.68	7.09	885	21.4	5.7	17.4	3.03	4.01	<DL	43.83	0.95
Whale Tail down deposit	2.9	0.02	8.13	<DL	640	79.8	2.52	57.7	1.05	11.07	<DL	61.06	4.44
Whale Tail down deposit	7.1	0.14	9.83	2.96	994	22.4	4.71	109.5	1.96	5.46	<DL	43.82	1.66
Whale Tail down deposit	3.1	<DL	35.9	0.21	1803	1.5	1.95	0.42	0.91	8.44	0.01	2.30	4.47
Whale Tail down deposit	3.3	0.02	19.5	0.32	4820	28.1	3.39	0.39	1.47	10.44	0.19	39.51	8.58
Whale Tail down deposit	3.07	0.01	12.7	0.34	5290	8.3	1.95	0.43	0.54	14.67	2.95	13.30	32.97
Whale Tail down deposit	3.08	0.04	12.21	1.88	896	23.1	2.32	0.81	4.89	7.3	0.07	38.46	4.75
Whale Tail down deposit	2.93	0.08	10.9	2.14	1160	28.2	5.4	20	5.54	8.54	0.01	45.92	2.67
Whale Tail down deposit	2.98	<DL	55.8	0.45	2241	7.2	1.78	<DL	0.5	14.55	0.25	5.91	8.76
Whale Tail down deposit	3.33	0.08	21.8	0.31	3430	23.0	2.32	0.11	1.4	6.99	1.8	97.08	16.47
Whale Tail down deposit	17.26	0.12	20.45	0.5	1654	18.0	1.94	0.14	1.04	5.37	0.01	20.31	5.04
Whale Tail down deposit	2.77	0.04	11.78	2.12	2088	42.1	5.61	0.25	0.27	5.47	0.29	93.92	5.31
Whale Tail down deposit	8.9	0.06	25.8	1.69	2322	41.7	4.49	0.16	0.3	9.26	0.06	82.22	5.63
Mustang	3.7	0.197	8.1	320	256	157.0	53.4	41.8	0.23	13.5	0.015	205.54	0.52
Mustang	3.1	0.45	8.31	0.104	508	258.0	75.9	9.55	0.34	16.6	0.002	591.03	0.41
Mustang	2.93	0.25	10	0.104	437	461.8	69.9	85	0.12	17.4	0.002	499.55	0.44
Mustang	2.58	0.364	9.38	0.105	281	185.1	51.5	88	0.31	16.7	0.006	232.78	0.44
Mustang	3.02	0.402	10.75	0.105	342	216.0	81.6	13.74	0.22	13.79	0.008	383.36	0.40
Woxi	10.201	0.057	0.957	98.398	3478	34.6	2.185	24.897	0.341	13.563	41.746	45.80	0.82
Woxi	14.419	0.117	4.074	116.091	5382	26.3	2.025	28.939	0.378	115.341	29.203	51.17	0.79
Woxi	7.217	0.061	3.788	129.487	7552	64.1	2.421	76.900	0.701	316.191	29.442	57.72	0.93
Woxi	12.444	0.034	4.830	100.330	7858	80.4	1.948	75.186	0.451	272.189	31.760	60.44	0.96

Appendix 3.2B (continued)

Deposit	Mg (ppm)	V (ppm)	Mn (ppm)	As (ppm)	Sr (ppm)	Y (ppm)	Nb (ppm)	Mo (ppm)	Ba (ppm)	Pb (ppm)	U (ppm)	REE	Eu anomaly
Woxi	6.703	0.179	0.208	3.581	319	94.5	1.541	27.097	0.036	1.780	0.462	24.14	0.55
Woxi	6.106	0.136	0.127	3.657	383	135.6	1.511	28.787	0.008	3.060	0.305	33.98	0.51
Woxi	6.170	0.121	0.245	2.379	394	80.3	1.506	24.587	0.430	2.381	0.194	30.23	0.62
Woxi	4.224	0.146	0.287	3.238	469	203.1	1.530	25.838	0.010	2.763	0.584	48.47	0.54
Woxi	6.817	0.134	0.786	12.756	292	421.1	1.528	21.548	1.044	1.299	0.188	237.35	0.58
Woxi	6.350	0.102	0.204	0.431	416	218.0	1.489	23.096	0.012	3.166	0.278	86.03	0.56
Woxi	5.828	0.102	0.382	0.656	349	634.5	1.567	17.921	0.251	4.039	0.299	345.91	0.56
Woxi	3.306	0.109	0.244	6.970	357	372.3	1.590	21.494	0.010	4.507	0.376	220.96	0.54
Woxi	3.496	0.133	0.117	0.284	326	108.5	1.541	13.132	0.006	3.431	0.273	31.56	0.57
Woxi	5.585	0.402	1.042	3.419	220	13.1	1.495	11.683	0.285	1.621	0.216	3.59	0.83
Woxi	7.675	0.175	0.176	23.275	429	89.0	1.491	8.815	0.021	1.154	0.140	35.30	0.56
Woxi	5.724	0.123	0.145	2.226	356	846.5	1.477	7.524	0.020	2.250	0.344	597.63	0.56
Woxi	4.892	0.093	0.161	9.851	348	246.6	1.406	9.168	0.177	2.329	0.316	97.16	0.54
Woxi	7.067	0.133	0.331	4.248	334	103.1	1.603	9.790	0.343	3.194	0.286	46.39	0.52
Macraes by Cave et al. (2017)	1.677	NA	5.152	NA	6294	223.5	NA	0.269	4.927	5.699	1.420	354.73	2.88
Macraes by Cave et al. (2017)	0.985	NA	3.395	NA	6089	139.7	NA	0.354	2.296	8.351	1.570	185.72	4.53
Macraes by Cave et al. (2017)	0.679	NA	10.238	NA	8155	79.4	NA	0.228	0.354	29.749	1.973	90.18	9.08
Macraes by Cave et al. (2017)	1.087	NA	3.133	NA	7139	101.4	NA	0.507	0.697	9.357	2.624	128.05	5.91
Macraes by Cave et al. (2017)	1.033	NA	3.697	NA	6390	46.9	NA	0.336	0.135	10.314	3.041	57.34	8.58
Macraes by Cave et al. (2017)	0.650	NA	2.052	NA	4861	198.6	NA	0.247	0.054	5.226	0.406	322.42	3.76
Macraes by Cave et al. (2017)	0.863	NA	6.616	NA	6920	175.5	NA	0.407	1.338	11.714	1.539	208.67	6.53
Macraes by Cave et al. (2017)	0.629	NA	2.702	NA	4152	1047.1	NA	0.450	0.159	5.240	0.016	2555.47	1.52
Macraes by Cave et al. (2017)	2.429	NA	2.809	NA	5416	98.9	NA	0.318	1.419	7.511	3.654	166.78	2.76
Macraes by Cave et al. (2017)	1.049	NA	3.600	NA	4989	38.9	NA	0.183	0.581	7.080	5.230	54.22	9.52

Appendix 3.2B (continued)

Deposit	Mg (ppm)	V (ppm)	Mn (ppm)	As (ppm)	Sr (ppm)	Y (ppm)	Nb (ppm)	Mo (ppm)	Ba (ppm)	Pb (ppm)	U (ppm)	REE	Eu anomaly
Macraes by Cave et al. (2017)	0.573	NA	2.760	NA	5240	70.7	NA	0.098	0.159	7.184	2.162	162.46	2.61
Macraes by Cave et al. (2017)	0.953	NA	3.848	NA	6774	90.7	NA	0.522	0.213	14.037	4.276	111.91	7.88
Macraes by Cave et al. (2017)	0.757	NA	2.878	NA	3239	1072.3	NA	0.272	0.059	3.873	0.034	2023.51	2.21
Macraes by Cave et al. (2017)	0.965	NA	1.264	NA	3619	410.5	NA	0.267	0.042	4.411	0.008	1157.85	2.49
Macraes by Cave et al. (2017)	0.804	NA	1.713	NA	3739	679.8	NA	0.220	0.043	4.707	0.037	1319.21	3.59
Macraes by Cave et al. (2017)	0.709	NA	2.969	NA	8621	48.5	NA	0.246	0.115	14.021	4.758	62.85	17.24
Macraes by Cave et al. (2017)	0.574	NA	3.341	NA	6976	278.3	NA	0.098	0.652	5.485	1.804	344.28	3.61
Macraes by Cave et al. (2017)	1.031	NA	12.612	NA	11943	156.0	NA	0.179	1.064	23.562	2.258	167.54	4.24
Macraes by Cave et al. (2017)	0.828	NA	13.080	NA	11487	124.6	NA	0.113	1.158	21.881	1.777	126.63	4.72
Macraes by Cave et al. (2017)	1.512	NA	7.272	NA	8485	94.6	NA	0.144	1.418	14.500	2.752	132.54	3.34
Macraes by Cave et al. (2017)	1.954	NA	6.368	NA	8403	72.1	NA	0.201	2.843	9.047	3.208	121.30	2.16
Macraes by Cave et al. (2017)	0.594	NA	3.754	NA	10191	51.8	NA	0.166	0.564	9.199	2.588	59.96	4.23
Macraes by Cave et al. (2017)	1.231	NA	7.986	NA	10378	98.5	NA	0.116	0.964	15.904	3.257	126.57	3.25
Macraes by Cave et al. (2017)	1.019	NA	3.531	NA	9419	98.0	NA	0.074	0.218	8.222	2.670	159.66	2.12
Macraes by Cave et al. (2017)	0.674	NA	10.043	NA	13354	73.0	NA	0.070	0.153	35.135	3.103	72.08	6.83
Macraes by Cave et al. (2017)	0.984	NA	2.209	NA	4780	215.6	NA	0.092	0.129	3.547	0.069	216.34	5.45
Macraes by Cave et al. (2017)	0.470	NA	7.204	NA	10007	58.6	NA	0.115	0.471	17.462	2.323	90.94	3.13

Appendix 3.2B (continued)

Deposit	Mg (ppm)	V (ppm)	Mn (ppm)	As (ppm)	Sr (ppm)	Y (ppm)	Nb (ppm)	Mo (ppm)	Ba (ppm)	Pb (ppm)	U (ppm)	REE	Eu anomaly
Macraes by Cave et al. (2017)	0.873	NA	5.838	NA	9113	105.7	NA	0.214	1.140	14.705	1.548	152.41	2.75
Macraes by Cave et al. (2017)	0.626	NA	6.157	NA	9540	186.9	NA	0.158	0.063	14.664	2.204	170.09	6.98
Macraes by Cave et al. (2017)	0.463	NA	2.181	NA	4869	91.7	NA	0.080	0.176	2.970	0.034	93.10	5.60
Macraes by Cave et al. (2017)	1.026	NA	3.442	NA	6742	526.0	NA	0.111	0.466	7.332	0.203	534.91	3.98
Macraes by Cave et al. (2017)	2.246	NA	3.013	NA	8899	49.5	NA	0.094	0.426	10.051	3.350	61.25	4.37
Macraes by Cave et al. (2017)	0.851	NA	7.474	NA	10585	58.0	NA	0.072	0.122	18.865	3.132	65.77	6.41
Macraes by Pickering (2018)	2.100	NA	2.800	0.700	6770	273	0.600	0.100	NA	4.000	0.700	493.40	1.32
Macraes by Pickering (2018)	6.600	NA	1.400	12.600	5412	600	1.300	0.200	NA	3.300	0.100	1552.20	0.89
Macraes by Pickering (2018)	53.000	NA	39.000	1.900	4603	864	1.500	0.200	NA	2.900	0.100	2061.90	0.92
Macraes by Pickering (2018)	3.300	NA	1.700	0.300	6577	174	0.500	0.200	NA	4.800	1.800	236.30	2.86
Macraes by Pickering (2018)	2.100	NA	2.600	0.200	6868	62	0.600	0.200	NA	6.000	1.800	104.90	2.96
Macraes by Pickering (2018)	71.000	NA	1.900	0.700	6559	71	0.600	0.300	NA	5.300	3.700	133.00	2.89
Macraes by Pickering (2018)	9.173	NA	2.100	0.300	8719	17	0.600	0.100	NA	8.600	2.400	29.40	5.42
Macraes by Pickering (2018)	7.800	NA	17.200	0.300	7971	35	0.600	0.100	NA	6.400	3.900	59.80	4.34
Macraes by Pickering (2018)	28.700	NA	3.200	6.500	5624	220	0.700	0.200	NA	4.500	0.300	447.30	1.67
Macraes by Pickering (2018)	3.700	NA	7.000	0.700	4832	222	0.700	0.100	NA	3.600	0.300	359.60	1.48
Macraes by Pickering (2018)	41.400	NA	167.000	1.800	4991	334	0.900	0.200	NA	3.800	0.700	898.80	0.90
Macraes by Pickering (2018)	1.600	NA	6.500	0.300	9110	75	0.600	0.100	NA	13.300	1.500	86.00	2.03

Appendix 3.2B (continued)

Deposit	Mg (ppm)	V (ppm)	Mn (ppm)	As (ppm)	Sr (ppm)	Y (ppm)	Nb (ppm)	Mo (ppm)	Ba (ppm)	Pb (ppm)	U (ppm)	REE	Eu anomaly
Macraes by Pickering (2018)	1.500	NA	3.100	0.200	7260	28	0.500	0.100	NA	7.100	1.700	29.00	7.48
Macraes by Pickering (2018)	1.800	NA	4.300	2.700	9100	57	0.500	0.100	NA	8.900	1.700	79.10	1.90
Macraes by Pickering (2018)	2.600	NA	4.900	2.500	8590	56	0.500	0.200	NA	7.300	1.800	60.20	2.24
Macraes by Pickering (2018)	48.200	NA	7.100	16.000	6630	120	0.600	0.100	NA	8.800	1.300	142.90	1.76
Macraes by Pickering (2018)	1.500	NA	3.200	0.200	7530	19	0.500	5.333	NA	6.200	1.800	20.70	2.65
Macraes by Pickering (2018)	5.200	NA	10.200	18.600	5585	227	0.500	0.200	NA	6.800	1.100	208.10	3.54
Macraes by Pickering (2018)	42.500	NA	8.700	3.300	6620	171	0.600	0.100	NA	7.100	1.300	183.60	2.14
Macraes by Pickering (2018)	1.500	NA	4.100	0.100	9690	39	0.500	0.100	NA	13.500	2.900	41.00	4.41
Macraes by Pickering (2018)	1.400	NA	3.200	0.200	7164	33	0.500	0.145	NA	6.200	2.200	34.20	4.24
Macraes by Pickering (2018)	1.500	NA	3.500	1.100	7840	116	0.500	0.100	NA	6.200	1.200	133.30	2.19
Macraes by Pickering (2018)	1.600	NA	1.600	1.900	8080	594	1.000	1.520	NA	7.600	0.700	1515.70	1.08
Macraes by Pickering (2018)	2.000	NA	2.400	0.300	8840	71	0.600	0.100	NA	8.300	2.700	90.10	3.73
Macraes by Pickering (2018)	169.000	NA	191.000	1.200	6420	106	0.500	0.300	NA	13.800	2.600	202.40	1.41
Macraes by Pickering (2018)	1.900	NA	1.700	1.000	6510	684	0.700	0.769	NA	4.900	0.100	1285.10	1.59
Macraes by Pickering (2018)	1.900	NA	3.400	0.200	9490	73	0.600	0.129	NA	12.600	2.600	90.10	2.89
Macraes by Pickering (2018)	2.600	NA	3.800	0.400	11280	66	0.600	0.135	NA	16.200	2.000	99.60	1.98
Macraes by Pickering (2018)	1.600	NA	1.900	1.000	6188	635	0.900	0.100	NA	4.200	0.100	1125.60	1.54
Macraes by Pickering (2018)	7.600	NA	13.900	1.000	8710	655	1.100	0.100	NA	12.900	0.500	1103.40	1.21

Appendix 3.2B (continued)

Deposit	Mg (ppm)	V (ppm)	Mn (ppm)	As (ppm)	Sr (ppm)	Y (ppm)	Nb (ppm)	Mo (ppm)	Ba (ppm)	Pb (ppm)	U (ppm)	REE	Eu anomaly
Macraes by Pickering (2018)	1.600	NA	5.700	0.200	12680	124	0.600	0.680	NA	25.200	2.200	146.70	2.98
Macraes by Pickering (2018)	1.500	NA	1.900	0.200	12110	25	0.600	0.100	NA	17.600	2.100	70.90	3.11
Macraes by Pickering (2018)	3.300	NA	5.900	8.500	8260	189	0.600	0.100	NA	12.300	1.100	281.90	1.44
Macraes by Pickering (2018)	4.900	NA	6.000	14.300	7440	281	0.900	0.100	NA	9.200	1.400	508.40	1.40
Macraes by Pickering (2018)	35.200	NA	5.500	12.300	8560	172	0.600	0.200	NA	10.200	1.700	261.20	1.51
Macraes by Pickering (2018)	11.900	NA	11.600	3.100	10540	150	0.700	0.100	NA	24.300	1.200	225.60	2.04
Macraes by Pickering (2018)	621.000	NA	8.800	27.000	10580	138	0.800	0.100	NA	16.500	2.000	242.90	1.26
Macraes by Pickering (2018)	3.100	NA	5.500	12.500	8182	547	0.900	0.100	NA	6.700	0.700	996.50	1.08
Macraes by Pickering (2018)	1.700	NA	3.200	0.900	15740	88	0.600	0.300	NA	32.000	2.900	117.20	1.63
Macraes by Pickering (2018)	17.800	NA	8.000	7.300	9860	287	1.000	0.100	NA	16.000	0.600	589.60	0.95
Macraes by Pickering (2018)	132.000	NA	6.500	116	6378	298	1.900	0.200	NA	6.000	0.100	691.70	0.92
Macraes by Pickering (2018)	3.600	NA	4.700	1.700	6373	219	1.100	0.200	NA	6.300	0.300	421.30	1.23
Macraes by Pickering (2018)	2.200	NA	8.500	3.500	6209	172	1.100	0.200	NA	8.800	0.200	440.00	1.08
Macraes by Pickering (2018)	4.300	NA	5.500	30.000	5570	185	0.700	0.200	NA	7.000	0.400	296.80	1.55
Macraes by Pickering (2018)	1.900	NA	4.400	0.700	6950	134	0.600	0.100	NA	5.700	1.000	162.20	2.61
Macraes by Pickering (2018)	1.900	NA	10.800	0.300	9100	85	0.600	0.100	NA	17.000	1.000	90.70	2.28
Macraes by Pickering (2018)	4.300	NA	6.600	2.600	6640	398	0.600	2.700	NA	9.500	0.300	469.90	1.03

Appendix 3.2B (continued)

Deposit	Mg (ppm)	V (ppm)	Mn (ppm)	As (ppm)	Sr (ppm)	Y (ppm)	Nb (ppm)	Mo (ppm)	Ba (ppm)	Pb (ppm)	U (ppm)	REE	Eu anomaly
Macraes by Pickering (2018)	2.000	NA	4.800	0.300	6649	86	0.500	0.100	NA	8.500	0.900	98.30	1.99
Macraes by Pickering (2018)	1.600	NA	5.900	0.500	9250	130	0.600	0.100	NA	15.800	1.100	147.10	1.78
Macraes by Pickering (2018)	2.100	NA	4.400	3.100	8030	226	0.600	0.100	NA	7.200	1.000	302.00	1.23
Macraes by Pickering (2018)	2.400	NA	4.000	2.200	6878	152	0.600	0.100	NA	5.900	1.200	206.90	1.40
Macraes by Pickering (2018)	1.600	NA	7.600	0.300	10550	132	0.600	4.224	NA	27.000	1.900	132.20	2.10
Macraes by Pickering (2018)	4.700	NA	4.800	47.000	9249	88	0.600	0.100	NA	20.000	1.200	111.10	2.15
Macraes by Pickering (2018)	17.000	NA	5.000	9.600	6409	221	0.700	0.100	NA	6.400	0.700	339.50	1.01
Macraes by Pickering (2018)	2.600	NA	3.800	6.300	4876	380	0.800	0.100	NA	3.300	0.100	672.60	0.99
Macraes by Pickering (2018)	3.200	NA	4.700	3.800	6238	185	0.700	0.200	NA	5.300	0.800	272.10	1.32
Macraes by Pickering (2018)	1.400	NA	3.400	0.200	9250	123	0.600	0.185	NA	10.900	0.900	150.90	1.78
Macraes by Pickering (2018)	177.000	NA	5.700	1.200	9510	59	0.600	43.029	NA	8.800	2.400	79.60	1.95
Macraes by Pickering (2018)	1.900	NA	5.300	0.200	9060	97	0.600	0.155	NA	7.400	1.600	121.00	2.37
Macraes by Pickering (2018)	1.400	NA	4.400	0.200	9500	64	0.600	0.123	NA	13.600	2.000	80.70	1.99
Macraes by Pickering (2018)	89.900	NA	3.400	3.300	5900	748	1.000	0.100	NA	4.600	0.100	1270.30	1.01
Macraes by Pickering (2018)	55.400	NA	3.700	2000	5135	527	0.900	0.200	NA	8.000	0.300	654.50	1.56
Macraes by Pickering (2018)	2.200	NA	3.500	0.600	8940	89	0.500	0.155	NA	10.200	4.200	136.50	2.04
Macraes by Pickering (2018)	339.000	NA	5.200	66.000	5127	603	1.500	0.100	NA	5.800	0.200	996.70	1.11

Appendix 3.2B (continued)

Deposit	Mg (ppm)	V (ppm)	Mn (ppm)	As (ppm)	Sr (ppm)	Y (ppm)	Nb (ppm)	Mo (ppm)	Ba (ppm)	Pb (ppm)	U (ppm)	REE	Eu anomaly
Macraes by Pickering (2018)	28.400	NA	3.000	48.000	5581	341	0.700	0.100	NA	5.700	0.400	449.70	2.05
Macraes by Pickering (2018)	17.100	NA	2.900	1.98	5102	386	0.900	0.100	NA	7.100	0.100	533.60	1.85
Macraes by Pickering (2018)	2.600	NA	11.400	3.000	6963	116	0.600	0.157	NA	7.400	1.200	121.90	1.90
Macraes by Pickering (2018)	52.500	NA	10.300	1.800	4217	416	0.800	0.100	NA	3.000	0.200	599.60	1.70
Macraes by Pickering (2018)	99.000	NA	6.200	340.0	6025	148	0.800	0.200	NA	12.800	1.400	254.00	1.38
Macraes by Pickering (2018)	21.400	NA	5.100	45.000	5360	278	0.700	0.100	NA	10.000	0.900	431.50	1.48
Macraes by Pickering (2018)	2.000	NA	3.300	3.100	6870	265	0.700	0.100	NA	10.400	1.000	443.70	1.28
Macraes by Pickering (2018)	260.000	NA	5.700	170.000	4982	745	1.300	0.100	NA	12.300	0.100	1127.70	1.17
Macraes by Pickering (2018)	1.500	NA	2.100	1.100	7008	93	0.600	2.600	NA	4.900	2.400	118.60	3.06
Macraes by Pickering (2018)	10.200	NA	5.400	14.500	9580	52	0.500	61.846	NA	21.200	1.400	55.50	4.15
Macraes by Pickering (2018)	2.300	NA	5.500	0.500	9890	181	0.700	0.100	NA	15.500	1.000	226.70	1.77
Macraes by Pickering (2018)	3.600	NA	3.700	0.500	6178	216	0.600	0.100	NA	4.300	0.300	169.40	2.72
Macraes by Pickering (2018)	1.800	NA	2.800	0.300	8040	54	0.500	0.148	NA	8.700	3.100	72.10	1.95
Macraes by Pickering (2018)	2.000	NA	2.600	0.300	8000	119	0.600	0.159	NA	6.000	1.800	115.60	2.62
Macraes by Pickering (2018)	1.600	NA	4.600	0.300	10020	87	0.500	0.100	NA	28.500	2.000	99.10	2.55
Macraes by Pickering (2018)	1.700	NA	1.600	0.100	8630	60	0.500	0.142	NA	8.500	2.700	62.70	4.06
Macraes by Pickering (2018)	2.500	NA	2.500	2.400	6523	403	0.800	0.352	NA	4.200	0.300	691.80	1.21

Appendix 3.2B (continued)

Deposit	Mg (ppm)	V (ppm)	Mn (ppm)	As (ppm)	Sr (ppm)	Y (ppm)	Nb (ppm)	Mo (ppm)	Ba (ppm)	Pb (ppm)	U (ppm)	REE	Eu anomaly
Macraes by Pickering (2018)	1.500	NA	3.300	0.200	13530	39	0.500	0.100	NA	20.600	2.400	54.40	1.59
Macraes by Pickering (2018)	1.400	NA	1.900	0.200	9930	76	0.600	2.229	NA	9.800	2.300	89.60	2.25
Macraes by Pickering (2018)	2.000	NA	2.800	1.100	10600	63	0.600	0.200	NA	10.600	2.200	80.00	2.07
Macraes by Pickering (2018)	2.100	NA	6.400	0.200	9570	49	0.600	0.100	NA	16.300	1.100	84.10	1.64
Macraes by Pickering (2018)	1.400	NA	3.500	0.400	8850	265	0.600	0.881	NA	24.400	2.200	288.70	2.57
Macraes by Pickering (2018)	2.600	NA	6.400	0.300	7850	139	0.600	0.100	NA	5.300	1.400	149.90	1.82
Macraes by Pickering (2018)	1.900	NA	5.100	0.500	8990	88	0.600	0.100	NA	8.300	2.100	115.60	1.55
Macraes by Pickering (2018)	1.500	NA	3.400	0.200	8130	32	0.500	0.135	NA	10.100	1.600	36.70	2.70
Macraes by Pickering (2018)	1.800	NA	3.400	0.400	5790	211	0.600	0.163	NA	5.200	0.200	336.30	1.54
Macraes by Pickering (2018)	10.300	NA	145.000	9.625	7430	250	0.500	0.100	NA	8.800	1.600	256.30	3.14
Macraes by Pickering (2018)	3.100	NA	2.000	0.400	7480	12	0.600	0.300	NA	4.900	6.200	22.90	1.55
Macraes by Pickering (2018)	92.000	NA	215.500	4.600	7330	120	0.700	0.300	NA	6.100	0.800	153.90	1.51
Macraes by Pickering (2018)	3.000	NA	3.200	0.600	9940	98	0.700	0.300	NA	7.900	0.900	83.30	2.61
Macraes by Pickering (2018)	3.300	NA	5.000	2.300	8350	201	0.900	0.300	NA	9.400	0.600	233.60	1.49
Macraes by Pickering (2018)	7.700	NA	4.500	1.300	6910	142	0.700	0.400	NA	4.600	0.700	121.00	2.44
Macraes by Pickering (2018)	308.000	NA	47.400	7.500	9180	497	2.300	1.100	NA	9.600	0.500	552.00	1.07
Macraes by Pickering (2018)	66.000	NA	107.000	2.500	7390	99	0.700	0.600	NA	4.200	1.200	119.10	1.33

Appendix 3.2B (continued)

Deposit	Mg (ppm)	V (ppm)	Mn (ppm)	As (ppm)	Sr (ppm)	Y (ppm)	Nb (ppm)	Mo (ppm)	Ba (ppm)	Pb (ppm)	U (ppm)	REE	Eu anomaly
Macraes by Pickering (2018)	101.000	NA	36.900	4.700	4340	384	1.200	0.300	NA	2.100	0.100	1037.80	0.76
Alta Lode-Bendigo	6.000	NA	0.900	50.0	4340	244	1.940	0.260	NA	12.600	NA	349.59	9.64
Alta Lode-Bendigo	2.172	NA	0.600	2.3	4700	486	2.080	0.320	NA	11.400	NA	955.90	2.79
Alta Lode-Bendigo	1.000	NA	0.700	2.1	4930	439	2.050	0.270	NA	18.600	NA	760.61	2.56
Alta Lode-Bendigo	1.000	NA	0.900	59.0	4730	429	2.080	0.340	NA	13.200	NA	723.97	3.13
Alta Lode-Bendigo	3.095	NA	0.700	3.6	4600	645	2.330	0.270	NA	11.900	NA	1277.26	2.47
Alta Lode-Bendigo	38.681	NA	0.500	20.2	5580	660	2.600	0.250	NA	14.100	NA	1379.92	1.79
Alta Lode-Bendigo	4.215	NA	0.600	45.9	5290	499	2.590	0.400	NA	13.500	NA	1018.65	2.14
Alta Lode-Bendigo	3.673	NA	0.600	1.6	5160	229	1.950	0.350	NA	12.200	NA	497.55	2.90
Alta Lode-Bendigo	4.614	NA	0.800	3.0	5050	136	2.050	0.370	NA	14.500	NA	187.92	21.08
Alta Lode-Bendigo	6.068	NA	0.600	1.7	3940	725	1.880	0.430	NA	12.000	NA	1464.53	2.49
Alta Lode-Bendigo	2.096	NA	0.400	2.0	3800	600	1.990	0.400	NA	12.200	NA	1158.60	2.26
Alta Lode-Bendigo	2.000	NA	0.800	13.3	4080	538	2.330	0.350	NA	12.900	NA	1100.48	2.41
Alta Lode-Bendigo	1.671	NA	0.700	24.4	4470	350	2.150	0.330	NA	12.000	NA	741.71	2.22
Alta Lode-Bendigo	1.956	NA	0.500	2.3	4910	510	2.240	0.340	NA	11.500	NA	1089.45	1.90
Alta Lode-Bendigo	2.204	NA	0.400	1.5	4260	485	2.440	0.240	NA	10.300	NA	1067.23	1.83
Alta Lode-Bendigo	4.000	NA	1.100	8.1	4670	187	1.830	0.420	NA	13.300	NA	379.38	3.97
Alta Lode-Bendigo	14.265	NA	0.800	69.0	4440	336	1.630	0.310	NA	15.800	NA	459.70	13.77
Alta Lode-Bendigo	4.108	NA	0.700	1.7	4560	334	2.320	0.300	NA	11.600	NA	580.37	5.40
Alta Lode-Bendigo	2.404	NA	0.500	2.2	3730	458	2.290	0.190	NA	9.000	NA	1004.43	2.07
Alta Lode-Bendigo	3.160	NA	0.600	1.2	4230	382	1.940	0.290	NA	9.900	NA	737.36	3.01
Alta Lode-Bendigo	3.640	NA	0.700	9.2	4440	308	1.650	0.190	NA	10.500	NA	497.51	6.25
Alta Lode-Bendigo	1.000	NA	1.000	47.3	4990	149	1.910	0.380	NA	21.200	NA	262.46	6.74
Alta Lode-Bendigo	4.720	NA	1.200	1.6	6400	172	2.190	0.340	NA	27.800	NA	245.64	9.64
Alta Lode-Bendigo	4.689	NA	1.100	9.3	4860	190	1.580	0.380	NA	20.500	NA	284.36	8.76
Alta Lode-Bendigo	4.766	NA	0.700	1.4	4670	325	2.020	0.250	NA	17.200	NA	635.52	3.13
Alta Lode-Bendigo	2.747	NA	0.500	2.0	3900	377	2.850	0.200	NA	9.700	NA	976.93	1.77
Alta Lode-Bendigo	2.289	NA	1.000	2.4	4380	372	2.640	0.440	NA	13.100	NA	777.94	2.33
Alta Lode-Bendigo	4.961	NA	1.000	2.4	4190	279	2.180	0.260	NA	13.600	NA	664.02	2.49
Alta Lode-Bendigo	3.984	NA	0.600	1.0	3230	416	2.020	0.230	NA	7.400	NA	964.31	2.46
Alta Lode-Bendigo	2.000	NA	1.500	117.0	4700	220	1.700	0.370	NA	17.100	NA	335.94	5.54

Appendix 3.2B (continued)

Deposit	Mg (ppm)	V (ppm)	Mn (ppm)	As (ppm)	Sr (ppm)	Y (ppm)	Nb (ppm)	Mo (ppm)	Ba (ppm)	Pb (ppm)	U (ppm)	REE	Eu anomaly
Alta Lode-Bendigo	12.779	NA	0.900	98.0	4710	215	1.990	0.300	NA	18.300	NA	356.10	6.85
Alta Lode-Bendigo	1.000	NA	0.900	76.0	4800	225	1.990	0.230	NA	18.200	NA	375.18	8.58
Alta Lode-Bendigo	3.777	NA	0.900	36.0	5080	197	1.810	0.120	NA	14.100	NA	305.20	9.98
Alta Lode-Bendigo	1.000	NA	0.800	80.0	4480	155	1.500	0.430	NA	13.500	NA	286.86	4.65
Alta Lode-Bendigo	1.000	NA	0.800	51.0	4300	176	1.780	0.230	NA	12.200	NA	308.35	6.67
Alta Lode-Bendigo	1.000	NA	0.500	2.3	3770	610	2.410	0.320	NA	9.900	NA	1522.68	1.71
Alta Lode-Bendigo	1.898	NA	0.600	1.3	4410	286	2.120	0.350	NA	10.200	NA	660.21	2.25
Alta Lode-Bendigo	3.248	NA	0.600	1.7	3820	255	2.080	0.210	NA	8.900	NA	611.34	2.10
Alta Lode-Bendigo	2.344	NA	0.700	15.0	3970	279	2.110	0.310	NA	10.400	NA	798.47	2.29
Alta Lode-Bendigo	3.160	NA	0.600	39.0	4510	269	2.070	0.330	NA	10.800	NA	692.74	1.96
Alta Lode-Bendigo	1.779	NA	0.600	17.0	4200	256	2.500	0.230	NA	11.500	NA	624.26	2.68
Alta Lode-Bendigo	2.586	NA	0.500	1.8	3820	336	2.430	0.390	NA	10.100	NA	898.33	2.09
Alta Lode-Bendigo	3.778	NA	0.600	52.0	3420	434	2.280	0.410	NA	9.700	NA	977.91	2.23
Alta Lode-Bendigo	7.609	NA	1.000	101.0	4760	246	1.820	0.270	NA	15.000	NA	419.94	5.56
Alta Lode-Bendigo	1.000	NA	1.200	134.0	4130	172	1.650	0.330	NA	17.000	NA	305.49	4.90
Alta Lode-Bendigo	1.000	NA	0.900	96.0	4560	297	1.820	0.300	NA	14.400	NA	424.65	8.22
Alta Lode-Bendigo	6.085	NA	1.100	1.0	5500	102	1.980	0.370	NA	29.300	NA	156.17	36.93
Alta Lode-Bendigo	6.159	NA	0.800	4.0	5800	151	1.760	0.230	NA	16.600	NA	239.62	14.95
Alta Lode-Bendigo	4.974	NA	0.700	33.1	4350	250	1.620	0.150	NA	15.000	NA	359.82	15.64
Alta Lode-Bendigo	27.000	NA	1.300	260.0	4250	164	1.940	0.520	NA	19.800	NA	326.25	5.29
Alta Lode-Bendigo	69.821	NA	0.400	68.0	4340	215	1.850	0.210	NA	9.180	NA	524.40	1.94
Alta Lode-Bendigo	2.928	NA	0.400	13.5	4820	246	1.840	0.360	NA	8.700	NA	582.75	2.22
Alta Lode-Bendigo	2.709	NA	0.600	1.9	4510	294	2.120	0.200	NA	7.750	NA	624.06	2.05
Alta Lode-Bendigo	3.839	NA	0.700	1.1	3380	282	1.890	0.310	NA	8.200	NA	606.82	2.89
Alta Lode-Bendigo	4.146	NA	0.600	1.3	3700	320	1.800	0.160	NA	9.700	NA	695.77	2.87
Alta Lode-Bendigo	2.000	NA	0.600	1.1	3570	257	1.790	0.250	NA	8.300	NA	593.72	2.65
Alta Lode-Bendigo	2.765	NA	0.600	1.5	3970	351	2.370	0.380	NA	10.700	NA	763.07	2.64
Alta Lode-Bendigo	3.360	NA	0.500	1.1	3530	335	2.240	0.190	NA	9.400	NA	684.29	2.69
Alta Lode-Bendigo	1.000	NA	0.800	7.4	3600	278	1.980	0.790	NA	9.200	NA	611.30	3.07
Alta Lode-Bendigo	2.871	NA	0.600	2.2	3600	268	1.820	0.430	NA	9.000	NA	588.84	2.69
Alta Lode-Bendigo	2.847	NA	0.700	22.7	4620	406	3.570	0.290	NA	12.300	NA	682.08	2.34
Alta Lode-Bendigo	7.208	NA	0.400	46.0	4820	482	4.490	0.200	NA	11.139	NA	694.28	1.98

Appendix 3.2B (continued)

Deposit	Mg (ppm)	V (ppm)	Mn (ppm)	As (ppm)	Sr (ppm)	Y (ppm)	Nb (ppm)	Mo (ppm)	Ba (ppm)	Pb (ppm)	U (ppm)	REE	Eu anomaly
Alta Lode-Bendigo	1.000	NA	0.600	16.4	4250	347	3.580	0.200	NA	13.200	NA	583.48	2.19
Alta Lode-Bendigo	1.000	NA	0.600	1.9	4190	207	2.160	0.360	NA	11.000	NA	548.86	2.12
Alta Lode-Bendigo	4.044	NA	0.500	2.1	3560	225	2.060	0.390	NA	9.500	NA	644.44	1.76
Alta Lode-Bendigo	2.996	NA	0.700	20.4	3480	255	1.880	0.330	NA	9.600	NA	584.82	2.33
Alta Lode-Bendigo	5.000	NA	0.900	58.0	4440	287	1.690	0.210	NA	15.200	NA	471.24	8.43
Alta Lode-Bendigo	14.605	NA	0.800	70.0	4370	600	2.610	0.360	NA	12.300	NA	1098.66	3.46
Alta Lode-Bendigo	20.919	NA	1.100	207.0	4940	139	1.860	0.530	NA	17.700	NA	260.53	5.25
Alta Lode-Bendigo	21.276	NA	0.800	146.0	4730	98	1.620	0.760	NA	15.600	NA	150.35	8.53
Alta Lode-Bendigo	5.000	NA	0.900	144.0	4620	223	1.800	0.520	NA	16.500	NA	478.02	2.41

<DL: below detection limit

NA: not analysed

Electronic Supplementary Materials associated with the chapter 4

AppendIx 4.1A Summary of all Sm-Nd isotope LASS-ICPMS analyses of scheelite crystals.

Sample ID	Sm ppm	Nd ppm	$^{147}Sm/^{144}Nd_0$	2SE on $^{147}Sm/^{144}Nd_0$	$^{143}Nd/^{144}Nd_0$	2SE on $^{143}Nd/^{144}Nd_0$	Age (t) in Ga	$^{143}Nd/^{144}Nd_t$	εNd_t
Celine-1	31.87	147.40	0.125863	0.000084	0.512508	0.000041	0.354	0.512216	**0.71**
Celine-2	19.50	96.30	0.11765	0.0003	0.512529	0.000049	0.354	0.512256	**1.49**
Celine-3	37.54	165.90	0.1332	0.00027	0.512553	0.00003	0.354	0.512244	**1.25**
Celine-4	25.13	129.40	0.11336	0.00067	0.512472	0.000041	0.354	0.512209	**0.57**
Celine-5	27.73	135.30	0.1186	0.00079	0.512533	0.000036	0.354	0.512258	**1.52**
Celine-6	21.11	101.93	0.1222	0.0001	0.512442	0.000056	0.354	0.512159	**-0.42**
Celine-7	24.58	129.05	0.11317	0.00023	0.512393	0.000046	0.354	0.512131	**-0.96**
Celine-8	24.15	116.59	0.12179	0.00046	0.5124	0.000039	0.354	0.512118	**-1.22**
Celine-9	21.56	105.63	0.11965	0.00023	0.512416	0.000056	0.354	0.512139	**-0.81**
Dublin Gulch-1	19.40	133.00	0.08812	0.00042	0.512103	0.000055	0.093	0.512049	**-9.11**
Dublin Gulch-2	23.54	165.40	0.08714	0.00018	0.512074	0.000056	0.093	0.512021	**-9.66**
Dublin Gulch-3	22.82	151.90	0.09227	0.00016	0.512089	0.000056	0.093	0.512033	**-9.43**
Dublin Gulch-4	29.64	214.60	0.08446	0.00032	0.512105	0.000047	0.093	0.512054	**-9.03**
Dublin Gulch-5	23.75	160.70	0.08926	0.00024	0.512042	0.000042	0.093	0.511988	**-10.31**
Dublin Gulch-6	29.58	210.20	0.085389	0.000058	0.512122	0.000043	0.093	0.512070	**-8.71**
Dublin Gulch-7	25.60	175.20	0.088934	0.000058	0.512105	0.000046	0.093	0.512051	**-9.08**
Fort Knox-1	10.64	52.55	0.113069	0.000073	0.512191	0.000067	0.092	0.512123	**-7.70**
Fort Knox-2	15.98	79.70	0.092095	0.000055	0.512206	0.000061	0.092	0.512151	**-7.16**
Fort Knox-3	38.61	144.90	0.12721	0.0009	0.512192	0.000067	0.092	0.512115	**-7.85**
Fort Knox-4	9.55	64.46	0.08979	0.00011	0.512154	0.000082	0.092	0.512100	**-8.15**
Fort Knox-5	37.54	164.80	0.13509	0.00018	0.51231	0.000037	0.092	0.512229	**-5.64**
Fort Knox-6	25.77	145.50	0.104083	0.000091	0.512192	0.00004	0.092	0.512129	**-7.58**
Fort Knox-7	31.94	157.00	0.120927	0.000073	0.5123	0.000042	0.092	0.512227	**-5.67**
Fort Knox-8	41.82	199.50	0.12594	0.00025	0.512279	0.000041	0.092	0.512203	**-6.13**
Fort Knox-9	31.13	148.23	0.12593	0.0004	0.5122	0.000036	0.092	0.512124	**-7.68**
Fort Knox-10	20.14	111.52	0.10477	0.00027	0.512144	0.00005	0.092	0.512081	**-8.52**
Fort Knox-11	45.28	213.04	0.128575	0.00009	0.512165	0.000032	0.092	0.512088	**-8.39**
Lened-1	17.86	120.40	0.08945	0.00033	0.511671	0.000052	0.096	0.511615	**-17.51**

AppendIx 4.1A (continued)

Sample ID	Sm ppm	Nd ppm	$^{147}Sm/^{144}Nd_0$	2SE on $^{147}Sm/^{144}Nd_0$	$^{143}Nd/^{144}Nd_0$	2SE on $^{143}Nd/^{144}Nd_0$	Age (t) in Ga	$^{143}Nd/^{144}Nd_t$	εNd_t
Lened-2	14.01	41.36	0.20302	0.00074	0.51172	0.00011	0.096	0.511592	**-17.95**
Lened-3	30.99	128.30	0.1454	0.0019	0.511622	0.000078	0.096	0.511531	**-19.16**
Lermontovskoe-1	38.30	145.90	0.1532	0.0014	0.512477	0.000034	0.112	0.512365	**-2.48**
Lermontovskoe-2	21.96	74.20	0.17741	0.00084	0.512573	0.000065	0.112	0.512443	**-0.95**
Lermontovskoe-3	17.75	99.70	0.1033	0.0011	0.512455	0.000043	0.112	0.512379	**-2.20**
Lermontovskoe-4	6.14	29.48	0.12217	0.0004	0.51252	0.00011	0.112	0.512430	**-1.20**
Lermontovskoe-5	22.20	104.10	0.12521	0.00084	0.512432	0.000043	0.112	0.512340	**-2.96**
Lermontovskoe-6	24.36	124.00	0.11429	0.00011	0.512511	0.000054	0.112	0.512427	**-1.26**
Lermontovskoe-7	18.50	59.32	0.18429	0.0008	0.512571	0.000068	0.112	0.512436	**-1.09**
Northern Dancer-1	259.34	610.61	0.2526	0.0011	0.512462	0.00002	0.118	0.512267	**-4.24**
Northern Dancer-2	269.89	582.39	0.27308	0.00027	0.51249	0.000022	0.118	0.512279	**-4.00**
Northern Dancer-3	193.86	482.24	0.24037	0.00055	0.512457	0.000022	0.118	0.512271	**-4.15**
Northern Dancer-4	255.64	610.61	0.2457	0.0013	0.512453	0.00002	0.118	0.512263	**-4.31**
Northern Dancer-5	253.86	604.72	0.25073	0.00048	0.512447	0.000022	0.118	0.512253	**-4.50**
Mactung-1	18.23	104.40	0.10303	0.00024	0.512143	0.000042	0.0975	0.512077	**-8.45**
Mactung-2	12.99	69.50	0.11128	0.00026	0.512111	0.000086	0.0975	0.512040	**-9.18**
Mactung-3	14.37	86.00	0.1003	0.00011	0.512079	0.000067	0.0975	0.512015	**-9.67**
Mactung-4	21.80	131.80	0.09951	0.00093	0.512111	0.000042	0.0975	0.512048	**-9.03**
Mactung-5	22.24	132.20	0.10136	0.00054	0.512097	0.000049	0.0975	0.512032	**-9.33**
Mactung-6	14.77	83.60	0.10788	0.00033	0.512082	0.00006	0.0975	0.512013	**-9.70**
Mactung-7	16.33	89.30	0.109274	0.00005	0.512084	0.000068	0.0975	0.512014	**-9.68**
Mactung-8	17.17	100.90	0.10109	0.00026	0.512182	0.000055	0.0975	0.512118	**-7.67**
Mactung-9	21.77	130.00	0.1013	0.0028	0.512118	0.000054	0.0975	0.512053	**-8.92**
Mactung-10	20.41	118.00	0.10267	0.00015	0.512107	0.000053	0.0975	0.512042	**-9.15**
Scheelite Dome-1	26.95	91.80	0.17223	0.00046	0.511536	0.00005	0.0925	0.511410	**-21.17**
Scheelite Dome-2	27.00	95.22	0.16972	0.00014	0.511392	0.000054	0.0925	0.511268	**-23.95**
Votosk-2-1	15.64	87.50	0.10534	0.00016	0.512503	0.000074	0.112	0.512426	**-1.29**
Votosk-2-2	19.79	102.60	0.114445	0.00009	0.512385	0.000049	0.112	0.512301	**-3.72**

AppendIx 4.1A (continued)

Sample ID	Sm ppm	Nd ppm	$^{147}Sm/^{144}Nd_0$	2SE on $^{147}Sm/^{144}Nd_0$	$^{143}Nd/^{144}Nd_0$	2SE on $^{143}Nd/^{144}Nd_0$	Age (t) in Ga	$^{143}Nd/^{144}Nd_t$	εNd_t
Votosk-2-3	12.16	97.90	0.07281	0.00084	0.51233	0.000064	0.112	0.512277	**-4.20**
Votosk-2-4	5.20	62.90	0.04942	0.00015	0.512321	0.000078	0.112	0.512285	**-4.04**
Votosk-2-5	20.85	99.00	0.12439	0.00054	0.512295	0.000053	0.112	0.512204	**-5.62**
Votosk-2-6	9.33	56.50	0.098	0.00023	0.512336	0.000067	0.112	0.512264	**-4.44**
Votosk-2-7	12.60	92.50	0.080465	0.000084	0.512316	0.000053	0.112	0.512257	**-4.58**
Votosk-2-8	9.52	91.13	0.06153	0.00047	0.512285	0.000045	0.112	0.512240	**-4.92**
Votosk-2-9	10.96	68.23	0.09587	0.00071	0.512254	0.000072	0.112	0.512184	**-6.01**
Votosk-2-10	15.41	116.31	0.0782	0.0017	0.512207	0.000045	0.112	0.512150	**-6.68**
Cantung_Ezone-1	16.30	83.25	0.1181	0.00012	0.511749	0.000055	0.0975	0.511674	**-16.33**
Cantung_Ezone-2	15.60	68.17	0.13487	0.00012	0.511723	0.000059	0.0975	0.511637	**-17.04**
Cantung_Ezone-3	13.91	64.58	0.129939	0.000074	0.511755	0.000066	0.0975	0.511672	**-16.36**
Cantung_Ezone-4	25.48	98.64	0.1553	0.00017	0.511768	0.000058	0.0975	0.511669	**-16.42**
Cantung_Ezone-5	41.10	114.12	0.21643	0.00023	0.511855	0.000047	0.0975	0.511717	**-15.48**
Cantung_Ezone-6	23.07	67.68	0.2067	0.0013	0.511932	0.000067	0.0975	0.511800	**-13.86**
Cantung_Ezone-7	20.54	86.23	0.144604	0.000041	0.511813	0.000061	0.0975	0.511721	**-15.41**
Cantung_Ezone-8	37.87	130.97	0.174339	0.000098	0.511896	0.000045	0.0975	0.511785	**-14.16**
Cantung_Ezone-9	15.11	65.02	0.13867	0.00023	0.511866	0.000058	0.0975	0.511778	**-14.30**
Cantung_Ezone-10	41.76	124.12	0.200987	0.000075	0.511861	0.000061	0.0975	0.511733	**-15.17**
Cantung_Ezone-11	15.10	68.29	0.13158	0.0002	0.511761	0.000063	0.0975	0.511677	**-16.26**
Cantung_open pit-1	55.90	99.60	0.3413	0.0043	0.512073	0.000051	0.0975	0.511855	**-12.78**
Cantung_open pit-2	45.00	95.80	0.284	0.0015	0.512054	0.000076	0.0975	0.511873	**-12.44**
Cantung_open pit-3	73.20	154.40	0.2882	0.0016	0.511937	0.000049	0.0975	0.511753	**-14.78**
Cantung_open pit-4	86.90	107.30	0.48733	0.00069	0.51211	0.000058	0.0975	0.511799	**-13.88**
Cantung_open pit-5	41.86	106.90	0.2339	0.0015	0.511876	0.000063	0.0975	0.511727	**-15.29**
Cantung_open pit-6	98.10	127.00	0.4656	0.0032	0.512097	0.000059	0.0975	0.511800	**-13.86**
Cantung_open pit-7	22.70	66.80	0.2046	0.0037	0.511931	0.000081	0.0975	0.511800	**-13.85**
Cantung_open pit-8	110.70	269.60	0.24776	0.0007	0.511881	0.000039	0.0975	0.511723	**-15.37**

Age corrected values calculated using the following formula: $^{143}Nd/^{144}Nd_t = {}^{143}Nd/^{144}Nd_0 - {}^{147}Sm/^{144}Nd_0 (e^{\lambda t} - 1)$, where $^{143}Nd/^{144}Nd_0$ and $^{147}Sm/^{144}Nd_0$ are the measured values, $\lambda = 0.00654$ Ga (White, 2015) and t = sample age. The εNd_t was calculated using CHUR $^{143}Nd/^{144}Nd_0 = 0.512638$ and

$^{147}Sm/^{144}Nd_0$ = 0.1960 (Bouvier et al., 2008) and the following formula: $\varepsilon Nd_t = ([^{143}Nd/^{144}Nd]sample_t - [^{143}Nd/^{144}Nd]CHUR_t / [^{143}Nd/^{144}Nd]CHUR_t * 10000)$.